Mathematical Problems in Engineering

Distributed Control and Estimation of Networked Agent Systems

Guest Editors: Wenwu Yu, Ming Cao, Guanrong Chen, Guanghui Wen, and Xinghuo Yu

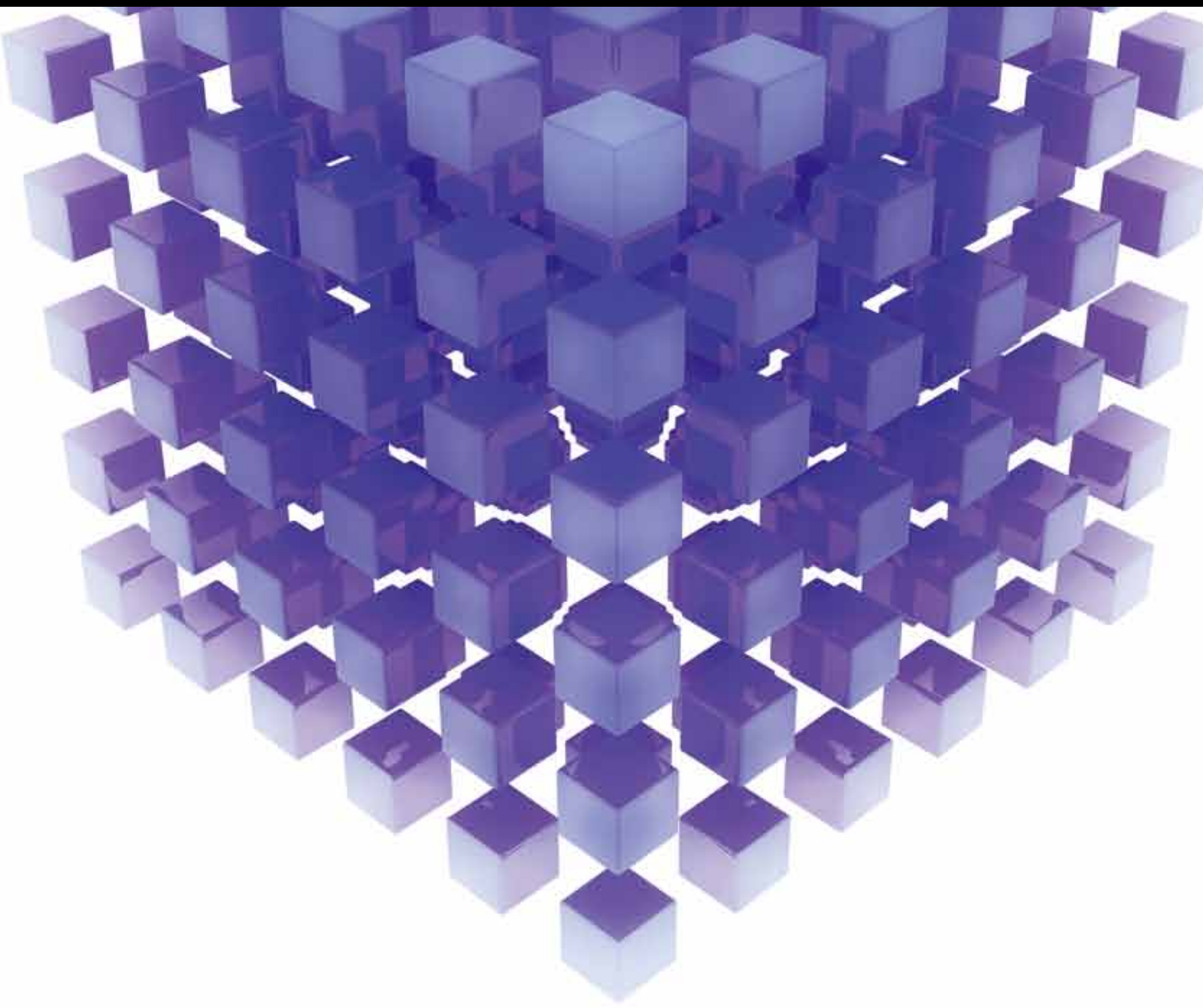

Distributed Control and Estimation of Networked Agent Systems

Mathematical Problems in Engineering

Distributed Control and Estimation of Networked Agent Systems

Guest Editors: Wenwu Yu, Ming Cao, Guanrong Chen, Guanghui Wen, and Xinghuo Yu

Editorial Board

Contents

Distributed Control and Estimation of Networked Agent Systems, Wenwu Yu, Ming Cao, Guanrong Chen, Guanghui Wen, and Xinghuo Yu
Volume 2013, Article ID 287917, 1 page

Synchronizability of Small-World Networks Generated from a Two-Dimensional Kleinberg Model, Yi Zhao, Jianwen Feng, and Jingyi Wang
Volume 2013, Article ID 451960, 7 pages

Impulsive Pinning Markovian Switching Stochastic Complex Networks with Time-Varying Delay, Chen Xu, Jingyi Wang, Jianwen Feng, and Yi Zhao
Volume 2013, Article ID 461924, 9 pages

A Hybrid Distributed Mutual Exclusion Algorithm for Cluster-Based Systems, Moharram Challenger, Elif Haytaoglu, Gorkem Tokatli, Orhan Dagdeviren, and Kayhan Erciyes
Volume 2013, Article ID 703414, 15 pages

Nonfragile Guaranteed Cost Control and Optimization for Interconnected Systems of Neutral Type, Heli Hu, Dan Zhao, and Qingling Zhang
Volume 2013, Article ID 586091, 15 pages

State Consensus Analysis and Design for High-Order Discrete-Time Linear Multiagent Systems, Yanrong Ge, Yangzhou Chen, Yaxiao Zhang, and Zhonghe He
Volume 2013, Article ID 192351, 13 pages

Design of an Attitude and Heading Reference System Based on Distributed Filtering for Small UAV, Long Zhao and Qing Yun Wang
Volume 2013, Article ID 498739, 8 pages

Capacity Analysis for Parallel Runway through Agent-Based Simulation, Yang Peng, Gao Wei, and Sun Jun-Qing
Volume 2013, Article ID 505794, 8 pages

Approximate Analytical Solutions of Fractional Perturbed Diffusion Equation by Reduced Differential Transform Method and the Homotopy Perturbation Method, Zhoujin Cui, Zisen Mao, Sujuan Yang, and Pinneng Yu
Volume 2013, Article ID 186934, 7 pages

Synchronization of Intermittently Coupled Dynamical Networks, Gang Zhang and Guanrong Chen
Volume 2013, Article ID 208609, 9 pages

Controllability of Second-Order Multiagent Systems with Multiple Leaders and General Dynamics, Bo Liu, Hongke Feng, Li Wang, Rong Li, Junyan Yu, Housheng Su, and Guangming Xie
Volume 2013, Article ID 587569, 6 pages

Improved Power Flow Algorithm for VSC-HVDC System Based on High-Order Newton-Type Method, Yanfang Wei, Qiang He, Yonghui Sun, Yanzhou Sun, and Cong Ji
Volume 2013, Article ID 235316, 10 pages

H_∞ Control of Network-Based Systems with Packet Disordering and Packet Loss Compensation, Jinna Li, Lifeng Wei, Chao Liu, and Haibin Yu
Volume 2013, Article ID 836314, 9 pages

Consensus of Continuous-Time Multiagent Systems with General Linear Dynamics and Nonuniform Sampling, Yanping Gao, Bo Liu, Min Zuo, Tongqiang Jiang, and Junyan Yu
Volume 2013, Article ID 718759, 7 pages

Optimal Bandwidth Scheduling of Networked Learning Control System Based on Nash Theory and Auction Mechanism, Xiang Yan, Hongbo Li, Lide Wang, and Ping Shen
Volume 2013, Article ID 540687, 8 pages

Distributed Robust H_∞ Consensus Control of Multiagent Systems with Communication Errors Using Dynamic Output Feedback Protocol, Xi Yang and Jinzhi Wang
Volume 2013, Article ID 979087, 12 pages

A Distributed Flow Rate Control Algorithm for Networked Agent System with Multiple Coding Rates to Optimize Multimedia Data Transmission, Shuai Zeng, Lemin Li, and Dan Liao
Volume 2013, Article ID 983637, 11 pages

Absolute Stability and Master-Slave Synchronization of Systems with State-Dependent Nonlinearities, Rong Li, Bo Liu, and Chao Liu
Volume 2013, Article ID 326560, 6 pages

Cooperative Control for Uncertain Multiagent Systems via Distributed Output Regulation, Lu Yu and Jinzhi Wang
Volume 2013, Article ID 898375, 11 pages

Bifurcation and Hybrid Control for A Simple Hopfield Neural Networks with Delays, Zisen Mao, Hao Wang, Dandan Xu, and Zhoujin Cui
Volume 2013, Article ID 315367, 8 pages

Controllability of Weighted and Directed Networks with Nonidentical Node Dynamics, Linying Xiang, Jonathan J. H. Zhu, Fei Chen, and Guanrong Chen
Volume 2013, Article ID 405034, 10 pages

Feature Selection in Decision Systems: A Mean-Variance Approach, Chengdong Yang, Wenyin Zhang, Jilin Zou, Shunbo Hu, and Jianlong Qiu
Volume 2013, Article ID 268063, 8 pages

Synchronization of *N* Different Chaotic Systems Based on Antisymmetric Structure, Xiangyong Chen and Jianlong Qiu
Volume 2013, Article ID 742765, 6 pages

The Effects of Decision-Making Processes and Population Turnover on the Formation of Social Networks, Zhijing Xu, Zhenghu Zu, Tao Zheng, Wendou Zhang, and Qing Xu
Volume 2013, Article ID 906785, 7 pages

Delayed Antiwindup Control Using a Decoupling Structure, Huawei Zhu, Guozheng Qin, Yingxin Yan, Zhichao Jiang, and Zhisheng Duan
Volume 2013, Article ID 248153, 7 pages

Hybrid Synchronization of General T-S Fuzzy Complex Dynamical Networks with Time-Varying Delay, Degang Xu, Weihua Gui, Panlei Zhao, and Chunhua Yang
Volume 2013, Article ID 384654, 8 pages

A Multiagent Dynamic Assessment Approach for Water Quality Based on Improved Q-Learning Algorithm, Jianjun Ni, Li Ren, Minghua Liu, and Daqi Zhu
Volume 2013, Article ID 812032, 7 pages

Second-Order Consensus in Multiagent Systems via Nonlinear Protocol, Huan Pan, Xiaohong Nian, and Ling Guo
Volume 2013, Article ID 978251, 7 pages

Hindawi Publishing Corporation
Mathematical Problems in Engineering
Volume 2013, Article ID 287917, 1 page
http://dx.doi.org/10.1155/2013/287917

Editorial

Distributed Control and Estimation of Networked Agent Systems

Wenwu Yu,[1] Ming Cao,[2] Guanrong Chen,[3] Guanghui Wen,[4] and Xinghuo Yu[5]

[1] *Department of Mathematics, Southeast University, Nanjing 210096, China*
[2] *Faculty of Mathematics and Natural Sciences, ITM, University of Groningen, 9747 AG Groningen, The Netherlands*
[3] *Department of Electronic Engineering, City University of Hong Kong, Hong Kong*
[4] *School of Engineering and Information Technology, The University of New South Wales at ADFA, Canberra, ACT 2600, Australia*
[5] *School of Electrical and Computer Engineering, RMIT University, Melbourne, VIC 3001, Australia*

Correspondence should be addressed to Wenwu Yu; wenwuyu@gmail.com

Received 24 September 2013; Accepted 24 September 2013

This special issue focuses on distributed control and estimation of networked agent systems. It is well known that, nowadays, most of the real-world large-scale systems can be modeled as networked agent systems, where examples include biological systems, multivehicle systems, and distributed sensor systems. Within this context, centralized control laws or estimation algorithms may be no longer valid since the size of such a networked agent system can be huge. Furthermore, each individual agent in such a networked system may have limited computational and sensing abilities; thus, distributed control and estimation design become necessary but challenging. Recently, distributed control and estimation of networked agent systems have been widely applied in various domains including distributed computing, formation control, spacecraft control, distributed sensor networks, and smart grids.

This special issue contains twenty-seven papers, most of which are related to distributed control and estimation of networked agent systems. In particular, six papers discuss coordination control for networked agent systems with communication constrains and higher-order dynamics. There are seven papers investigating synchronization in complex networks. In addition, modeling, identification, and optimization of networked agent systems are studied in another set of three papers. Furthermore, dynamics and control of networked systems are discussed in five papers. To apply dynamics and control of networked systems into some practical problems, six papers studied some potential applications in social network, water quality, UAVs, and so on.

It should be noted that the selected topics and published papers in this special issue are not a comprehensive study in distributed control and estimation of networked agent systems. However, they do provide some recent advances covering many topics in this field, which could benefit the current research to some extent.

Wenwu Yu
Ming Cao
Guanrong Chen
Guanghui Wen
Xinghuo Yu

Hindawi Publishing Corporation
Mathematical Problems in Engineering
Volume 2013, Article ID 451960, 7 pages
http://dx.doi.org/10.1155/2013/451960

Research Article

Synchronizability of Small-World Networks Generated from a Two-Dimensional Kleinberg Model

Yi Zhao,[1] Jianwen Feng,[1] and Jingyi Wang[2]

[1] *College of Mathematics and Computational Science, Shenzhen University, Shenzhen 518060, China*
[2] *College of Information and Engineering, Shenzhen University, Shenzhen 518060, China*

Correspondence should be addressed to Jianwen Feng; fengjw@szu.edu.cn

Received 5 June 2013; Accepted 26 July 2013

Academic Editor: Wenwu Yu

This paper investigates the synchronizability of small-world networks generated from a two-dimensional Kleinberg model, which is more general than NW small-world network. The three parameters of the Kleinberg model, namely, the distance of neighbors, the number of edge-adding, and the edge-adding probability, are analyzed for their impacts on its synchronizability and average path length. It can be deduced that the synchronizability becomes stronger as the edge-adding probability increases, and the increasing edge-adding probability could make the average path length of the Kleinberg small-world network go smaller. Moreover, larger distance among neighbors and more edges to be added could play positive roles in enhancing the synchronizability of the Kleinberg model. The lorentz oscillators are employed to verify the conclusions numerically.

1. Introduction

A complex network is a large set of nodes (or vertices) connected by a set of links (or edges) such as coupled biological and chemical system, neural networks, social interacting species, the Internet, and the World Wide Web. Recently, increasing interest has been devoted to the study of collective behaviors in complex networks for its widely applications in real world. Among the studies on the complex network, synchronization phenomena attract the interests of most scientists and engineers. Loosely speaking, synchronization is the process in which two (or more) dynamical systems seek to adjust a certain prescribed property of their motion to a common behavior in the limit as time tends to infinity either by virtue of coupling or by forcing. Synchronization of complex networks is an important mathematical problem in both the physical and biological sciences since it has potential applications to diverse fields such as communications security, seismology, and parallel image processing [1–6].

Complex networks could be classified as many types. Among them, synchronization on small-world networks has attracted considerable attention since the pioneering work of Stanley Milgram in the 1960s [7]. A small-world network can be generated by either random edge-rewiring, which gives WS small-world network [8], or random edge-adding, which yields the NW small-world network [9]. The Kleinberg small-world network, in which the edge-adding probabilities are proportional to the length of the edge to be added, could be seen as a more general NW small-world network.

Various literatures have already been devoted to the studies on synchronizability of small-world networks. In the research articles [10–13], the synchronizability of a small-world network generated by randomly adding a fraction of long-range shortcuts to a ring network is investigated. It can be deduced from the theoretical analysis and numerical simulation that the synchronizability of the small-world network becomes stronger as the edge-adding probability p grows larger. In [14], Tang et al. found that the synchronizability of the network as a function of the distance is fluctuant and there exist some distances that have almost no impact on the synchronizability when they investigated the impact of edge-adding number and edge-adding distance on both synchronizability and average path length of NW small-world networks generated from ring networks via random edge-adding. Moreover, the relationship between the synchronizability and the average path length of a small-world network

is studied in [15–18]. The analysis and numerical simulations show that the synchronizability of the small-world network grows as p increases and the average path length becomes smaller as p goes larger. Therefore, it can be deduced that the decreasing in the average path length may result in the increasing synchronizability. These phenomena are interesting, and a natural question is that whether other small-world networks have similar properties, which motivates us to take a two-dimensional Kleinberg small-world network [19] as an example and investigate the impact factors of such network. It should be mentioned that the synchronizability of an undirected Kleinberg small-world network was investigated in [20]. However, the Kleinberg model is built as a directed network in [19]. Thus, the directions of the edge-adding in building the Kleinberg model are considered in this paper. Moreover, [20] only discussed the relationship between the edge-adding probability and the synchronizability of the small-world network, while in this paper the three parameters of the Kleinberg model, namely, the distance of neighbours, the number of edge-adding, and the edge-adding probability, would be analyzed for their impacts on its synchronizability and average path length. Actually, this paper improves the results in [20].

In this paper, we investigate the impacts of the distance of neighbors, the number of edge-adding and the edge-adding probability on the synchronizability of the Kleinberg small-world network. The Kleinberg small-world network is an $N \times N$ two-dimensional one. We add q edges on the nodes with certain probability Π. Then, we could get some conclusions about impact factor on the synchronizability and the average path length of the Kleinberg small-world network, which are complementary to the studies on the synchronizability of the small-world networks.

2. Preliminaries

First of all, we build a Kleinberg small-world network in the way introduced in [19]. Figure 1 also comes from [19], and we redraw it in our case to be studied. A Kleinberg small-world network is composed of the set of lattice points in an $N \times N$ square, which are denoted as $\{(i, j) : i \in \{1, 2, \ldots, N\}, j \in \{1, 2, \ldots, N\}\}$. The lattice distance between two nodes (i, j) and (k, l) is defined to be the number of "lattice steps," which could be written as $d((i, j), (k, l)) = |k - i| + |l - j|$. Let p and q be positive integers. The node u is connected with every other node within lattice distance p, and we name it local contact. We also construct edges from u to q other nodes using independent random trials, which are called the long-range contacts. The probability of edge connected between u and v is proportional to $[d(u, v)]^{-\alpha}$, where α is a given constant. Precisely speaking, this probability of the connections between u and v is denoted as Π_{uv}, and

$$\Pi_{uv} = \frac{[d(u, v)]^{-\alpha}}{\sum_v [d(u, v)]^{-\alpha}}. \tag{1}$$

Figure 1 shows basic structures of a 10×10 Kleinberg small-world network. In Figure 1(b), there are two long-rang contacts from a node "a" to a node "b" and a node "c". Actually, two long-range contacts are added to every node in this network if $q = 2$.

Actually, this model could be interpreted in the point of "geography" in [19]. Individuals live on a grid and know their neighbors for some number of steps in all directions; they also have some number of acquaintances distributed more broadly across the grid. If we fixed p and q and let the value of the exponent α vary, we would have a one-parameter family of network models. When $\alpha = 0$, the uniform distribution over long-range contacts could be obtained, which means long-range contacts are chosen independently of their position on the grid. In this sense, the Kleinberg small-world network could be seen as a kind of NW small-world network. As α increases, the long-range contacts of a node become more and more clustered in their vicinity on the grid. Thus, α could be seen as a basic structural parameter measuring how widely "networked" the underlying society of nodes is. Considering that α could reveal some basic properties of the Kleinberg network, in this paper, we investigate the effect of adding-edges probabilities, namely, the effect of the parameter α on the synchronizability of the Kleinberg small-world network. Moreover, two other parameters of the Kleinberg small-world network, namely, the distance of neighbors and the number of edge-adding, are also considered for their influences of synchronizability.

Next, the synchronizability analysis of the complex dynamical system follows [21]. The complex dynamical system considered in this paper consists of coupled continuous-time nonlinear oscillators. Since chaotic behaviors are common since the intrinsic nonlinearity exists in each individual oscillator, chaotic synchronization is addressed by choosing the parameters of each oscillator such that it exhibits a chaotic attractor in order to be general. Then, the network of $N \times N$ identical dynamics nodes considered in this paper can be written as

$$x_i = F(x_i) + c \sum_{j=1}^{N \times N} a_{ij} H(x_j). \tag{2}$$

Here, if the node is located at (k, l) in the network, we denote the index $i = N(k - 1) + l$, and thus, $i \in \{1, 2, 3, \ldots, N^2\}$. $x_i \in R^n$ is the state vector of the ith node in all $N \times N$ nodes. c is a positive constant coupling strength. $F(\cdot) : R^n \to R^n$ is a well-defined nonlinear function and $H(\cdot) : R^n \to R^n$ is a coupling function. $A = (a_{ij})_{N^2 \times N^2}$ is a coupling matrix determined by the connection topology. That is, $a_{ij} = 1$ if the node i and j have connections, and $a_{ij} = 0$ otherwise. Moreover, it is required that $a_{ii} = -\sum_{j=1, j \neq i}^{N^2} a_{ij}$ for any $i \in 1, 2, \ldots, N^2$. Note that A is not necessarily symmetric since our considered network is directed. Moreover, there is only one zero eigenvalue of the matrix A such that the eigenvalues can be sorted as

$$0 = \lambda_1 > \operatorname{Re} \lambda_2 \geq \operatorname{Re} \lambda_3 \geq \cdots \geq \operatorname{Re} \lambda_{N^2}. \tag{3}$$

Let $ds/dt = F(s)$, and $s(t)$ is automatically a solution of (2). Then, the synchronous state is defined as $x_1 = x_2 = \cdots = x_{N^2} = s$. Let $\xi_i = x_i(t) - s$. For the system described by (2), the variational equations governing the time evolution of the set

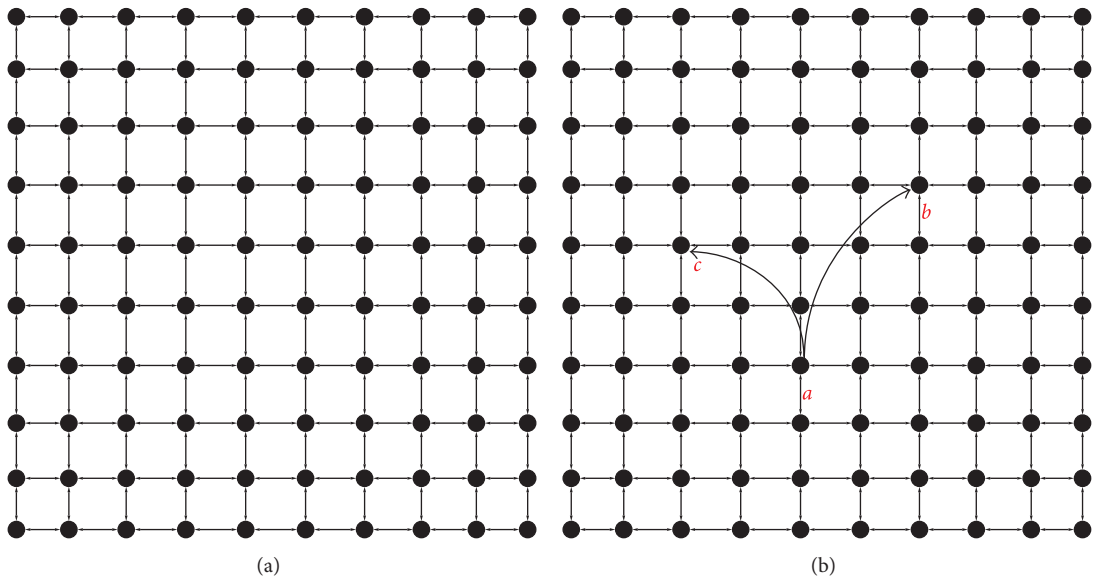

Figure 1: (a) A two-dimensional Kleinberg network with 10×10 nodes, the distance of local contacts $p = 1$, and it has no long-range contacts thus $q = 0$. (b) The contacts of a node "a" with the distance of local contacts $p = 1$ and the number of long-range contacts $q = 2$. "ab" and "ac" are the two long-range contacts.

of infinitesimal vectors about the synchronous solution $\xi_i(t)$ are

$$\xi_i = DF(s)\,\xi_i + c\sum_{j=1}^{N^2} a_{ij} DH(s)\,\xi_j, \quad i = 1, 2, \ldots, N^2, \tag{4}$$

where $DF(s)$ and $DH(s)$ are the $n \times n$ Jacobian matrices of the corresponding vector functions evaluated at $s(t)$, respectively. Let $\xi = \{\xi_1, \xi_2, \ldots, \xi_{N^2}\}$. Then, (4) can be rewritten as

$$\dot{\xi} = DF(s)\,\xi + cDH(s)\,\xi A. \tag{5}$$

By using Jordan transformation with respect to the coupling matrix A, we have

$$\Lambda = P^{-1}AP = \begin{pmatrix} 0 & & & \\ & B_1 & & \\ & & \ddots & \\ & & & B_l \end{pmatrix}, \tag{6}$$

where P is composed of the eigenvectors of A. And B_i in (6) are blocks of the form

$$B_i = \begin{pmatrix} \lambda & & & \\ 1 & \lambda & & \\ & \ddots & \ddots & \\ & & 1 & \lambda \end{pmatrix}, \tag{7}$$

where λ is one of the eigenvalues of A.

Letting $\eta = \{\eta_1, \eta_2, \ldots, \eta_{N^2}\} = \xi(P^{-1})^T$ and employing (6), (5) could also be written as

$$\dot{\eta} = DF(s)\,\eta + cDH(s)\,\eta\Lambda^T. \tag{8}$$

Then, each block of the Jordan canonical form corresponds to a subject of these columns in η, which obeys a subset of equations in (8). For instance, if block B_i is $m \times m$, and suppose the corresponding columns of η are denoted by $\eta_1, \eta_2, \ldots, \eta_m$, which could be seen as the modes of perturbations in the generalized eigenspace associated with eigenvalue λ_i, then the equations have the following form

$$\begin{aligned} \dot{\eta}_1 &= [DF(s) + k_i DH(s)]\,\eta_1, \\ \dot{\eta}_2 &= [DF(s) + k_i DH(s)]\,\eta_2 + cDH(s)\,\eta_1, \\ &\vdots \\ \dot{\eta}_m &= [DF(s) + k_i DH(s)]\,\eta_m + cDH(s)\,\eta_{m-1}, \end{aligned} \tag{9}$$

where $k_i = c\lambda_i$. Each block of the previous decoupled equation (9) is structurally the same with only the factor of k_i being different [21].

Define k as a normalized coupling parameter that takes values in the set $\{k = c\lambda_i : i = 1, 2, \ldots, N^2\}$. Denote $L(k)$ as the largest Lyapunov exponent, which is determined from (9). In order to achieve the synchronization of the network, $L(k)$ is required to be negative. It can be explained that a small disturbance from the synchronization state will diminish exponentially so that the synchronous solution is stable. On the contrary, the synchronous solution is unstable and cannot be realized physically if $L(k)$ is positive because small perturbations from the synchronous state will lead to trajectories that diverge from the state. For the reasons mentioned above, in order to achieve the synchronization of the coupled oscillator network (2), all normalized coupling parameters $k = c\lambda_i$ for $i = 2, \ldots, N^2$ should fall in a region in which $L(k)$ should be negative. This region is called the synchronized region. In case that the synchronized region is bounded, namely, $\widetilde{k} < -\operatorname{Re} k < \widehat{k}$, then from (3), we have

$$\widetilde{k} < -c\operatorname{Re}\lambda_2 \le -c\operatorname{Re}\lambda_3 \le \cdots \le -c\operatorname{Re}\lambda_{N^2} < \widehat{k}. \tag{10}$$

When the spread in the eigenvalue $\operatorname{Re}\lambda_i$ goes smaller, it becomes easier that all the numbers $-c\operatorname{Re}\lambda_3$ fall into the bounded region $\widetilde{k} < k < \widehat{k}$, which means that the synchronizability of the network is better. Thus, we need the ratio of eigenvalue satisfying

$$R = \frac{\operatorname{Re}\lambda_{N^2}}{\operatorname{Re}\lambda_2} < \frac{\widehat{k}}{\widetilde{k}} \tag{11}$$

to be smaller. In case that the synchronized region is unbounded, then $\widetilde{k} < -c\operatorname{Re}\lambda_i < \infty$ for $i = 1, 2, \ldots, N^2$. Thus, the synchronizability of the network is better if the eigenvalue $\operatorname{Re}\lambda_2$ is smaller. Thus, $\operatorname{Re}\lambda_2$ and $\operatorname{Re}\lambda_{N^2}/\operatorname{Re}\lambda_2$ are used as the measure to evaluate the synchronizability of the network.

3. Influencing Factors the Synchronizability of a Network

An extensive numerical analysis is employed to investigate the influences of the distance of neighbors, the number of edge-adding, and the edge-adding probability on the network synchronizability. The Kleinberg small-world networks we considered have 10×10 nodes and 15×15 nodes, respectively. Identical dynamics are assumed for all the nodes in the Kleinberg small-world network.

Let $p = 1, 2$, which means that each node in the Kleinberg small-world network is connected with its nearest neighbors in distance 1 or in distance 2. They form the local contacts. Then, q long-range contacts are added with the probability Π defined in (1). Thus, different q and α would result in different corresponding Laplacian matrix. The eigenvalues of such Laplacian matrix could be calculated. Since the nodes with long-range contacts added are chosen randomly, the Laplacian matrix would be different on each trial. Thus, in the simulation, 100 and 225 different realizations were performed and the results were averaged.

Let $q = 1, 2$, respectively, for the network with 10×10 nodes and 15×15 nodes. The parameter α in (1) on the probability of adding the long-range contacts is chosen from 0.1 to 10 with step size 0.1. Their corresponding Laplacian eigenvalues $\operatorname{Re}\lambda_2$ and $\operatorname{Re}\lambda_{N^2}/\operatorname{Re}\lambda_2$ as a function of α are found, which was shown in Figures 2 and 3, respectively.

Figures 2 and 3 reveal that the values of $\operatorname{Re}\lambda_2$ and $\operatorname{Re}\lambda_{N^2}/\operatorname{Re}\lambda_2$ are continuously and monotonically increasing as α increases. It means that the synchronizability of the Kleinberg small-world network becomes stronger as the edge-adding probability increases. Note that when $\alpha = 0$, Kleinberg small-world network could be seen as the NW small-world network. This result corresponds with the observations in references [10–13]. Also, we can see from Figures 2 and 3 that the synchronizability is enhanced as the number of long-range contacts q and the distance of neighbours p increase. It could be explained that the average path length is reduced as more long-range contacts are built and more short-range contacts are constructed. We illustrate this relationship in Figure 4.

It is well known that as the distance of the edges added increases, the synchronizability of the network becomes stronger since the average path length is shortened. The probability of edge-adding between u and v is proportional to $[d(u, v)]^{-\alpha}$, which is to say that the shorter distance of the edge-adding has larger probabilities than the longer distance of edge-adding for any given α. Then, it can be concluded that if α is fixed, the synchronizability of the Kleinberg small-world network would be better though the probability of edge adding will become smaller. Figures 2, 3, and 4 show that if q is fixed, in other words, q edges would be added into the network, the synchronizability becomes weaker as we take a larger value of α. Then, it means that if distance of the edge-adding and the number of edges are fixed, the synchronizability is enhanced as the probability of the edge-adding increases. Meanwhile, in the Kleinberg small-world network, the probabilities of the long-range contacts decrease as the distance between two nodes increases, especially for

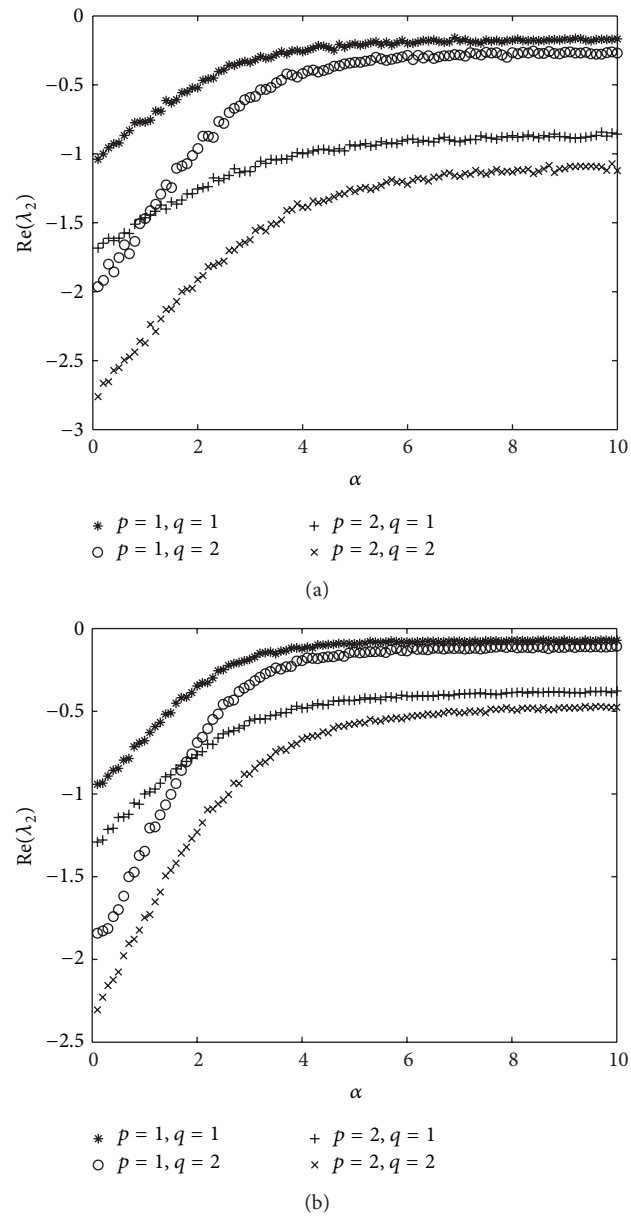

Figure 2: The relationship between $\operatorname{Re}\lambda_2$ and α for the Kleinberg small-world network with (a) 10×10 nodes and (b) 15×15 nodes.

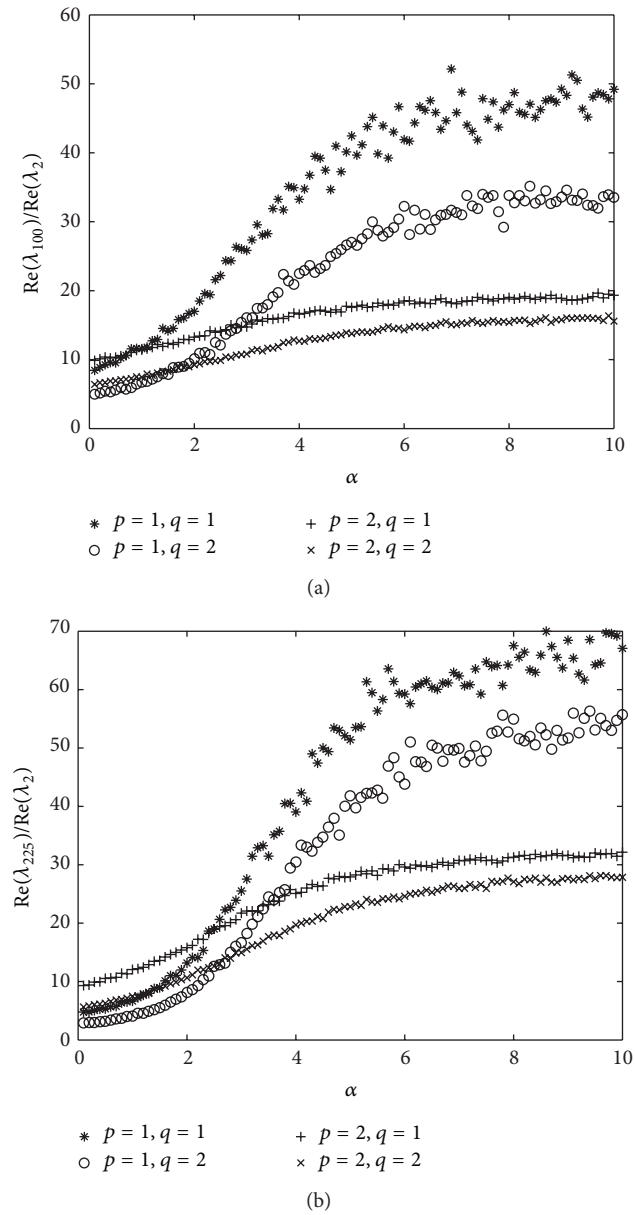

FIGURE 3: The relationship between $\operatorname{Re}\lambda_{N^2}/\operatorname{Re}\lambda_2$ and α for the Kleinberg small-world network with (a) 10×10 nodes and (b) 15×15 nodes.

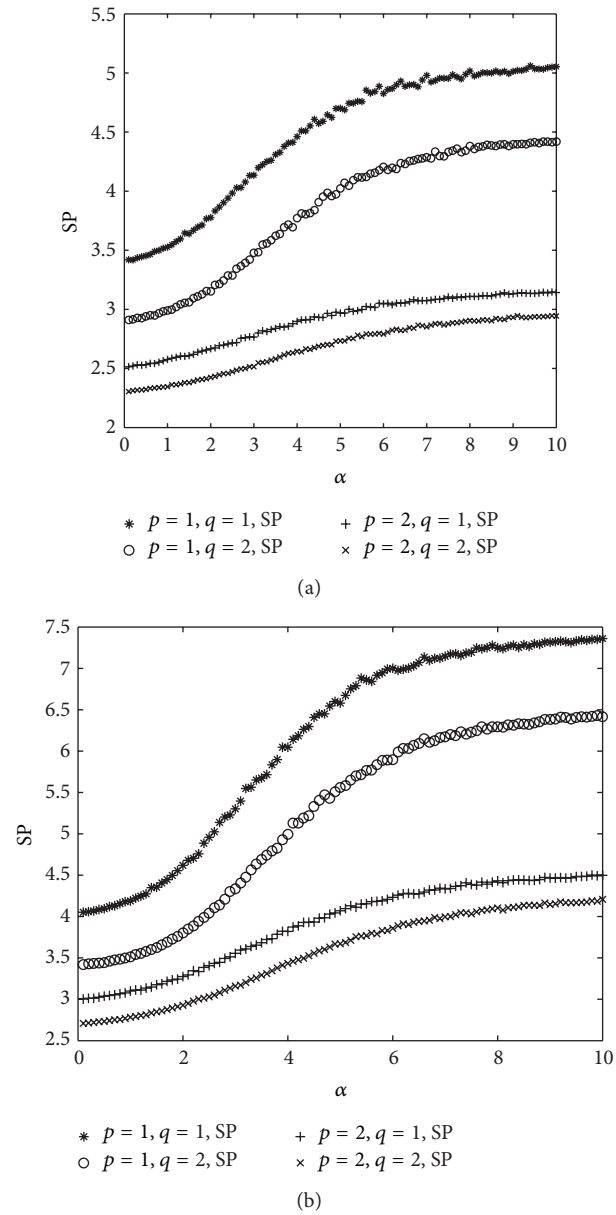

FIGURE 4: The average path length as a function of α with different values of p and q for the Kleinberg small-world network with (a) 10×10 nodes and (b) 15×15 nodes.

large α. As α increases, the long-range contacts of a node become more and more clustered in their vicinity on the grid.

4. Numerical Simulation for Lorentz Oscillators

The linearly coupled Kleinberg small-world network containing identical Lorentz oscillators is used for numerical simulations. Such oscillators can be written as

$$F(x_i) = \begin{cases} \alpha_s(x_{i2} - x_{i1}), \\ \gamma_s x_{i1} - x_{i1}x_{i3} - x_{i2}, \\ x_{i1}x_{i2} - \beta_s x_{i3}, \end{cases} \tag{12}$$

for $i = 1, 2, \ldots, N^2$. Here, $\alpha_s = 10$, $\beta_s = 8/3$, and $\gamma_s = 28$. Let

$$H = \begin{bmatrix} 1 & 0 & 0 \\ 1 & 0 & 0 \\ 0 & 0 & 0 \end{bmatrix}. \tag{13}$$

In the simulation, we consider a network with $N = 10$ (100 nodes). Define the error term as

$$E(t) = \sqrt{\frac{2}{N^2(N^2-1)}\sum_{j>i}\left\|x_i(t) - x_j(t)\right\|^2}. \tag{14}$$

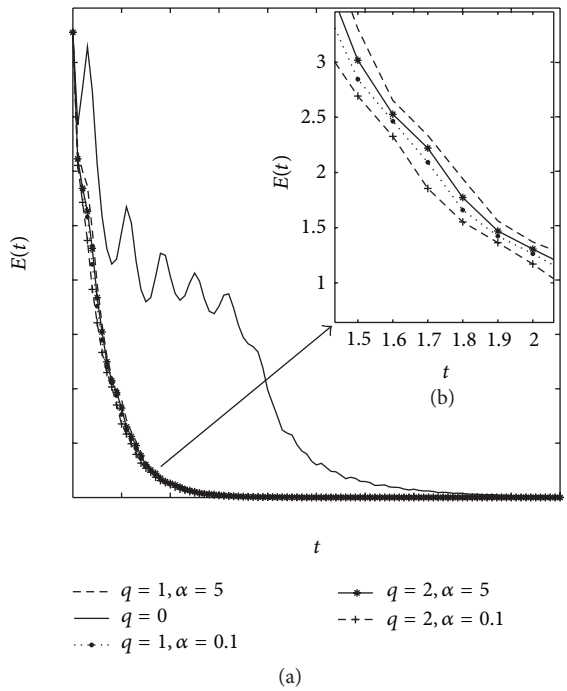

Figure 5: The errors of synchronization among 10×10 different Lorentz dynamics oscillators over time for $p = 1$, $q = 0, 1, 2$, and $\alpha = 0.1, 5$, respectively. The inset is an amplified figure on some time interval.

If $\lim_{t\to\infty} E(t) = 0$, the complex network achieves synchronization. We consider that the synchronizability would be better if $E(t)$ goes to zero faster.

For the network (2), let the coupling strength $c = 70$, the distance of local contacts $p = 1$, the number of long-range contacts $q = 0, 1, 2$, and the parameter $\alpha = 0.1, 5$ in the probability of edge-adding (1), respectively. Figure 5 shows how $E(t)$ evolved in network with the same initial values chosen randomly in the interval $[-10, 10]$. It can be seen from Figure 5 that the synchronizability of the network is enhanced as the number of long-range contacts increases, and the synchronizability of the network becomes better as α goes smaller, which means that longer distance of the edge-adding could still enhance the synchronizability though the probabilities of longer distance of the edge-adding are small compared with the probabilities of shorter distance of edge-adding. Moreover, it can be seen that the synchronizability goes better as the number of edges added becomes larger.

5. Conclusion

The impact factors of synchronizability of two-dimensional Kleinberg small-world network are investigated in this paper. Through mathematical analysis and numerical simulations, we show that the Kleinberg small-world network shares similar properties as NW small-world networks but Kleinberg small-world network is more general. Namely, we see that synchronizability of two-dimensional Kleinberg small-world network is enhanced as the edge-adding probability increases, and the average path length of the Kleinberg small-world network decreases with the increasing edge-adding probability. Moreover, larger distance among neighbors and more edges to be added could play positive roles in enhancing the synchronizability of the Kleinberg model. A network of Lorentz oscillators is taken to make numerical simulations in order to verify the observed phenomena.

Acknowledgments

The authors thank the referees and the editor for their valuable comments on this paper. This work is supported by the Natural Science Foundation of China (Grant no. 61273220), Guangdong Education University Industry Cooperation Projects (Grant no. 2009B090300355) and the Shenzhen Basic Research Project (JC201006010743A, JCYJ20120613105730482), and 2011 Foundation for Distinguished Young Talents in Higher Education of Guangdong (LYM11115).

References

[1] S. H. Strogatz and I. Stewart, "Coupled oscillators and biological synchronization," *Scientific American*, vol. 269, no. 6, pp. 102–109, 1993.

[2] C. M. Gray, "Synchronous oscillations in neuronal systems: mechanisms and functions," *Journal of Computational Neuroscience*, vol. 1, no. 1-2, pp. 11–38, 1994.

[3] L. Glass, "Synchronization and rhythmic processes in physiology," *Nature*, vol. 410, no. 6825, pp. 277–284, 2001.

[4] M. S. de Vieira, "Chaos and synchronized chaos in an earthquake model," *Physical Review Letters*, vol. 82, no. 1, pp. 201–204, 1999.

[5] S. H. Wang, J. Y. Kuang, J. H. Li, Y. L. Luo, H. P. Lu, and G. Hu, "Chaos-based secure communications in a large community," *Physical Review E*, vol. 66, no. 6, Article ID 065202, 2002.

[6] D. Yu, M. Righero, and L. Kocarev, "Estimating topology of networks," *Physical Review Letters*, vol. 97, no. 18, Article ID 188701, 2006.

[7] S. Milgram, "The small world problem," in *Psychology Today*, vol. 2, pp. 60–67, Sussex Publishers, 1967.

[8] D. J. Watts and S. H. Strogatz, "Collective dynamics of small-world networks," *Nature*, vol. 393, no. 6684, pp. 440–442, 1998.

[9] M. E. J. Newman and D. J. Watts, "Renormalization group analysis of the small-world network model," *Physics Letters A*, vol. 263, no. 4–6, pp. 341–346, 1999.

[10] X. F. Wang and G. Chen, "Synchronization in small-world dynamical networks," *International Journal of Bifurcation and Chaos in Applied Sciences and Engineering*, vol. 12, no. 1, pp. 187–192, 2002.

[11] F. Qi, Z. Hou, and H. Xin, "Ordering chaos by random shortcuts," *Physical Review Letters*, vol. 91, no. 6, Article ID 064102, 2003.

[12] V. N. Belykh, I. V. Belykh, and M. Hasler, "Connection graph stability method for synchronized coupled chaotic systems," *Physica D*, vol. 195, no. 1-2, pp. 159–187, 2004.

[13] I. V. Belykh, V. N. Belykh, and M. Hasler, "Blinking model and synchronization in small-world networks with a time-varying coupling," *Physica D*, vol. 195, no. 1-2, pp. 188–206, 2004.

[14] L. Tang, J. Lu, and G. Chen, "Synchronizability of small-world networks generated from ring networks with equal-distance edge additions," *Chaos*, vol. 22, no. 2, Article ID 023121.

[15] T. Nishikawa, A. E. Motter, Y.-C. Lai, and F. C. Hoppensteadt, "Heterogeneity in oscillator networks: are smaller worlds easier to synchronize?" *Physical Review Letters*, vol. 91, no. 1, Article ID 014101, 2003.

[16] M. Zhao, T. Zhou, B.-H. Wang, G. Yan, H.-J. Yang, and W.-J. Bai, "Relations between average distance, heterogeneity and network synchronizability," *Physica A*, vol. 371, no. 2, pp. 773–780, 2006.

[17] X. F. Wang, X. Li, and G. Chen, *Complex Network and Application*, Tsinghua University Press, Beijing, China, 2006.

[18] X. F. Wang, X. Li, and G. Chen, *Network Science: An Introduction*, Higher Education Press, Beijing, China, 2012.

[19] J. Kleinberg, "The small-world phenomenon: an algorithm perspective," in *Proceedings of the 32nd Annual ACM Symposium on Theory of Computing*, 2000.

[20] Y. Zhao, J. W. Feng, and J. Y. Wang, "On synchronizability of kleinberg small world networks," in *Proceedings of 8th International Conference on Computational Intelligence and Security*, pp. 204–208, 2012.

[21] T. Nishikawa and A. E. Motter, "Maximum performance at minimum cost in network synchronization," *Physica D*, vol. 224, no. 1-2, pp. 77–89, 2006.

Hindawi Publishing Corporation
Mathematical Problems in Engineering
Volume 2013, Article ID 461924, 9 pages
http://dx.doi.org/10.1155/2013/461924

Research Article

Impulsive Pinning Markovian Switching Stochastic Complex Networks with Time-Varying Delay

Chen Xu,[1,2] Jingyi Wang,[1] Jianwen Feng,[2] and Yi Zhao[2]

[1] *College of Information Engineering, Shenzhen University, Shenzhen 518060, China*
[2] *College of Mathematics and Computational Science, Shenzhen University, Shenzhen 518060, China*

Correspondence should be addressed to Chen Xu; xuchen_szu@szu.edu.cn

Received 26 April 2013; Revised 28 June 2013; Accepted 7 July 2013

Academic Editor: Wenwu Yu

The synchronization problem of stochastic complex networks with Markovian switching and time-varying delays is investigated by using impulsive pinning control scheme. The complex network possesses noise perturbations, Markovian switching, and internal and outer time-varying delays. Sufficient conditions for synchronization are obtained by employing the Lyapunov-Krasovskii functional method, Itô's formula, and the linear matrix inequality (LMI). Numerical examples are also given to demonstrate the validity of the theoretical results.

1. Introduction and Model Description

Collective behaviors in complex networks and systems have attracted increasing attention in recent years due to their wide applications in physics, mathematics, engineering, biology, and so forth (see [1, 2] and references therein). While complex networks are ubiquitously found in nature and in the modern world, such as neural networks, socially interacting animal species, power networks, wireless sensor networks, Internet, and the World Wide Web.

In the past few decades, the synchronization problems in complex networks have attracted increasing attention. Many synchronization patterns have been studied, including complete synchronization [3], cluster synchronization [4–6], phase synchronization [7], and partial synchronization [8]. There are several control methods to guide the dynamics of a complex network to a desired state, such as adaptive control [9], feedback control [10], intermittent control [11], fuzzy control [12], impulsive control [13, 14], and pinning control [5, 6, 15, 16]. Synchronization of complex networks holds particular promise for applications to many fields [17–21].

Synchronization in complex dynamical networks is realized via information exchanges among the interconnect nodes [22]. The signal traveling along real physical system is usually perturbed randomly by the environmental elements, such as noises, the structures of the interconnections, time delays, and the positions of nodes [9]. One popular model is the Markovian switching model driven by continuous-time Markov chains in the sciences and industries (see [23–26] and references therein). In [23, 24], Mao et al. studied stability and controllability of stochastic differential delay equations with Markovian switching, while [25, 26] discussed the exponential stability of stochastic delayed neural networks. Liu et al. [26], on the other hand, investigated the synchronization of discrete-time stochastic complex networks with Markovian jumping and mode-dependent mixed time delays. In [16], Wang et al. investigated the mean-square exponential synchronization of stochastic complex networks with Markovian switching and time-varying delays by using the pinning control method, which is described as

$$\begin{aligned} dx_i(t) &= \Bigg\{ f\left(t, x_i(t), x_i(t-\tau(t))\right) \\ &\quad + \sum_{j=1, i\neq j}^{N} a_{ij}(r(t))\, \Sigma\left(x_j(t) - x_i(t)\right) \end{aligned}$$

$$+\sum_{j=1,i\neq j}^{N} b_{ij}(r(t))\Sigma\left(x_j(t-\tau_c(t))-x_i(t-\tau_c(t))\right)$$
$$+u_i(t)\Bigg\}dt$$
$$+\sigma_i\left(x(t),x(t-\tau(t)),x(t-\tau_c(t)),r(t)\right)dw_i(t),$$
$$i=1,2,\ldots,N, \tag{1}$$

where $u_i(t)$ $(i = 1,2,\ldots,N)$ are the linear state feedback controllers that are defined by

$$u_i(t)=\begin{cases}-\varepsilon_i\left(x_i(t)-s(t)\right), & i=1,2,\ldots,l,\\ 0, & i=l+1,l+2,\ldots,N,\end{cases} \tag{2}$$

and $\varepsilon_i > 0$ $(i = 1,2,\ldots,l)$ are the control gains.

Pinning control has been proved to be effective for the synchronization of complex dynamical networks with continuous state coupling [15, 16, 27]. In many systems, the impulsive effect is a common phenomenon due to instantaneous perturbations at certain moments [27, 28]. Impulsive control strategies have been widely used to stabilize and synchronize coupled complex dynamical systems, such as signal processing system, computer networks, automatic control systems, and telecommunications [13]. In [27], pinning impulsive strategy is proposed for the synchronization of stochastic dynamical networks with nonlinear coupling. Zhou et al. studied synchronization in complex delayed dynamical networks with impulsive effects in [28]. And Zhu et al., in [29], investigated the exponential stability of a class of stochastic neural networks with both Markovian jump parameters and mixed fixed time delays. Can the stochastic dynamical network with Markovian switching and time-varying delays be synchronized by impulsive pinning control? This paper is devoted to solving this problem.

In this paper, we study the synchronization of stochastic complex networks with Markovian switching by using the impulse control method. We consider a kind of stochastic complex networks with internal time-varying delayed couplings, Markovian switching, and Wiener processes. By applying the Lyapunov-Krasovskii functional method, Itö's formula and the linear matrix inequality (LMI), some sufficient conditions for synchronization of these networks are derived. Numerical examples are finally given to demonstrate the effectiveness of the proposed impulsive pinning strategy.

Notations. Throughout this paper, $\mathbb{R}^n$ will denote the n-dimensional Euclidean space and $\mathbb{R}^{n\times n}$ the set of all $n\times n$ real matrices. The superscript T will denote the transpose of a matrix or a vector. And $\mathrm{Tr}(\cdot)$ stands for the trace of the corresponding matrix. $\mathbf{1}_n = (1,1,\ldots,1)^T \in \mathbb{R}^n$, and I_n is the n-dimensional identity matrix. For square matrices M, the notation $M > 0$ (<0) will mean that M is a positive-definite (negative-definite) matrix. $\lambda_{\max}(A)$ and $\lambda_{\min}(A)$ will denote the greatest and least eigenvalues of a symmetric matrix, respectively. $\check{p} = \max\{p_1,p_2,\ldots,p_n\}$, and $\widehat{p} = \min\{p_1,p_2,\ldots,p_n\}$.

2. Preliminaries

Let $(\Omega,\mathcal{F},\{\mathcal{F}_t\}_{t\geq 0},\mathcal{P})$ be a complete probability space with a filtration $\{\mathcal{F}_t\}_{t\geq 0}$ that is right continuous with $\mathcal{F}_0$ containing all the $\mathcal{P}$-null sets. $C([-\tau,0];\mathbb{R}^n)$ will denote the family of continuous functions ϕ from $[-\tau,0]$ to $\mathbb{R}^n$ with the uniform norm $\|\phi\|^2 = \sup_{-\tau\leq s\leq 0}\phi(s)^T\phi(s)$. And $C^2_{\mathcal{F}_0}([-\tau,0];\mathbb{R}^n)$ denotes the family of all $\mathcal{F}_0$ measurable, $C([-\tau,0];\mathbb{R}^n)$-valued stochastic variables $\xi = \{\xi(\theta) : -\tau\leq\theta\leq 0\}$ such that $\int_{-\tau}^{0}\mathbb{E}\|\xi(s)\|^2 ds \leq \infty$, where $\mathbb{E}$ stands for the correspondent expectation operator with respect to the given probability measure $\mathcal{P}$.

Consider a complex network consisting of N identical nodes with Markovian switching

$$dx_i(t)=\Bigg\{f\left(x_i(t),x_i(t-\tau(t))\right)$$
$$+\sum_{j=1}^{N}a_{ij}^{[r(t)]}\Sigma x_j(t)$$
$$+\sum_{j=1}^{N}b_{ij}^{[r(t)]}\Sigma x_j(t-\tau_c(t))\Bigg\}dt$$
$$+\sigma_i^{[r(t)]}\left(x(t),x(t-\tau(t)),x(t-\tau_c(t))\right)dw(t),$$
$$i=1,2,\ldots,N, \tag{3}$$

where $x_i(t) = (x_{i1}(t),x_{i2}(t),\ldots,x_{in}(t))^T \in \mathbb{R}^n$ is the state vector of the ith node of the network, $f(x_i(t),x_i(t-\tau(t))) = [f_1(x_i(t),x_i(t-\tau(t))), f_2(x_i(t),x_i(t-\tau(t))),\ldots,f_n(x_i(t),x_i(t-\tau(t)))]^T$ is a continuous vector-valued function, $\Sigma = \mathrm{diag}\{\varrho_1,\varrho_2,\ldots,\varrho_n\}$ is an inner coupling matrix of the networks that satisfies $\varrho_j > 0$, $j = 1,2,\ldots,n$, and $r(t)$ are the continuous-time Markov processes that describe the evolution of the nodes at time t. Here, $A^{[r(t)]} = [a_{ij}^{[r(t)]}] \in \mathbb{R}^{n\times n}$ and $B^{[r(t)]} = [b_{ij}^{[r(t)]}] \in \mathbb{R}^{n\times n}$ are the outer coupling matrices of the network at time t at nodes $r(t)$, $t-\tau_c(t)$, respectively, such that $a_{ij}^{[r(t)]} \geq 0$ for $i\neq j$, $a_{ii}^{[r(t)]} = -\sum_{j=i,j\neq i}^{N}a_{ij}^{[r(t)]}$, $b_{ij}^{[r(t)]} \geq 0$ for $i\neq j$ and $b_{ii}^{[r(t)]} = -\sum_{j=i,j\neq i}^{N}b_{ij}^{[r(t)]}$. Figure 1 shows the topology structures of the switching networks for 5 nodes. $\tau(t)$ is the inner time-varying delay satisfying $\tau \geq \tau(t) \geq 0$ and $\tau_c(t)$ is the coupling time-varying delay satisfying $\tau_c \geq \tau_c(t) \geq 0$. Finally, $\sigma_i^{[r(t)]}(x(t),x(t-\tau(t)),x(t-\tau_c(t))) = \sigma_i^{[r(t)]}(x_1(t),\ldots,x_n(t),x_1(t-\tau(t)),\ldots,x_n(t-\tau(t)),x_1(t-\tau_c(t)),\ldots,x_n(t-\tau_c(t))) \in \mathbb{R}^{n\times n}$ and $w(t) = (w_1(t),w_2(t),\ldots,w_n(t))^T \in \mathbb{R}^n$ is a bounded vector-form Weiner process, satisfying

$$\mathbb{E}w_j(t)=0,\qquad \mathbb{E}w_j^2(t)=1,$$
$$\mathbb{E}w_j(t)w_j(s)=0\quad(s\neq t). \tag{4}$$

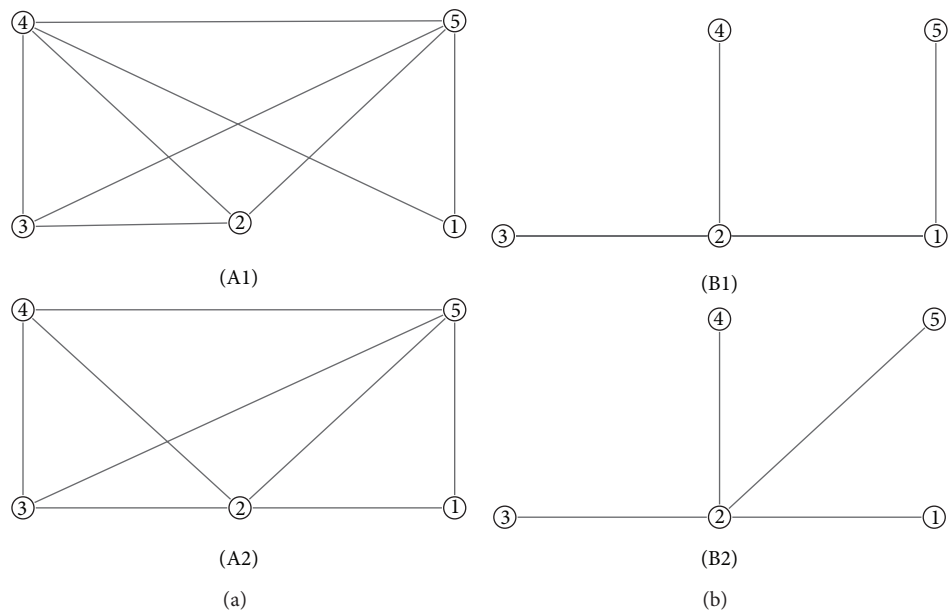

Figure 1: The topology structures of the switching networks for 5 nodes; (A1) and (A2) the topology structures of the coupling matrix A^1 and A^2, respectively; (B1) and (B2) the topology structures of the coupling matrix B^1 and B^2, respectively.

Let $r(t)$, $t > 0$ be a right-continuous Markov chain on a probability space that takes values in a finite state space $S = 1, 2, \ldots, M$ with a generator $\Gamma = [\gamma_{ij}] \in \mathbb{R}^{M\times M}$ given by

$$P\{r(t+\Delta) = j \mid r(t) = i\} = \begin{cases} \gamma_{ij}\Delta + o(\Delta) & \text{if } i \neq j, \\ 1 + \gamma_{ii}\Delta + o(\Delta) & \text{if } i = j, \end{cases} \tag{5}$$

for some $\Delta > 0$. Here $\gamma_{ij} \geq 0$ is the transition rate from i to j if $i \neq j$ and $\gamma_{ii} = -\sum_{i\neq j}\gamma_{ij}$, In this paper, $A^{[r]}$ is assumed to be symmetric and irreducible, and $B^{[r]}$ is assumed to be symmetric, for $r = 1, 2, \ldots, M$.

The initial conditions associated with (3) are

$$x_i(s) = \xi_i(s), \quad -\check{\tau} \leq s \leq 0, \quad i = 1, 2, \ldots, N, \tag{6}$$

where $\check{\tau} = \max\{\tau(t), \tau_c(t)\}$, $\xi_i \in C^b_{\mathcal{F}_0}([-\check{\tau}, 0], \mathbb{R}^n)$ with the norm $\|\xi_i\|^2 = \sup_{-\check{\tau}\leq s\leq 0}\xi_i(s)^T\xi_i(s)$.

The impulse controllers are defined by

$$\begin{gathered} \Delta x_i(t_k) = x_i(t_k^+) - x_i(t_k^-) = \epsilon_{ik}x_i(t_k^-), \\ t = t_k, \quad k \in Z^+, \quad i = 1, 2, \ldots, N, \end{gathered} \tag{7}$$

where ϵ_{ik} are constants, and $\{t_1, t_2, t_3, \ldots\}$ is the impulsive sequence of strictly increasing impulsive instants satisfying $\lim_{k\to\infty} t_k = +\infty$, and $t_k - t_{k-1} = T$ for $k > 1$.

In the case that system (3) reaches synchronization, that is, $x_1(t) = x_2(t) = \cdots = x_N(t) = s(t)$, we have the following synchronized state equation:

$$\begin{aligned} ds(t) = {} & f(s(t), s(t-\tau(t)))\,dt \\ & + \sigma(s(t), s(t-\tau(t)))\,dw(t). \end{aligned} \tag{8}$$

In the paper, we would control the system (3) to the desired trajectory $s(t)$. Define $e_i(t) = x_i(t) - s(t)$ ($i = 1, 2, \ldots, N$) as the synchronization error. Then, according to the controller (7), the error system is

$$\begin{aligned} de_i(t) = {} & \Bigg\{ f(x_i(t), x_i(t-\tau(t))) - f(s(t), s(t-\tau(t))) \\ & + \sum_{j=1}^{N} a_{ij}^{[r(t)]}\Sigma e_j(t) + \sum_{j=1}^{N} b_{ij}^{[r(t)]}\Sigma e_j(t-\tau_c(t)) \Bigg\} dt \\ & + \sigma_i^{[r(t)]}(e(t), e(t-\tau(t)), e(t-\tau_c(t)))\,dw(t), \\ & t \neq t_k, \quad k \in Z^+, \quad i = 1, 2, \ldots, N, \\ \Delta e_i(t_k) = {} & \epsilon_{ik}e_i(t_k^-), \quad t = t_k, \quad k \in Z^+, \quad i = 1, 2, \ldots, N, \end{aligned} \tag{9}$$

where $\sigma_i^{[r(t)]}(e(t), e(t-\tau(t)), e(t-\tau_c(t))) = \sigma_i^{[r(t)]}(x(t), x(t-\tau(t)), x(t-\tau_c(t))) - \sigma(s(t), s(t-\tau(t)))$.

Definition 1 (see [16, 27]). The complex network (3) is said to be exponentially synchronized in mean square if the trivial solution of system (9) is such that

$$\sum_{i=1}^{N}\mathbb{E}\|e_i(t, t_0, \xi_i)\|^2 \leq Ke^{-\kappa t}, \tag{10}$$

for some $K > 0$ and $\kappa > 0$ under any initial data $\xi_i \in \mathscr{C}^b_{\mathcal{F}_0}([-\check{\tau}, 0]; \mathbb{R}^n)$.

Definition 2 (see [9, 11, 16]). A continuous function $f(x, y) : \mathbb{R}^n \times \mathbb{R}^n \to \mathbb{R}^n$ is said to belong to the function class QUAD,

denoted by $f \in \mathrm{QUAD}(P, \Delta, \eta, \theta)$ for some given matrix $\Sigma = \mathrm{diag}\{\varrho_1, \varrho_2, \ldots, \varrho_n\}$ if there exists a positive definite diagonal matrix $P = \mathrm{diag}\{p_1, p_2, \ldots, p_n\}$, a diagonal matrix $\Delta = \mathrm{diag}\{\delta_1, \delta_2, \ldots, \delta_n\}$ and constants $\eta > 0, \theta > 0$ such that $f(\cdot)$ satisfies the condition

$$\begin{aligned}(x-y)^T P\left(\left(f(x,z)-f(y,w)\right)-\Delta\Sigma(x-y)\right)\\ \le -\eta(x-y)^T(x-y)+\theta(z-w)^T(z-w)\end{aligned} \tag{11}$$

for all $x, y, z, w \in \mathbb{R}^n$.

The following assumptions are usual and will be used throughout this paper for establishing the synchronization conditions [9, 11, 16].

(H1) $\tau(t)$ and $\tau_c(t)$ are bounded and continuously differentiable functions such that $0 < \tau(t) \le \tau$, $\dot{\tau}(t) < \overline{\tau} < 1$, $0 < \tau_c(t) \le \tau_c$ and $\dot{\tau}_c(t) < \overline{\tau}_c < 1$. Let $\check{\overline{\tau}} = \max\{\overline{\tau}, \overline{\tau}_c\}$.

(H2) There exist positive definite constant matrices $\Upsilon_{i1}^{[r]}$, $\Upsilon_{i2}^{[r]}$ and $\Upsilon_{i3}^{[r]}$ for $i = 1, 2, \ldots, N$ and $r = 1, 2, \ldots, M$ such that

$$\begin{aligned}&\mathrm{Tr}\left[\sigma_i^{[r]}\left(e(t), e(t-\tau(t)), e\left(t-\tau_c(t)\right)\right)^T\right.\\ &\quad\left.\times\sigma_i^{[r]}\left(e(t), e(t-\tau(t)), e\left(t-\tau_c(t)\right)\right)\right]\\ &\le \sum_{j=1}^{N} e_j(t)^T\Upsilon_{i1}^{[r]}e_j(t)\\ &\quad+\sum_{j=1}^{N} e_j(t-\tau(t))^T\Upsilon_{i2}^{[r]}e_j(t-\tau(t))\\ &\quad+\sum_{j=1}^{N} e_j\left(t-\tau_c(t)\right)^T\Upsilon_{i3}^{[r]}e_j\left(t-\tau_c(t)\right).\end{aligned} \tag{12}$$

Remark 3. Considering Definition 2 and assumption (H2), there exists a unique solution of (9) under the initial data $\xi_i \in \mathscr{C}^b_{\mathscr{F}_0}([-\tau, 0]; \mathbb{R}^n)$ (see [23, 24]).

Lemma 4 (see [23, 24]). *Consider a stochastic delayed differential equation with Markovian switching of the form*

$$\begin{aligned}dx(t) = f(x(t), x(t-\tau), r(t))\,dt\\ +\sigma(x(t), x(t-\tau), r(t))\,d\omega(t)\end{aligned} \tag{13}$$

on $t \ge 0$ with initial value $x_0 = \xi \in C^b_{F_0}([-\tau, 0]; \mathbb{R}^n)$, where

$$f : \mathbb{R}^n \times \mathbb{R}^n \times S \to \mathbb{R}^n, \qquad \sigma : \mathbb{R}^n \times \mathbb{R}^n \times S \to \mathbb{R}^{n\times m}. \tag{14}$$

Let $C^{2,1}(\mathbb{R}_+ \times \mathbb{R}^n; \mathbb{R}_+)$ be the family of all the nonnegative functions $V(t, x, r)$ on $\mathbb{R}_+ \times \mathbb{R}^n \times S$ that are twice continuously differentiable in x and once differentiable in t. Let $V \in C^{2,1}(\mathbb{R}_+ \times \mathbb{R}^n \times S; \mathbb{R}_+)$. Define an operator $\mathscr{L}V$ from $\mathbb{R}^n \times \mathbb{R}_+ \times S$ to $\mathbb{R}^n$ by

$$\begin{aligned}\mathscr{L}V(t,x,r) = V_t(t,x,r) + V_x(t,x,r)f(x,r)\\ +\frac{1}{2}\mathrm{Tr}\left[\sigma(x,r)^T V_{xx}\sigma(x,r)\right]\\ +\sum_{j=1}^{M}\gamma_{ij}V(t,x,j),\end{aligned} \tag{15}$$

where $V_t(t, x, r) = \partial V(t, x, r)/\partial t$, $V_x(t, x, r) = (\partial V(t, x, r)/\partial x_1, \ldots, \partial V(t, x, r)/\partial x_n)$, and $V_{xx}(t, x, r) = (\partial^2 V(t, x, r)/\partial x_i x_j)_{n\times n}$. If $V \in C^{2,1}(\mathbb{R}_+ \times \mathbb{R}^n \times S; \mathbb{R}_+)$, and then

$$\mathbb{E}V(t, x(t), r) = \mathbb{E}V(t_0, x(t_0), r) + \mathbb{E}\int_{t_0}^{t}\mathscr{L}V(s, x(s), r)\,ds \tag{16}$$

for all $\infty > t > t_0 \ge 0$, as long as the expectations of the integrals exist.

3. Main Result

In this section, we will deduce our main results.

Theorem 5. *Let assumptions (H1) and (H2) be true and let $f \in \mathrm{QUAD}(P, \Delta, \eta, \theta)$. If there exist positive constants α_r and β_r such that*

$$\begin{gathered}\begin{bmatrix} A^{[r]} + \check{\delta}I_N - \alpha_r I_N & \dfrac{B^{[r]}}{2} \\ \dfrac{B^{[r]}}{2} & -\beta_r I_N\end{bmatrix} \le 0, \quad \text{for } r = 1, 2, \ldots, M,\\ \check{\tau} \le \theta T, \quad \check{\tau} \le (1-\theta)T, \quad 0 \le \check{\overline{\tau}} \le 1 - \frac{\check{q}\left(\check{b}+\check{c}\right)}{1+\theta},\\ \varphi(\check{\tau}+T) + 2\ln\frac{\check{q}}{\widehat{q}}\left|1+\epsilon_v\right| - \gamma T < 0,\\ \left(\frac{1}{b_1+c_1}, \frac{1}{b_2+c_2}, \ldots, \frac{1}{b_M+c_M}\right)^T > \widetilde{\Gamma}^{-1}\mathbf{1}_M,\end{gathered} \tag{17}$$

where

$$\begin{gathered}\varphi = 1 + \theta + \gamma\check{q} + \frac{\check{b}\check{q}}{1-\overline{\tau}}e^{\gamma\tau} + \frac{\check{c}\check{q}}{1-\overline{\tau}_c}e^{\gamma\tau_c},\\ \widetilde{\Gamma} = \mathrm{diag}\{a_1, a_2, \ldots, a_M\} + \Gamma,\\ \check{a} = \max_{r\in S} a_r, \qquad a_r = \frac{\lambda_{\max}\left(-2\eta I_n + \check{p}\sum_{i=1}^{N}\Upsilon_{i1}^{[r]} + 2\alpha_r P\Sigma\right)}{\check{p}},\\ \check{b} = \max_{r\in S} b_r, \qquad b_r = \frac{\lambda_{\max}\left(\sum_{i=1}^{N} P\Upsilon_{i2}^{[r]} + 2\theta I_N\right)}{\widehat{p}},\\ \check{c} = \max_{r\in S} c_r, \qquad c_r = \frac{\lambda_{\max}\left(\sum_{i=1}^{N} P\Upsilon_{i3}^{[r]} + 2\beta_r P\Sigma\right)}{\widehat{p}},\end{gathered} \tag{18}$$

then the solutions $e_1(t), e_2(t), \ldots,$ and $e_N(t)$ of system (9) *are exponentially stable in mean square. It means that the complex dynamical network* (3) *can be exponentially controlled to the objective trajectory $s(t)$ under the controllers* (7).

Proof. By (44), there exists a sufficiently small constant $\theta > 0$ such that

$$\left(\frac{1}{b_1+c_1}, \frac{1}{b_2+c_2}, \ldots, \frac{1}{b_M+c_M}\right)^T \geq (1+\theta)\,\widetilde{\Gamma}^{-1}\mathbf{1}. \tag{19}$$

Set $(1+\theta)\widetilde{\Gamma}^{-1}\mathbf{1} = q = (q_1, q_2, \ldots, q_M)^T$. Then $\widetilde{\Gamma}q = (1+\theta)\mathbf{1}_M$, that is,

$$(b_r + c_r)\, q_r \leq 1, \qquad a_r q_r + \sum_{s=1}^{M} \gamma_{rs} q_s = 1 + \theta. \tag{20}$$

For $1 \leq r \leq M$, define the Lyapunov-Krasovskii function

$$V(e(t), r) = q_r \frac{1}{2} \sum_{i=1}^{N} e_i(t)^T P e_i(t), \tag{21}$$

and let $\widetilde{e}^k(t) = (e_{1k}(t), e_{2k}(t), \ldots, e_{Nk}(t))^T$, $k = 1, 2, \ldots, n$. For any $t \in (t_{k-1}, t_k]$, $k = 1, 2, \ldots$, by Lemma 4, we have

$$\begin{aligned}
&\mathscr{L}V(e(t), r) \\
&= q_r \sum_{i=1}^{N} e_i(t)^T P \Big\{ f(x_i(t), x_i(t-\tau(t))) \\
&\qquad - f(s(t), s(t-\tau(t))) + \sum_{j=1}^{N} a_{ij}^{[r]} \Sigma e_j(t) \\
&\qquad + \sum_{j=1}^{N} b_{ij}^{[r]} \Sigma e_j(t-\tau_c(t)) \Big\} \\
&\quad + \frac{1}{2} q_r \sum_{i=1}^{N} \mathrm{Tr}\Big\{ \sigma_i(x(t), x(t-\tau(t)), x(t-\tau_c(t)), r)^T \\
&\qquad \times P \sigma_i(x(t), x(t-\tau(t)), x(t-\tau_c(t)), r) \Big\} \\
&\quad + \sum_{s=1}^{M} \gamma_{rs} q_s \frac{1}{2} \sum_{i=1}^{N} e_i(t)^T P e_i(t) \\
&\leq q_r \Big\{ -\eta \sum_{i=1}^{N} e_i(t)^T e_i(t) + \theta \sum_{i=1}^{N} e_i(t-\tau(t))^T e_i(t-\tau(t)) \\
&\qquad + \sum_{k=1}^{n} p_k \varrho_k \delta_k \widetilde{e}^k(t)^T \widetilde{e}^k(t) + \sum_{k=1}^{n} p_k \varrho_k \widetilde{e}^k(t)^T A^{[r]} \widetilde{e}^k(t) \\
&\qquad + \sum_{k=1}^{n} p_k \varrho_k \widetilde{e}^k(t)^T B^{[r]} \widetilde{e}^k(t-\tau_c(t)) \\
&\qquad + \frac{1}{2} \check{p} \sum_{j=1}^{N} \Big[\sum_{i=1}^{N} e_i(t)^T \Upsilon_{j1}^{[r]} e_i(t) \\
&\qquad\qquad + \sum_{i=1}^{N} e_i(t-\tau(t))^T \Upsilon_{j2}^{[r]} e_i(t-\tau(t)) \\
&\qquad\qquad + \sum_{i=1}^{N} e_i(t-\tau_c(t))^T \Upsilon_{j3}^{[r]} e_i(t-\tau_c(t)) \Big] \Big\} \\
&\qquad + \sum_{s=1}^{M} \gamma_{rs} q_s \frac{1}{2} \sum_{i=1}^{N} e_i(t)^T P e_i(t) \\
&= q_r \Big\{ \sum_{i=1}^{N} e_i(t)^T \Big(-\eta I_N + \frac{1}{2} \check{p} \sum_{j=1}^{N} \Upsilon_{j1}^{[r]} + \alpha_r P \Sigma \Big) e_i(t) \\
&\qquad + \sum_{i=1}^{N} e_i(t-\tau(t))^T \Big(\theta + \frac{1}{2} \check{p} \sum_{j=1}^{N} \Upsilon_{j2}^{[r]} \Big) e_i(t-\tau(t)) \\
&\qquad + \sum_{i=1}^{N} e_i(t-\tau_c(t))^T \Big(\frac{1}{2} \check{p} \sum_{j=1}^{N} \Upsilon_{j3}^{[r]} + \beta_r P \Sigma \Big) e_i(t-\tau_c(t)) \Big\} \\
&\qquad + \sum_{s=1}^{M} \gamma_{rs} q_s \frac{1}{2} \sum_{i=1}^{N} e_i(t)^T P e_i(t) \\
&\qquad + q_r \Big\{ \sum_{k=1}^{n} p_k \varrho_k \widetilde{e}^k(t)^T \big[A^{[r]} + (\check{\delta} - \alpha_r) I_N \big] \widetilde{e}^k(t) \\
&\qquad + \sum_{k=1}^{n} p_k \varrho_k \widetilde{e}^k(t)^T B^{[r]} \widetilde{e}^k(t-\tau_c(t)) \\
&\qquad - \sum_{k=1}^{n} p_k \varrho_k \widetilde{e}^k(t-\tau_c(t))^T \beta_r \widetilde{e}^k(t-\tau_c(t)) \Big\} \\
&\leq q_r \Big\{ \sum_{i=1}^{N} e_i(t)^T \Big(-\eta I_N + \frac{1}{2} \check{p} \sum_{j=1}^{N} \Upsilon_{j1}^{[r]} + \alpha_r P \Sigma \Big) e_i(t) \\
&\qquad + \sum_{i=1}^{N} e_i(t-\tau(t))^T \Big(\theta I_N + \frac{1}{2} \check{p} \sum_{j=1}^{N} \Upsilon_{j2}^{[r]} \Big) e_i(t-\tau(t)) \\
&\qquad + \sum_{i=1}^{N} e_i(t-\tau_c(t))^T \Big(\frac{1}{2} \check{p} \sum_{j=1}^{N} \Upsilon_{j3}^{[r]} + \beta_r P \Sigma \Big) e_i(t-\tau_c(t)) \Big\} \\
&\qquad + \sum_{s=1}^{M} \gamma_{rs} q_s \frac{1}{2} \sum_{i=1}^{N} e_i(t)^T P e_i(t).
\end{aligned} \tag{22}$$

Let

$$E(t) = \frac{1}{2} \sum_{i=1}^{N} e_i(t)^T P e_i(t); \tag{23}$$

then we have

$$\begin{aligned}
\mathscr{L}V(t) &\leq a_r q_r E(t) + b_r q_r E(t-\tau(t)) \\
&\quad + c_r q_r E(t-\tau_c(t)) + \sum_{s=1}^{M} \gamma_{rs} q_s E(t),
\end{aligned} \tag{24}$$

and by (20), we have

$$\mathscr{L}V(t) \leq (1+\theta) E(t) + \check{b}\check{q} E(t-\tau(t)) + \check{c}\check{q} E(t-\tau_c(t)). \tag{25}$$

Define

$$W(t) = e^{\gamma t} V(t). \tag{26}$$

Use (25) to compute the operator

$$\begin{aligned}\mathscr{L}W(t) &= e^{\gamma t}\left[\gamma V(t) + \mathscr{L}V(t)\right] \\ &\le e^{\gamma t}\left[\gamma\check{q}E(t) + (1+\theta)E(t)\right. \\ &\qquad \left. + \check{b}\check{q}E(t-\tau(t)) + \check{c}\check{q}E(t-\tau_c(t))\right].\end{aligned} \tag{27}$$

The generalized Itô's formula gives

$$e^{\gamma t}\mathbb{E}V(t) = e^{\gamma t_0}\mathbb{E}V(t_0) + \mathbb{E}\int_{t_0}^{t}\mathscr{L}W(s)\,ds, \tag{28}$$

for any $t_k > t > t_0 > t_{k-1} \ge 0$. Hence we have

$$\begin{aligned}e^{\gamma t}\mathbb{E}V(t) &\le e^{\gamma t_0}\mathbb{E}V(t_0) \\ &\quad + \mathbb{E}\int_{t_0}^{t} e^{\gamma s}\left[\gamma\check{q}E(s) + (1+\theta)E(s)\right. \\ &\qquad \left. + \check{b}\check{q}E(s-\tau(s)) + \check{c}\check{q}E(s-\tau_c(s))\right]ds \\ &\le \check{q}e^{\gamma t_0}\mathbb{E}E(t_0) + (\gamma\check{q} + 1 + \theta) \\ &\quad \times \int_{t_0}^{t} e^{\gamma s}\mathbb{E}E(s)\,ds \\ &\quad + \check{b}\check{q}e^{\gamma\tau}\int_{t_0}^{t} e^{\gamma(s-\tau(s))}\mathbb{E}E(s-\tau(s))\,ds \\ &\quad + \check{c}\check{q}e^{\gamma\tau_c}\int_{t_0}^{t} e^{\gamma(s-\tau_c(s))}\mathbb{E}E(s-\tau_c(s))\,ds.\end{aligned} \tag{29}$$

By changing variable $s - \tau(s) = u$, we have

$$\begin{aligned}&\int_{t_0}^{t} e^{\gamma(s-\tau(s))}\mathbb{E}E(s-\tau(s))\,ds \\ &\quad = \int_{t_0-\tau(t_0)}^{t-\tau(t)} e^{\gamma u}\mathbb{E}E(u)\frac{du}{1-\dot{\tau}(t)} \\ &\quad \le \frac{1}{1-\overline{\tau}}\int_{t_0-\tau}^{t} e^{\gamma u}\mathbb{E}E(u)\,du.\end{aligned} \tag{30}$$

Similarly, we have

$$\int_{t_0}^{t} e^{\gamma(s-\tau_c(s))}\mathbb{E}E(s-\tau(s))\,ds \le \frac{1}{1-\overline{\tau}_c}\int_{t_0-\tau_c}^{t} e^{\gamma u}\mathbb{E}E(u)\,du. \tag{31}$$

Substituting (30) and (31) into (29), we get

$$e^{\gamma t}\mathbb{E}V(t) \le q_r e^{\gamma t_0}\mathbb{E}V(t_0) + \varphi\int_{t_0-\check{\tau}}^{t} e^{\gamma u}\mathbb{E}E(u)\,du. \tag{32}$$

By using Gronwall inequality, we have

$$\mathbb{E}E(t) \le \frac{\check{q}}{\widehat{q}}\mathbb{E}E(t_0)\,e^{\varphi(t-t_0+\check{\tau})+\gamma(t_0-t)}. \tag{33}$$

On the other hand, from the construction of $E(t)$, we have

$$E(t_k) \le (1+\epsilon_k)^2 E(t_k^-), \tag{34}$$

where $|1+\epsilon_k| = \max_{i=1,2,\ldots,N}|1+\epsilon_{ik}|$.

According to (33)-(34), let $k = \lfloor (t-t_0)/T \rfloor$, for any $t \in [t_{k-1}, t_k)$, and we get

$$\begin{aligned}\mathbb{E}V(t) &\le \frac{\check{q}}{\widehat{q}}\mathbb{E}E(t_k)\,e^{\varphi(t-t_k+\check{\tau})+\gamma(t_k-t)} \\ &\le \frac{\check{q}}{\widehat{q}}\mathbb{E}V(t_{k-1}^-)\,e^{\varphi(t-t_{k-1}+\check{\tau})+\gamma(t_k-t)+2\ln|1+\epsilon_{k-1}|} \\ &\le \cdots \le \left(\frac{\check{q}}{\widehat{q}}\right)^{k-1}\mathbb{E}E(0)\,e^{\varphi(t+k\check{\tau})-\gamma t+\sum_{v=1}^{k-1}2\ln|1+\epsilon_v|}.\end{aligned} \tag{35}$$

Let $|1+\epsilon| = \max_{v\in Z^+}|1+\epsilon_v|$, and we have

$$\mathbb{E}E(t) \le \mathbb{E}E(0)\,e^{\varphi(t+k\check{\tau})-\gamma t+2(k-1)\ln(\check{q}/\widehat{q})|1+\epsilon|}. \tag{36}$$

Using condition (43) of Theorem 5, there exist a number η such that $\mathbb{E}E(t) \le \mathbb{E}E(t_0)e^{-\eta t}$. Hence, $\mathbb{E}\|e_i(t)\| \le (E(t_0)/\check{p})^{1/2}e^{-(\eta/2)(t-t_0)}$. The proof of Theorem 5 is completed. □

Remark 6. The stochastic networks studied before are without topological switch, and the time delays are always assumed to be fixed. However, for the sake of applications in the real work, these two points above should be taken into consideration. Of course, it will enhance the difficulties of the investigations on this network. For example, if the network has Markovian switching topology, the structure of the network is fast varying and the Lyapunov function is hard to be determined. By using the Lyapunov-Krasovskii functional, Itö's formula, and LMI, the exponential stability criterion of the pinning impulsive controlled Markovian switching stochastic dynamical network with time-varying delays was obtained. This also showed that the impulsive pinning control is a kind of cheap control strategy for guiding complex dynamical networks to the objective trajectory.

To make Theorem 5 more applicative, we give the following corollaries.

When complex dynamic networks (3) are considered without coupled delay time ($B^{[r(t)]} = B$), we can get the following corollary.

Corollary 7. *Let assumptions (H1) and (H2) be true and let $f \in \mathrm{QUAD}(P,\Delta,\eta,\theta)$. If there exist positive constants α_r and β_r such that*

$$\begin{gathered}A^{[r]} + \check{\delta}I_N - \alpha_r I_N \le 0, \quad \text{for } r = 1,2,\ldots,M, \\ \tau \le \theta T, \qquad \tau \le (1-\theta)T, \qquad 0 \le \overline{\tau} \le 1 - \frac{\check{q}\check{b}}{1+\theta}, \\ \varphi(\check{\tau}+T) + 2\ln\frac{\check{q}}{\widehat{q}}|1+\epsilon| - \gamma T < 0, \\ \left(\frac{1}{b_1}, \frac{1}{b_2}, \ldots, \frac{1}{b_M}\right)^T > \widetilde{\Gamma}^{-1}\mathbf{1}_M,\end{gathered} \tag{37}$$

where

$$\varphi = 1 + \theta + \gamma\check{q} + \frac{\check{b}\check{q}}{1-\overline{\tau}}e^{\gamma\tau},$$
$$\widetilde{\Gamma} = \operatorname{diag}\{a_1, a_2, \ldots, a_M\} + \Gamma,$$
$$\check{a} = \max_{r\in S} a_r, \qquad a_r = \frac{\lambda_{\max}\left(-2\eta I_n + \check{p}\sum_{i=1}^{N}\Upsilon_{i1}^{[r]} + 2\alpha_r P\Sigma\right)}{\check{p}},$$
$$\check{b} = \max_{r\in S} b_r, \qquad b_r = \frac{\lambda_{\max}\left(\sum_{i=1}^{N} P\Upsilon_{i2}^{[r]} + 2\theta I_N\right)}{\widehat{p}}, \tag{38}$$

then the solutions $e_1(t), e_2(t), \ldots,$ and $e_N(t)$ of system (9) are exponentially stable in mean square.

In another case, when we consider the system (3) without Markov switching, that is, $A^{[r(t)]} = A$, $B^{[r(t)]} = B$, and $\sigma_i^{[r(t)]}(e(t), e(t-\tau(t)), e(t-\tau_c(t))) = \sigma_i(e(t), e(t-\tau(t)), e(t-\tau_c(t)))$, we can get another corollary.

Corollary 8. *Let assumptions (H1) and (H2) be true and let $f \in \mathrm{QUAD}((P, \Delta, \eta, \theta)$. If there exist positive constants α and β such that*

$$\begin{bmatrix} A + \check{\delta}I_N - \alpha I_N & \frac{B}{2} \\ \frac{B}{2} & -\beta I_N \end{bmatrix} \le 0,$$
$$\check{\tau} \le \theta T, \qquad \check{\tau} \le (1-\theta)T, \qquad 0 \le \check{\overline{\tau}} \le 1 - \frac{b+c}{a}, \tag{39}$$
$$\varphi(\check{\tau} + T) + 2\ln\left|1 + \epsilon_v\right| - \gamma T < 0,$$
$$b + c < a,$$

where

$$\varphi = a + \gamma + \frac{b}{1-\overline{\tau}}e^{\gamma\tau} + \frac{c}{1-\overline{\tau}_c}e^{\gamma\tau_c},$$
$$a = \frac{\lambda_{\max}\left(-2\eta I_n + \check{p}\sum_{i=1}^{N}\Upsilon_{i1} + 2\alpha P\Sigma\right)}{\check{p}},$$
$$b = \frac{\lambda_{\max}\left(\sum_{i=1}^{N} P\Upsilon_{i2} + 2\theta I_N\right)}{\widehat{p}}, \tag{40}$$
$$c = \frac{\lambda_{\max}\left(\sum_{i=1}^{N} P\Upsilon_{i3} + 2\beta_r P\Sigma\right)}{\widehat{p}},$$

then the solutions $e_1(t), e_2(t), \ldots,$ and $e_N(t)$ of system (9) are exponentially stable in mean square.

Furthermore, when we address the system (3) with fixed time delays, that is, $\tau(t) = \tau$, $\tau_c(t) = \tau_c$, the following corollary also can be obtained.

Corollary 9. *Let assumptions (H1) and (H2) be true and let $f \in \mathrm{QUAD}(P, \Delta, \eta, \theta)$. If there exist positive constants α_r and β_r such that*

$$\begin{bmatrix} A^{[r]} + \check{\delta}I_N - \alpha_r I_N & \frac{B^{[r]}}{2} \\ \frac{B^{[r]}}{2} & -\beta_r I_N \end{bmatrix} \le 0, \quad \text{for } r = 1, 2, \ldots, M, \tag{41}$$
$$\check{\tau} \le \theta T, \qquad \check{\tau} \le (1-\theta)T, \tag{42}$$
$$\varphi(\check{\tau} + T) + 2\ln\frac{\check{q}}{\widehat{q}}\left|1 + \epsilon_v\right| - \gamma T < 0, \tag{43}$$
$$\left(\frac{1}{b_1 + c_1}, \frac{1}{b_2 + c_2}, \ldots, \frac{1}{b_M + c_M}\right)^T > \widetilde{\Gamma}^{-1}\mathbf{1}_M, \tag{44}$$

where

$$\varphi = 1 + \theta + \gamma\check{q} + \check{b}\check{q}e^{\gamma\tau} + \check{c}\check{q}e^{\gamma\tau_c},$$
$$\widetilde{\Gamma} = \operatorname{diag}\{a_1, a_2, \ldots, a_M\} + \Gamma,$$
$$\check{a} = \max_{r\in S} a_r, \qquad a_r = \frac{\lambda_{\max}\left(-2\eta I_n + \check{p}\sum_{i=1}^{N}\Upsilon_{i1}^{[r]} + 2\alpha_r P\Sigma\right)}{\check{p}},$$
$$\check{b} = \max_{r\in S} b_r, \qquad b_r = \frac{\lambda_{\max}\left(\sum_{i=1}^{N} P\Upsilon_{i2}^{[r]} + 2\theta I_N\right)}{\widehat{p}},$$
$$\check{c} = \max_{r\in S} c_r, \qquad c_r = \frac{\lambda_{\max}\left(\sum_{i=1}^{N} P\Upsilon_{i3}^{[r]} + 2\beta_r P\Sigma\right)}{\widehat{p}}, \tag{45}$$

then the solutions $e_1(t), e_2(t), \ldots,$ and $e_N(t)$ of system (9) are exponentially stable in mean square.

Remark 10. In [29], the exponential stability of a class of stochastic neural networks with both Markovian jump parameters and mixed fixed time delays were investigated. Therefore, we could see our results as a further research about the stochastic dynamic network of [29].

4. Numerical Simulation

In this section, we present some numerical simulation results that validate the theorem in the previous section.

Consider the chaotic delayed neural network

$$\begin{aligned} ds(t) = {} & \{-Cs(t) + Af(s(t)) + Bg(s(t-\tau(t)))\}\,dt \\ & + \sigma(s(t), s(t-\tau(t)))\,dw(t), \end{aligned} \tag{46}$$

where $f(s) = g(s) = \tanh(s)$, $\tau(t) = 1$, $\sigma(s(t), s(t-\tau(t))) = \operatorname{diag}\{s_1(t), s_2(t)\}$,

$$C = \begin{bmatrix} 1 & 0 \\ 0 & 1 \end{bmatrix}, \qquad A = \begin{bmatrix} 2 & -0.1 \\ -5 & 4.5 \end{bmatrix},$$
$$B = \begin{bmatrix} -1.5 & -0.1 \\ -0.2 & -4 \end{bmatrix}. \tag{47}$$

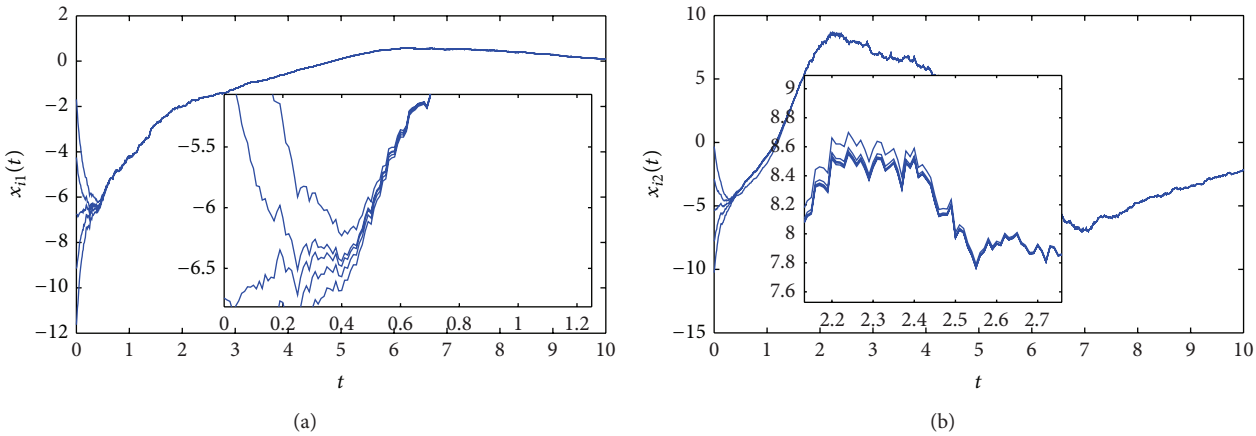

FIGURE 2: The trajectories of the state variables of x_{i1} and x_{i2} $(i = 1, 2, \ldots, 5)$ in system (48) by impulse control.

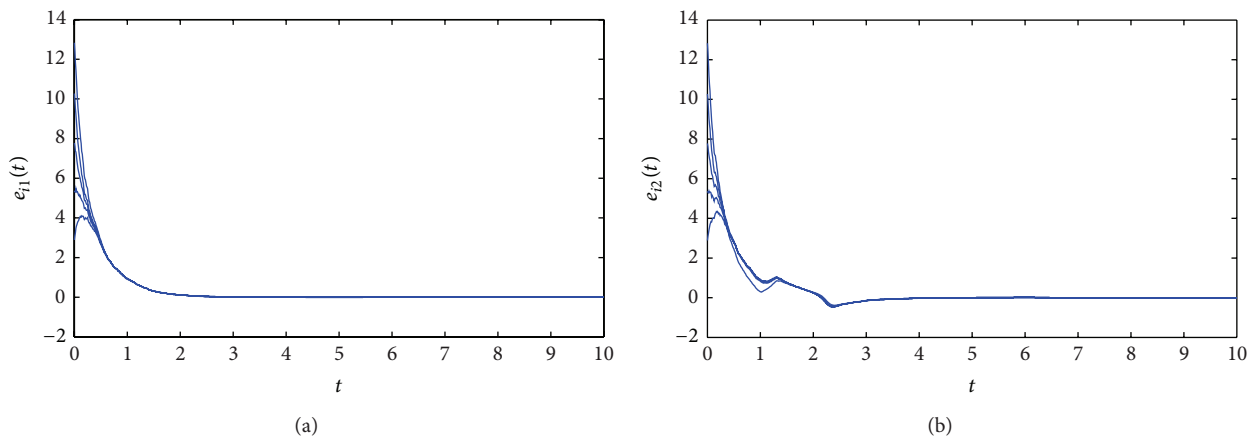

FIGURE 3: The time evolution of e_{i1} and e_{i2} $(i = 1, 2, \ldots, 5)$ in system (48) by impulse control.

Taking $P = \mathrm{diag}\{1, 2\}$ and $\Delta = \mathrm{diag}\{5, 11, 5\}$, we have $\eta = 0.15$ and $\theta = 3.25$ so that condition (11) is satisfied. Thus

$$\begin{aligned} dx_i(t) = &\left\{ f\left(x_i(t), x_i(t-\tau(t))\right) + \sum_{j=1}^{5} a_{ij}^{[r]} \Sigma x_j(t) \right. \\ &\left. + \sum_{j=1}^{5} b_{ij}^{[r]} \Sigma x_j\left(t-\tau_c(t)\right) \right\} dt \\ &+ \sigma_i^{[r]}\left(x(t), x(t-\tau(t)), x\left(t-\tau_c(t)\right)\right) dw_i(t), \\ &\qquad i = 1, 2, \ldots, 5, \quad r = 1, 2, \end{aligned} \tag{48}$$

and $\Gamma = \left[\begin{smallmatrix} -3 & 3 \\ 2 & -2 \end{smallmatrix}\right]$, $\tau_c(t) = 0.1(e^t/(1+e^t))$,

$$\begin{aligned} &\sigma_i^{[1]}\left(x(t), x(t-\tau(t)), x\left(t-\tau_c(t)\right)\right) \\ &\quad = 0.1\,\mathrm{diag}\left\{x_{i1}(t), x_{i2}(t)\right\}, \\ &\sigma_i^{[2]}\left(x(t), x(t-\tau(t)), x\left(t-\tau_c(t)\right)\right) \\ &\quad = 0.1\,\mathrm{diag}\left\{x_{i1}(t-\tau(t)), x_{i2}(t-\tau(t))\right\}. \end{aligned} \tag{49}$$

Computations then yield $\tau = 1$, $\overline{\tau} = 0$, $\tau_c = 0.1$, $\overline{\tau}_c = 0.1$ and $\Upsilon_{ij} = 0.1 I_2$ for $i = 1, 2, \ldots, N$. Then the solutions of inequalities (41)–(44) are (by using the Matlab LMI toolbox) $\alpha_1 = 2.500$, $\beta_1 = 0.001$, $a_1 = 4.305$, $b_1 = 5.055$, $c_1 = 0.109$; $\alpha_2 = 4.006$, $\beta_2 = 0.009$, $a_2 = 5.105$, $b_2 = 5.030$, and $c_2 = 0.065$.

The initial conditions for this simulation are $x_{ij}(t_0)$ which are constants, for $i = 1, 2, \ldots, 5$, $j = 1, 2$ and the trajectories of the impulse control gains are shown in Figure 2. Figure 3 shows the time evolution of the synchronization errors with impulse control.

5. Conclusion

In this paper, we investigated the synchronization problem for stochastic complex networks with Markovian switching and nondelayed and time-varying delayed hybrid couplings. We achieved synchronization by applying an impulse control scheme to a small fraction of the nodes and derived sufficient conditions for stability of synchronization. Finally, we considered some numerical examples that illustrate the theoretical analysis.

Acknowledgments

This work was supported by the National Science Foundation of China under Grant nos. 61070087 and 61273220,

Guangdong Education University Industry Cooperation Projects (2009B090300355), and Shenzhen Basic Research Project (JC201006010743A and JCYJ20120613105730482). The authors are very grateful to the reviewers and the editor for their valuable comments and suggestions to improve the presentation of the paper.

References

[1] M. E. J. Newman, "The structure and function of complex networks," *SIAM Review*, vol. 45, no. 2, pp. 167–256, 2003.

[2] A. Arenas, A. Díaz-Guilera, J. Kurths, Y. Moreno, and C. Zhou, "Synchronization in complex networks," *Physics Reports A*, vol. 469, no. 3, pp. 93–153, 2008.

[3] R. Tönjes and B. Blasius, "Perturbation analysis of complete synchronization in networks of phase oscillators," *Physical Review E*, vol. 80, Article ID 026202, 7 pages, 2009.

[4] W. Lu, B. Liu, and T. Chen, "Cluster synchronization in networks of coupled nonidentical dynamical systems," *Chaos*, vol. 20, no. 1, Article ID 013120, 12 pages, 2010.

[5] J. Feng, J. Wang, C. Xu, and F. Austin, "Cluster synchronization of nonlinearly coupled complex networks via pinning control," *Discrete Dynamics in Nature and Society*, vol. 2011, Article ID 262349, 23 pages, 2011.

[6] J. Wang, J. Feng, C. Xu, and Y. Zhao, "Cluster synchronization of nonlinearly-coupled complex networks with nonidentical nodes and asymmetrical coupling matrix," *Nonlinear Dynamics*, vol. 67, no. 2, pp. 1635–1646, 2012.

[7] M. G. Rosenblum, A. S. Pikovsky, and J. Kurths, "Phase synchronization of chaotic oscillators," *Physical Review Letters*, vol. 76, no. 11, pp. 1804–1807, 1996.

[8] C. Van Vreeswijk, "Partial synchronization in populations of pulse-coupled oscillators," *Physical Review E*, vol. 54, no. 5, pp. 5522–5537, 1996.

[9] X. Yang and J. Cao, "Adaptive pinning synchronization of complex networks with stochastic perturbations," *Discrete Dynamics in Nature and Society*, vol. 2010, Article ID 416182, 21 pages, 2010.

[10] J. Lu, X. Wu, X. Han, and J. Lü, "Adaptive feedback synchronization of a unified chaotic system," *Physics Letters A*, vol. 329, no. 4-5, pp. 327–333, 2004.

[11] J. Wang, J. Feng, C. Xu, and Y. Zhao, "Exponential synchronization of stochastic perturbed complex networks with time-varying delays via periodically intermittent pinning," *Communications in Nonlinear Science and Numerical Simulation*, vol. 18, no. 11, pp. 3146–3157, 2013.

[12] Z. Li, X. Cao, and N. Ding, "Adaptive fuzzy control for synchronization of nonlinear teleoperators with stochastic time-varying communication delays," *IEEE Transactions on Fuzzy Systems*, vol. 19, no. 4, pp. 745–757, 2011.

[13] T. Yang, *Impulsive Control Theory*, vol. 272 of *Lecture Notes in Control and Information Sciences*, Springer, Berlin, Germany, 2001.

[14] G. Zhang, Z. Liu, and Z. Ma, "Synchronization of complex dynamical networks via impulsive control," *Chaos*, vol. 17, no. 4, Article ID 043126, 9 pages, 2007.

[15] T. Chen, X. Liu, and W. Lu, "Pinning complex networks by a single controller," *IEEE Transactions on Circuits and Systems I*, vol. 54, no. 6, pp. 1317–1326, 2007.

[16] J. Wang, C. Xu, J. Feng, M. K. Kwong, and F. Austin, "Mean-square exponential synchronization of Markovian switching stochastic complex networks with time-varying delays by pinning control," *Abstract and Applied Analysis*, vol. 2012, Article ID 298095, 18 pages, 2012.

[17] S. H. Strogatz and I. Stewart, "Coupled oscillators and biological synchronization," *Scientific American*, vol. 269, pp. 102–109, 1993.

[18] C. Gray, "Synchronous oscillations in neuronal systems: mechanisms and functions," *Journal of Computational Neuroscience*, vol. 1, no. 1-2, pp. 11–38, 1994.

[19] M. de Sousa Vieira, "Chaos and synchronized chaos in an earthquake model," *Physical Review Letters*, vol. 82, no. 1, pp. 201–204, 1999.

[20] R. Olfati-Saber, J. A. Fax, and R. M. Murray, "Consensus and cooperation in networked multi-agent systems," *Proceedings of the IEEE*, vol. 95, no. 1, pp. 215–233, 2007.

[21] O. Askari-Sichani and M. Jalili, "Large-scale global optimization through consensus of opinions over complex networks," *Complex Adaptive Systems Modeling*, vol. 1, no. 1, p. 11, 2013.

[22] J. Lu, D. W. C. Ho, and J. Kurths, "Consensus over directed static networks with arbitrary finite communication delays," *Physical Review E*, vol. 80, no. 6, Article ID 066121, 2009.

[23] X. Mao, "Stability of stochastic differential equations with Markovian switching," *Stochastic Processes and their Applications*, vol. 79, no. 1, pp. 45–67, 1999.

[24] C. Yuan and X. Mao, "Robust stability and controllability of stochastic differential delay equations with Markovian switching," *Automatica*, vol. 40, no. 3, pp. 343–354, 2004.

[25] Y. Sun and J. Cao, "Stabilization of stochastic delayed neural networks with Markovian switching," *Asian Journal of Control*, vol. 10, no. 3, pp. 327–340, 2008.

[26] Y. Liu, Z. Wang, and X. Liu, "On synchronization of discrete-time markovian jumping stochastic complex networks with mode-dependent mixed time-delays," *International Journal of Modern Physics B*, vol. 23, no. 3, pp. 411–434, 2009.

[27] J. Lu, J. Kurths, J. Cao, N. Mahdavi, and C. Huang, "Synchronization control for nonlinear stochastic dynamical networks: pinning impulsive strategy," *IEEE Transactions on Neural Networks and Learning Systems*, vol. 23, no. 2, pp. 285–292, 2012.

[28] J. Zhou, L. Xiang, and Z. Liu, "Synchronization in complex delayed dynamical networks with impulsive effects," *Physica A*, vol. 384, no. 2, pp. 684–692, 2007.

[29] Q. Zhu and J. Cao, "Exponential stability of stochastic neural networks with both Markovian jump parameters and mixed time delays," *IEEE Transactions on Systems, Man, and Cybernetics, Part B*, vol. 41, no. 2, pp. 341–353, 2011.

Hindawi Publishing Corporation
Mathematical Problems in Engineering
Volume 2013, Article ID 703414, 15 pages
http://dx.doi.org/10.1155/2013/703414

Research Article

A Hybrid Distributed Mutual Exclusion Algorithm for Cluster-Based Systems

Moharram Challenger,[1,2] Elif Haytaoglu,[1] Gorkem Tokatli,[1] Orhan Dagdeviren,[1] and Kayhan Erciyes[3]

[1] *International Computer Institute, Ege University, 35100 Izmir, Turkey*
[2] *Department of Computer Engineering, Shabestar Branch, Islamic Azad University, 53815 Shabestar, Iran*
[3] *Department of Computer Engineering, Izmir University, 35140 Izmir, Turkey*

Correspondence should be addressed to Moharram Challenger; m.challenger@gmail.com

Received 26 April 2013; Accepted 10 June 2013

Academic Editor: Guanghui Wen

Distributed mutual exclusion is a fundamental problem which arises in various systems such as grid computing, mobile ad hoc networks (MANETs), and distributed databases. Reducing key metrics like message count per any critical section (CS) and delay between two CS entrances, which is known as synchronization delay, is a great challenge for this problem. Various algorithms use either permission-based or token-based protocols. Token-based algorithms offer better communication costs and synchronization delay. Raymond's and Suzuki-Kasami's algorithms are well-known token-based ones. Raymond's algorithm needs only $O(\log_2(N))$ messages per CS and Suzuki-Kasami's algorithm needs just one message delivery time between two CS entrances. Nevertheless, both algorithms are weak in the other metric, synchronization delay and message complexity correspondingly. In this work, a new hybrid algorithm is proposed which gains from powerful aspects of both algorithms. Raysuz's algorithm (the proposed algorithm) uses a clustered graph and executes Suzuki-Kasami's algorithm intraclusters and Raymond's algorithm interclusters. This leads to have better message complexity than that of pure Suzuki-Kasami's algorithm and better synchronization delay than that of pure Raymond's algorithm, resulting in an overall efficient DMX algorithm pure algorithm.

1. Introduction

Using shared resources among different processes is a primary need in distributed systems. For this reason, distributed mutual exclusion (DMX) has drawn great attention over the years and a good number of algorithms have been proposed in this area. These algorithms are used in distributed systems such as mobile ad hoc networks (MANETs), sensor networks [1, 2], grids, and distributed databases. Messages sent for acquiring and releasing CS are an important measure for DMX algorithms and have a great effect on system's overall performance. Safety, liveness, and fairness are the main requirements for any mutual exclusion algorithm. Lamport's algorithm [3] and Ricart-Agrawala's (RA) [4] algorithm are considered as two of the most important fair distributed mutual exclusion algorithms in the literature. Generally, DMX algorithms can be classified into two major groups, token-based algorithms and permission-based ones. In the first case, a node enters a CS after receiving permission from all of the nodes in its set for the critical section. For token-based algorithms, however, processes are on a logical ring and possession of a system-wide unique token provides the right to enter a critical section. Suzuki-Kasami's algorithm [5] and Raymond's tree-based algorithm [6] are milestone token-based algorithms.

Suzuki-Kasami's algorithm has a low synchronization delay of one message between each two consecutive CS entrances, meanwhile its message communication number per any CS is N and that is fairly high for vast distributed systems which can restrict system scalability. On the other hand, Raymond's algorithm requires low message communication

for each CS entrance, but its delay is order of $O(\log_2(N))$ messages between two consecutive CS entrances.

In this study, a new hybrid DMX algorithm is proposed that is called Raysuz. Raysuz's algorithm uses a clustered graph infrastructure. Suzuki-Kasami's algorithm is run inside the clusters and Raymond's algorithm is run among cluster leaders. Therefore it has better synchronization delay than pure Raymond's algorithm and better message complexity than pure Suzuki-Kasami's algorithm.

In addition, cluster leaders collect internal CS requests and serve them once they receive token from other clusters. This prevents ping-pong style communication of token which is the matter of issue in Raymond's algorithm. Also using shortest paths inside clusters, Raysuz's algorithm gains even better performance than Suzuki-Kasami's algorithm too.

In rest of the paper, we have presented related work in Section 2. In Section 3, the new hybrid algorithm is described both formally and informally. The description of the algorithm is supported by the sample scenario in this section. Then in Section 4, the proposed algorithm is evaluated. Finally, in Section 5, we discuss the proposed algorithm and conclude the paper.

2. The Literature Study

In this section the related studies are elaborated and some performance metrics are discussed which are used in comparison of related algorithms.

2.1. Related Work. DMX algorithms can be classified as permission-based and token-based. In the permission based approaches, if a node needs to enter the CS, it should take permission from all other nodes. There are many algorithms which use this approach, for example, the studies of Singhal [7], Maekawa [8], Agrawal and El Abbadi [9], and Lodha and Kshemkalyani [10]. In the Lamport's algorithm, a node which needs to enter CS should broadcast its CS request, wait for acknowledge from all nodes, and finally enter the CS. After exiting CS, the node should broadcast a release message indicating *I have exited the CS*. This algorithm sends $3(N-1)$ messages for each CS [3].

In order to reduce message complexity, Ricart Agrawala has made improvements to Lamport's algorithm which sends only $2(N-1)$ messages per each CS [4]. Ricart Agrawala achieved this by removing *release message* step of Lamport's algorithm. Instead, the node exiting the CS only sends release message to the nodes which have sent request messages and wait for permission. A queue for holding requests that come from other nodes is also added to the algorithm.

Agrawal and El Abbadi [9] and Maekawa [8] have proposed quorrum-based algorithms which dramatically reduce the message complexity and belong to permission-based approach [8, 9]. Agrawal and El Abbadi use tree-structured quorums which require permission from only $O(\log_2(N))$ nodes in best case, and $O(N)$ in the worst case. Maekawa proposed a new DMX algorithm which only uses $c\ \sqrt[2]{N}$ messages to create a mutual exclusion in a computer network. The network consists of number of subsets whose intersection set is not empty. DMX algorithms in [11–15] are also permission-based algorithms.

Additionally, there are also a number of algorithms which use token-based DMX approach [5, 6, 16–21]. Main idea of token-based algorithms is that the node having the token will have opportunity to enter CS. One of the most popular approaches is Suzuki-Kasami's algorithm [5] which uses N messages per each CS. Another one is Raymond's tree based algorithm [6] which reduces the message complexity using its dynamic tree structure. Raymond's and Suzuki-Kasami's algorithms are basis for our new approach which is described in Sections 2.2 and 2.3. In [22], a new DMX algorithm which is based on path reversal is proposed.

Although many DMX algorithms exist, the state-of-the-art technologies still require adapted DMX algorithms for their circumstances. For example, Edmondson et al. [23] propose a QoS-enabled DMX algorithm for public clouds [24].

2.2. Performance Metrics. Performance bounds of DMX algorithms can vary due to the network load. When a few number of nodes want to enter a CS, the network is assumed as lightly loaded; otherwise it can be called highly loaded. There exist some metrics for evaluating performance and efficiency of DMX algorithms. "*number of messages per request*" is one of them which denotes the total number of messages used for entering CS. It is a critical metric for determining limits of required network bandwidth. Another key metric is "*response time*" which implies the time interval between one node's requesting of a CS permission and entering the CS. The last metric is "*synchronization delay.*" It denotes the latency between one node exiting and the next permitted node entering the CS.

2.3. Suzuki-Kasami's and Raymond's Algorithms. One of the most important token-based DMX algorithms is Suzuki-Kasami's algorithm [5]. It works on fully connected network and its main idea is to reduce the synchronization delay. The algorithm has three data structures. The first one is N-sized array named *request* which is used for holding requests of all nodes in the network. The number of requests which is made by some node i is stored in i_{th} place of request array. When a new request comes from node j, j_{th} element of the request array is incremented by one. The other two structures are stored only in token. One of them is an N-sized array named *last* which holds the number of CS entrances for each node. *SuzQ* is a queue for holding node identities that are waiting for the token.

When node i wants to enter the CS, it increments its request number on the *request* array and broadcasts it. Upon receiving request from node i, any node $j \neq i$ updates its ith element of *request* array with new value of variable in arriving message. After exiting the CS, a node compares the *last* and *request* arrays and enqueues node v if v_{th} element of request array is one more than the v_{th} element of *last* array and v does not already exist in queue.

Suzuki-Kasami's synchronization delay is lower than Raymond's algorithm (0 or T) but its "*number of messages*

per request" is higher than many of the other token-based algorithms (N).

Considering message complexity, Raymond's algorithm is one of the most powerful algorithms amongst token-based solutions for DMX [6]. The algorithm is based on unrooted minimum spanning tree. The tree can be physically or logically built. Each node does not need to know about all the network topology; they only have to know about their neighbors.

Entering a CS for a node requires having the *PRIVILEGE*. Every node in the tree has a variable named *HOLDER* indicating the direction to its neighbor which is on the shortest path to the node that has the *PRIVILEGE*. If the node owns the *PRIVILEGE*, its *HOLDER* variable shows itself. If a nonprivileged node wants to enter the CS, it sends *REQUEST* message to *HOLDER*. When a nonprivileged node receives the *REQUEST* message from its neighbor, it sends the *REQUEST* message to its *HOLDER* node. This process continues until the *REQUEST* message reaches the privileged node. When the privileged node receives request message and finishes executing its CS, it becomes a nonprivileged node and sends *PRIVILEGE* message to the sender. If the privileged node receives a *REQUEST* message while executing its CS, it sends *PRIVILEGE* message to the sender after it finishes CS.

As can be inferred from the description of the algorithm, the "*number of messages per request*" is decreased dramatically in comparison with the other DMX algoritms. However, this improvement comes with a trade-off. While achieving a reasonable decrease on the "*number of messages per request,*" "*synchronization delay*" increases. In Table 1, performance metrics of Raymond's tree-based algorithm are shown as well as information for some other algorithms.

2.4. Comparison. In this section, some of the DMX algorithms are evaluated with respect to performance metrics and their results, as shown in Table 1. In centralized algorithm, three messages are sent per any CS both in high and low network loads [16]. Its synchronization delay is measured as $2T$. Its primary drawback is known as single point of failure. However, Lamport's algorithm requires $3(N-1)$ messages per CS, and its synchronization delay is only T [3]. Ricart and Agrawala (RA) have made an improvement and their algorithm uses only $2(N-1)$ messages per CS both in high and low network loads. Also, it has synchronization delay of only T [4].

Maekawa's algorithm is quorum based and sends $3\sqrt[2]{N}$ messages and $5\sqrt[2]{N}$ messages per any CS for low load and high loads, respectively [8]. Its synchronization delay is evaluated as $2T$. Another quorum-based algorithm, Agrawal and El Abbadi's algorithm, uses $O(\log_2(N))$ messages per CS in low load and $(N/2)$ messages per CS in high load [9]. Suzuki-Kasami's algorithm, which is one of the token-based algorithms, uses N messages per CS in low load, and its synchronization delay is to be measured as T [5]. While Suzuki-Kasami's algorithm uses N messages per CS, Raymond's tree-based algorithm uses only $O(\log_2(N))$ messages per CS. Although synchronization delay of Suzuki-Kasami's algorithm is only T, Raymond's algorithm spends $4T$ as synchronization delay [6].

Table 1: Comparing different DMX algorithms.

Algorithm	Criteria		
	Number of messages per CS (low load)	Number of messages per CS (high load)	Synch (CS) delay
Permission based			
Centralized	3	3	$2T$
Message passing			
Lamport	$3(N-1)$	$3(N-1)$	T
Ricart-Agrawala	$2(N-1)$	$2(N-1)$	T
Singhal	$N-1$	$3/2(N-1)$	T
Lodha	$N-1$	$2(N-1)$	T
Quorum based			
Maekawa	$3\sqrt{N}$	$5\sqrt{N}$	$2T$
Agrawal-El Abbadi	$\log_2(N)$	$N/2$	—
Token passing			
Token ring	$N/2$	—	$N/2$
Suzuki-Kasami	N	N	T
Raymond	$\log_2(N)$	$\log_2(N)$	$4T$

As a result, Suzuki-Kasami's algorithm and Raymond's algorithm have less synchronization delay and less message count per CS, respectively. Their message count per CS and synchronization delay is not efficient correspondingly and we have dealt with these weaknesses.

3. Raysuz Algorithm

Suzuki-Kasami's algorithm is known to have lower synchronization delay than Raymond's with the expense of higher message complexity. Raymond's algorithm has much less message complexity, but synchronization delay is higher because of using only the edges of the minimum spanning tree (MST).

In this section, we propose an algorithm which combines the better sides of these algorithms. Initially, the nodes are grouped in clusters and each cluster has a leader node. Suzuki-Kasami's algorithm is used inside clusters and Raymond's algorithm is used to pass token among the cluster leaders. Among the leaders, token can travel only on the edges belonging to the MST paths, but inside clusters shortest paths can be used. The high message traffic of broadcasting CS requests of Suzuki-Kasami's algorithm is decreased by limiting broadcast only inside the clusters. Each cluster leader will be responsible for requesting token from outer clusters and dealing with their requests.

3.1. System Model and Data Structures. Before explaining the algorithm, we describe the system model. Each node has a unique ID and it can only communicate with its neighbors via edges. We also assume that communication channels have FIFO structure. Asynchronous communication model is used

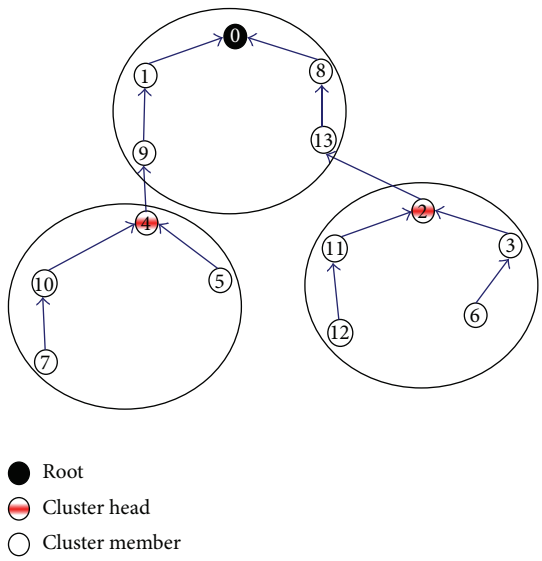

Figure 1: An example network clustered with DSTA.

in this algorithm. It is supposed that the communication channel and nodes are failure free and there are no malicious nodes. We suppose that all of the edges in the network have the same weight. However, other assumptions will not violate our results. Interested readers for weighted graphs and analysis of clustering complex networks with distributed preference mechanism can refer to [25].

Distributed spanning tree-based clustering algorithm (DSTA) [26] can be implemented to cluster the network. DSTA constructs clusters with controllable diameter and the spanning tree of cluster heads (leaders) directing to the root (sink) node as the backbone. The depth parameter of the DSTA is used to adjust the diameter of the clusters. The root node sends *PARENT*(*nhops*) message to its immediate neighbors to start the execution of the DSTA algorithm. When a node first receives *PARENT*(*nhops*) message, it sends *PARENT*(*nhops* + 1 mod *depth*) message to its neighbors. The recipients of the message with *nhops* = 0 are the *CLUSTERHEADS*, and those with *nhops* ≤ *depth* are the *MEMBER* nodes. Figure 1 shows an example network clustered with DSTA, where *depth* = 2. The borders of the clusters are circled and the communication edges are shown with lines.

Inside clusters, Suzuki-Kasami's algorithm is used to pass the token. Broadcasting requests for token in this algorithm will be achieved by unicasting them on the shortest paths for each node in the cluster. The leader only spectate the internal token passing operations. Token passing between clusters is made by cluster leaders using Raymond's algorithm. When internal requests take place, the leader node in the cluster will be responsible for requesting and taking token from other cluster leaders. When the token is in the cluster and other clusters need it, the leader of the cluster steals token from its cluster and sends it to the leader of related cluster.

The ordinary and leader nodes must hold some variables in order to run the algorithm. These variables are as follows.

(i) *Dir*: each node holds the direction which shows the leader of the cluster having the token. This variable helps cluster leaders requests to reach the cluster which has the token.

(ii) *TokInside*: this variable is held by the leader nodes. It states whether the token is inside the cluster or not.

(iii) *Asked*: this variable states whether a Raymond's algorithm token request has been made or not. Using this variable prevents sending token requests for each incoming request. It is used by cluster leaders and other nodes who are making token transfer on the transfer path.

(iv) *RequestArray*: it is an array which is used in the same way as Suzuki-Kasami's algorithm. Related array element is incremented for each internal Suzuki-Kasami's algorithm request.

(v) *LastArray*: this array is used in the same way as *last* array in Suzuki-Kasami's algorithm. It holds the number of times each node in cluster has entered the CS. Nodes increment their array element after finishing critical section. There is only one *LastArray* for each cluster and it travels with internal tokens.

(vi) *SuzQ*: it is the queue which is used by nodes that are waiting to enter CS in the same cluster, the same as Suzuki-Kasami's algorithm. It also travels with internal token, which is always sent to head of this queue. New requests from the same cluster are detected by comparing *request* and *last* arrays and there requester nodes are added to this queue by nodes exiting CS.

(vii) *RaymQ*: this queue is the same as Raymond's algorithm. During the token travel among the cluster leaders, the nodes in the path use this queue. Cluster leaders forward their token to the head of this queue after their clusters have finished their jobs. Ordinary nodes in the path also help the transfer of token by using this queue.

There are also several message types, used in the proposed algorithm, which are listed below.

(i) *InTok*: a token message which lives in the clusters.

(ii) *ExTok*: a token message which travels between cluster leaders.

(iii) *InReq*: it denotes internal Suzuki-Kasami's algorithm requests made within the clusters.

(iv) *ExReq*: it denotes external token requests (handled using Raymond's algorithm) which are sent by the cluster leaders.

(v) *Pulse*: this input denotes the need of entering CS. Only ordinary nodes can have pulse and enter CS.

3.2. Informal Description of Raysuz's Algorithm. In Raysuz's algorithm, we have two types of nodes, namely, ordinary and leader. Ordinary nodes only have information about their own neighbors and use Suzuki-Kasami's algorithm to enter the CS. These nodes broadcast a CS request to their cluster

using the shortest path routing with all possible edges. When the nodes acquire the *InTok*, these nodes will do the same procedure as that of Suzuki-Kasami's algorithm. The only difference between ordinary nodes in pure Suzuki-Kasami's algorithm and Raysuz's algorithm is that the ordinary nodes in the proposed algorithm use Raymond's algorithm procedures to transfer external CS requests and external token between cluster leaders. When an external CS request comes to a node, this node adds the requester to its *RaymQ* and if another external CS request has not been sent earlier, it sends an external CS request towards the direction in *Dir*. Whenever an external token arrives at the node, it sends this token to the head of *RaymQ*, probably itself.

Leader nodes are dedicated to request token from other clusters. The leader nodes can process two threads in order to act as leader and ordinary nodes simultaneously. Their job is to send external token requests when their cluster needs token and give the token back when other clusters need it. They send external requests and external token according to Raymond's algorithm routines. When there is an internal Suzuki-Kasami's algorithm request, *InReq*, inside the cluster, the cluster leader sends an external request to direction, *Dir*, if the token is not in the cluster. Each node in the path will forward the message up to the leader of the cluster having the token. When the leader of the token owner cluster receives the external request, *ExReq*, it sends an ordinary Suzuki-Kasami's request to its cluster, takes the token in its turn, and sends it to the requester. Cluster leaders add a level of indirection and obtain the illusion that there are only cluster leaders which are implementing Raymond's algorithm. They also hide the outer system from their cluster nodes. When the token is outside the cluster, the ordinary nodes will believe that the token is in their cluster leader.

As mentioned above, this clustered algorithm combines the low *synchronization delay* feature of Suzuki-Kasami's algorithm and low message complexity feature of Raymond's algorithms. When an external requests arrives, the cluster leader does not grab and does not send the token immediately. Instead, it makes a Suzuki-Kasami's algorithm request to take and send the token. This behaviour ensures that significant amount of internal CS demands which have arrived before external requests are fulfilled. This prevents token to travel along the graph for each request like in a ping-pong style communication, thus reducing token travelling distance for each request and reducing *synchronization delay* in comparison with pure Raymond's algorithm. Moreover, using the shortest paths for Suzuki-Kasami's operations fastens the token travelling inside the cluster, therefore reduces the *synchronization delay* and *number of messages per request*.

3.3. Formal Description of Raysuz's Algorithm. In this section, Raysuz's algorithm is illustrated formally as two finite state machines (FSM) for both leader and ordinary nodes. The related FSMs for leader and ordinary nodes can be seen in Figures 2 and 3, respectively. The pseudocode of these algorithms and used legends are provided in Table 3, Algorithm 1, and Algorithm 2.

3.3.1. The Leader Node. As it can be seen in the FSM of Figure 2, the leader node has three states, *IDLE*, *WAITEXTOKEN,* and *INTOKENSTEAL*.

IDLE. The leader nodes are in *IDLE* state when the token is in the cluster and there are no external requests, or the token is outside and there are no internal nodes which need to enter CS currently. When the token is inside and external request arrives, leader node makes a Suzuki-Kasami's algorithm request, adds the requester's ID to *RaymQ,* and passes to *INTOKENSTEAL* state. If the token is not inside the cluster and an internal Suzuki-Kasami's algorithm request arrives, the leader adds itself to *RaymQ* and sends an external request to the direction of *Dir* (if not previously sent) and transits to *WAITEXTOKEN* state.

INTOKENSTEAL. The leader nodes are in *INTOKENSTEAL* state when they are waiting for the internal token to send to external requester. When the internal token arrives, the leader looks at its *RaymQ* and *SuzQ* sizes. If their sizes both are one (which is the same the leader itself), it means that there is no more external or internal requester waiting for the token. Therefore, it sends the token to the requester and updates the direction to it and finally goes to *IDLE* state. If one of the queues is greater than one, it means that the token is needed back, either for internal CS demands or external requests. In this case, the leader puts itself into its *RaymQ* and sends external request just after sending the token and finally it transits to *WAITEXTOKEN* state.

WAITEXTOKEN. The leader nodes are in this state when they are waiting for the external token either for internal CS demands or external requests. When the external token for another cluster arrives to the leader, it just forwards the token to head of *RaymQ*, changes direction, and transits its state to *IDLE*. If the external token arrives to the leader, it looks at the size of its *RaymQ*. In case the size of its *RaymQ* is one, this means there are no other external requests waiting, so it creates and sends the internal token to its cluster and goes to *IDLE* state. If it is greater than one, this means that there are other clusters waiting for the token, thus it makes a Suzuki-Kasami's algorithm request just after sending the token into its cluster and goes to *INTOKENSTEAL* state.

The routine which takes place in a leader of any cluster is clearly defined in the Algorithm 1. This algorithm consists of six steps. Step one is triggered when the cluster has no token inside and the leader receives a request, either from outside or inside cluster. In both cases, it transits to *WAITEXTOKEN* state but in earlier case the leader puts external request in the *RaymQ* while in latter case it puts its own request in this queue.

Step two describes the state which occurs when the token owner cluster's leader receives a token request. The actions to take place are determined with regard to whether the request comes from intracluster or not. The former one forces leader to operate ordinary Suzuki-Kasami's algorithm's related part. In the other case, the leader makes Suzuki-Kasami's request

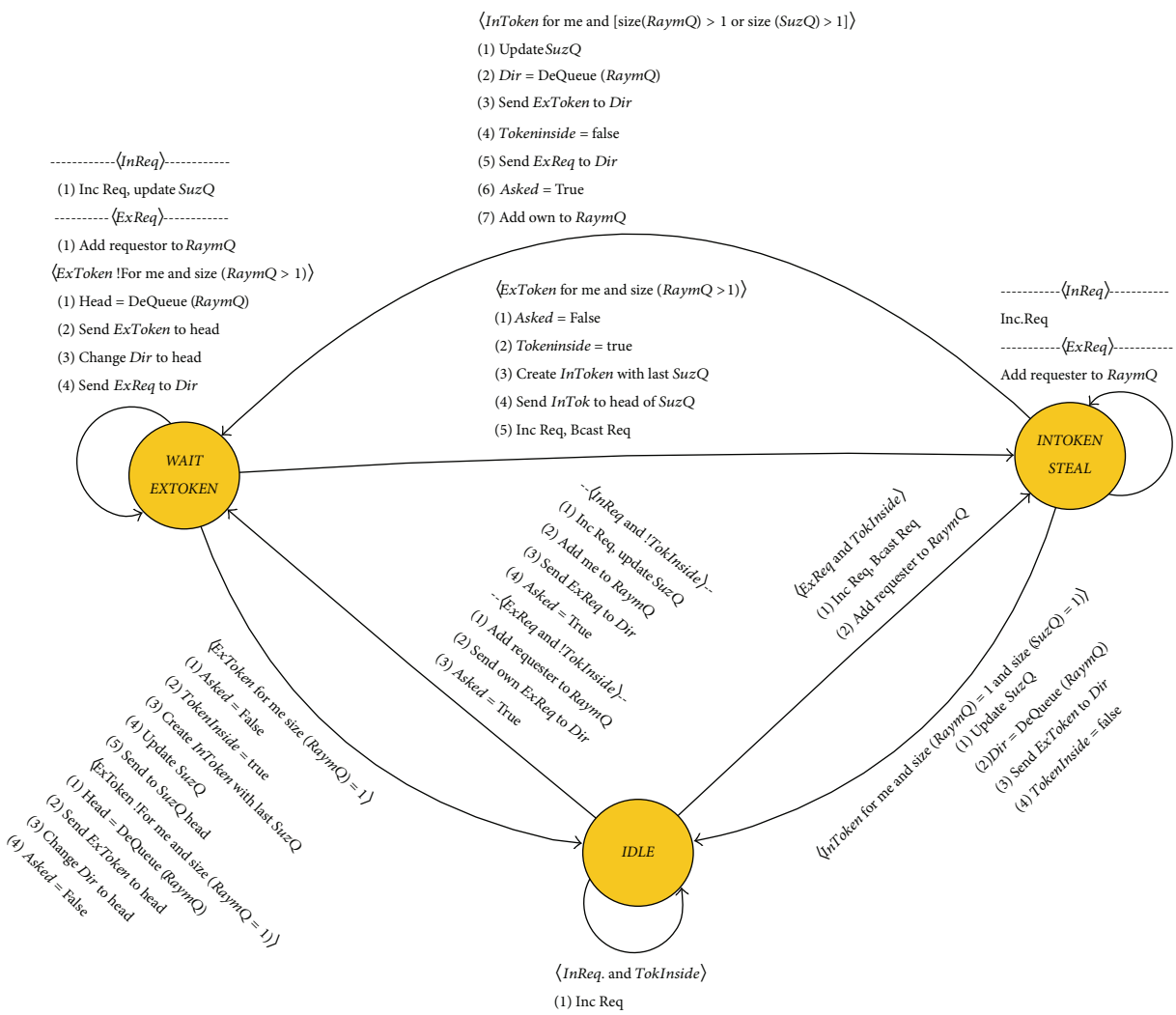

Figure 2: Leader nodes' finite state machine.

on behalf of the original requester to steal the token from its own cluster to send it outside of the cluster (to the origin of the request). At this point, the leader's state is changed to *INTOKENSTEAL* state.

In step three the leader which is in token steal state receives it and sends the token to the requester's cluster. Until receiving the token, this leader reacts with a new request from other clusters, if any, in step four. Step five deals with the leaders that are waiting for the external token and receive a request from other clusters. Nevertheless, the actions listed in step six will be taken if this leader gets the token for its cluster.

3.3.2. The Ordinary Node. The ordinary node has also three states, *IDLE*, *HAVEREQUEST,* and *HAVETOKEN*.

IDLE. This state means that the ordinary node does not have a CS demand. It follows Raymond's algorithm routine when external requests or the external token arrives. When a pulse indicating CS demand arrives, it makes Suzuki-Kasami's algorithm request and goes to *HAVEREQUEST* state.

HAVEREQUEST. The node waits for the token in this state. When internal token arrives, it enters the CS. Upon exiting the CS, it checks the *SuzQ*. If it is empty, this means there are no token waiting nodes in the cluster. Thus, it goes to *HAVETOKEN* state. If *SuzQ* is not empty, it sends the token to the head of *SuzQ* and goes to *IDLE* state.

HAVETOKEN. This state means that there are no more token waiting nodes in the cluster and the token remains at the node after the CS; then it can freely enter the CS whenever it needs. When an internal request arrives, it sends the token to the requester and transits to *IDLE* state.

The routine which takes place in an ordinary node is defined in the algorithm of Algorithm 2. This algorithm contains seven steps. The first step deals with any idle or token requested ordinary node which receives a request from any other node. In second step, the actions required upon receiving an external token for idle nodes or nodes which have just requested a token are listed. The event of receiving

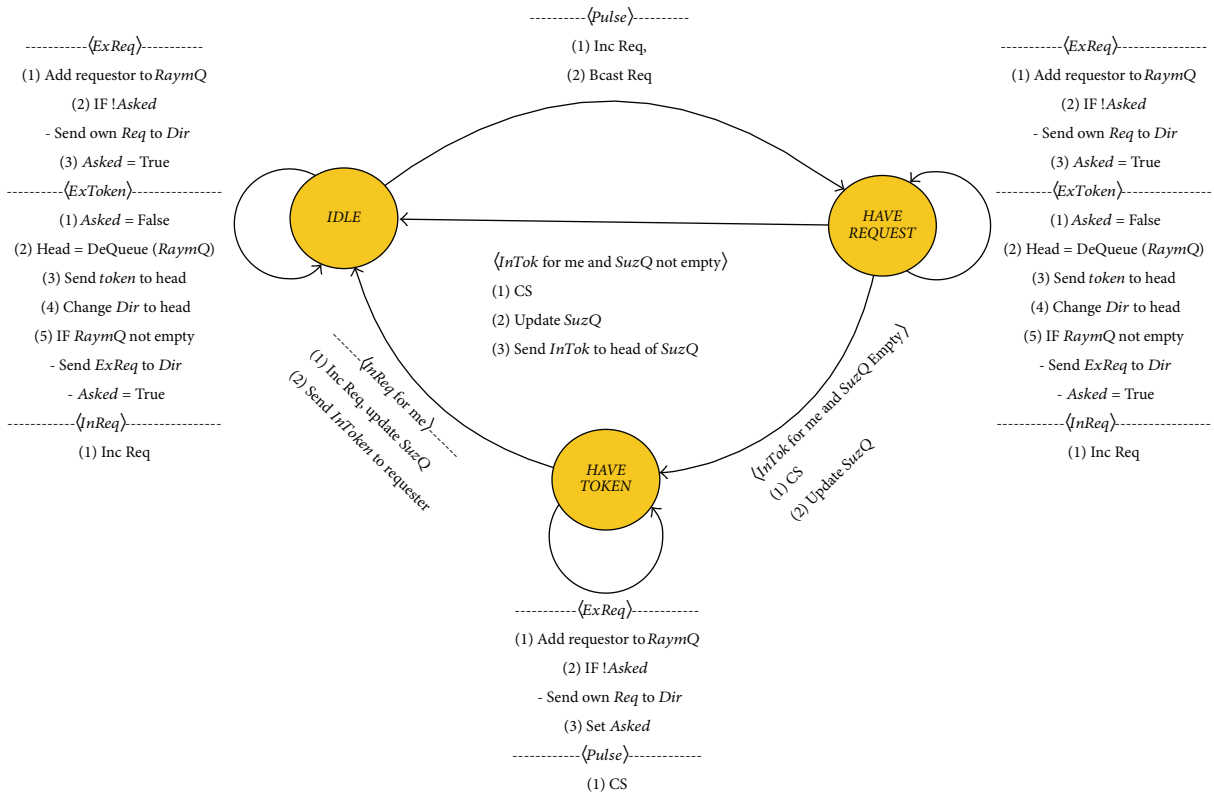

Figure 3: Ordinary Nodes' Finite State Machine.

a pulse enforces the idle node to have a request in the third step.

The fourth and fifth steps demonstrate the original related part of Suzuki-Kasami's algorithm in which any requested node receives the token. Finally, the sixth and seventh steps handle receiving request and pulse, respectively, for an ordinary node which is in the *HAVETOKEN* state.

3.4. A Sample Scenario Using Raysuz's Algorithm. For clarity of Raysuz's algorithm, we present a sample scenario for the algorithm execution. According to the algorithm, the network is clustered by an algorithm such as [26, 27]. In this scenario, initially, the token belongs to a node T, in cluster C_0. There are some requests from other nodes in this scenario: firstly, N_0 in C_0 requests the token. Then the other node, N_1 in C_1, asks for the token shortly after N_0's request. Meanwhile, N_2 in C_2 also wants to grab the token. This scenario shows how the algorithm deals with these requests.

The first event of the scenario can be seen in Figure 4(a). Firstly, node N_0, which needs the token, makes a Suzuki-Kasami request and broadcasts it to its cluster. Since it is the first node which has requested the token, it receives the token immediately as shown in event 1 in Figure 4(b). After that, node N_1 in cluster C_1 requests the token from its own cluster with broadcasting a Suzuki-Kasami's request as shown in event 2 in Figure 4(b). Due to lack of the tokens in this cluster C_1's leader L_1 sends the request to the leader of the cluster which is the owner of the token, L_0, as in Figure 5(a). After L_0 receives the token request, it makes a Suzuki-Kasami request as it does for itself, as shown in event 1 in Figure 5(b). Shortly after that, node N_2 from another cluster, C_2, wants the token and makes a request to its own cluster as shown in event 2 in Figure 5(b). Since the token is not in C_2, its leader, L_2, sends the request to N_0's cluster leader as shown in event 1 in Figure 5(c).

At this point, N_0 has the token and N_1 and N_2 are waiting for it. When N_0 quits the critical section, it sends the token to the leader of its cluster as shown with event 2 in Figure 5(c) and the leader forwards it to the leader of C_1 accompanied with a request (for request of N_2) as shown in event 1 in Figure 5(d). Upon receiving the token by L_1, it delivers the token to N_1, which has asked for it, and then L_1 broadcasts an internal request in its cluster to steal the token and send it back to L_0 as shown in event 2 in Figure 5(d).

As soon as N_1 exits the critical section, due to prior internal request, it sends the token to L_1 as shown in event 1 in Figure 5(e). Afterwards, the leader returns the token to L_0 as shown in event 2 in Figure 5(e). Then, L_0, according to the requests saved in its queue, sends the token to L_2, which delivers it to N_2 as shown in events 3 and 4, respectively, in Figure 5(e).

Now, we examine this scenario deeply according to algorithm's detail to understand what is going on in this algorithm. When node N_0 makes a Suzuki-Kasami request as is shown in Figure 4(a), L_0 only increases the request array in

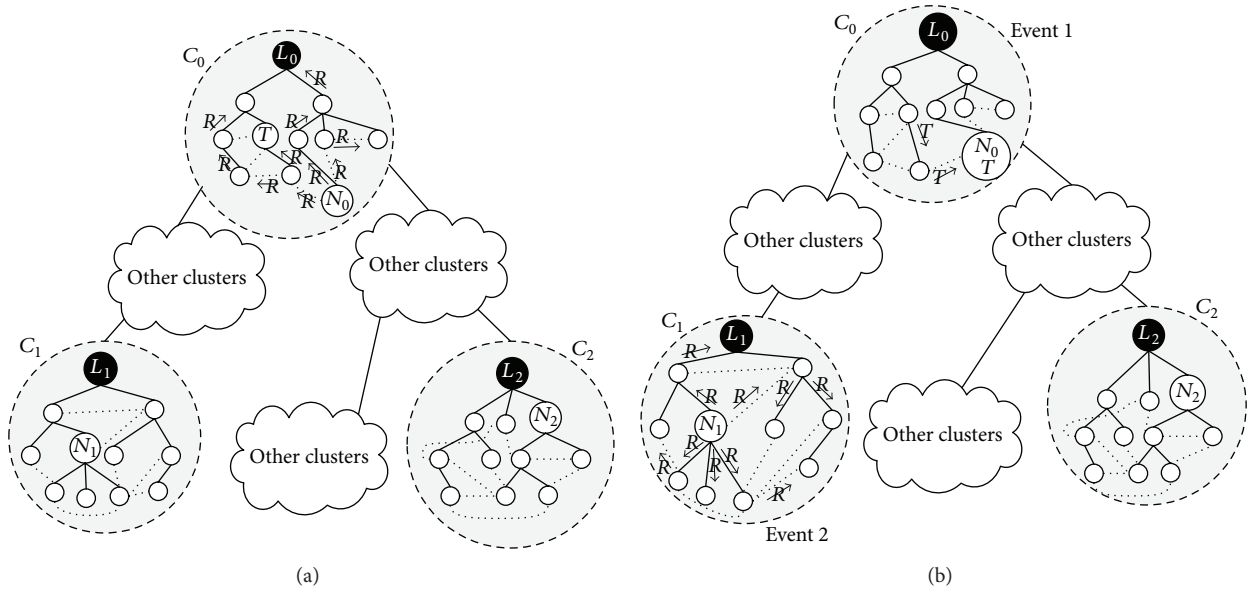

Figure 4: Scenario for Suzuki-Kasami's part of the Raysuz algorithm.

the same way as an ordinary node does in the same cluster. So far everything is straightforward. Then node N_1 in C_1 makes a request in its cluster to enter the CS; see Figure 4(b). Before N_1 requests for the token, N_0 receives the token from the token holder node, as shown in Figure 4(b).

At this time, in C_1, L_1 which is aware of the token absence prepares a request to get token and sends it to node whose identity is the same as the *Dir*'s content, as shown in Figure 5(a). Upon receiving the external request from N_1, L_0 adds N_1's request to its *RaymQ* and prepares a request to get the token from its own cluster. This is achieved by making a Suzuki-Kasami request as shown in event 1 of Figure 5(b), as if L_0 wants the token for itself to give it to N_1. While L_0 is dealing with acquiring the token, another node, N_2 in C_2, needs to enter the CS, so it makes a Suzuki-Kasami request as shown with event 2 in Figure 5(b). After some while, L_2 sends an external request to L_0 to get the token as shown in event 1 in Figure 5(c). Then L_0 adds this node (L_2) to its own *RaymQ*. In this way, L_0 knows that there is another node, N_2, which wants to grab the token after N_1. Later on, N_0 sends back the token to L_0 as shown in event 2 in Figure 5(c).

Now, L_0 has the token and dequeues *RaymQ* and sets *Dir* variable with dequeued node. Afterwards, it sends the token to dequeued node which is the first external node which wants token from L_0. Since the *RaymQ* is not empty, L_0 also sends an external request along with the token as shown in event 1 in Figure 5(d).

As L_1 receives the request and the token, it queues the external request to the *RaymQ* and forwards the token to the N_1 using *SuzQ*. Taking the request into consideration, L_1 also broadcasts a Suzuki-Kasami request in the cluster, as can be seen in event 2 of Figure 5(d). Since there is no other internal request in C_1, after exiting the CS, N_1 forwards the token to the L_1 as shown in event 1 of Figure 5(e).

At this point, L_1's *RaymQ* is not empty, so it sends the token to the *RaymQ*'s head (in this case L_0 with dequeuing it as shown in event 2 of Figure 5(e)). Analogous to the previous event, L_0 sends the token to L_2 using its *RaymQ* as shown in event 3 of Figure 5(e).

Finally, L_2, receiving an external token, sends the token to the head of *SuzQ* which is N_2 as shown in event 4 in Figure 5(e). In this way, three nodes received the token in order and the scenario is accomplished.

4. Analysis of the Proposed Algorithm

In this section, we present the theoretical analysis of Raysuz's algorithm along with relevant proofs. This theoretical analysis contains correctness, message complexity, energy consumption, synchronization delay, and response time for the proposed algorithm.

4.1. Correctness of Raysuz's Algorithm. The correctness of Raysuz's algorithm is examined according to safety and liveness attributes of the algorithm.

4.1.1. Safety. Safety of Raysuz's algorithm is analyzed from the single token existence and mutual exclusion points of view, which will be discussed in Theorem 3.

Lemma 1. *In Raysuz's algorithm at most one token exists in the network concurrently.*

Proof. Assume the contrary. In this case, there exists more than one token in the network concurrently. Therefore, according to finite-state machine given in Figure 3, more than one ordinary node should be in *HAVETOKEN* state. Assume that these nodes are in the same cluster. Suzuki-Kasami's algorithm is used in intracluster communication; thus multiple token existence is impossible [5].

On the other hand, assume that more than one node belonging to different clusters is in the CS at the same time.

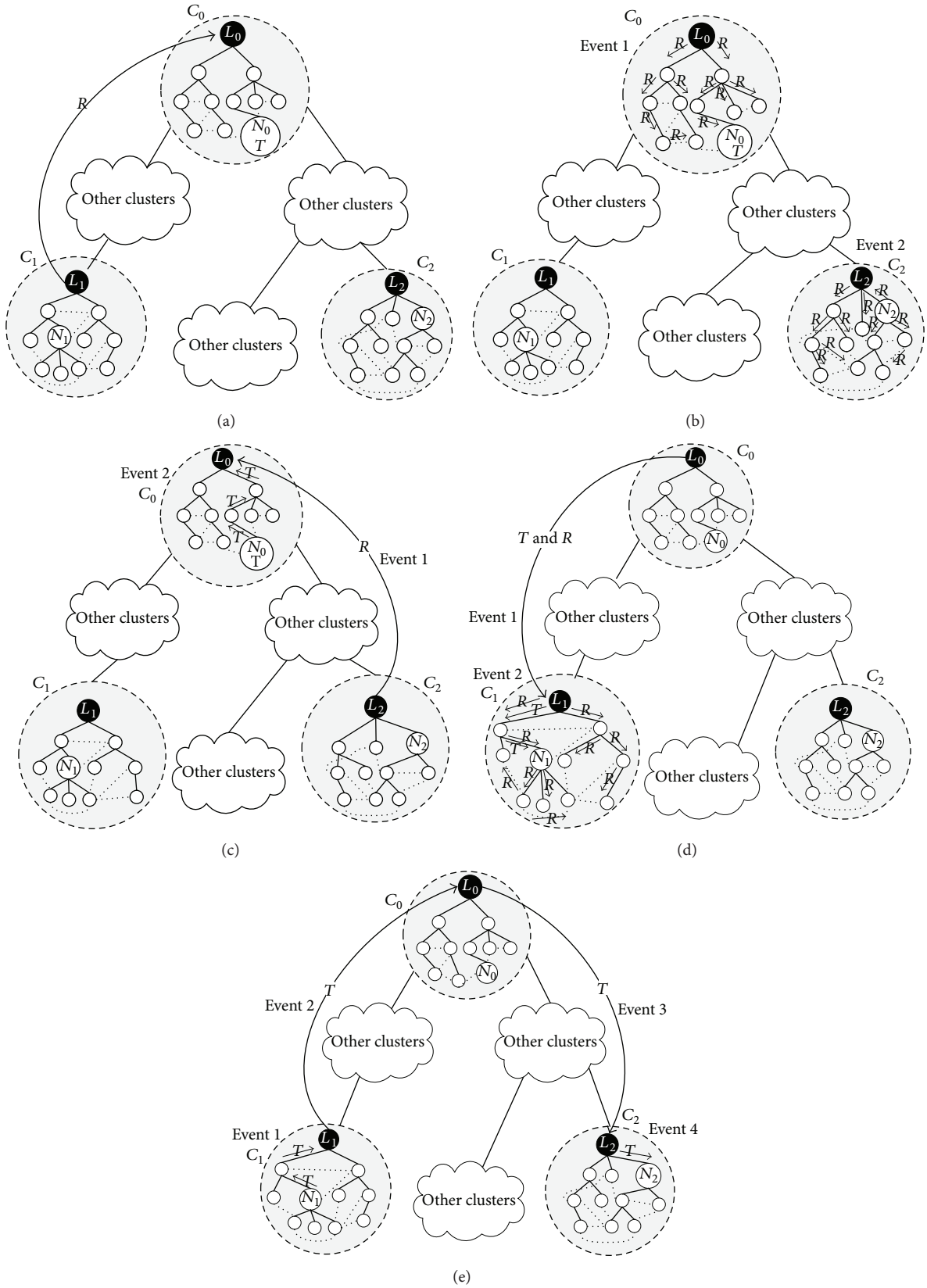

Figure 5: Scenario for Raymond's part of the Raysuz algorithm.

In this case, according to pseudocode of leader node in Algorithm 1, multiple leaders should be in *INTOKENSTEAL* state. Since Raymond's algorithm is used for intracluster communications, this is also not possible [6].

There is no other possibility; therefore we contradict our assumption. □

Lemma 2. *At most one node can be in the CS at any time, ensuring mutual exclusion.*

Proof. Assume the contrary, that more than one node can execute CS at any time concurrently. In Raysuz's algorithm, when a node receives token, it enters CS. If there is more than one token in the network, then more than one node can execute CS at the same time. However, it is proven in Lemma 1 that this case is not possible. Therefore, we contradict our assumption. □

Theorem 3. *There always exists exactly one token in Raysuz algorithm, which also provides at most one node entering CS at any time, thus satisfying Safety attribute.*

Proof. The theorem holds since Lemmas 1 and 2 are true. □

4.1.2. Liveness

Theorem 4. *Raysuz's algorithm is deadlock- and starvation-free.*

Proof. We use Suzuki-Kasami's algorithm for intracluster communication and Raymond's algorithm for intercluster, communication. Both algorithms are deadlock- and starvation free which is proven in [5, 6]. Thus, Raysuz's algorithm is deadlock- and starvation-free. □

4.2. Message Complexity. The message complexities of Raysuz's, Raymond's and Suzuki-Kasami's algorithms are comparatively explained in this section. We assume the topology of the network as multihop cluster tree, where there are C clusters and N nodes.

In the graph consisting of N nodes, the mean distance between any two nodes (also mean unicast distance between two nodes), $E(L_u)$, is almost surely of order $O(\log_2(N)/\log_2(d))$, where d is the weighted average of the sum of squares of the expected degrees [28].

We consider the power law graphs with lots of nodes, so d is a very small value in comparison with N. Thus we use the complexity $O(\log_2(N))$ instead of $O(\log_2(N)/\log_2(d)$ as a mean distance between two arbitrary nodes.

4.2.1. The Worst Case. In Raymond's algorithm, token requester and token holder nodes will be on the farthest sides in the worst situation. In this case, request message will travel up to the root and down to the token holder. Similarly, token holder will send token back in the same path. Thus, the message complexity for a request is $N-1+N-1 = 2N-2 = O(N)$.

In Suzuki-Kasami's algorithm on a tree, the requester will broadcast request on tree, which uses a total of $N-1$ messages. Then the token holder node will receive request and send token to requester using the shortest path routing information in messages. Therefore, the total message count for a request is: $N-1+N-1 = 2N-2 = O(N)$. Raysuz's algorithm has six phases for requesting and entering CS. The phases and number of messages sent in each phase are described as follows.

(i) Requester node sends request to its leader: intra cluster requests are broadcasted along the tree, and one message will be sent for each node in cluster except the requester. This requires $N/C-1 = O(N/C)$ messages.

(ii) Leader forwards the request to the token holder node's cluster: in this phase, the two token leaders will communicate. In the worst situation, these leaders will be in the farthest sides of the tree. Then, the distance between them will be $N-1 = O(N)$, which is also the number of messages needed in this phase.

(iii) Token holder leader makes Suzuki-Kasami's request: the leader of the token holding cluster will broadcast request to its cluster to take the token. This broadcast needs $N/C-1 = O(N/C)$ messages.

(iv) Token holder node sends token to its leader: the token holder node will send token to leader at the cluster root using $O(N/C)$ messages.

(v) Token holder cluster's leader sends token to requester's leader: similar to phase 2, the two token leaders will communicate. Thus, the number of messages needed is $N-1 = O(N)$.

(vi) Token requester node's leader sends token to the requester node using $O(N/C)$ messages.

The total of these phases yields $O(N)$.

4.2.2. The Best Case. The best case situation occurs when only the token holder node wants to enter CS. In this case, no message transmission is needed. Therefore, the number of messages needed for Raymond's, Suzuki-Kasami's and Raysuz's algorithm is 0 in the best case.

4.2.3. The General Case. The general case for message complexity is elaborated in this section. The required notation is shown in Table 2. We assume that underlying topology is a balanced tree with height $O(\log_2(N))$.

LHL denotes the level of the token holder leader in the tree. *LHN* denotes the level of token holder node. *LRN* is level of requesting node and *LRL* is the level of requesting leader.

In Raymond's algorithm, request message will travel $LRN+LHN$ hops. Similarly, the token will travel back $LHN+LRN$ hops, resulting in a total of $2(LRN+LHN)$ messages travelling through the path. This yields $O(\log_2(N))$ message complexity for Raymond's algorithm. According to Suzuki-Kasami's algorithm, $N-1$ messages are needed to broadcast the request. The token will be sent to requester in *LHN* number of messages, resulting in $N-1+O(\log_2(N)) = O(N)$ messages.

Table 2: Legends of the analysis.

Legend	Description
LHL	Level of the token holder leader
LRL	Level of requesting leader
LHN	Level of the token holder node
LRN	Level of requesting node

Table 3: Legends of the algorithms.

Legend	Description
L_j	Any leader j
L_{hold}	Leader's cluster holding token
$L_{waitExToken}$	Leader who sent request
$L_{tokenSteal}$	Leader who sends Suzuki-Kasami's request to inner cluster
C_j	Cluster j
P_j	Process j
O_j	Any node
O_{idle}	The node which is not interested in token
$O_{haveToken}$	The node which has the token
$O_{haveRequest}$	The node which has requested the token

In Raysuz's algorithm, we have the same 6 phases as in Section 4.2.1.

(i) The requester node sends request to its leader (using Suzuki-Kasami's algorithm) with $N/C - 1$ messages.

(ii) The leader forwards the request to token holder cluster's leader in $LRL + LHL$ number of messages.

(iii) Token holder leader broadcasts Suzuki-Kasami's algorithm request to take the token. The number of messages needed is $N/C - 1$.

(iv) Token holder node sends token to its cluster leader using $LHN - LHL$ messages.

(v) Token holder cluster leader sends token to leader of token requester node in $LRL + LHL$ number of messages.

(vi) Leader of token requesting node sends message to requesting node in $LRN - LRL$ number of messages.

The total of these phases results is $N/C - 1 + LRL + LHL + N/C - 1 + LHN - LHL + LRL + LHL + LRN - LRL = 2N/C - 2 + LRL + LHL + LHN + LRN = O(N/C + \log_2(N))$.

For example, if the number of clusters, C, is big enough, then the average message complexity becomes $\Omega(\log_2(N))$.

4.3. Energy Consumption. Energy consumption is important for wireless systems and especially for MANETs where nodes are battery-powered. Generally transceiver is the dominant energy consumer, so that transmitted byte counts should be minimized to maximize the network lifetime. With regard to this, our energy consumption analysis depends on message size and message complexity. We first analyze message size of Raysuz's algorithm and then we analyze the worst case, the best case, and the general case for the transmitted bit count.

The complexities of size of *ExTok*, *InReq*, *ExReq*, and *Pulse* messages are $O(\log_2(N))$ bits since these messages include constant number of fields (such as *source*, *destination*, and *requestor*) and each of these fields can be represented with numbers in $[0, N]$. On the other hand, the *InTok* message's size is $O(N/C\ \log_2(N))$ bits since Suzuki-Kasami token should include information about all nodes in the cluster.

4.3.1. The Worst Case. In Raymond's algorithm, $O(N)$ messages are sent at the worst case. Since the message size in Raymond's algorithm is $O(\log_2(N))$ bits, the transmitted bit count of Raymond's algorithm is $O(N\log_2(N))$ bits.

At the worst case, the message complexity of Suzuki-Kasami's algorithm is $O(N)$. Token includes information of all nodes, so that the size of the token is $O(N\log_2(N))$ bits. In this case, $O(N^2\log_2(N))$ bits are transmitted in total.

Raysuz's algorithm has six phases in the worst case as given in Section 4.2.1. The transmitted bit count of each phase is added to find the total value as follows: $O(N/C)\ O(N/C\log_2(N)) + O(N)\ O(\log_2(N)) + O(N/C)\ O(N/C\log_2(N)) + O(N/C)\ O(N/C\log_2(N)) + O(N)\ O(\log_2(N)) + O(N/C)\ O(N/C\log_2(N)) = O((N/C)^2\log_2(N))$. At the worst case for $C = 1$, the complexity of transmitted bit count is $O(N^2\log_2(N))$ bits.

4.3.2. The Best Case. At the best case, token holder wants to enter CS. No transmissions are needed; thus, the transmitted bit counts of Raymond's, Suzuki-Kasami's and Raysuz's algorithm are 0 bits.

4.3.3. The General Case. In the general case, Suzuki-Kasami's and Raymond's transmitted byte counts are $O(N^2\log_2(N))$ bits and $O(\log_2(N)^2)$ bits, respectively. The general case of Raysuz's algorithm can be found by adding the complexities of intracluster and intercluster operations as follows: $O(N/C)\ O(N/C\log_2(N)) + O(N/C+\log_2(N))\ O(\log_2(N)) = O((N/C)^2\log_2(N) + (N/C+\log_2(N))\log_2(N))$. For $C = 1$, the worst case equals $O(N^2\log_2(N))$ bits, the same as the value given in Section 4.3.1. For $C = N$, $\Omega(\log_2(N)^2)$ bits are the lower bound of the general case.

4.4. Synchronization Delay. In synchronization delay formulations, we have used notation T to indicate the unit time for sending a message.

4.4.1. The Worst Case. The worst case synchronization delay of Suzuki-Kasami's algorithm is NT for a network consisting of N nodes, since distance of any two nodes is at most N. Thus synchronization delay of Suzuki-Kasami's algorithm is $O(N)$ at the worst case. The worst synchronization delay of Raymond's algorithm is NT, resulting in $O(N)$ time complexity which is equal to diameter of the tree at the worst case.

The worst case of Raysuz's algorithm has 3 phases. In the first phase token holder finishes executing CS and sends token to its leader. This phase requires $O(N/C)$ time. In the second phase, the token holding leader sends token to leader

Step 1. Upon a leader $L_j \neq L_{hold}$ receives request from process P_i and $L_j = L_{idle}$
1.1 if $P_i \cap C_j = \emptyset$
1.1.1 add P_i to *RaymQ*
1.1.2 send L_j's request to *Dir* (as an external request)
1.2 else
1.2.1 increase corresponding request array element by 1
1.2.2 enqueue *RaymQ* with L_j
1.2.3 send *ExReq* to *Dir*
1.3 end if
1.4 $L_j = L_{waitExToken}$
Step 2. Upon a $L_j = L_{hold}$ receive request from process P_i
2.1 if $P_i \cap C_j = \emptyset$ **then**
2.1.1 increase jth element of request array and broadcast request
2.1.2 enqueue P_i to *RaymQ*
2.1.3 $L_j = L_{inTokenSteal}$
2.2 else
2.2.1 increase ith element of request array by 1
2.3 end if
Step 3. Upon a $L_j = L_{inTokenSteal}$ receive *InToken* for L_j
3.1 if *RaymQ*.length > 1 or *SuzQ*.length > 1 **then**
3.1.1 update *SuzQ*
3.1.2 dequeue *RaymQ* and set *Dir* with dequeued node
3.1.3 send *ExToken* and *ExReq* to *Dir*
3.1.4 enqueue *RaymQ* with L_j
3.1.5 $L_j = L_{waitExToken}$
3.2 else
3.2.1 update *SuzQ*
3.2.2 dequeue *RaymQ* and set *Dir* with dequeued node
3.2.3 send *ExToken* to *Dir*
3.2.4 $L_j = L_{idle}$
3.3 end if
Step 4. Upon a $L_j = L_{inTokenSteal}$ receive request from P_j
4.1 if $P_i \cap C_j = \emptyset$ **then**
4.1.1 add P_j to *RaymQ*
4.2 else
4.2.1 increase jth element of request array
4.3 end if
Step 5. Upon a $L_j = L_{waitExToken}$ and receives request from P_i
5.1 if $P_i \cap C_j = \emptyset$
5.1.1 enqueue P_i to *RaymQ*
5.2 else
5.2.1 increase corresponding request array element by 1
5.2.2 Update *SuzQ*
5.3 end if
Step 6. Upon a $L_j = L_{waitExToken}$ and receives *ExToken* for L_j
6.1 update *SuzQ* and last and add them in *InToken*

Algorithm 1: Raysuz's algorithm for leader node.

of the requester. This phase needs $O(N)$ time. In the last phase, token requester's leader sends token to the requester. This requires $O(N/C)$ time. Consequently, the total messages needed in these three phases are $O(N)$ time which is needed at the worst case.

4.4.2. The Best Case. The best case situation occurs when requester node is the token holder node. In this case, Raymond's, Suzuki-Kasami's, and Raysuz's algorithm will have 0 synchronization delay.

4.4.3. General Case. In Suzuki-Kasami's algorithm, the best case and general case have the same delay. The synchronization delay of Suzuki-Kasami's algorithm is $\log_2(N)T$ in general case for power law graphs. In Raymond's algorithm, synchronization delay is $(LHN + LRN)T = 2\log_2(N)T$ in general case.

In Raysuz's algorithm, the first phase takes $(LHN - LHL)T$ time. The second and the third phases require $(LRL + LHL)T$ and $(LRN - LRL)T$, respectively. The total time is: $(LHN + LRL + LRN)T = 2\log_2(N)T$.

Step 1. Upon $O_j = O_{idle}$ or $O_j = O_{haveRequest}$ and receives request from P_i
  1.1 if $P_i \cap C_j = \emptyset$ **then**
    1.1.1 enqueue P_i to *RaymQ*
    1.1.2 if !*Asked*
      1.1.2.1 send own request to *Dir*
      1.1.2.2 set *Asked* True
    1.1.3 end if
  1.2 else
    1.2.1 increase corresponding *request* array element by 1
  1.3 end if
Step 2. Upon $O_j = O_{idle}$ or $O_j = O_{haveRequest}$ and receives *ExToken*
  2.1 set *Asked* False
  2.2 dequeue *RaymQ* and set *Dir* with dequeued node
  2.3 send *ExToken* to *Dir*
  2.4 if *RaymQ*.length ≥ 1 **then**
    2.4.1 send *ExReq* to *Dir*
    2.4.2 set *Asked* True
  2.5 end if
Step 3. Upon $O_j = O_{idle}$ and receives *Pulse*
  3.1 increase corresponding *request* array element by 1 and broadcast request
  3.2 $O_j = O_{haveRequest}$
Step 4. Upon $O_j = O_{haveRequest}$ receives *InToken* for O_j and *SuzQ*.length = 0
  4.1 enter CS
  4.2 update *SuzQ*
  4.3 send *InToken* to head of *SuzQ*
  4.4 set *Dir* as head
Step 5. Upon $O_j = O_{haveRequest}$ receives *InToken* for O_j and *SuzQ*.length > 0
  5.1 enter CS
  5.2 update *SuzQ*
  5.3 $O_j = O_{haveToken}$
Step 6. Upon $O_j = O_{haveToken}$ receives request from P_i
  6.1 if $P_i \cap C_j = \emptyset$ **then**
    6.1.1 enqueue P_i to *RaymQ*
    6.1.2 if !*Asked*
      6.1.2.1 send own *request* to *Dir*
      6.1.2.2 set *Asked* True
    6.1.3 end if
  6.2 else
    6.2.1 increase corresponding *request* array element by 1
    6.2.2 update *SuzQ*
    6.2.3 send *InToken* to P_i
    6.2.4 $O_j = O_{idle}$
  6.3 end if
Step 7. Upon $O_j = O_{haveToken}$ and receives *Pulse*
  7.1 enter CS

Algorithm 2: Raysuz's algorithm for ordinary node.

This case is for intercluster token transmission between two leaf clusters. The fact is that the token transmissions are not always from end to end nodes. So, the synchronization delay is less than $O(\log_2(N))$. Furthermore, due to the locality of reference, in high load critical section request, a good number of requests will arise in the clusters, there exist C clusters in the system each having N/C nodes. In these cases, the synchronization delay is as much as the best case which is much less than $O(\log_2(N))$.

4.4.4. Clustering Effect on Raysuz's Algorithm. Raysuz's algorithm takes the advantage of using clusters and applying Suzuki-Kasami's algorithm inside the clusters. In some cases, nodes that are close to the token owner node are more likely to make CS request than further nodes. This locality of reference property leads to have lower synchronization delay using Suzuki-Kasami's algorithm inside clusters.

Assume that the requester and the token holder node are in the same cluster. Then, in the worst case, the token

requester will wait for the next node of its cluster to enter CS. This takes $\log_2(N/C)T$ time.

However, in Raymond's algorithm, the worst case time is $\log_2(N)T$. It can be seen that Raysuz's algorithm has lower synchronization delay when requester is in the same cluster.

4.5. Response Time. At the worst case, the response of time of Raysuz's algorithm is $2\log_2(N/C)T$ for intracluster communications and $O(\log_2(N)T)$ for intercluster communications. The response times of Raymond's and Suzuki's algorithms are $2\log_2(N)T$ at the worst case. As explained in previous section, Raysuz is favorable when requests are mostly made by nodes that are in the same cluster as the token requestor.

4.6. Fairness. A distributed mutex algorithm can be stated as fair if CS requests are always satisfied in the increasing order of their request timestamps. Raymond's algorithm [6] is known to be not fair in certain situations. One of these situations can be stated as follows.

Assume that nodes a and b are in the same cluster and node a is the token holder and cluster leader of node b. Also, nodes c and d are in the same cluster and the leader of these nodes is denoted as node e. This topology can be seen in Figure 6. Considering this topology, suppose that the CS requests are made in d, b, and c chronological order. The leaders of the requesters hear the requests and send requests to the token holding cluster, node a. Node a sends the token to the direction of d and immediately sends a request to grab and send token to node b. Node e which is the leader of node d receives the token and forwards it to d. After node d exits the CS, it immediately sends the token to node c, since they are in the same cluster and Suzuki-Kasami's part of Raysuz is processed. Meanwhile, node e makes Suzuki-Kasami's request, since it has received a request from node a (which belongs to node b). After c exits CS, e takes the token back and sends to a, which will finally send token to b. In this scenario, c enters CS before b while b has sent request earlier.

Our proposed algorithm uses Raymond's algorithm for intercluster communications; therefore, intercluster operations are unfair as in Raymond's algorithm. Intracluster requests are satisfied fairly as in Suzuki-Kasami's algorithm. On the whole, unfairness of Raysuz's algorithm is generally lower than, and in the worst cases the same as the unfairness of Raymond's algorithm.

Kanrar and Chaki [29] had solved the unfairness issue by adding extensions to original Raymond's algorithm. The same approach can be applied to Raysuz's algorithm easily; therefore, the unfairness issue can be solved.

5. Discussion and Conclusion

In this work, we have proposed a new token-based hybrid DMX algorithm. The algorithm works on a clustered graph and executes Suzuki-Kasami's algorithm in the clusters, meanwhile running Raymond's algorithm between cluster's leaders. It stores the CS requests in clusters and serves them whenever token arrives into the cluster.

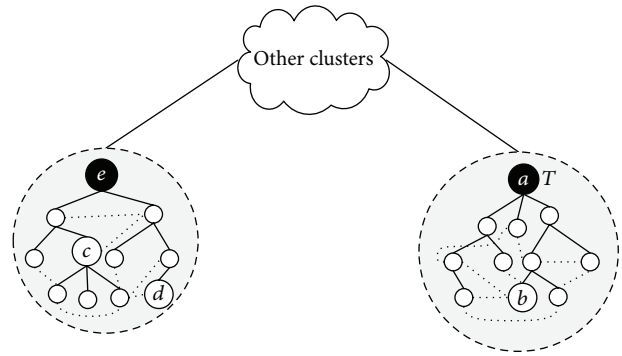

Figure 6: The topology of the scenario.

In general, Raysuz's algorithm has a stronger fairness property than Raymond's algorithm. In the worst case scenario, the algorithm is as fair as Raymond's algorithm. However, there are algorithms to make Raymond's algorithm fair which can also be added into Raysuz's algorithm [29]. Instead, Raysuz algorithm gives better message complexity than pure Suzuki-Kasami's algorithm and better CS delay than pure Raymond's algorithm. In addition, storing CS request and serving them as soon as external token arrives leads to preventing ping-pong style token communication in intraclusters which can be matter of issue in Raymond's algorithm.

Using positive points of both Raymond's and Suzuki-Kasami's algorithms makes it possible to balance the amount of message communication (increasing with bigger clusters) and the synchronization delay (increasing with smaller clusters). Therefore, having a parameter like cluster size as a tuning variable can make desired balance between CS delay and communication messages. Thus, the algorithm will be useful for both interactive systems with multiusers, in which traffic reduction is important, and real-time systems, in which lower CS delay is critical. In the real distributed systems, usually networks are not fully connected. The proposed algorithm uses Suzuki-Kasami's algorithm and customizes it by finding an MST in the clusters and using the shortest paths in them.

The reduction of message count used in the communication leads to have lower energy consumption. This is an important issue for wireless systems in general and makes our algorithm more suitable to be used in MANETs. Also, using clusters and executing CS in the clusters can lead to have less energy consumptions. Group mutual exclusion [30] is another field that can be adapted to proposed algorithm [3, 31]. In any cluster, CS executions can be considered as groups of nodes which tend to enter a CS.

Acknowledgment

The authors would like to thank the anonymous reviewers for their accurate comments on the previous version of the paper. The authors have been able to improve both their work and the paper significantly by taking these anonymous reviewers' critical comments into account.

References

[1] J. Mou, W. Zhou, T. Wang, C. Ji, and D. Tong, "Consensus of the distributed varying scale wireless sensor networks," *Mathematical Problems in Engineering*, vol. 2013, Article ID 862518, 9 pages, 2013.

[2] D. Y. Kim and M. Jeon, "Robust distributed Kalman filter for wireless sensor networks with uncertain communication channels," *Mathematical Problems in Engineering*, vol. 2012, Article ID 238597, 12 pages, 2012.

[3] L. Lamport, "Time, clocks, and the ordering of events in a distributed system," *Communications of the ACM*, vol. 21, no. 7, pp. 558–565, 1978.

[4] G. Ricart and A. K. Agrawala, "An optimal algorithm for mutual exclusion in computer networks," *Communications of the ACM*, vol. 24, no. 1, pp. 9–17, 1981.

[5] I. Suzuki and T. Kasami, "A distributed mutual exclusion algorithm," *ACM Transactions on Computer Systems*, vol. 3, no. 4, pp. 344–349, 1985.

[6] K. Raymond, "A tree-based algorithm for distributed mutual exclusion," *ACM Transactions on Computer Systems*, vol. 7, no. 1, pp. 61–77, 1989.

[7] M. Singhal, "A heuristically-aided algorithm for mutual exclusion for distributed systems," *IEEE Transactions on Computers*, vol. 38, no. 5, pp. 70–78, 1989.

[8] M. Maekawa, "A root N algorithm for mutual exclusion in decentralized systems," *ACM Transactions on Computer Systems*, vol. 3, no. 2, pp. 145–159, 1985.

[9] D. Agrawal and A. El Abbadi, "An efficient solution to the distributed mutual exclusion problem," *ACM Transactions on Computer Systems*, vol. 9, no. 1, pp. 1–20, 1991.

[10] S. Lodha and A. Kshemkalyani, "A fair distributed mutual exclusion algorithm," *IEEE Transactions on Parallel and Distributed Systems*, vol. 11, no. 6, pp. 537–549, 2000.

[11] O. S. F. Carvalho and G. Roucairol, "On mutual exclusion in computer networks," *Communications of the ACM*, vol. 26, no. 2, pp. 146–147, 1983.

[12] A. Goscinski, "Two algorithms for mutual exclusion in real-time distributed computer systems," *Journal of Parallel and Distributed Computing*, vol. 9, no. 1, pp. 77–82, 1990.

[13] Y. Chang, "Design of mutual exclusion algorithms for real-time distributed systems," *Journal of Inforamtion Science and Engineering*, vol. 11, no. 4, pp. 527–548, 1994.

[14] M. Challenger, P. Bayat, and M. R. Meybodi, "A reliable optimization on distributed mutual exclusion algorithm," in *Proceedings of the 2nd International Conference on Testbeds and Research Infrastructures for the Development of Networks and Communities (TRI-DENTCOM '06)*, pp. 566–574, Barcelona, Spain, 2006.

[15] M. Challenger, V. Khalilpour, P. Bayat, and M. R. Meibodi, "A new robust centralized DMX algorithm," in *Proceedings of the IASTED International Conference on Parallel and Distributed Computing and Networks (PDCN '07)*, pp. 367–374, Innsbruck, Austria, February 2007.

[16] A. S. Tanenbaum, *Distributed Operating System, Pearson Education*, 2007.

[17] G. Hosseinabadi and N. H. Vaidya, "Exploiting opportunistic overhearing to improve performance of mutual exclusion in wireless Ad Hoc networks," in *Wired/Wireless Internet Communication*, vol. 7277 of *Lecture Notes in Computer Science*, pp. 162–173, 2012.

[18] P. Chaudhuri and T. Edward, "An $O(\sqrt{n})$ distributed mutual exclusion algorithm using queue migration," *Journal of Universal Computer Science*, vol. 12, no. 2, pp. 140–159, 2006.

[19] F. Mueller, "Prioritized token-based mutual exclusion for distributed systems," in *Proceedings of the 12th International Parallel Processing Symposium and 9th Symposium on Parallel and Distributed Processing*, pp. 791–795, April 1998.

[20] M. L. Neilsen and M. Mizuno, "A dag-based algorithm for distributed mutual exclusion," in *Proceedings of the 11th International Conference on Distributed Computing Systems*, pp. 354–360, May 1991.

[21] M. Naimi and M. Trehel, "A distributed algorithm for mutual exclusion based on data structures and fault tolerance," in *Proceedings of the 6th International Phoenix IEEE International Conference on Computer Communications*, pp. 35–39, Scottsdale, Ariz, USA, 1987.

[22] M. Naimi, M. Trehel, and A. Arnold, "A log (N) distributed mutual exclusion algorithm based on path reversal," *Journal of Parallel and Distributed Computing*, vol. 34, no. 1, pp. 1–13, 1996.

[23] J. Edmondson, D. Schmidt, and A. Gokhale, "QoS-enabled distributed mutual exclusion in public clouds," in *On the Move to Meaningful Internet Systems: OTM*, vol. 7045 of *Lecture Notes in Computer Science*, pp. 542–559, 2011.

[24] M. Chen, W. Cai, and L. Ma, "Cloud computing platform for an online model library system," *Mathematical Problems in Engineering*, vol. 2013, Article ID 369056, 7 pages, 2013.

[25] G. Wen and Z. Duan, "Dynamics behaviors of weighted local-world evolving networks with extended links," *International Journal of Modern Physics C*, vol. 20, no. 11, pp. 1719–1735, 2009.

[26] K. Erciyes, D. Ozsoyeller, and O. Dagdeviren, "Distributed algorithms to form cluster based spanning trees in wireless sensor networks," in *Proceedings of the 8th International Conference of Computational Science (ICCS '08)*, vol. 5101 of *Lecture Notes in Computer Science*, pp. 519–528, Springer, 2008.

[27] Q. Min and R. Zimmermann, "VCA: an energy-efficient voting-based clustering algorithm for sensor networks," *Journal of Universal Computer Science*, vol. 13, no. 1, pp. 87–109, 2007.

[28] F. Chung and L. Lu, "The average distance in a random graph with given expected degrees," *Internet Mathematics*, vol. 1, no. 1, pp. 91–113, 2003.

[29] S. Kanrar and N. Chaki, "Modified Raymond's algorithm for priority (MRA-P) based mutual exclusion in distributed systems," in *Proceedings of the 3rd International Conference on Distributed Computing and Internet Technology (ICDCIT '06)*, pp. 325–332, 2006.

[30] A. Swaroop and A. K. Singh, "A token-based group mutual exclusion algorithm for cellular wireless networks," in *Proceedings of the Annual IEEE India Conference (IN-DICON '09)*, pp. 1–4, 2009.

[31] A. Housni and M. Trehel, "Distributed mutual exclusion token-permission based by prioritized groups," in *Proceedings of the ACS/IEEE International Conference on Computer Systems and Applications*, pp. 253–259, 2001.

Hindawi Publishing Corporation
Mathematical Problems in Engineering
Volume 2013, Article ID 586091, 15 pages
http://dx.doi.org/10.1155/2013/586091

Research Article

Nonfragile Guaranteed Cost Control and Optimization for Interconnected Systems of Neutral Type

Heli Hu,[1] Dan Zhao,[2] and Qingling Zhang[3]

[1] *Key Laboratory of Manufacturing Industrial Integrated Automation, Shenyang University, Shenyang 110044, China*
[2] *Department of Fundamental Teaching, Shenyang Institute of Engineering, Shenyang 110136, China*
[3] *Institute of Systems Science, Northeastern University, Shenyang, Liaoning 110004, China*

Correspondence should be addressed to Heli Hu; huheli2002@yahoo.com.cn

Received 4 April 2013; Accepted 19 June 2013

Academic Editor: Ming Cao

The design and optimization problems of the nonfragile guaranteed cost control are investigated for a class of interconnected systems of neutral type. A novel scheme, viewing the interconnections with time-varying delays as effective information but not disturbances, is developed to decrease the conservatism. Many techniques on decomposing and magnifying the matrices are utilized to obtain the guaranteed cost of the considered system. Also, an algorithm is proposed to solve the nonlinear problem of the interconnected matrices. Based on this algorithm, the minimization of the guaranteed cost of the considered system is obtained by optimization. Further, the state feedback control is extended to the case in which the underlying system is dependent on uncertain parameters. Finally, two numerical examples are given to illustrate the proposed method, and some comparisons are made to show the advantages of the schemes of dealing with the interconnections.

1. Introduction

Time delays often arise in the processing state, input or related variables of dynamic systems. Particularly, when the state derivative also contains time delay, the considered systems are called neutral systems [1]. The outstanding characteristic of neutral systems is the fact that such systems contain the same highest order derivatives for the state vector $x(t)$, at both time t and past time(s) $t_s \leq t$. Many engineering systems can be represented as neutral equation [2–10], such as heat exchangers, robots in contact with rigid environments [11], distributed networks containing lossless transmission lines [12], and population ecology [13]. Therefore, great interest has been devoted to analysis and synthesis of a class of neutral delay systems. The delay-dependent stability criteria for stochastic systems of neutral type are studied in [3, 6]. The difference between them is that the exponential stability problem is investigated in the former, and the robust stochastic stability, stabilization, and H_∞ control problems are considered in the other. Furthermore, the improved stability criteria for neutral systems are established by the method of a memory state feedback control [2] and by the method of a robust H_∞ reduced order filter in [4]. In the context of infinite-dimensional linear systems modeled by neutral functional differential equations, a periodic output feedback is studied in [14] and the stabilization of neutral systems with delayed control is the main work. As the further results, in [15–17], the stability and H_∞ performance analysis, the finite-time H_∞ control, and the reliable stabilization for uncertain switched systems of neutral type are investigated, respectively.

On the other hand, interconnected systems appear in a variety of engineering applications including power systems, large structures and manufacturing systems, and their applications, such as [18–21]. In [18], Mukaidani investigates the stability of a class of nonlinear large-scale systems and proposes a suboptimal guaranteed cost control instead of solving the nonconvex optimization problem. But the time delays are invariant and not involved in the interconnections. Furthermore, the scheme of counteracting the interconnections to simplify the problem may add conservatism in some cases. In [19], Mahmoud and Xia propose a generalized approach to stabilization of systems which are composed of

linear time delay subsystems coupled by linear time-varying interconnections. The decentralized structure of dissipative state-feedback controllers is designed to render the closed-loop interconnected system delay-dependent asymptotically stable with strict dissipativity. However, the optimization problem for the dissipativity β_j is not taken into account. In [20], a decentralized control scheme for a class of linear large-scale interconnected systems with norm-bounded time-varying parameter uncertainties is designed under a class of control failures. It is worth noting that the considered systems do not include any time delay, and the optimization problem for the guaranteed cost $J(x,u)$ is not investigated.

To the best of the authors' knowledge, the nonfragile guaranteed cost control and optimization for neutral interconnected systems have not yet been investigated, which motivates the present study. One contribution of this paper is that a novel scheme, viewing the interconnections with time-varying delays as effective information but not disturbances, is developed to decrease the conservatism. The other contribution lies in the fact that an algorithm is proposed to solve the nonlinear constraint problem caused by the interconnected matrices. In this paper, the designed control is the state feedback control with gain perturbations. Also, the guaranteed cost of the considered system can be obtained by solving the corresponding matrix inequality. Based on the proposed algorithm, the minimization of the guaranteed cost of the considered system can be obtained by optimization. particuraly, the matrix $E_i^{1/2}$ is introduced to denote the square root matrix of symmetric positive semidefinite matrix $E_i \geq 0$, that is, $E_i^{1/2} = V_i H_i^{1/2} V_i^T$ with V_i the eigenvector matrix of E_i satisfying $V_i V_i^T = I$ and H_i the diagonal eigenvalues matrix of E_i.

The remainder of the paper is organized as follows. The nonfragile control problem formulation is described in Section 2. In Section 3, the guaranteed cost control with gain perturbations and optimization are investigated for unperturbed and uncertain neutral interconnected systems. The numerical examples, the simulation results, and some comparisons are presented in Section 4. The conclusion is provided in Section 5.

2. Problem Formulation

Consider the following uncertain neutral interconnected systems composed of N subsystems:

$$\begin{aligned}\dot{x}_i(t) - \sum_{j=1, j\neq i}^{N} A_{ij} x_j\left(t-\tau_{ij}(t)\right) &= \left[A_i + \Delta A_i(t)\right] x_i(t) \\ &\quad + \left[A_{i\sigma_i} + \Delta A_{i\sigma_i}(t)\right] x_i\left(t-\sigma_i(t)\right) \\ &\quad + \left[A_{i\eta_i} + \Delta A_{i\eta_i}(t)\right] \dot{x}_i\left(t-\eta_i(t)\right) \\ &\quad + \left[B_i + \Delta B_i(t)\right] u_i(t) \\ &\quad + \left[B_{i\delta_i} + \Delta B_{i\delta_i}(t)\right] u_i\left(t-\delta_i(t)\right),\end{aligned}$$

$$x_i(t) = \phi_i(t), \quad t \in [-l, 0], \; i = 1, 2, \ldots, N, \tag{1}$$

where $x_i(t) \in \Re^{n_i}$ and $u_i(t) \in \Re^{m_i}$ are the state vector and the input vector of the ith subsystem, respectively. $\sum_{j=1, j\neq i}^{N} A_{ij} x_j(t-\tau_{ij}(t))$ is the interconnections between the ith subsystem and the other $N-1$ subsystems, in which A_{ij} is known interconnected matrices of appropriate dimensions, and $x_j(t-\tau_{ij}(t))$ implies the interconnections between the ith subsystem and the other $N-1$ subsystems have different time-varying delays $\tau_{ij}(t)$, $j = 1, 2, \ldots, N$, $j \neq i$. A_i, $A_{i\sigma_i}$, $A_{i\eta_i}$, B_i, and $B_{i\delta_i}$ are known constant matrices of appropriate dimensions. $\phi_i(t)$ is the initial condition. Assume that there exist constants f_{i0}, g_{i0}, h_{i0}, l_{i0}, f_i, g_i, h_i, l_i, and l satisfying

$$\begin{aligned} &0 \leq \sigma_i(t) \leq f_{i0}, && 0 \leq \eta_i(t) \leq g_{i0}, \\ &0 \leq \delta_i(t) \leq h_{i0}, && 0 \leq \tau_{ij}(t) \leq l_{i0}, \\ &\dot{\sigma}_i(t) \leq f_i < 1, && \dot{\eta}_i(t) \leq g_i < 1, \\ &\dot{\delta}_i(t) \leq h_i < 1, && \dot{\tau}_{ij}(t) \leq l_i < 1, \\ &l = \max\{f_{i0}, g_{i0}, h_{i0}, l_{i0}\}, && i, j = 1, 2 \ldots, N, \; j \neq i. \end{aligned} \tag{2}$$

Time-varying parametric uncertainties $\Delta A_i(t)$, $\Delta A_{i\sigma_i}(t)$, $\Delta A_{i\eta_i}(t)$, $\Delta B_i(t)$, and $\Delta B_{i\delta_i}(t)$ are assumed to be of the following form:

$$\begin{aligned}&\left[\Delta A_i(t) \;\; \Delta A_{i\sigma_i}(t) \;\; \Delta A_{i\eta_i}(t) \;\; \Delta B_i(t) \;\; \Delta B_{i\delta_i}(t)\right] \\ &\quad = C_i F_i(t) \left[D_{i1} \;\; D_{i\sigma_i} \;\; D_{i\eta_i} \;\; D_{i2} \;\; D_{i\delta_i}\right],\end{aligned} \tag{3}$$

where C_i, D_{i1}, $D_{i\sigma_i}$, $D_{i\eta_i}$, D_{i2}, and $D_{i\delta_i}$ are constant matrices of appropriate dimensions, and $F_i(t)$ is the unknown matrix function satisfying $F_i^T(t)F_i(t) \leq I_{n_i}$, for all $t \geq 0$.

Construct the following state feedback control with gain perturbations:

$$u_i(t) = -\left(K_i + \Delta K_i\right) x_i(t), \tag{4}$$

where $K_i \in \Re^{m_i \times n_i}$ is the control gain to be designed, and ΔK_i is a perturbed matrix satisfying $\Delta K_i = M_i \overline{F}_i(t) N_i$, where M_i and N_i are known matrices of appropriate dimensions, and $\overline{F}_i(t)$ satisfies $\overline{F}_i^T(t)\overline{F}_i(t) \leq I_{m_i}$, for all $t \geq 0$; the resulting

closed-loop uncertain neutral interconnected systems are obtained:

$$\begin{aligned}\dot{x}_i(t) - \sum_{j=1,j\neq i}^{N} A_{ij}x_j\left(t-\tau_{ij}(t)\right) &= \left[A_i - B_i\left(K_i+\Delta K_i\right) + \Delta A_i(t)\right.\\ &\quad \left.-\Delta B_i(t)\left(K_i+\Delta K_i\right)\right]x_i(t)\\ &\quad + \left[A_{i\sigma_i} + \Delta A_{i\sigma_i}(t)\right]x_i\left(t-\sigma_i(t)\right)\\ &\quad + \left[A_{i\eta_i} + \Delta A_{i\eta_i}(t)\right]\dot{x}_i\left(t-\eta_i(t)\right)\\ &\quad + \left[-B_{i\delta_i}\left(K_i+\Delta K_i\right) - \Delta B_{i\delta_i}(t)\left(K_i+\Delta K_i\right)\right]\\ &\quad \times x_i\left(t-\delta_i(t)\right).\end{aligned} \tag{5}$$

Define the following quadratic cost function:

$$J = \sum_{i=1}^{N}\int_0^{\infty}\left[x_i^T(t)S_{i1}x_i(t) + u_i^T(t)S_{i2}u_i(t)\right]dt, \tag{6}$$

where $S_{i1} \in \mathfrak{R}^{n_i\times n_i}$ and $S_{i2} \in \mathfrak{R}^{m_i\times m_i}$ are two given symmetric positive definite matrices.

One objective of this paper is to design a control (4) and determine a scalar J_u satisfying the following two conditions:

(a) the closed-loop system (5) is asymptotically stable,

(b) $J \le J_u$.

If the aforementioned control gain K_i and constant J_u exist, control (4) is the decentralized nonfragile guaranteed cost control and J_u is the guaranteed cost for the considered system.

The other is to find out J^*, the minimization of the guaranteed cost J_u.

Lemma 1 (see [8]). *Let Z, X, S, and Y be matrices of appropriate dimensions. Assuming that Z is symmetric and $S^TS \le I$, then $Z + XSY + Y^TS^TX^T < 0$ if and only if there exists a scalar $\varepsilon > 0$ satisfying*

$$\begin{aligned}Z + \varepsilon XX^T + \varepsilon^{-1}Y^TY &= Z + \varepsilon^{-1}(\varepsilon X)(\varepsilon X)^T\\ &\quad + \varepsilon^{-1}Y^TY < 0.\end{aligned} \tag{7}$$

Lemma 2 (see [8]). *For any constant matrix $P > 0$ and differentiable vector function $x_i(t)$ with appropriate dimensions, one has*

$$\begin{aligned}&\left[\int_{t-\sigma_i(t)}^{t}\dot{x}_i(s)\,ds\right]^T P\left[\int_{t-\sigma_i(t)}^{t}\dot{x}_i(s)\,ds\right]\\ &\quad \le f_{i0}\int_{t-\sigma_i(t)}^{t}\dot{x}_i^T(s)P\dot{x}_i(s)\,ds\\ &\quad \le f_{i0}\int_{t-f_{i0}}^{t}\dot{x}_i^T(s)P\dot{x}_i(s)\,ds.\end{aligned} \tag{8}$$

3. Main Result

3.1. Nonfragile Guaranteed Cost Control and Optimization for Unperturbed Neutral Interconnected Systems. For convenience, firstly consider the following unperturbed neutral interconnected systems with time-varying delays:

$$\begin{aligned}\dot{x}_i(t) - \sum_{j=1,j\neq i}^{N} A_{ij}x_j\left(t-\tau_{ij}(t)\right) &= A_ix_i(t) + A_{i\sigma_i}x_i\left(t-\sigma_i(t)\right)\\ &\quad + A_{i\eta_i}\dot{x}_i\left(t-\eta_i(t)\right)\\ &\quad + B_iu_i(t) + B_{i\delta_i}u_i\left(t-\delta_i(t)\right),\\ x_i(t) = \phi_i(t), \quad t\in[-l,0],\ i = 1,2,\ldots,N.\end{aligned} \tag{9}$$

Now a sufficient condition for existence of the decentralized nonfragile guaranteed cost control (4) for unperturbed neutral interconnected systems (9) with cost function (6) is presented in the following results.

Theorem 3. *Assume $\|A_{i\eta_i}\| < 1$. If there exist a positive number ε_{i1}, some symmetric positive definite matrices Q_{ik} $(k = 0,1,2)$, $\overline{W}_{ji}$, W_{ij}, and matrix X_i such that the following inequality holds:*

$$\Gamma_i = \begin{bmatrix}\Gamma_{11}^i & \Gamma_{12}^i & 0 & \Gamma_{14}^i & \Gamma_{15}^i & \Gamma_{16}^i\\ * & \Gamma_{22}^i & 0 & \Gamma_{24}^i & 0 & \Gamma_{26}^i\\ * & * & \Gamma_{33}^i & 0 & 0 & 0\\ * & * & * & \Gamma_{44}^i & 0 & \Gamma_{46}^i\\ * & * & * & * & \Gamma_{55}^i & 0\\ * & * & * & * & * & \Gamma_{66}^i\end{bmatrix} < 0; \tag{10}$$

then control (4) with $K_i = X_iQ_{i0}^{-1}$ is the decentralized nonfragile guaranteed cost control of unperturbed neutral interconnected systems (9) with the following guaranteed cost:

$$\begin{aligned}J_u = \sum_{i=1}^{N}\Bigg[&\phi_i^T(0)Q_{i0}^{-1}\phi_i(0)\\ &+ \int_{-\sigma_i(0)}^{0}\phi_i^T(s)Q_{i0}^{-1}Q_{i1}Q_{i0}^{-1}\phi_i(s)\,ds\\ &+ \frac{1}{1-g_i}\int_{-\eta_i(0)}^{0}\dot{\phi}_i^T(s)\dot{\phi}_i(s)\,ds\\ &+ f_{i0}\int_{-f_{i0}}^{0}(s+f_{i0})\dot{\phi}_i^T(s)\dot{\phi}_i(s)\,ds\\ &+ \int_{-\delta_i(0)}^{0}\phi_i^T(s)Q_{i0}^{-1}Q_{i2}Q_{i0}^{-1}\phi_i(s)\,ds\\ &+ \frac{1}{1-l_i}\sum_{j=1,j\neq i}^{N}\int_{-\tau_{ij}(0)}^{0}\phi_j^T(s)W_{ij}\phi_j(s)\,ds\Bigg],\end{aligned} \tag{11}$$

where

$$\Gamma_{11}^{i} = A_i Q_{i0} + Q_{i0} A_i^T - B_i X_i - X_i^T B_i^T + Q_{i1} + Q_{i2} + E_i,$$

$$\Gamma_{12}^{i} = \left[A_{i\sigma_i} Q_{i0} \quad A_{i\eta_i} \quad 0 \quad -B_{i\delta_i} X_i \right], \qquad \Gamma_{16}^{i} = \left[\varepsilon_{i1} B_i M_i \quad \varepsilon_{i1} B_{i\delta_i} M_i \quad -Q_{i0} N_i^T \quad 0 \right],$$

$$\Gamma_{14}^{i} = \left[Q_{i0} A_i^T - X_i^T B_i^T \quad Q_{i0} \quad -X_i^T \quad Q_{i0} A_i^T E_i^{1/2} \quad -X_i^T B_i^T E_i^{1/2} \quad 0 \quad 0 \quad 0 \right],$$

$$\Gamma_{22}^{i} = \operatorname{diag}\left\{ -(1-f_i) Q_{i1}, -I_{n_i}, -I_{n_i}, -(1-h_i) Q_{i2} \right\},$$

$$\Gamma_{24}^{i} = \begin{bmatrix} Q_{i0} A_{i\sigma_i}^T & 0 & 0 & 0 & 0 & Q_{i0} A_{i\sigma_i}^T E_i^{1/2} & 0 & 0 \\ A_{i\eta_i}^T & 0 & 0 & 0 & 0 & 0 & A_{i\eta_i}^T E_i^{1/2} & 0 \\ 0 & 0 & 0 & 0 & 0 & 0 & 0 & 0 \\ -X_i^T B_{i\delta_i}^T & 0 & 0 & 0 & 0 & 0 & 0 & -X_i^T B_{i\delta_i}^T E_i^{1/2} \end{bmatrix},$$

$$\Gamma_{15}^{i} = \left[\underbrace{Q_{i0} \quad \cdots \quad Q_{i0}}_{N-1} \right], \qquad \Gamma_{26}^{i} = \begin{bmatrix} 0 & 0 & 0 & 0 \\ 0 & 0 & 0 & 0 \\ 0 & 0 & 0 & 0 \\ 0 & 0 & 0 & -Q_{i0} N_i^T \end{bmatrix},$$

$$E_i = \sum_{j=1, j\neq i}^{N} A_{ij} A_{ij}^T, \qquad \Gamma_{33}^{i} = \begin{bmatrix} \Psi_{11}^{i} & \cdots & \Psi_{1\,i-1}^{i} & \Psi_{1\,i+1}^{i} & \cdots & \Psi_{1N}^{i} \\ \vdots & \ddots & \vdots & \vdots & \vdots & \vdots \\ * & * & \Psi_{i-1\,i-1}^{i} & \Psi_{i-1\,i+1}^{i} & \cdots & \Psi_{i-1\,N}^{i} \\ * & * & * & \Psi_{i+1\,i+1}^{i} & \cdots & \Psi_{i+1\,N}^{i} \\ \vdots & \vdots & \vdots & \vdots & \ddots & \vdots \\ * & * & * & * & * & \Psi_{NN}^{i} \end{bmatrix},$$

$$\Gamma_{44}^{i} = \operatorname{diag}\left\{ -e_{i1}^{-1} I_{n_i}, -S_{i1}^{-1}, -S_{i2}^{-1}, -e_{i1}^{-1} I_{n_i}, -e_{i1}^{-1} I_{n_i}, -e_{i1}^{-1} I_{n_i}, -e_{i1}^{-1} I_{n_i}, -e_{i1}^{-1} I_{n_i} \right\},$$

$$\Gamma_{46}^{i} = \begin{bmatrix} \varepsilon_{i1} B_i M_i & \varepsilon_{i1} B_{i\delta_i} M_i & 0 & 0 \\ 0 & 0 & 0 & 0 \\ \varepsilon_{i1} M_i & 0 & 0 & 0 \\ 0 & 0 & 0 & 0 \\ \varepsilon_{i1} E_i^{1/2} B_i M_i & 0 & 0 & 0 \\ 0 & 0 & 0 & 0 \\ 0 & 0 & 0 & 0 \\ 0 & \varepsilon_{i1} E_i^{1/2} B_{i\delta_i} M_i & 0 & 0 \end{bmatrix},$$

$$e_{i1} = \frac{1}{1-g_i} + f_{i0}^2, \qquad e_{i2} = 1 + \frac{5}{1-g_i} + 5 f_{i0}^2,$$

$$\Gamma_{55}^{i} = \operatorname{diag}\left\{ -(1-l_1) \overline{W}_{1\,i}, \ldots, -(1-l_{i-1}) \overline{W}_{i-1\,i}, -(1-l_{i+1}) \overline{W}_{i+1\,i}, \ldots, -(1-l_N) \overline{W}_{Ni} \right\},$$

$$\Gamma_{66}^{i} = \operatorname{diag}\left\{ -\varepsilon_{i1} I_{n_i}, -\varepsilon_{i1} I_{n_i}, -\varepsilon_{i1} I_{n_i}, -\varepsilon_{i1} I_{n_i} \right\},$$

$$\Psi_{11}^{i} = e_{i2} I_{n_1} - W_{i1} + e_{i1} A_{i1}^T A_{i1},$$

$$\Psi_{1\,i-1}^{i} = e_{i1} A_{i1}^T A_{i\,i-1}, \qquad \Psi_{1\,i+1}^{i} = e_{i1} A_{i1}^T A_{i\,i+1},$$

$$\Psi_{1N}^{i} = e_{i1} A_{i1}^T A_{iN}, \qquad \Psi_{i-1\,i-1}^{i} = e_{i2} I_{n_{i-1}} - W_{i\,i-1} + e_{i1} A_{i\,i-1}^T A_{i\,i-1},$$

$$\Psi_{i-1\,i+1}^{i} = e_{i1} A_{i\,i-1}^T A_{i\,i+1}, \qquad \Psi_{i-1\,N}^{i} = e_{i1} A_{i\,i-1}^T A_{iN},$$

$$\Psi_{i+1\,i+1}^{i} = e_{i2} I_{n_{i+1}} - W_{i\,i+1} + e_{i1} A_{i\,i+1}^T A_{i\,i+1},$$

$$\Psi^{i}_{i+1\,N} = e_{i1}A^{T}_{i\,i+1}A_{iN}, \qquad \Psi^{i}_{NN} = e_{i2}I_{n_N} - W_{iN} + e_{i1}A^{T}_{iN}A_{iN},$$
$$\overline{W}_{ji} = W^{-1}_{ji}, \quad i, j = 1, 2 \ldots, N, \;\; j \neq i. \tag{12}$$

Proof. Choose $P_{i0} = Q^{-1}_{i0}$, $P_{i1} = Q^{-1}_{i0}Q_{i1}Q^{-1}_{i0}$, and $P_{i2} = Q^{-1}_{i0}Q_{i2}Q^{-1}_{i0}$, and construct the following Lyapunov functional:

$$\begin{aligned} V(x(t), t) &= \sum_{i=1}^{N} \Bigg[x_i^T(t) P_{i0} x_i(t) \\ &\quad + \int_{t-\sigma_i(t)}^{t} x_i^T(s) P_{i1} x_i(s)\, ds \\ &\quad + \frac{1}{1-g_i} \int_{t-\eta_i(t)}^{t} \dot{x}_i^T(s) \dot{x}_i(s)\, ds \\ &\quad + f_{i0} \int_{t-f_{i0}}^{t} (s - (t - f_{i0})) \dot{x}_i^T(s) \dot{x}_i(s)\, ds \\ &\quad + \int_{t-\delta_i(t)}^{t} x_i^T(s) P_{i2} x_i(s)\, ds \\ &\quad + \frac{1}{1-l_i} \sum_{j=1, j\neq i}^{N} \int_{t-\tau_{ij}(t)}^{t} x_j^T(s) W_{ij} x_j(s)\, ds \Bigg]. \end{aligned} \tag{13}$$

Obviously, $V(x(t), t) > 0$ for all $x_i(t) \neq 0$. Differentiating $V(x(t), t)$ along the trajectories of the unperturbed neutral interconnected systems (9) with control (4) and applying (2) and Lemma 2 yield

$$\begin{aligned} \dot{V}(x(t), t) &\leq \sum_{i=1}^{N} \Bigg\{ x_i^T(t) \left(P_{i0}A_i + A_i^T P_{i0} \right) x_i(t) \\ &\quad + 2x_i^T(t) P_{i0} A_{i\sigma_i} x_i(t - \sigma_i(t)) \\ &\quad + 2x_i^T(t) P_{i0} A_{i\eta_i} \dot{x}_i(t - \eta_i(t)) \\ &\quad - 2x_i^T(t) P_{i0} B_i (K_i + \Delta K_i) x_i(t) \\ &\quad - 2x_i^T(t) P_{i0} B_{i\delta_i} (K_i + \Delta K_i) \\ &\quad \times x_i(t - \delta_i(t)) + 2x_i^T(t) P_{i0} \\ &\quad \times \sum_{j=1, j\neq i}^{N} A_{ij} x_j(t - \tau_{ij}(t)) \\ &\quad + x_i^T(t) P_{i1} x_i(t) - (1 - f_i) x_i^T \\ &\quad \times (t - \sigma_i(t)) P_{i1} x_i(t - \sigma_i(t)) \\ &\quad + \left(\frac{1}{1-g_i} + f_{i0}^2 \right) \\ &\quad \times \Bigg[x_i^T(t) A_i^T + x_i^T(t - \sigma_i(t)) A_{i\sigma_i}^T \\ &\quad + \dot{x}_i^T(t - \eta_i(t)) A_{i\eta_i}^T \\ &\quad - x_i^T(t) (K_i + \Delta K_i)^T B_i^T - x_i^T \\ &\quad \times (t - \delta_i(t)) (K_i + \Delta K_i)^T B_{i\delta_i}^T \\ &\quad + \sum_{j=1, j\neq i}^{N} x_j^T(t - \tau_{ij}(t)) A_{ij}^T \Bigg] \\ &\quad \times \Bigg[A_i x_i(t) + A_{i\sigma_i} x_i(t - \sigma_i(t)) \\ &\quad + A_{i\eta_i} \dot{x}_i(t - \eta_i(t)) \\ &\quad - B_i (K_i + \Delta K_i) x_i(t) \\ &\quad - B_{i\delta_i} (K_i + \Delta K_i) x_i(t - \delta_i(t)) \\ &\quad + \sum_{j=1, j\neq i}^{N} A_{ij} x_j(t - \tau_{ij}(t)) \Bigg] \\ &\quad - \dot{x}_i^T(t - \eta_i(t)) \dot{x}_i(t - \eta_i(t)) \\ &\quad - \left[\int_{t-\sigma_i(t)}^{t} \dot{x}_i(s) ds \right]^T \left[\int_{t-\sigma_i(t)}^{t} \dot{x}_i(s)\, ds \right] \\ &\quad + x_i^T(t) P_{i2} x_i(t) - (1 - h_i) x_i^T \\ &\quad \times (t - \delta_i(t)) P_{i2} x_i(t - \delta_i(t)) \\ &\quad + \frac{1}{1-l_i} \sum_{j=1, j\neq i}^{N} x_j^T(t) W_{ij} x_j(t) \\ &\quad - \sum_{j=1, j\neq i}^{N} x_j^T(t - \tau_{ij}(t)) W_{ij} x_j(t - \tau_{ij}(t)) \Bigg\}. \end{aligned} \tag{14}$$

According to Lemma 1 and the following the fact:

$$\sum_{i=1}^{N}\frac{1}{1-l_i}\sum_{j=1,j\neq i}^{N}x_j^T(t)W_{ij}x_j(t) = \sum_{i=1}^{N}x_i^T(t)\sum_{j=1,j\neq i}^{N}\frac{1}{1-l_j}W_{ji}x_i(t), \tag{15}$$

one can obtain

$$\begin{aligned}
&\sum_{i=1}^{N}\Bigg\{2x_i^T(t)P_{i0}\sum_{j=1,j\neq i}^{N}A_{ij}x_j\left(t-\tau_{ij}(t)\right)+2e_{i1}\\
&\quad\times\Big[x_i^T(t)A_i^T+x_i^T(t-\sigma_i(t))A_{i\sigma_i}^T\\
&\qquad+\dot{x}_i^T(t-\eta_i(t))A_{i\eta_i}^T-x_i^T(t)\\
&\qquad\times(K_i+\Delta K_i)^TB_i^T-x_i^T(t-\delta_i(t))\\
&\qquad\times(K_i+\Delta K_i)^TB_{i\delta_i}^T\Big]\\
&\quad\times\sum_{j=1,j\neq i}^{N}A_{ij}x_j\left(t-\tau_{ij}(t)\right)+e_{i1}\\
&\quad\times\sum_{j=1,j\neq i}^{N}x_j^T\left(t-\tau_{ij}(t)\right)A_{ij}^T\\
&\quad\times\sum_{j=1,j\neq i}^{N}A_{ij}x_j\left(t-\tau_{ij}(t)\right)\\
&\quad+\frac{1}{1-l_i}\sum_{j=1,j\neq i}^{N}x_j^T(t)W_{ij}x_j(t)\\
&\quad-\sum_{j=1,j\neq i}^{N}x_j^T\left(t-\tau_{ij}(t)\right)\\
&\quad\times W_{ij}x_j\left(t-\tau_{ij}(t)\right)\Bigg\}\\
&\le\sum_{i=1}^{N}\Bigg\{x_i^T(t)\Bigg[P_{i0}E_iP_{i0}+e_{i1}A_i^TE_iA_i\\
&\qquad+e_{i1}(K_i+\Delta K_i)^T\\
&\qquad\times B_i^TE_iB_i(K_i+\Delta K_i)\\
&\qquad+\sum_{j=1,j\neq i}^{N}\frac{1}{1-l_j}W_{ji}\Bigg]\\
&\quad\times x_i(t)+e_{i1}x_i^T(t-\sigma_i(t))\\
&\quad\times A_{i\sigma_i}^TE_iA_{i\sigma_i}x_i(t-\sigma_i(t))\\
&\quad+e_{i1}x_i^T(t-\delta_i(t))(K_i+\Delta K_i)^T\\
&\quad\times B_{i\delta_i}^TE_iB_{i\delta_i}(K_i+\Delta K_i)x_i(t-\delta_i(t))\\
&\quad+e_{i1}\dot{x}_i^T(t-\eta_i(t))A_{i\eta_i}^TE_iA_{i\eta_i}\dot{x}_i(t-\eta_i(t))\\
&\quad+\sum_{j=1,j\neq i}^{N}x_j^T\left(t-\tau_{ij}(t)\right)\\
&\quad\times\left(e_{i2}I-W_{ij}\right)x_j\left(t-\tau_{ij}(t)\right)+e_{i1}\\
&\quad\times\sum_{j=1,j\neq i}^{N}x_j^T\left(t-\tau_{ij}(t)\right)A_{ij}^T\\
&\quad\times\sum_{j=1,j\neq i}^{N}A_{ij}x_j\left(t-\tau_{ij}(t)\right)\Bigg\}.
\end{aligned}\tag{16}$$

Therefore, it follows from (14) and (16) that

$$\begin{aligned}
&\dot{V}(x(t),t)+\sum_{i=1}^{N}\Big[x_i^T(t)S_{i1}x_i(t)+x_i^T(t)(K_i+\Delta K_i)^T\\
&\qquad\times S_{i2}(K_i+\Delta K_i)x_i(t)\Big]\\
&\le\sum_{i=1}^{N}\xi_i^T\Upsilon_i\xi_i,
\end{aligned}\tag{17}$$

where

$$\begin{aligned}
\xi_i^T=\Big[&\ x_i^T(t)\ \ x_i^T(t-\sigma_i(t))\ \ \dot{x}_i^T(t-\eta_i(t))\ \ \textstyle\int_{t-\sigma_i(t)}^{t}\dot{x}_i^T(s)\,ds\ \ x_i^T(t-\delta_i(t))\ \ x_1^T(t-\tau_{i1}(t))\\
&\cdots\ x_{i-1}^T(t-\tau_{i\,i-1}(t))\ \ x_{i+1}^T(t-\tau_{i\,i+1}(t))\ \cdots\ x_N^T(t-\tau_{iN}(t))\Big],
\end{aligned}$$

$$\Upsilon_i=\begin{bmatrix}\Omega_i & 0\\ * & \Gamma_{33}^i\end{bmatrix}+\begin{bmatrix}G_{i1}\\0\end{bmatrix}(e_{i1}I_{n_i})\begin{bmatrix}G_{i1}^T & 0\end{bmatrix}+\begin{bmatrix}G_{i2}\\0\end{bmatrix}S_{i1}\begin{bmatrix}G_{i2}^T & 0\end{bmatrix}+\begin{bmatrix}G_{i3}\\0\end{bmatrix}S_{i2}\begin{bmatrix}G_{i3}^T & 0\end{bmatrix},$$

$$\Omega_i = \begin{bmatrix} \Omega_{11}^i & \Omega_{12}^i & \Omega_{13}^i & 0 & \Omega_{15}^i \\ * & \Omega_{22}^i & 0 & 0 & 0 \\ * & * & \Omega_{33}^i & 0 & 0 \\ * & * & * & \Omega_{44}^i & 0 \\ * & * & * & * & \Omega_{55}^i \end{bmatrix},$$

$$\Omega_{12}^i = P_{i0}A_{i\sigma_i}, \qquad \Omega_{13}^i = P_{i0}A_{i\eta_i}, \qquad \Omega_{44}^i = -I_{n_i},$$

$$\begin{aligned} \Omega_{11}^i = {} & P_{i0}A_i + A_i^T P_{i0} - P_{i0}B_i\left(K_i + \Delta K_i\right) - \left(K_i + \Delta K_i\right)^T B_i^T P_{i0} + P_{i1} + P_{i2} \\ & + P_{i0}E_iP_{i0} + e_{i1}A_i^T E_i A_i + e_{i1}\left(K_i + \Delta K_i\right)^T B_i^T E_i B_i\left(K_i + \Delta K_i\right) \\ & + \sum_{j=1, j\neq i}^{N} \frac{1}{1-l_j} W_{ji}, \end{aligned}$$

$$\Omega_{15}^i = -P_{i0}B_{i\delta_i}\left(K_i + \Delta K_i\right), \qquad \Omega_{22}^i = -\left(1 - f_i\right)P_{i1} + e_{i1}A_{i\sigma_i}^T E_i A_{i\sigma_i},$$

$$\Omega_{33}^i = -I_{n_i} + e_{i1}A_{i\eta_i}^T E_i A_{i\eta_i},$$

$$\Omega_{55}^i = -\left(1 - h_i\right)P_{i2} + e_{i1}\left(K_i + \Delta K_i\right)^T B_{i\delta_i}^T E_i B_{i\delta_i}\left(K_i + \Delta K_i\right),$$

$$G_{i1} = \left[A_i - B_i(K_i + \Delta K_i) \quad A_{i\sigma_i} \quad A_{i\eta_i} \quad 0 \quad -B_{i\delta_i}(K_i + \Delta K_i)\right]^T,$$

$$G_{i2} = \left[I_{n_i} \quad 0 \quad 0 \quad 0 \quad 0\right]^T,$$

$$G_{i3} = \left[-(K_i + \Delta K_i) \quad 0 \quad 0 \quad 0 \quad 0\right]^T. \tag{18}$$

Define

$$\overline{\Upsilon}_i = \begin{bmatrix} \Omega_i & 0 & \overline{\Upsilon}_{13}^i \\ * & \Gamma_{33}^i & 0 \\ * & * & \overline{\Upsilon}_{33}^i \end{bmatrix}, \tag{19}$$

where $\overline{\Upsilon}_{13}^i = [G_{i1} \quad G_{i2} \quad G_{i3}]$, $\overline{\Upsilon}_{33}^i = \mathrm{diag}\{-e_{i1}^{-1}I_{n_i}, -S_{i1}^{-1}, -S_{i2}^{-1}\}$.

Pre- and postmultiplying the matrix $\overline{\Upsilon}_i$ in (19) by U_i^T and U_i, where $U_i = \mathrm{diag}\{Q_{i0}, Q_{i0}, I_{n_i}, I_{n_i}, Q_{i0}, I_{n_1}, \ldots, I_{n_{i-1}}, I_{n_{i+1}}, \ldots, I_{n_N}, I_{n_i}, I_{n_i}, I_{m_i}\}$, the following matrix is obtained:

$$\overline{\overline{\Upsilon}}_i = \begin{bmatrix} \overline{\Omega}_i & 0 & \overline{\overline{\Upsilon}}_{13}^i \\ * & \Gamma_{33}^i & 0 \\ * & * & \overline{\Upsilon}_{33}^i \end{bmatrix}, \tag{20}$$

where

$$\overline{\Omega}_i = \begin{bmatrix} \overline{\Omega}_{11}^i & \overline{\Omega}_{12}^i & \overline{\Omega}_{13}^i & 0 & \overline{\Omega}_{15}^i \\ * & \overline{\Omega}_{22}^i & 0 & 0 & 0 \\ * & * & \Omega_{33}^i & 0 & 0 \\ * & * & * & \Omega_{44}^i & 0 \\ * & * & * & * & \overline{\Omega}_{55}^i \end{bmatrix},$$

$$\overline{\Omega}_{12}^i = A_{i\sigma_i}Q_{i0}, \qquad \overline{\Omega}_{13}^i = A_{i\eta_i},$$

$$\begin{aligned} \overline{\Omega}_{11}^i = {} & A_iQ_{i0} + Q_{i0}A_i^T - B_i\left(K_i + \Delta K_i\right)Q_{i0} \\ & - Q_{i0}\left(K_i + \Delta K_i\right)^T B_i^T + Q_{i1} + Q_{i2} \\ & + E_i + e_{i1}Q_{i0}A_i^T E_i A_i Q_{i0} + e_{i1}Q_{i0} \\ & \times \left(K_i + \Delta K_i\right)^T B_i^T E_i B_i\left(K_i + \Delta K_i\right)Q_{i0} \\ & + Q_{i0}\sum_{j=1, j\neq i}^{N} \frac{1}{1-l_j} W_{ji}Q_{i0}, \end{aligned}$$

$$\overline{\Omega}_{15}^i = -B_{i\delta_i}\left(K_i + \Delta K_i\right)Q_{i0},$$

$$\overline{\Omega}_{22}^i = -\left(1 - f_i\right)Q_{i1} + e_{i1}Q_{i0}A_{i\sigma_i}^T E_i A_{i\sigma_i}Q_{i0},$$

$$\overline{\overline{\Omega}}_{55}^{i} = -(1-h_i)Q_{i2} + e_{i1}Q_{i0} \times (K_i+\Delta K_i)^T B_{i\delta_i}^T E_i B_{i\delta_i}(K_i+\Delta K_i)Q_{i0},$$

$$\overline{\overline{\Upsilon}}_{13}^{i} = \begin{bmatrix} Q_{i0}A_i^T - Q_{i0}(K_i+\Delta K_i)^T B_i^T & Q_{i0} & -Q_{i0}(K_i+\Delta K_i)^T \\ Q_{i0}A_{i\sigma_i}^T & 0 & 0 \\ A_{i\eta_i}^T & 0 & 0 \\ 0 & 0 & 0 \\ -Q_{i0}(K_i+\Delta K_i)^T B_{i\delta_i}^T & 0 & 0 \end{bmatrix}. \tag{21}$$

Define

$$\Theta_i = \begin{bmatrix} \overline{\overline{\Omega}}_i & 0 & \overline{\overline{\Upsilon}}_{13}^{i} & \Xi_i & \Theta_{15}^{i} \\ * & \Gamma_{33}^{i} & 0 & 0 & 0 \\ * & * & \overline{\Upsilon}_{33}^{i} & 0 & 0 \\ * & * & * & \Theta_{44}^{i} & 0 \\ * & * & * & * & \Theta_{55}^{i} \end{bmatrix}, \tag{22}$$

where

$$\overline{\overline{\Omega}}_i = \begin{bmatrix} \overline{\overline{\Omega}}_{11}^{i} & \overline{\Omega}_{12}^{i} & \overline{\Omega}_{13}^{i} & 0 & \overline{\Omega}_{15}^{i} \\ * & \overline{\overline{\Omega}}_{22}^{i} & 0 & 0 & 0 \\ * & * & \overline{\overline{\Omega}}_{33}^{i} & 0 & 0 \\ * & * & * & \Omega_{44}^{i} & 0 \\ * & * & * & * & \overline{\overline{\Omega}}_{55}^{i} \end{bmatrix},$$

$$\Xi_i = \begin{bmatrix} \Xi_{11}^{i} & \Xi_{12}^{i} & 0 & 0 & 0 \\ 0 & 0 & \Xi_{23}^{i} & 0 & 0 \\ 0 & 0 & 0 & \Xi_{34}^{i} & 0 \\ 0 & 0 & 0 & 0 & 0 \\ 0 & 0 & 0 & 0 & \Xi_{55}^{i} \end{bmatrix},$$

$$\Theta_{15}^{i} = \begin{bmatrix} \Gamma_{15}^{i} \\ 0 \\ 0 \\ 0 \\ 0 \end{bmatrix},$$

$$\Theta_{44}^{i} = \operatorname{diag}\left\{-e_{i1}^{-1}I_{n_i}, -e_{i1}^{-1}I_{n_i}, -e_{i1}^{-1}I_{n_i}, -e_{i1}^{-1}I_{n_i}, -e_{i1}^{-1}I_{n_i}\right\},$$

$$\Theta_{55}^{i} = \Gamma_{55}^{i},$$

$$\overline{\overline{\Omega}}_{11}^{i} = A_iQ_{i0} + Q_{i0}A_i^T - B_i(K_i+\Delta K_i)Q_{i0} - Q_{i0}(K_i+\Delta K_i)^T B_i^T + Q_{i1} + Q_{i2} + E_i,$$

$$\overline{\overline{\Omega}}_{22}^{i} = -(1-f_i)Q_{i1}, \qquad \overline{\overline{\Omega}}_{33}^{i} = -I_{n_i},$$

$$\overline{\overline{\Omega}}_{55}^{i} = -(1-h_i)Q_{i2}, \qquad \Xi_{11}^{i} = Q_{i0}A_i^T E_i^{1/2},$$

$$\Xi_{12}^{i} = -Q_{i0}(K_i+\Delta K_i)^T B_i^T E_i^{1/2},$$

$$\Xi_{23}^{i} = Q_{i0}A_{i\sigma_i}^T E_i^{1/2}, \qquad \Xi_{34}^{i} = A_{i\eta_i}^T E_i^{1/2},$$

$$\Xi_{55}^{i} = -Q_{i0}(K_i+\Delta K_i)^T B_{i\delta_i}^T E_i^{1/2}. \tag{23}$$

The following equality is obvious:

$$\Theta_i = \begin{bmatrix} \Gamma_{11}^{i} & \Gamma_{12}^{i} & 0 & \Gamma_{14}^{i} & \Gamma_{15}^{i} \\ * & \Gamma_{22}^{i} & 0 & \Gamma_{24}^{i} & 0 \\ * & * & \Gamma_{33}^{i} & 0 & 0 \\ * & * & * & \Gamma_{44}^{i} & 0 \\ * & * & * & * & \Gamma_{55}^{i} \end{bmatrix} + \Lambda_i^T R_{i1} \$_i + \$_i^T R_{i1}^T \Lambda_i, \tag{24}$$

where

$$\Lambda_i = \begin{bmatrix} M_i^T B_i^T & 0 & 0 & \Lambda_{14}^{i} & 0 \\ M_i^T B_{i\delta_i}^T & 0 & 0 & \Lambda_{24}^{i} & 0 \end{bmatrix},$$

$$\$_i = \begin{bmatrix} -N_iQ_{i0} & 0 & 0 & 0 & 0 \\ 0 & \$_{22}^{i} & 0 & 0 & 0 \end{bmatrix},$$

$$R_{i1} = \operatorname{diag}\left\{\overline{F}_i(t), \overline{F}_i(t)\right\}, \tag{25}$$

$$\Lambda_{14}^{i} = \begin{bmatrix} M_i^T B_i^T & 0 & M_i^T & 0 & M_i^T B_i^T E_i^{1/2} & 0 & 0 & 0 \end{bmatrix},$$

$$\Lambda_{24}^{i} = \begin{bmatrix} M_i^T & B_{i\delta_i}^T & 0 & 0 & 0 & 0 & 0 & 0 & M_i^T B_{i\delta_i}^T E_i^{1/2} \end{bmatrix},$$

$$\$_{22}^{i} = \begin{bmatrix} 0 & 0 & 0 & -N_iQ_{i0} \end{bmatrix}.$$

By Lemma 1 and Schur complement formula, the condition $\Gamma_i < 0$ in (10) is equivalent to $\Theta_i < 0$ in (24). By Schur complement formula with $\Theta_i < 0$, one can obtain $\overline{\overline{\Upsilon}}_i < 0$ in (20). The condition $\overline{\overline{\Upsilon}}_{ii} < 0$ is equivalent to $\overline{\Upsilon}_i < 0$. Again, by Schur complement formula with $\overline{\Upsilon}_i < 0$, one can obtain $\Upsilon_i < 0$. From the condition $\Upsilon_i < 0$ in (17), there exists a constant $\rho_i > 0$, such that

$$\dot{V}(x(t), t) \le \sum_{i=1}^{N} -\rho_i \|x_i(t)\|^2. \tag{26}$$

By conditions (13) and (26) and $\|A_{i\eta_i}\| < 1$, one can conclude that system (9) with (2) and (4) is asymptotically stable. From (17) with $\Upsilon_i < 0$, one can obtain

$$\begin{aligned}\int_0^\infty \dot{V}(x(t),t)\,dt &= \lim_{t\to\infty} V(x(t),t) - V(x(0),0) \\ &\le -\sum_{i=1}^N \int_0^\infty \left[x_i^T(t) S_{i1} x_i(t) + u_i^T(t) S_{i2} u_i(t)\right] dt.\end{aligned} \tag{27}$$

Therefore, the following equalities hold:

$$\begin{aligned}&\lim_{t\to\infty} V(x(t),t) = 0, \\ &\sum_{i=1}^N \int_0^\infty \left[x_i^T(t) S_{i1} x_i(t) + u_i^T(t) S_{i2} u_i(t)\right] dt \\ &\qquad \le V(x(0),0) = J_u.\end{aligned} \tag{28}$$

This completes the proof. □

Remark 4. It is obvious that for every subsystem, the corresponding Γ_i in (10) is an LMI with obtained matrices $\overline{W}_{ji}$ ($\overline{W}_{ji} = W_{ji}^{-1}$) and W_{ij} in the last inequality (i.e., the inequality $\Gamma_{i-1} < 0$). Hence, the decentralized nonfragile control (4) and the guaranteed cost J_u in (11) can be obtained by finding feasible set to $\Gamma_i < 0$ with *feasp* in [22] one by one.

Remark 5. Obviously, the guaranteed cost J_u in (11) cannot be directly optimized by using the toolbox of *mincx* in [22]. One reason is that inequalities (10) with variable matrices W_{ij} and $\overline{W}_{ji}$ ($\overline{W}_{ji} = W_{ji}^{-1}$) are not a group of LMIs but N coupled nonlinear inequalities. Another reason is that J_u is a nonconvex function with respect to the optimization variables.

The following algorithm is given to solve the nonlinear problem of inequalities (10).

Algorithm 6. Choose constant matrices $W_{ij} > 0$ and $\overline{W}_{ji} > 0$ satisfying $\Psi_{jj}^i < 0$ in Γ_i, where $\overline{W}_{ji} = W_{ji}^{-1}$, $i, j = 1, 2 \ldots, N$, $j \ne i$.

It is needed to simultaneously select $N \times (N-1)$ constant matrices $W_{ij} > 0$ and $\overline{W}_{ji} > 0$ ($\overline{W}_{ji} = W_{ji}^{-1}$) satisfying $\Psi_{jj}^i < 0$. For simplicity, one can choose W_{ij} and $\overline{W}_{ji}$ to be positive definite diagonal matrices according to the eigenvalues of $e_{i2} I_{n_j} + e_{i1} A_{ij}^T A_{ij}$ due to $\Psi_{jj}^i = e_{i2} I_{n_j} - W_{ij} + e_{i1} A_{ij}^T A_{ij}$. The chosen entries need to be as small as possible, because

$$\frac{1}{1-l_i} \sum_{j=1, j\ne i}^N \int_{-\tau_{ij}(0)}^0 x_j^T(s) W_{ij} x_j(s)\,ds \tag{29}$$

is involved in J_u. However, if there is no solution to inequalities (10), the large scalars can be considered.

In the sequel, instead of solving the nonconvex optimization problem, a suboptimal method of minimizing the guaranteed cost J_u, based on Algorithm 6, is presented.

Theorem 7. *Consider unperturbed system* (9) *with cost function* (6)*, and assume* $\|A_{i\eta_i}\| < 1$. *If the following optimization problem:*

$$\min \sum_{i=1}^N \left[\alpha_i + \operatorname{Tr}\left(U_{i1}^T \Phi_{i1} U_{i1} + U_{i2}^T \Phi_{i2} U_{i2}\right)\right] \tag{30}$$

subject to LMI (10) *with Algorithm 6, and*

$$\begin{aligned}&\begin{bmatrix} -\alpha_i & \phi_i^T(0) \\ * & -Q_{i0} \end{bmatrix} < 0, \\ &\begin{bmatrix} -2Q_{i0} + Q_{i1} & I_{n_i} \\ * & -\Phi_{i1} \end{bmatrix} < 0, \\ &\begin{bmatrix} -2Q_{i0} + Q_{i2} & I_{n_i} \\ * & -\Phi_{i2} \end{bmatrix} < 0\end{aligned} \tag{31}$$

has a solution set ($\alpha_i > 0, \varepsilon_{i1} > 0, Q_{ik} > 0$ $(k = 0, 1, 2), \Phi_{i1} > 0, \Phi_{i2} > 0, X_i$), *where* $\int_{-\sigma_i(0)}^0 \phi_i(s)\phi_i^T(s)ds = U_{i1}U_{i1}^T$, $\int_{-\delta_i(0)}^0 \phi_i(s)\phi_i^T(s)ds = U_{i2}U_{i2}^T$, $(1/(1-g_i)) \int_{-\eta_i(0)}^0 \dot{\phi}_i^T(s)\dot{\phi}_i(s)ds = L_{i1}$, $f_{i0} \int_{-f_{i0}}^0 (s + f_{i0})\dot{\phi}_i^T(s)\dot{\phi}_i(s)ds = L_{i2}$, $(1/(1-l_i)) \sum_{j=1, j\ne i}^N \int_{-\tau_{ij}(0)}^0 \phi_j^T(s) W_{ij} \phi_j(s)ds = L_{i3}$, *then control* (4) *with* $K_i = X_i Q_{i0}^{-1}$ *is the decentralized nonfragile guaranteed cost control of unperturbed system* (9) *with the minimization of the guaranteed cost* J_u *as follows:*

$$\begin{aligned}J^* = \min &\left(\sum_{i=1}^N \left[\alpha_i + \operatorname{Tr}\left(U_{i1}^T \Phi_{i1} U_{i1} + U_{i2}^T \Phi_{i2} U_{i2}\right)\right]\right) \\ &+ \sum_{i=1}^N \left(L_{i1} + L_{i2} + L_{i3}\right).\end{aligned} \tag{32}$$

Proof. Applying the Schur complement formula to LMIs (31) leads to $\phi_i^T(0) Q_{i0}^{-1} \phi_i(0) < \alpha_i$, $-2Q_{i0} + Q_{i1} + \Phi_{i1}^{-1} < 0$, $-2Q_{i0} + Q_{i2} + \Phi_{i2}^{-1} < 0$, respectively.

Noting that [8]

$$\begin{aligned}\left[Q_{i0} - \Phi_{i1}^{-1}\right] \Phi_{i1} \left[Q_{i0} - \Phi_{i1}^{-1}\right] &= Q_{i0}\Phi_{i1}Q_{i0} - 2Q_{i0} + \Phi_{i1}^{-1} \ge 0, \\ \left[Q_{i0} - \Phi_{i2}^{-1}\right] \Phi_{i2} \left[Q_{i0} - \Phi_{i2}^{-1}\right] &= Q_{i0}\Phi_{i2}Q_{i0} - 2Q_{i0} + \Phi_{i2}^{-1} \ge 0,\end{aligned} \tag{33}$$

the following inequalities are obtained

$$\begin{aligned}P_{i1} &= Q_{i0}^{-1} Q_{i1} Q_{i0}^{-1} < \Phi_{i1}, \\ P_{i2} &= Q_{i0}^{-1} Q_{i2} Q_{i0}^{-1} < \Phi_{i2}.\end{aligned} \tag{34}$$

Further, one can obtain

$$\begin{aligned}
&\int_{-\sigma_i(0)}^{0} \phi_i^T(s) P_{i1} \phi_i(s)\, ds \\
&\quad = \operatorname{Tr}\left(\int_{-\sigma_i(0)}^{0} \phi_i(s) \phi_i^T(s) P_{i1}\right) ds \\
&\quad = \operatorname{Tr}\left(U_{i1}^T P_{i1} U_{i1}\right) \le \operatorname{Tr}\left(U_{i1}^T \Phi_{i1} U_{i1}\right), \\
&\int_{-\delta_i(0)}^{0} \phi_i^T(s) P_{i2} \phi_i(s)\, ds \\
&\quad = \operatorname{Tr}\left(\int_{-\delta_i(0)}^{0} \phi_i(s) \phi_i^T(s) P_{i2}\right) ds \\
&\quad = \operatorname{Tr}\left(U_{i2}^T P_{i2} U_{i2}\right) \le \operatorname{Tr}\left(U_{i2}^T \Phi_{i2} U_{i2}\right), \\
&\frac{1}{1-g_i} \int_{-\eta_i(0)}^{0} \dot{\phi}_i^T(s) \dot{\phi}_i(s)\, ds = L_{i1}, \\
&f_{i0} \int_{-f_{i0}}^{0} (s + f_{i0}) \dot{\phi}_i^T(s) \dot{\phi}_i(s)\, ds = L_{i2}, \\
&\frac{1}{1-l_i} \sum_{j=1, j\ne i}^{N} \int_{-\tau_{ij}(0)}^{0} \phi_j^T(s) W_{ij} \phi_j(s)\, ds = L_{i3}.
\end{aligned} \tag{35}$$

Therefore, it follows from (11) that

$$\begin{aligned}
J_u \le &\sum_{i=1}^{N} \left[\alpha_i + \operatorname{Tr}\left(U_{i1}^T \Phi_{i1} U_{i1} + U_{i2}^T \Phi_{i2} U_{i2}\right)\right] \\
&+ \sum_{i=1}^{N} \left(L_{i1} + L_{i2} + L_{i3}\right).
\end{aligned} \tag{36}$$

The minimization of the right hand of inequality (36) implies the minimization of the guaranteed cost J_u for unperturbed system (9). This completes the proof. □

3.2. Nonfragile Guaranteed Cost Control for Uncertain Neutral Interconnected Systems

Theorem 8. *Consider uncertain neutral interconnected systems* (1) *with* (2), (3), *and* (4). *If there exist positive numbers* $\varepsilon_{i1} > 0$, $\varepsilon_{i2} > 0$, *and* $\varepsilon_{i3} > 0$, *some symmetric positive definite matrices* Q_{ik} $(k = 0, 1, 2)$, $\overline{W}_{ji}$, W_{ij}, *and matrix* X_i *such that the following inequalities hold:*

$$\overline{\overline{\Gamma}}_i = \begin{bmatrix} \Gamma_i & \overline{\Gamma}_i \\ * & \widetilde{\Gamma}_i \end{bmatrix} < 0, \tag{37}$$

$$\begin{bmatrix} -I_{n_i} + \varepsilon_{i3} D_{i\eta_i}^T D_{i\eta_i} & A_{i\eta_i}^T & 0 \\ * & -I_{n_i} & C_i \\ * & * & -\varepsilon_{i3} I_{n_i} \end{bmatrix} < 0, \tag{38}$$

then control (4) *with* $K_i = X_i Q_{i0}^{-1}$ *is the decentralized nonfragile guaranteed cost control of uncertain neutral interconnected systems* (1) *with the guaranteed cost in* (11), *where* $\overline{\Gamma}_i = [\varepsilon_{i2}\Pi_{i1} \;\; \Pi_{i2}]$,

$$\Pi_{i1} = \begin{bmatrix} \overline{\Gamma}_{11}^i \\ 0 \\ 0 \\ \overline{\Gamma}_{41}^i \\ 0 \\ 0 \end{bmatrix}, \qquad \Pi_{i2} = \begin{bmatrix} \overline{\Gamma}_{12}^i \\ \overline{\Gamma}_{22}^i \\ 0 \\ 0 \\ 0 \\ \overline{\Gamma}_{62}^i \end{bmatrix},$$

$$\overline{\Gamma}_{22}^i = \begin{bmatrix} 0 & 0 & Q_{i0} D_{i\sigma_i}^T & 0 & 0 & 0 \\ 0 & 0 & 0 & D_{i\eta_i}^T & 0 & 0 \\ 0 & 0 & 0 & 0 & 0 & 0 \\ 0 & 0 & 0 & 0 & -X_i^T D_{i\delta_i}^T & 0 \end{bmatrix},$$

$$\overline{\Gamma}_{11}^i = [C_i \;\; C_i \;\; C_i \;\; C_i \;\; C_i \;\; C_i],$$

$$\overline{\Gamma}_{12}^i = \left[Q_{i0} D_{i1}^T \;\; -X_i^T D_{i2}^T \;\; 0 \;\; 0 \;\; 0 \;\; 0\right],$$

$$\overline{\Gamma}_{41}^i = \begin{bmatrix} C_i & C_i & C_i & C_i & C_i & C_i \\ 0 & 0 & 0 & 0 & 0 & 0 \\ 0 & 0 & 0 & 0 & 0 & 0 \\ E_i^{1/2} C_i & 0 & 0 & 0 & 0 & 0 \\ 0 & E_i^{1/2} C_i & 0 & 0 & 0 & E_i^{1/2} C_i \\ 0 & 0 & E_i^{1/2} C_i & 0 & 0 & 0 \\ 0 & 0 & 0 & E_i^{1/2} C_i & 0 & 0 \\ 0 & 0 & 0 & 0 & E_i^{1/2} C_i & 0 \end{bmatrix},$$

$$\overline{\Gamma}_{62}^i = \begin{bmatrix} 0 & 0 & 0 & 0 & 0 & \varepsilon_{i1} M_i^T D_{i2}^T \\ 0 & 0 & 0 & 0 & \varepsilon_{i1} M_i^T D_{i\delta_i}^T & 0 \\ 0 & 0 & 0 & 0 & 0 & 0 \\ 0 & 0 & 0 & 0 & 0 & 0 \end{bmatrix},$$

$$\widetilde{\Gamma}_i = \operatorname{diag}\left\{\underbrace{-\varepsilon_{i2} I_{n_i}, \ldots, -\varepsilon_{i2} I_{n_i}}_{12}\right\}. \tag{39}$$

Proof. From condition (10) with unperturbed neutral interconnected systems (9), one can obtain the corresponding condition to stabilize uncertain neutral interconnected systems (1) as follows:

$$\Sigma_i = \Gamma_i + \Pi_{i1} R_{i2} \Pi_{i2}^T + \Pi_{i2} R_{i2}^T \Pi_{i1}^T < 0, \tag{40}$$

where $R_{i2} = \operatorname{diag}\{F_i(t), F_i(t), F_i(t), F_i(t), F_i(t), F_i(t)\}$.

By Lemma 1 and Schur complement formula, the condition $\overline{\overline{\Gamma}}_i < 0$ in (37) is equivalent to $\Sigma_i < 0$ in (40). For the same reason, (38) is equivalent to

$$\left[A_{i\eta_i} + \Delta A_{i\eta_i}(t)\right]^T \left[A_{i\eta_i} + \Delta A_{i\eta_i}(t)\right] < I_{n_i}. \tag{41}$$

This implies that uncertain neutral interconnected systems (1) are Lipschitz in the term $\dot{x}_i(t - \eta_i(t))$ with Lipschitz constant less than 1 [8]. By the same derivation of Theorem 3, one can complete this proof. □

The decentralized nonfragile guaranteed cost control (4) and the minimization of the guaranteed cost J_u for uncertain

neutral interconnected systems (1) are determined by the following theorem.

Theorem 9. *Consider uncertain neutral interconnected systems* (1) *with* (2), (3), (4), *and cost function* (6). *If the following optimization problem:*

$$\min \sum_{i=1}^{N} \left[\alpha_i + \operatorname{Tr}\left(U_{i1}^T \Phi_{i1} U_{i1} + U_{i2}^T \Phi_{i2} U_{i2}\right)\right] \tag{42}$$

is subject to LMI (37) *with Algorithm 6,* (38), *and* (31) *has a solution set* ($\alpha_i > 0$, $\varepsilon_{i1} > 0$, $\varepsilon_{i2} > 0$, $\varepsilon_{i3} > 0$, $Q_{ik} > 0$ $(k = 0, 1, 2)$, $\Phi_{i1} > 0$, $\Phi_{i2} > 0$, X_i), *then control* (4) *with* $K_i = X_i Q_{i0}^{-1}$ *is the decentralized nonfragile guaranteed cost control for uncertain neutral interconnected systems* (1) *with the minimization* J^* *of the guaranteed cost* J_u *in* (32).

Remark 10. Reference [18] develops a scheme of counteracting the interconnections to simplify the problem, which may add conservatism in some cases. Compared with the approach of treating the interconnections in [18], we utilize an approach of magnifying the terms associated interconnections; for details, one can see the derivation of inequality (16). To some extent, it may reduce the conservatism of the results derived in the paper.

4. Illustrative Examples

In this section, some examples are presented to show the validity of the control approach and the advantages of the schemes of dealing with the interconnections.

Example 1. To illustrate the design method of the decentralized nonfragile guaranteed cost control and the optimization approach of the guaranteed cost for uncertain neutral interconnected system, consider uncertain neutral interconnected systems (1) composed of two third-order subsystems:

$$A_1 = \begin{bmatrix} 1.1221 & 70.1414 & -5.1247 \\ 4.1437 & -1.1203 & 3.1243 \\ 2.4589 & -0.5671 & -2.2548 \end{bmatrix},$$

$$A_{1\sigma_1} = \begin{bmatrix} -0.0321 & 0.0012 & -0.0123 \\ 0.1325 & -0.0321 & -0.0246 \\ 0.0348 & 0.0023 & 0.0236 \end{bmatrix},$$

$$A_{1\eta_1} = \begin{bmatrix} 0.2236 & -0.2011 & -0.0321 \\ 0.2134 & 0.0271 & -0.1282 \\ 0.0123 & 0.5621 & -0.0124 \end{bmatrix},$$

$$B_1 = \begin{bmatrix} -2.1231 & -4.0126 \\ -1.1245 & 3.4725 \\ 0.1243 & -9.3417 \end{bmatrix},$$

$$B_{1\delta_1} = \begin{bmatrix} 0.1012 & -0.0219 \\ 0.1427 & -0.0537 \\ -0.0531 & 0.05324 \end{bmatrix},$$

$$A_{12} = \begin{bmatrix} -0.0898 & 0.0161 & -0.0682 \\ -0.0359 & 0.0205 & -0.0542 \\ -0.0205 & 0.0176 & 0.0814 \end{bmatrix},$$

$$C_1 = \begin{bmatrix} 0.0680 & -0.0655 & 0.0283 \\ -0.0086 & -0.0381 & 0.0889 \\ 0.0422 & 0.0088 & 0.0366 \end{bmatrix},$$

$$D_{11} = \begin{bmatrix} -0.0051 & 0.0429 & 0.0464 \\ 0.0792 & -0.0749 & -0.0321 \\ -0.0579 & 0.0900 & 0.0946 \end{bmatrix},$$

$$D_{1\sigma_1} = \begin{bmatrix} -0.0212 & 0.0481 & -0.0933 \\ -0.0991 & 0.0896 & 0.0941 \\ -0.0347 & -0.0204 & -0.0837 \end{bmatrix},$$

$$D_{12} = \begin{bmatrix} 0.0928 & -0.0609 \\ -0.0390 & 0.0897 \\ -0.0874 & -0.0064 \end{bmatrix},$$

$$D_{1\eta_1} = \begin{bmatrix} -0.0501 & 0.0860 & -0.0565 \\ -0.0311 & -0.0913 & 0.0185 \\ 0.0068 & 0.0621 & -0.0214 \end{bmatrix},$$

$$M_1 = \begin{bmatrix} 0.01 & 0.01 & 0.01 \\ 0.01 & 0.01 & 0.01 \end{bmatrix},$$

$$D_{1\delta_1} = \begin{bmatrix} -0.0175 & 0.0086 \\ 0.0172 & 0.0621 \\ 0.0142 & -0.0739 \end{bmatrix},$$

$$N_1 = \operatorname{diag}\{1, 1, 1\},$$

$$\sigma_1(t) = 0.1 * (2 + \sin(t)),$$

$$\eta_1(t) = 0.2 * (1 + \cos(t)),$$

$$\delta_1(t) = 0.3 * (1 + \sin(t)),$$

$$\tau_{12}(t) = 0.1 * (1 + \cos(t)),$$

$$A_2 = \begin{bmatrix} 8.1906 & 0.4571 & 2.5678 \\ -0.4724 & -4.4540 & 1.4527 \\ 0.4561 & -2.4561 & -5.9568 \end{bmatrix},$$

$$A_{2\sigma_2} = \begin{bmatrix} 0.0614 & 0.0973 & -0.0627 \\ -0.0819 & -0.0535 & -0.0848 \\ -0.0844 & -0.0895 & 0.0602 \end{bmatrix},$$

$$A_{2\eta_2} = \begin{bmatrix} 0.1147 & -0.0218 & 0.0157 \\ -0.1254 & 0.0282 & -0.0515 \\ 0.0919 & -0.0763 & -0.2169 \end{bmatrix},$$

$$B_2 = \begin{bmatrix} 9.7954 & -1.3341 \\ -7.5894 & -1.0482 \\ -0.0893 & -0.3494 \end{bmatrix},$$

$$B_{2\delta_2} = \begin{bmatrix} -0.0349 & -0.0189 \\ -0.0854 & -0.0231 \\ 0.0312 & 0.0993 \end{bmatrix},$$

$$A_{21} = \begin{bmatrix} -0.2898 & 0.3161 & -0.0682 \\ -0.0359 & 0.0205 & -0.0542 \\ -0.0205 & 0.3176 & 0.3814 \end{bmatrix},$$

$$C_2 = \begin{bmatrix} 0.0387 & 0.0738 & 0.0668 \\ -0.0441 & 0.0863 & -0.0823 \\ -0.0909 & 0.0750 & 0.0727 \end{bmatrix},$$

$$D_{21} = \begin{bmatrix} 0.0417 & 0.0333 & 0.0483 \\ 0.0805 & -0.0888 & 0.0914 \\ 0.0205 & -0.0677 & 0.0988 \end{bmatrix},$$

$$D_{2\sigma_2} = \begin{bmatrix} -0.0149 & -0.0275 & -0.0303 \\ -0.0488 & 0.0497 & -0.0892 \\ -0.0614 & 0.0711 & -0.0632 \end{bmatrix},$$

$$D_{22} = \begin{bmatrix} -0.0860 & -0.0073 \\ 0.0380 & 0.0673 \\ 0.0462 & 0.0578 \end{bmatrix},$$

$$D_{2\eta_2} = \begin{bmatrix} -0.0103 & -0.0529 & -0.0389 \\ 0.0136 & 0.0132 & -0.0028 \\ 0.0579 & -0.0099 & -0.0987 \end{bmatrix},$$

$$D_{2\delta_2} = \begin{bmatrix} 0.0566 & 0.0541 \\ -0.0304 & -0.0335 \\ 0.0894 & 0.0378 \end{bmatrix},$$

$$M_2 = M_1, \qquad N_2 = N_1,$$
$$\sigma_2(t) = 0.12 * (1 + \cos(t)),$$
$$\eta_2(t) = 0.1 * (2 + \sin(t)),$$
$$\delta_2(t) = 0.2 * (1 + \cos(t)),$$
$$\tau_{21}(t) = 0.2 * (2 + \sin(t)). \tag{43}$$

Let

$$\begin{aligned} S_{11} &= \operatorname{diag}\{0.3, 0.3, 0.3\}, \\ S_{12} &= \operatorname{diag}\{0.5, 0.5\}, \\ S_{21} &= \operatorname{diag}\{0.1, 0.1, 0.1\}, \\ S_{22} &= \operatorname{diag}\{1, 1\}, \end{aligned} \tag{44}$$

and give the following initial condition:

$$\begin{aligned} \phi_1(t) &= \left[-0.1e^{2t} \quad 0.15 \quad 0.2t + 0.05\right]^T, \\ \phi_2(t) &= \left[0.2e^{t} \quad -0.06 + 0.2t \quad 0.06\right]^T. \end{aligned} \tag{45}$$

According to Algorithm 6, W_{12} and W_{21} are chosen as follows:

$$\begin{aligned} W_{12} &= \operatorname{diag}\{7.7378, 7.7123, 7.7253\}, \\ W_{21} &= \operatorname{diag}\{6.9514, 9.0184, 7.2122\}. \end{aligned} \tag{46}$$

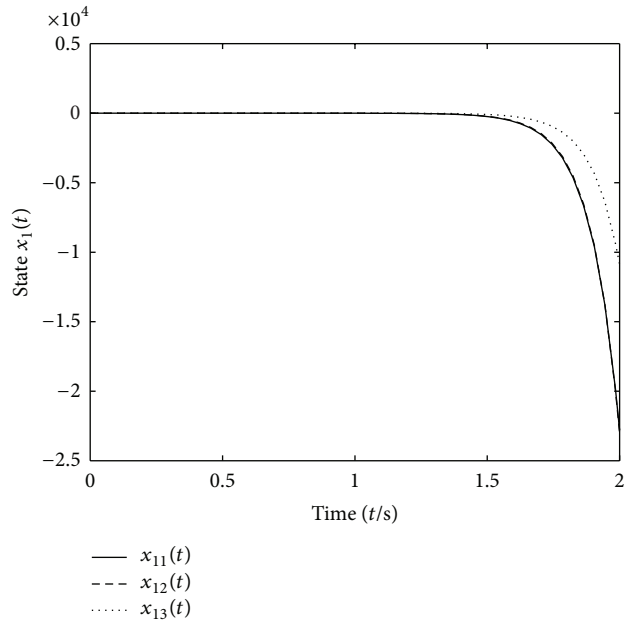

Figure 1: State response of the first open-loop subsystem.

Solving the optimization problem (42) subject to condition LMI (37) with Algorithm 6, (38), and (31), one can obtain

$$\begin{aligned} K_1 &= \begin{bmatrix} -3.9594 & -1.2404 & -1.2278 \\ -0.6353 & -0.0710 & -0.6896 \end{bmatrix}, \\ K_2 &= \begin{bmatrix} 1.0313 & 0.0551 & 0.1222 \\ -4.5397 & 0.3862 & -1.8594 \end{bmatrix}, \\ J^* &= 1.3053. \end{aligned} \tag{47}$$

The simulation results are shown in Figures 1–6 based on the above parameters. From Figures 1 and 2, one can see that the uncertain neutral systems (1) without controller are divergent. From Figures 3 and 4, one can see that the nonlinear neutral systems (1) with control law (4) are indeed well stabilized. The control signals $u_1(t)$ and $u_2(t)$ are rather smooth in Figures 5 and 6.

Example 2. To the best of the authors' knowledge, the nonfragile control and optimization for neutral interconnected systems have not been studied. But in order to show the advantages of the schemes of dealing with the interconnections, the authors have to simplify the model of neutral interconnected systems (1) to compare with the existing results.

In contrast to the model of system (13a) in [18], let

$$A_{1\eta_1} = 0, \qquad D_{1\eta_1} = 0,$$
$$M_1 = 0, \qquad N_1 = 0,$$
$$\sigma_1(t) = 0.3, \qquad \eta_1(t) = 0,$$

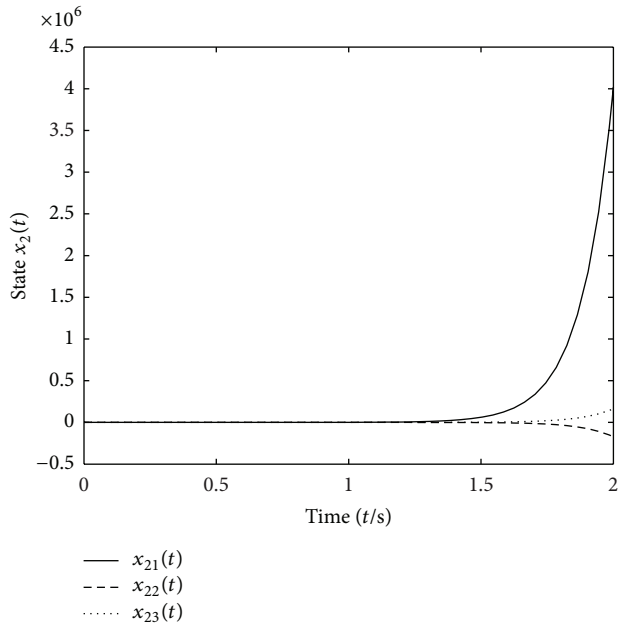

Figure 2: State response of the second open-loop subsystem.

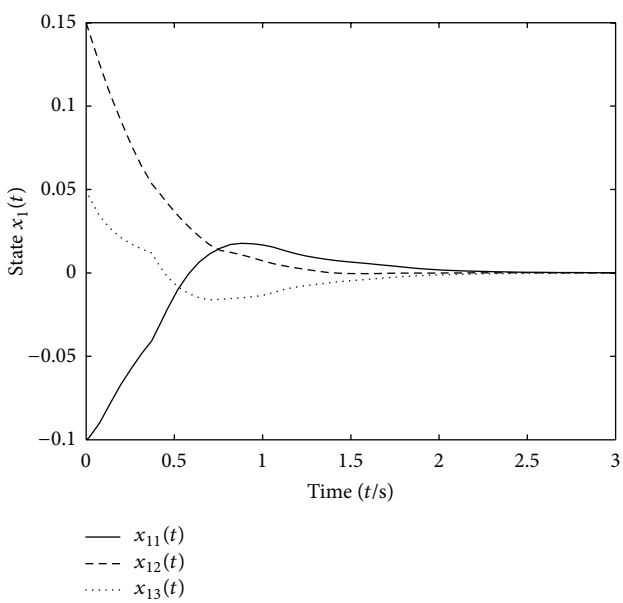

Figure 3: State response of the first closed-loop subsystem.

$$\delta_1(t) = 0.6, \qquad \tau_{12}(t) = 0,$$
$$A_{2\eta_2} = 0, \qquad D_{2\eta_2} = 0,$$
$$M_2 = 0, \qquad N_2 = 0, \qquad \sigma_2(t) = 0.24,$$
$$\eta_2(t) = 0, \qquad \delta_2(t) = 0.3, \qquad \tau_{21}(t) = 0, \tag{48}$$

and other parameters be the same as Example 1.

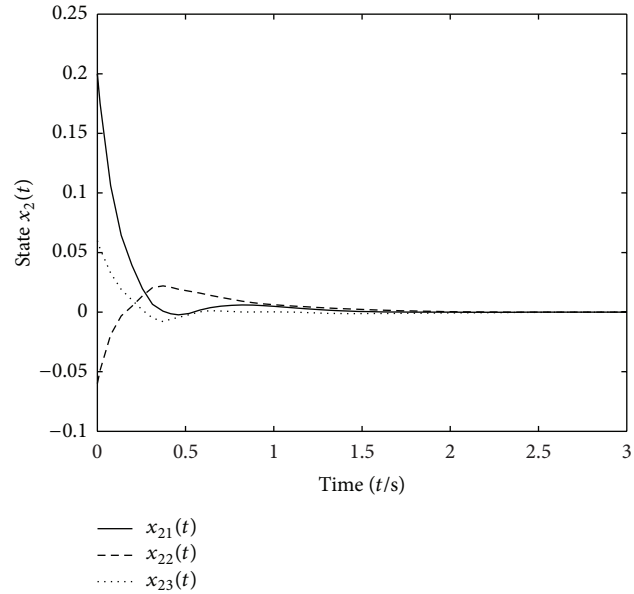

Figure 4: State response of the second closed-loop subsystem.

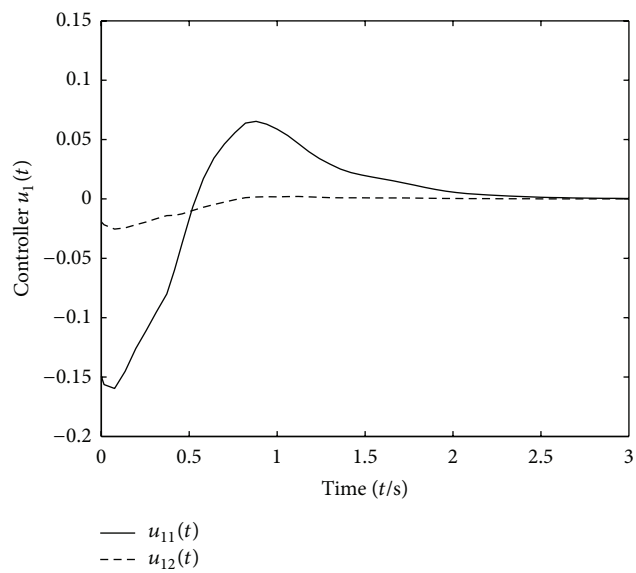

Figure 5: Control signal of the first subsystem.

Solving the optimization problem (42) subject to condition LMI (37) with Algorithm 6 and (31), the minimization of the guaranteed cost J_u is given by

$$J^* = 0.9429. \tag{49}$$

Since system (13a) in [18] is a nonlinear large-scale system, the authors choose the nonlinear vector function $g_{ij} = W_{ij}x_j$ satisfying the assumptions in [18] and $G_{ij} = \mathrm{diag}\{1, 1, 1\}$, $D_{ij} = E_{ij} = 0$. By Theorem 4.2 in [18], one can obtain the minimization J^* as follows:

$$J^* = 2.2627. \tag{50}$$

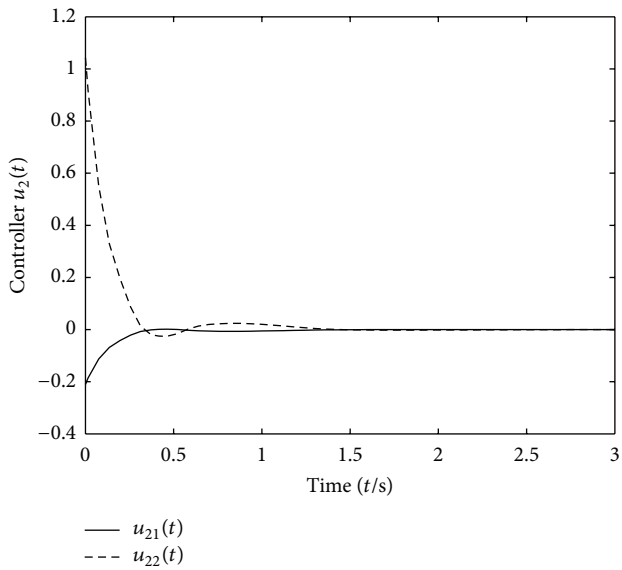

Figure 6: Control signal of the second subsystem.

Remark 11. It is clear from Example 2 that the minimization of the guaranteed cost provided by Theorem 9 in this paper is less than that of [18]. Viewing from this point, the results derived in this paper have the less conservatism.

5. Conclusion

The nonfragile guaranteed cost control and optimization are complex and challenging for uncertain interconnected systems of neutral type. In this paper, the sufficient conditions for the existence of the decentralized nonfragile guaranteed cost control for unperturbed and uncertain neutral interconnected systems are derived, which are presented in terms of coupled nonlinear inequalities. A novel algorithm is proposed to solve the nonlinear problems of coupled inequalities (10). Also, a good optimization scheme is introduced to solve the nonconvex problem of the guaranteed cost. Two numerical examples with the corresponding simulation results and the comparison results have elucidated the validity of the present control approach and the advantages of the schemes of dealing with the interconnections over the existing results in the literature.

Acknowledgments

This research is supported by Natural Science Foundation of China (no. 61104106), Science Foundation of Department of Education of Liaoning Province (no. L2012422), and Start-up Fund for Doctors of Shenyang University (no. 1120212340).

References

[1] V. Kolmanovskii and A. Myshkis, *Introduction to the Theory and Applications of Functional Differential Equations*, Kluwer Academic, Dordrecht, The Netherlands, 1999.

[2] S. Zhou and L. Zhou, "Improved exponential stability criteria and stabilisation of T-S model-based neutral systems," *IET Control Theory & Applications*, vol. 4, no. 12, pp. 2993–3002, 2010.

[3] L. Huang and X. Mao, "Delay-dependent exponential stability of neutral stochastic delay systems," *IEEE Transactions on Automatic Control*, vol. 54, no. 1, pp. 147–152, 2009.

[4] A. Alif, M. Darouach, and M. Boutayeb, "Design of robust H_∞ reduced-order unknown-input filter for a class of uncertain linear neutral systems," *IEEE Transactions on Automatic Control*, vol. 55, no. 1, pp. 6–19, 2010.

[5] H. R. Karimi, "Robust delay-dependent H_∞ control of uncertain time-delay systems with mixed neutral, discrete, and distributed time-delays and Markovian switching parameters," *IEEE Transactions on Circuits and Systems I*, vol. 58, no. 8, pp. 1910–1923, 2011.

[6] W. H. Chen, W. X. Zheng, and Y. Shen, "Delay-dependent stochastic stability and H_∞-control of uncertain neutral stochastic systems with time delay," *IEEE Transactions on Automatic Control*, vol. 54, no. 7, pp. 1660–1667, 2009.

[7] J. Yang, W. Luo, G. Li, and S. Zhong, "Reliable guaranteed cost control for uncertain fuzzy neutral systems," *Nonlinear Analysis: Hybrid Systems*, vol. 4, no. 4, pp. 644–658, 2010.

[8] C. H. Lien, "Non-fragile guaranteed cost control for uncertain neutral dynamic systems with time-varying delays in state and control input," *Chaos, Solitons and Fractals*, vol. 31, no. 4, pp. 889–899, 2007.

[9] C. H. Lien and K. W. Yu, "Non-fragile H_∞ control for uncertain neutral systems with time-varying delays via the LMI optimization approach," *IEEE Transactions on Systems, Man, Cybernetics B*, vol. 37, no. 2, pp. 493–499, 2007.

[10] S. Y. Xu, J. Lam, J. L. Wang, and G. H. Yang, "Non-fragile positive real control for uncertain linear neutral delay systems," *Systems & Control Letters*, vol. 52, no. 1, pp. 59–74, 2004.

[11] S. I. Niculescu, *Delay Effects on Stability: A Robust Control Approach*, vol. 269 of *Lecture Notes in Control and Information Sciences*, Springer, Berlin, Germany, 2001.

[12] R. K. Brayton, "Bifurcation of periodic solutions in a nonlinear difference-differential equations of neutral type," *Quarterly of Applied Mathematics*, vol. 24, pp. 215–224, 1966.

[13] Y. Kuang, *Delay Differential Equations with Applications in Population Dynamics*, vol. 191 of *Mathematics in Science and Engineering*, Academic Press, Boston, Mass, USA, 1993.

[14] T.-J. Tarn, T. Yang, X. Zeng, and C. Guo, "Periodic output feedback stabilization of neutral systems," *IEEE Transactions on Automatic Control*, vol. 41, no. 4, pp. 511–521, 1996.

[15] G. Chen, Z. Xiang, and M. S. Mahmoud, "Stability and H_∞ performance analysis of switched stochastic neutral systems," *Circuits, Systems, and Signal Processing*, vol. 32, no. 1, pp. 387–400, 2013.

[16] Z. Xiang, Y. N. Sun, and M. S. Mahmoud, "Robust finite-time H_∞ control for a class of uncertain switched neutral systems," *Communications in Nonlinear Science and Numerical Simulation*, vol. 17, no. 4, pp. 1766–1778, 2012.

[17] Z. Xiang, Y. N. Sun, and Q. Chen, "Robust reliable stabilization of uncertain switched neutral systems with delayed switching," *Applied Mathematics and Computation*, vol. 217, no. 23, pp. 9835–9844, 2011.

[18] H. Mukaidani, "An LMI approach to decentralized guaranteed cost control for a class of uncertain nonlinear large-scale delay systems," *Journal of Mathematical Analysis and Applications*, vol. 300, no. 1, pp. 17–29, 2004.

[19] M. S. Mahmoud and Y. Xia, "A generalized approach to stabilization of linear interconnected time-delay systems," *Asian Journal of Control*, vol. 14, no. 6, pp. 1539–1552, 2012.

[20] G. Pujol, J. Rodellar, J. Rossell, and F. Pozo, "Decentralised reliable guaranteed cost control of uncertain systems: an LMI design," *IET Control Theory and Applications*, vol. 1, no. 3, pp. 779–785, 2007.

[21] D. Zhao, Q. L. Zhang, H. L. Hu, and C. Y. Zhao, "Non-fragile guaranteed cost control for uncertain neutral large-scale interconnected systems," *Journal of Systems Engineering and Electronics*, vol. 21, no. 4, pp. 635–642, 2010.

[22] P. Gahinet, A. Nemirovski, A. J. Laub, and M. Chilali, *LMI Control Toolbox User's Guide*, The Math Works, Natick, Mass, USA, 1995.

Hindawi Publishing Corporation
Mathematical Problems in Engineering
Volume 2013, Article ID 192351, 13 pages
http://dx.doi.org/10.1155/2013/192351

Research Article

State Consensus Analysis and Design for High-Order Discrete-Time Linear Multiagent Systems

Yanrong Ge,[1,2] Yangzhou Chen,[1] Yaxiao Zhang,[1] and Zhonghe He[1]

[1] *College of Electronic Information and Control Engineering, Beijing University of Technology, Beijing 100124, China*
[2] *College of Physics Science and Information Engineering, Hebei Normal University, Shijiazhuang 050024, China*

Correspondence should be addressed to Yangzhou Chen; yzchen@bjut.edu.cn

Received 17 April 2013; Accepted 17 June 2013

Academic Editor: Guanghui Wen

The paper deals with the state consensus problem of high-order discrete-time linear multiagent systems (DLMASs) with fixed information topologies. We consider three aspects of the consensus analysis and design problem: (1) the convergence criteria of global state consensus, (2) the calculation of the state consensus function, and (3) the determination of the weighted matrix and the feedback gain matrix in the consensus protocol. We solve the consensus problem by proposing a linear transformation to translate it into a partial stability problem. Based on the approach, we obtain necessary and sufficient criteria in terms of Schur stability of matrices and present an analytical expression of the state consensus function. We also propose a design process to determine the feedback gain matrix in the consensus protocol. Finally, we extend the state consensus to the formation control. The results are explained by several numerical examples.

1. Introduction

In recent years, the consensus problem of multiagent systems (MASs) has been becoming a significant research topic because of its broad practical applications, including the work load balance in a network of parallel computers [1], the clock synchronization [2], distributed decision [3], consensus filtering and estimation in sensor networks [4–6], rendezvous, and the formation of various moving objects [7–11] such as underwater vehicles, aircrafts, satellites, mobile robots, and intelligent vehicles in automated highway systems, to name only a few. Hence, its study has captured attention of the researchers from different disciplines.

MASs are comprised of locally interacting agents equipped with dedicated sensing, computing, and communication devices. The consensus problem of MASs is to design a distributed control law for each agent, using only information from itself and its neighbors, such that all agents achieve an agreement on some quantities of interest. To design and analyse this class of systems, one needs to consider three essential elements: (1) a dynamic model describing the states of the agents, which can be either continuous time or discrete time, linear or nonlinear, homogeneous or heterogeneous, time varying or time invariant, low order or high order; (2) an information topology describing communication network between the agents, which can be either undirected or directed, fixed or switched; (3) a protocol (control input) for each of the agents describing how the agents interact on each other according to the given information topology, which can be synchronous or asynchronous, with or without time delay.

Up to now, numerous researches have been done for continuous-time MASs in different settings from the above cases [10, 12–18]. This paper focuses on the study of high-order discrete-time linear multiagent systems (DLMASs) by proposing a linear transformation to translate the consensus problem into a partial stability problem. Although this approach can be extended to any setting from the above cases, we pay our attention only to the case of fixed information topology and in the absence of time delay for giving prominence to the trait of the approach. Here we give an overview mainly to the DLMASs.

Reference [19] first proposed an interesting model for self-propelled particle systems, where all agents move in a plane with the same speed but different headings, and showed that in the model all agents might eventually move in the same

direction despite the absence of centralized coordination. Reference [20] further gave a mathematically rigorous qualitative analysis. Then, a theoretical explanation was given for the consensus behavior of Vicsek model on the basis of graph theory in [21, 22]. A necessary and sufficient condition was given for the average consensus criterion in [23]. Reference [24] further considered the case of switching network topologies for the average consensus. The average consensus was investigated for the systems with uncertain communication environments and time-varying topologies in [25] and with communication constraints in [26]. Reference [27] presented convergence results for the time-varying protocol in the absence or presence of communication delays. Reference [28] proposed an asynchronous time-varying consensus protocol. Reference [29] further discussed nonlinear systems with time-dependent communication links. References [30, 31] addressed the case with both time-varying delays and switching information topologies and provided a class of effective consensus protocols by repeatedly using the same state information at two time steps.

The researches mentioned above were limited to first-order systems. The extension to second-order systems was done for the systems with time-varying delays and time-varying interaction topology in [32], and for the systems with nonuniform time-delays and dynamically changing topologies in [33].

Recent researches were turned to the high-order DLMASs in [34–39]. Reference [34] studied a class of dynamic average consensus algorithms that allow a group of agents to track the average of their reference inputs. Reference [35] proposed an observer-type protocol based on the relative outputs of neighboring agents. Reference [36] studied the convergence speed for the high-order systems with random networks and arbitrary weights. Reference [37] addressed the high-order systems with or without delays. These researches were focused on the consensus convergence criteria for the proposed protocols. Another significant topic is the design of the gain matrices of the protocols in [38, 39].

This paper deals with both analysis and design problems of the state consensus for general high-order DLMASs. Compared with the existing works, the contributions of the paper are summarized as follows. Firstly, motivated by [12], we improve the protocol by adding a self-feedback of the agent to achieve the expected consensus dynamics, whereas [13] introduced the internal model to change the given dynamic to achieve the expected consensus dynamics and [14, 15] introduced the virtual leader to guide the multiagent systems to achieve the expected consensus dynamics. Secondly, we propose a state linear transformation to translate the consensus problem into a partial stability problem. The approach is motivated by the error variable method or the state space decomposition method in [12, 16]. However, our improvement can more spontaneously and conveniently deal with various settings of the consensus problems. Based on the partial stability theory, we educe new necessary and sufficient consensus convergence criteria in terms of stability of matrices and moreover give an explicit analytical expression of the state consensus function based on the different contributions of the initial states of the agents and the protocols. Thirdly, based on stability theorem, we give a design procedure to determine the gain matrices in the protocol on the basis of algebraic Riccati inequality similarly to [38, 39]. Fourthly, we extend the state consensus results to the formation control problem.

The remainder of the paper is organized as follows. Section 2 introduces some basic concepts and notations, and formulates the problem under investigation. Section 3 firstly introduces a linear transformation which translates the consensus problem of the multiagent systems into a partial stability problem of the corresponding transformed system, and then educes a new necessary and sufficient condition for the multiagent system to achieve global state consensus and presents an analytical expression of the state consensus function. Section 4 shows a design procedure to determine the gain matrices in the state consensus protocol. Section 5 extends the approach for the analysis and design of the state consensus to the formation control problem. Section 6 gives numerical examples to explain the theoretical results. Section 7 concludes the paper. All the proofs of the results are deposited in the appendix for the sake of reading.

2. Problem Description

Before stating the consensus problem, we give some basic concepts and notations. Let $\mathbb{R}^{n\times n}$ and $\mathbb{C}^{n\times n}$ be the sets of $n \times n$ real matrices and complex matrices, respectively. Matrices, if not explicitly stated, have appropriate dimensions in all settings. The superscript "T" means transpose for real matrices, and the superscript "H" means conjugate transpose for complex matrices. I_n presents the identity matrix of dimension n, and sometimes I is used for simplicity. $\mathbf{1}_N$ denotes the vector of dimension N with all entries equal to one. 0 is applied to denote zero matrices/vectors of any size, with zero components. A matrix $A \in \mathbb{C}^{n\times n}$ is said to be Schur stable if all of its eigenvalues have magnitude less than 1. The Kronecker product is denoted by $\otimes$ and the Hadamard product by $\circ$ in [40]. The following properties of the Kronecker product will be used: (1) $(A\otimes B)(C\otimes D) = AC\otimes BD$; (2) $(A+B)\otimes C = A\otimes C+B\otimes C$; (3) $(A\otimes B)^{-1} = A^{-1}\otimes B^{-1}$.

We consider DLMASs with N homogeneous agents and assume they are described by

$$x_i^+ = Ax_i + Bu_i, \quad i = 1, \ldots, N, \tag{1}$$

where $A \in \mathbb{R}^{n\times n}$, $B \in \mathbb{R}^{n\times m}$, (A, B) is assumed to be stabilizable, $x_i = x_i(k) \in \mathbb{R}^n$ is the state of the current time k, $x_i^+ = x_i(k+1)$ denotes the state at the next time $k+1$, and $u_i = u_i(k) \in \mathbb{R}^m$ is the control input of the current time k.

The control input u_i will be constructed based on the available information of the agent i. Let $\mathcal{N}_i$ denote the index set of the agents which can send their state information to the agent i. We call the set $\mathcal{N} = \{\mathcal{N}_i : i = 1, \ldots, N\}$ the information topology of the DLMASs (1). It is well known that one can use a digraph $G = (V, E)$ to express the information topology $\mathcal{N}$, where $V = \{1, \ldots, N\}$ is the index set of N agents, $E \subseteq V \times V$ is the set of directed edges to describe the information interaction between agents; that is, $(j, i) \in E \Leftrightarrow j \in \mathcal{N}_i$. Based on the directed edges, one can construct

an adjacency matrix $A = [a_{ij}]_{N\times N}$, whose entries are defined as $a_{ij} = 0$ for $j = i$, $a_{ij} = 1$ for $j \in \mathcal{N}_i$, and $a_{ij} = 0$ for $j \notin \mathcal{N}_i$. The corresponding in-degree matrix and graph Laplacian are defined as $D = \mathrm{diag}\{\deg_1, \ldots, \deg_N\}$ and $L = D - A$, respectively, where $\deg_i = \sum_{j=1}^{N} a_{ij}$ is the in-degree of the vertex i. A directed spanning tree of the digraph G is a tree covering all the vertices of the digraph. The following results are well known.

Lemma 1 (see [22]). *The Laplacian matrix $L \in \mathbb{R}^{N\times N}$ has the following properties: (1) all of the eigenvalues of L are either in the open right half complex plan or equal to 0; (2) 0 is a simple eigenvalue of L if and only if the digraph G contains a directed spanning tree.*

Given the information topology $\mathcal{N}$, we construct the following linear consensus protocol:

$$u_i = K_1 x_i + K_2 \sum_{j\in\mathcal{N}_i} w_{ij}\left(x_j - x_i\right), \quad i = 1, \ldots, N, \tag{2}$$

where $K_1, K_2 \in \mathbb{R}^{m\times n}$ are feedback gain matrices to be determined, which are relative to the consensus state and the convergence rate, respectively. $W =: [w_{ij}]_{N\times N}$ is a weighted matrix associated with the information topology $\mathcal{N}$. For the sake of expression, we also define the weighted adjacency matrix $A_w = A \circ W$ by using Hadamard product of matrices and the weighted Laplacian $L_w = D_w - A_w$ with weights w_{ij}, where $D_w = \mathrm{diag}\{\deg_1, \ldots, \deg_N\}$ is the corresponding weighted in-degree matrix with weighted in-degrees $\deg_i = \sum_{j\in\mathcal{N}_i} w_{ij}$.

Definition 2. For the given information topology $\mathcal{N}$, the DLMASs (1) are said to achieve global state consensus via the protocol (2) if for any given initial state $x_i(0)$, $i = 1, \ldots, N$, there exists an n-dimensional vector function $\xi(k)$ depending on the initial states such that $\lim_{k\to\infty}\|x_i(k) - \xi(k)\| = 0$. The function $\xi(k)$ is called a state consensus function.

In this paper, we will address the following three aspects of the state consensus problem: (i) to give criteria of global state consensus, that is, for any given information topology $\mathcal{N}$, weighted matrix W and feedback gain matrices K_1 and K_2 to find the conditions of the DLMASs (1) achieving global state consensus via the protocol (2); (ii) to calculate the state consensus function $\xi(k)$ if the DLMASs (1) achieve global state consensus via the protocol (2); (iii) to determine the matrices K_1 and K_2 such that the DLMASs (1) achieve global state consensus via the protocol (2).

First of all, we transform the state consensus problem to the partial stability problem. Then, based on the partial stability theorem framework, we educe new necessary and sufficient consensus convergence criteria and state a procedure to determine the gain matrices in the protocol on the basis of algebraic Riccati inequality. We also give an explicit analytical expression of the state consensus function based on the respective contributions of the initial states and the protocols. Finally, we extend the results to formation control.

3. State Consensus Analysis

In this section, we first introduce a linear transformation which translates the consensus problem of the multiagent systems into a partial stability problem of the corresponding transformed system. Then, we educe a necessary and sufficient condition for the DLMASs (1) to achieve global state consensus via the protocol (2), and present an analysis expression of the state consensus function. Finally, we discuss some interesting remarks and corollaries based on the result.

Let $x = [x_1^T, \ldots, x_N^T]^T$. The dynamics of the DLMASs (1) with the protocol (2) is described by

$$x^+ = \Psi x, \tag{3}$$

where

$$\Psi = I_N \otimes \left(A + BK_1\right) - L_w \otimes BK_2. \tag{4}$$

We propose a state linear transformation for the linear system (3) as follows:

$$\overline{x} = Tx, \tag{5}$$

where the block matrix $T \in \mathbb{R}^{nN\times nN}$ is defined as

$$T =: \begin{bmatrix} \widetilde{T} \\ \mathbf{1}_N^T \otimes I_n \end{bmatrix}, \qquad \widetilde{T} = \begin{bmatrix} T_1 \\ \vdots \\ T_{N-1} \end{bmatrix}. \tag{6}$$

And the matrix $T_i = [T_{i1}, \ldots, T_{iN}]$, $i = 1, \ldots, N-1$, is chosen such that the following two conditions are satisfied:

(1) the row vectors in each of the matrices T_i are linearly independent, respectively;

(2) the identities $T_i(\mathbf{1}_N \otimes I_n) = 0$, $i = 1, \ldots, N-1$, are held.

Lemma 3. *The inverse T^{-1} of the matrix T admits the following form:*

$$\begin{aligned} T^{-1} &= \begin{bmatrix} \overline{T}_{11} & \cdots & \overline{T}_{1,N-1} & N^{-1}I_n \\ \vdots & \ddots & \vdots & \vdots \\ \overline{T}_{N-1,1} & \cdots & \overline{T}_{N-1,N-1} & N^{-1}I_n \\ \overline{T}_{N,1} & \cdots & \overline{T}_{N,N-1} & N^{-1}I_n \end{bmatrix} \\ &=: \left[\overline{T}_1 \ \cdots \ \overline{T}_{N-1} \ N^{-1}\mathbf{1}_N \otimes I_n\right] \\ &=: \left[\widehat{T} \ N^{-1}\mathbf{1}_N \otimes I_n\right], \end{aligned} \tag{7}$$

where $\overline{T}_{ij}$, $i = 1, \ldots, N$, $j = 1, \ldots, N-1$, are the $n \times n$ blocks indefinitely described.

Using the linear transformation (5), we transform the linear system (3) into the following system:

$$\overline{x}^+ = T\Psi T^{-1}\overline{x}, \tag{8}$$

or the form of two equations

$$\begin{aligned} y^{+} &= \widetilde{T}\Psi\widehat{T}y + N^{-1}\widetilde{T}\Psi\left(\mathbf{1}_N \otimes I_n\right)z, \\ z^{+} &= \left(\mathbf{1}_N^T \otimes I_n\right)\Psi\widehat{T}y + N^{-1}\left(\mathbf{1}_N^T \otimes I_n\right)\Psi\left(\mathbf{1}_N \otimes I_n\right)z, \end{aligned} \tag{9}$$

where $\overline{x} = [y^T, z^T]^T$, $y = [\overline{x}_1^T, \ldots, \overline{x}_{N-1}^T]^T$, and $z = \overline{x}_N$.

We show that the state consensus problem of the DLMASs (1) with the protocol (2) can be transformed into a partial stability problem.

Definition 4 (see [41]). The linear system (8) is said to be asymptotically stable with respect to y (or asymptotically y-stable in short) if $\lim_{k\to\infty} y(k) = 0$ for any bounded initial state $\overline{x}(0)$ of the system (8).

Lemma 5. *Under the given information topology $\mathcal{N}$, the DLMASs* (1) *achieve global state consensus via the protocol* (2) *if and only if the equilibrium point $\overline{x} = 0$ of the linear system* (8) *is asymptotically y-stable. Moreover, the state consensus function of the agents is $\xi(k) = N^{-1}\sum_{i=1}^{N} x_i(k) = N^{-1}\overline{x}_N(k)$.*

Lemma 5 builds a bridge between the consensus problem and the partial stability problem. Now we focus on the asymptotical y-stability of the linear system (8). We can verify the following lemma.

Lemma 6. *The system* (9) *is of the following form:*

$$\begin{aligned} y^{+} &= \overline{A}y, \quad y \in \mathbb{R}^{n(N-1)}, \\ z^{+} &= \overline{C}y + \overline{D}z, \quad z \in \mathbb{R}^{n}, \end{aligned} \tag{10}$$

where $\overline{A} = \widetilde{T}(I_N \otimes (A + BK_1) - L_w \otimes BK_2)\widehat{T}$, $\overline{C} = -(\mathbf{1}_N^T L_w \otimes BK_2)\widehat{T}$, and $\overline{D} = A + BK_1$.

Combining Lemma 5 with Lemma 6, we directly get the following theorem.

Theorem 7. *Under the given information topology $\mathcal{N}$, the DLMASs* (1) *achieve global state consensus via the protocol* (2) *if and only if matrix $\overline{A}$ in* (10) *is Schur stable. Moreover, the state consensus function is*

$$\begin{aligned} \xi(k) = N^{-1}\Bigg(&\left(\sum_{j=0}^{k-1}(A + BK_1)^j \overline{C}\,\overline{A}^{k-1-j}\right)\widetilde{T} \\ &+ \mathbf{1}_N^T \otimes (A + BK_1)^k\Bigg)x(0). \end{aligned} \tag{11}$$

Subsequently, we give some interesting remarks and corollaries based on the result.

Remark 8. Since $\widehat{T}\widetilde{T} = (I_N - N^{-1}\mathbf{1}_N\mathbf{1}_N^T) \otimes I_n$, the result of Theorem 7 is in fact independent of the choice of the matrix T although both $\overline{A}$ and formula (11) in Theorem 7 contain $\widetilde{T}$ and $\widehat{T}$. Hence, for simplicity, we take it in the following form:

$$\begin{aligned} T &= \begin{bmatrix} 1 & -1 & 0 & \cdots & 0 \\ 0 & 1 & -1 & \cdots & 0 \\ \vdots & \vdots & \ddots & \vdots & \vdots \\ 0 & \cdots & 0 & 1 & -1 \\ 1 & 1 & 1 & \cdots & 1 \end{bmatrix} \otimes I_n \\ &:= \begin{bmatrix} \widetilde{T}_0 \\ \mathbf{1}_N^T \end{bmatrix} \otimes I_n. \end{aligned} \tag{12}$$

The corresponding inverse matrix is

$$\begin{aligned} T^{-1} &= \frac{1}{N}\begin{bmatrix} N-1 & N-2 & \cdots & 1 & 1 \\ -1 & N-2 & \cdots & 1 & 1 \\ \vdots & \vdots & \ddots & \vdots & \vdots \\ -1 & -2 & \cdots & 1 & 1 \\ -1 & -2 & \cdots & -(N-1) & 1 \end{bmatrix} \otimes I_n \\ &:= \begin{bmatrix} \widehat{T}_0 & N^{-1}\mathbf{1}_N \end{bmatrix} \otimes I_n. \end{aligned} \tag{13}$$

Thus, we can write $\overline{A}$ and $\overline{C}$ into

$$\begin{aligned} \overline{A} &= I_{N-1} \otimes (A + BK_1) - \widetilde{T}_0 L_w \widehat{T}_0 \otimes BK_2, \\ \overline{C} &= -\mathbf{1}_N^{\mathrm{T}} L_w \widehat{T}_0 \otimes BK_2. \end{aligned} \tag{14}$$

Corollary 9. *Under the given information topology $\mathcal{N}$, the DLMASs* (1) *achieve global consensus via the protocol* (2) *if and only if all the matrices $A + BK_1 - \lambda_i BK_2$ are Schur stable, where λ_i, $i = 1, \ldots, N-1$, are the eigenvalues of the matrix $\widetilde{T}_0 L_w \widehat{T}_0$. Moreover, the state consensus function is expressed by*

$$\xi(k) = \left(\eta^T \otimes (A + BK_1)^k\right)x(0), \quad i = 1, \ldots, N, \tag{15}$$

where η satisfies $\eta^T L_w = 0$ and $\eta^T \mathbf{1}_N = 1$.

One can verify that as $k \to \infty$ the state consensus functions in formulas (11) and (15) are the same.

Remark 10. From Schur stability of $\overline{A}$ in the formula (14), we can conclude that if $A + BK_1$ is not Schur stable, it is a necessary condition of the consensus that the digraph G expressing the information topology $\mathcal{N}$ has a directed spanning tree. In fact, since the condition of directed spanning tree is equivalent to Hurwitz stability of $-\widetilde{T}_0 L_w \widehat{T}_0$, a lack of directed spanning tree means that $-\widetilde{T}_0 L_w \widehat{T}_0$ has a zero eigenvalue. In this case, we transform $\overline{A}$ into its Jordan form via the matrix $U \otimes I_n$, where U is the matrix such that $U^{-1}\widetilde{T}_0 L_w \widehat{T}_0 U = J$ is the Jordan form, and thus we have

$$\left(U^{-1} \otimes I_n\right)\overline{A}\left(U \otimes I_n\right) = I_{N-1} \otimes (A + BK_1) - J \otimes BK_2. \tag{16}$$

One can verify that the eigenvalues of $A + BK_1$ are the members of the eigenvalues of $\overline{A}$, and thus $\overline{A}$ is not Schur

stable if $A + BK_1$ is not Schur stable. On the other hand, if $A + BK_1$ is Schur stable, one can take $K_2 = 0$ to make the DLMASs (1) achieve global consensus, which implies that for any initial states all the agents always converge to the equilibrium point 0.

Hence, from the formula (16) we can educe another global consensus criterion.

Corollary 11. *If $A + BK_1$ is not Schur stable, then under the given information topology $\mathcal{N}$, the DLMASs* (1) *achieve global state consensus via the protocol* (2) *if and only if $\widetilde{T}_0 L_w \widehat{T}_0$ has $N-1$ eigenvalues with positive real part λ_i, $i = 1, \ldots, N-1$, and the matrices $A + BK_1 - \lambda_i BK_2$, $i = 1, \ldots, N-1$, are Schur stable.*

Remark 12. If the state consensus function in (11) is a constant vector equal to the average of the initial states of all the agents, the consensus is called the average consensus. From the formula (11) we educe the following result on the average consensus.

Corollary 13. *The DLMASs* (1) *achieve global average consensus via the protocol* (2) *if and only the matrix $\overline{A}$ is Schur stable and $(\sum_{j=0}^{k-1}(A+BK_1)^j \overline{C}\,\overline{A}^{k-1-j})\widetilde{T} + \mathbf{1}_N^T \otimes (A+BK_1)^k = \mathbf{1}_N^T \otimes I_n$.*

If $A + BK_1 = I_n$, then the last condition in Corollary 13 becomes $\mathbf{1}_N^T L_w = 0$, or equivalently, the digraph G is either undirected connected or directed strong connected and balanced. More specially, if L_w is a symmetric matrix (equivalently, the digraph G becomes undirected connected), the condition $\mathbf{1}_N^T L_w = 0$ is satisfied and thus the average consensus is achieved.

Remark 14. When $A = I_n$, $K_1 = 0$, and $B = I_n$, the DLMASs (1) are called a single-integrator one. In this case, $\overline{A} = I_{(N-1)n} - \widetilde{T}_0 L_w \widehat{T}_0 \otimes K_2$ and $\overline{C} = -\mathbf{1}_N^T L_w \widehat{T}_0 \otimes K_2$. We educe the following result.

Corollary 15. *Under the given information topology $\mathcal{N}$, the single-integrator DLMASs* (1) *achieve global state consensus via the protocol* (2) *if and only if the following two conditions are held simultaneously: (1) the matrix $-\widetilde{T}_0 L_w \widehat{T}_0$ is Hurwitz stable; that is, the digraph G admits a directed spanning tree; (2) the products $\lambda_i \mu_j$, $i = 1, \ldots, N-1$, $j = 1, \ldots, n$, are in the open unit circle of the complex plane with the centre at $(1, 0)$, where λ_i, $i = 1, \ldots, N-1$, are the eigenvalues of the matrix $\widetilde{T}_0 L_w \widehat{T}_0$ and μ_j, $j = 1, \ldots, n$, are the eigenvalues of the matrix K_2. The corresponding consensus function* (11) *becomes a constant vector*

$$\xi = N^{-1}\left(\mathbf{1}_N^T \otimes I_n - \mathbf{1}_N^T L_w \widehat{T}_0 \left(\widetilde{T}_0 L_w \widehat{T}_0\right)^{-1} \widetilde{T}_0 \otimes I_n\right) x(0). \tag{17}$$

Moreover, the single-integrator DLMASs (1) *achieve global average consensus via the protocol* (2) *if and only both of the above conditions are satisfied and in addition $\mathbf{1}_N^T L_w = 0$.*

Remark 16. When $A = \left[\begin{smallmatrix} 1 & 1 \\ 0 & 1 \end{smallmatrix}\right] \otimes I_n$, $B = \left[\begin{smallmatrix} 0 \\ 1 \end{smallmatrix}\right] \otimes I_n$, and $K_1 = 0$, the DLMASs (1) are called a double-integrator one, whose state vector can be seen as consisting of the position and velocity in the n dimensional space $\mathbb{R}^n$.

Corollary 17. *Under the given information topology $\mathcal{N}$, the double-integrator DLMASs* (1) *achieve global state consensus via the protocol* (2) *if and only if $\overline{A}$ is Schur stable. Moreover, the consensus function is*

$$\begin{aligned}
\xi(k) &= N^{-1}\left\{\left(\overline{C}\left(I_{2(N-1)n} - \overline{A}\right)^{-1} + \begin{bmatrix} 0 & kI_n \\ 0 & 0 \end{bmatrix} \overline{C}\left(I_{2(N-1)n} - \overline{A}\right)^{-1}\right.\right. \\
&\quad \left.\left. - \begin{bmatrix} 0 & I_n \\ 0 & 0 \end{bmatrix} \overline{C}\left(I_{2(N-1)n} - \overline{A}\right)^{-2}\right)\widetilde{T} \right. \\
&\quad \left. + \mathbf{1}_N^T \otimes \begin{bmatrix} I_n & kI_n \\ 0 & I_n \end{bmatrix}\right\} x(0).
\end{aligned} \tag{18}$$

The consensus function above can be decomposed into the position consensus function

$$\begin{aligned}
\xi_1(k) = N^{-1}\left\{\left([I_n \;\; 0]\,\overline{C}\left(I_{2(N-1)n} - \overline{A}\right)^{-1}\right.\right. \\
+ [0 \;\; kI_n]\,\overline{C}\left(I_{2(N-1)n} - \overline{A}\right)^{-1} \\
\left. - [0 \;\; I_n]\,\overline{C}\left(I_{2(N-1)n} - \overline{A}\right)^{-2}\right)\widetilde{T} \\
\left. + \mathbf{1}_N^T \otimes [I_n \;\; kI_n]\right\} x(0),
\end{aligned} \tag{19}$$

which is a linear function of discrete time k, and the constant velocity consensus function is as follows:

$$\begin{aligned}
\xi_2(k) = N^{-1}\left\{\left([0 \;\; I_n]\,\overline{C}\left(I_{2(N-1)n} - \overline{A}\right)^{-1}\right)\widetilde{T}\right. \\
\left. + \mathbf{1}_N^T \otimes [0 \;\; I_n]\right\} x(0).
\end{aligned} \tag{20}$$

Similarly, we can define the velocity average consensus, that is, if the DLMASs (1) achieve global consensus via the protocol (2), and the velocity consensus function is a constant vector equal to the average of the initial velocities of all the agents.

Corollary 18. *Under the given information topology $\mathcal{N}$, the double-integrator DLMASs* (1) *achieve global velocity average consensus via the protocol* (2) *if and only the matrix $\overline{A}$ is Schur stable and $[0 \;\; I_n]\,\overline{C} = 0$.*

It is obvious that if $\mathbf{1}_N^T L_w = 0$, then $\overline{C} = 0$; that is, the last condition in Corollary 18 is satisfied, and thus, the state consensus function becomes

$$\xi(k) = N^{-1}\mathbf{1}_N^T \otimes \begin{bmatrix} I_n & kI_n \\ 0 & I_n \end{bmatrix} x(0). \tag{21}$$

4. Design of Gain Matrices

In this section, we discuss the third problem, that is, how to determine the weighted matrix W and the gain matrices K_1 and K_2, such that the DLMASs (1) achieve global state consensus via the protocol (2).

Theorem 7 shows that the matrices W, K_1, and K_2 should be taken to ensure that the matrix $\overline{A}$ is Schur stable. Furthermore, from Corollary 11 we see that if the matrix W with respect to the information topology $\mathcal{N}$ has been given, we need only to design the gain matrices K_1 and K_2 to ensure that the matrices $A + BK_1 - \lambda_i BK_2$ are Schur stable, where λ_i, $i = 1, \ldots, N-1$, are the eigenvalues of the matrix $\widetilde{T}_0 L_w \widehat{T}_0$. The matrix K_1 is often taken to obtain an expected consensus dynamics. The matrix K_2 is designed to achieve state consensus and expected convergence rate. Its design needs the following lemma.

Lemma 19 (see [38]). *Supposing that the matrix $\widehat{A} = A + BK_1$ is not Schur stable but $(\widehat{A}, B)$ is stabilizable, then there is a critical value $\delta_c \in (0, 1]$, such that for any number δ with $0 < \delta < \delta_c$ the modified Riccati inequality*

$$\widehat{A}^T P \widehat{A} - P - \left(1 - \delta^2\right) \widehat{A}^T PB\left(B^T PB\right)^{-1} B^T P \widehat{A} < 0 \qquad (22)$$

admits a positive definite matrix solution P, where δ_c depends on the unstable eigenvalues of the matrix $\widehat{A}$.

We define functions $\delta_i(\omega) = 1 - \omega\lambda_i$ and $\delta(\omega) = \max_{i\in\{1,\ldots,N-1\}} |\delta_i(\omega)|$. Motivated by [38], we get the following theorem.

Theorem 20. *Supposing that the matrix (A, B) is stabilizable, the gain matrix K_1 has been taken such that the expected consensus dynamic matrix $A + BK_1$ is not Schur stable, and the weighted matrix W with respect to the information topology $\mathcal{N}$ is given such that $-\widetilde{T}_0 L_w \widehat{T}_0$ is Hurwitz stable with $N-1$ eigenvalues $-\lambda_i$, $i = 1, \ldots, N-1$; then, for the DLMASs (1) to achieve state consensus via the protocol (2), the matrix K_2 can be designed as $K_2 = \omega(B^T PB)^{-1} B^T P(A + BK_1)$, where ω is an arbitrary constant satisfying $\delta = \delta(\omega) < \delta_c$, $\delta_c \in (0, 1]$ is a critical value which depends on the unstable eigenvalues of the matrix $A + BK_1$, and $P^T = P > 0$ is a solution of the algebraic Riccati inequality (22).*

Based on Theorem 20, we give the following algorithm of determining the feedback gain matrices K_1 and K_2 in the protocol (2).

Algorithm 21. Design procedure of the gain matrices K_1 and K_2.

Step 1. Verify the stabilizability condition of (A, B) and the spanning tree condition of the information topology $\mathcal{N}$. If neither of them is satisfied, then stop. Otherwise, design the weighted Laplacian L_w such that $-\widetilde{T}_0 L_w \widehat{T}_0$ is Hurwitz stable with $N-1$ eigenvalues $-\lambda_i$, $i = 1, \ldots, N-1$.

Step 2. Design K_1 such that $\widehat{A} = A + BK_1$ is the matrix of the expected consensus dynamics of the DLMASs (1) and is not Schur stable.

Step 3. Calculate all the eigenvalues of $\widehat{A}$, which are composed of the stable eigenvalues $\lambda_i^s(\widehat{A})$, $i = 1, \ldots, n_s$ and unstable ones $\lambda_i^u(\widehat{A})$, $i = 1, \ldots, n_u$, $n_s + n_u = n$.

Step 4. Calculate the critical value $\delta_c \in (0, 1]$. If B is invertible, then $\delta_c = (\max_{i=\{1,\ldots,n_u\}} |\lambda_i^u(\widehat{A})|)^{-1}$. If B is of rank one, then $\delta_c = (\prod_{i=\{1,\ldots,n_u\}} |\lambda_i^u(\widehat{A})|)^{-1}$. Otherwise, apply Wonham decomposition to the unstable part (A_u, B_u) of $(\widehat{A}, B)$ to convert the multiple input system to m single input subsystems, where m is the number of the Jordan blocks of matrix A_u. Specifically, there is a nonsingular real matrix Q with a compatible dimension such that $\widetilde{A} = Q^{-1} A_u Q$ and $\widetilde{B} = Q^{-1} B_u$ take the form

$$\widetilde{A} = \begin{bmatrix} A_1 & * & * & * \\ 0 & A_2 & \cdots & * \\ \vdots & \vdots & \ddots & \vdots \\ 0 & 0 & \cdots & A_m \end{bmatrix}, \qquad \widetilde{B} = \begin{bmatrix} b_1 & * & * & * \\ 0 & b_2 & \cdots & * \\ \vdots & \vdots & \ddots & \vdots \\ 0 & 0 & \cdots & b_m \end{bmatrix}, \qquad (23)$$

where the symbol $*$ denotes possibly nonzero parts and (A_j, b_j) with $A_j \in \mathbb{R}^{n_j \times n_j}$ and $b_j \in \mathbb{R}^{n_j}$ for all $j \in \{1, \ldots, m\}$ is controllable and $\sum_{j=1}^m n_j = n_u$. In this case, δ_c is lower bounded by $\delta_c \geq (\prod_i |\lambda_i^u(A_{m^*})|)^{-1}) = \delta_c'$, where the index m^* is defined by $m^* = \arg\max_{j=\{1,\ldots,m\}} (\prod_i |\lambda_i^u(A_j)|)$ and A_j is the Jordan block of the unstable part of matrix $\widehat{A}$.

Step 5. Calculate the value ω such that $\delta(\omega) = \max_{i\in\{1,\ldots,N-1\}} |\delta_i(\omega)|$.

Step 6. Solve (22) with $\delta = \delta(\omega)$ for a positive definite matrix P.

Step 7. Calculate the matrix $K_2 = \omega(B^T PB)^{-1} B^T P(A + BK_1)$.

5. Application to Formation Control

In this section, the consensus approach is modified to solve the formation control problem of the DLMASs (1). Let $h = \begin{bmatrix} h_1^T & h_2^T & \cdots & h_N^T \end{bmatrix}^T \in \mathbb{R}^{nN}$ describe a constant formation of the agent network in a reference coordinate frame, where $h_i \in \mathbb{R}^n$ is the formation variable corresponding to the agent i. The variable $h_i - h_j$ denotes the relative formation vector between the agents i and j, which is assumed to be independent of the reference coordinate.

We modify the consensus protocol (2) and propose a distributed formation protocol as follows:

$$u_i = K_1 x_i + K_2 \sum_{j\in\mathcal{N}_i} w_{ij} \left(x_j - x_i - \left(h_j - h_i\right)\right), \quad i = 1, \ldots, N. \qquad (24)$$

Definition 22. Under the given information topology $\mathcal{N}$, the DLMASs (1) achieve the given formation h via the protocol

(24) if $\|(x_i(k) - x_j(k)) - (h_i - h_j)\| \to 0$ as $k \to \infty$, for all $i, j = 1, \ldots, N$, that is, if there is a function $\xi(k)$ such that $\|x_i(k) - h_i - \xi(k)\| \to 0$ as $k \to \infty$, for all $i = 1, \ldots, N$, where $\xi(k)$ is called reference state consensus function.

Theorem 23. *Under the given information topology $\mathcal{N}$, the DLMASs* (1) *achieve the formation h via the protocol* (24) *if and only if the matrix $I_{N-1} \otimes (A + BK_1) - \widetilde{T}_0 L_w \widehat{T}_0 \otimes BK_2$ is Schur stable and $(\widetilde{T}_0 \otimes (A + BK_1 - I_n))h = 0$. Moreover, the reference state consensus function is*

$$\xi(k) = N^{-1}\left(\left(\sum_{j=0}^{k-1}(A + BK_1)^j \overline{C}\,\overline{A}^{k-1-j}\right)\widetilde{T} + \mathbf{1}_N^T \otimes (A + BK_1)^k\right) x(0). \tag{25}$$

Similarly to Corollary 11, we get the following corollary for the formation control.

Corollary 24. *Under the given information topology $\mathcal{N}$, the DLMASs* (1) *achieve the formation h via the protocol* (24) *if and only if all the matrices $A + BK_1 - \lambda_i BK_2$ are Schur stable and $(\widetilde{T}_0 \otimes (A + BK_1 - I_n))h = 0$, where λ_i, $i = 1, \ldots, N-1$, are the eigenvalues of the matrix $\widetilde{T}_0 L_w \widehat{T}_0$.*

Remark 25. Note that not all kinds of formation structure can be achieved for the DLMASs (1) by using the protocol (24). The achievable formation structures have to satisfy the constraints $(\widetilde{T}_0 \otimes (A + BK_1 - I_n))h = 0$. The formation protocol (24) for a given achievable formation h can be constructed analogously by using the Algorithm 21 in Section 4.

6. Numerical Examples

In this section, we give some illustrative examples.

Example 26 (state consensus analysis). We consider the DLMASs (1) consisting of four agents described by the following matrices:

$$A = \begin{bmatrix} 2 & \frac{\sqrt{2}}{2} & \frac{-\sqrt{2}}{2} \\ \frac{-1}{2} & \frac{\sqrt{2}}{4} & \frac{3\sqrt{2}}{4} \\ 1 & 0 & 0 \end{bmatrix}, \qquad B = \begin{bmatrix} 1 \\ \frac{-1}{2} \\ 1 \end{bmatrix}. \tag{26}$$

Supposed that we are given the information topology $\mathcal{N} = \{\{4\}, \{1\}, \{2\}, \{3\}\}$, the weights $w_{ij} = 0.5$, and the gain matrices $K_1 = [-1, -\sqrt{2}/2, \sqrt{2}/2]$ and $K_2 = [0.4444, -0.4714, 0.1571]$, we are required to verify the consensus convergence.

The matrix $\overline{A}$ is Schur stable since its eigenvalues are $0.3482 \pm 0.7182i$, $0.8746 \pm 0.2786i$, $0.7885 \pm 0.4643i$, $0.7728 \pm 0.5782i$, and 0.0001. Therefore, according to Theorem 7, the DLMASs (1) with the matrices in (26) achieve global consensus via the protocol (2) under the given information topology $\mathcal{N}$ and the gain matrix K_1, K_2. For the initial states $x_1(0) = [0, 0.6, 0.6]^T$, $x_2(0) = [1.2, 1.5, 1.8]^T$, $x_3(0) = [1.8, 2.4, 2.1]^T$, and $x_4(0) = [3.0, 2.7, 3.6]^T$, the corresponding state consensus function in (11) is $\xi(k) = [1.5, 2.7094\cos(0.7854k - 1.6296), 2.7094\cos(0.7854k - 0.0588)]^T$. Figure 1 shows the state trajectories of the agents and the trajectory of the state consensus function marked by circles.

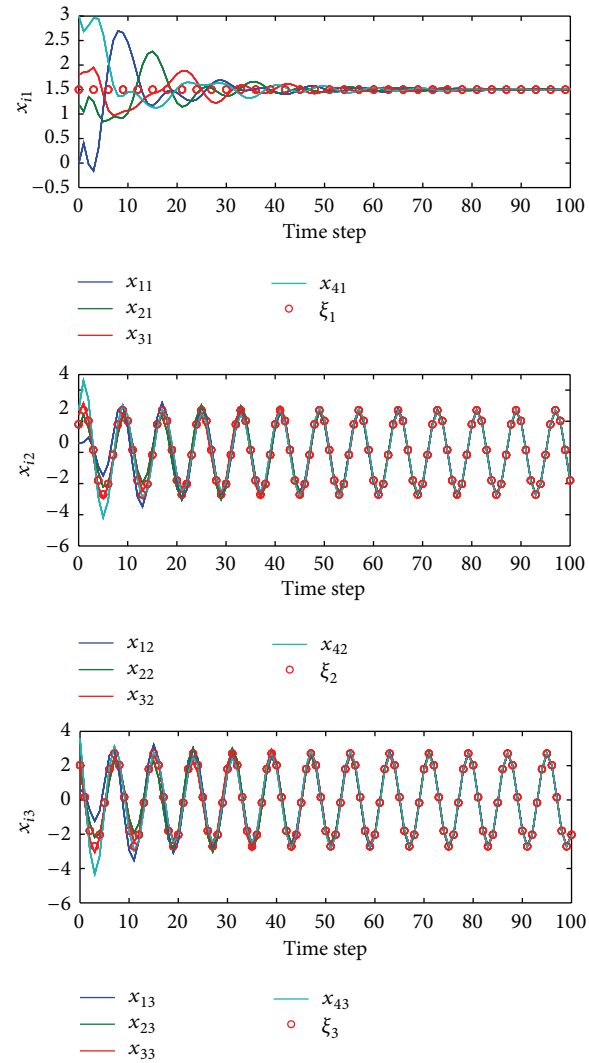

Figure 1: State trajectories of DLMASs.

Example 27 (gain matrices design for a formation control). The consensus problem of multiagent systems has many practical applications, such as formation control of mobile robots and cooperative control of unmanned airborne vehicles. In this example, we consider that DLMASs consisting of four mobile robots are described as

$$\begin{aligned} x_i^+ &= x_i + v_i, \\ v_i^+ &= v_i + u_i, \quad i = 1, \ldots, 4, \end{aligned} \tag{27}$$

where $x_i \in \mathbb{R}^2$, $v_i \in \mathbb{R}^2$, and $u_i \in \mathbb{R}^2$ are the position, the velocity, and the acceleration input of the robot i, respectively.

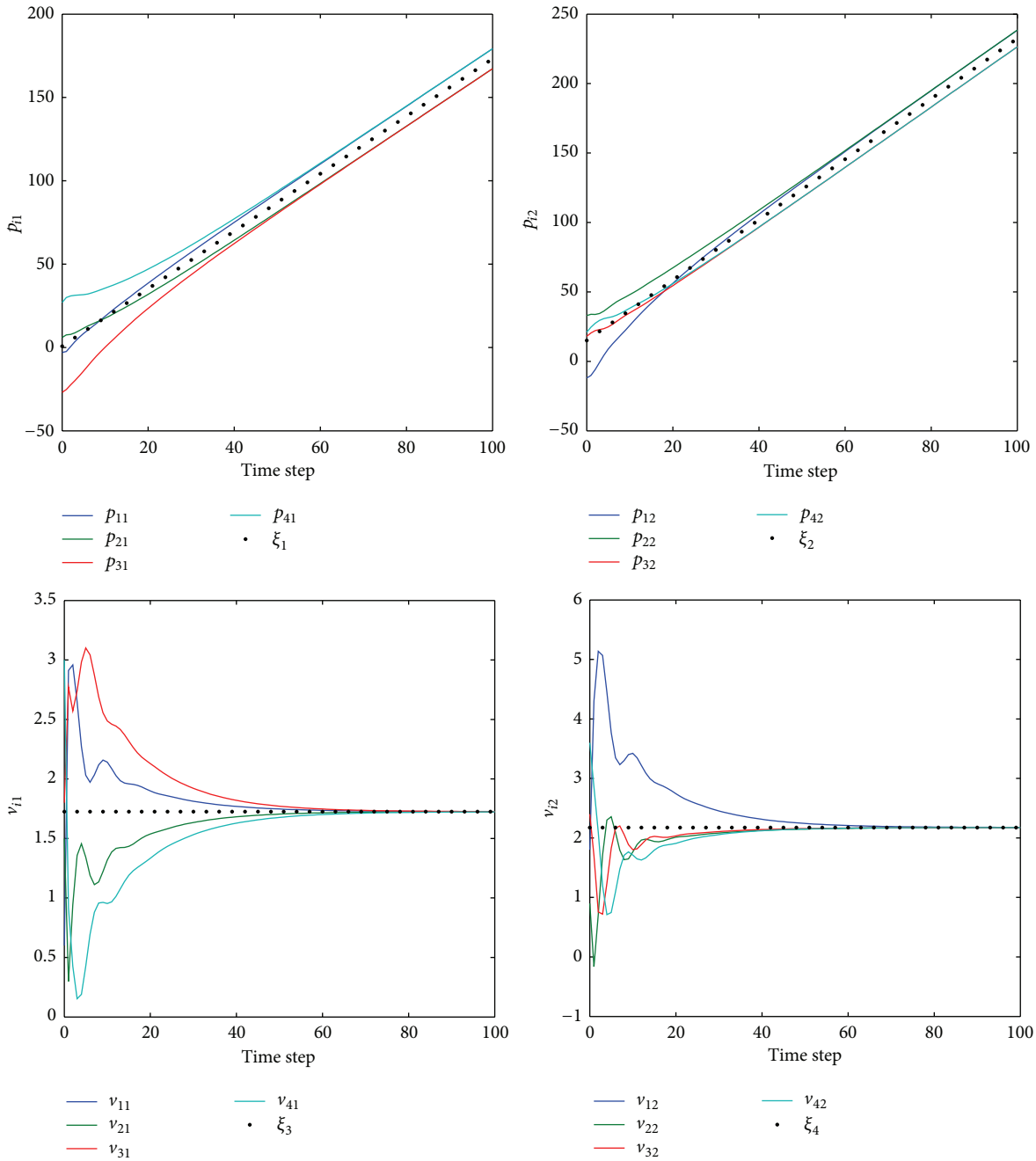

FIGURE 2: Position and velocity trajectories of mobile robots.

The information topology and the weights are the same as in Example 26. The eigenvalues of the matrix $\widetilde{T}_0 L_w \widetilde{T}_0$ are $\lambda_1 = 0.5 + 0.5i$, $\lambda_2 = 0.5 - 0.5i$, and $\lambda_3 = 1$. We choose $h_1 = [6, 6, 0, 0]^T$, $h_2 = [-6, 6, 0, 0]^T$, $h_3 = [-6, -6, 0, 0]^T$, and $h_4 = [6, -6, 0, 0]^T$ for the formation h of the mobile robots. Note that (A, B) in (27) is stabilizable. The eigenvalues of matrix A are 1 (4 multiples). We assume that the expected consensus dynamics of the agents is not changed, and thus, we have $K_1 = 0$. It is easy to verify that the formation h satisfies the constraints $(\widetilde{T}_0 \otimes (A + BK_1 - I_n))h = 0$. One can get $\delta_c = 1$ through Step 4 of the Algorithm 21. By Step 5, one can obtain $\omega = 1.0$, and the corresponding $\delta(\omega) = \sqrt{2}/2 < \delta_c$. The modified Riccati inequality (22) admits a solution

$$P = \begin{bmatrix} 88 & 17 & 0 & 0 \\ 17 & 248 & 0 & 0 \\ 0 & 0 & 88 & 17 \\ 0 & 0 & 17 & 248 \end{bmatrix} \times 10^{-4}. \tag{28}$$

The corresponding control gain is calculated as follows:

$$K_2 = \begin{bmatrix} 0 & 0 & 0.0686 & 1.0686 \\ 0.0686 & 1.0686 & 0 & 0 \end{bmatrix}. \tag{29}$$

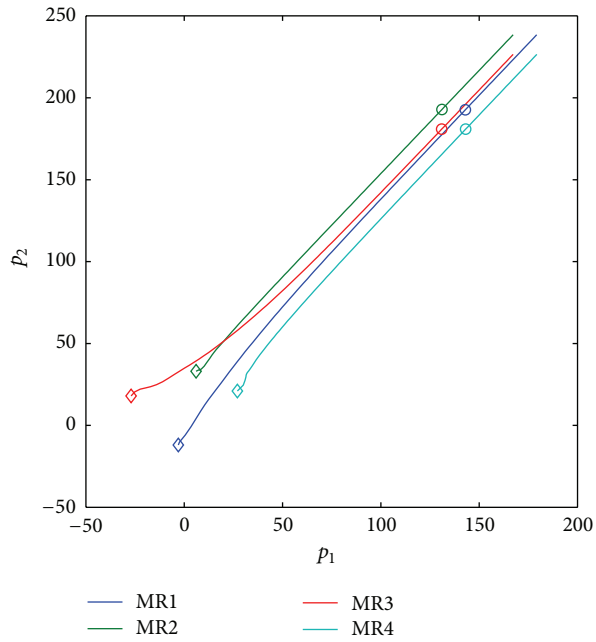

FIGURE 3: Formation of four mobile robots.

The eigenvalues of matrix $\overline{A}$ are $0.5336 \pm 0.5392i$ (2 multiples), $0.9321 \pm 0.0049i$ (2 multiples), 0.9314 (2 multiples), and 0 (2 multiples), that is, the matrix $\overline{A}$ is Schur stable. By Theorem 23, the system (27) via the protocol (24) achieves the formation h.

For the initial states $x_1(0) = [-9, 0.6, -18, 1.8]^T$, $x_2(0) = [12, 1.5, 27, 0.9]^T$, $x_3(0) = [-21, 1.8, 24, 2.4]^T$, and $x_4(0) = [21, 3, 27, 3.6]^T$, we get the reference state consensus function $\xi(k) = [0.75 + 1.725k, 1.725, 15 + 2.175k, 2.175]^T$ according to (25). Figure 2 shows the position and velocity trajectories of the mobile robots and the trajectory of the reference state consensus function marked by dots, and Figure 3 shows the formation evolution trajectories. From Figure 3 it is clear to see that the mobile robots achieve the expected formation, where the symbol diamond denotes the initial position, and the symbol circle denotes the position at the moment $k = 80$ of the mobile robots, respectively.

7. Conclusions

We considered the state consensus problem of high-order discrete-time linear multiagent systems with fixed directed information topology. A linear transformation approach was proposed to translate the consensus problem of multiagent systems into a partial stability problem of the corresponding transformed systems. We have shown that the approach is powerful in dealing with the three aspects of the consensus problem: (1) the criteria of global state consensus, (2) the calculation of the state consensus function, and (3) the determination the weighted matrix and the feedback gain matrix. Precisely, we have educed new necessary and sufficient consensus criteria in terms of Schur stability of a matrix related to the weighted Laplacian matrix and presented an analytical expression of the state consensus function. In addition, we have stated a design process of determining the feedback gain matrix under the condition of each agent being stabilizable. The consensus algorithm has been further applied to solve the formation control problem of multiagent systems.

Though the work in this paper focuses on the high-order discrete-time linear multiagent systems with fixed information topology and without time delay, it is undoubted that the approach can be easily extended to more complex cases, which will be dealt with in the future works.

Appendix

Proof of Lemma 3. Assuming the inverse to be $T^{-1} = \left[\overline{T}_1 \ \cdots \ \overline{T}_{N-1} \ \overline{T}_N\right]^T$ with columns $\overline{T}_i$, $i = 1, \ldots, N$, we prove that the equality $\overline{T}_N = N^{-1}\mathbf{1}_N \otimes I_n$ is correct. Since the matrix T^T is invertible and thus each column of $\overline{T}_N$ can be linearly represented by the columns of the matrix T^T, so the matrix $\overline{T}_N$ can be represented by $q_1 + q_2$, where each column of the matrix q_1 can be linearly represented by matrices T_i^T, $i = 1, \ldots, N-1$, and q_2 by those of the matrix $\mathbf{1}_N \otimes I_n$. Left multiplying $\overline{T}_N = q_1 + q_2$ by q_1^T gets $q_1^T\overline{T}_N = q_1^T q_1 + q_1^T q_2$. Because of $TT^{-1} = I_{Nn}$, one has $T_i\overline{T}_N = 0$, $i = 1, \ldots, N-1$, which implies $q_1^T\overline{T}_N = 0$. On the other hand, from the equalities $T_i(\mathbf{1}_N \otimes I_n) = 0$, $i = 1, \ldots, N-1$, one gets $T_i q_2 = 0$, $i = 1, \ldots, N-1$, which means $q_1^T q_2 = 0$. Hence, from the equality $q_1^T\overline{T}_N = q_1^T q_1 + q_1^T q_2$, one deduces $q_1^T q_1 = 0$, that is, $q_1 = 0$ and thus $\overline{T}_N = q_2$. In other words, one can write $\overline{T}_N$ into $\overline{T}_N = (\mathbf{1}_N \otimes I_n)\alpha$, where α is a matrix of the order $n \times n$. From the identity $T\overline{T} = I_{Nn}$, one has $(\mathbf{1}_N \otimes I_n)^T = I_n$, and thus, from $\overline{T}_N = (\mathbf{1}_N \otimes I_n)\alpha$ one can get $I_n = N\alpha$, that is, $\alpha = N^{-1}I_n$. Finally, one has the expression $\overline{T}_N = N^{-1}\mathbf{1}_N \otimes I_n$. □

Proof of Lemma 5. In fact, if there is $\xi(k; x(0))$ such that $\lim_{k\to\infty}\|x_i(k; x_i(0)) - \xi(k; x(0))\| = 0$, $i = 1, \ldots, N$, it follows that $\lim_{k\to\infty}\|\overline{x}_i(k)\| = 0$, $i = 1, \ldots, N-1$, in virtue of $\overline{x}_i = T_i(x - \mathbf{1}_N \otimes \xi)$, $i = 1, \ldots, N$, and therefore the necessary has been proved. Conversely, by virtue of Lemma 3, one can verify $x_i = \sum_{j=1}^{N-1}\overline{T}_{ij}\overline{x}_j + N^{-1}\overline{x}_N$, $i = 1, \ldots, N-1$. So from $\lim_{k\to\infty}\|\overline{x}_i(k)\| = 0$, $i = 1, \ldots, N-1$, it follows that $\lim_{k\to\infty}\|x_i(k) - \xi(k)\| = 0$, $i = 1, \ldots, N$, where $\xi(k) = N^{-1}\sum_{i=1}^{N} x_i(k) = N^{-1}\overline{x}_N(k)$, and thus, the sufficiency has been verified. □

Proof of Lemma 6. By observation, we only need to show that $\widetilde{T}\Psi(\mathbf{1}_N \otimes I_n) = 0$, $(\mathbf{1}_N^T \otimes I_n)\Psi\widehat{T} = -(\mathbf{1}_N^T L_w \otimes BK_2)\widehat{T}$, and $(\mathbf{1}_N^T \otimes I_n)\Psi(\mathbf{1}_N \otimes I_n) = N(A + BK_1)$. In fact, since $L_w\mathbf{1}_N = 0$, $(\mathbf{1}_N^T \otimes I_n)\widehat{T} = 0$, and $\widetilde{T}(\mathbf{1}_N \otimes I_n) = 0$, we have that

$$\begin{aligned}
&\widetilde{T}\Psi\left(\mathbf{1}_N \otimes I_n\right) \\
&\quad = \widetilde{T}\left(I_N \otimes (A + BK_1) - L_w \otimes BK_2\right)\left(\mathbf{1}_N \otimes I_n\right) \\
&\quad = \widetilde{T}\left(I_N \otimes (A + BK_1)\right)\left(\mathbf{1}_N \otimes I_n\right) \\
&\quad = \widetilde{T}\left(\mathbf{1}_N \otimes (A + BK_1)\right) = 0,
\end{aligned}$$

$$\begin{aligned}
&\left(\mathbf{1}_N^T \otimes I_n\right)\Psi\widehat{T} \\
&\quad = \left(\mathbf{1}_N^T \otimes I_n\right)\left(I_N \otimes (A+BK_1) - L_w \otimes BK_2\right)\widehat{T} \\
&\quad = \left(\mathbf{1}_N^T \otimes (A+BK_1) - \mathbf{1}_N^T L_w \otimes BK_2\right)\widehat{T} \\
&\quad = -\left(\mathbf{1}_N^T L_w \otimes BK_2\right)\widehat{T}, \\
&\left(\mathbf{1}_N^T \otimes I_n\right)\Psi\left(\mathbf{1}_N \otimes I_n\right) \\
&\quad = \left(\mathbf{1}_N^T \otimes I_n\right)\left(I_N \otimes (A+BK_1) - L_w \otimes BK_2\right)\left(\mathbf{1}_N \otimes I_n\right) \\
&\quad = \left(\mathbf{1}_N^T \otimes I_n\right)\left(I_N \otimes (A+BK_1)\right)\left(\mathbf{1}_N \otimes I_n\right) \\
&\quad = \left(\mathbf{1}_N^T \mathbf{1}_N\right) \otimes (A+BK_1) = N(A+BK_1).
\end{aligned} \tag{A.1}$$

Thus, system (9) becomes

$$\begin{aligned}
y^+ &= \widetilde{T}\Psi\widehat{T}y, \\
z^+ &= -\left(\mathbf{1}_N^T L_w \otimes BK_2\right)\widehat{T}y + (A+BK_1)z.
\end{aligned} \tag{A.2}$$

Denoting $\overline{A} = \widetilde{T}\Psi\widehat{T}$, $\overline{C} = -(\mathbf{1}_N^T L_w \otimes BK_2)\widehat{T}$, and $\overline{D} = A+BK_1$, where $\Psi = I_N \otimes (A+BK_1) - L_w \otimes BK_2$, we get (10). □

Proof of Theorem 7. The necessary and sufficient condition is verified directly by using the Lemmas 5 and 6. Now we focus on the calculation of the state consensus function. The first equation in (10) gives $y(k) = \overline{A}^k y(0)$. From the second equation in (10) we have

$$\begin{aligned}
z(k) &= \overline{C}y(k-1) + \overline{D}z(k-1) \\
&= \overline{C}y(k-1) + \overline{D}\,\overline{C}y(k-2) + \cdots \\
&\quad + \overline{D}^{k-1}\overline{C}y(0) + \overline{D}^k z(0).
\end{aligned} \tag{A.3}$$

Substituting $y(k) = \overline{A}^k y(0)$, $y(0) = \widetilde{T}x(0)$, $\overline{D} = A + BK_1$ and $z(0) = (\mathbf{1}_N^T \otimes I_n)x(0)$ into the above formula, one gets $z(k) = ((\sum_{j=0}^{k-1}(A+BK_1)^j\overline{C}\,\overline{A}^{k-1-j})\widetilde{T} + \mathbf{1}_N^T \otimes (A+BK_1)^k)x(0)$. Thus, by Lemma 5 one has the state consensus function in (11). □

Proof of Corollary 9. First of all, one easily verifies that the Schur stability of $\overline{A}$ is equivalent to Schur stability of all the matrices $A + BK_1 - \lambda_i BK_2$ by transforming $\overline{A}$ into its Jordan form. We focus on the calculation of the state consensus function. Rewrite the system (3) as $x^+ = (I_N \otimes (A+BK_1) - L_w \otimes BK_2)x$. So for the left eigenvector η with the property $\eta^T\mathbf{1}_N = 1$ of the Laplacian L_w with respect to the zero eigenvalue, we obtain $(\eta^T \otimes I_n)x^+ = (A+BK_1)(\eta^T \otimes I_n)x$. When the consensus is achieved, we have that $\xi(k) = (\eta^T \otimes I_n)x(k)$ and thus the state consensus function is $\xi(k) = (A+BK_1)^k(\eta^T \otimes I_n)x(0)$, which can be written into the form (15). □

Proof of Corollary 15. In this case, the two conditions in Corollary 11 become: (1) the matrix $-\widetilde{T}_0 L_w \widehat{T}_0$ is Hurwitz stable, that is, the digraph G admits a directed spanning tree; (2) for all the eigenvalues λ_i, $i = 1, \ldots, N-1$, of the matrix $\widetilde{T}_0 L_w \widehat{T}_0$, all the matrix $I_n - \lambda_i K_2$ are Schur stable. Let μ_j, $j = 1, \ldots, n$, be the eigenvalues of the matrix K_2. Hence, the Schur stability of the matrix $I_n - \lambda_i K_2$ is equivalent to that the products $\lambda_i\mu_j$, $i = 1, \ldots, N-1$, $j = 1, \ldots, n$, are in the open unit circle of the complex plane with the centre at $(1, 0)$.

Now we calculate the state consensus function. In this case, the state consensus function becomes $\xi(k) = N^{-1}\{\overline{C}(I_{(N-1)n} - \overline{A}^k)(I_{(N-1)n} - \overline{A})^{-1}\widetilde{T} + \mathbf{1}_N^T \otimes I_n\}x(0)$. Since $\overline{A}$ is Schur stable, instead of the previous state consensus function $\xi(k)$, we take the following state consensus value $\xi = N^{-1}\{\overline{C}(I_{(N-1)n} - \overline{A})^{-1}\widetilde{T} + \mathbf{1}_N^T \otimes I_n\}x(0)$. Since $\widetilde{T} = \widetilde{T}_0 \otimes I_n$, $\overline{A} = I_{(N-1)n} - \widetilde{T}_0 L_w \widehat{T}_0 \otimes K_2$, and $\overline{C} = -\mathbf{1}_N^T L_w \widehat{T}_0 \otimes K_2$, and noticing that $(\widetilde{T}_0 L_w \widehat{T}_0 \otimes K_2)^{-1} = (\widetilde{T}_0 L_w \widehat{T}_0)^{-1} \otimes K_2^{-1}$, the previous state consensus value can be written into (17). □

Proof of Corollary 17. Since

$$A^j = \begin{bmatrix} 1 & j \\ 0 & 1 \end{bmatrix} \otimes I_n, \tag{A.4}$$

Equation (11) becomes

$$\begin{aligned}
&\xi(k) \\
&\quad = N^{-1}\left(\left(\sum_{j=0}^{k-1}\begin{bmatrix} I_n & jI_n \\ 0 & I_n \end{bmatrix}\overline{C}\,\overline{A}^{k-1-j}\right)\widetilde{T}\right. \\
&\qquad \left. + \mathbf{1}_N^T \otimes \begin{bmatrix} I_n & kI_n \\ 0 & I_n \end{bmatrix}\right)x(0) \\
&\quad = N^{-1}\left(\left(\overline{C}\sum_{j=0}^{k-1}\overline{A}^{k-1-j} + \sum_{j=0}^{k-1}\begin{bmatrix} 0 & jI_n \\ 0 & 0 \end{bmatrix}\overline{C}\,\overline{A}^{k-1-j}\right)\widetilde{T}\right. \\
&\qquad \left. + \mathbf{1}_N^T \otimes \begin{bmatrix} I_n & kI_n \\ 0 & I_n \end{bmatrix}\right)x(0).
\end{aligned} \tag{A.5}$$

Letting

$$X = \sum_{j=0}^{k-1}\begin{bmatrix} 0 & jI_n \\ 0 & 0 \end{bmatrix}\overline{C}\,\overline{A}^{k-1-j} \tag{A.6}$$

and $j' = j + 1$, we get

$$\begin{aligned}
X &= \sum_{j'=1}^{k}\begin{bmatrix} 0 & (j'-1)I_n \\ 0 & 0 \end{bmatrix}\overline{C}\,\overline{A}^{k-1-j'+1} \\
&= \sum_{j'=1}^{k}\begin{bmatrix} 0 & j'I_n \\ 0 & 0 \end{bmatrix}\overline{C}\,\overline{A}^{k-1-j'+1} - \begin{bmatrix} 0 & I_n \\ 0 & 0 \end{bmatrix}\overline{C}\left(I_{2(N-1)n} - \overline{A}^k\right) \\
&= \sum_{j'=0}^{k-1}\begin{bmatrix} 0 & j'I_n \\ 0 & 0 \end{bmatrix}\overline{C}\,\overline{A}^{k-1-j'+1} + \begin{bmatrix} 0 & kI_n \\ 0 & 0 \end{bmatrix}\overline{C} \\
&\quad - \begin{bmatrix} 0 & I_n \\ 0 & 0 \end{bmatrix}\overline{C}\left(I_{2(N-1)n} - \overline{A}^k\right)\left(I_{2(N-1)n} - \overline{A}\right)^{-1}
\end{aligned}$$

$$= X\overline{A} + \begin{bmatrix} 0 & kI_n \\ 0 & 0 \end{bmatrix} \overline{C} - \begin{bmatrix} 0 & I_n \\ 0 & 0 \end{bmatrix} \overline{C} \left(I_{2(N-1)n} - \overline{A}^k \right) \times \left(I_{2(N-1)n} - \overline{A} \right)^{-1}. \tag{A.7}$$

Thus, we have the following:

$$X = \begin{bmatrix} 0 & kI_n \\ 0 & 0 \end{bmatrix} \overline{C} \left(I_{2(N-1)n} - \overline{A} \right)^{-1} - \begin{bmatrix} 0 & I_n \\ 0 & 0 \end{bmatrix} \overline{C} \left(I_{2(N-1)n} - \overline{A}^k \right) \left(I_{2(N-1)n} - \overline{A} \right)^{-2}. \tag{A.8}$$

Substituting it into (A.5), we get

$$\begin{aligned} \xi(k) &= N^{-1} \left\{ \left(\overline{C} \left(I_{2(N-1)n} - \overline{A}^k \right) \left(I_{2(N-1)n} - \overline{A} \right)^{-1} + \begin{bmatrix} 0 & kI_n \\ 0 & 0 \end{bmatrix} \overline{C} \left(I_{2(N-1)n} - \overline{A} \right)^{-1} - \begin{bmatrix} 0 & I_n \\ 0 & 0 \end{bmatrix} \overline{C} \left(I_{2(N-1)n} - \overline{A}^k \right) \left(I_{2(N-1)n} - \overline{A} \right)^{-2} \right) \widetilde{T} \right. \\ &\quad \left. + \mathbf{1}_N^T \otimes \begin{bmatrix} I_n & kI_n \\ 0 & I_n \end{bmatrix} \right\} x(0). \end{aligned} \tag{A.9}$$

If $\overline{A}$ is Schur stable, the consensus function above can be replaced by

$$\begin{aligned} \xi(k) &= N^{-1} \left\{ \left(\overline{C} \left(I_{2(N-1)n} - \overline{A} \right)^{-1} + \begin{bmatrix} 0 & kI_n \\ 0 & 0 \end{bmatrix} \overline{C} \left(I_{2(N-1)n} - \overline{A} \right)^{-1} - \begin{bmatrix} 0 & I_n \\ 0 & 0 \end{bmatrix} \overline{C} \left(I_{2(N-1)n} - \overline{A} \right)^{-2} \right) \widetilde{T} \right. \\ &\quad \left. + \mathbf{1}_N^T \otimes \begin{bmatrix} I_n & kI_n \\ 0 & I_n \end{bmatrix} \right\} x(0). \end{aligned} \tag{A.10}$$

□

Proof of Theorem 20. Supposed that the matrices L_w and K_1 have been given, by Corollary 11, we need only to verify that the matrix K_2 ensures that all the matrices $A + BK_1 - \lambda_i BK_2$ are Schur stable, where λ_i, $i = 1, \ldots, N-1$, are the eigenvalues of the matrix $\widetilde{T}_0 L_w \widehat{T}_0$.

It is clear that there exists $\omega > 0$ such that $|\delta_i(\omega)| \le \delta(\omega) < \delta_c$, $i = 1, \ldots, N-1$. We can verify that the following systems $\xi_i(k+1) = (A + BK_1 - \lambda_i BK_2)\xi_i(k)$, $i = 1, \ldots, N-1$, admit a common Lyapunov function $V(\xi_i) = \xi_i^H P \xi_i$. In fact, let $K_2 = \omega(B^T PB)^{-1} B^T P(A + BK_1)$, then we have that

$$\begin{aligned} \Delta V(\xi_i) &= V(\xi_i(k+1)) - V(\xi_i(k)) \\ &= \xi_i^H(k) \left(\left((A + BK_1) - \lambda_i \omega B \left(B^T PB \right)^{-1} B^T P(A + BK_1) \right)^H \times P \left((A + BK_1) - \lambda_i \omega B (B^T PB)^{-1} B^T P \times (A + BK_1) \right) - P \right) \xi_i(k) \\ &= \xi_i^H(k) \left((A + BK_1)^T P (A + BK_1) - P - \left(\left(\lambda_i^H + \lambda_i \right) \omega + \lambda_i^H \lambda_i \omega^2 \right) \times (A + BK_1)^T PB \left(B^T PB \right)^{-1} B^T P (A + BK_1) \right) \xi_i(k) \\ &= \xi_i^H(k) \left((A + BK_1)^T P (A + BK_1) - P - \left(1 - |\delta_i(\omega)|^2 \right) (A + BK_1)^T PB \left(B^T PB \right)^{-1} \times B^T P (A + BK_1) \right) \xi_i(k) \\ &\le \xi_i^H(k) \left((A + BK_1)^T P (A + BK_1) - P - (1 - \delta_i(\omega)) (A + BK_1)^T PB \left(B^T PB \right)^{-1} \times B^T P (A + BK_1) \right) \xi_i(k) \\ &< 0. \end{aligned} \tag{A.11}$$

That is, all the matrices $A + BK_1 - \lambda_i BK_2$, $i = 1, \ldots, N-1$, are Schur stable. □

Proof of Theorem 23. Let $\widetilde{x}_i = x_i - h_i$, $i = 1, \ldots, N$. Then the DLMASs (1) reach the formation h if and only if $\|(\widetilde{x}_i(k) - \widetilde{x}_j(k)\| \to \infty$ as $k \to \infty$, for all $i, j = 1, \ldots, N$. So the formation problem on the variables x_i is transformed to the consensus problem on the variables $\widetilde{x}_i$.

From (1), one gets $\widetilde{x}_i^+ = x_i^+ - h_i = A(\widetilde{x}_i + h_i) + Bu_i - h_i$, $i = 1, \ldots, N$. Substituting the protocol (24) and writing it into the vector form, we have that

$$\widetilde{x}^+ = \left(I_N \otimes (A + BK_1) - L_w \otimes BK_2 \right) \widetilde{x} + \left(I_N \otimes (A + BK_1 - I_n) \right) h. \tag{A.12}$$

Introducing the state linear transformation $\overline{x} = T\widetilde{x}$ for the linear system (A.12), one obtains

$$\overline{x}^+ = T \left(I_N \otimes (A + BK_1) - L_w \otimes BK_2 \right) T^{-1} \overline{x} + T \left(I_N \otimes (A + BK_1 - I_n) \right) h. \tag{A.13}$$

Let $y = [\overline{x}_1^T, \ldots, \overline{x}_{N-1}^T]^T$, then

$$y^+ = \left(I_{N-1} \otimes (A + BK_1) - \widetilde{T}_0 L_w \widehat{T}_0 \otimes BK_2 \right) y + \left(\widetilde{T}_0 \otimes I_N \right) \left(I_N \otimes (A + BK_1 - I_n) \right) h \tag{A.14}$$

is held. Since $y = 0$ must be the equilibrium point if the DLMASs (1) reach the formation h, one has $(\widetilde{T}_0 \otimes (A + BK_1 - I_n))h = 0$. The residuary proof is similar to that of Theorem 7. □

Acknowledgments

This work is partially supported by the National Natural Science Foundation of China (61079001 and 61273006), National High Technology Research and Development Program of China (863 Program) (2011AA110301), Specialized Research Fund for the Doctoral Program of Higher Education of China (20111103110017), Hebei Province Science and Technology Research and Development Planning Project (10203548D), and Hebei Province Science and Technology Conditions Building Program (11963546D).

References

[1] N. A. Lynch, *Distributed Algorithms*, Morgan Kaufmann, San Francisco, Calif, USA, 1997.

[2] J. Chen, M. Yu, L. H. Dou, and M. G. Gan, "A fast averaging synchronization algorithm for clock oscillators in nonlinear dynamical network with arbitrary time-delays," *Acta Automatica Sinica*, vol. 36, no. 6, pp. 873–880, 2010.

[3] J. N. Tsitsiklis and M. Athans, "Convergence and asymptotic agreement in distributed decision problems," *IEEE Transactions on Automatic Control*, vol. 29, no. 1, pp. 42–50, 1984.

[4] R. Carli, A. Chiuso, L. Schenato, and S. Zampieri, "Distributed Kalman filtering based on consensus strategies," *IEEE Journal on Selected Areas in Communications*, vol. 26, no. 4, pp. 622–633, 2008.

[5] E. Serpedin and Q. M. Chaudhari, *Synchronization in Wireless Sensor Networks: Parameter Estimation, Performance Benchmarks and Protocols*, Cambridge University Press, New York, NY, USA, 2009.

[6] R. Olfati-Saber and P. Jalalkamali, "Coupled distributed estimation and control for mobile sensor networks," *IEEE Transactions on Automatic Control*, vol. 57, no. 10, pp. 2609–2614, 2012.

[7] R. W. Beard, J. Lawton, and F. Y. Hadaegh, "A coordination architecture for spacecraft formation control," *IEEE Transactions on Control Systems Technology*, vol. 9, no. 6, pp. 777–790, 2001.

[8] W. Kang and H. H. Yeh, "Co-ordinated attitude control of multi-satellite systems," *International Journal of Robust and Nonlinear Control*, vol. 12, no. 2-3, pp. 185–205, 2002.

[9] J. A. Fax and R. M. Murray, "Information flow and cooperative control of vehicle formations," *IEEE Transactions on Automatic Control*, vol. 49, no. 9, pp. 1465–1476, 2004.

[10] W. Ren, "On consensus algorithms for double-integrator dynamics," *IEEE Transactions on Automatic Control*, vol. 53, no. 6, pp. 1503–1509, 2008.

[11] A. Karimoddini, H. Lin, B. M. Chen, and T. H. Lee, "Hybrid formation control of the unmanned aerial vehicles," *Mechatronics*, vol. 21, no. 5, pp. 886–898, 2011.

[12] J. X. Xi, N. Cai, and Y. S. Zhong, "Consensus problems for high-order linear time-invariant swarm systems," *Physica A*, vol. 389, no. 24, pp. 5619–5627, 2010.

[13] P. Wieland, R. Sepulchre, and F. Allgöwer, "An internal model principle is necessary and sufficient for linear output synchronization," *Automatica*, vol. 47, no. 5, pp. 1068–1074, 2011.

[14] W. Ren, K. L. Moore, and Y. Q. Chen, "High-order and model reference consensus algorithms in cooperative control of multi-vehicle systems," *Journal of Dynamic Systems, Measurement and Control*, vol. 129, no. 5, pp. 678–688, 2007.

[15] Z. K. Li, Z. H. Duan, G. R. Chen, and L. Huang, "Consensus of multiagent systems and synchronization of complex networks: a unified viewpoint," *IEEE Transactions on Circuits and Systems I*, vol. 57, no. 1, pp. 213–224, 2010.

[16] J. X. Xi, Z. Y. Shi, and Y. S. Zhong, "Output consensus analysis and design for high-order linear swarm systems: partial stability method," *Automatica*, vol. 48, no. 9, pp. 2335–2343, 2012.

[17] G. H. Wen, Z. S. Duan, W. W. Yu, and G. R. Chen, "Consensus in multi-agent systems with communication constraints," *International Journal of Robust and Nonlinear Control*, vol. 22, no. 2, pp. 170–182, 2012.

[18] G. H. Wen, Z. K. Li, Z. S. Duan, and G. R. Chen, "Distributed consensus control for linear multi-agent systems with discontinuous observations," *International Journal of Control*, vol. 86, no. 1, pp. 95–106, 2013.

[19] T. Vicsek, A. Czirók, E. Ben-Jacob, I. Cohen, and O. Shochet, "Novel type of phase transition in a system of self-driven particles," *Physical Review Letters*, vol. 75, no. 6, pp. 1226–1229, 1995.

[20] A. V. Savkin, "Coordinated collective motion of groups of autonomous mobile robots: analysis of Vicsek's model," *IEEE Transactions on Automatic Control*, vol. 49, no. 6, pp. 981–982, 2004.

[21] A. Jadbabaie, J. Lin, and A. S. Morse, "Coordination of groups of mobile autonomous agents using nearest neighbor rules," *IEEE Transactions on Automatic Control*, vol. 48, no. 6, pp. 988–1001, 2003.

[22] W. Ren and R. W. Beard, "Consensus seeking in multiagent systems under dynamically changing interaction topologies," *IEEE Transactions on Automatic Control*, vol. 50, no. 5, pp. 655–661, 2005.

[23] L. Xiao and S. Boyd, "Fast linear iterations for distributed averaging," *Systems & Control Letters*, vol. 53, no. 1, pp. 65–78, 2004.

[24] D. B. Kingston and R. W. Beard, "Discrete-time average-consensus under switching network topologies," in *Proceedings of the American Control Conference*, pp. 3551–3557, June 2006.

[25] T. Li and J. F. Zhang, "Consensus conditions of multi-agent systems with time-varying topologies and stochastic communication noises," *IEEE Transactions on Automatic Control*, vol. 55, no. 9, pp. 2043–2057, 2010.

[26] T. Li, M. Y. Fu, L. H. Xie, and J. F. Zhang, "Distributed consensus with limited communication data rate," *IEEE Transactions on Automatic Control*, vol. 56, no. 2, pp. 279–292, 2011.

[27] V. D. Blondel, J. M. Hendrickx, A. Olshevsky, and J. N. Tsitsiklis, "Convergence in multiagent coordination, consensus, and flocking," in *Proceedings of the 44th IEEE Conference on Decision and Control, and the European Control Conference (CDC-ECC '05)*, pp. 2996–3000, December 2005.

[28] L. Fang, P. J. Antsaklis, and A. Tzimas, "Asynchronous consensus protocols: Preliminary results, simulations and open questions," in *Proceedings of the 44th IEEE Conference on Decision and Control, and the European Control Conference (CDC-ECC '05)*, pp. 2194–2199, December 2005.

[29] L. Moreau, "Stability of multiagent systems with time-dependent communication links," *IEEE Transactions on Automatic Control*, vol. 50, no. 2, pp. 169–182, 2005.

[30] F. Xiao and L. Wang, "State consensus for multi-agent systems with switching topologies and time-varying delays," *International Journal of Control*, vol. 79, no. 10, pp. 1277–1284, 2006.

[31] F. Xiao and L. Wang, "Consensus protocols for discrete-time multi-agent systems with time-varying delays," *Automatica*, vol. 44, no. 10, pp. 2577–2582, 2008.

[32] Y. P. Gao, J. W. Ma, M. Zuo, T. Q. Jiang, and J. P. Du, "Consensus of discrete-time second-order agents with time-varying topology and time-varying delays," *Journal of the Franklin Institute*, vol. 349, no. 8, pp. 2598–2608, 2012.

[33] P. Lin and Y. M. Jia, "Consensus of second-order discrete-time multi-agent systems with nonuniform time-delays and dynamically changing topologies," *Automatica*, vol. 45, no. 9, pp. 2154–2158, 2009.

[34] M. H. Zhu and S. Martínez, "Discrete-time dynamic average consensus," *Automatica*, vol. 46, no. 2, pp. 322–329, 2010.

[35] Z. K. Li, Z. H. Duan, and G. R. Chen, "Consensus of discrete-time linear multi-agent systems with observer-type protocols," *Discrete and Continuous Dynamical Systems B*, vol. 16, no. 2, pp. 489–505, 2011.

[36] F. L. Sun, Z. H. Guan, X. S. Zhan, and F. S. Yuan, "Consensus of second-order and high-order discrete-time multi-agent systems with random networks," *Nonlinear Analysis: Real World Applications*, vol. 13, no. 5, pp. 1979–1990, 2012.

[37] Q. Z. Huang, "Consensus analysis of multi-agent discrete-time systems," *Acta Automatica Sinica*, vol. 38, no. 7, pp. 1127–1133, 2012.

[38] K. Y. You and L. H. Xie, "Network topology and communication data rate for consensusability of discrete-time multi-agent systems," *IEEE Transactions on Automatic Control*, vol. 56, no. 10, pp. 2262–2275, 2011.

[39] G. X. Gu, L. Marinovici, and F. L. Lewis, "Consensusability of discrete-time dynamic multiagent systems," *IEEE Transactions on Automatic Control*, vol. 57, no. 8, pp. 2085–2089, 2012.

[40] R. A. Horn and C. R. Johnson, *Matrix Analysis*, Cambridge University Press, Cambridge, UK, 1985.

[41] V. I. Vorotnikov, *Partial Stability and Control*, Birkhäuser, Basel, Switzerland, 1998.

Hindawi Publishing Corporation
Mathematical Problems in Engineering
Volume 2013, Article ID 498739, 8 pages
http://dx.doi.org/10.1155/2013/498739

Research Article

Design of an Attitude and Heading Reference System Based on Distributed Filtering for Small UAV

Long Zhao[1] and Qing Yun Wang[2]

[1] *Science and Technology on Aircraft Control Laboratory, Beihang University, Beijing 100191, China*
[2] *School Aeronautic Science and Engineering, Beihang University, Beijing 100191, China*

Correspondence should be addressed to Qing Yun Wang; nmqingyun@163.com

Received 8 April 2013; Accepted 22 May 2013

Academic Editor: Wenwu Yu

A development procedure for a low-cost attitude and heading reference system (AHRS) based on the distributed filter has been proposed. The AHRS consists of three single-axis accelerometers, three single-axis gyroscopes, and one 3-axis digital compass. The initial attitude estimation is readily accomplished by using the complementary filtering. The attitude estimation for UAV flying in the real time is realized by using the three low orders EKF. The validation results show that the estimated orientations of the developed AHRS are within the acceptable region, and AHRS can give a stabilized attitude and heading information for a long time.

1. Introduction

Recent advances in autonomous vehicle technologies have made unmanned aerial vehicles (UAV) to become an attractive solution for the modern military and civilian applications such as aerial surveying, pipeline and power line inspection, post-disaster assessment, remote sensing, and cruise missiles [1, 2]. A 2011 report by the Teal Group, who is specialized in aerospace market analysis, forecasts that UAV expenditures worldwide will double within the next ten years to reach $11.3 billion dollars annually in 2020 [3]. By 2018, analysts expect that over 15,000 UAVs could be operating within United States Airspace [4]. Commonly, it needs to know the UAV's orientation, velocity, and position to be operated, whether manually or with computer assistance. When cost or weight is an issue, inertial navigation using very accurate inertial sensors has been excluded. Instead, low-cost systems using inertial sensors based on microelectromechanical systems (MEMS) have been widely used. To ensure safe and reliable flight of UAV, an accurate attitude and heading reference system (AHRS) is a key component and can give information about the UAV's orientation in three-dimensional spaces. MEMS-based AHRS are of low cost, light weight, and consume little power. However, the advantages of inexpensive MEMS sensors are coupled with the drawback of having greater potential error in reported roll, pitch, and yaw due to increased sensor noise and drift. Most of the previous works at fusing are based on inertial sensors with GPS for attitude determination [5, 6]. However, GPS signals are susceptible to interference and deception. GPS is unreliable in hostile jammed environments or caused by shadowing effects since the possibility of the outage of GPS. More importantly, the transmitters cannot afford long-term, stable, and reliable positioning information because of the risk of destruction. Recently, many AHRS based on low-cost MEMS gyroscopes, accelerometers, and magnetometers have been developed [7–10]. A number of estimation filters have been proposed since 1970s. The basic idea is to blend several different measurements to obtain the best approximation of the signals. Although many filtering techniques have been proposed and studied to design observers for attitude determination [11–15], the Extended Kalman Filter (EKF) is still one of the most well-known and widely adopted filtering algorithms to design such estimators [16, 17]. The Kalman filter provides the best estimates based on the system dynamics and a priori knowledge of the noise characteristics of the signals. However, EKF divergence due to the linearization of the system and large-state initialization error is a frequent stumbling

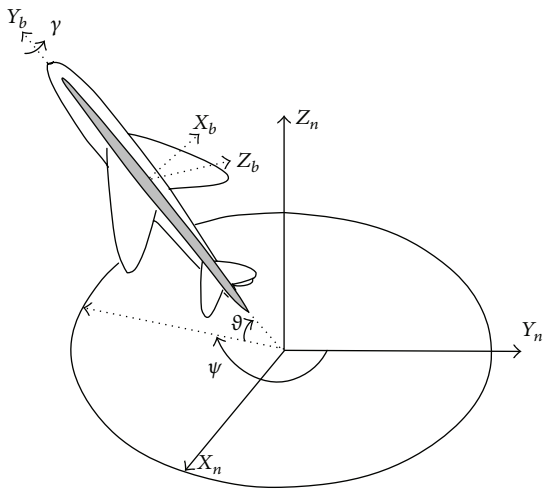

Figure 1: b frame, n frame, and Euler angles.

block to the implementation of the filter. Major difficulties when implementing a centralized Kalman filter (CKF) on a microcontroller arise from the complexity caused by the need for inverting certain matrices. This problem is exacerbated by the need to implement an EKF in case the system is nonlinear and with a large number of states. In contrast to the CKF, the distributed filter is simple, easy to implement, and it has been successfully used for decades on a low-performance microcontroller [18].

The attitude and heading estimation filter proposed in this work is based on the distributed filtering theory, initial attitude estimation is based on the complementary filtering theory, and the real-time attitude estimation will use the three low orders EKF for UAV flying.

The paper is organized as follows. The design of attitude estimation filter is presented in Section 2. Section 3 focuses on the implementation of the attitude estimation filter. Experimental results obtained during UAV flying are presented in Section 4 to illustrate the performance of the proposed AHRS. Concluding remarks and future work are pointed out in Section 5.

2. Problem Statement and System Design

The Euler angles describe the body-axis orientation of UAV body coordinate frame (b frame) in North, East, and Up navigation coordinates frame (n frame). Here, ψ is the yaw angle, ϑ is the pitch angle, and γ is the roll angle, as illustrated in Figure 1. The initial attitude and heading of the UAV are needed to initialize the AHRS. When UAV is stationary, Initial attitude and heading of UAV are computed by accelerators and digital compass. The calculation formulas are described as follows:

$$\gamma = \tan^{-1}\left(\frac{f_x^b}{\left(-f_z^b\right)}\right),$$

$$\theta = \tan^{-1}\left(\frac{f_y^b}{\left(\sqrt{f_x^{b2} + f_z^{b2}}\right)}\right),$$

$$\widehat{\psi}_m = \tan^{-1}\left(\frac{m_x^b \cos\widehat{\gamma} + m_z^b \sin\widehat{\gamma}}{m_x^b \sin\widehat{\gamma}\sin\widehat{\vartheta} + m_y^b \cos\widehat{\vartheta} - m_z^b \cos\widehat{\gamma}\sin\widehat{\vartheta}}\right), \tag{1}$$

where, f_x^b, f_y^b, and f_z^b are the specific force of the accelerometers in body coordinate frame (b frame). m_x^b, m_y^b, and m_z^b are the components of the magnetic field strength in body coordinate frame.

However, stationary UAV is difficult owing to wind and engine vibration in actual test, the initial attitude and heading are seriously influenced by high-frequency noise when the initial attitude and heading are computed by using (1). When the condition of UAV is stationary or low dynamic, the attitude and heading of UAV are accurate and have good low-pass property. However, the error of attitude and heading computed from the gyroscopes output is large since it is easily influenced by drift of the gyroscope. There is complementary property between the attitude derived from the gyroscope outputs and the attitude derived from the accelerometer outputs. The complementary filters theory provides an estimate of the true signal by employing two complementary high-pass and low-pass filters, and an unknown signal can be estimated using corrupted measurements from one or more sensors whose information naturally stands in distinct and complementary frequency bands [19–21]. The initial attitude estimation filter based on complementary filter is to pass the attitude derived from the gyroscope through a high-pass filter and the attitude derived from the accelerometer through a low-pass filter and then to fuse those signals to obtain the estimated attitude; thus, compensating for the drift on the gyroscope and for the slow dynamics of the accelerometer, the block is shown in Figure 2.

The real attitude and heading are processed on an embedded processor in actual flying test, major difficulties when implementing a centralized extended Kalman filter (CEKF) on a embedded processor arise from the complexity caused by the need of the Jacobian matrix computing and the system equation linearizing, and this problem is exacerbated by the need to implement an EKF with a large number of states. To solve this problem, the attitude and heading estimation filter based on the distributed filtering is designed and completed, three low-order parallel EFK are implemented on the ARM 9 embedded processor. The block diagram of the orientation estimating filter based on the distributed filtering is shown in Figure 3.

3. Attitude and Heading Estimation Filter

3.1. Initial Alignment Filter. Complementary filters have been widely used to combine two independent noisy measurements of the same signal, where each measurement is corrupted by different types of spectral noise [19]. The complementary filters have first-order filter and second-order

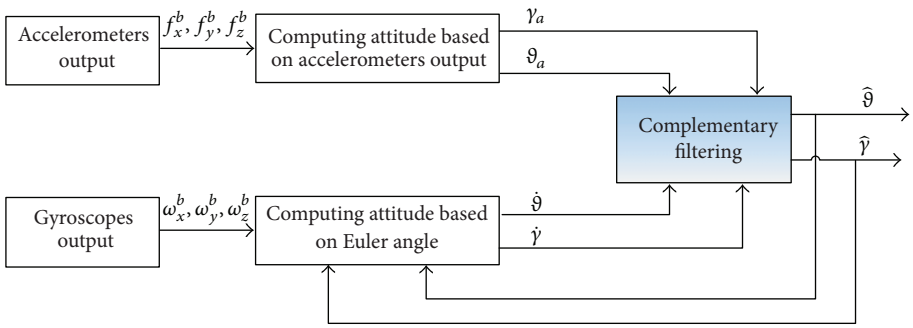

Figure 2: Flow diagram of complementary filtering.

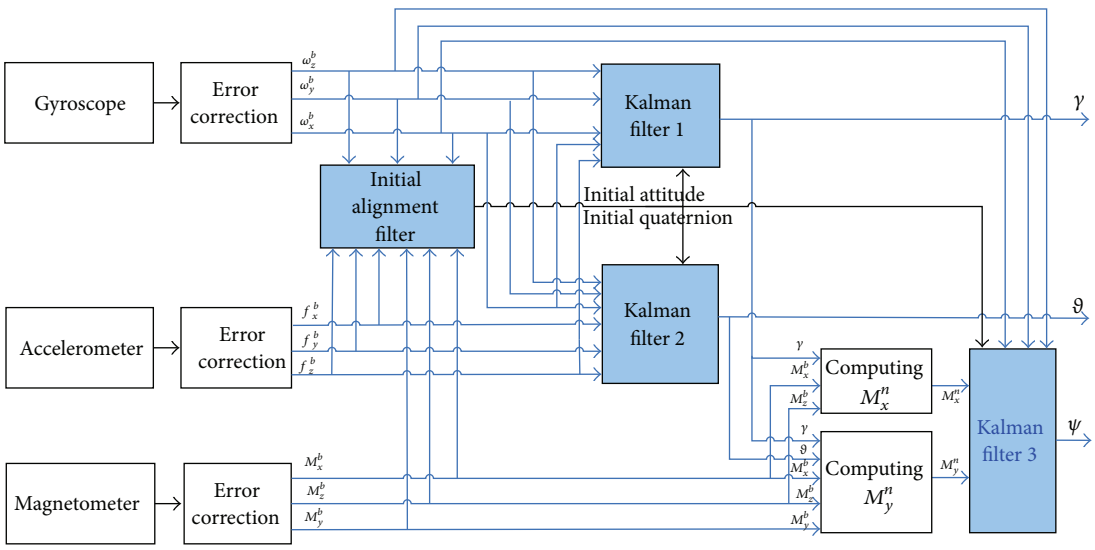

Figure 3: Design of the orientation estimating filter based on the distributed filtering.

filter; the second-order complementary filter consists of a second-order high-pass filter and a second-order low-pass filter. The second-order complementary filter of the attitude is described as follows [22]:

$$\begin{aligned}\hat{\gamma} &= \frac{\omega_0^2\left(2\varsigma/\omega_0\right)D}{D^2+2\varsigma\omega_0 D+\omega_0^2}\gamma_a + \frac{D^2}{D^2+2\varsigma\omega_0 D+\omega_0^2}\gamma,\\ \hat{\vartheta} &= \frac{\omega_0^2\left(2\varsigma/\omega_0\right)D}{D^2+2\varsigma\omega_0 D+\omega_0^2}\vartheta_a + \frac{D^2}{D^2+2\varsigma\omega_0 D+\omega_0^2}\vartheta,\end{aligned} \tag{2}$$

where D is the differential operator, ω_0 is the natural frequency, and ς is the damping ratio.

With the estimated roll and pitch, the yaw can be derived from the measured strength of the magnetic field in body coordinate frame by the digital compass:

$$\begin{aligned}\hat{\psi}_m &= \tan^{-1}\left(\frac{M_x^n}{M_y^n}\right)\\ &= \tan^{-1}\left(\frac{m_x^b\cos\hat{\gamma}+m_z^b\sin\hat{\gamma}}{m_x^b\sin\hat{\gamma}\sin\hat{\vartheta}+m_y^b\cos\hat{\vartheta}-m_z^b\cos\hat{\gamma}\sin\hat{\vartheta}}\right),\end{aligned} \tag{3}$$

where m_x^n, m_y^n, and m_z^n are the components of the magnetic field strength in navigation coordinate frame (n frame). The relationship between real heading ψ_m and $\hat{\psi}_m$ is described as follows [23]:

$$\psi_m = \begin{cases}\hat{\psi}_m, & M_y^n > 0,\ \hat{\psi}_m > 0,\\ \hat{\psi}_m + 2\pi, & M_y^n > 0,\ \hat{\psi}_m < 0,\\ \hat{\psi}_m + \pi, & M_y^n < 0.\end{cases} \tag{4}$$

3.2. Attitude and Heading Estimation Filter. According to the initial attitude and heading, the initial strapdown attitude matrix is computed as follow [23]:

$$\begin{aligned}T_b^n &= \begin{bmatrix}T_{11} & T_{12} & T_{13}\\ T_{21} & T_{22} & T_{23}\\ T_{31} & T_{32} & T_{33}\end{bmatrix}\\ &= \begin{bmatrix}q_0^2+q_1^2-q_2^2-q_3^2 & 2(q_1q_2-q_0q_3) & 2(q_1q_3+q_0q_2)\\ 2(q_1q_2+q_0q_3) & q_0^2-q_1^2+q_2^2-q_3^2 & 2(q_2q_3-q_0q_1)\\ 2(q_1q_3-q_0q_2) & 2(q_2q_3+q_0q_1) & q_0^2-q_1^2-q_2^2+q_3^2\end{bmatrix}.\end{aligned} \tag{5}$$

Table 1: The error between AHRS outputs and the reference values for the dynamic test on the ground.

	Pitch angle error (°)		Roll angle error (°)		Yaw angle error (°)	
	Mean	Variance	Mean	Variance	Mean	Variance
Dynamic test	−0.017	0.069	−0.056	0.089	−0.013	0.150

Attitude and heading estimation depend on the updated quaternion; the system state equation selected the system state $X = [q_0 \;\; q_1 \;\; q_2 \;\; q_3]^T$ is built as follows:

$$\begin{aligned}\dot{X} &= \begin{bmatrix}\dot{q}_0\\ \dot{q}_1\\ \dot{q}_2\\ \dot{q}_3\end{bmatrix} = \frac{1}{2}\begin{bmatrix}0 & -\widehat{\omega}_x^b & -\widehat{\omega}_y^b & -\widehat{\omega}_z^b\\ \widehat{\omega}_x^b & 0 & \widehat{\omega}_z^b & -\widehat{\omega}_y^b\\ \widehat{\omega}_y^b & -\widehat{\omega}_z^b & 0 & \widehat{\omega}_x^b\\ \widehat{\omega}_z^b & \widehat{\omega}_y^b & -\widehat{\omega}_x^b & 0\end{bmatrix}\begin{bmatrix}q_0\\ q_1\\ q_2\\ q_3\end{bmatrix}\\ &= \frac{1}{2}\begin{bmatrix}0 & -\omega_x^b & -\omega_y^b & -\omega_z^b\\ \omega_x^b & 0 & \omega_z^b & -\omega_y^b\\ \omega_y^b & -\omega_z^b & 0 & \omega_x^b\\ \omega_z^b & \omega_y^b & -\omega_x^b & 0\end{bmatrix}\begin{bmatrix}q_0\\ q_1\\ q_2\\ q_3\end{bmatrix}\\ &\quad + \frac{1}{2}\begin{bmatrix}q_1 & q_2 & q_3\\ -q_0 & q_3 & -q_2\\ -q_3 & -q_0 & q_1\\ q_2 & -q_1 & -q_1\end{bmatrix}\begin{bmatrix}\delta_x^b\\ \delta_y^b\\ \delta_z^b\end{bmatrix}\\ &= F(t)X(t) + G(t)W(t),\end{aligned} \tag{6}$$

where $\widehat{\omega}^b = \left[\widehat{\omega}_x^b \;\; \widehat{\omega}_y^b \;\; \widehat{\omega}_z^b\right]^T = \left[\omega_x^b - \delta_x^b \;\; \omega_y^b - \delta_y^b \;\; \omega_z^b - \delta_z^b\right]^T$, $\omega^b = \left[\omega_x^b \;\; \omega_y^b \;\; \omega_z^b\right]^T$, and $\delta^b = \left[\delta_x^b \;\; \delta_y^b \;\; \delta_z^b\right]^T$ is the ideal value, real output value, and drift of gyroscopes in body coordinate frame (b frame), respectively. $F(t)$ is the state transition matrix; $G(t)$ is the covariance matrix of noise.

According to (1) and (5), the measurement equation is built by the attitude derived from the gyroscope output and the attitude derived from the accelerometers output. The measurement equation is described as follows:

$$Z(t) = \begin{bmatrix}Z_1(t)\\ Z_2(t)\\ Z_3(t)\end{bmatrix} = \begin{bmatrix}\Delta\psi\\ \Delta\vartheta\\ \Delta\gamma\end{bmatrix} = \begin{bmatrix}\psi_m - \psi_q\\ \vartheta_a - \vartheta_q\\ \gamma_a - \gamma_q\end{bmatrix} = H(t,q) + V(t), \tag{7}$$

where $Z(t) = [\delta\psi \;\; \delta\vartheta \;\; \delta\lambda]^T$ is the error of the attitude and heading. ψ_m is the yaw derived from the digital compass. ϑ_a and γ_a is respectively the pitch, and roll derived from the accelerators; the computing equations are described in (1) ψ_q, ϑ_q, and γ_q is respectively the yaw, pitch, and roll derived

Figure 4: Self-developed autopilot from DNC.

from the quaternion, the computing equation is described as follows [23]:

$$\begin{aligned}\psi_q &= \tan^{-1}\left(\frac{2(q_1q_2 - q_0q_3)}{q_0^2 - q_1^2 + q_2^2 - q_3^2}\right),\\ \vartheta_q &= \sin^{-1}(2q_2q_3 + 2q_0q_1),\\ \gamma_q &= \tan^{-1}\left(\frac{2(q_1q_3 - q_0q_2)}{q_0^2 - q_1^2 - q_2^2 + q_3^2}\right).\end{aligned} \tag{8}$$

The measurement matrix (See Appendix) is obtained by linearizing (6) and (7):

$$\begin{aligned}H &= \left[\frac{\partial\Delta\psi}{\partial X} \;\; \frac{\partial\Delta\vartheta}{\partial X} \;\; \frac{\partial\Delta\gamma}{\partial X}\right]^T,\\ \frac{\partial\Delta\psi}{\partial X} &= \left[\frac{\partial\Delta\psi}{\partial q_0} \;\; \frac{\partial\Delta\psi}{\partial q_1} \;\; \frac{\partial\Delta\psi}{\partial q_2} \;\; \frac{\partial\Delta\psi}{\partial q_3}\right],\\ \frac{\partial\Delta\vartheta}{\partial X} &= \left[\frac{\partial\Delta\vartheta}{\partial q_0} \;\; \frac{\partial\Delta\vartheta}{\partial q_1} \;\; \frac{\partial\Delta\vartheta}{\partial q_2} \;\; \frac{\partial\Delta\vartheta}{\partial q_3}\right],\\ \frac{\partial\Delta\gamma}{\partial X} &= \left[\frac{\partial\Delta\gamma}{\partial q_0} \;\; \frac{\partial\Delta\gamma}{\partial q_1} \;\; \frac{\partial\Delta\gamma}{\partial q_2} \;\; \frac{\partial\Delta\gamma}{\partial q_3}\right].\end{aligned} \tag{9}$$

The quaternion is updated by (6) and (7), the principal value of pitch, roll and yaw are derived from the updated T_b^n [23], for example,

$$\begin{aligned}\vartheta_p &= \sin^{-1}(T_{32}),\\ \gamma_p &= \tan^{-1}\left(\frac{-T_{31}}{T_{33}}\right),\\ \psi_p &= \tan^{-1}\left(\frac{-T_{12}}{T_{22}}\right).\end{aligned} \tag{10}$$

Table 2: The attitude error between AHRS outputs and MIMU/GPS integrated system outputs for flight test.

	Pitch angle error (°)		Roll angle error (°)		Yaw angle error (°)	
	Mean	Variance	Mean	Variance	Mean	Variance
Flighting test	1.84	3.73	−1.12	4.43	—	—

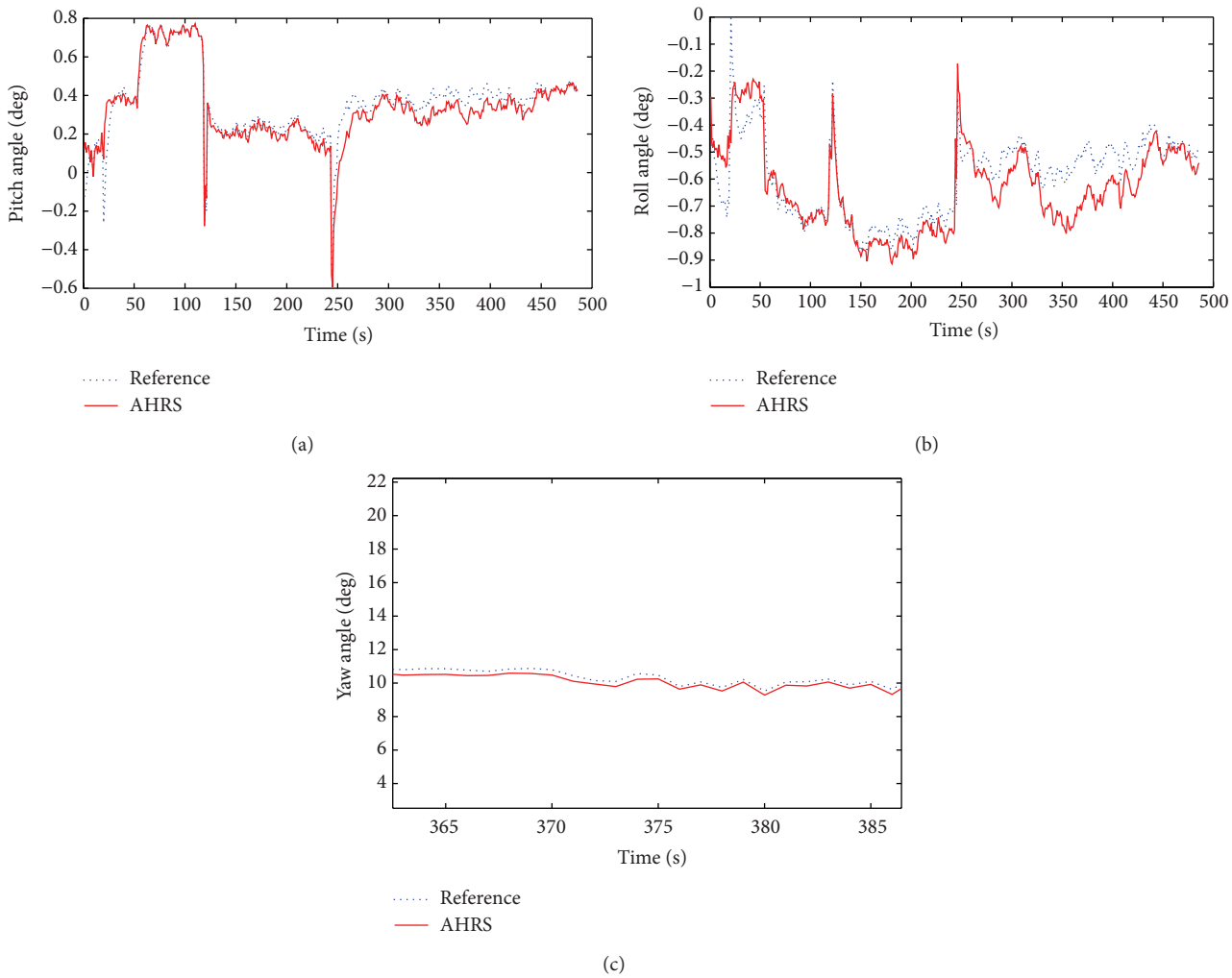

Figure 5: AHRS outputs and the reference values for the dynamic test on the ground, (a) pitch, (b) roll, and (c) yaw.

The domain of yaw, pitch, and roll is $[0^\circ \ 360^\circ]$, $[-90^\circ \ 90^\circ]$ and $[-180^\circ \ 180^\circ]$, respectively. The domain and range of pitch are the same; the real value of pitch is the principal value, for example, $\vartheta = \vartheta_p$. The real value of yaw and roll is computed as follows, respectively [23],

$$\gamma = \begin{cases} \gamma_p, & T_{33} > 0, \\ \gamma_p + \pi, & T_{33} < 0, \ \gamma_p < 0, \\ \gamma_p - \pi, & T_{33} < 0, \ \gamma_p > 0, \end{cases}$$
$$\psi = \begin{cases} \psi_p, & T_{22} < 0, \\ \psi_p + 2 \cdot \pi, & T_{22} > 0, \ \psi_p > 0, \\ \psi_p + \pi, & T_{22} > 0, \ \psi_p < 0. \end{cases} \tag{11}$$

4. Experimental Test and Results Analysis

Experiments are conducted using an autopilot self-developed from Digital Navigation Center (DNC), BUAA (see Figure 4). This system is composed of three single-axis accelerometers, three single-axis gyroscopes, one 3-axis digital compass, one barometer, one airspeed meter, and one Global Positioning System (GPS) receiver. In order to test the proposed attitude and heading calculation method based on distributed filtering, the dynamic test on the ground and flying test are implemented by using the autopilot from DNC. In the process of dynamic testing, the autopilot is put on the ground, the pitch and roll of UAV do not change, the autopilot is turned around the z axis from the initial yaw to 360°, the yaw is turned to make a quarter turn, and the autopilot is

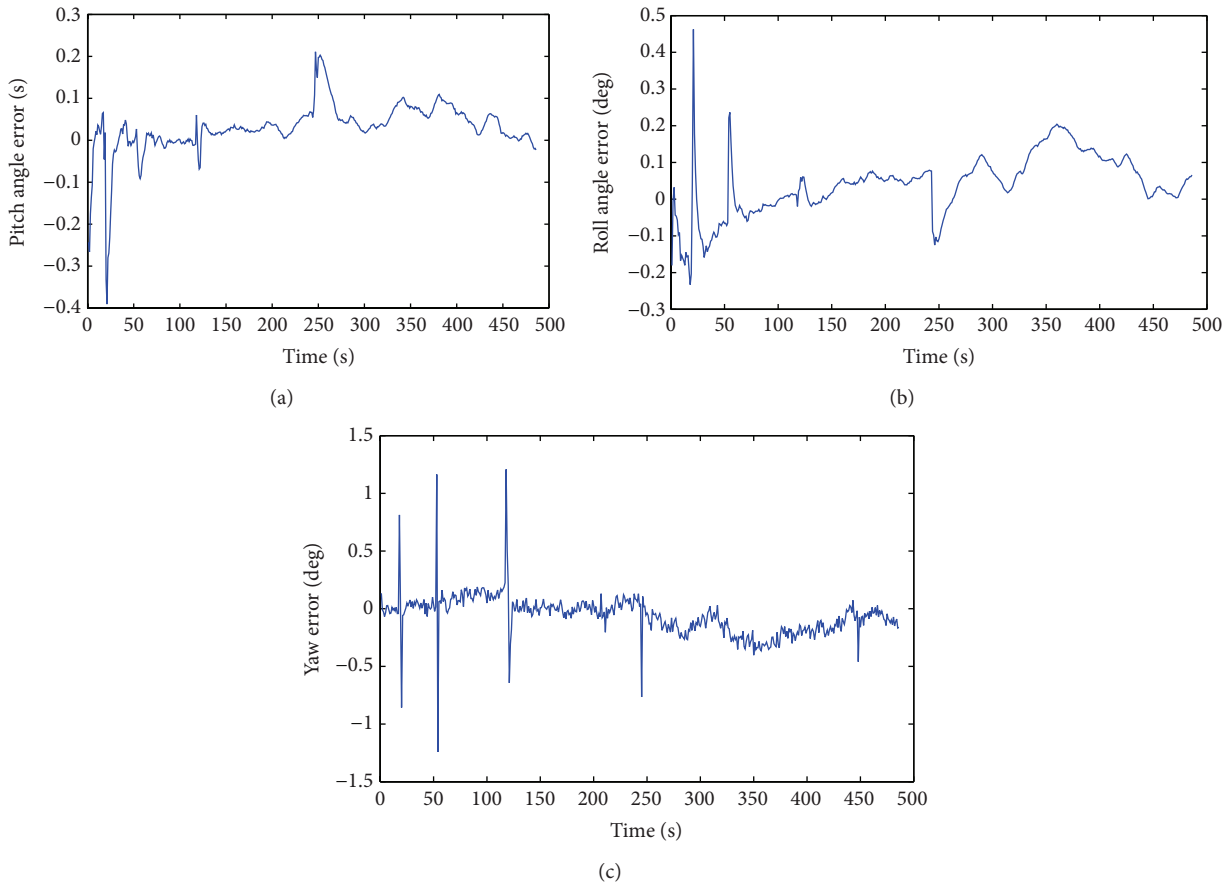

Figure 6: The error between AHRS outputs and the reference values for the dynamic test on the ground, (a) pitch error, (b) roll error, and (c) yaw error.

stationary for a period of time. The outputs of the AHRS and the reference values for the dynamic test on the ground is represented in Figure 5. The error between of AHRS outputs and the reference values are represented in Figure 6 and Table 1.

Seen from Figures 5 and 6, and Table 1 the attitude calculated output from the AHRS system this paper proposed is stable and can track the reference value. The pitch, roll, and yaw have big fluctuation because when the yaw is turned manually, the MIMU cannot maintain horizontality, and the precision of pitch, roll, and yaw is 0.069°, 0.089°, and 0.15°, respectively.

In order to further test the AHRS system this article proposed, the flight test is carried out using a fixed-wing UAV. After the plane takes off through manual manipulation, the condition is changed to automated driving condition during aircruise phases and the acceleration, gyroscope, and magnetic compass data are stored in an SD card. The test verification is based on the actual data and the results are shown in Figure 7 and Table 2.

Seen from Figure 7 and Table 2, the attitude calculated output from the AHRS system this paper proposed is also stable under the dynamic condition through actual flight test. The attitude error between AHRS outputs and reference value is small and the precisions of pitch and roll are 3.73° and 4.43°, respectively. So, AHRS can give a stabilized attitude and heading information in long time.

5. Conclusions

In this paper, based on the distributed filter, the low-cost attitude and heading reference system has been developed. The dynamic test on the ground and actual flight test are implemented, and the test results show that the presented AHRS based on the distributed filter can give the stabilized attitude and heading information for a long time and can implement the automatic flight control of UAV.

Appendix

The attitude and heading based on quaternion were updated as follows:

$$\psi = \tan^{-1}\left(\frac{2\left(q_1q_2 - q_0q_3\right)}{q_0^2 - q_1^2 + q_2^2 - q_3^2}\right),$$

$$\vartheta = \sin^{-1}\left(2q_2q_3 + 2q_0q_1\right),$$

$$\gamma = \tan^{-1}\left(\frac{2\left(q_1q_3 - q_0q_2\right)}{q_0^2 - q_1^2 - q_2^2 + q_3^2}\right),$$

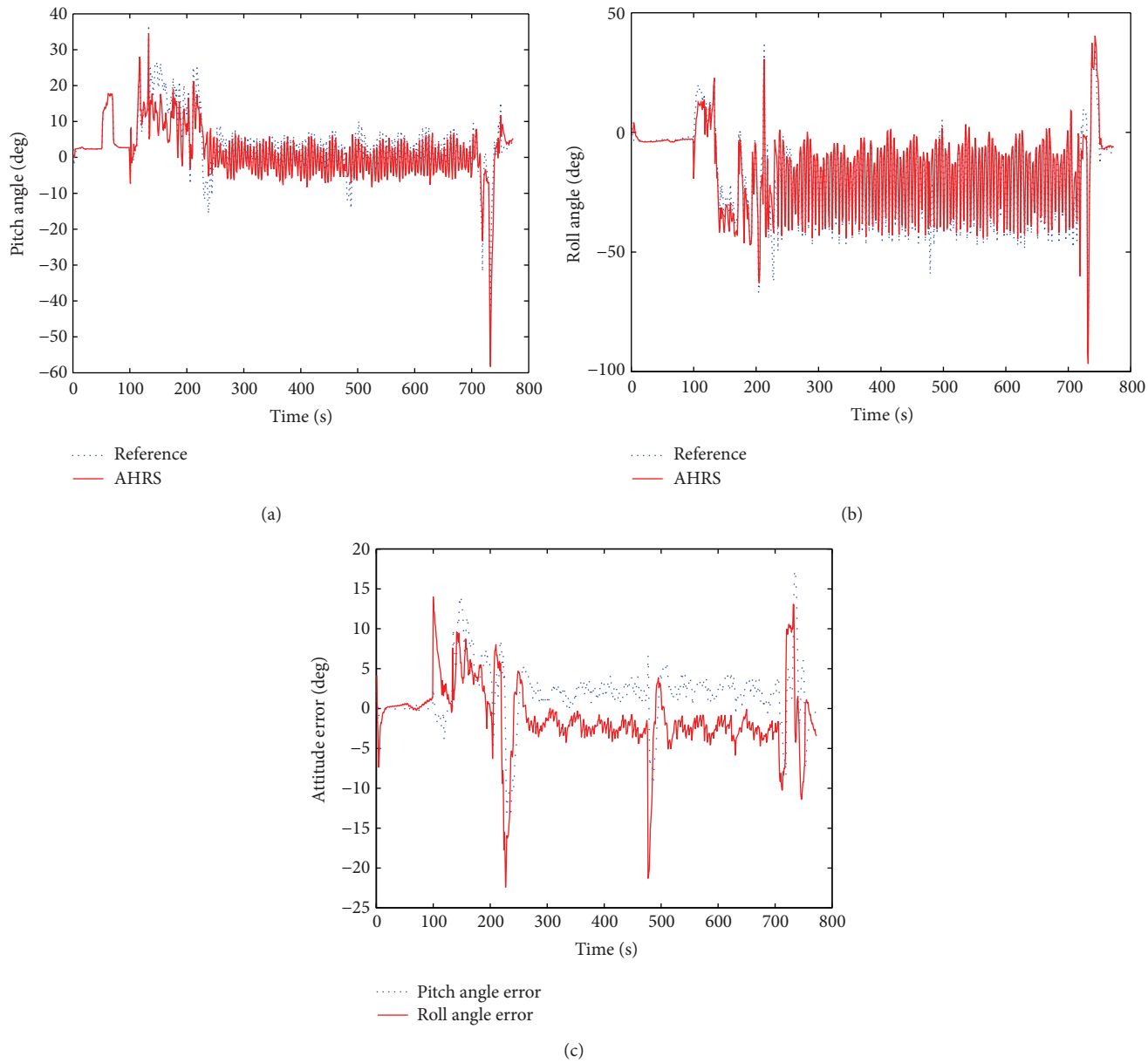

Figure 7: Results of AHRS for fixed-wing UAV flight test, (a) pitch, (b) roll, and (c) attitude error.

$$\frac{\partial\psi}{\partial q_0} = \frac{-2q_3\left(q_0^2 - q_1^2 + q_2^2 - q_3^2\right) - 4q_0\left(q_1q_2 - q_0q_3\right)}{4(q_1q_2 - q_0q_3)^2 + (q_0^2 - q_1^2 + q_2^2 - q_3^2)^2},$$

$$\frac{\partial\psi}{\partial q_1} = \frac{2q_2\left(q_0^2 - q_1^2 + q_2^2 - q_3^2\right) + 4q_1\left(q_1q_2 - q_0q_3\right)}{4(q_1q_2 - q_0q_3)^2 + (q_0^2 - q_1^2 + q_2^2 - q_3^2)^2},$$

$$\frac{\partial\psi}{\partial q_2} = \frac{2q_1\left(q_0^2 - q_1^2 + q_2^2 - q_3^2\right) - 4q_2\left(q_1q_2 - q_0q_3\right)}{4(q_1q_2 - q_0q_3)^2 + (q_0^2 - q_1^2 + q_2^2 - q_3^2)^2},$$

$$\frac{\partial\psi}{\partial q_3} = \frac{-2q_0\left(q_0^2 - q_1^2 + q_2^2 - q_3^2\right) + 4q_3\left(q_1q_2 - q_0q_3\right)}{4(q_1q_2 - q_0q_3)^2 + (q_0^2 - q_1^2 + q_2^2 - q_3^2)^2},$$

$$\frac{\partial\vartheta}{\partial q_0} = \frac{2q_1}{\sqrt{1 - (2(q_0q_1 + q_2q_3))^2}},$$

$$\frac{\partial\vartheta}{\partial q_1} = \frac{2q_0}{\sqrt{1 - (2(q_0q_1 + q_2q_3))^2}},$$

$$\frac{\partial\vartheta}{\partial q_2} = \frac{2q_3}{\sqrt{1 - (2(q_0q_1 + q_2q_3))^2}},$$

$$\frac{\partial\vartheta}{\partial q_3} = \frac{2q_2}{\sqrt{1 - (2(q_0q_1 + q_2q_3))^2}},$$

$$\frac{\partial\gamma}{\partial q_0} = \frac{-2q_2\left(q_0^2 - q_1^2 - q_2^2 + q_3^2\right) - 4q_0\left(q_1q_3 - q_0q_2\right)}{4(q_1q_3 - q_0q_2)^2 + \left(q_0^2 - q_1^2 - q_2^2 + q_3^2\right)^2},$$

$$\frac{\partial\gamma}{\partial q_1} = \frac{2q_3\left(q_0^2 - q_1^2 - q_2^2 + q_3^2\right) + 4q_1\left(q_1q_3 - q_0q_2\right)}{4(q_1q_3 - q_0q_2)^2 + \left(q_0^2 - q_1^2 - q_2^2 + q_3^2\right)^2},$$

$$\frac{\partial\gamma}{\partial q_2} = \frac{-2q_0\left(q_0^2 - q_1^2 - q_2^2 + q_3^2\right) + 4q_2\left(q_1q_3 - q_0q_2\right)}{4(q_1q_3 - q_0q_2)^2 + \left(q_0^2 - q_1^2 - q_2^2 + q_3^2\right)^2},$$

$$\frac{\partial\gamma}{\partial q_3} = \frac{2q_1\left(q_0^2 - q_1^2 - q_2^2 + q_3^2\right) - 4q_3\left(q_1q_3 - q_0q_2\right)}{4(q_1q_3 - q_0q_2)^2 + \left(q_0^2 - q_1^2 - q_2^2 + q_3^2\right)^2}. \tag{A.1}$$

Acknowledgments

This project is supported by the Key Program of the National Natural Science Foundation of China (Grant no. 61039003), the National Natural Science Foundation of China (Grant no. 41274038), the Aeronautical Science Foundation of China (Gratis no. 20100851018), and the Aerospace Innovation Foundation of China (CASC201102).

References

[1] T. H. Cox, C. J. Nagy, M. A. Skoog, and I. A. Somers, "Civil UAV capabil it y assessment," *The National Aeronautics and Space Administration*, pp. 1–10, 2006.

[2] Z. Wachter, "A cost effective motion platform for performance testing of MEMS-based attitude and heading reference systems," *Journal of Intelligent & Robotic Systems*, vol. 70, no. 411, pp. 1–9, 2013.

[3] S. J. Zaloga, D. Rockwell, and P. Finnegan, *World Unmanned Aerial Vehicle Systems Market Profile and Forecast*, Teal Group Corporation, 2011.

[4] R. Schneiderman, "Unmanned drones are flying high in the military/aerospace sector," *IEEE Signal Processing Magazine*, vol. 29, no. 1, pp. 8–11, 2012.

[5] R. Wolf, G. W. Hein, B. Eissfeller, and E. Loehnert, "Integrated low cost GPS/INS attitude determination and position location system," in *Proceedings of the 9th International Technical Meeting of the Satellite Division of the Institute of Navigation (ION GPS '96)*, pp. 975–981, September 1996.

[6] Y. Li, A. Dempster, B. H. Li, J. L. Wang, and C. Rizos, "A low-cost at t itude heading reference system by combinat ion of GPS and magnetometers and MEMS inert ial sensors for mobile applicat ions," *Journal of Global Positioning Systems*, vol. 5, no. 1-2, pp. 88–95, 2006.

[7] P. Martin and E. Salaün, "Design and implementation of a low-cost aided attitude and heading reference system," in *Proceedings of the AIAA Guidance, Navigation, and Control Conference*, 2008.

[8] W. Geiger, J. Bartholomeyczik, U. Breng et al., "MEMS IMU for AHRS applications," in *Proceedings of the IEEE/ION Position, Location and Navigation Symposium (PLANS '08)*, pp. 225–231, May 2008.

[9] S. Sukkarieh, P. Gibbens, B. Grocholsky, K. Willis, and H. F. Durrant-Whyte, "Low-cost, redundant inertial measurement unit for unmanned air vehicles," *International Journal of Robotics Research*, vol. 19, no. 11, pp. 1089–1103, 2000.

[10] L. Sherry, C. Brown, B. Motazed, and D. Vos, "Performance of automotive-grade MEMS sensors in low cost AHRS for general aviation," in *Proceeding of the 22nd Digital Avionics Systems Conference*, vol. 2, pp. 12.C.2/1–12.C.2/5, October 2003.

[11] M. L. Psiaki, "Attitude-determination filtering via extended quaternion estimation," *Journal of Guidance, Control, and Dynamics*, vol. 23, no. 2, pp. 206–214, 2000.

[12] J. L. Marins, X. Yun, E. R. Bachmann, R. B. McGhee, and M. J. Zyda, "An extended Kalman filter for quaternion-based orientation estimation using MARG sensors," in *Proceedings of the IEEE/RSJ International Conference on Intelligent Robots and Systems*, pp. 2003–2011, November 2001.

[13] J. L. Crassidis, "Sigma-point Kalman filtering for integrated GPS and inertial navigation," *IEEE Transactions on Aerospace and Electronic Systems*, vol. 42, no. 2, pp. 750–756, 2006.

[14] R. D. Van Merwe, E. A. Wan, and S. I. Julier, "Sigma-point kalman filters for nonlinear estimation and sensor-fusion—applications to integrated navigation," in *Proceedings of the AIAA Guidance, Navigation, and Control Conference*, pp. 1735–1764, August 2004.

[15] C. Hide, T. Moore, and M. Smith, "Adaptive Kalman filtering for low-cost INS/GPS," *Journal of Navigation*, vol. 56, no. 1, pp. 143–152, 2003.

[16] J. L. Crassidis, F. Landis Markley, and Y. Cheng, "Survey of nonlinear attitude estimation methods," *Journal of Guidance, Control, and Dynamics*, vol. 30, no. 1, pp. 12–28, 2007.

[17] F. L. Markley, "Attitude error representations for Kalman filtering," *Journal of Guidance, Control, and Dynamics*, vol. 26, no. 2, pp. 311–317, 2003.

[18] J. L. Speyer, "Computation and transmission requirements for a decentralized Linear-Quadratic-Gaussian control problem," *IEEE Transaction on Automatic Control*, vol. 24, no. 2, pp. 266–269, 1979.

[19] D. W. Jung and P. Tsiotras, *Inertial Attitude and Position Reference System Development for a Small UAV*, American Institute of Aeronautics and Astronautics, 2007.

[20] W. T. Higgins Jr., "A comparison of complementary and Kalman filtering," *IEEE Transactions on Aerospace and Electronic Systems*, vol. 11, no. 3, pp. 321–325, 1975.

[21] J. F. Vasconcelos, C. Silvestre, P. Oliveira, P. Batista, and B. Cardeira, "Discrete time-varying attitude complementary filter," in *Proceedings of the American Control Conference (ACC '09)*, pp. 4056–4061, June 2009.

[22] Y.-C. Lai, S.-S. Jan, and F.-B. Hsiao, "Development of a low-cost attitude and heading reference system using a three-axis rotating platform," *Sensors*, vol. 10, no. 4, pp. 2472–2491, 2010.

[23] Z. Chen, *Strapdown Inertial Navigation System*, China Astronautic Publishing House, 1986.

Hindawi Publishing Corporation
Mathematical Problems in Engineering
Volume 2013, Article ID 505794, 8 pages
http://dx.doi.org/10.1155/2013/505794

Research Article

Capacity Analysis for Parallel Runway through Agent-Based Simulation

Yang Peng,[1] Gao Wei,[2] and Sun Jun-Qing[1]

[1] *School of Computer Science and Technology, Tianjin University of Technology, Tianjin 300191, China*
[2] *Civil Aviation University of China, Tianjin 300300, China*

Correspondence should be addressed to Yang Peng; pqxx@sina.com

Received 28 March 2013; Revised 18 June 2013; Accepted 18 June 2013

Academic Editor: Ming Cao

Parallel runway is the mainstream structure of China hub airport, runway is often the bottleneck of an airport, and the evaluation of its capacity is of great importance to airport management. This study outlines a model, multiagent architecture, implementation approach, and software prototype of a simulation system for evaluating runway capacity. Agent Unified Modeling Language (AUML) is applied to illustrate the inbound and departing procedure of planes and design the agent-based model. The model is evaluated experimentally, and the quality is studied in comparison with models, created by SIMMOD and Arena. The results seem to be highly efficient, so the method can be applied to parallel runway capacity evaluation and the model propose favorable flexibility and extensibility.

1. Introduction

Airports play a key role in the commercial aviation system by allowing airlines and their customers to converge. However, since the early 1970s, the peaking of traffic at airports has been a problem of increasing concern to airport operators around the world. This challenge is most pronounced in the runways, where multiple traffic flows converge within a confined region. A failure to manage these runways effectively can start a causal chain wherein an accumulating bottleneck effect leads to fighting delays, unused runway capacity, and increased controller workload which, in turn, leads to increased financial and environmental costs.

An airport's capacity may be broadly defined as its ability to handle a given volume. While a runway system capacity is defined as the hourly rate of aircraft operations which may be reasonably expected to be accommodated by a single or a combination of runways under given local conditions [1]. Congestion occurs when demand approaches or exceeds capacity. Nonintersecting runways, whose extended centre lines have an angle of convergence/divergence of 15 degrees or less, are called near parallel runways. The use of parallel runways to increase aerodrome capacity is a common concept at busy aerodromes.

Results in this study are mainly focused on parallel runways, conducted using an agent-based simulation software called AnyLogic. Given its capabilities for modeling at a very high level of detail and closely representing reality in terms of applicable separation standards and air traffic management procedures. Agent based model is created to simulate proposed alternative. Using the methodology proposed here, the baseline and the different alternatives were evaluated in terms of design functionality and overall utilization of potential capacity.

2. Literature Review

2.1. Capacity Estimation Models. The primary analytical models used to estimate runway capacity include the LMI runway capacity model and the FAA airfield capacity model [2]. The LMI capacity model is an analytical model for computing the capacity of a runway system. Its fundamental

building block is a model that computes the capacity of a single runway. The FAA airfield capacity model is an analytic model which calculates the capacity of a runway system, but it assumes that all random variables in the model are normally distributed and a 5% probability of violation of separation requirements is used in determining spacing of runway operations, using these normal distributions. A hybrid of these two models, with the logic of the LMI model and the extension to multiple runways featured in the FAA model, is expected to be very useful in providing quick estimates of runway system capacity [3].

A distinction between analytical and simulation models is made based on the methodology used to compute capacity, delay, or other such metrics. Analytical models are primarily sought to provide estimates of capacity by manipulation of the representation formulated. These models tend to have a low level of detail [4].

Simulation of the airport environment is increasingly applied to obtain more realistic estimates of capacity by randomizing the various input parameters. Many commercial simulation tools for air traffic are available, for example, SIMMOD and TAAM. These tools dedicated to airport types of simulation seek to generate traffic flows through the airports, which are modeled and configured to represent actual constraints and uncertainties. Observations from these flows allow appropriate measures of capacity and/or delay to be computed. Simulations tend to have a much higher level of detail including conflict resolution, airport taxiway, and gate selection, to deal with more tactical issues.

In many applications these commercial simulation tools will satisfy the simulation objectives, but when microsimulation becomes an issue to consider, very few models analyze air traffic metrics in combination with capacity and safety. With regard to microsimulation, we are concerned with events such as wake-vortex separation violations, simultaneous runway occupancies (SRO's), and collisions on a runway. Furthermore, the aviation system is a complicated stochastic system.

2.2. Agent-Based Systems for Air-Traffic Control and Management. Agent-based computing is one of the powerful technologies for the development of distributed complex systems [5, 6]. Many researchers believe that agents represent the most important new paradigm for software development since object-oriented design [7], and the concept of intelligent agents has already found a diverse range of applications in transportation systems.

The geographical and functional distribution and the highly dynamic nature of air traffic control (ATC) make it an ideal candidate with many potential applications that can be modeled with MAS [8], such as air traffic flow management [9]. The optimal aircraft sequencing using intelligent scheduling (OASIS) presented in [10] is a real-time agent-oriented system developed to support air traffic management. OASIS distributes air traffic control (ATC) tasks into two classes of autonomous and cooperating agents: aircraft agents and global agents. Each aircraft agent associates with an arriving aircraft and performs computation or reasoning relevant to the aircraft. The system helps alleviate air traffic congestion by maximizing runway utilization through arranging landing aircrafts into an optimal order and monitoring the progress of each individual aircraft in real time.

An agent-based model enables modeling of every individual throughout the complete simulation lifecycle in complex scenarios, so, to follow these domestic properties, an agent-based simulation is created to provide the necessary information for parallel runways.

3. Operational Conceptions and Considerations

The impetus for considering operations on parallel or near-parallel instrument runways is provided by the need to increase capacity at busy aerodromes. The procedures for airports with multiple parallel runways are similar, with added safeguards to ensure that an aircraft is safely separated from those approaching the adjacent parallel runway. The relation among many parallel runways can be turned to the relation between two parallel runways. So we only focus our research on two parallel runways.

In order to enable evaluation of capacity of parallel runway, it is necessary to model the details of how arriving aircraft is guided through the final stage, including their behavior and interactions. Modeling of the agents was accomplished by comparison with a set of baseline operational data and consultation with subject matter experts.

3.1. Modes of Operation

3.1.1. Simultaneous Parallel Approaches. Independent parallel approaches: simultaneous approaches to parallel or near-parallel instrument runways where radar separation minima between aircraft on adjacent extended runway centre lines are not prescribed. Dependent parallel approaches: simultaneous approaches to parallel or near-parallel instrument runways where radar separation minima between aircraft on adjacent extended runway centre lines are prescribed.

3.1.2. Simultaneous Parallel Departures/Departures. Independent parallel departures: simultaneous departures from parallel or near-parallel instrument runways. Segregated parallel departures: simultaneous operations on parallel or near-parallel instrument runways. Under this mode, one runway is used exclusively for approaches and the other runway is used exclusively for departures. There may be semimixed operations; that is, one runway is used exclusively for departures, while the other runway is used for a mixture of approaches and departures; or, one runway is used exclusively for approaches while the other is used for a mixture of approaches and departures.

3.2. Safeguards for Parallel Runway. In order to obtain reliable and valid model to evaluate the capacity, it was necessary to collect these regulations in a systematic and controlled manner. Therefore, various aircraft controls are described in this section.

3.2.1. Separation Control. The separations imposed between aircraft by terminal controllers can be characterized by the interarrival separation distribution of aircraft as they fly along the final approach course. This distribution is a good measure of the applied separations since it is sensitive not only to the average separations applied, but also to the variability of the applied separations around the average. The variability of aircraft separations can have many sources, including the different required minimums between different aircraft types and the deviation of aircraft from their assigned routes and speeds. All of these sources are captured by the interarrival separation distribution along the final approach. The final approach is particularly important because it is where aircraft are moving most slowly, are most closely spaced, and have their routes most constrained.

To avoid the situation where a faster aircraft catches up with a slower aircraft, an extraseparation is required for the following faster aircraft at the beginning of its final approach. FAA has an official separation requirement for each aircraft mix, and the separations are chosen to avoid a wake vortex encounter. The target separation at the threshold is drawn from a Gaussian distribution $\sim N(\mu, \sigma^2)$, where the mean μ is given in Tables 1 and 2 based on the leader and trailer aircraft types, and the standard deviation σ is assumed to be 0.39 nm. The actual separation at the threshold depends on several factors including aircraft speed and time of arrival at the final approach fix.

3.2.2. Runway Entrance Control. The minimal time between an aircraft that wants to takeoff (takeoff lasts about 30 seconds) and an aircraft that wants to land is about 3 minutes. If the time difference is smaller, aircraft at the ground have to hold until the runway is vacated.

3.2.3. Runway Balance Control. The model flow manager chooses a landing runway for each inbound aircraft based on the need to balance throughput on the available runways. Balancing the throughput on all the runways of an airport is important because overwhelming one runway while another remains underutilized will lower the overall throughput of the airport. In order to choose which runway would be best, based on balancing considerations, the model flow manager first calculates an estimated demand on each runway and then decides whether reassigning the aircraft to other than the nearest runway would be desirable. The estimated demand is calculated as a weighted moving average constructed so that nearer flights contribute more to the estimated demand than distant flights.

Once estimated demands have been calculated for each available runway, the flow manager will reassign the incoming flight to the runway with the lowest estimated demand if the demand estimate on that runway is lower than the demand estimate on the nearest runway by at least a specified amount called the demand barrier. The demand barrier used in the simulations is 2 flights per hour. The purpose of the demand barrier is to ensure that flights are not reassigned to other than their closest runway unless there is a clear advantage in doing so.

Table 1: Separation standard matrix (nautical mile).

Leader	Trailer		
	Heavy	Large	Small
Heavy	4	5	6
Large	2.5	2.5	4
Small	2.5	2.5	2.5

Table 2: Hypothetical reduced separation (nautical mile).

Leader	Trailer		
	Heavy	Large	Small
Heavy	3.3	3.3	3.3
Large	2.5	2.5	4
Small	2.5	2.5	2.5

4. Architecture of MAS

4.1. Agent-Oriented Parallel Runway Architecture. Agent-based modeling develops computational representation of a complex system by modeling each of the components or subsystems as agents and it models the rules for possible actions and interaction between these agents.

To formulate the evaluation model, we created the following pseudoagent. The developed model considers each subsystem as an independent type of agent that acts based on its local knowledge and its interaction with other agents.

(1) Runway agent is applied to simulate the runway and it was afforded statistical methods to recorder the utilization rate of the runway.

(2) Runway entrance agent is applied to simulate the entrance of the runway and it was embedded in the runway agent.

(3) Departure agent is applied to simulate the departure aircraft. Different aircraft types are modeled through database of aircraft performance parameters.

(4) Departure environment agent is applied to simulate the surrounding condition of the departure aircraft. The departure aircraft can learn the surrounding information from this agent, and it is embedded in the departure agent.

(5) Arrival agent is applied to simulate the departure aircraft.

(6) Arrival environment agent is applied to simulate the surrounding condition of the arrival aircraft.

(7) Departure track agent is applied to simulate the approach line of aircraft, it can record the quantity of arrival aircraft at any time.

(8) Arrival track agent is applied to simulate the approach line of aircraft.

(9) Rule agent receives and converts the regulation data, for example, the miss distance between aircraft.

(10) Control agent balances the arrival and departure aircraft.

Considering that UML is a language widely accepted, we will design the architecture of the agent-oriented parallel runway system at this part by AUML. The AUML is extended from UML with agent-related modeling techniques, to enhance the modeling capabilities of UML [11]. Figure 1 shows the group membership hierarchy on which the design of the runway system is based. To describe the simulation model in more detail, some entities are further decomposed to virtual agents. For example, the arrival aircraft is decomposed to arrival agent and the corresponding arrival environment agent; in this way the model can be applied to more complicated condition without much change, as is shown in Figure 2. The main features of the important agents presented in this architecture are specified in the following sections.

4.2. Agent Description

4.2.1. Arrival Agent. An agent will be created for each arrival aircraft. Therefore, in response to the arrival of an aircraft (arrival agent creation event) the system will create a new arrival agent instance for this aircraft. Each arrival agent faces a safe problem. In this problem, a strict set of rules must be followed, and arrival agent may get a copy of the rules from rule agent through communication and can get the position and characteristics information of nearby-arrival agents through its arrival environment agent. Also, the agent has to coordinate with the other service agents in order to resolve any conflicts. This arrival agent must have the following information: the ID of assigned runway to the aircraft, the aircraft characteristics, the operation time assigned to the different operations (approach/landing).

4.2.2. Runway Agent. Each aircraft will be assigned to a specific runway. Each one of the runway is controlled by a runway agent. To do this, the agent will have to manage the runway assigned and the corresponding runway entrance agents, informing the control agent and the corresponding aircraft agent when necessary.

When an arrival agent approaches to the target runway, it will have to communicate with runway agent to check the state of the runway. If the runway is not locked by departure agent and no aircraft will take the runway upon its arrival to the runway, the aircraft will continue its approach processes; otherwise' it will have to hover at its current position.

4.2.3. Control Agent. The main goal of this agent is to determine the appropriate allocation for the arrival/departure aircrafts to specific time and runway. While an arrival agent is created, it has to wait in the approach queue for the instruction of the control agent before it moves to the target runway, so do departure aircraft.

The control agent will try to obtain the most appropriate scheduling to balance the arrival and departure stream. At this point, the agent will search the information of aircrafts at approach/departure queues. The agent will have to know the following information in order to perform its task: the length of the approach/departure queues and the cumulative waiting time and max waiting time of aircrafts of the approach/departure queues.

4.3. Agent Communication. One of the most important tasks is the coordination and the negotiation between the agents. Each one is in charge of one independent part of the system. The message interchange between agents forming the system is not based on the most popular foundation for intelligent physical agents specifications (FIPA-ACL). Instead, we apply the regular interobject communication facilities of the simulation environment for agents: calling methods, sending messages via ports, linking continuously changing variables, and so forth.

The interaction between agents, while arrival aircraft approaches to the runway, is shown in Figure 3.

While arrival aircraft is created, it gets target runway and obstacle aircraft information from control agent. The aircraft registers its information to the arrival track agent and approaches to the runway, as soon as it gets permission from the control agent. During the approach process, the aircraft checks whether the distance to obstacle aircraft satisfies the safety rules. If the distance is too short, the aircraft will hold on current position, until it is safe for it to move forward again. Upon the final approach stage, the aircraft communicates with the runway agent and departure aircrafts to make sure that the runway will be available when it reaches the runway, and no departure aircraft has locked the runway.

5. Developing Models in AnyLogic

5.1. Simulation Control and Data Collection. The simulation approach used in this paper is based on the software tool AnyLogic. AnyLogic is a programming and simulation environment based on Java that is matching with unified modeling language (UML) inherently and the model based on AnyLogic possesses the open architecture as [12] characterizes. AnyLogic focuses on agent-based approach and business simulation and allows the user to combine different techniques and approaches.

The example problem is considered in this case study to conduct simulation although the model being developed is independent of the problem structure. The example is drawn partially with minor modifications from Bei Jing airport runway structure, the structure information of the parallel runway is stored in the database, and the distance between runways can be manually changed during simulation. Figure 4 shows the parallel runway structure.

Validation of the computer simulation is a critical step since the reliability of predictions derived from it depends on the fidelity of the simulation to actual operations. It is a good idea to compare the simulation results of the model with real airport operation data, but the data is hard to collect. So, we verify the multiagent model through comparison with SIMMOD model and Arena model. The screenshot for multiagent-based parallel runway simulation model is presented in Figure 5. Several versions of the model have been

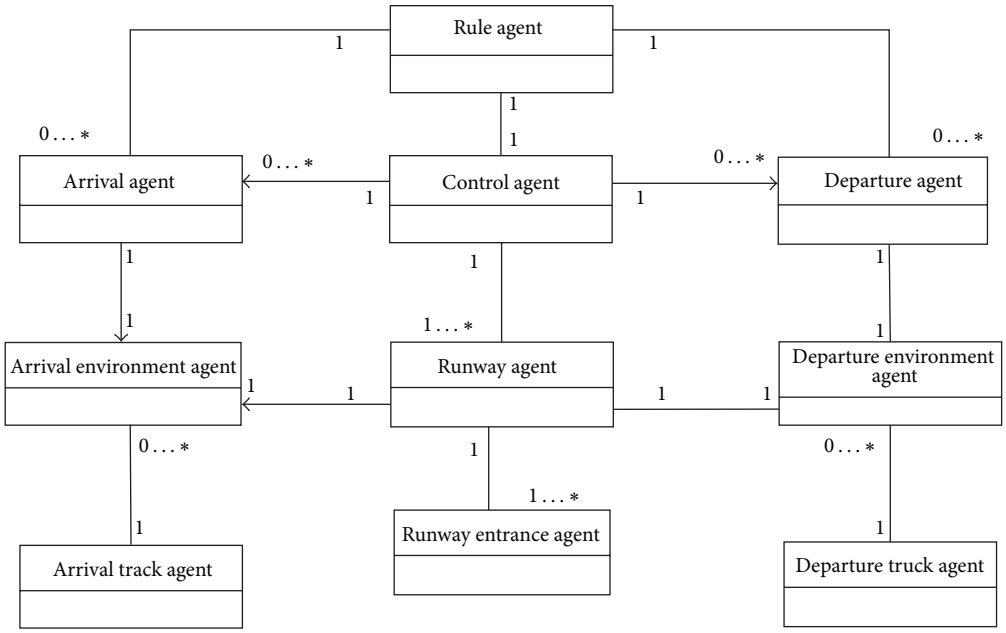

Figure 1: Agent Class Diagram.

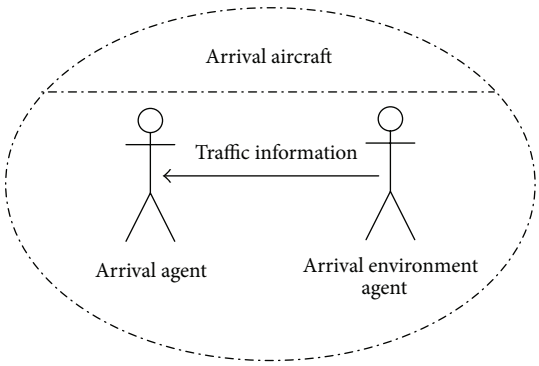

Figure 2: Collaboration of Virtual Agents.

simulated allowing a comparison of runway capacity under different operation modes.

The experimenter's display is essentially an electronic map of an area. All aircraft are shown as symbols at their proper locations. In a separate window on the screen, a variety of information about the subject aircraft is displayed. This information is received from the model and is shown as a reference for the experimenter. Information about pseudoaircraft can be displayed, including the waypoints the pseudoaircraft is flying through.

5.2. Numerical Experiments. Small aircrafts are seldom used in recent years at Chinese aviation market, so we suppose that only large and heavy aircraft were available at the simulation experiments. Some of the important parameters of the aircraft are displayed at Tables 3 and 4.

Being one of the oldest and most commonly used air traffic simulation modeling tools, SIMMOD outputs were used as the baseline for expected results. The average delay of aircrafts is used to measure the quality of a scenario after execution and to compare with other scenarios.

Table 3: Scenario data.

	Aircraft types	
	Medium	Heavy
Arrival velocity km/h	314	334
Take-off velocity km/h	309	315
Mixindex%	63.4	36.6

One of the main benefits of a simulation model is the wealth of information derived from each simulation run. Each scenario is repeated for 20 times, and the averaged simulation results are then presented to illustrate the use of the model developed.

5.3. Results and Analysis. In the case of independent arrival, the distance between parallel runways is over 1035 m, and the

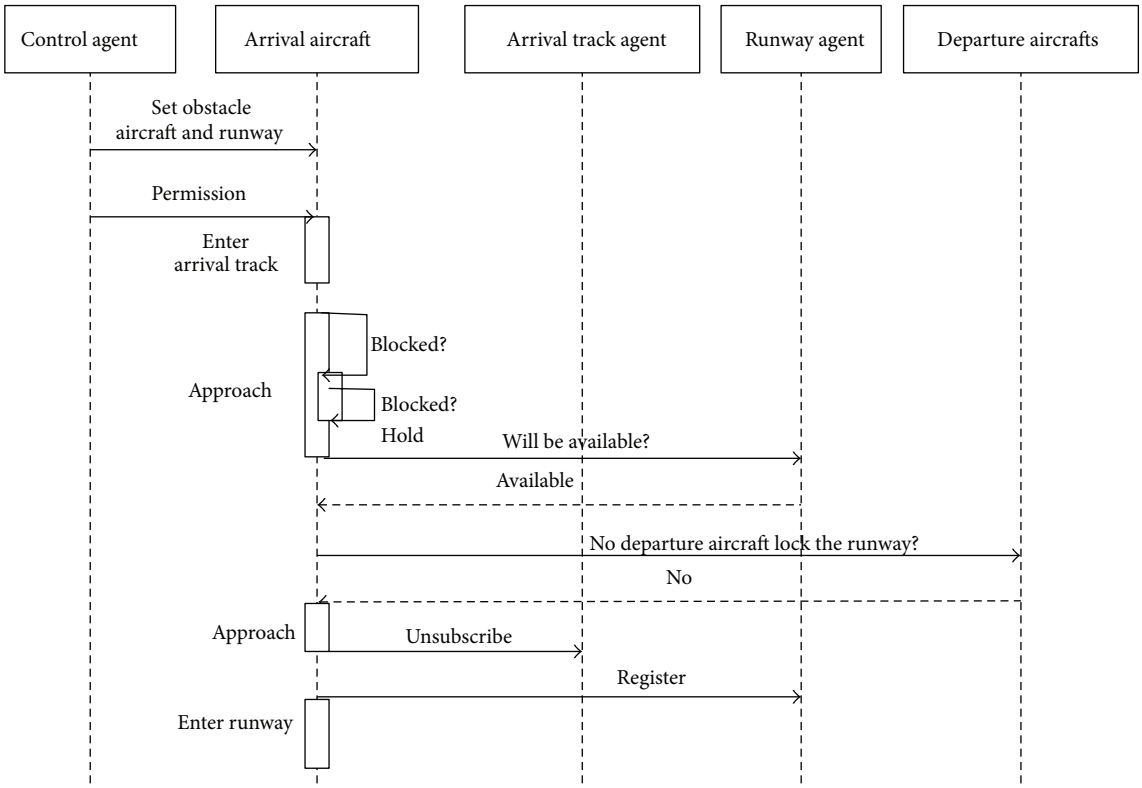

Figure 3: Message sequence diagram.

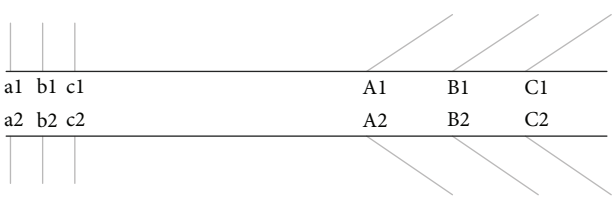

Figure 4: Runway Structure.

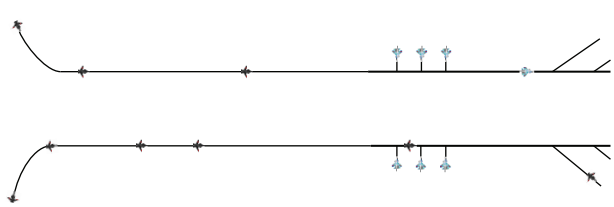

Figure 5: Screenshot of the model.

Table 4: Taxiway choice parameters.

First runway	Ratio of medium aircraft that taxi to A1, B1, and C1	0.4, 0.3, 0.3
	Ratio of medium aircraft that taxi to A1, B1, and C1	0.2, 0.3, 0.5
Second runway	Ratio of heavy aircraft that taxi to A1, B1, and C1	0.3, 0.4, 0.3
	Ratio of heavy aircraft that taxi to A1, B1, and C1	0.2, 0.2, 0.6

initial arrival rate is 10 aircrafts per hour. Then the arrival rate will gradually rise to an unrealistically high level. As expected, the level resulted in all flights being delay. The resulting delay distribution is depicted in Figure 6.

As can be seen form Figure 6, the results of the models are quite similar when the density of arrival aircraft is small. While the arrival rate turns to unsustainable heavy, the distinction turns to be clear. This fact ensures that a simulation validated against airport arrival operations will have been stress tested in high-density traffic situations. The results of multiagent model are in accordance with those of SIMMOD, but the results of the Arena and SIMMOD are significantly different.

Suppose that the tolerable level of average delay is 4 minutes, and the corresponding capacity is regarded as runway practical capacity. Figure 7 shows the simulation results of dependant approach scenarios.

Clearly there are differences between the results of Arena and SIMMOD models for this scenario, and, by inspection of the confidence intervals, it is clear that the results of agent and SIMMOD are similar. The most important reason for the difference lies in the technique used to implement origin-destination routing and separation control. While agent-based model uses a monitoring technology, checking the distance between nearby aircraft at any time. Arena uses a trigger technology, checking the distance at particular moment or

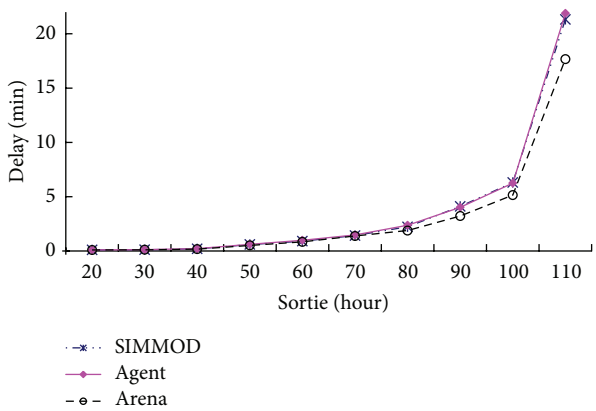

Figure 6: Comparison of delays under independent parallel approaches.

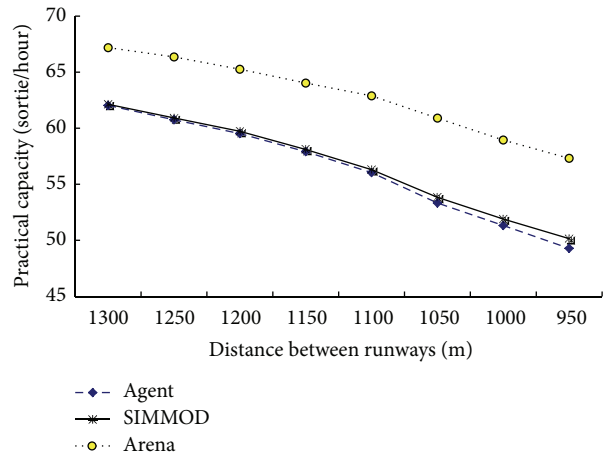

Figure 7: Comparison of capacities under dependent parallel approaches.

particular position. Consequently, Arena required each intersection to have hard-coded turning movement percentages. The reason for not implementing routing and separation mechanism in Arena to match that in Agent model is the complexity of the cooperative logic and component in a microscopic level system. From this, it is very difficult to determine specific vehicle turning directions at each intersection, which results in shorter separation for aircrafts. Due to the nature of the routing technique utilized in Arena, there was no way to assign specific destinations for aircrafts each origin. Because of this, there was no guarantee that destination volumes in Arena would match those established separation rules.

The purpose of introducing agents into parallel runway simulation is to increase the flexibility and the ability of the system to deal with uncertainty in a dynamic environment. Through the above comparison, we can see that the multiagent model consists of multiple functional stationary agents that are intelligent and cooperative. Interoperability is critically needed in making decisions based on information across systems, organizational and jurisdictional boundaries, or application scenarios in which the integration of multiple agent systems is needed.

6. Conclusions

This research applied agent-based modeling approach to the simulation of parallel runway system. The simulation model that seeks aircrafts and runway interactions using individual agents that attempt to fulfill a specific objective is developed. The coordination between agents is achieved through protocols. The hierarchical architecture makes it possible to examine and understand how approach mode and architecture decisions might affect the parallel runway capacity. Regarding the proposed model, the movement of aircrafts at taxiway should be also included at the multiagent model in future research.

Conflict of Interests

Yang Peng, Gao Wei, and Sun Jun-Qing declare that they have no proprietary, financial, professional, or other personal interests of any nature or kind in any product, service, and/or company that could be construed as influencing the position presented in, or the review of, the paper.

Acknowledgment

This work is financially supported by National Nature Science Foundation of China under the Grant 61201234, Tianjin City, Board of Education Scientific Research Plan Project under the Grant 20110416, and the Basic Research Universities Special Fund Operations ZXH2010D011, ZXH2012G002.

References

[1] B. Jiang, M. Hu, and Y. Tian, "Further research of airport runway capacity evaluation," *Journal of Traffic and Transportation Engineering*, vol. 2, no. 3, pp. 80–883, 2003.

[2] H.-Q. Guo and J.-F. Zhu, "Calculation models of capacity and delay for y closely spaced parallel runway," *Journal of Traffic and Transportation Engineering*, vol. 18, no. 14, pp. 68–72, 2008.

[3] W. Wang, M. Wang, and X. Qian, "Study on method of determination of centrally distance and threshold staggering manner for closely spaced parallel runways of airport," *Journal of Civil Aviation University of China*, vol. 29, no. 2, pp. 23–26, 2011.

[4] S. Alam, H. A. Abbass, and M. Barlow, "ATOMS: air traffic operations and management simulator," *IEEE Transactions on Intelligent Transportation Systems*, vol. 9, no. 2, pp. 209–225, 2008.

[5] F. Zambonelli and H. van Dyke Parunak, "Signs of a revolution in computer science and software engineering," in *Proceedings of the 3rd International Conference on Engineering Societies in the Agents World III (ESAW '02)* , pp. 13–28, Springer, Berlin, Germany, 2003.

[6] S. Wollkind, J. Valasek, and T. R. Ioerger, "Automated conflict resolution for air traffic management using cooperative multi-agent negotiation," in *Proceedings of the American Institute of Aeronautics and Astronautics Conference on Guidance, Navigation and Control (AIAA '04)*, pp. 1078–1088, August 2004.

[7] M. Luck, "Guest editorial: challenges for agent-based computing," *Autonomous Agents and Multi-Agent Systems*, vol. 9, no. 3, pp. 199–201, 2004.

[8] B. Burmeister, A. Haddadi, and G. Matylis, "Application of multi-agent systems in traffic and transportation," *IEE Proceedings*, vol. 144, no. 1, pp. 51–60, 1997.

[9] K. Tumer and A. Agogino, "Distributed agent-based air traffic flow management," in *Proceedings of the 6th International Joint Conference on Autonomous Agents and Multiagent Systems (AAMAS '07)*, pp. 342–349, May 2008.

[10] M. Ljungberg and A. Lucas, "The OASIS air traffic management system," in *Proceedings of the 2nd Paciffic Rim International Conference on Artificial Intelligence*, Seoul, South Korea, 1992.

[11] N. Mani, V. Garousi, and B. H. Far, "A UML-based conversion tool for monitoring and testing multi-agent systems," in *Proceedings of the 20th IEEE International Conference on Tools with Artificial Intelligence (ICTAI '08)*, pp. 212–219, Dayton, Ohio, USA, November 2008.

[12] L. Bin, L. Wen-feng, and Z. Yu, "Study on modeling of container terminal logistics system using agent-based computing and knowledge Discovery," in *Proceedings of International Symposium on Advances in Computer and Sensor Networks and Systems*, pp. 164–171, Aardvark Global Publishing, Sandy, Utah, USA, 2008.

Hindawi Publishing Corporation
Mathematical Problems in Engineering
Volume 2013, Article ID 186934, 7 pages
http://dx.doi.org/10.1155/2013/186934

Research Article

Approximate Analytical Solutions of Fractional Perturbed Diffusion Equation by Reduced Differential Transform Method and the Homotopy Perturbation Method

Zhoujin Cui,[1] Zisen Mao,[2] Sujuan Yang,[2] and Pinneng Yu[2]

[1] *Jiangsu Maritime Institute, Nanjing 211100, China*
[2] *Institute of Science, PLA University of Science and Technology, Nanjing 211101, China*

Correspondence should be addressed to Zisen Mao; maozisen@126.com

Received 23 March 2013; Accepted 6 May 2013

Academic Editor: Guanghui Wen

The approximate analytical solutions of differential equations with fractional time derivative are obtained with the help of a general framework of the reduced differential transform method (RDTM) and the homotopy perturbation method (HPM). RDTM technique does not require any discretization, linearization, or small perturbations and therefore it reduces significantly the numerical computation. Comparing the methodology (RDTM) with some known technique (HPM) shows that the present approach is effective and powerful. The numerical calculations are carried out when the initial conditions in the form of periodic functions and the results are depicted through graphs. The two different cases have studied and proved that the method is extremely effective due to its simplistic approach and performance.

1. Introduction

Various fields of science and engineering deal with dynamical systems (see [1, 2]), some of which can be described by fractional-order equations (see [3–5] and the references therein). The last two decades have witnessed a great progress in fractional calculus and fractional-order dynamical systems. It has been found that fractional calculus is a mathematical tool that works adequately for anomalous social and physical systems with nonlocal, frequency- and history-dependent properties, and for intermediate states such as soft materials, which are neither idea solid nor idea fluid (see [3, 4, 6]). Differential equations with fractional-order derivatives/integrals are called fractional differential equations, and they have found many successful applications in viscoelasticity, heat conduction, electromagnetic wave, diffusion wave, control theory, and so on (see [7–9] and the references therein).

Bistable systems play an important role in the study of spatial patterns. A typical example, which appears in population dynamics, leads to

$$\frac{\partial u}{\partial t} = \frac{\partial^2 u}{\partial x^2} + u - u^3, \tag{1}$$

referred to as the classical Fisher-Kolmogorov (FK) equation. In investigating such spatial patterns, a key role is played by a model equation, which is simpler than the full equation describing the process. Recently, interest has turned to higher-order model equations involving bistable dynamics, such as the extended Fisher-Kolmogorov (EFK) equation

$$\frac{\partial u}{\partial t} = -\gamma \frac{\partial^4 u}{\partial x^4} + \frac{\partial^2 u}{\partial x^2} + u - u^3, \quad \gamma > 0, \tag{2}$$

proposed by Coullet et al. [10] in 1987 as well as by Dee and Van Saarloos [11] in 1988. The EFK equation has appeared in

studies of phase transitions, for instance, near a Lifshitz point (cf. Zimmerman [12]). Another well-known equation of this type is the Swift-Hohenberg equation

$$\frac{\partial u}{\partial t} = \alpha u - \left(1 + \frac{\partial^2}{\partial x^2}\right)^2 u - u^3, \quad \alpha > 0, \tag{3}$$

proposed in 1977.

Whereas the EFK equation and the SH equation involve fourth-order spatial derivatives, certain phase-field models lead to even-higher-order spatial gradients. The following equation

$$\frac{\partial u}{\partial t} = \frac{\partial^6 u}{\partial x^6} + A\frac{\partial^4 u}{\partial x^4} + B\frac{\partial^2 u}{\partial x^2} + u - u^3, \tag{4}$$

studied by Gardner and Jones [13] and Caginalp and Fife [14], in which A and B are constants. In this paper, we consider the initial value problem (IVP) of perturbed diffusion equation with fractional time derivative

$$\begin{gathered} D_t^\alpha u = \frac{\partial^6 u}{\partial x^6} + A\frac{\partial^4 u}{\partial x^4} + B\frac{\partial^2 u}{\partial x^2} + u - u^2, \\ u(x,0) = \varphi(x), \end{gathered} \tag{5}$$

where the fractional derivative in (5) is in the sense of Caputo and $0 \le \alpha < 1$.

Historically, comparatively little was known about the extraordinary range of behavior presented by the solutions of nonlinear partial differential equations. Except for a few special cases, it is impossible to find a closed form solution for a fractional differential equation. Effective methods for solving such equations are needed. So approximate and numerical techniques must be used.

The homotopy perturbation method (HPM) is relatively new approach to provide an analytical approximation to linear or nonlinear problem. This method was first presented by He [15, 16] and applied to various nonlinear problems [17, 18]. The basic difference of this method from the other perturbation techniques is that it does not require small parameters in the equation, which overcomes the limitations of the traditional perturbation techniques. Recently, the application of this method is extended for fractional differential equations [5, 19–21]. Zhou [22] was the first one to use differential transform method (DTM) in engineering applications. He employed DTM in solution of initial boundary value problems in electric circuit analysis. This method constructs an analytical solution in the form of a polynomial. It is different from the traditional high order Taylor series method, which requires symbolic computation of necessary derivatives of the data functions. The differential transform is an iterative procedure for obtaining analytical differential equations. The concept of DTM has broadened to problems involving partial differential equations and systems of differential equations [23, 24]. Some researchers have lately applied DTM for analysis of uniform and non-uniform beams [25–27]. Recently, the application of reduced differential transform method is successfully extended to obtain analytical approximate solutions to linear and nonlinear ordinary differential equations of fractional order [28–30].

In this paper, we try to find an approximate analytical solution of (5) for fractional time derivatives with the help of powerful analytical method. We use the reduced differential transform method (RDTM) and homotopy perturbation method (HPM) to obtain the solutions and compare them with each other. We know that the HPM method is based on the use of homotopy parameter for classification of most favorable values of parameters in between $[0,1]$. While, RDTM technique does not require any parameter, discretization, linearization, or small perturbations and therefore it reduces significantly the numerical computation. For the standard cases, comparing the methodology with some known techniques shows that the present approach is effective and powerful.

2. Preliminaries

There are several approaches to define the fractional calculus, for example, Riemann-Liouville, Gruunwald-Letnikow, Caputo, and Generalized Functions approach. For the readers' convenience, definitions of fractional integral/derivative and some preliminary results are given in this section.

Definition 1 (see [6]). The fractional integral of order $\alpha \ge 0$ of a function $u(x,t)$ is given by

$$I^\alpha u(x,t) = \frac{1}{\Gamma(\alpha)} \int_0^t (t-s)^{\alpha-1} u(x,s)\, ds, \tag{6}$$

provided that the right side is point-wise defined on $(0,+\infty)$, where $\Gamma(\cdot)$ is the well-known gamma function.

Definition 2 (see [6]). The Caputo derivative of order $s > 0$ of a continuous function $u(x,t)$ is defined to be

$${}^{C}D_t^s u(x,t) = \frac{1}{\Gamma(n-s)} \int_0^t \frac{u^{(n)}(x,\tau)}{(t-\tau)^{s-n+1}} d\tau, \tag{7}$$

where $n = [s] + 1$, provided that the right side is point-wise defined on $(0,+\infty)$.

Definition 3 (see [6]). The Riemann-Liouville derivative of order $s > 0$ of a continuous function $u(x,t)$ is defined to be

$${}^{RL}D_t^s u(x,t) = \frac{1}{\Gamma(n-s)} \frac{d^n}{dt^n} \left[\int_0^t \frac{u(x,\tau)}{(t-\tau)^{s-n+1}} d\tau \right], \tag{8}$$

where $n = [s] + 1$, provided that the right side is point-wise defined on $(0,+\infty)$.

Riemann-Liouville fractional derivative is mostly used by mathematicians but this approach is not suitable for real world physical problems since it requires the definition of fractional order initial conditions, which have no physically meaningful explanation yet. Caputo introduced an alternative definition, which has the advantage of defining integer order initial conditions for fractional order differential equations. We have chosen the Caputo fractional derivative

because it allows traditional initial and boundary conditions to be included in the formulation of the problem. And some other properties of fractional derivative can be found in [4, 6].

The relation between the Riemann-Liouville operator and Caputo operator is given by

$$ {}^{C}D_t^s u(x,t) = {}^{RL}D_t^s \left[u(x,t) - \sum_{i=1}^{n-1} u^{(i)}(x,0) \frac{t^i}{i!} \right]. \quad (9) $$

By using (9), from (8), we obtain fractional derivative in the Caputo sense as follows:

$$ {}^{C}D_t^s u(x,t) = \frac{1}{\Gamma(n-s)} \frac{d^n}{dt^n} \times \left[\int_0^t \frac{\omega(x,\tau) - \sum_{i=1}^{n-1} u^{(i)}(x,0)\left(\tau^i/i!\right)}{(t-\tau)^{s-n+1}} d\tau \right]. \quad (10) $$

Let us expand the analytical and continuous function $u(x,t)$ in terms of a fractional power series as follows:

$$ u(x,t) = \sum_{k=0}^{\infty} U_k(x) t^{k/\alpha}, \quad (11) $$

where α is the order of fraction and $U_k(x)$ is the fractional differential transform of $u(x,t)$.

Since the initial conditions are implemented to the integer order derivatives, the transformations of the initial conditions are defined as follows:

$$ U_k(x) = \begin{cases} \text{if } \left(\frac{k}{\alpha}\right) \in Z^+, \frac{1}{(k/\alpha)!} \\ \times \left[\frac{d^{k/\alpha}}{dt^{k/\alpha}} u(x,t) \right]_{t=0} & \text{for } k = 0, 1, 2, \ldots, (\alpha s - 1) \\ \text{if } \left(\frac{k}{\alpha}\right) \in R \setminus Z^+, & 0. \end{cases} \quad (12) $$

The following theorems that can be deduced from (7) and (8) are given below.

Theorem 4. *If $w(x,t) = x^m t^n u(x,t)$, then $W_K(x) = x^m U_{k-n}(x)$.*

Theorem 5. *If $w(x,t) = u(x,t)v(x,t)$, then*

$$ W_K(x) = \sum_{r=0}^{k} U_r(x) V_{k-r}(x) = \sum_{r=0}^{k} U_{k-r}(x) V_r(x). \quad (13) $$

Theorem 6. *If $w(x,t) = (\partial^m/\partial x^m)u(x,t)$, then $W_K(x) = (\partial^m/\partial x^m)U_k(x)$.*

Theorem 7. *If $w(x,t) = (\partial^\beta/\partial t^\beta)u(x,t)$, then $W_K(x) = (\Gamma(\beta + 1 + k/\alpha)/\Gamma(1 + k/\alpha))U_{k+\alpha\beta}(x)$.*

3. Solution of the Problem by the RDTM and HPM

To illustrate the basic ideas of HPM [15], we consider the following general nonlinear differential equation:

$$ A(y) - f(r) = 0, \quad r \in \Omega, \quad (14) $$

with boundary conditions

$$ B\left(y, \frac{\partial y}{\partial n}\right) = 0, \quad r \in \Gamma, \quad (15) $$

where A is a general differential operator, B is a boundary operator, $f(r)$ is a known analytic function, and Γ is the boundary of the domain Ω.

The operator A can be generally divided into two parts L and N, where L is linear, while N is nonlinear. Therefore (14) can be written as follows:

$$ L(y) + N(y) - f(r) = 0. \quad (16) $$

We construct a homotopy of (14) $y(r,p) : \Omega \times [0,1] \to \mathfrak{R}$ which satisfies

$$ H(y,p) = (1-p)[L(y) - L(y_0)] + p[A(y) - f(r)] = 0, \quad p \in [0,1], \ r \in \Omega, \quad (17) $$

which is equivalent to

$$ H(y,p) = L(y) - L(y_0) + pL(y_0) + p[N(y) - f(r)] = 0, \quad (18) $$

where $p \in [0,1]$ is an embedding parameter, and y_0 is an initial guess approximation of (14) which satisfies the boundary conditions. It follows from (17) and (18) that

$$ \begin{aligned} H(y,0) &= L(y) - L(y_0) = 0, \\ H(y,1) &= A(y) - f(r) = 0. \end{aligned} \quad (19) $$

Thus, the changing process of p from 0 to 1 is just that of $y(r,p)$ from $y_0(r)$ to $y(r)$. In topology this is called deformation and $L(y) - L(y_0)$ and $A(y) - f(r)$ are called homotopic. Here the embedding parameter is introduced much more naturally, unaffected by artificial factors; further it can be considered as a small parameter for $0 \le p \le 1$. So it is very natural to assume that the solution of (18) and (19) can be expressed as

$$ y(t) = y_0(t) + py_1(t) + p^2 y_2(t) + \cdots. \quad (20) $$

The approximate solutions of the original equations can be obtained by setting $p = 1$; that is,

$$ y(t) = \lim_{p \to 1} \sum_{n=0}^{\infty} p^n y_n(t) = y_0(t) + y_1(t) + y_2(t) + \cdots. \quad (21) $$

The convergence of series (21) has been proved by He in his paper [15].

Because of the knowledge of various perturbation methods that low-order approximate solution leads to high accuracy, there requires no infinite series. Then after a series of recurrent calculation by using Mathematica software, we will get approximate solutions of fractional model (5).

According to HPM, we construct the following homotopy of (5)

$$D_t^\alpha u = p\left[\frac{\partial^6 u}{\partial x^6} + A\frac{\partial^4 u}{\partial x^4} + B\frac{\partial^2 u}{\partial x^2} + u - u^2\right], \quad (22)$$

where the homotopy parameter p is considered to be small, $0 \le p \le 1$.

Assuming the solution of (22) has the form

$$u(x,t) = u_0 + pu_1 + p^2u_2 + p^3u_3 + \cdots, \quad (23)$$

when $p \to 1$, (23) becomes the approximate solution of (5). Substituting (23) into (22) and equating the terms with identical powers of p, we obtain the following set of linear differential equations:

$$\begin{aligned} &p^0 : D_t^\alpha u_0 = 0,\\ &p^1 : D_t^\alpha u_1 = D_{xxxxxx}u_0 + AD_{xxxx}u_0 + BD_{xx}u_0 + u_0 - u_0^2,\\ &p^2 : D_t^\alpha u_2 = D_{xxxxxx}u_1 + AD_{xxxx}u_1 + BD_{xx}u_1 + u_1 - 2u_0u_1, \end{aligned} \quad (24)$$

and so on. The method is based on applying the operators I_t^α (the inverse operators of the Caputo derivative D_t^α) on both sides of the above linear differential equations. Using this selection we obtain the successive approximations and the solution may be obtained.

Finally, we approximate the analytical solutions of $u(x,t)$ by the truncated series

$$u(x,t) = \lim_{N\to\infty}\sum_{n=0}^{N-1} u_n(x,t). \quad (25)$$

For the illustration of the methodology of the reduced differential transform method, we write (5) in the standard operator form

$$L(u(x,t)) - R(u(x,t)) + N(u(x,t)) = 0, \quad (26)$$

with initial condition

$$u(x,0) = \varphi(x), \quad (27)$$

where $L(u(x,t)) = (\partial^\alpha/\partial t^\alpha)u(x,t)$ is the fractional time derivative operator and $R(u(x,t)) = \partial^6 u/\partial x^6 + A(\partial^4 u/\partial x^4) + B(\partial^2 u/\partial x^2) + u$ is linear operator and $N(u(x,t)) = u^2$ is nonlinear operator.

According to the RDTM and Theorems 6 and 7, we can construct the following iteration formula for (26):

$$\frac{\Gamma(\alpha+1+k/q)}{\Gamma(1+k/q)}U_{k+\alpha q}(x) = R(U_k(x)) - N(U_k(x)). \quad (28)$$

For the convenience of readers, we can give the first few nonlinear term are

$$\begin{aligned} N(U_0(x)) &= U_0^2(x),\\ N(U_1(x)) &= 2U_0(x)U_1(x),\\ N(U_2(x)) &= 2U_0(x)U_2(x) + U_1^2(x). \end{aligned} \quad (29)$$

From initial condition, we write

$$U_0(x) = \varphi(x). \quad (30)$$

Substituting (30) into (28) and by a straight forward iterative calculations, we get the following $U_k(x)$ values:

$$\begin{aligned} U_0(x,t) &= \varphi(x),\\ U_1(x,t) &= \left[\varphi^{(6)}(x) + A\varphi^{(4)}(x) + B\varphi^{(2)}(x)\right.\\ &\quad \left. + \varphi(x) - (\varphi(x))^2\right] \times \frac{t^\alpha}{\Gamma(\alpha+1)}, \end{aligned} \quad (31)$$

and so on. Then the inverse transformation of the set of values $\{U_k(x)\}_{k=0}^n$ gives approximation solution as

$$\tilde{u}_n(x,t) = \sum_{k=0}^{n} U_k(x)t^k, \quad (32)$$

where n is order of approximation solution.

Therefore, the exact solution of problem is given by

$$u(x,t) = \lim_{n\to\infty}\tilde{u}_n(x,t). \quad (33)$$

4. Numerical Results and Discussion

Here, we take three different values of $\varphi(x)$ and comparing the results of RDTM and HPM in the form of three- and two dimensional figures for each case, we would see that RDTM and HPM solutions are in excellent agreement. In this section we assume that $A = B = 1$.

Case Study 1. $\varphi(x) = 4\,\mathrm{sech}(\mu x)$. See Figures 1 and 2.

Case Study 2. $\varphi(x) = \pi + \mu\cos(\beta x)$. See Figures 3 and 4.

5. Conclusions

In this paper, RDTM and HPM are successfully applied to find the solution of the fractional differential equation and standard motion with different initial conditions. Unlike the traditional methods, the solutions here are given in series 9 form. The approximate solution to the equation was computed without any need for special transformations, linearization, or discretization. In addition, we compare these two methods and show that the results of the RDTM method are in excellent agreement with results of the HPM method and the obtained numerical solutions are shown graphically. We use the mathematical simulation to calculate the functions obtained from the RDTM and HPM. It was shown that RDTM and HPM methods are powerful tools for solving analytically of nonlinear equations.

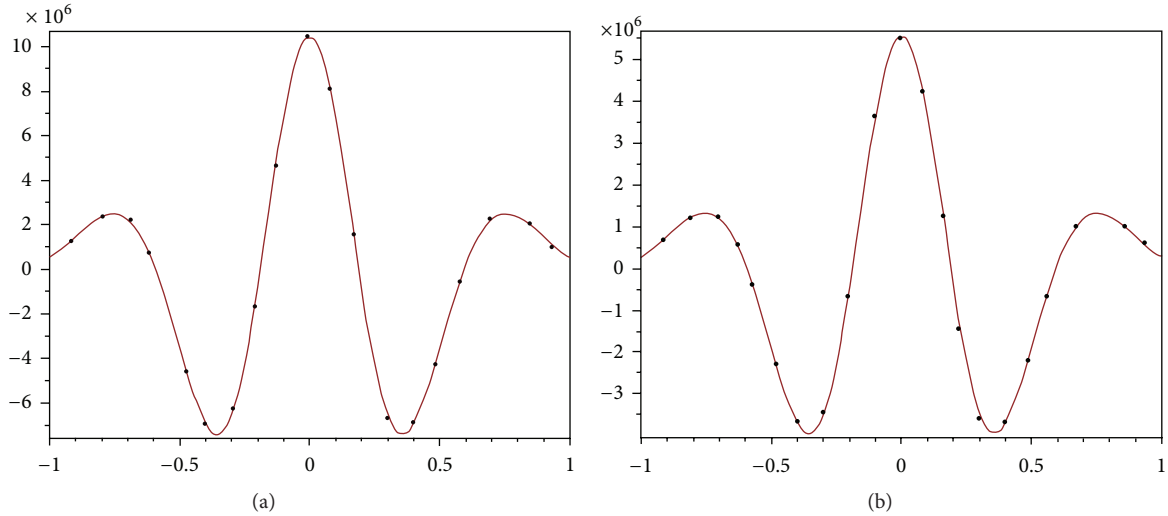

Figure 1: The comparison of the results of the RDTM and HPM for $\alpha = 1/4$ and $\alpha = 3/4$ at $t = 0.8$ and $\mu = 1$.

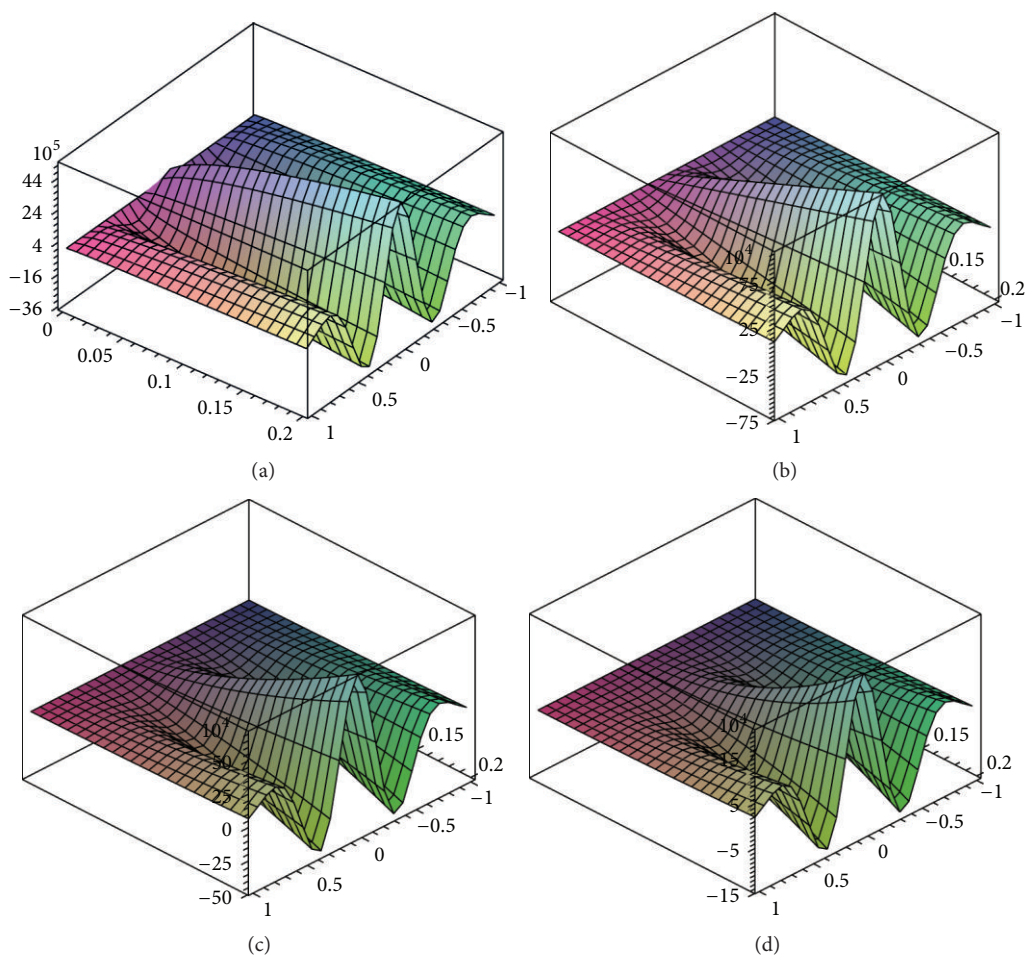

Figure 2: Results of the HPM for $\alpha = 1/4$, $1/2$, $3/4$ and 1 and $\mu = 1$.

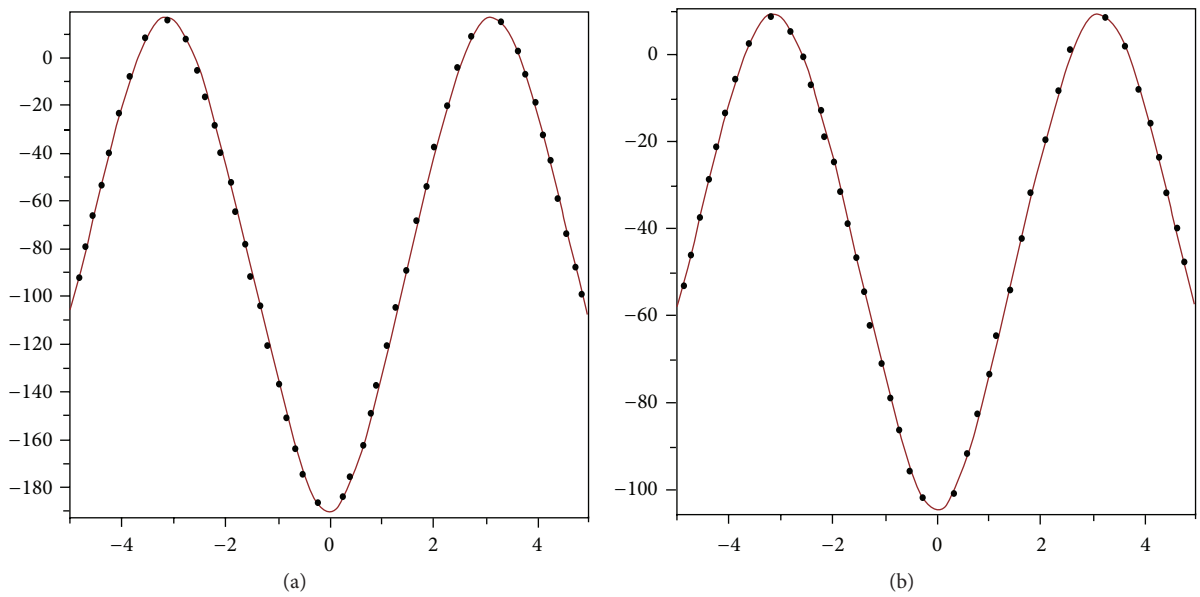

Figure 3: The comparison of the results of the RDTM and HPM for $\alpha = 1/4$ and $\alpha = 3/4$ at $t = 0.8$ and $\beta = \mu = 1$.

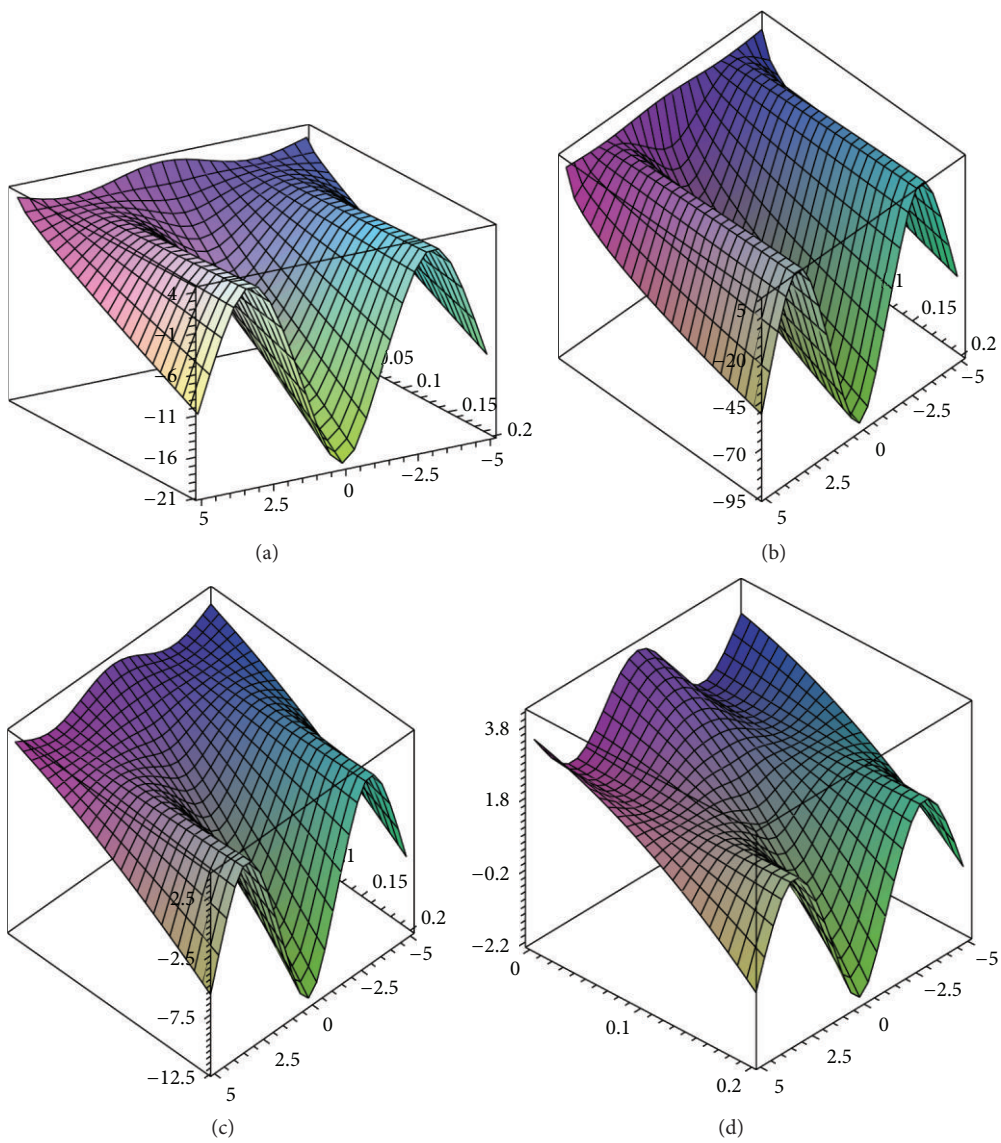

Figure 4: Results of the HPM for $\alpha = 1/4, 1/2, 3/4$ and 1 and $\beta = \mu = 1$.

Acknowledgments

This project was supported by the National Natural Science Foundation of China (no. 41206163), Open Research Program of State Key Laboratory of Tropical Oceanography (South China Sea Institute of Oceanology Chinese Academy of Sciences) (no. LTO1205), and the Pre-research Foundation of PLA University of Science and Technology.

References

[1] G. Wen and Z. Duan, "Dynamics behaviors of weighted local-world evolving networks with extended links," *International Journal of Modern Physics C*, vol. 20, no. 11, pp. 1719–1735, 2009.

[2] G. Wen, Z. Duan, W. Yu, and G. Chen, "Consensus of second-order multi-agent systems with delayed nonlinear dynamics and intermittent communications," *International Journal of Control*, vol. 86, no. 2, pp. 322–331, 2013.

[3] S. G. Samko, A. A. Kilbas, and O. I. Marichev, *Fractional Integrals and Derivatives. Theory and Applications*, Gordon and Breach, London, UK, 1993.

[4] V. Kiryakova, *Generalized Fractional Calculus and Applications*, vol. 301 of *Pitman Research Notes in Mathematics Series*, Longman Scientific & Technical, Harlow, UK, 1994.

[5] Z. Cui, Z. Yang, and Z. Rui, "Application of homotopy perturbation method to nonlinear fractional population dynamics models," *International Journal of Applied Mathematics and Computation*, vol. 4, pp. 403–412, 2012.

[6] I. Podlubny, *Fractional Differential Equations*, vol. 198 of *Mathematics in Science and Engineering*, Academic Press, San Diego, Calif, USA, 1999.

[7] R. Hilfer, *Applications of Fractional Calculus in Physics*, World Scientific, Singapore, 2000.

[8] M. Xu and W. Tan, "Intermediate processes and critical phenomena: theory, method and progress of fractional operators and their applications to modern mechanics," *Science in China G*, vol. 49, no. 3, pp. 257–272, 2006.

[9] Z. Cui, P. Yu, and W. Zong, "Dynamical behaviors and chaos in a new fractional-order financial system," in *Proceedings of the 5th International Workshop on Chaos-Fractals Theories and Applications (IWCFTA '12)*, pp. 109–113, 2012.

[10] P. Coullet, C. Elphick, and D. Repaux, "Nature of spatial chaos," *Physical Review Letters*, vol. 58, no. 5, pp. 431–434, 1987.

[11] G. T. Dee and W. Van Saarloos, "Bistable systems with propagating fronts leading to pattern formation," *Physical Review Letters*, vol. 60, no. 25, pp. 2641–2644, 1988.

[12] W. Zimmermann, "Propagating fronts near a Lifshitz point," *Physical Review Letters*, vol. 66, no. 11, p. 1546, 1991.

[13] R. A. Gardner and C. K. R. T. Jones, "Traveling waves of a perturbed diffusion equation arising in a phase field model," *Indiana University Mathematics Journal*, vol. 39, no. 4, pp. 1197–1222, 1990.

[14] G. Caginalp and P. Fife, "Higher-order phase field models and detailed anisotropy," *Physical Review B*, vol. 34, no. 7, pp. 4940–4943, 1986.

[15] J.-H. He, "Homotopy perturbation technique," *Computer Methods in Applied Mechanics and Engineering*, vol. 178, no. 3-4, pp. 257–262, 1999.

[16] J. H. He, "A new perturbation technique which is also valid for large parameters," *Chaos, Solitons and Fractals*, vol. 26, pp. 827–833, 2005.

[17] J. H. He, "Homotopy perturbation method for bifurcation of nonlinear problems," *International Journal of Nonlinear Sciences and Numerical Simulation*, vol. 6, no. 2, pp. 207–208, 2005.

[18] X. Li, M. Xu, and X. Jiang, "Homotopy perturbation method to time-fractional diffusion equation with a moving boundary condition," *Applied Mathematics and Computation*, vol. 208, no. 2, pp. 434–439, 2009.

[19] S. Momani and Z. Odibat, "Homotopy perturbation method for nonlinear partial differential equations of fractional order," *Physics Letters A*, vol. 365, no. 5-6, pp. 345–350, 2007.

[20] S. Das, P. K. Gupta, and Rajeev, "A fractional predator-prey model and its solution," *International Journal of Nonlinear Sciences and Numerical Simulation*, vol. 10, no. 7, pp. 873–876, 2009.

[21] S. Das and P. K. Gupta, "A mathematical model on fractional Lotka-Volterra equations," *Journal of Theoretical Biology*, vol. 277, pp. 1–6, 2011.

[22] J. K. Zhou, *Differential Transformation and Its Applications for Electrical CircuIts*, Huazhong University Press, Wuhan, China, 1986.

[23] M.-J. Jang, C.-L. Chen, and Y.-C. Liu, "Two-dimensional differential transform for partial differential equations," *Applied Mathematics and Computation*, vol. 121, no. 2-3, pp. 261–270, 2001.

[24] F. Ayaz, "Solutions of the system of differential equations by differential transform method," *Applied Mathematics and Computation*, vol. 147, no. 2, pp. 547–567, 2004.

[25] S. H. Ho and C. K. Chen, "Analysis of general elastically end restrained non-uniform beams using differential transform," *Applied Mathematical Modelling*, vol. 22, no. 4-5, pp. 219–234, 1998.

[26] O. O. Ozdemir and M. O. Kaya, "Flapwise bending vibration analysis of a rotating tapered cantilever Bernoulli-Euler beam by differential transform method," *Journal of Sound and Vibration*, vol. 289, no. 1-2, pp. 413–420, 2006.

[27] S. Çatal, "Solution of free vibration equations of beam on elastic soil by using differential transform method," *Applied Mathematical Modelling*, vol. 32, no. 9, pp. 1744–1757, 2008.

[28] A. Arikoglu and I. Ozkol, "Solution of fractional differential equations by using differential transform method," *Chaos, Solitons and Fractals*, vol. 34, no. 5, pp. 1473–1481, 2007.

[29] Y. Keskin and G. Oturanç, "Reduced differential transform method for partial differential equations," *International Journal of Nonlinear Sciences and Numerical Simulation*, vol. 10, no. 6, pp. 741–749, 2009.

[30] Y. Keskin and G. Oturanç, "Reduced differential transform method for generalized KdV equations," *Mathematical & Computational Applications*, vol. 15, no. 3, pp. 382–393, 2010.

Hindawi Publishing Corporation
Mathematical Problems in Engineering
Volume 2013, Article ID 208609, 9 pages
http://dx.doi.org/10.1155/2013/208609

Research Article

Synchronization of Intermittently Coupled Dynamical Networks

Gang Zhang[1] and Guanrong Chen[2]

[1] *College of Mathematics and Information Science, Hebei Normal University, Shijiazhuang 050016, China*
[2] *Department of Electronic Engineering, City University of Hong Kong, Kowloon, Hong Kong*

Correspondence should be addressed to Gang Zhang; gzhang_math@163.com

Received 17 April 2013; Accepted 5 June 2013

Academic Editor: Wenwu Yu

This paper investigates the synchronization phenomenon of an intermittently coupled dynamical network in which the coupling among nodes can occur only at discrete instants and the coupling configuration of the network is time varying. A model of intermittently coupled dynamical network consisting of identical nodes is introduced. Based on the stability theory for impulsive differential equations, some synchronization criteria for intermittently coupled dynamical networks are derived. The network synchronizability is shown to be related to the second largest and the smallest eigenvalues of the coupling matrix, the coupling strength, and the impulsive intervals. Using the chaotic Chua system and Lorenz system as nodes of a dynamical network for simulation, respectively, the theoretical results are verified and illustrated.

1. Introduction

A complex dynamical network is a large set of interconnected nodes, in which each node is typically a nonlinear dynamical system. Many real systems in nature and engineering, such as physical, biological, technological, and social systems, can be described by various models of complex dynamical networks. Complex dynamical networks, therefore, have become a significant research topic for studying nonlinear dynamics in various fields of sciences and humanities today [1–7].

One of the most remarkable phenomena in complex dynamical networks is the synchronization of dynamical nodes, which has been extensively investigated in recent years [8–32]. Wang and Chen [8, 9] presented a unified dynamical network model and investigated its synchronization in small-world and scale-free networks. Belykh et al. [11, 12] proposed an effective method for determining the global stability of synchronization in dynamical networks with different topologies, which combines the Lyapunov function approach with graph-theoretic reasoning. Restrepo et al. [19] studied the emergence of coherence in large-scale complex networks of interacting heterogeneous dynamical systems and showed that the largest eigenvalue of the network adjacency matrix plays a key role in determining the transition to coherence. Zhou et al. [20–22] derived some synchronization criteria for general complex delayed dynamical networks. Recently, synchronization of complex dynamical networks with impulsive control has been extensively studied [23–32]. For example, Guan et al. [23, 24] proposed a hybrid impulsive and switching control strategy and investigated the stabilization of complex networks. Liu et al. [25] proposed an impulsive synchronization scheme for an uncertain dynamical network. Zhang et al. [26] designed an effective impulsive controller to achieve impulsive synchronization for a complex dynamical network with unknown coupling. Lu et al. [27] investigated the problem of globally exponential synchronization of impulsive dynamical network, with a unified impulsive synchronization criterion derived by proposing a concept of average impulsive interval. Tang et al. [29] investigated the pinning synchronization problem of stochastic impulsive networks. Zhou et al. [30] proposed an impulsive control approach for analyzing pinning stability in a complex delayed dynamical network comprised of linearly coupled dynamical systems with coupling delays. Han et al. [31] and Sun et al. [32] derived some distributed impulsive control schemes for various impulsively coupled complex dynamical systems with or without delays.

However, the aforementioned work and most other existing research focus on the networks whose couplings are invariable or continuously varying in time. In the real world, there are many networks in which the coupling among nodes is intermittent. For example, in neural networks, the connections among neurons are usually cut-off type or extremely faint. There are prominent impulsive interactions among neurons when they are stimulated by certain signals, and the interactions are not identical due to the differences of stimulating signals. This type of networks is referred to as intermittently coupled dynamical networks. Note that the structure of such networks is time varying, and the interactions among nodes can only take place when some conditions are satisfied which are usually described by a group of discrete time sequences. To the best of our knowledge, there are few theoretical results about intermittently coupled dynamical networks in the current literature.

In this paper, an intermittently coupled dynamical network consisting of identical nodes is investigated. In the network, the coupling among nodes can only occur at discrete instants, and the coupling configuration of the network is varying at different instants. Based on the stability theory for impulsive differential equations, some synchronization criteria are obtained, showing that the synchronizability of the intermittently coupled dynamical network is related to the second largest and the smallest eigenvalues of the coupling matrix, the coupling strength, and the impulsive intervals. It turns out that the analytical results about the second largest and the smallest eigenvalues of the coupling matrix are consistent with other known results about complex dynamical networks [8, 9, 19].

The rest of the paper is organized as follows. In Section 2, an intermittently coupled dynamical network model is introduced, and some necessary definitions and preliminary lemmas are presented. The main results of the paper are given in Section 3, where some synchronization criteria for the network model are derived. In Section 4, using the chaotic Chua system and Lorenz system as nodes of a dynamical network, respectively, numerical simulations are performed to illustrate and verify the theoretical results. Finally, conclusions are drawn in Section 5.

2. Model Description and Preliminaries

Consider an intermittently coupled dynamical network consisting of N identical nodes, with each node being an n-dimension dynamical system, described by

$$\dot{x}_i(t) = f(x_i(t)) + \sum_{k=1}^{\infty} U_i(t; x_1, \ldots, x_N)\,\delta(t - t_k), \quad i = 1, 2, \ldots, N, \tag{1}$$

where $x_i = (x_{i1}, x_{i2}, \ldots, x_{in})^T \in R^n$ is the state vector of node i, $f : R^n \to R^n$ is continuously differentiable, $U_i(t; x_1, x_2, \ldots, x_N) : R \times R^{nN} \to R^n$ are coupling functions, time sequence $\{t_k\}_{k=1}^{\infty}$ satisfies $0 < t_1 < t_2 < \cdots < t_k < t_{k+1} < \cdots$, $\lim_{k\to\infty} t_k = \infty$, and $\delta(\cdot)$ is a Dirac delta function defined by

$$\delta(t - t_k) = \begin{cases} \infty, & t = t_k, \\ 0, & t \neq t_k, \end{cases} \tag{2}$$

satisfying the identities $\int_{-\infty}^{+\infty} \delta(t)dt = 1$ and $\int_{-\infty}^{+\infty} g(t)\delta(t - t_0)dt = g(t_0)$ for any continuous function $g(t)$. Suppose that the function f satisfies the following condition.

(**A1**) There exists a positive scalar L such that, for any $x, y \in R^n$,

$$\|f(x) - f(y)\| \le L\|x - y\|. \tag{3}$$

In this paper, we consider the dynamical network with time-varying diffusive coupling at discrete instants. Let

$$U_i(t_k; x_1, \ldots, x_N) = c \sum_{j=1, j\neq i}^{N} a_{ij}(t_k)\,\Gamma\left[x_j(t_k) - x_i(t_k)\right], \tag{4}$$

where constant $c > 0$ is the coupling strength, $A(t_k) = (a_{ij}(t_k)) \in R^{N\times N}$ is the outer-coupling matrix which represents the coupling configuration of network (1) at instant t_k, and $a_{ij}(t_k)$ is defined as follows: if there is a connection between nodes i and j $(i \neq j)$, then $a_{ij}(t_k) = a_{ji}(t_k) = 1$, otherwise, $a_{ij}(t_k) = a_{ji}(t_k) = 0$ $(i \neq j)$; the diagonal elements are defined by

$$a_{ii}(t_k) = -\sum_{j=1, j\neq i}^{N} a_{ij}(t_k) = -\sum_{j=1, j\neq i}^{N} a_{ji}(t_k), \quad i = 1, 2, \ldots, N, \tag{5}$$

and $\Gamma = \mathrm{diag}\{\gamma_1, \gamma_2, \ldots, \gamma_n\} \in R^{n\times n}$ is the inner-linking matrix. Let $\Gamma = \mathrm{diag}\{1, 1, \ldots, 1\}$. Thus, (4) becomes

$$U_i(t_k; x_1, x_2, \ldots, x_N) = c \sum_{j=1}^{N} a_{ij}(t_k)\,\Gamma x_j(t_k). \tag{6}$$

Assume that network (1) is connected at instants $t_1, t_2, \ldots$, in the sense that there is no isolated cluster; that is, $A(t_k)$ is an irreducible matrix.

Lemma 1 (see [14]). *Suppose that the outer-coupling matrix $A = (a_{ij}) \in R^{N\times N}$ satisfies the above-mentioned conditions. Then,*

(i) *0 is an eigenvalue of matrix A of multiplicity 1, associated with eigenvector $(1/\sqrt{N}, 1/\sqrt{N}, \ldots, 1/\sqrt{N})^T$;*

(ii) *all the other eigenvalues of A are real-valued and are strictly negative.*

Lemma 1 implies that the outer-coupling matrix $A(t_k)$ of network (1) at instant t_k has a 0 eigenvalue of multiplicity 1, with $\lambda_N(t_k) \le \cdots \le \lambda_2(t_k) < \lambda_1(t_k) = 0$.

Remark 2. According to matrix theory, there exists an orthogonal matrix $B(t_k)$ such that $A(t_k) = B^T(t_k)\Lambda(t_k)B(t_k)$, where $\Lambda(t_k) = \mathrm{diag}\{\lambda_1(t_k), \ldots, \lambda_N(t_k)\}$. It is easy to see that the first column of $B^T(t_k)$ can be chosen as the eigenvector $(1/\sqrt{N}, 1/\sqrt{N}, \ldots, 1/\sqrt{N})^T$ corresponding to the zero eigenvalue of $A(t_k)$.

Next, network (1) is rewritten as the following impulsive differential equations:

$$\begin{aligned} \dot{x}_i(t) &= f(x_i(t)), \quad t \neq t_k,\ i = 1, 2, \ldots, N, \\ \Delta x_i(t_k) &= c\sum_{j=1}^{N} a_{ij}(t_k)\, x_j(t_k), \quad t = t_k,\ k = 1, 2, \ldots, \end{aligned} \tag{7}$$

where $\Delta x_i(t_k) = x_i(t_k^+) - x_i(t_k^-)$ is the "jump" in the state variable at instant t_k, with $x_i(t_k^+) = \lim_{t\to t_k^+} x(t)$, $x_i(t_k^-) = \lim_{t\to t_k^-} x(t)$. For simplicity, assume that $x_i(t_k^-) = x_i(t_k)$, which means $x_i(t)$ is continuous from the left.

Definition 3. The synchronization manifold is presented as $\mathbf{S} = \{(x_1^T, x_2^T, \ldots, x_N^T)^T \in R^{nN} : x_i = x_j,\ i, j = 1, 2, \ldots N\}$, where $x_i \in R^n$, $i = 1, 2, \ldots, N$.

Definition 4. The coupled system (6) is said to achieve synchronization if, for all $i, j = 1, 2, \ldots, N$, $\lim_{t\to\infty}\|x_i(t) - x_j(t)\| = 0$.

From Definitions 3 and 4, it can be easily seen that the intermittently coupled system (7) achieves synchronization if and only if the synchronization manifold $\mathbf{S}$ for the coupled system (7) is globally asymptotically stable.

3. Synchronization of the Intermittently Coupled Network

Let $\overline{x}(t) = (1/N)\sum_{j=1}^{N} x_j(t)$ and $\overline{X}(t) = [\overline{x}^T(t), \ldots, \overline{x}^T(t)]^T \in \mathbf{S}$, which can be regarded as a projection of $X(t) = [x_1^T(t), \ldots, x_N^T(t)]^T$ on the synchronization manifold. The dynamical equation of $\overline{x}(t)$ can be written as

$$\dot{\overline{x}}(t) = \frac{1}{N}\sum_{i=1}^{N}\dot{x}_i(t) = \frac{1}{N}\sum_{i=1}^{N} f(x_i(t)), \quad t \neq t_k. \tag{8}$$

On the other hand,

$$\begin{aligned} \overline{x}(t_k^+) &= \frac{1}{N}\sum_{i=1}^{N} x_i(t_k^+) \\ &= \frac{1}{N}\sum_{i=1}^{N}\left[x_i(t_k) + c\sum_{j=1}^{N} a_{ij}(t_k)\, x_j(t_k)\right] \\ &= \frac{1}{N}\sum_{i=1}^{N} x_i(t_k) + \frac{c}{N}\sum_{j=1}^{N}\left[\sum_{i=1}^{N} a_{ij}(t_k)\right] x_j(t_k) \\ &= \overline{x}(t_k), \quad k = 1, 2, \ldots. \end{aligned} \tag{9}$$

Define the synchronization error of node i as $e_i(t) = x_i(t) - \overline{x}(t)$, $i = 1, 2, \ldots, N$. Obviously, $\sum_{i=1}^{N} e_i(t) = 0$.

For $t \neq t_k$, $k = 1, 2, \ldots$, one has

$$\begin{aligned} \dot{e}_i(t) &= f(x_i(t)) - \frac{1}{N}\sum_{j=1}^{N} f(x_i(t)) \\ &= f(x_i(t)) - f(\overline{x}(t)) + \frac{1}{N}\sum_{j=1}^{N}\left[f(\overline{x}(t)) - f(x_j(t))\right] \\ &= \widetilde{f}(e_i(t)) - \frac{1}{N}\sum_{j=1}^{N}\widetilde{f}(e_j(t)), \end{aligned} \tag{10}$$

where $\widetilde{f}(e_i(t)) = f(\overline{x}(t) + e_i(t)) - f(\overline{x}(t))$.

According to assumption (**A1**), it can be easily shown that

$$\left\|\widetilde{f}(e_i(t))\right\| \leq L\left\|e_i(t)\right\|, \quad i = 1, 2, \ldots, N. \tag{11}$$

For $t = t_k$, $k = 1, 2, \ldots$, one has

$$\begin{aligned} e_i(t_k^+) &= x_i(t_k^+) - \overline{x}(t_k^+) \\ &= x_i(t_k) + c\sum_{j=1}^{N} a_{ij}(t_k)\, x_j(t_k) - \overline{x}(t_k) \\ &= e_i(t_k) + c\sum_{j=1}^{N} a_{ij}(t_k)\, e_j(t_k). \end{aligned} \tag{12}$$

Therefore, the error dynamical system can be described as

$$\begin{aligned} \dot{e}_i(t) &= \widetilde{f}(e_i(t)) - \frac{1}{N}\sum_{j=1}^{N}\widetilde{f}(e_j(t)), \quad t \neq t_k, \\ e_i(t_k^+) &= e_i(t_k) + c\sum_{j=1}^{N} a_{ij}(t_k)\, e_j(t_k), \quad k = 1, 2, \ldots, \end{aligned} \tag{13}$$

where $i = 1, 2, \ldots, N$.

Let $e(t) = [e_1^T(t), \ldots, e_N^T(t)]^T \in R^{nN}$. It is easily seen that the stability of the synchronization manifold is equivalent to $e(t) \to 0$ as $t \to \infty$. In the following, we directly investigate the dynamical behaviors of the error dynamical system (13).

Theorem 5. *Let $P \in R^{n\times n}$ be a symmetric and positive definite matrix, with $\lambda_{\max}(P)$ and $\lambda_{\min}(P)$ being the largest and the smallest eigenvalues, respectively. Suppose that there exists a constant $\xi > 1$ and, for all $k = 1, 2, \ldots$,*

$$\frac{\lambda_{\min}(P)\exp^{-2L\sqrt{(\lambda_{\max}(P)/\lambda_{\min}(P))}(t_{k+1}-t_k)}}{\lambda_{\max}(P)\,\lambda(t_k)} \geq \xi > 1, \tag{14}$$

where $\lambda(t_k) = \max\{(1 + c\lambda_i(t_k))^2 \mid i = 2, N\}$, $\lambda_2(t_k)$ and $\lambda_N(t_k)$ are the second largest and the smallest eigenvalues of matrix $A(t_k)$, respectively, and the constant $c > 0$ is the coupling strength. Then, the trivial solution of the error dynamical system (21) *is asymptotically stable, implying that network* (1) *achieves synchronization.*

Proof. Construct a Lyapunov function as

$$V(t,e) = e^T(t)(I_N \otimes P)e(t) = \sum_{i=1}^{N} e_i^T(t) P e_i(t), \tag{15}$$

where $\otimes$ denotes the Kronecker product operator.

For $t \neq t_k$, taking Dini's derivative along the trajectories of (13) gives

$$\begin{aligned} D^+V(t,e) &= \sum_{i=1}^{N} 2e_i^T(t) P\dot{e}_i(t) \\ &= \sum_{i=1}^{N} 2e_i^T(t) P\left[\tilde{f}(e_i(t)) - \frac{1}{N}\sum_{j=1}^{N}\tilde{f}(e_j(t))\right] \\ &= \sum_{i=1}^{N} 2e_i^T(t) P\tilde{f}(e_i(t)) \\ &\leq \sum_{i=1}^{N} \frac{1}{L}\sqrt{\lambda_{\min}(P)\lambda_{\max}(P)}\tilde{f}^T(e_i(t))\tilde{f}(e_i(t)) \\ &\quad + \frac{L}{\sqrt{\lambda_{\min}(P)\lambda_{\max}(P)}} e_i^T(t) P^T P e_i(t) \\ &\leq \sum_{i=1}^{N} L\sqrt{\lambda_{\min}(P)\lambda_{\max}(P)}\frac{e_i^T(t) P e_i(t)}{\lambda_{\min}(P)} \\ &\quad + L\sqrt{\frac{\lambda_{\max}(P)}{\lambda_{\min}(P)}} e_i^T(t) P e_i(t) \\ &= 2L\sqrt{\frac{\lambda_{\max}(P)}{\lambda_{\min}(P)}} V(t,e). \end{aligned} \tag{16}$$

For $t = t_k$, one has

$$\begin{aligned} e(t_k^+) &= \left(e_1^T(t_k^+), e_2^T(t_k^+), \ldots, e_N^T(t_k^+)\right)^T \\ &= e(t_k) + cA^T(t_k) \otimes I_n e(t_k) \\ &= \left[I_N \otimes I_n + cA^T(t_k) \otimes I_n\right] e(t_k). \end{aligned} \tag{17}$$

Therefore,

$$\begin{aligned} V(t_k^+, e) &= e^T(t_k^+)(I_N \otimes P)e(t_k^+) \\ &= e^T(t_k)\left[(I_N + cA(t_k)) \otimes I_n\right]^T (I_N \otimes P) \\ &\quad \times \left[(I_N + cA(t_k)) \otimes I_n\right] e(t_k) \\ &\leq \lambda_{\max}(P) e^T(t_k)\left[(I_N + cA(t_k)) \otimes I_n\right]^T \\ &\quad \times \left[(I_N + cA(t_k)) \otimes I_n\right] e(t_k) \\ &= \lambda_{\max}(P) e^T(t_k)\left[(I_N + cA(t_k))^2 \otimes I_n\right] e(t_k). \end{aligned} \tag{18}$$

Based on the property of the matrix $A(t_k)$ mentioned in Remark 2, there exits an orthogonal matrix $B(t_k)$ such that $A(t_k) = B^T(t_k)\Lambda(t_k)B(t_k)$, where

$$\Lambda(t_k) = \operatorname{diag}\{\lambda_1(t_k), \ldots, \lambda_N(t_k)\} \tag{19}$$

and the first column of $B^T(t_k)$ is the eigenvector $(1/\sqrt{N}, \ldots, 1/\sqrt{N})^T$ corresponding to the zero eigenvalue of $A(t_k)$. Let $\eta(t_k) = (\eta_1^T(t_k), \ldots, \eta_N^T(t_k))^T = (B(t_k) \otimes I_n)e(t_k)$. Then,

$$\eta_1(t_k) = \frac{1}{\sqrt{N}}\sum_{j=1}^{N} e_j(t_k) = \mathbf{0}. \tag{20}$$

Therefore,

$$\eta(t_k) = \left(\mathbf{0}, \eta_2^T(t_k), \ldots, \eta_N^T(t_k)\right)^T. \tag{21}$$

Let $\lambda(t_k) = \max\{(1 + c\lambda_i(t_k))^2 \mid i = 2, N\}$, where $\lambda_2(t_k)$ and $\lambda_N(t_k)$ are the second largest and the smallest eigenvalues of matrix $A(t_k)$, respectively. It follows from (18) and (21) that

$$\begin{aligned} V(t_k^+, e) &\leq \lambda_{\max}(P) e^T(t_k) \\ &\quad \times \left[\left(B^T(t_k)(I_N + c\Lambda(t_k))^2 B(t_k)\right) \otimes I_n\right] e(t_k) \\ &= \lambda_{\max}(P)\eta^T(t_k)\left((I_N + c\Lambda(t_k))^2 \otimes I_n\right)\eta(t_k) \\ &= \lambda_{\max}(P)\sum_{i=1}^{N}\eta_i^T(t_k)(1 + c\lambda_i(t_k))^2\eta_i(t_k) \\ &\leq \lambda_{\max}(P)\lambda(t_k)\sum_{i=1}^{N}\eta_i^T(t_k)\eta_i(t_k) \\ &= \lambda_{\max}(P)\lambda(t_k) e^T(t_k)\left(B^T(t_k) \otimes I_n\right) \\ &\quad \times (B(t_k) \otimes I_n) e(t_k) \\ &\leq \frac{\lambda_{\max}(P)}{\lambda_{\min}(P)}\lambda(t_k) e^T(t_k)(I_N \otimes P) e(t_k) \\ &= \frac{\lambda_{\max}(P)}{\lambda_{\min}(P)}\lambda(t_k) V(t_k, e). \end{aligned} \tag{22}$$

Let $S_\rho = \{x \in R^n : ||x|| < \rho\}$. Since $||e(t_k^+)|| = ||[(I_N + cA(t_k)) \otimes I_n]e(t_k)|| \leq ||(I_N + cA(t_k)) \otimes I_n||||e(t_k)||$ and $||(I_N + cA(t_k)) \otimes I_n|| < \infty$, there exists a $\rho_0 > 0$ such that $e(t_k) \in S_{\rho_0}$ implies $e(t_k^+) \in S_\rho$ for all k.

Since P is a symmetric and positive definite matrix, one has

$$\lambda_{\min}(P)\sum_{i=1}^{n} e_i^T(t) e_i(t) \leq V(t,e) \leq \lambda_{\max}(P)\sum_{i=1}^{n} e_i^T(t) e_i(t). \tag{23}$$

Thus, by the well-known comparison Theorem [33], the asymptotic stability of the trivial solution of the impulsive

dynamical system (13) follows from the comparison system below:

$$\begin{aligned}
\dot{\omega}(t) &= 2L\sqrt{\frac{\lambda_{\max}(P)}{\lambda_{\min}(P)}}\,\omega(t), \quad t \neq t_k,\\
\omega(t_k^+) &= \frac{\lambda_{\max}(P)}{\lambda_{\min}(P)}\lambda(t_k)\,\omega(t_k), \quad t = t_k,\ k = 1,2,\ldots,\\
\omega(t_0^+) &= \omega_0.
\end{aligned} \tag{24}$$

Therefore, by the stability criterion for impulsive differential equations [34], there exists a constant $\xi > 1$ such that

$$\ln\frac{\lambda_{\max}(P)}{\lambda_{\min}(P)}\lambda(t_k)\,\xi + 2L\sqrt{\frac{\lambda_{\max}(P)}{\lambda_{\min}(P)}}\,(t_{k+1} - t_k) \leq 0, \tag{25}$$

namely,

$$\frac{\lambda_{\min}(P)\exp^{-2L\sqrt{(\lambda_{\max}(P)/\lambda_{\min}(P))}(t_{k+1}-t_k)}}{\lambda_{\max}(P)\,\lambda(t_k)} \geq \xi > 1. \tag{26}$$

Hence, the trivial solution of error dynamical system (13) is asymptotically stable, implying that network (1) achieves synchronization. □

Remark 6. For a dynamical network consisting of N nodes, the number of possible coupling matrices which represent the coupling configurations of the network is finite. Therefore, one may define

$$\lambda^{\max} = \max_{k=1,2,\ldots}\lambda_2(t_k), \qquad \lambda^{\min} = \min_{k=1,2,\ldots}\lambda_N(t_k), \tag{27}$$

and $\lambda = \max\{(1 + c\lambda^{\max})^2, (1 + c\lambda^{\min})^2\}$. It is obvious that $\lambda(t_k) \leq \lambda$ for all $k = 1, 2, \ldots$.

Remark 7. The synchronizability of network (1) is determined by the second largest eigenvalue $\lambda_2(t_k)$ and the smallest eigenvalue $\lambda_N(t_k)$ of the coupling matrix, the coupling strength c, and impulsive intervals $\sigma_k = t_{k+1} - t_k$, $k = 1, 2, \ldots$.

4. Numerical Simulations

In this section, two illustrative examples about the chaotic Chua system and Lorenz system, respectively, are given to demonstrate the theoretical results obtained above. Without loss of generality, let the impulses be equidistant and separated by a constant interval $\sigma > 0$.

Example 1. The chaotic Chua system is used as nodes of a dynamical network, which is described by

$$\begin{pmatrix}\dot{x}\\ \dot{y}\\ \dot{z}\end{pmatrix} = \begin{pmatrix}\alpha[y - x - \varphi(x)]\\ x - y + z\\ -\beta y\end{pmatrix}, \tag{28}$$

where α, β are two parameters and $\varphi(x) = bx + 0.5(a - b)(|x+1| - |x-1|)$ represents a piecewise-linear diode, where

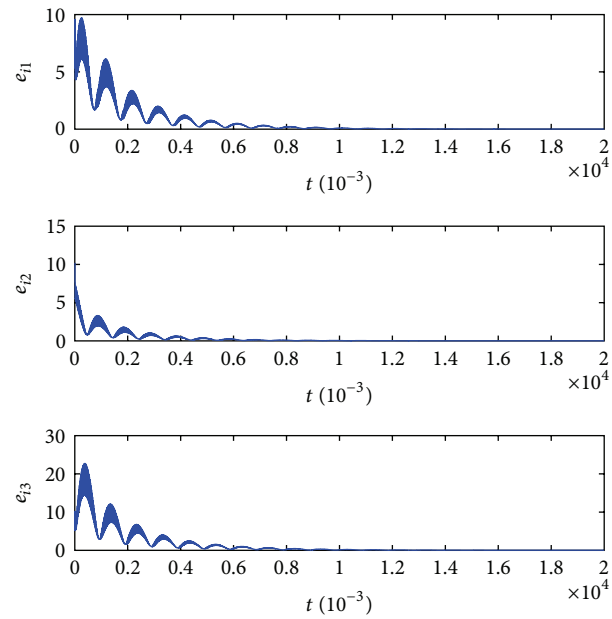

Figure 1: $N = 100$, $\sigma = 0.01$, and $c = 0.01$.

$a < b < 0$ are two constants. It is well known that Chua system is chaotic when $\alpha = 9.22$, $\beta = 15.99$, $a = -1.25$, and $b = -0.76$.

The intermittently coupled dynamical network is described by

$$\begin{aligned}
\dot{x}_i(t) &= f(x_i(t)), \quad t \neq t_k,\\
\Delta x_i(t_k) &= c\sum_{j=1}^{N} a_{ij}(t_k)\,x_j(t_k), \quad t = t_k,\ k = 1,2,\ldots,
\end{aligned} \tag{29}$$

where

$$f(x_i(t)) = \begin{pmatrix}\alpha[x_{i2} - x_{i1} - \varphi(x_{i1})]\\ x_{i1} - x_{i2} + x_{i3}\\ -\beta x_{i2}\end{pmatrix}. \tag{30}$$

The outer-coupling matrix $A(t_k) = (a_{ij}(t_k)) \in R^{N\times N}$ represents the coupling configuration of the dynamical network at instant t_k and is defined as follows.

When k is odd, the dynamical network has nearest-neighbor coupling, so

$$A(t_k) = A_1 = \begin{pmatrix}-2 & 1 & 0 & \cdots & 0 & 1\\ 1 & -2 & 1 & \cdots & 0 & 0\\ \vdots & \vdots & \vdots & \vdots & \vdots & \vdots\\ 1 & 0 & 0 & \cdots & 1 & -2\end{pmatrix}. \tag{31}$$

When k is even, the dynamical network has star coupling, so

$$A(t_k) = A_2 = \begin{pmatrix}-N+1 & 1 & 1 & \cdots & 1 & 1\\ 1 & -1 & 0 & \cdots & 0 & 0\\ \vdots & \vdots & \vdots & \vdots & \vdots & \vdots\\ 1 & 0 & 0 & \cdots & 0 & -1\end{pmatrix}. \tag{32}$$

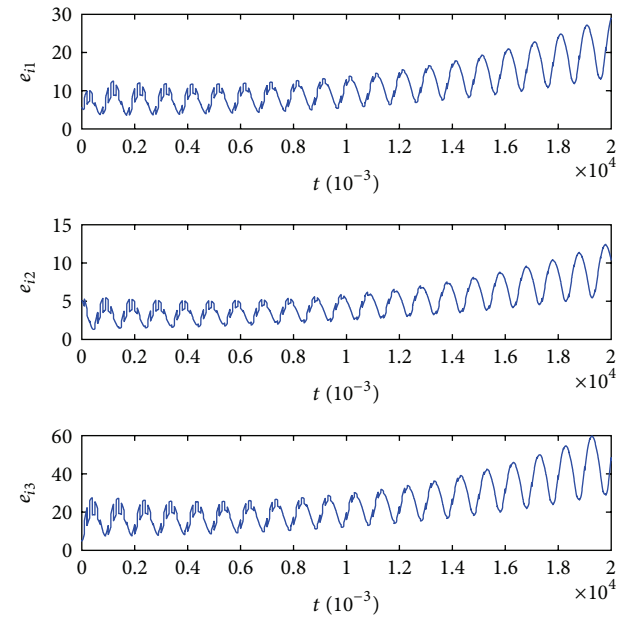

Figure 2: $N = 100$, $\sigma = 0.05$, and $c = 0.01$.

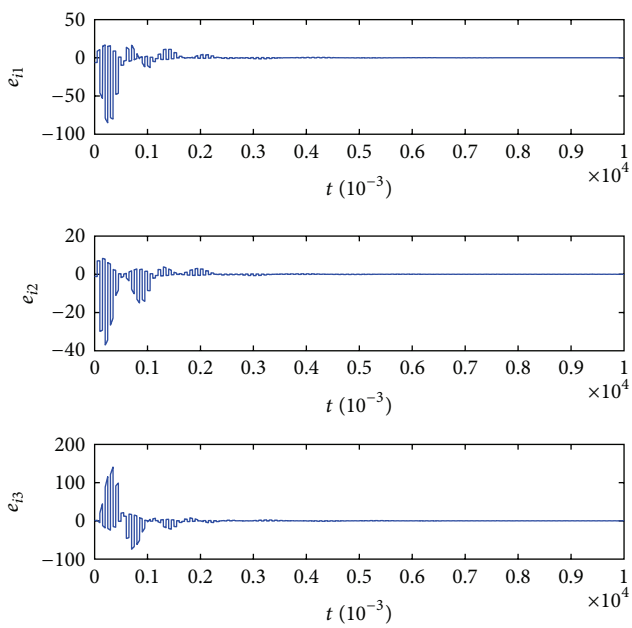

Figure 3: $N = 100$, $\sigma = 0.05$, and $c = 0.05$.

In the simulation, we choose $N = 100$. The initial values of these systems are chosen randomly from interval $[-20, 20]$. For a small impulsive interval $\sigma > 0$, the synchronization of network (29) can be achieved by choosing an appropriate coupling strength c. The numerical simulation results are shown in Figures 1–5, where $e_{ij} = \sum_{i=2}^{N} |x_{ij} - x_{1j}|/(N-1)$, $j = 1, 2, 3$.

In Figure 1, $\sigma = 0.01$ and $c = 0.01$. One can see that the state errors between node 1 and node i, $i = 2, 3, \ldots, 100$, tend to zero asymptotically as time evolves, implying that network (29) achieves synchronization. When $\sigma = 0.05$ and

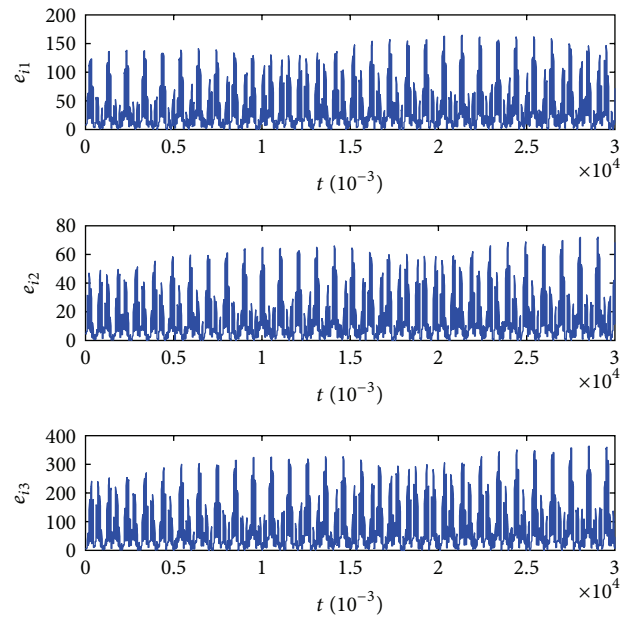

Figure 4: $N = 100$, $\sigma = 0.05$, and $c = 0.06$.

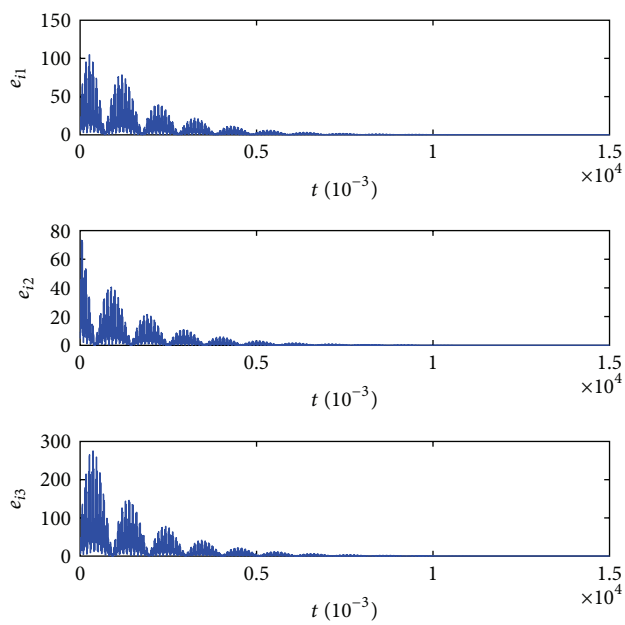

Figure 5: $N = 100$, $\sigma = 0.01$, and $c = 0.06$.

$c = 0.01$, network (29) cannot achieve synchronization, as shown in Figure 2. Figure 3 shows that network (29) achieves synchronization with $\sigma = 0.05$ and $c = 0.05$. Figure 4 shows that network (29) cannot achieve synchronization where $\sigma = 0.05$ and $c = 0.06$. Figure 5 shows that network (29) achieves synchronization with $\sigma = 0.01$ and $c = 0.06$.

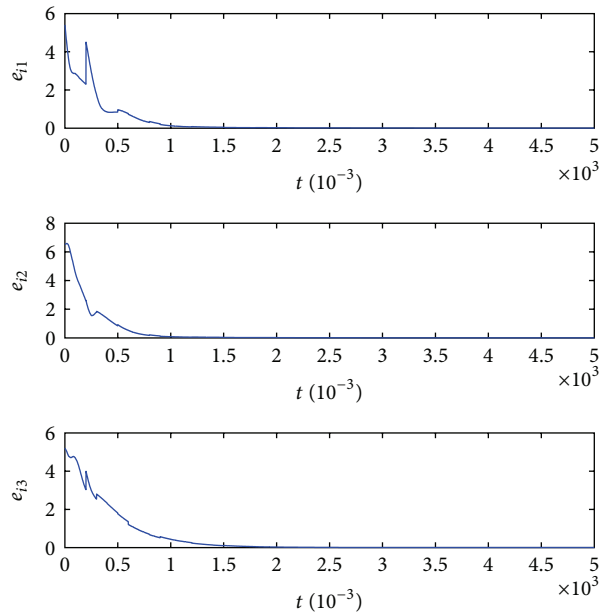

FIGURE 6: $N = 200$, $\sigma = 0.1$, and $c = 0.01$.

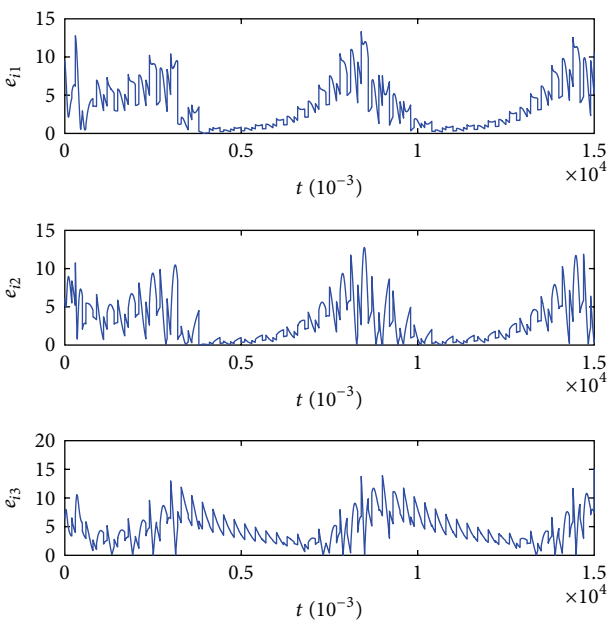

FIGURE 7: $N = 200$, $\sigma = 0.1$, and $c = 0.015$.

Example 2. The chaotic Lorenz system is used as nodes of a dynamical network, which is described by

$$\begin{pmatrix} \dot{x} \\ \dot{y} \\ \dot{z} \end{pmatrix} = \begin{pmatrix} a(y-x) \\ cx - xz - y \\ xy - bz \end{pmatrix}, \tag{33}$$

with a chaotic attractor when $a = 10$, $b = 8/3$, and $c = 28$.

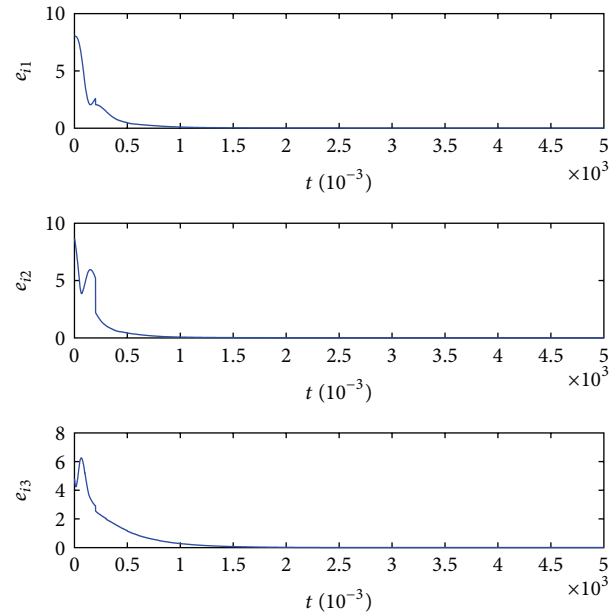

FIGURE 8: $N = 50$, $\sigma = 0.1$, and $c = 0.015$.

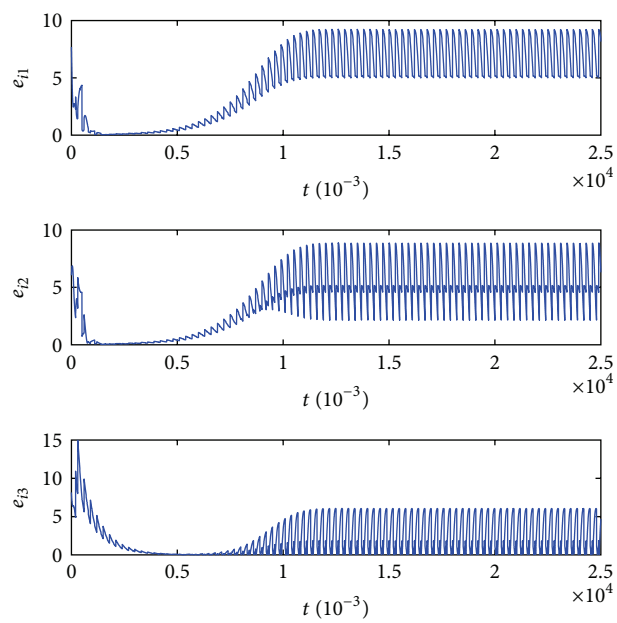

FIGURE 9: $N = 50$, $\sigma = 0.1$, and $c = 0.055$.

The intermittently coupled dynamical network is described by

$$\begin{aligned} \dot{x}_i(t) &= f(x_i(t)), \quad t \neq t_k, \ k = 1, 2, \ldots, \\ \Delta x_i(t_k) &= c \sum_{j=1}^{N} a_{ij}(t_k)\, x_j(t_k), \quad t = t_k, \end{aligned} \tag{34}$$

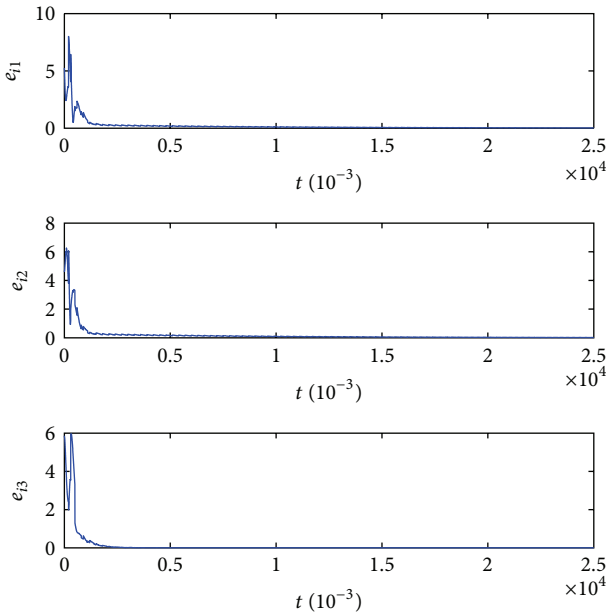

Figure 10: $N = 50$, $\sigma = 0.1$, and $c = 0.048$.

where

$$f(x_i(t)) = \begin{pmatrix} a(x_{i2} - x_{i1}) \\ cx_{i1} - x_{i1}x_{i3} - x_{i2} \\ x_{i1}x_{i2} - bx_{i3} \end{pmatrix}. \tag{35}$$

Let $l \equiv k \bmod 3$. The outer-coupling matrix $A(t_k) = (a_{ij}(t_k)) \in R^{N\times N}$ is defined as follows.

When $l = 1$, the dynamical network has global coupling, and its outer-coupling matrix is

$$A(t_k) = A_{gc} = \begin{pmatrix} -N+1 & 1 & 1 & \cdots & 1 \\ 1 & -N+1 & 1 & \cdots & 1 \\ \vdots & \vdots & \vdots & \vdots & \vdots \\ 1 & 1 & 1 & \cdots & -N+1 \end{pmatrix}. \tag{36}$$

When $l = 2$, the dynamical network has nearest-neighbor coupling, with

$$A(t_k) = A_1 = \begin{pmatrix} -2 & 1 & 0 & \cdots & 0 & 1 \\ 1 & -2 & 1 & \cdots & 0 & 0 \\ \vdots & \vdots & \vdots & \vdots & \vdots & \vdots \\ 1 & 0 & 0 & \cdots & 1 & -2 \end{pmatrix}. \tag{37}$$

When $l = 0$, the dynamical network has star coupling, with

$$A(t_k) = A_2 = \begin{pmatrix} -N+1 & 1 & 1 & \cdots & 1 & 1 \\ 1 & -1 & 0 & \cdots & 0 & 0 \\ \vdots & \vdots & \vdots & \vdots & \vdots & \vdots \\ 1 & 0 & 0 & \cdots & 0 & -1 \end{pmatrix}. \tag{38}$$

In the simulation, we choose $\sigma = 0.1$. The initial values of these systems are chosen randomly from interval $[-20, 20]$. The numerical simulation results indicate that the synchronizability of network (34) is related to the coupling strength c and the number of nodes N, as shown in Figures 6–10, where $e_{ij} = \sum_{i=2}^{N} |x_{ij} - x_{1j}|/(N-1)$, $j = 1, 2, 3$. For the coupling matrices of this network (34), the spectral width of eigenvalues will be broadened with increasing N. Therefore, the synchronizability of the network will be weakened if the node number increases sharply.

In Figure 6, $N = 200$ and $c = 0.01$. One can see that the state errors tend to zero asymptotically as time evolves, implying that network (34) achieves synchronization. When $N = 200$ and $c = 0.015$, network (34) cannot achieve synchronization, as illustrated in Figure 7. When $N = 50$ and $c = 0.015$, network (34) achieves synchronization, as shown in Figure 8. When $N = 50$ and $c = 0.055$, network (34) cannot achieve synchronization, as shown in Figure 9. Figure 10 demonstrates that network (34) achieves synchronization when $N = 50$ and $c = 0.048$.

5. Conclusions

This paper investigates the synchronization phenomenon of an intermittently coupled dynamical network, in which the coupling among nodes can occur only at discrete instants and the coupling configuration of the network is varying at different instants. For such an intermittently coupled dynamical network consisting of identical nodes, based on the stability theory for impulsive differential equations, some synchronization conditions are derived. It is shown that the synchronizability of the network is related to the second largest eigenvalue and the smallest eigenvalue of the coupling matrix, the coupling strength, and the impulsive intervals. It is worth noting that the analytical results about the second largest and the smallest eigenvalues of the coupling matrix are consistent with most existing criteria for complex dynamical networks. Finally, by employing the chaotic Chua system and Lorenz system as nodes of a dynamical network, respectively, numerical simulations are carried out to illustrate and verify the theoretical results.

Acknowledgments

The authors gratefully acknowledge the support of the National Natural Science Foundation of China (NNSF) through Grant no. 10972011, the Natural Science Foundation of Hebei Province of China through Grant no. A2010001943, and the Hong Kong Research Grants Council through GRF Grant City U1114/11E.

References

[1] P. Erdős and A. Rényi, "On the evolution of random graphs," *Publications of the Mathematical Institute of the Hungarian Academy of Sciences*, vol. 5, pp. 17–61, 1960.

[2] D. J. Watts and S. H. Strogatz, "Collective dynamics of small-world networks," *Nature*, vol. 393, no. 6684, pp. 440–442, 1998.

[3] M. E. J. Newman and D. J. Watts, "Scaling and percolation in the small-world network model," *Physical Review E*, vol. 60, no. 6, pp. 7332–7342, 1999.

[4] M. E. J. Newman, "The structure and function of complex networks," *SIAM Review*, vol. 45, no. 2, pp. 167–256, 2003.

[5] A. L. Barabási and R. Albert, "Emergence of scaling in random networks," *Science*, vol. 286, no. 5439, pp. 509–512, 1999.

[6] A. L. Barabsi, R. Albert, H. Jeong, and G. Bianconi, "Power-law distribution of the world wide web," *Science*, vol. 287, no. 5461, p. 2115, 2000.

[7] R. Albert and A. L. Barabási, "Statistical mechanics of complex networks," *Reviews of Modern Physics*, vol. 74, no. 1, pp. 47–97, 2002.

[8] X. F. Wang and G. Chen, "Synchronization in scale-free dynamical networks: robustness and fragility," *IEEE Transactions on Circuits and Systems I*, vol. 49, no. 1, pp. 54–62, 2002.

[9] X. F. Wang and G. Chen, "Synchronization in small-world dynamical networks," *International Journal of Bifurcation and Chaos in Applied Sciences and Engineering*, vol. 12, no. 1, pp. 187–192, 2002.

[10] T. Nishikawa, A. E. Motter, Y. Lai, and F. C. Hoppensteadt, "Heterogeneity in oscillator networks: are smaller worlds easier to synchronize?" *Physical Review Letters*, vol. 91, no. 1, Article ID 014101, pp. 1–4, 2003.

[11] V. N. Belykh, I. V. Belykh, and M. Hasler, "Connection graph stability method for synchronized coupled chaotic systems," *Physica D*, vol. 195, no. 1-2, pp. 159–187, 2004.

[12] I. Belykh, V. Belykh, and M. Hasler, "Generalized connection graph method for synchronization in asymmetrical networks," *Physica D*, vol. 224, no. 1-2, pp. 42–51, 2006.

[13] J. Lü, X. Yu, and G. Chen, "Chaos synchronization of general complex dynamical networks," *Physica A*, vol. 334, no. 1-2, pp. 281–302, 2004.

[14] C. Li and G. Chen, "Synchronization in general complex dynamical networks with coupling delays," *Physica A*, vol. 343, no. 1–4, pp. 263–278, 2004.

[15] J. Cao and J. Lu, "Adaptive synchronization of neural networks with or without time-varying delay," *Chaos*, vol. 16, no. 1, Article ID 013133, p. 6, 2006.

[16] W. Xia and J. Cao, "Adaptive synchronization of a switching system and its applications to secure communications," *Chaos*, vol. 18, no. 2, Article ID 023128, p. 15, 2008.

[17] W. Yu, G. Chen, J. Cao, J. Lu, and U. Parlitz, "Parameter identification of dynamical systems from time series," *Physical Review E*, vol. 75, no. 6, Article ID 067201, 2007.

[18] Z. Ma, Z. Liu, and G. Zhang, "A new method to realize cluster synchronization in connected chaotic networks," *Chaos*, vol. 16, no. 2, Article ID 023103, p. 9, 2006.

[19] J. G. Restrepo, E. Ott, and B. R. Hunt, "Emergence of synchronization in complex networks of interacting dynamical systems," *Physica D*, vol. 224, no. 1-2, pp. 114–122, 2006.

[20] J. Zhou and T. Chen, "Synchronization in general complex delayed dynamical networks," *IEEE Transactions on Circuits and Systems I*, vol. 53, no. 3, pp. 733–744, 2006.

[21] J. Zhou, T. Chen, and L. Xiang, "Adaptive synchronization of coupled chaotic delayed systems based on parameter identification and its applications," *International Journal of Bifurcation and Chaos in Applied Sciences and Engineering*, vol. 16, no. 10, pp. 2923–2933, 2006.

[22] J. Zhou, T. Chen, and L. Xiang, "Robust synchronization of delayed neural networks based on adaptive control and parameters identification," *Chaos, Solitons and Fractals*, vol. 27, no. 4, pp. 905–913, 2006.

[23] Z. Guan, J. Hill, and X. Shen, "On hybrid impulsive and switching systems and application to nonlinear control," *IEEE Transactions on Automatic Control*, vol. 50, no. 7, pp. 1058–1062, 2005.

[24] Z. Guan and H. Zhang, "Stabilization of complex network with hybrid impulsive and switching control," *Chaos, Solitons & Fractals*, vol. 37, no. 5, pp. 1372–1382, 2008.

[25] B. Liu, X. Liu, G. Chen, and H. Wang, "Robust impulsive synchronization of uncertain dynamical networks," *IEEE Transactions on Circuits and Systems I*, vol. 52, no. 7, pp. 1431–1441, 2005.

[26] G. Zhang, Z. Liu, and Z. Ma, "Synchronization of complex dynamical networks via impulsive control," *Chaos*, vol. 17, no. 4, Article ID 043126, p. 9, 2007.

[27] J. Lu, D. W. C. Ho, and J. Cao, "A unified synchronization criterion for impulsive dynamical networks," *Automatica*, vol. 46, no. 7, pp. 1215–1221, 2010.

[28] Y. Yang and J. Cao, "Exponential synchronization of the complex dynamical networks with a coupling delay and impulsive effects," *Nonlinear Analysis. Real World Applications. An International Multidisciplinary Journal*, vol. 11, no. 3, pp. 1650–1659, 2010.

[29] Y. Tang, S. Y. S. Leung, W. K. Wong, and J. Fang, "Impulsive pinning synchronization of stochastic discrete-time networks," *Neurocomputing*, vol. 73, no. 10–12, pp. 2132–2139, 2010.

[30] J. Zhou, Q. Wu, and L. Xiang, "Pinning complex delayed dynamical networks by a single impulsive controller," *IEEE Transactions on Circuits and Systems I*, vol. 58, no. 12, pp. 2882–2893, 2011.

[31] X. Han, J.-A. Lu, and X. Wu, "Synchronization of impulsively coupled systems," *International Journal of Bifurcation and Chaos in Applied Sciences and Engineering*, vol. 18, no. 5, pp. 1539–1549, 2008.

[32] W. Sun, F. Austin, J. Lü, and S. Chen, "Synchronization of impulsively coupled complex systems with delay," *Chaos*, vol. 21, no. 3, Article ID 033123, 2011.

[33] T. Yang, *Impulsive Control Theory*, Springer, Berlin, Germany, 2001.

[34] V. Lakshmikantham, D. D. Bainov, and P. S. Simeonov, *Theory of Impulsive Differential Equations*, World Scientific, Singapore, 1989.

Hindawi Publishing Corporation
Mathematical Problems in Engineering
Volume 2013, Article ID 587569, 6 pages
http://dx.doi.org/10.1155/2013/587569

Research Article

Controllability of Second-Order Multiagent Systems with Multiple Leaders and General Dynamics

Bo Liu,[1] Hongke Feng,[1] Li Wang,[2] Rong Li,[3] Junyan Yu,[4] Housheng Su,[5] and Guangming Xie[6]

[1] *College of Science, North China University of Technology, Beijing 100144, China*
[2] *Beijing Key Lab of Urban Intelligent Traffic Control Technology, North China University of Technology, Beijing 100144, China*
[3] *Department of Applied Mathematical Sciences, Shanghai Finance University, Shanghai 201209, China*
[4] *College of Mathematical Science, University of Electronic Science and Technology of China, Chengdu 611731, China*
[5] *Department of Control Science and Engineering, Key Laboratory of Image Processing and Intelligent Control of Education Ministry of China, Huazhong University of Science and Technology, Wuhan 430074, China*
[6] *Intelligent Control Laboratory, Center for Systems and Control, Department of Industrial Engineering and Management, College of Engineering, Peking University, Beijing 100871, China*

Correspondence should be addressed to Bo Liu; liuboer@163.com

Received 3 April 2013; Accepted 3 June 2013

Academic Editor: Ming Cao

This paper proposes a new second-order discrete-time multiagent model and addresses the controllability of second-order multiagent system with multiple leaders and general dynamics. The leaders play an important role in governing the other member agents to achieve any desired configuration. Some sufficient and necessary conditions are given for the controllability of the second-order multiagent system. Moreover, the speed controllability of the second-order multiagent system with general dynamics is discussed. Particularly, it is shown that the controllability of the whole system relies on the number of leaders and the connectivity between the leaders and the members. Numerical examples illustrate the theoretical results.

1. Introduction

Controllability is one of the fundamental issues for coordinated control of multiagent systems which is partly due to the wide applications in communication and computation, as well as cooperative control [1–19].

So far, the issue of controllability shows new features and difficulties, and is still lacking in studies. In [4], the issue of controllability was firstly investigated by the nearest neighbor rules. Tanner had obtained necessary and sufficient conditions of the controllability for first-order multiagent dynamic systems regarding an agent as a leader or the external input. In [5, 7], the controllability for multiagent systems was investigated by the graph theoretic characterization. Moreover, Ji et al. [17] analyzed the multiagent controllability using tree topology. Jafari et al. [18] studied the structural controllability of multiagent systems. In [9, 15, 16], the authors discussed the controllability of discrete-time multiagent systems with a single leader or multiple leaders on fixed networks and switching networks, respectively, and obtained the necessary or sufficient controllable conditions for multiagent systems. References [10, 14] studied the controllability of continuous-time multiagent systems with time-delay and switching topology, respectively.

However, most of the recent research work focuses on the controllability of single integrator or first-order multiagent dynamic systems, such as [4–19]. But the controllability of double integrator or second-order multiagent dynamic systems was seldom studied. Motivated by the works above, in this paper, we focus on discussing the controllability of second-order discrete-time multiagent systems with general dynamic topology. Some sufficient and necessary conditions for controllability are presented. The main contributions of our paper lie in the following. (1) A novel model of

discrete-time multiagent system is a second-order. (2) The influence of leaders on the followers is investigated. (3) The controllability of such second-order discrete-time system with multiple leaders and general dynamics is considered, which cannot be found in the recent literatures. (4) The controllability and the speed controllability of the second-order multiagent system are discussed, respectively. (5) A sufficient and necessary condition for controllability of the second-order system is presented.

This paper is organized as follows. In Section 2, we present some concepts in graph theory. Section 3 gives the model to be studied. In Section 4, main results are presented. In Section 5, numerical examples and simulations are provided to illustrate the theoretical results. A conclusion is made in Section 6.

2. Preliminaries

In this section, some basic definitions and concepts in graph theory [20] are first introduced.

Let $\mathscr{G} = (\mathscr{V}, \mathscr{E}, A)$ be an undirected graph of order n with the set of nodes $\mathscr{V} = \{1, 2, 3, \ldots, n\}$ and the set of edges $\mathscr{E} \subseteq \mathscr{V} \times \mathscr{V}$. An edge of $\mathscr{G}$ is denoted by (i, j), which is an unordered pair of distinct nodes of $\mathscr{V}$. If $i, j \in \mathscr{V}$, and $(i, j) \in \mathscr{E}$, then we say that j is a neighbor of i or i and j are adjacent. The neighborhood set of node i is denoted by $\mathscr{N}_i = \{j \in \mathscr{V} : (i, j) \in \mathscr{E}\}$. $A = [a_{ij}] \in \mathbb{R}^{n\times n}$, where $a_{ij} > 0 \Leftrightarrow (j, i) \in \mathscr{E}$, and a_{ij} is called the coupling weight of edge (i, j).

Any undirected graph can be represented by its adjacency matrix A, which is a symmetric matrix. A diagonal matrix $D = \operatorname{diag}\{d_1, d_2, \ldots, d_n\} \in R^{n\times n}$ is a degree matrix of $\mathscr{G}$ with its diagonal elements $d_i = \sum_{j\in\mathscr{N}_i} a_{ij}$, $i = 1, 2, \ldots, n$.

Then, the Laplacian of the graph $\mathscr{G}$ (or matrix A) is defined as

$$L = D - A \in R^{n\times n}. \tag{1}$$

3. Model

Consider a second-order multiagent system with $N + n_l$ agents, labeled the first N agents from 1 to N as followers and the remainder n_l agents from $N + 1$ to $N + n_l$ as leaders, and each agent moves according to the following dynamics:

$$\begin{aligned} x_i(k+1) &= x_i(k) + v_i(k), \\ v_i(k+1) &= v_i(k) + u_i(k), \end{aligned} \tag{2}$$

with

$$\begin{aligned} u_i(k) = &-\sum_{i\in\mathscr{N}_{i_j}} a_{ij}\left(v_i(k) - v_j(k)\right) \\ &-\sum_{p\in\mathscr{N}_{i_p}} \gamma_{ip} b_{ip}\left(v_i(k) - v_p(k)\right), \quad k \in J_k, \end{aligned} \tag{3}$$

where $x_i \in \mathbb{R}^m$ is the state of agent i ($i \in \underline{N} \triangleq \{N+1, \ldots, N+n_l\}$) and $x_p \in \mathbb{R}^m$ is the state of agent p ($p \in \underline{N+n_l} - \underline{N}$, $\underline{N+n_l} \triangleq \{1, 2, \ldots, N\}$). $\mathscr{N}_i$ presents the neighbor set of agent i. $\mathscr{N}_{i_j} \bigcup \mathscr{N}_{i_p} = \mathscr{N}_i$, and $\mathscr{N}_{i_j} \bigcap \mathscr{N}_{i_p} = \emptyset$. J_k is a discrete-time index set. The coupling matrix $A = [a_{ij}] \in \mathbb{R}^{N\times N}$ with $a_{ij} \geq 0$ and $a_{ii} = 0$ represents the coupling strength among the followers, and $B = [b_{ip}] \in \mathbb{R}^{N\times n_l}$ with $b_{ip} > 0$ represents the coupling strength from the leaders to the followers. $\gamma_{ip} = 1$ if there is information from leader p to follower i; otherwise $\gamma_{ip} = 0$.

Throughout this paper, it is assumed that the leader can influence the member followers but cannot be influenced by its neighbors.

Suppose $z = (x_1, x_2, \ldots, x_N, v_1, v_2, \ldots, x_N)^T$ and $y = (x_{N+1}, x_{N+2}, \ldots, x_{N+n_l}, v_{N+1}, v_{N+2}, \ldots, v_{N+n_l})^T$ be the state vector of all the followers and all the leaders, respectively. Then, (2) can be rewritten as

$$z(k+1) = Gz(k) + Hy(k), \quad k \in J_k, \tag{4}$$

where

$$G = \begin{pmatrix} I & I \\ 0 & F \end{pmatrix}, \qquad H = \begin{pmatrix} 0 & 0 \\ 0 & P \end{pmatrix}, \tag{5}$$

$F = I - L - R$, I is the $N \times N$ identity matrix,

$$R = \operatorname{diag}\left\{\sum_p \gamma_{1p} b_{1p}, \sum_p \gamma_{2p} b_{2p}, \ldots, \sum_p \gamma_{Np} b_{Np}\right\} \in \mathbb{R}^{N\times N},$$

$$P = \begin{bmatrix} \gamma_{1(N+1)} b_{1(N+1)} & \gamma_{1(N+2)} b_{1(N+2)} & \cdots & \gamma_{1(N+n_l)} b_{1(N+n_l)} \\ \gamma_{2(N+1)} b_{2(N+1)} & \gamma_{2(N+2)} b_{2(N+2)} & \cdots & \gamma_{2(N+n_l)} b_{2(N+n_l)} \\ \vdots & \vdots & \ddots & \vdots \\ \gamma_{N(N+1)} b_{N(N+1)} & \gamma_{N(N+2)} b_{N(N+2)} & \cdots & \gamma_{N(N+n_l)} b_{N(N+n_l)} \end{bmatrix}. \tag{6}$$

For simplicity, we denote (6) as

$$P = \left[p_{N+1}, p_{N+2}, \ldots, p_{N+n_l}\right] \in \mathbb{R}^{N\times n_l}, \tag{7}$$

where

$$\begin{aligned} p_p = \left(\gamma_{1p} b_{1p}, \gamma_{2p} b_{2p}, \ldots, \gamma_{Np} b_{Np}\right)^T \in \mathbb{R}^{N\times 1}, \\ q \in \underline{N+n_l} - \underline{N}, \end{aligned} \tag{8}$$

and the matrix $L = [l_{ij}]$ with

$$l_{ij} = \begin{cases} -a_{ij}, & i \neq j \text{ and } j \in \mathscr{N}_{i_j} \\ \sum_{j\in\mathscr{N}_{i_j}} a_{ij}, & i = j \\ 0, & \text{otherwise.} \end{cases} \tag{9}$$

It can be easily seen that the matrix L satisfies the following:

(i) the off-diagonal elements are all negative or zero;

(ii) the row sums are equal to the column sums with the value of zero.

4. Main Results

In the following, we first give the definition of controllability in second-order discrete-time system and the classical criterion of controllability.

Definition 1. A nonzero state z_0 of system (4) is controllable at the initial time $h \in J_k$ if there exists a finite time $l \in J_k, l > h$ and a control input $y(k)$, such that $z(h) = z_0$ and $z(l) = 0$. If any nonzero state z_0 of system (4) is controllable, then system (4) is said to be controllable. If $x(h) = x_0$ and $x(l) = 0$, then system (4) is position controllable, and if $v(h) = v_0$ and $v(l) = 0$, then system (4) is speed controllable.

Definition 2 (controllability matrix). The controllability matrix of system (4) is given by

$$Q = \left[H \;\; GH \;\; G^2H \;\; \cdots \;\; G^{2N-1}H\right], \tag{10}$$

where matrix $Q \in \mathbb{R}^{2N\times Nn_l}$.

Lemma 3 (Rank test for controllability). *System* (4) *is controllable if* Rank $(Q) = 2N$.

Lemma 4 (PBH rank test for discrete-time systems). *System* (4) *is controllable if* (4) *satisfies one of the following conditions:*

(i) $\operatorname{rank}(sI - G, H) = 2N$, *for all* $s \in \mathbb{C}$;

(ii) $\operatorname{rank}(\lambda_i I - G, H) = 2N$, *where* λ_i, *for all* $i = 1, 2, \ldots, 2N$, *is the eigenvalue of matrix* G.

In general, for second-order multiagent systems, the controllable matrix is too hard to calculate. Therefore, we can use the PBH rank rest to justify the controllability of such system. In the following, we will give a more simple and convenient theorem using the PBH rank rest.

Theorem 5. *System* (4) *is controllable if* Rank $(P) = m$.

Proof. By Lemma 4, system (4) is controllability if $\operatorname{rank}(\lambda_i I - G, H) = 2N$, where λ_i, for all $i = 1, 2, \ldots, 2N$, is the eigenvalue of matrix G. Then, it is obvious to see that

$$\operatorname{rank}\left(\lambda_i \mathbf{I} - G \;\; H\right) = \operatorname{rank}\begin{pmatrix} \lambda_i I - I & -I & 0 \\ 0 & \lambda_i I - F & P \end{pmatrix} = 2N, \tag{11}$$

if $\operatorname{Rank}(P) = m$. □

Remark 6. From Theorem 5, we can find that the second-order multiagent system (4) is controllable if $n_l \geq N$ (n_l is the number of leaders and N the number of followers); otherwise, the system is always uncontrollable.

Remark 7. Notice that the direct consequence of Theorem 5 is that the controllability of the network (4) of a group of agents relies only on the connectivity between the leaders and members, regardless of the connectivity of the members in the network.

Corollary 8. *If* Rank $(P) = N$, *system* (4) *is speed controllable.*

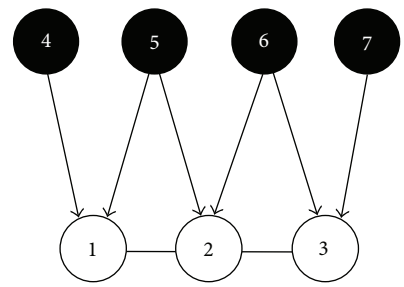

Figure 1: The network topology 1.

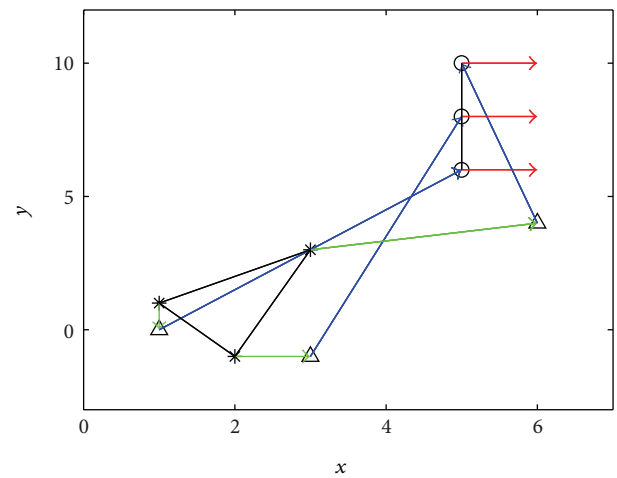

Figure 2: A straight line configuration with speed.

Under the symmetry condition of the adjacent matrix A, we can have the following result.

Theorem 9. *System* (4) *is speed controllable if and only if the following conditions hold.*

(i) *The eigenvalues of* F *are all distinct.*

(ii) *All the eigenvectors of* F *are not orthogonal to at least one column in* P *simultaneously.*

The proof of Lemma 3 is similar to that of [15, Theorem 1], here omitted.

Remark 10. From Corollary 8 and Theorem 9, it can be easily seen that even though system (4) is speed controllable, system (4) cannot be completely controllable.

5. Numerical Examples and Simulations

This section presents some numerical examples and simulations to illustrate the theoretical results.

Example 1. Consider a seven-agent network with agents 4–7 as the leaders, where the topology of the network is described by Figure 1. From Figure 1, we can see that the number of the leaders is more than that of the followers. For simplicity, let

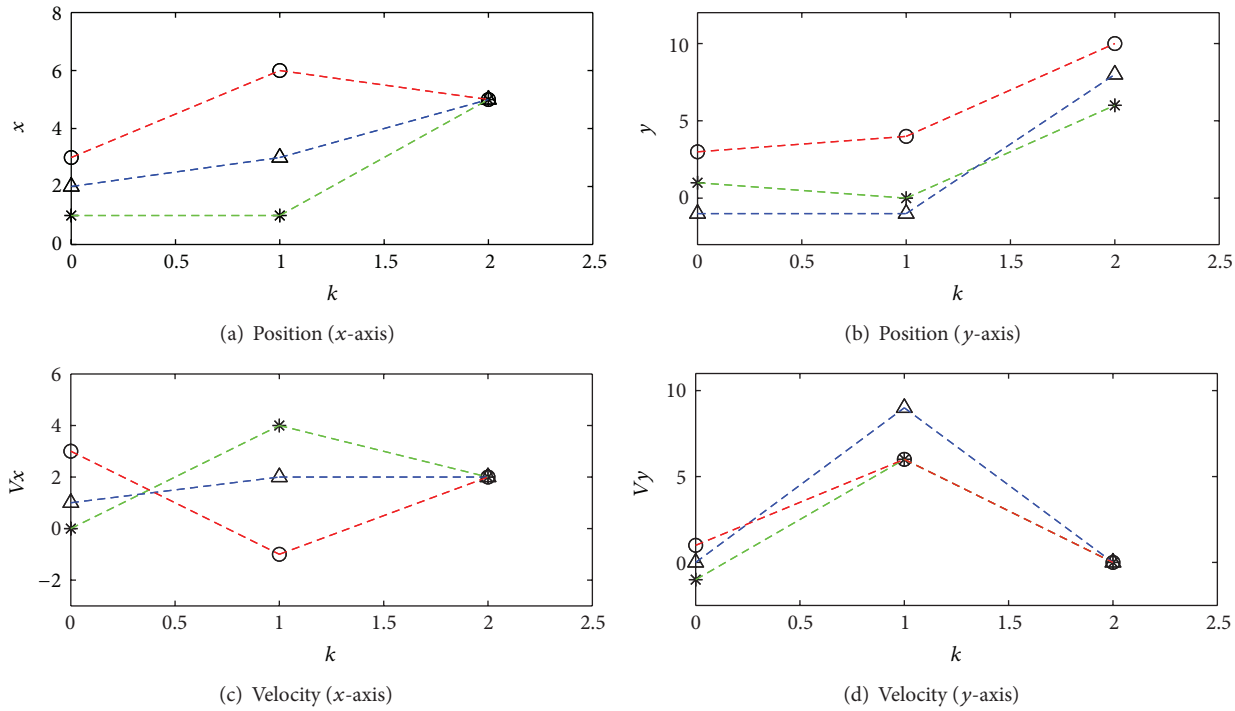

(a) Position (x-axis)

(b) Position (y-axis)

(c) Velocity (x-axis)

(d) Velocity (y-axis)

Figure 3: Second-order controllability.

$a_{ij} = b_{ip} = 1$ for $i, j = 1, 2, 3$ and $p = 4, 5, 6, 7$. According to Figure 1, the second-order multiagent system (4) is defined by

$$G = \begin{bmatrix} 1 & 0 & 0 & 1 & 0 & 0 \\ 0 & 1 & 0 & 0 & 1 & 0 \\ 0 & 0 & 1 & 0 & 0 & 1 \\ 0 & 0 & 0 & -2 & 1 & 0 \\ 0 & 0 & 0 & 1 & -3 & 1 \\ 0 & 0 & 0 & 0 & 1 & -2 \end{bmatrix}, \qquad H = \begin{bmatrix} 0 & 0 & 0 & 0 \\ 0 & 0 & 0 & 0 \\ 0 & 0 & 0 & 0 \\ 1 & 1 & 0 & 0 \\ 0 & 1 & 1 & 0 \\ 0 & 0 & 1 & 1 \end{bmatrix}, \tag{12}$$

with

$$L = \begin{bmatrix} 1 & -1 & 0 \\ -1 & 2 & -1 \\ 0 & -1 & 1 \end{bmatrix}, \qquad R = \begin{bmatrix} 2 & 0 & 0 \\ 0 & 2 & 0 \\ 0 & 0 & 2 \end{bmatrix}, \qquad P = \begin{bmatrix} 1 & 1 & 0 & 0 \\ 0 & 1 & 1 & 0 \\ 0 & 0 & 1 & 1 \end{bmatrix}. \tag{13}$$

By computing, $\mathrm{Rank}(P) = 3$ and $\mathrm{Rank}(Q) = \mathrm{Rank}\left[H \;\; GH \;\; G^2H \;\; \cdots \;\; G^{2N-1}H\right] = 6$, then system (4) is indeed controllable.

Figures 2 and 3 show the simulation results of formation control of the second-order network. The follower agents (the black star dots) move from a random initial configuration to desired ones: aligning in a straight line (the black circles) with controllable speed as shown in Figures 2 and 3, respectively.

Example 2. A five-agent network with agents 4 and 5 as the leaders and with fixed topology described by the graph in Figure 4. From Figure 4, we can see that the number of the leaders is less than that of the followers.

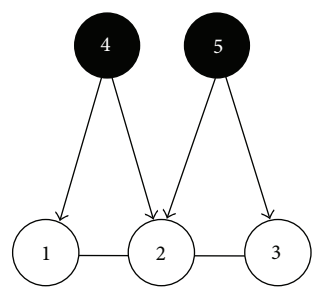

Figure 4: The network topology 2.

From Figure 1, the second-order multiagent system (4) is given by

$$G = \begin{bmatrix} 1 & 0 & 0 & 1 & 0 & 0 \\ 0 & 1 & 0 & 0 & 1 & 0 \\ 0 & 0 & 1 & 0 & 0 & 1 \\ 0 & 0 & 0 & -1 & 1 & 0 \\ 0 & 0 & 0 & 1 & -3 & 1 \\ 0 & 0 & 0 & 0 & 1 & -1 \end{bmatrix}, \qquad H = \begin{bmatrix} 0 & 0 \\ 0 & 0 \\ 0 & 0 \\ 1 & 0 \\ 1 & 1 \\ 0 & 1 \end{bmatrix}, \tag{14}$$

with

$$L = \begin{bmatrix} 1 & -1 & 0 \\ -1 & 2 & -1 \\ 0 & -1 & 1 \end{bmatrix}, \qquad R = \begin{bmatrix} 1 & 0 & 0 \\ 0 & 2 & 0 \\ 0 & 0 & 1 \end{bmatrix}, \qquad P = \begin{bmatrix} 1 & 0 \\ 1 & 1 \\ 0 & 1 \end{bmatrix}. \tag{15}$$

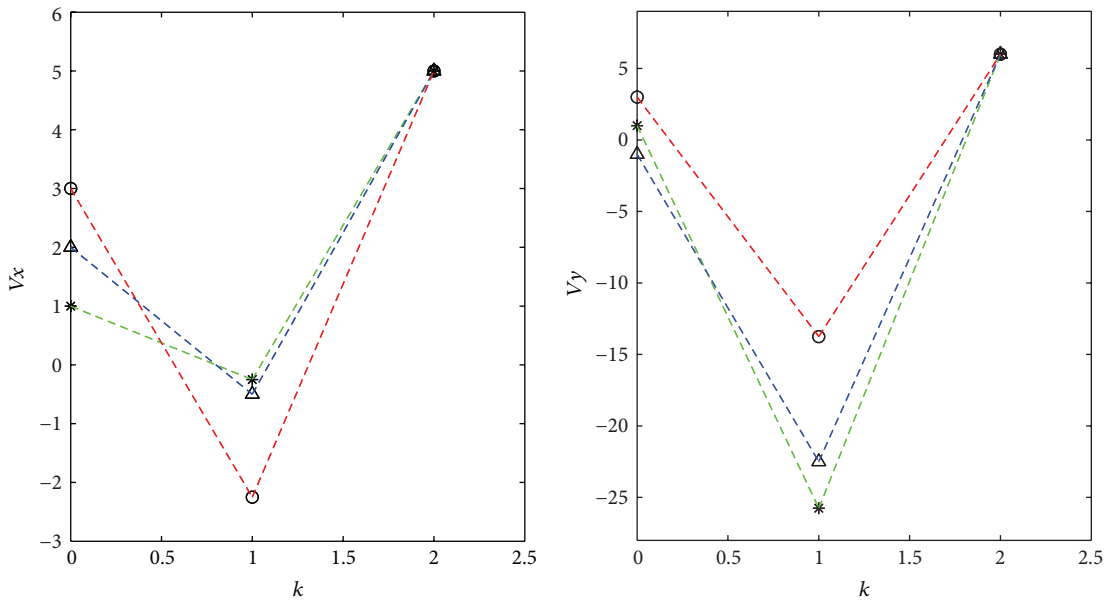

(a) Velocity (x-axis) (b) Velocity (y-axis)

Figure 5: Speed controllability.

Using Matlab calculation, the eigenvalues of F are

$$\operatorname{eig}(F) = \{-3.7321, -1, -0.2679\},$$

$$U^T = \begin{bmatrix} -0.3251 & 0.8881 & -0.3251 \\ -0.7071 & -0.0000 & 0.7071 \\ 0.6280 & 0.4597 & 0.6280 \end{bmatrix}, \tag{16}$$

$$U^T P = \begin{bmatrix} 0.5630 & 0.5630 \\ -0.7071 & 0.7071 \\ 1.0877 & 1.0877 \end{bmatrix}.$$

It is obvious that the eigenvalues of F are all different, and the elements of $U^T P$ are all nonzero. Therefore, system (4) is speed controllable. However, $\operatorname{Rank}(P) = 2$ and $\operatorname{Rank}(Q) = \operatorname{Rank}\left[H \;\; GH \;\; G^2H \;\; \cdots \;\; G^{2N-1}H\right] = 5$, then system (4) is uncontrollable.

Figure 5 shows the simulation results of the second-order network. It is easily seen that the speeds of the system are controllable, but the positions of the system are uncontrollable. Therefore, the whole second-order system is uncontrollable.

6. Conclusion

This paper has studied the controllability of discrete-time second-order multiagent systems with multiple leaders and general dynamic topology. By applying the PBH rank test technique, some effective sufficient and necessary conditions for the controllability of the multiagent discrete-time systems are obtained. The results in this paper show that the controllability of discrete-time second-order multiagent systems can only depend on the information from the leaders to the followers, regardless of the connectivity of the members in the network. These studies are helpful in understanding the dynamics of interconnected systems. However, for discrete-time second-order multiagent systems, as in cases often encountered in practice, it is usually difficult to deal with the controllability problem due to complexity of the topology and lack of theoretical tools. Our main result shows an advantage of the second-order topology scheme. We anticipate that our solutions to the above-described problems will offer a theoretical basis and valuable ideas for future applications of networked multiagent systems in the field of coordination control, including formation control and tracking problems.

Acknowledgments

This work was supported by National Natural Science Foundation (61170113, 61203150, 61104141, 60774089, 10972003, 61174116), Science and Technology Development Plan Project of Beijing Education Commission (no. KM201310009011), the Funding Project for Academic Human Resources Development in Institutions of Higher Learning Under the Jurisdiction of Beijing Municipality (PHR201108055), the Program for New Century Excellent Talents in University from Chinese Ministry of Education under Grant NCET-12-0215, the National High Technology Research and Development Program of China 863 (no. 2012AA112401), and the Research Fund for the Doctoral Program of Higher Education (RFDP) under Grant no. 20100142120023. This work was also supported by the Foundation Grant of Guangxi Key Laboratory of Automobile Components and Vehicle Technology (13-A-03-01) and the Opening Project of Guangxi Key Laboratory of Automobile Components and Vehicle Technology (2012KFZD03).

References

[1] W. Ren and R. W. Beard, "Consensus seeking in multiagent systems under dynamically changing interaction topologies," *Institute of Electrical and Electronics Engineers*, vol. 50, no. 5, pp. 655–661, 2005.

[2] H. Su, X. Wang, and Z. Lin, "Flocking of multi-agents with a virtual leader," *Institute of Electrical and Electronics Engineers*, vol. 54, no. 2, pp. 293–307, 2009.

[3] H. Su, G. Chen, X. Wang, and Z. Lin, "Adaptive second-order consensus of networked mobile agents with nonlinear dynamics," *Automatica*, vol. 47, no. 2, pp. 368–375, 2011.

[4] H. G. Tanner, "On the controllability of nearest neighbor interconnections," in *Proceedings of the 43rd IEEE Conference on Decision and Control (CDC '04)*, pp. 2467–2472, December 2004.

[5] M. Ji and M. Egerstedt, "A graph theoretic characterization of controllability for multi-agent systems," *IEEE Transactions on Robotics*, vol. 23, no. 4, pp. 693–703, 2007.

[6] B. Liu, G. Xie, T. Chu, and L. Wang, "Controllability of interconnected systems via switching networks with a leader," in *Proceedings of the IEEE International Conference on Systems, Man and Cybernetics*, vol. 5, pp. 3912–3916, October 2006.

[7] Z. Ji, H. Lin, and T. H. Lee, "A graph theory based characterization of controllability for multi-agent systems with fixed topology," in *Proceedings of the 47th IEEE Conference on Decision and Control (CDC '08)*, pp. 5262–5267, Cancun, Mexico, December 2008.

[8] M. Zamani and H. Lin, "Structural controllability of multi-agent systems," in *Proceedings of the American Control Conference (ACC '09)*, pp. 5743–5748, St. Louis, Mo, USA, June 2009.

[9] B. Liu, T. Chu, L. Wang, and G. Xie, "Controllability of a leader-follower dynamic network with switching topology," *Institute of Electrical and Electronics Engineers*, vol. 53, no. 4, pp. 1009–1013, 2008.

[10] Z. Ji, Z. Wang, H. Lin, and Z. Wang, "Controllability of multi-agent systems with time-delay in state and switching topology," *International Journal of Control*, vol. 83, no. 2, pp. 371–386, 2010.

[11] R. Lozano, M. W. Spong, J. A. Guerrero, and N. Chopra, "Controllability and observability of leader-based multi-agent systems," in *Proceedings of the 47th IEEE Conference on Decision and Control (CDC '08)*, pp. 3713–3718, Cancun, Mexico, December 2008.

[12] L. Wang, F. Jiang, G. Xie, and Z. Ji, "Controllability of multi-agent systems based on agreement protocols," *Science in China F*, vol. 52, no. 11, pp. 2074–2088, 2009.

[13] F. Jiang, L. Wang, G. Xie, Z. Ji, and Y. Jia, "On the controllability of multiple dynamic agents with fixed topology," in *Proceedings of the American Control Conference (ACC '09)*, pp. 5665–5670, St. Louis, Mo, USA, June 2009.

[14] B. Liu, T. Chu, L. Wang, Z. Zuo, G. Chen, and H. Su, "Controllability of switching networks of multi-agent systems," *International Journal of Robust and Nonlinear Control*, vol. 22, no. 6, pp. 630–644, 2012.

[15] B. Liu, N. Hu, J. Zhang, and H. Su, "Controllability of discrete-time multi-agent systems with multiple leaders on fixed networks," *Communications in Theoretical Physics*, vol. 58, pp. 856–862, 2012.

[16] B. Liu, W. Hu, and Z. Jie, "Controllability of discrete-time multi-agent systems with leaders via switching topology," *Applied Mechanics and Materials*, vol. 128-129, pp. 92–95, 2012.

[17] Z. Ji, H. Lin, T. H. Lee, and Q. Ling, "Multi-agent controllability with tree topology," in *Proceedings of the American Control Conference (ACC '10)*, pp. 850–855, Baltimore, Md, USA, July 2010.

[18] S. Jafari, A. Ajorlou, A. G. Aghdam, and S. Tafazoli, "On the structural controllability of multi-agent systems subject to failure: a graph-theoretic approach," in *Proceedings of the 49th IEEE Conference on Decision and Control (CDC '10)*, pp. 4565–4570, Atlanta, Ga, USA, December 2010.

[19] Y. Liu, J. Slotine, and A. Barabási, "Controllability of complex networks," *Nature*, vol. 473, no. 7346, pp. 167–173, 2011.

[20] C. Godsil and G. Royle, *Algebraic Graph Theory*, vol. 207, Springer, New York, NY, USA, 2001.

Hindawi Publishing Corporation
Mathematical Problems in Engineering
Volume 2013, Article ID 235316, 10 pages
http://dx.doi.org/10.1155/2013/235316

Research Article

Improved Power Flow Algorithm for VSC-HVDC System Based on High-Order Newton-Type Method

Yanfang Wei,[1] Qiang He,[2] Yonghui Sun,[3] Yanzhou Sun,[1] and Cong Ji[4]

[1] *School of Electrical Engineering and Automation, Henan Polytechnic University, Jiaozuo 454000, China*
[2] *Economics and Business College, Qingdao Technological University, Qingdao 266520, China*
[3] *College of Energy and Electrical Engineering, Hohai University, Nanjing 210098, China*
[4] *Jiangsu Frontier Electric Technology Co., Ltd., Nanjing 211102, China*

Correspondence should be addressed to Yanfang Wei; weiyanfang@hpu.edu.cn

Received 4 April 2013; Accepted 12 May 2013

Academic Editor: Guanghui Wen

Voltage source converter (VSC) based high-voltage direct-current (HVDC) system is a new transmission technique, which has the most promising applications in the fields of power systems and power electronics. Considering the importance of power flow analysis of the VSC-HVDC system for its utilization and exploitation, the improved power flow algorithms for VSC-HVDC system based on third-order and sixth-order Newton-type method are presented. The steady power model of VSC-HVDC system is introduced firstly. Then the derivation solving formats of multivariable matrix for third-order and sixth-order Newton-type power flow method of VSC-HVDC system are given. The formats have the feature of third-order and sixth-order convergence based on Newton method. Further, based on the automatic differentiation technology and third-order Newton method, a new improved algorithm is given, which will help in improving the program development, computation efficiency, maintainability, and flexibility of the power flow. Simulations of AC/DC power systems in two-terminal, multi-terminal, and multi-infeed DC with VSC-HVDC are carried out for the modified IEEE bus systems, which show the effectiveness and practicality of the presented algorithms for VSC-HVDC system.

1. Introduction

Voltage source converter (VSC) based high-voltage direct-current (HVDC) is a new technology of HVDC transmission system. Based on pulse width modulation and VSC, the VSC-HVDC system has many merits and attracted wide publicity worldwide [1–3]. Since the first pilot project application in 1997, the VSC-HVDC system is widely applied in interconnected power system, the connection of distributed generation to power grid, the supply of electric power to islands or offshore drilling platform, the distribution of power to urban power network, and so forth.

The main advantages of VSC-HVDC system are as follows: no synchronization problem of AC system, the feature of supplying power to passive network, the simultaneous and independent control for active power and reactive power, the easy achievement of inversion for power flow, the more flexible control modes, the suitable application for multi-terminal and multi-infeed system, and so on. In the near future, a series of new VSC-HVDC transmission system will be built and put into operation worldwide [1, 4]. As a fundamental analytical method for operation and analyzing of power system, the reliable power flow calculation algorithm is an indispensable tool for AC/DC interconnected power systems [5–10]. A great deal of research has been conducted in this field. Now there are two critical methods for the power flow analysis of AC/DC systems, the unified iteration technique and the alternative iteration technique [10–14]. The former has the precision of quadratic convergence and has the better convergence for a variety of control modes of HVDC system. But the realization of the control modes switching for HVDC system is difficult. The latter has the trait of easy programming, especially for the varying process of HVDC control modes. But the alternative iteration technique is sensitive to the operation ways and control modes of the HVDC system and is inclined to the convergence problem.

The Newton method is a fundamental and important technology to solve the power flow of power system [6–9, 15–17]. In [6], a Newton-Raphson power flow algorithm is proposed for the VSC-HVDC system. In [7], the steady power flow of VSC-HVDC is presented based on Newton method and alternative iteration technique. In [8], an optimal power flow (OPF) model suitable for VSC-HVDC system is presented based on Newton-Raphson algorithm. In [9], based on Newton method, a new model that considers the operational constraints associated with the MVA ratings of the converters for OPF analysis of VSC-HVDC system is introduced. In these papers, the modeling approach based on Newton algorithm only has the first-order or quadratic convergence, and the convergence precision needs to be further improved.

In recent years, the solution of nonlinear equation has made great progress, especially the modified Newton method with high-order convergence performance [18–23]. In [23], the power flow algorithm with cubic convergence is analyzed for power system. Despite the fact that a great many improved algorithms for power flow analysis of AC/DC interconnected networks with VSC-HVDC have been presented in many aspects, few papers use the Newton method of high-order convergence to analyze the power flow of VSC-HVDC system. Moreover, with the VSC-HVDC adding to AC/DC system, the kind and number of the system variables are multiplied, causing the modeling of AC/DC system to become more complex. And with the increase of DC line of VSC-HVDC, the dimension and scale of Jacobian matrix and equations of AC/DC system are increased obviously, causing the efficiency of hand codes to decrease. The automatic differentiation (AD) technology overcomes the shortcomings of hand codes. Compared with other differential methods, such as numerical differentiation and symbolic differentiation methods, the AD has the advantages of no truncation error, the exact solution of Jacobian matrix, the less work of hand codes, and so on [24–26]. Motivated by the above discussions, we will investigate the problem of power flow for AC/DC systems with VSC-HVDC. Novel third-order and sixth-order convergence of power flow technique based on Newton method will be derived, and the AD technology will be introduced in this paper based on third-order Newton method to raise the efficiency of programming. The effectiveness of the presented arithmetics for VSC-HVDC system is also discussed. These results and observations will help promote the practical applications of high-order Newton-type method in AC/DC systems with VSC-HVDC.

The remaining of this paper is arranged as follows. In Section 2, a mathematical model for the VSC-HVDC system is presented, in which all the AC system equations, the VSC equations, and the control modes of VSC are analyzed basing on steady model. In Section 3, the power flow and converter equations of VSC-HVDC, the mathematical description of Newton method, third-order and sixth-order convergence of Newton-type methods, and the improved third-order Newton method based on automatic differentiation are presented. In Section 4, the methods are applied to the modified IEEE bus test systems with VSC-HVDC. This paper ends with a conclusion finally.

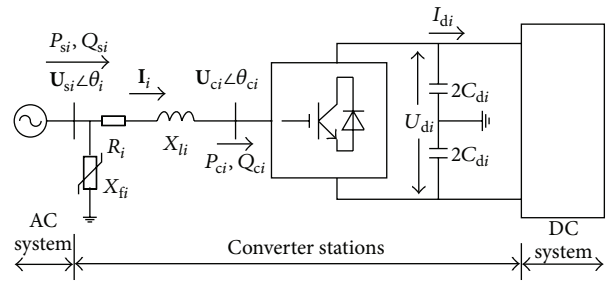

Figure 1: Schematic diagram of steady state physical model for multi-terminal VSC-HVDC.

2. Mathematical Steady Model of VSC-HVDC System

2.1. Per-Unit Value System of VSC-HVDC. For the simulation and calculation of AC/DC hybrid power systems, the unified per-unit value system should be adopted both for AC system and DC system. In this paper the per-unit value system is introduced as follows [7]:

$$\begin{aligned} P_{\mathrm{dB}} &= S_{\mathrm{B}}, \\ U_{\mathrm{dB}} &= U_{\mathrm{B}}, \\ I_{\mathrm{dB}} &= \sqrt{3} I_{\mathrm{B}}, \\ R_{\mathrm{dB}} &= Z_{\mathrm{B}}, \end{aligned} \tag{1}$$

where S_{B}, P_{dB} are the reference power of AC system and DC system, respectively. U_{B}, I_{B}, and Z_{B} are the reference voltage, reference current, and reference impedance of AC side of the converter, respectively. U_{dB}, I_{dB}, and R_{dB} are the reference voltage, reference current, and reference impedance of DC side of the converter, respectively.

2.2. Mathematical Steady Model of VSC-HVDC System. The VSC-HVDC system consists of at least two VSC stations, one operating as a rectifier station and the other as an inverter station. The VSC stations can be connected as two-terminal, multi-terminal, or multi-infeed DC system with VSC-HVDC, depending on the various different applications fields [1–3]. The steady state physical model for a multi-terminal DC system with VSC-HVDC is shown schematically in Figure 1. The steady models of VSC-HVDC are given in the per-unit system (p.u.) as follows:

$$\mathbf{I}_i = \frac{\mathbf{U}_{si} - \mathbf{U}_{ci}}{R_i + jX_{li}}, \tag{2}$$

$$\widetilde{S_{si}} = P_{si} + jQ_{si} = \mathbf{U}_{si}\mathbf{I}_i^*, \tag{3}$$

$$P_{si} = -\left|Y_i\right| U_{si} U_{ci} \cos\left(\delta_i + \alpha_i\right) + \left|Y_i\right| U_{si}^2 \cos\alpha_i, \tag{4}$$

$$Q_{si} = -|Y_i| U_{si} U_{ci} \sin(\delta_i + \alpha_i) + |Y_i| U_{si}^2 \sin\alpha_i + \frac{U_{si}^2}{X_{fi}}, \quad (5)$$

$$P_{ci} = |Y_i| U_{si} U_{ci} \cos(\delta_i - \alpha_i) - |Y_i| U_{ci}^2 \cos\alpha_i, \quad (6)$$

$$Q_{ci} = -|Y_i| U_{si} U_{ci} \sin(\delta_i - \alpha_i) - |Y_i| U_{ci}^2 \sin\alpha_i, \quad (7)$$

$$P_{di} = U_{di} I_{di} = |Y_i| U_{si} U_{ci} \cos(\delta_i - \alpha_i) - |Y_i| U_{ci}^2 \cos\alpha_i, \quad (8)$$

$$U_{ci} = \frac{\sqrt{6} M_i U_{di}}{4}. \quad (9)$$

The variables in the equations of (2)–(9) are referenced to the literature [14].

2.3. Steady-State Control Modes of VSC-HVDC. Owning to having full controllable power electronic switch semiconductors such as insulated gate bipolar transistor and gate turn-off thyristor, VSC-HVDC has the ability to independent control active and reactive power at its terminal. So for each VSC, a couple of regular used control goals can be set [27].

(1) AC active power control: determines the active power exchanged with the AC system.

(2) DC voltage control: is used to keep the DC voltage control constant.

(3) AC reactive power control: determines the reactive power exchanged with the AC system.

(4) AC voltage control: instead of controlling reactive power, AC voltage can be directly controlled, determining the voltage of the system bus.

The general used control means of VSC include the following four categories:

① constant DC voltage control, constant AC reactive power control;

② constant DC voltage control, constant AC voltage control;

③ constant AC active power control, constant AC reactive power control;

④ constant AC active power control, constant AC voltage control.

3. The Improved Power Flow Algorithms of AC/DC Systems with VSC-HVDC Based on High-Order Newton-Type Method

3.1. Steady Mathematical Model of Power Flow Calculation of VSC-HVDC System. For the AC/DC systems with VSC-HVDC, the power flow equations are given as follows [14].

Pure AC bus equation

$$\begin{aligned} \Delta P_{ai} &= P_{ai} - U_{ai} \sum_{j\in i} U_j \left(G_{ij} \cos\theta_{ij} + B_{ij} \sin\theta_{ij}\right), \\ \Delta Q_{ai} &= Q_{ai} - U_{ai} \sum_{j\in i} U_j \left(G_{ij} \sin\theta_{ij} - B_{ij} \cos\theta_{ij}\right). \end{aligned} \quad (10)$$

DC bus equation

$$\begin{aligned} \Delta P_{ti} &= P_{ti} - U_{ti} \sum_{j\in i} U_j \left(G_{ij} \cos\theta_{ij} + B_{ij} \sin\theta_{ij}\right), \\ \Delta Q_{ti} &= Q_{ti} - U_{ti} \sum_{j\in i} U_j \left(G_{ij} \sin\theta_{ij} - B_{ij} \cos\theta_{ij}\right). \end{aligned} \quad (11)$$

VSC converter equation

$$\begin{aligned} \Delta d_{k1} &= P_{tk} + \frac{\sqrt{6}}{4} M_k U_{tk} U_{dk} |Y| \cos(\delta_k + \alpha_k) \\ &\quad - U_{tk}^2 |Y| \cos\alpha_k, \\ \Delta d_{k2} &= Q_{tk} + \frac{\sqrt{6}}{4} M_k U_{tk} U_{dk} |Y| \sin(\delta_k + \alpha_k) \\ &\quad - U_{tk}^2 |Y| \sin\alpha_k - \frac{U_{tk}^2}{X_{fk}}, \\ \Delta d_{k3} &= U_{tk} I_{dk} - \frac{\sqrt{6}}{4} M_k U_{tk} U_{dk} |Y| \cos(\delta_k - \alpha_k) \\ &\quad + \frac{3}{8} (M_k U_{dk})^2 |Y| \cos\alpha_k, \\ \mathbf{I}_d &= \mathbf{G}_d \mathbf{U}_d. \end{aligned} \quad (12)$$

DC network equation

$$\Delta d_{k4} = \pm I_{dk} - \sum_{s=1}^{n_{AC}} g_{dks} U_{ds} = 0. \quad (13)$$

The variables in the equations of (10)–(13) are referenced to the literature [14].

3.2. The Mathematical Description of Newton Method. The mathematical description of multivariable iterative form for Newton method is given by

$$\begin{aligned} \Delta x^{(k)} &= -\left[F'\left(x^{(k)}\right)^{-1}\right] F'\left(x^{(k)}\right), \\ x^{(k+1)} &= x^{(k)} + \Delta x^{(k)}. \end{aligned} \quad (14)$$

The formula (14) has the second-order convergence [23, 28].

The equivalence form of linear equation solution for (14) is given by

$$\begin{aligned} \left[F'\left(x^{(k)}\right)\right] \Delta x^{(k)} &= -F'\left(x^{(k)}\right), \\ x^{(k+1)} &= x^{(k)} + \Delta x^{(k)}, \end{aligned} \quad (15)$$

where $F'(x^{(k)})$ is the matrix variable of first-order partial derivative of $F(x)$ and k is the number of iterations.

3.3. The Newton-Type Method of Third-Order Convergence (Algorithm 1). The single variable iterative algorithm format based on modified Newton-type method is given by

$$x_{k+1} = x_k - \frac{f\left(x_k + f(x_k)/f'(x_k)\right) - f(x_k)}{f'(x_k)}. \quad (16)$$

The iterative format of (16) has the trait of third-order convergence [29].

The multivariable matrix equivalent form of (16) is given by

$$\begin{aligned} F'\left(x^{(k)}\right)\Delta x^{(k)} &= -F\left(x^{(k)}\right), \\ \tilde{x}^{(k+1)} &= x^{(k)} - \Delta x^{(k)}, \\ F'\left(x^{(k)}\right)\Delta \tilde{x}^{(k)} &= -F'\left(\tilde{x}^{(k+1)}\right) + F\left(x^{(k)}\right), \\ x^{(k+1)} &= x^{(k)} + \Delta \tilde{x}^{(k)}. \end{aligned} \tag{17}$$

The gotten Jacobian matrix and its triangular factorization are being utilized fully in the algorithm iterative process of (17).

3.4. The Newton-Type Method of Third-Order Convergence (Algorithm 2). Another single variable iterative algorithm format with third-order convergence based on Newton-type method is given by:

$$\begin{aligned} x_{k+1} &= x_k - 0.5 f\left(x_k\right) \\ &\quad \times \left[\frac{1}{f'\left(x_k - f\left(x_k\right)/f'\left(x_k\right)\right)} + \frac{1}{f'\left(x_k\right)}\right]. \end{aligned} \tag{18}$$

The iterative format of (18) has the trait of third-order convergence [30].

The multivariable matrix equivalent form of (18) is given by:

$$\begin{aligned} F'\left(x^{(k)}\right)\Delta x^{(k)} &= -F\left(x^{(k)}\right), \\ \tilde{x}^{(k+1)} &= x^{(k)} + \Delta x^{(k)}, \\ F'\left(x^{(k+1)}\right)\Delta \tilde{x}^{(k)} &= -F\left(x^{(k)}\right), \\ x^{(k+1)} &= x^{(k)} + 0.5\left(\Delta x^{(k)} + \Delta \tilde{x}^{(k)}\right). \end{aligned} \tag{19}$$

3.5. The Newton-Type Method of Sixth-Order Convergence. For the above presented Algorithm 1 and Algorithm 2, the two iterative formats have the advantages for fast convergence speed of Newton method and less computations of simplified Newton method. The application of Algorithm 1 and Algorithm 2 is a two-step process.

Step 1. The prediction based on the Newton method [23]

$$\begin{aligned} \Delta x^{(k)} &= -\left[F'\left(x^{(k)}\right)\right]^{-1} F\left(x^{(k)}\right), \\ \tilde{x}^{(k+1)} &= x^{(k)} + \Delta x^{(k)}. \end{aligned} \tag{20}$$

Step 2. The correction for the obtained predicted value of $\tilde{x}^{(k+1)}$

$$\begin{aligned} \Delta \tilde{x}^{(k)} &= -\left[F'\left(x^{(k)}\right)\right]^{-1}\left[F\left(x^{(k)}\right) + F\left(\tilde{x}^{(k+1)}\right)\right], \\ x^{(k+1)} &= x^{(k)} + \Delta \tilde{x}^{(k)}. \end{aligned} \tag{21}$$

The simplified realization of the iterative procedure for (20) and (21) is given by

$$\begin{aligned} y_k &= x_k - \frac{f\left(x_k\right)}{f'\left(x_k\right)}, \\ z_k &= x_k - \frac{2f\left(x_k\right)}{f'\left(x_k\right) + f'\left(y_k\right)}, \end{aligned} \tag{22}$$

where z_k is the iterative result of x_{k+1} at the k iterative cycle.

An effective implement of the iterative process of (22) is given by [31]

$$x_{k+1} = z_k - \frac{f\left(z_k\right)}{f'\left(z_k\right)}. \tag{23}$$

The approximate value of $f'(x)$ at z_k is given by

$$f'\left(z_k\right) \approx \frac{f'\left(x_k\right)\left(3f'\left(y_k\right) - f'\left(x_k\right)\right)}{f'\left(x_k\right) + f'\left(y_k\right)}. \tag{24}$$

The (16) or (18), (23), and (24) comprise the new sixth-order convergence method [31]:

$$\begin{aligned} y_k &= x_k - \frac{f\left(x_k\right)}{f'\left(x_k\right)}, \\ z_k &= x_k - \frac{2f\left(x_k\right)}{f'\left(x_k\right) + f'\left(y_k\right)}, \\ x_{k+1} &= z_k - \frac{f\left(z_k\right)}{f'\left(x_k\right)} \frac{f'\left(x_k\right) + f'\left(y_k\right)}{3f'\left(y_k\right) - f'\left(x_k\right)}. \end{aligned} \tag{25}$$

3.6. The Automatic Differentiation Algorithm Based on Third-Order Newton-Type Method. The AD technique could always be decomposed to complex computations of basic functions and basic mathematical operations, such as the four arithmetic operations of add, subtract, multiply, and divide, the basic functions of trigonometric function, exponential function, and logarithmic function. Here an instance is given to illustrate the application of AD. The function expression of a certain model is given by

$$f(x) = \sin x_1 + e^{x_1 x_2}. \tag{26}$$

The independent variables and intermediate variables of (26) are given in Table 1. For the use of independent variables and intermediate variables, the function of (26) is decomposed to a series of basic functions. If the value of independent variables is given, the exact value of y is gotten by top-down solution order in Table 1. Given the value of $\dot{x}_1$ and $\dot{x}_2$, the differentiation of (26) can be obtained mechanically through the chain rule of differentiation calculation. At present, there are two main modes for the application of AD, the forward mode and the backward mode, as shown in Table 2. And in Table 2, $x_{i,j} = \partial x_i/\partial x_j$, $p_i = \partial y/\partial x_i$.

Now there are two kinds of implementation method for AD, the source code transform method and operator

Table 1: Independent variables and intermediate variables of (26).

Independent variables	Intermediate variables
x_1	$x_3 = \sin x_1$
x_2	$x_4 = x_1 x_2$
	$x_5 = e^{x_4}$
	$x_6 = x_3 + x_5$
	$y = x_6$

Table 2: Forward and backward mode.

Forward mode	Backward mode
$\dot{x}_3 = \mathrm{con}(x_1) \cdot \dot{x}_1$	$p_1 = p_1 + x_{3,1} p_3$
$\dot{x}_4 = \dot{x}_1 x_2 + x_1 \dot{x}_2$	$p_1 = p_1 + x_{4,1} p_4$, $p_2 = p_2 + x_{4,2} p_4$
$\dot{x}_5 = x_5 \dot{x}_4$	$p_4 = p_4 + x_{5,4} p_5$
$\dot{x}_6 = \dot{x}_3 + \dot{x}_5$	$p_3 = p_3 + x_{6,3} p_6$, $p_5 = p_5 + x_{6,5} p_6$
$\dot{y} = \dot{x}_6$	$p_7 = 1$

overloading method. The typical representative softwares for the former is ADIFOR and ADIC. The typical representative software for the latter is ADOL-C and ADC. The method of ADOL-C realizes the differentiation of C++ program automatically by using operator overloading and can calculate any order derivative by forward and backward mode. In this paper, the ADOL-C method is used to realize the differential operation [32].

The steps of the improved AD algorithm based on third-order Newton method are listed below.

Step 1. Read network parameter, including bus number, active and reactive power of load, compensate capacitance, branch number of line, resistor and reactance in series, and ratio and impedance of transformer.

Step 2 (initialization). Form the admittance matrix of the DC and AC systems.

Step 3. Distribute space for AD and state active variables, including independent variables and dependent variables.

Step 4. Transmit the value of system variable to active variable.

Step 5. Form the expression of dependent variable by using independent variable.

Step 6. Judge the maximum of imbalance equation whether to meet the error precision or not. If yes, exit the loop. If not, the loop goes on.

Step 7. Call the function of Jacobian and Hessian of AD.

Step 8. Solve the equation of (17) or (19).

Return to Step 3.

4. Case Studies

In this part, in order to validate the correctness and suitability of the proposed algorithms, three sections are presented.

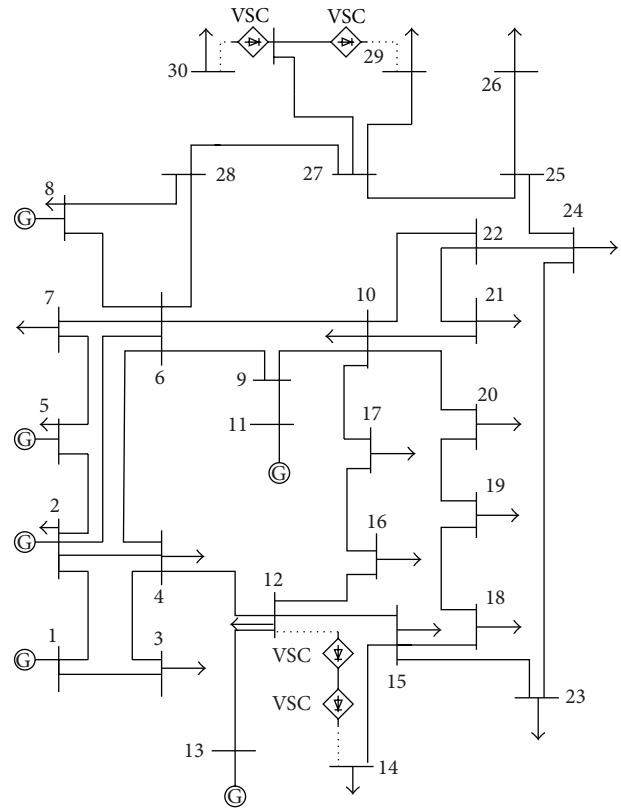

Figure 2: The modified IEEE-30 bus AC/DC system with VSC-HVDC.

(1) For the modified high-order Newton methods, the modified IEEE 30-bus system with two-terminal and multi-infeed VSC-HVDC is analyzed in detail firstly.

(2) Then the simulation results of performance comparisons for the improved high-order Newton methods are presented among the modified IEEE 5-bus, IEEE 9-bus, IEEE 14-bus, IEEE 57-bus, and IEEE 118- bus text systems.

(3) At last, the AD based on third-order Newton method is evaluated for the modified IEEE 30-bus system with two-terminal of VSC-HVDC.

4.1. The Modified IEEE 30-Bus System with Two-Terminal and Multi-Infeed VSC-HVDC. The proposed method has been applied to the modified IEEE 30-bus system [33]. The wiring diagram is shown in Figure 2. In this section, two cases are considered and compared. In Figure 2, the dotted lines represent the possible positions of VSC stations, and the specific positions are located as follows.

(1) In the system with two-terminal VSC-HVDC, the VSC1 and VSC2 are connected to AC line of bus 29 and bus 30, respectively.

(2) In the system with two-infeed VSC-HVDC, the VSC1, VSC2, VSC3, and VSC4 are connected to AC line of bus 12, bus 14, bus 29, and bus 30, respectively.

Table 3: Results of the power flow calculation of AC system.

Control mode	Method	Bus Number 1		2		3		4	
		V	θ	V	θ	V	θ	V	θ
① + ③	Newton	1.0600	0	1.0450	−5.5025	1.0333	−8.1365	1.0271	−9.8132
	Algorithm 1	1.0600	0	1.0450	−5.5025	1.0333	−8.1365	1.0271	−9.8132
	Algorithm 2	1.0600	0	1.0450	−5.5025	1.0333	−8.1365	1.0271	−9.8132
	Sixth-order Newton	1.0600	0	1.0450	−5.5025	1.0333	−8.1365	1.0271	−9.8132
① + ④	Newton	1.0600	0	1.0450	−5.5012	1.0340	−8.1415	1.0279	−9.8187
	Algorithm 1	1.0600	0	1.0450	−5.5012	1.0340	−8.1415	1.0279	−9.8187
	Algorithm 2	1.0600	0	1.0450	−5.5012	1.0340	−8.1415	1.0279	−9.8187
	Sixth-order Newton	1.0600	0	1.0450	−5.5012	1.0340	−8.1415	1.0279	−9.8187
② + ③	Newton	1.0600	0	1.0450	−5.5013	1.0341	−8.1434	1.0281	−9.8208
	Algorithm 1	1.0600	0	1.0450	−5.5013	1.0341	−8.1434	1.0281	−9.8208
	Algorithm 2	1.0600	0	1.0450	−5.5013	1.0341	−8.1434	1.0281	−9.8208
	Sixth-order Newton	1.0600	0	1.0450	−5.5013	1.0341	−8.1434	1.0281	−9.8208
② + ④	Newton	1.0600	0	1.0450	−5.4996	1.0344	−8.1435	1.0284	−9.8208
	Algorithm 1	1.0600	0	1.0450	−5.4996	1.0344	−8.1435	1.0284	−9.8208
	Algorithm 2	1.0600	0	1.0450	−5.4996	1.0344	−8.1435	1.0284	−9.8208
	Sixth-order Newton	1.0600	0	1.0450	−5.4996	1.0344	−8.1435	1.0284	−9.8208

Table 4: Results of the power flow calculation of DC system.

DC variable		Converter number	Control mode ① + ③	① + ④	② + ③	② + ④
U_d	Newton	VSC_1	2.0000	2.0000	2.0000	2.0000
		VSC_2	1.9994	1.9994	1.9994	1.9994
	Algorithm 1	VSC_1	2.0000	2.0000	2.0000	2.0000
		VSC_2	1.9994	1.9994	1.9994	1.9994
	Algorithm 2	VSC_1	2.0000	2.0000	2.0000	2.0000
		VSC_2	1.9994	1.9994	1.9994	1.9994
	Sixth-order Newton	VSC_1	2.0000	2.0000	2.0000	2.0000
		VSC_2	1.9994	1.9994	1.9994	1.9994
δ	Newton	VSC_1	0.3556	0.3402	0.3381	0.3322
		VSC_2	−0.3701	−0.2960	−0.3495	−0.3047
	Algorithm 1	VSC_1	0.0062	0.0059	0.0059	0.0058
		VSC_2	−0.0065	−0.0052	−0.0061	−0.0053
	Algorithm 2	VSC_1	0.0062	0.0059	0.0059	0.0058
		VSC_2	−0.0065	−0.0052	−0.0061	−0.0053
	Sixth-order Newton	VSC_1	0.0062	0.0059	0.0059	0.0058
		VSC_2	−0.0065	−0.0052	−0.0061	−0.0053
M	Newton	VSC_1	0.7663	0.7838	0.8282	0.8257
		VSC_2	0.7574	0.8188	0.7794	0.8161
	Algorithm 1	VSC_1	0.7663	0.7838	0.8282	0.8257
		VSC_2	0.7574	0.8188	0.7794	0.8161
	Algorithm 2	VSC_1	0.7663	0.7838	0.8282	0.8257
		VSC_2	0.7574	0.8188	0.7794	0.8161
	Sixth-order Newton	VSC_1	0.7663	0.7838	0.8282	0.8257
		VSC_2	0.7574	0.8188	0.7794	0.8161

Table 5: Comparisons of iteration times and computing time.

Control mode	Iteration times				Computing time (ms)			
	Newton	Algorithm 1	Algorithm 2	Sixth-order Newton	Newton	Algorithm 1	Algorithm 2	Sixth-order Newton
① + ③	4	3	3	2	8.6885	8.8367	0.1040	12.6763
① + ④	4	3	3	2	9.8464	5.6506	0.1023	9.5408
② + ③	4	3	3	1.5*	9.3356	5.6121	0.1045	8.4520
② + ④	4	3	3	1.5*	9.4767	5.6403	0.0990	8.2271

Table 6: Comparison of iteration times and computing time.

Control mode		Iteration times				Computing time (ms)			
$VSC_1 + VSC_2$	$VSC_3 + VSC_4$	Newton	Algorithm 1	Algorithm 2	Sixth-order Newton	Newton	Algorithm 1	Algorithm 2	Sixth-order Newton
① + ③	① + ③	4	3	3	1.5	10.0649	8.6786	0.1186	0.4648
① + ③	① + ④	4	3	3	1.5	9.4347	6.8694	0.1110	0.4870
① + ③	② + ③	4	3	3	1.5	9.4438	6.0041	0.1086	0.4399
① + ③	② + ④	4	3	3	1.5	9.8407	6.7326	0.1136	0.4384
① + ④	① + ④	4	3	3	1.5	9.4073	6.3733	0.1164	0.4885
① + ④	② + ③	4	3	3	1.5	10.1531	5.9505	0.1113	0.4499
① + ④	② + ④	4	3	3	1.5	5.8884	6.0551	0.1121	0.4273
② + ③	② + ③	4	3	3	1.5	9.7429	5.8435	0.1330	0.4283
② + ③	② + ④	4	3	3	1.5	9.8400	6.1026	0.1216	0.3860
② + ④	② + ④	4	3	3	1.5	9.7773	6.2020	0.1168	0.4181

4.1.1. The Modified IEEE 30-Bus System with Two-Terminal VSC-HVDC. The results of the power flow calculation of the AC system and DC system under different control modes for Newton, third-order and sixth-order Newton methods are shown in Tables 3 and 4. In Table 3, the simulation results of bus number of 1, 2, 3, and 4 are presented only, and the other buses of the modified IEEE 30-bus system are not included for the sake of brevity. There are two methods of third-order Newton in Tables 3 and 4, Algorithm 1, and Algorithm 2. In Table 3, the "Newton" method is the algorithm in the references of [5–10], the unit of V is p.u., and the unit of θ is $^\circ$.

It can be seen from Table 3 the voltage amplitudes of bus 1 and bus 2 are all the same for the proposed four methods. This is due to the node type of bus 1 and bus 2 for the IEEE 30-bus system. Bus 1 is the equilibrium node. And Bus 2 is the PV node. So in the iterative process of the proposed different methods, if the generators of bus 1 and bus 2 have not reached the limit of reactive power, the voltage amplitudes of bus 1 and bus 2 remain the same.

In Table 4, the DC variables of Ud are the same for different control modes and Newton methods; the reason is that for the general used four control modes of VSC, all the mode combinations of ① + ③, ① + ④, ② + ③, and ② + ④ contain the constant DC voltage control category. As a result, in the operation process of VSC-HVDC system, the DC voltage of VSC remains constant.

Both in Tables 3 and 4, for the proposed algorithms of Newton, Algorithm 1, Algorithm 2, and sixth-order Newton method, the results of the power flow calculation for the four different control modes remain the same fundamentally. And the operational parameters of DC system are all in the normal range. The simulation results also illustrate the flexible application of the third-order and sixth-order Newton methods for the AC/DC system with VSC-HVDC.

The comparisons of iteration times and computing time for the four proposed Newton methods are shown in Table 5. In Table 5, the * indicates that the criterion for convergence is met only at the front half iteration procedure. As seen in Table 5, for the modified IEEE 30-bus text system with two-terminal VSC-HVDC, the iteration times of sixth-order Newton method are evidently less than other Newton methods. And the CPU computing time of the third-order Newton of Algorithm 2 is smaller than other Newton methods under four different control modes. The reason is that for the modified IEEE 30-bus text system, the computation task of Jacobian matrix formation and triangular factorization for high-order Newton method is less than Newton method.

4.1.2. The Modified IEEE 30-Bus System with Multi-Infeed VSC-HVDC. For the flexible control performance and particular technical advantages, the VSC-HVDC is suitable for application in multi-infeed system [5, 34]. In this section, the comparison of iteration times and computing time under different control modes for improved Newton methods is shown in Table 6 for the modified IEEE 30-bus system with two-infeed VSC-HVDC. For two-infeed VSC-HVDC, the combinations ways of VSC have ten different types, as shown in Table 6.

It can be seen from Table 6, both for the iteration times and the computing time, the high-order Newton-type of

Table 7: The topology and parameter settings for different IEEE text systems.

Topology	Two-terminal										Two-infeed				Three-terminal					
Modified test system	IEEE-5		IEEE-9		IEEE-14		IEEE-57		IEEE-118		IEEE-14				IEEE-14			IEEE-57		
Bus number	VSC_1	VSC_2	VSC_1	VSC_2	VSC_1	VSC_2	VSC_1	VSC_2	VSC_1	VSC_2	VSC_1	VSC_2	VSC_3	VSC_4	VSC_1	VSC_2	VSC_3	VSC_1	VSC_2	VSC_3
	4	5	8	9	13	14	56	57	75	118	12	14	29	30	12	13	14	55	56	41

Table 8: Performance comparison for different text systems.

Topology	Modified test system	Iteration times			Computing time (ms)		
		Newton	Algorithm 1	Sixth-order Newton	Newton	Algorithm 1	Sixth-order Newton
Two-terminal	IEEE-5	5	4	1.5	4.8287	4.4651	5.3692
Two-terminal	IEEE-9	4	3	1.5	3.1646	2.2094	2.7866
Two-terminal	IEEE-14	4	3	1.5	4.1375	2.6509	4.1890
Two-infeed	IEEE-14	4	3	1.5	4.3529	3.1544	3.9907
Three-terminal	IEEE-14	4	3	1.5	4.3546	2.9592	4.1260
Two-terminal	IEEE-57	4	4	2	22.0698	14.2854	23.6236
Three-terminal	IEEE-57	4	4	2	28.9858	24.7143	29.0658
Two-terminal	IEEE-118	4	3	1.5	120.8938	70.8048	115.1420

Table 9: Results of the power flow calculation of DC system.

DC variable		Converter number	Control modes of ① + ③
U_d	Algorithm 1 + AD	VSC_1	2.0000
		VSC_2	1.9994
	Algorithm 2 + AD	VSC_1	2.0000
		VSC_2	1.9994
δ	Algorithm 1 + AD	VSC_1	0.0062
		VSC_2	−0.0064
	Algorithm 2 + AD	VSC_1	0.0062
		VSC_2	−0.0064
M	Algorithm 1 + AD	VSC_1	0.7677
		VSC_2	0.7589
	Algorithm 2 + AD	VSC_1	0.7677
		VSC_2	0.7589

third-order and sixth-order Newton methods is less than the Newton method. And the advantage of computing time for Algorithm 2 is obvious. Table 6 also shows the proposed high-order methods suitable for the AC/DC systems with multi-infeed VSC-HVDC.

4.2. The Simulations of Modified IEEE 5-, 9-, 14-, 57-, and 118-Bus Systems. The modified IEEE 5-, 9-, 14-, 57-, and 118-bus systems are analyzed in this section [33]. The topology and parameter settings for those different IEEE text systems are shown in Table 7. The simulation results of performance comparisons for those IEEE text systems among improved Newton methods are shown in Table 8. The system topologies of two-terminal, two-infeed, and three-terminal are analyzed in this section.

It can be seen in Table 8, as the size and scale of the IEEE text systems grow, the iteration times keep mostly unchangeable for the third-order Newton and sixth-order Newton methods. And the computing time of the third-order or sixth-order Newton method is less than the Newton method. The validity and usability of the proposed improved Newton method suitable for VSC-HVDC system are certified.

4.3. The Simulation Results of AD Based on Third-Order Newton Method. In this part, the simulation results for AD algorithm based on Algorithm 1 and Algorithm 2 of third-order Newton method are presented. The IEEE-30 bus text system with two-terminal VSC-HVDC is employed to demonstrate the validity of the proposed AD algorithm. The results of the power flow calculation of DC system of control mode ① + ③ are shown in Table 9. The comparison of iteration times and computing time for the proposed AD algorithm is shown in Table 10.

From the results of Tables 9 and 10, the following can be seen.

(1) Compared with the results of Algorithm 1 and Algorithm 2 of third-order Newton method, as shown in Table 4, the improved AD algorithm satisfies the operation requirements of VSC parameter.

(2) Compared with the results of Table 5, for the iteration times and computing time, the improved AD algorithm has certain advantages.

(3) The result shows that AD technology is suitable for use in the third-order Newton method of VSC-HVDC system. And the application of AD technology reduces the work of hand code greatly. The efficiency of code programming is improved.

Table 10: Comparison of iteration times and computing time

Control mode	Iteration times		Computing time (ms)	
% VSC_1 + VSC_2	Algorithm 1 + AD	Algorithm 2 + AD	Algorithm 1 + AD	Algorithm 2 + AD
① + ③	2	2	0.15	0.31
① + ④	2	2	0.31	0.31
② + ③	2	2	0.31	0.32
② + ④	2	2	0.31	0.32

5. Conclusions

In this paper, based on the steady mathematical model of VSC-HVDC, the modified third-order Newton and sixth-order Newton methods have been presented to calculate the power flow of AC/DC systems with VSC-HVDC. The multivariate iteration matrix forms of the presented algorithms suitable for VSC-HVDC system are given. The proposed high-order Newton method has the third-order and sixth-order convergence, without solving the Hessian matrix. The task of the calculation is greatly reduced, and the efficiency is improved. Based on the third-order Newton method, the automatic differentiation technology is used to increase the efficiency of hand code. Some numerical examples on the modified IEEE bus systems with two-terminal, multi-terminal, and multi-infeed VSC-HVDC have demonstrated the computational performance of the power flow algorithms with incorporation of VSC-HVDC models.

Acknowledgments

This work is supported in part by the National Natural Science Foundation of China (Grant no. 61104045 and U1204506), in part by the Youth Project of National Social Science Fund (Grant no. 09CJY007), and in part by the Fundamental Research Funds for the Central Universities of China (Grant no. 2012B03514).

References

[1] N. Flourentzou, V. G. Agelidis, and G. D. Demetriades, "VSC-based HVDC power transmission systems: an overview," *IEEE Transactions on Power Electronics*, vol. 24, no. 3, pp. 592–602, 2009.

[2] P. Haugland, *It's Time to Connect—Technical Description of HVDC Light Technology*, ABB, 2008.

[3] A. L. P. de Oliveira, C. E. Tibúrcio, M. N. Lemes, and D. Retzmann, "Prospects of Voltage-Sourced Converters (VSC) applications in DC transmission systems," in *Proceedings of the IEEE/PES Transmission and Distribution Conference and Exposition: Latin America (T and D-LA '10)*, pp. 491–495, Sao Paulo, Brazil, November 2010.

[4] J. M. Maza-Ortega, A. Gomez-Exposito, M. Barragan-Villarejo, E. Romero-Ramos, and A. Marano-Marcolini, "Voltage source converter-based topologies to further integrate renewable energy sources in distribution systems," *IET Renewable Power Generation*, vol. 6, no. 6, pp. 435–445, 2012.

[5] X. P. Zhang, "Multiterminal voltage-sourced converter-based HVDC models for power flow analysis," *IEEE Transactions on Power Systems*, vol. 19, no. 4, pp. 1877–1884, 2004.

[6] C. Angeles-Camacho, O. L. Tortelli, E. Acha, and C. R. Fuerte-Esquivel, "Inclusion of a high voltage DC-voltage source converter model in a Newton-Raphson power flow algorithm," *IEE Proceedings: Generation, Transmission and Distribution*, vol. 150, no. 6, pp. 691–696, 2003.

[7] C. Zheng, X. Zhou, R. Li, and C. Sheng, "Study on the steady characteristic and algorithm of power flow for VSC-HVDC," *Proceedings of the CSEE*, vol. 25, no. 6, pp. 1–5, 2005.

[8] A. Pizano-Martinez, C. R. Fuerte-Esquivel, H. Ambriz-Pérez, and E. Acha, "Modeling of VSC-based HVDC systems for a Newton-Raphson OPF algorithm," *IEEE Transactions on Power Systems*, vol. 22, no. 4, pp. 1794–1803, 2007.

[9] A. Pizano-Martinez, C. R. Fuerte-Esquivel, and C. Angeles-Camacho, "Voltage source converter based high-voltage DC system modeling for optimal power flow studies," *Electric Power Components and Systems*, vol. 40, no. 3, pp. 312–320, 2012.

[10] C. Liu, B. Zhang, Y. Hou, F. F. Wu, and Y. Liu, "An improved approach for AC-DC power flow calculation with multi-infeed DC systems," *IEEE Transactions on Power Systems*, vol. 26, no. 2, pp. 862–869, 2011.

[11] X. Wang, Y. Song, and M. Irving, *Modern Power Systems Analysis*, Springer, Berlin, Germany, 2008.

[12] J. Beerten, S. Cole, and R. Belmans, "Generalized steady-state vsc mtdc model for sequential ac/dc power flow algorithms," *IEEE Transactions on Power Systems*, vol. 27, no. 2, pp. 821–829, 2012.

[13] T. Smed, G. Andersson, G. B. Sheble, and L. L. Grigsby, "A new approach to AC/DC power flow," *IEEE Transactions on Power Systems*, vol. 6, no. 3, pp. 1238–1244, 1991.

[14] Y. Wei, Z. Zheng, Y. Sun, Z. Wei, and G. Sun, "Voltage stability bifurcation analysis for AC/DC systems with VSC-HVDC," *Abstract and Applied Analysis*, vol. 2013, Article ID 387167, 9 pages, 2013.

[15] C. R. Fuerte-Esquivel, E. Acha, and H. Ambriz-Pérez, "A comprehensive Newton-Raphson UPFC model for the quadratic power flow solution of practical power networks," *IEEE Transactions on Power Systems*, vol. 15, no. 1, pp. 102–109, 2000.

[16] H. Ambriz-Perez, E. Acha, and C. R. Fuerte-Esquivel, "Advanced SVC models for Newton-Raphson load flow and Newton optimal power flow studies," *IEEE Transactions on Power Systems*, vol. 15, no. 1, pp. 129–136, 2000.

[17] C. R. Fuerte-Esquivel and E. Acha, "A Newton-type algorithm for the control of power flow in electrical power networks," *IEEE Transactions on Power Systems*, vol. 12, no. 4, pp. 1474–1480, 1997.

[18] M. A. Noor, K. I. Noor, E. Al-Said, and M. Waseem, "Some new iterative methods for nonlinear equations," *Mathematical Problems in Engineering*, vol. 2010, Article ID 198943, 12 pages, 2010.

[19] P. Tang and X. Wang, "An iteration method with generally convergent property for cubic polynomials," *International Journal of Bifurcation and Chaos*, vol. 19, no. 1, pp. 395–401, 2009.

[20] A. Cordero, J. L. Hueso, E. Martínez, and J. R. Torregrosa, "Increasing the convergence order of an iterative method for nonlinear systems," *Applied Mathematics Letters*, vol. 25, no. 12, pp. 2369–2374, 2012.

[21] D. Herceg and D. Herceg, "Means based modifications of Newton's method for solving nonlinear equations," *Applied Mathematics and Computation*, vol. 219, no. 11, pp. 6126–6133, 2013.

[22] F. Soleymani, S. Karimi Vanani, and A. Afghani, "A general three-step class of optimal iterations for nonlinear equations," *Mathematical Problems in Engineering*, vol. 2011, Article ID 469512, 10 pages, 2011.

[23] Z. Y. Sun, Y. Sun, and W. H. Ning, "Power flow algorithm with cubic convergence," *Power System Protection and Control*, vol. 37, no. 4, pp. 5–8+28, 2009.

[24] T. Orfanogianni and R. Bacher, "Using automatic code differentiation in power flow algorithms," *IEEE Transactions on Power Systems*, vol. 14, no. 1, pp. 138–144, 1999.

[25] M. Bartholomew-Biggs, S. Brown, B. Christianson, and L. Dixon, "Automatic differentiation of algorithms," *Journal of Computational and Applied Mathematics*, vol. 124, no. 1-2, pp. 171–190, 2000.

[26] Q. Jiang, G. Geng, C. Guo, and Y. Cao, "An efficient implementation of automatic differentiation in interior point optimal power flow," *IEEE Transactions on Power Systems*, vol. 25, no. 1, pp. 147–155, 2010.

[27] S. Cole, *Steady-State and Dynamic Modeling of VSC-HVDC Systems for Power System Simulation*, K. U. Leuven, Leuven, Belgium, 2010.

[28] A. M. Ostrowski, *Solution of Equations in Euclidean and Banach Spaces*, Academic Press, New York, NY, USA, 1973.

[29] J. Kou, Y. Li, and X. Wang, "A modification of Newton method with third-order convergence," *Applied Mathematics and Computation*, vol. 181, no. 2, pp. 1106–1111, 2006.

[30] H. H. H. Homeier, "On Newton-type methods with cubic convergence," *Journal of Computational and Applied Mathematics*, vol. 176, no. 2, pp. 425–432, 2005.

[31] S. K. Parhi and D. K. Gupta, "A sixth order method for nonlinear equations," *Applied Mathematics and Computation*, vol. 203, no. 1, pp. 50–55, 2008.

[32] A. Walther and A. Griewank, *A Package for the Automatic Differentiation of Algorithms Written in C/C++*, 2009, http://www.coin-or.org/projects/ADOL-C.xml.

[33] *Power Systems Test Case Archive*, University of Washington, http://www.ee.washington.edu/research/pstca/.

[34] Y. Wei, Z. Wei, and G. Sun, "A commentary on voltage stability of multi-infeed AC/DC system with VSC-HDVC," in *Proceedings of the Asia-Pacific Power and Energy Engineering Conference (APPEEC '11)*, pp. 1–4, Wuhan, China, March 2011.

Hindawi Publishing Corporation
Mathematical Problems in Engineering
Volume 2013, Article ID 836314, 9 pages
http://dx.doi.org/10.1155/2013/836314

Research Article

H_∞ Control of Network-Based Systems with Packet Disordering and Packet Loss Compensation

Jinna Li,[1,2] Lifeng Wei,[3] Chao Liu,[4] and Haibin Yu[2]

[1] *Lab of Operation and Control, Shenyang, University of Chemical Technology, Liaoning 110142, China*
[2] *Lab of Industrial Control Networks and Systems, Shenyang Institute of Automation, Chinese Academy of Sciences, Liaoning 110016, China*
[3] *College of Information Engineering, Shenyang University of Chemical Technology, Liaoning 110142, China*
[4] *Institute of Systems Science, Northeastern University, Shenyang, Liaoning 110004, China*

Correspondence should be addressed to Jinna Li; lijinna_721@126.com

Received 3 April 2013; Accepted 14 May 2013

Academic Editor: Guanghui Wen

Compensation scheme-based H_∞ control is investigated for networked control systems with packet disordering and packet loss. Since the existence of packet disordering and packet loss inevitably degrades the control performance of networked control systems, it is worth studying a control scheme to compensate for them, such that the control performance can be improved. Thus, a compensation control strategy is first proposed following this direction. Next, a mathematical model of networked control systems with Markovian property is constructed due to the signals executed by the plant subject to Markovian chain. Based on it, a sufficient condition for stochastic stability of networked control systems with uncertain parameters as well as compensation strategy is presented, and an adaptive controller is designed based on linear matrix inequality (LMI) technique. Finally, a numerical example and simulations are given to illustrate the effectiveness of the proposed method.

1. Introduction

Networked control systems (NCSs), in which nodes communicate over communication networks, have attracted lots of researchers' attention [1–4]. Since networks-based control gives rise to many advantages including low cost, easy maintenance, and flexible system structure, the successful application of NCSs can be found in a wide range of areas such as industrial automation, intelligent transportation system, and smart grid. However, packet disordering and packet dropout inevitably exist in the transmission of signals. They are recognized to be two main causes for performance deterioration or even instability of NCSs, hence, considerable research has been done (see, e.g. [5–21] and the references therein).

So far, the majority of NCSs research has focused on controller design to provide sufficient stability conditions for NCSs with packet loss. A lot of effort has also been taken for modeling NCSs in presence of packet losses as asynchronous dynamic systems or Markovian jumping systems [5, 6]. With further study on packet loss, some effective compensation strategies for packet loss that occurred during communication are proposed to improve control performance of NCSs. Predictive control is a typical method with wich the control prediction generator provides a set of future control predictions to enable the closed-loop system to achieve the desired control performance leading to removing the effects of data dropout [7–11]. Another typical compensation methodology for packet loss is observer-based state estimation [12]. In addition, [13] proposed a packet dropout-based compensation scheme, namely, the latest control signal is used for compensation if the ideal control input is missing. However, note that, in all of the aforementioned literature, packet disordering is not considered, but packet disordering and packet loss coexist in packets delivered network communication.

Packet disordering means that a packet sent earlier may arrive at the destination node later or vice versa. Packet disordering of NCSs has drawn an increasing attention [10, 14–21]. In [14], packets that arrived late at control nodes were discarded, and stability and H_∞ compensation control

were investigated. However, the packet disordering is not described clearly. In [15, 16], the sampling instants of received signals were compared to describe packet disordering, and stability analysis and synthesis were studied. Some literature using the similar method can be found in the existing reported results (e.g., [17]). Recently, [10, 18] proposed an active compensation for packet disordering; that is, the latest control actions applied to the plant are available by comparing the time stamps of packets. The so called compensation method has been also presented in [19–21], where the latest signals are executed by the plant by defining an operator constructing a mapping between the newest signals and packet displacement values. However, note that a situation where no new control actions arrive at the actuator may occur due to packet disordering and packet loss during a sampling interval. In this case, it is critical how to control the plant. To the best of the authors' knowledge, this problem has been not fully investigated to date, which motivates this work for proposing a new compensation scheme.

The specific problem addressed in this paper is the compensation control when the newest signal is not available for NCSs due to the packet disordering and packet loss. The highlighted method is that control inputs are determined by defining some operators associated with packet displacements; that is, the latest control input is chosen when no new signals arrive at the actuator during the sampling interval $((k-1)T, kT]$; otherwise, the newest signal controls the plant. After that, a Markovian jumping model of NCSs is put forward. Stability analysis and the controller synthesis are thoroughly investigated and the adaptive controller design is obtained in terms of linear matrix inequalities (LMI). A numerical example is provided to demonstrate the effectiveness of the proposed approach.

The rest of the paper is organized as follows. Section 2 is concerned with problem statement. In this section, a compensation control scheme is proposed, and a model of networked control systems is constructed. Section 3 investigates the stability and H_∞ control for NCSs with packet disordering and packet losses. The results of numerical simulation are presented in Section 4. Conclusions are stated in Section 5.

Notation. R^n denotes the n dimensional Euclidean space. $\mathbf{P} > \mathbf{0}$ means that matrix $\mathbf{P}$ is real symmetric and positive definite, and $\mathbf{I}$ is the identity matrix of appropriate dimensions. The subscript "T" denotes the matrix transpose. In symmetric block matrices, we use "$*$" to represent a term that is induced by symmetry, and diag$(\cdots)$ stands for a block-diagonal matrix. $\|\mathbf{x}\|$ stands for the standard l_2 norm of vector $\mathbf{x}$; that is, $\|\mathbf{x}\| = (\mathbf{x}^{\mathrm{T}}\mathbf{x})^{1/2}$.

2. Problem Statement

The following system is considered:

$$\begin{aligned} \mathbf{x}_{k+1} &= \overline{\mathbf{A}}\mathbf{x}_k + \overline{\mathbf{B}}\mathbf{u}_k + \mathbf{D}_1\mathbf{w}_k \\ \mathbf{z}_k &= \mathbf{C}\mathbf{x}_k + \mathbf{D}_2\mathbf{w}_k, \end{aligned} \tag{1}$$

where $\mathbf{x}_k = \mathbf{x}(kT) \in \Re^n$, $\mathbf{u}_k = \mathbf{u}(kT) \in \Re^M$, and $\mathbf{z}_k = \mathbf{z}(kT) \in \Re^P$ are the state vector, control input vector, and controlled output vector, respectively. T is the sampling period. $\overline{\mathbf{A}} = \mathbf{A} + \Delta\mathbf{A}$, $\overline{\mathbf{B}} = \mathbf{B} + \Delta\mathbf{B}$, $(\Delta\mathbf{A} \;\; \Delta\mathbf{B}) = \mathbf{D}\mathbf{F}(k)(\mathbf{E}_1 \;\; \mathbf{E}_2)$, $\mathbf{A}, \mathbf{B}, \mathbf{C}, \mathbf{D}, \mathbf{D}_1, \mathbf{D}_2, \mathbf{E}_1$, and $\mathbf{E}_2$ are some constant matrices of appropriate dimensions, and $\mathbf{F}^T(k)\mathbf{F}(k) \le \mathbf{I}$. $\mathbf{w}_k = \mathbf{w}(kT) \in \iota_2[0, \infty]$ denotes the exogenous disturbance signal.

The state feedback controller can be expressed as

$$\mathbf{u}_k = \mathbf{K}\mathbf{x}_k, \tag{2}$$

where $\mathbf{K}$ is some constant matrix of appropriate dimensions.

Here, we assume that sensor and actuator are time-driven synchronously, the period is identical and equal to T, and the controller is event-driven. Since the states of systems and control signals are transmitted over the communication networks with limited bandwidth, the packet disordering and intermittent packet dropouts are inevitable in the communication channels. To describe the phenomenon of packet disordering and design compensation scheme, we define the displacement values of packets and some operators determining the control actions. The details are as follows.

Without loss of generalization, we consider a sequence of packets $\mathbf{x}_{k-h}, \mathbf{x}_{k-h+1}, \ldots, \mathbf{x}_k$ transmitted over the network from the sensor, where h is a given integer. The maximum delay bound is an alternative solution to h. For $\mathbf{x}_{k-h}, \mathbf{x}_{k-h+1}, \ldots, \mathbf{x}_k$, it is well known that the corresponding expected arrival sequence numbers are $1, 2, \ldots, h+1$. Then, the expected arrival sequence number of packet $\mathbf{x}_{k-i}$ is $h + 1 - i$ $(i = 0, 1, \ldots, h)$ is easily obtained. A receive_index l $(l = 1, 2, \ldots, h+1)$ is assigned to each nonduplicate packet as it arrives at the point of measurement, which we refer to as the destination (actuator) since the control is event-driven. To describe the newest signal executed by the plant, we assume that packets which have not appeared or lost during the sampling interval $((k-1)T, kT]$ arrive at the actuator in order after the kT time instant, and their receive_index values are 1 more than the real values. Moreover, if the sampled packets behind p (p is some positive integer) lost packets arrive at the plant before the kT time instant (including kT time instant), their receive index values are p more than the real values. $R_k(i)$ and $d_k(h+1-i)$ denote the receive_index and displacement value of packet $\mathbf{x}_{k-i}$, respectively. For packet $\mathbf{x}_{k-i}$ arriving at the actuator before the kT instant (including kT instant), if $d_k(h+1-i) \neq 0$, then a "disordering event" has occurred in communication. Packet $\mathbf{x}_{k-i}$ is late if $d_k(h+1-i) > 0$, early if $d_k(h+1-i) < 0$, and in order if $d_k(h+1-i) = 0$ (see [19–21]). To guarantee the newest signals being executed by the plant, the packets that arrive at the actuator late are discarded. Define the following operators:

$$\delta\left(d_k\left(h+1-i\right)\right) = \begin{cases} 1 & d_k\left(h+1-i\right) \le 0 \\ 0 & d_k\left(h+1-i\right) > 0, \end{cases} \tag{3}$$

$$\theta_k\left(i\right) = \prod_{j=0}^{i-1}\left(1 - \delta\left(d_k\left(h+1-j\right)\right)\right)\delta\left(d_k\left(h+1-i\right)\right), \tag{4}$$

Table 1: An example in Figure 1.

	x_{k-2}	x_{k-1}	x_k
Exception values	1	2	3
Receive_index	2	3	4
Displacement values	1	1	1
Parameters		$\theta_k(-1) = 1$ $\theta_k(0) = 0$ $\theta_k(1) = 0$ $\theta_k(2) = 0$	

Table 2: An example in Figure 2.

	x_{k-1}	x_{k-1}	x_k
Exception values	1	2	3
Receive_index	1	3	4
Displacement values	0	1	1
Parameters		$\theta_k(-1) = 0$ $\theta_k(0) = 0$ $\theta_k(1) = 0$ $\theta_k(2) = 1$	

where $\prod_{j=0}^{-1}(1 - \delta(d_k(h + 1 - j))) = 1$ $(i = 0, 1, \ldots, h)$. The function of $\theta_k(i)$ $(i = 0, 1, \ldots, h)$ is to guarantee that the newest signal is executed if it has arrived at the actuator during the interval $((k - 1)T, kT]$. Moreover, note that it may happen not to receive new signal due to late coming packet or packet loss; thus we design the following controller:

$$\mathbf{u}_k = \sum_{i=0}^{h} \theta_k(i)\, \mathbf{K}\mathbf{x}_{k-i} + \theta_k(-1)\, \mathbf{u}_{k-1}, \tag{5}$$

where

$$\theta_k(-1) = \begin{cases} 1 & d_k(h + 1 - i) > 0, \\ & \forall i\, (i = 0, 1, \ldots, h) \\ 0 & \text{otherwise.} \end{cases} \tag{6}$$

Remark 1. As a matter of fact, the operators $\theta_k(i)$ $(i = -1, 0, \ldots, h)$ are defined for the purpose of selecting control input. Note that $\theta_k(i) = 1$ or 0, and $\sum_{i=-1}^{h} \theta_k(i) = 1$. $\theta_k(i) = 1$ or $\theta_k(i) = 0$ $(i = 0, 1, \ldots, h)$, which is determined in terms of the displacement values of packets. More detailed explanations can be found in the examples in Figures 1 and 2, Tables 1 and 2. Since we choose event-triggered controller, once $\mathbf{x}_{k-i}$ arrives at the controller, control action $\mathbf{K}\mathbf{x}_{k-i}$ is sent to the actuator. When the displacement values of all packets $d_k(h + 1 - i) > 0$ $(i = 0, 1, \ldots, h)$; that is, there are no new signals arriving the actuator during sampling interval $((k - 1)T, kT]$, $\theta_k(-1)$ is set to be 1 by (6) and other $\theta_k(i) = 0$ $(i = 0, 1, \ldots, h)$ hold due to (4), which indicates the control input $\mathbf{u}_{k-1}$ to act on the plant (see Figure 1 and Table 1). Otherwise, $\theta_k(-1) = 0$ and there exists one $\theta_k(i) = 1$ $(i = 0, 1, \ldots, h)$. In this context, the newest control signal $\mathbf{K}\mathbf{x}_{k-i}$ is regarded as the control action $\mathbf{u}_k$. It is worth pointing out that the packet disordering, random time-varying transmission delay, and packet loss are taken into account in the suggested compensation control scheme (5), simultaneously. From this point of view, it is readily seen that the proposed control scheme (5) is quite general.

For further understanding compensation control scheme (5), we study two examples shown in Figures 1 and 2 which illustrate the arriving timing of signals transmitted. Expected arrival sequence numbers, assigned receive_index values, and displacement values for a sequence transmitted,

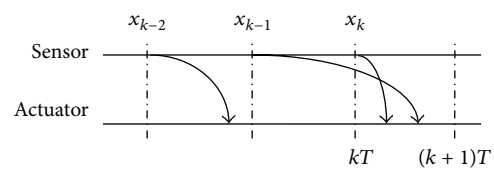

Figure 1: Timing diagram of signals transmitting in the example with packet disordering.

corresponding to Figures 1 and 2, are given in Tables 1 and 2, respectively. In the two examples, we choose $h = 2$, which means that a group of 3 packets is used as the studying object. From Table 1, we find that, packets $\mathbf{x}_{k-2}$, $\mathbf{x}_{k-1}$ and $\mathbf{x}_k$ are displaced by one unit from their positions, then all of displacement values are equal to 1. In this context, the actuator does not receive new signal during the sampling interval $((k - 1)T, kT]$, which can be seen in Figure 1. By (3), (4), and (6), we obtain $\theta_k(-1) = 1$ and $\theta_k(0) = \theta_k(1) = \theta_k(2) = 0$. And by (5), the control input $\mathbf{u}_{k-1}$ acts on the plant, which is entirely consistent with the proposed compensation control scheme that the latest control action is utilized to control the plant when no new signal is available during the sampling interval $((k - 1)T, kT]$. In Figure 2, note that packet $\mathbf{x}_{k-1}$ has lost. Similarly, by calculating, we obtain $\theta_k(2) = 1$ and $\theta_k(0) = \theta_k(1) = \theta_k(-1) = 0$. Then, $\mathbf{K}\mathbf{x}_{k-2}$ is used as the newest control input by virtue of (5). Obviously, this result accords with the actual situation shown in Figure 2.

Remark 2. Similar to [13], we execute the compensation control scheme. However, there are two distinct differences from [13]. The first one is that the stability analysis and compensation strategy are investigated in the presence of both packet loss and packet disordering simultaneously. In this sense, the theory method presented in this paper extends the results presented in [13], since packet disordering is not taken into account in [13]. The second difference is that an operator deciding how to choose control actions is clearly defined based on the displacement values of packets, while [13] control strategy is proposed in terms of delay information.

Remark 3. Compared with the existing studies on NCSs with packet disordering [10, 14–21], a key difference is

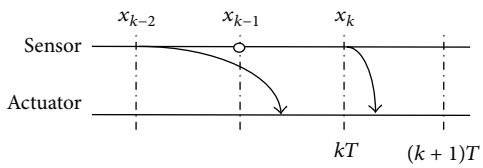

Figure 2: Timing diagram of signals transmitting in the example with packet loss.

that a compensation control scheme is proposed when no new signal arrives at the actuator.

The closed-loop system can be obtained by substituting (5) into (1):

$$\begin{aligned} \mathbf{x}_{k+1} &= \overline{\mathbf{A}}x_k + \overline{\mathbf{B}}\left(\sum_{i=0}^{h}\theta_k(i)\,\mathbf{K}x_{k-i} + \theta_k(-1)\,\mathbf{u}_{k-1}\right) \\ &\quad + \mathbf{D}_1\mathbf{w}_k \\ \mathbf{z}_k &= \mathbf{C}\mathbf{x}_k + \mathbf{D}_2\mathbf{w}_k. \end{aligned} \tag{7}$$

Letting $\xi_k^{\mathrm{T}} = [\mathbf{x}_k^{\mathrm{T}} \;\; \mathbf{x}_{k-1}^{\mathrm{T}} \cdots \mathbf{x}_{k-h}^{\mathrm{T}}]$ and $\eta_k^{\mathrm{T}} = [\xi_k^{\mathrm{T}} \;\; \mathbf{u}_{k-1}^{\mathrm{T}}]$, (7) is expressed as

$$\begin{aligned} \xi_{k+1} &= \mathbf{A}_{11,k}\xi_k + \mathbf{A}_{12,k}\mathbf{u}_{k-1} + \widetilde{\mathbf{D}}_1\mathbf{w}_k \\ \mathbf{u}_k &= \mathbf{A}_{21,k}\xi_k + \theta_k(-1)\,\mathbf{u}_{k-1}, \end{aligned} \tag{8}$$

where

$$\begin{aligned} \mathbf{A}_{11,k} &= \begin{bmatrix} \overline{\mathbf{A}} + \mathbf{M}_0 & \mathbf{M}_1 & \cdots & \mathbf{M}_{h-1} & \mathbf{M}_h \\ \mathbf{I} & \mathbf{0} & \cdots & \mathbf{0} & \mathbf{0} \\ \vdots & \vdots & \ddots & \vdots & \vdots \\ \mathbf{0} & \mathbf{0} & \cdots & \mathbf{I} & \mathbf{0} \end{bmatrix}, \\ \mathbf{A}_{12,k} &= \begin{bmatrix} \overline{\mathbf{B}}\theta_k(-1) \\ \mathbf{0} \\ \vdots \\ \mathbf{0} \end{bmatrix}, \qquad \widetilde{\mathbf{D}}_1 = \begin{bmatrix} \mathbf{D}_1 \\ \mathbf{0} \\ \vdots \\ \mathbf{0} \end{bmatrix}, \\ \mathbf{A}_{21,k} &= \left[\theta_k(0)\,\mathbf{K} \;\; \theta_k(1)\,\mathbf{K} \;\; \cdots \;\; \theta_k(h)\,\mathbf{K}\right], \\ \mathbf{M}_i &= \overline{\mathbf{B}}i_k(i)\,\mathbf{K} \quad (i = 0, 1, \ldots, h). \end{aligned} \tag{9}$$

Further, we have

$$\begin{aligned} \eta_{k+1} &= \overline{\mathbf{A}}_k\eta_k + \overline{\mathbf{D}}_1\mathbf{w}_k \\ \mathbf{z}_k &= \widehat{\mathbf{C}}\eta_k + \mathbf{D}_2\mathbf{w}_k, \end{aligned} \tag{10}$$

where

$$\begin{aligned} \overline{\mathbf{A}}_k &= \begin{bmatrix} \Gamma & \mathbf{R} \\ \Lambda(\theta_k(0), \ldots, \theta_k(h))\,\overline{\mathbf{K}} & \theta_k(-1)\,\mathbf{I} \end{bmatrix}, \\ \mathbf{R} &= \widehat{\mathbf{D}}\mathbf{F}(k)\,\mathbf{E}_2\theta_k(-1) + \widehat{\mathbf{B}}\theta_k(-1), \\ \Gamma &= \widehat{\mathbf{A}} + \widehat{\mathbf{B}}\Lambda(\theta_k(0), \ldots, \theta_k(h))\,\overline{\mathbf{K}} \\ &\quad + \widehat{\mathbf{D}}\mathbf{F}(k)\left(\widehat{\mathbf{E}}_1 + \mathbf{E}_2\Lambda(\theta_k(0), \ldots, \theta_k(h))\,\overline{\mathbf{K}}\right), \\ \Lambda(\theta_k(0), \ldots, \theta_k(h)) &= \left[\theta_k(0)\,\mathbf{I} \;\; \cdots \;\; \theta_k(h)\,\mathbf{I}\right], \\ \overline{\mathbf{K}} &= \operatorname{diag}\left\{\underbrace{\mathbf{K}, \mathbf{K}, \ldots, \mathbf{K}}_{(h+1)}\right\}, \qquad \widehat{\mathbf{C}} = \left[\mathbf{C} \;\; \mathbf{0} \;\; \cdots \;\; \mathbf{0}\right], \\ \widehat{\mathbf{A}} &= \begin{bmatrix} \mathbf{A} & \mathbf{0} & \cdots & \mathbf{0} & \mathbf{0} \\ \mathbf{I} & \mathbf{0} & \cdots & \mathbf{0} & \mathbf{0} \\ \vdots & \vdots & \ddots & \vdots & \vdots \\ \mathbf{0} & \mathbf{0} & \cdots & \mathbf{I} & \mathbf{0} \end{bmatrix}, \qquad \widehat{\mathbf{B}} = \begin{bmatrix} \mathbf{B} \\ \mathbf{0} \\ \vdots \\ \mathbf{0} \end{bmatrix}, \\ \widehat{\mathbf{E}}_1 &= \left[\mathbf{E} \;\; \mathbf{0} \;\; \cdots \;\; \mathbf{0}\right], \\ \widehat{\mathbf{D}} &= \begin{bmatrix} \mathbf{D} \\ \mathbf{0} \\ \vdots \\ \mathbf{0} \end{bmatrix}, \qquad \overline{\mathbf{D}}_1 = \begin{bmatrix} \widetilde{\mathbf{D}}_1 \\ \mathbf{0} \end{bmatrix}. \end{aligned} \tag{11}$$

It is well known that the newest signals executed by plant may be subject to some probability distribution [6]; here we will assume that the newest signals transmitted over communication network are subject to Markovian chain. Define $\mathbf{d}_k = [\theta_k(-1), \theta_k(0), \ldots, \theta_k(h)]^{\mathrm{T}}$; since $\theta_k(i) = 1$ or 0 $(i = -1, 0, \ldots, h)$ and $\sum_{i=-1}^{h}\theta_k(i) = 1$, then, there are $h+2$ possible values for $\mathbf{d}_k$, obviously. Similar to our prior effort [21], for ease of notation, we define a vector-valued function $f : \mathbf{d}_k \rightarrow \sigma(k)$ to map the vector $\mathbf{d}_k$ into a scalar number $\sigma(k) \in \mathfrak{I} = \{1, 2, \ldots, r\}$, where $r = h+2$. $\sigma(k) = i$ also denotes the No. i $(i \in \mathfrak{I})$ subsystem of NCS (10). Moreover, transition probability associated with the newest signals executed is defined as $\pi_{ij} = \operatorname{Prob}(\sigma(k+1) = j \mid \sigma(k) = i)$, where $\sigma(k) = i$ denotes $\mathbf{d}_k = [0, \ldots, 1, \ldots, 0]^{\mathrm{T}}$, namely, $\theta_k(i-2) = 1$. Obviously, $\sum_{j\in\mathfrak{I}}\pi_{ij} = 1$. Thus, (10) is a Markovian jumping system.

Remark 4. In this paper, the stability analysis and H_∞ controller design are investigated on the premise that transition probability matrix is fully known. Actually, the analysis and control methods for NCSs with uncertain transition probabilities have been developed, and we can refer to [22, 23].

3. Stability Analysis and H_∞ Controller Design

In this section, we will present a sufficient condition for H_∞ control and the design of the controller gains $\mathbf{K}_i$ $(i = 1, 2, \ldots, r)$ adapting to No. i switched subsystem.

Lemma 5 (see [24]). *For any matrices* $\mathbf{W}$, $\mathbf{M}$, $\mathbf{N}$, $\mathbf{F}(k)$ *with* $\mathbf{F}^T(k)\mathbf{F}(k) < \mathbf{I}$, *and any scalar* $\varepsilon > 0$, *the following inequality holds:*

$$\begin{aligned}&\mathbf{W} + \mathbf{M}\mathbf{F}(k)\mathbf{N} + \mathbf{N}^{\mathrm{T}}\mathbf{F}^{\mathrm{T}}(k)\mathbf{M}^{\mathrm{T}}\\&\quad\le \mathbf{W} + \varepsilon\mathbf{M}\mathbf{M}^{\mathrm{T}} + \varepsilon^{-1}\mathbf{N}^{\mathrm{T}}\mathbf{N}.\end{aligned} \tag{12}$$

Theorem 6. *For given scalars* h *and* $\gamma > 0$, *matrices* $\mathbf{K}_i$, *if there exist matrices* $\mathbf{P}_i > \mathbf{0}$, $\mathbf{Q}_i > \mathbf{0}$ $(i \in \mathfrak{J})$, *such that*

$$\begin{bmatrix}\Upsilon_1 & \Upsilon_2\\ * & \Upsilon_3\end{bmatrix} < 0, \tag{13}$$

then the closed-loop system (10) *is stochastic stable with an* H_∞ *norm bound* γ, *where* $\Upsilon_1 = \sum_{j\in\mathfrak{J}}\pi_{ij}\overline{\mathbf{A}}_k^{\mathrm{T}}\mathbf{W}_j\overline{\mathbf{A}}_k + \gamma^{-1}\widehat{\mathbf{C}}^{\mathrm{T}}\widehat{\mathbf{C}} - \mathbf{W}_i$, $\Upsilon_2 = \sum_{j\in\mathfrak{J}}\pi_{ij}\overline{\mathbf{A}}_k^{\mathrm{T}}\mathbf{W}_j\overline{\mathbf{D}}_1 + \gamma^{-1}\widehat{\mathbf{C}}^{\mathrm{T}}\mathbf{D}_2$, $\Upsilon_3 = \sum_{j\in\mathfrak{J}}\pi_{ij}\overline{\mathbf{D}}_1^{\mathrm{T}}\mathbf{W}_j\overline{\mathbf{D}}_1 + \gamma^{-1}\mathbf{D}_2^{\mathrm{T}}\mathbf{D}_2 - \gamma\mathbf{I}$.

Proof. Without loss of generalization, we set $\sigma(k)$ to be i. Choosing a Lyapunov-Krasovskii functional candidate which is given by

$$V_k = \eta_k^{\mathrm{T}}\mathbf{W}_i\eta_k, \tag{14}$$

where

$$\mathbf{W}_i = \begin{bmatrix}\mathbf{P}_i & \mathbf{0}\\ \mathbf{0} & \mathbf{Q}_i\end{bmatrix}, \tag{15}$$

we can obtain

$$\begin{aligned}EV_{k+1} - V_k = &\sum_{j\in\mathfrak{J}}\pi_{ij}\left(\overline{\mathbf{A}}_k\eta_k + \overline{\mathbf{D}}_1\mathbf{w}_k\right)^{\mathrm{T}}\mathbf{W}_j\\&\times\left(\overline{\mathbf{A}}_k\eta_k + \overline{\mathbf{D}}_1\mathbf{w}_k\right) - \eta_k^{\mathrm{T}}\mathbf{W}_i\eta_k.\end{aligned} \tag{16}$$

Let $\mathbf{e}_k = \left[\eta_k^{\mathrm{T}}\ \ \mathbf{w}_k^{\mathrm{T}}\right]^{\mathrm{T}}$; we can obtain $EV_{k+1} - V_k = \mathbf{e}_k^{\mathrm{T}}\Theta_i\mathbf{e}_k$, where

$$\Theta_i = \begin{bmatrix}-\mathbf{W}_i + \sum_{j\in\mathfrak{J}}\pi_{ij}\overline{\mathbf{A}}_k^{\mathrm{T}}\mathbf{W}_j\overline{\mathbf{A}}_k & \sum_{j\in\mathfrak{J}}\pi_{ij}\overline{\mathbf{A}}_k^{\mathrm{T}}\mathbf{W}_j\overline{\mathbf{D}}_1\\ * & \sum_{j\in\mathfrak{J}}\pi_{ij}\overline{\mathbf{D}}_1^{\mathrm{T}}\mathbf{W}_j\overline{\mathbf{D}}_1\end{bmatrix}. \tag{17}$$

And

$$\gamma^{-1}\mathbf{z}_k^{\mathrm{T}}\mathbf{z}_k - \gamma\mathbf{w}_k^{\mathrm{T}}\mathbf{w}_k + EV_{k+1} - V_k = \eta_k^{\mathrm{T}}\left(\Theta_i + \Lambda\right)\eta_k, \tag{18}$$

where

$$\Lambda = \begin{bmatrix}\gamma^{-1}\widehat{\mathbf{C}}^{\mathrm{T}}\widehat{\mathbf{C}} & \gamma^{-1}\widehat{\mathbf{C}}^{\mathrm{T}}\mathbf{D}_2\\ * & \gamma^{-1}\mathbf{D}_2^{\mathrm{T}}\mathbf{D}_2 - \gamma\mathbf{I}\end{bmatrix}. \tag{19}$$

If (13) is satisfied, we have $(\Theta_i + \Lambda) < \mathbf{0}$. Further, we can obtain

$$\gamma^{-1}\mathbf{z}_k^{\mathrm{T}}\mathbf{y}_k - \gamma\mathbf{w}_k^{\mathrm{T}}\mathbf{w}_k + EV_{k+1} - V_k < \mathbf{0}. \tag{20}$$

Then, $\gamma^{-1}\mathbf{z}_k^{\mathrm{T}}\mathbf{y}_k - \gamma\mathbf{w}_k^{\mathrm{T}}\mathbf{w}_k < -(EV_{k+1} - V_k)$. Summing up both sides of the above inequality from $k = 0$ to $k = n$, using the zero initial condition, we have $\sum_{k=0}^{n}\|\mathbf{z}_k\|^2 < \gamma^2\sum_{k=0}^{n}\|\mathbf{w}_k\|^2 - \gamma EV_{n+1}$ for all n. Letting $n \to \infty$, we have

$$\|\mathbf{z}_k\|_2^2 < \gamma^2\|\mathbf{w}_k\|_2^2. \tag{21}$$

If $\mathbf{w}_k \equiv \mathbf{0}$ and (13) holds, it is clear that $\Gamma_i = -\mathbf{W}_i + \sum_{j\in\mathfrak{J}}\pi_{ij}\overline{\mathbf{A}}_k^{\mathrm{T}}\mathbf{W}_j\overline{\mathbf{A}}_k < 0$ can be implied by (13), then

$$EV_{k+1} - V_k \le -\beta\mathbf{x}_k^{\mathrm{T}}\mathbf{x}_k, \tag{22}$$

where $\beta = \min\{\lambda_{\min}(-\Gamma_i), i \in \mathfrak{J}\}$. Summing up both sides of the above inequality from $k = 0$ to $k = \hbar$ and Letting $\hbar \to \infty$, we can see that for any $\hbar > 1$

$$\begin{aligned}&\lim_{\hbar\to\infty} EV(\hbar + 1) - V(\varphi_0, s_0)\\&\quad\le -\beta\lim_{\hbar\to\infty}\sum_{k=0}^{\hbar}E\left(\mathbf{x}_k^{\mathrm{T}}\mathbf{x}_k\right)\end{aligned} \tag{23}$$

or

$$\lim_{\hbar\to\infty}\sum_{k=0}^{\hbar}E\left(\mathbf{x}_k^{\mathrm{T}}\mathbf{x}_k\right) \le \lim_{\hbar\to\infty}\frac{1}{\beta}V(\varphi_0, s_0) < \infty, \tag{24}$$

where φ_0 and s_0 are the initial condition of the system. The stochastic stability is obtained. This completes the proof. □

For the purpose of controller design, we give Theorem 7.

Theorem 7. *For a given scalar* h_1, *if there exist matrices* $\mathbf{X}_i > \mathbf{0}$, $\mathbf{Y}_i$, *and* $\mathbf{F}_i$ $(i \in \mathfrak{J})$, *such that*

$$\begin{bmatrix}-\mathbf{S}_i & \mathbf{0} & \Xi_{i1} & \mathbf{S}_i\widehat{\mathbf{C}}^T & \widehat{\mathbf{H}}_i^T\\ * & -\gamma\mathbf{I} & \Xi_{i2} & \mathbf{D}_2^T & \mathbf{0}\\ * & * & \Xi_{i3} & \mathbf{0} & \mathbf{0}\\ * & * & * & -\gamma\mathbf{I} & \mathbf{0}\\ * & * & * & * & -\varepsilon\mathbf{I}\end{bmatrix} < \mathbf{0}, \tag{25}$$

then $\mathbf{K}_i$ $(\overline{\mathbf{K}}_i = \mathbf{F}_i\mathbf{X}_i^{-1}, \overline{\mathbf{K}}_i = \mathrm{diag}(\mathbf{K}_i, \mathbf{K}_i, \ldots, \mathbf{K}_i))$ *are adaptive controller gains with an* H_∞ *norm bound* γ, *where*

$$\begin{aligned}\Xi_{i1} &= \left[\rho_{i1}\mathbf{N}_i^T\ \ \rho_{i2}\mathbf{N}_i^T\ \ \cdots\ \ \rho_{ir}\mathbf{N}_i^T\right],\\ \Xi_{i2} &= \left[\rho_{i1}\overline{\mathbf{D}}_1^T\ \ \rho_{i2}\overline{\mathbf{D}}_1^T\ \ \cdots\ \ \rho_{ir}\overline{\mathbf{D}}_1^T\right],\\ \Psi_i &= \begin{bmatrix}\Psi_{i,11} & \Psi_{i,12} & \cdots & \Psi_{i,1r}\\ * & \Psi_{i,22} & \cdots & \Psi_{i,2r}\\ * & * & \ddots & \vdots\\ * & * & * & \Psi_{i,rr}\end{bmatrix},\\ \Xi_{i3} &= \mathrm{diag}\left(-\mathbf{S}_1, -\mathbf{S}_2, \ldots, -\mathbf{S}_r\right) + \Psi_i,\\ \rho_{ij} &= \sqrt{\pi_{ij}}\quad (j = 1, 2, \ldots, r),\\ \mathbf{N}_i &= \begin{bmatrix}\widehat{\mathbf{A}}_k\mathbf{X}_i + \widehat{\mathbf{B}}\Lambda_i\mathbf{F}_i & \widehat{\mathbf{B}}\theta_k(-1)\mathbf{Y}_i\\ \Lambda_i\mathbf{F}_i & \theta_k(-1)\mathbf{Y}_i\end{bmatrix},\\ \widehat{\mathbf{H}}_i &= \left[\widehat{\mathbf{E}}_1\mathbf{X}_i + \mathbf{E}_2\Lambda_i\mathbf{F}_i\ \ \mathbf{E}_2\theta_k(-1)\mathbf{Y}_i\right],\\ \Psi_{i,lj} &= \rho_{il} * \rho_{ij}\varepsilon\widetilde{\mathbf{D}}\widetilde{\mathbf{D}}^T\quad (l, j = 1, 2, \ldots, r).\end{aligned} \tag{26}$$

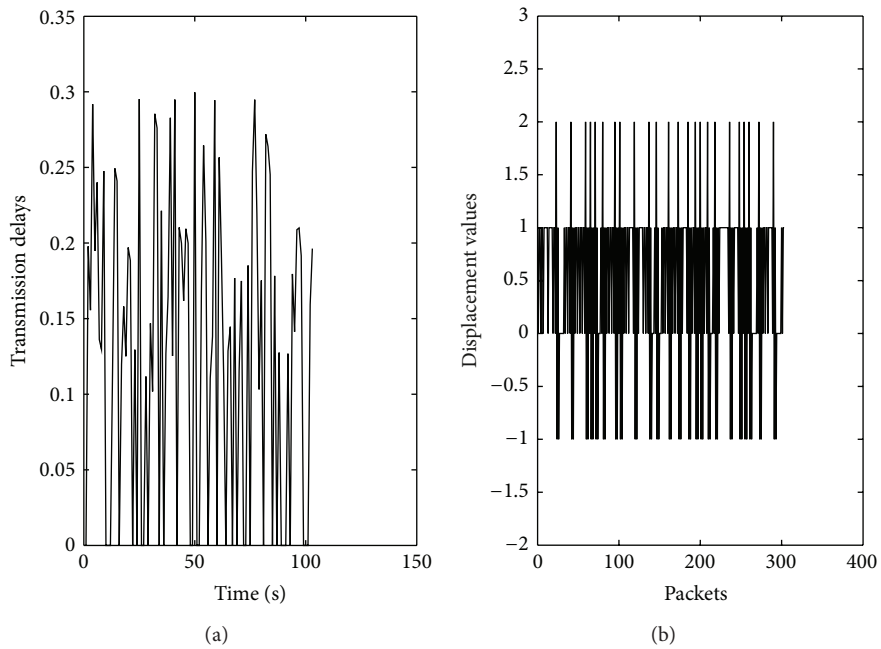

Figure 3: Transmission delay (a) and displacement values (b).

Proof. By Schur complement and Lemma 5, (13) is equivalent to

$$\begin{bmatrix} -\mathbf{W}_i & \mathbf{0} & \Lambda_{i1} & \widehat{\mathbf{C}}^{\mathrm{T}} & \mathbf{H}_i^{\mathrm{T}} \\ * & -\gamma\mathbf{I} & \Xi_{i2} & \mathbf{D}_2^{\mathrm{T}} & \mathbf{0} \\ * & * & \Lambda_{i3} & \mathbf{0} & \mathbf{0} \\ * & * & * & -\gamma\mathbf{I} & \mathbf{0} \\ * & * & * & * & -\varepsilon\mathbf{I} \end{bmatrix} < \mathbf{0}, \tag{27}$$

where

$$\begin{aligned} \Lambda_{i1} &= \left[\rho_{i1}\widehat{\mathbf{A}}_k^{\mathrm{T}} \quad \rho_{i2}\widehat{\mathbf{A}}_k^{\mathrm{T}} \quad \cdots \quad \rho_{ir}\widehat{\mathbf{A}}_k^{\mathrm{T}}\right], \\ \Lambda_{i3} &= \operatorname{diag}\left(-\mathbf{W}_1, -\mathbf{W}_2, \ldots, -\mathbf{W}_r\right) + \Psi_i, \\ \mathbf{H}_i &= \left[\widehat{\mathbf{E}}_1 + \mathbf{E}_2\Lambda_i\overline{\mathbf{K}}_i \quad \mathbf{E}_2\theta_k(-1)\right]. \end{aligned} \tag{28}$$

Pre- and postmultiplying both sides of (27) with $\operatorname{diag}(\mathbf{W}_i^{-1}, \underbrace{\mathbf{I}, \ldots, \mathbf{I}}_{r+3})$ and its transpose, letting $\mathbf{X}_i = \mathbf{P}_i^{-1}$, $\mathbf{Y}_i = \mathbf{Q}_i^{-1}$, $\mathbf{S}_i = \mathbf{W}_i^{-1}$, $\overline{\mathbf{K}}_i\mathbf{X}_i = \mathbf{F}_i$ $(i = 1, 2, \ldots r)$, (25) can be derived. Theorem 7 is completed. □

4. Numerical Examples

In this section, we verify the effectiveness of the control strategy proposed for NCSs with packet disordering and packet loss. First, we show the control results for NCSs with packet disordering and packet loss under two cases. One is in the absence of structural uncertainty, and the other is with uncertain structure. One can clearly see that the method proposed has good robustness. Second, comparative studies are performed to demonstrate clearly the advantages enjoyed by the suggested compensation scheme described in this paper.

Example 1. Consider the following unstable system:

$$\begin{aligned} \mathbf{x}_{k+1} &= \left(\begin{bmatrix} 0.0885 & -0.0659 \\ -0.1538 & 0.2977 \end{bmatrix} + \Delta\mathbf{A}\right)\mathbf{x}_k \\ &\quad + \left(\begin{bmatrix} 0.5234 \\ -0.0990 \end{bmatrix} + \Delta\mathbf{B}\right)\mathbf{u}_k \\ &\quad + \begin{bmatrix} 1.2544 \\ 0.5317 \end{bmatrix}\mathbf{w}_k \\ \mathbf{z}_{k+1} &= \left[0.0690 \quad -0.3554\right]\mathbf{x}_k + 0.3304\mathbf{w}_k, \end{aligned} \tag{29}$$

where

$$\begin{aligned} \mathbf{D} &= \begin{bmatrix} 0.3885 \\ 0.3112 \end{bmatrix}, \qquad \mathbf{E}_1 = \left[0.3237 \quad -0.2128\right] \\ \mathbf{E}_2 &= 0.5243. \end{aligned} \tag{30}$$

The transmission delays and displacement values of packets delivered over network are shown in Figure 3. It should be explained that delay determines the arrival orders of packets, based on which displacement values of packets are calculated. Clearly, the bound of transmission delay $h = 2$ under assuming sampling period $0.15s$. Based on the displacement values of packets, thus the jumping process taking values in a finite set $\mathfrak{I} = \{1, 2, 3, 4\}$, standing for $\mathfrak{I} = \{[1, 0, 0, 0], [0, 1, 0, 0], [0, 0, 1, 0], [0, 0, 0, 1]\}$, governs the switching among the different system modes, then $r = 4$. $[1, 0, 0, 0] \rightarrow 1$ means no new signal arrives at the actuator, $u(k-1)$ acts on the plant; $[0, 1, 0, 0] \rightarrow 2$ means the newest signal $\mathbf{K}_2\mathbf{x}_k$ transmitted over network is executed by the plant at kT time instant, the rest may be deduced by analogy; $[0, 0, 0, 1] \rightarrow 4$ means the newest signal $\mathbf{K}_4\mathbf{x}_{k-2}$ transmitted over network is executed by the plant at kT time instant.

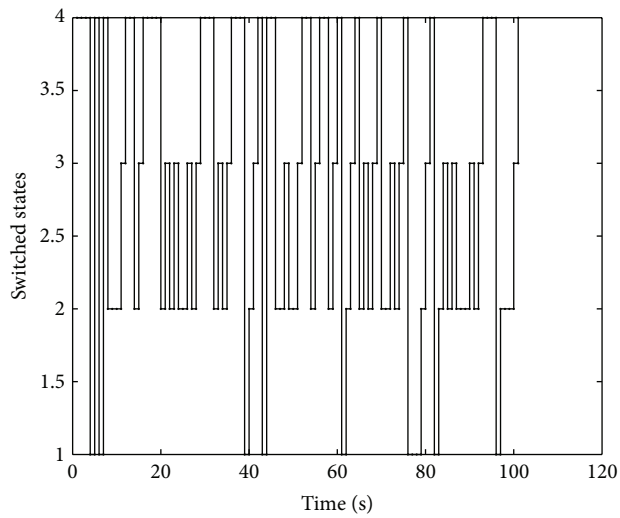

Figure 4: Markovian process of NCS with packet disordering and dropouts competition.

Thus, the newest signals executed by the plant are subject to Markovian process, whose switched states are shown in Figure 4 and transition probability matrix is given as follows:

$$\begin{bmatrix} 0.2000 & 0.5000 & 0 & 0.3000 \\ 0 & 0.2941 & 0.7059 & 0 \\ 0 & 0.4167 & 0 & 0.5833 \\ 0.2500 & 0.2813 & 0 & 0.4688 \end{bmatrix}. \tag{31}$$

4.1. Verification of Compensation Scheme. First, we consider the systems without structural uncertainty in NCS. By Theorem 7, we obtain the following adaptive controller gains

$$\begin{aligned} \mathbf{K}_2 &= \begin{bmatrix} -0.3271 & 0.5110 \end{bmatrix} \\ \mathbf{K}_3 &= 1.0e-03 * \begin{bmatrix} 0.1137 & -0.1898 \end{bmatrix} \\ \mathbf{K}_4 &= 1.0e-03 * \begin{bmatrix} -0.0474 & 0.1103 \end{bmatrix}. \end{aligned} \tag{32}$$

Second, if the uncertainty exists in the NCSs, by Theorem 7, we also obtain the corresponding adaptive controller gains

$$\begin{aligned} \mathbf{K}_2 &= \begin{bmatrix} -0.3903 & 0.5512 \end{bmatrix} \\ \mathbf{K}_3 &= \begin{bmatrix} -0.2038 & 0.3679 \end{bmatrix} \\ \mathbf{K}_4 &= \begin{bmatrix} -0.2869 & 0.3902 \end{bmatrix}. \end{aligned} \tag{33}$$

We choose the uncertain parameter $F(k) = \sin(k)$. At the initial state value $\mathbf{x}_0 = [-1 - 3]^{\mathrm{T}}$, the states and output response of the NCS, without uncertainty and with uncertainty under the network environment in the presence of packet disordering and packet loss competition, are shown in Figures 5 and 6, respectively. Compared with the result given in Figure 5, the NCS with uncertainty can be also stabilized quickly using the competition controller designed in this paper though there exist packet disordering and packet dropout in communication network. This makes it clear that the proposed control scheme has a good robustness.

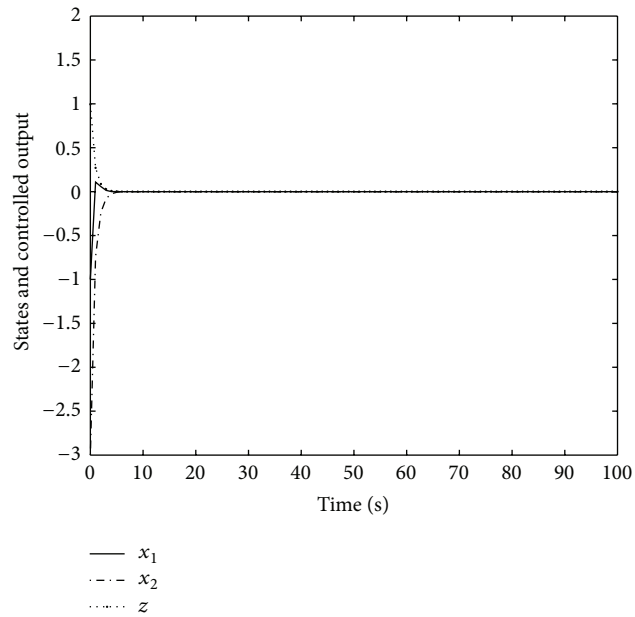

Figure 5: State and output response of the system.

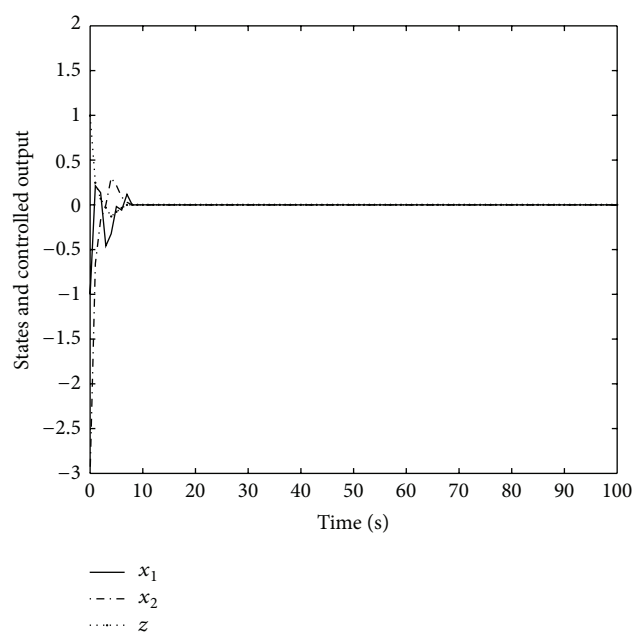

Figure 6: State and output response of the system.

4.2. Control Performance Comparison. It should be pointed out that the discrete-time system in this example can be inverted into a continuous-time system in [14, 20] if sampling period $T = 0.1s$ is given. If $\mathbf{w}_k \neq \mathbf{0}$, the H_∞ norm bounds and corresponding controller gains are shown in Table 3 ("—" denotes that the conditions are infeasible). Obviously, a more optimal H_∞ norm bound is obtained in this paper than those in [14, 20] since the competition scheme is performed when no signal is available by the plant due to packet disordering

Table 3: Comparison of convergence time.

	H_∞ norm bound	Controller gain
[14]	—	—
[20]	1.5	$\mathbf{K} = 1.0 * 10^{-7}$ $\begin{bmatrix} 0.1278 & -0.0714 \end{bmatrix}$
This paper	0.6977	$\mathbf{K}_2 = [-0.4867 \quad 0.7869]$ $\mathbf{K}_3 = [0 \quad 0]$ $\mathbf{K}_4 = [0 \quad 0]$

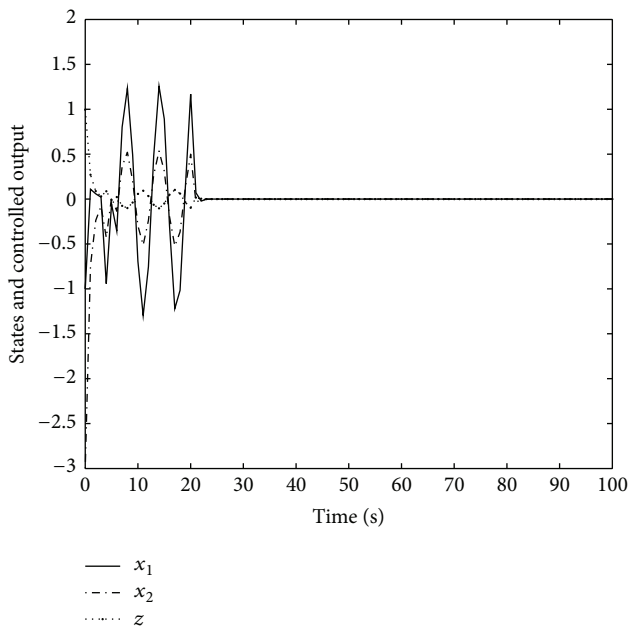

Figure 7: Curves of state and output response of the system subject to exogenous disturbance.

and packet loss. At the initial state value $\mathbf{x}_0 = \begin{bmatrix} -1 & -3 \end{bmatrix}^{\mathrm{T}}$, the disturbance input $\mathbf{w}(t)$ is as follows:

$$\mathbf{w}(t) = \begin{cases} \sin(t) & 5s \le t < 20s \\ 0 & \text{otherwise}, \end{cases} \tag{34}$$

the state and output response of the NCS in the presence of packet disordering and packet loss are shown in Figure 7.

5. Conclusions

In this paper, we are concerned with H_∞ control of NCSs with compensation scheme. The aim of devised control scheme is that the effect of packet disordering and packet loss on control performance is eliminated. The main idea is that we first describe the packet disordering and give the compensation scheme when there are no new signals executed by the plant during the sampling interval $((k-1)T, kT]$. Second, a model of NCSs with Markovian jumping property is presented. Furthermore, the stochastic stability and controller design are discussed. Finally, a numerical example and simulations are given to illustrate the advantages and the effectiveness of the developed theory.

Acknowledgments

The authors would like to acknowledge the National Natural Science Foundation of China under Grants 61104093, 61174119, 61034006, and 60774070, the Special Program for Key Basic Research Founded by MOST under Grant 2010CB334705, the National High Technology Research and Development Program of China (863 Program) under Grant 2011AA040101, and Scientific Research Project of Liaoning Province of China under Grants L2012141, L2011064.

References

[1] J. Zhang, P. Shi, and Y. Xia, "Fuzzy delay compensation control for T-S fuzzy systems over network," *IEEE Transaction on Cybernetics*, vol. 43, no. 1, pp. 259–268, 2013.

[2] Y. Sun and J. Xu, "Finite-time boundedness and stabilization of networked control systems with time delay," *Mathematical Problems in Engineering*, vol. 2012, Article ID 705828, 12 pages, 2012.

[3] H. Li, Z. Sun, M. Chow, and F. Sun, "Gain-scheduling-based state feedback integral control for networked control systems," *IEEE Transactions on Industrial Electronics*, vol. 58, no. 6, pp. 2465–2472, 2011.

[4] G.-P. Liu, J.-X. Mu, D. Rees, and S.-C. Chai, "Design and stability analysis of networked control systems with random communication time delay using the modified MPC," *International Journal of Control*, vol. 79, no. 4, pp. 288–297, 2006.

[5] W. Zhang, M. S. Branicky, and S. M. Phillips, "Stability of networked control systems," *IEEE Control Systems Magazine*, vol. 21, no. 1, pp. 84–97, 2001.

[6] P. Seiler and R. Sengupta, "An H_∞ approach to networked control," *IEEE Transactions on Automatic Control*, vol. 50, no. 3, pp. 356–364, 2005.

[7] G. Liu, Y. Xia, J. Chen, D. Rees, and W. Hu, "Networked predictive control of systems with random network delays in both forward and feedback channels," *IEEE Transactions on Industrial Electronics*, vol. 54, no. 3, pp. 1282–1297, 2007.

[8] Y. Zhang and S. Li, "Networked model predictive control based on neighbourhood optimization for serially connected large-scale processes," *Journal of Process Control*, vol. 17, no. 1, pp. 37–50, 2007.

[9] R. Wang, G. Liu, W. Wang, D. Rees, and Y.-B. Zhao, "Guaranteed cost control for networked control systems based on an improved predictive control method," *IEEE Transactions on Control Systems Technology*, vol. 18, no. 5, pp. 1226–1232, 2010.

[10] Y. Zhao, G. Liu, and D. Rees, "Design of a packet-based control framework for networked control systems," *IEEE Transactions on Control Systems Technology*, vol. 17, no. 4, pp. 859–865, 2009.

[11] J. Zhang, Y. Xia, and P. Shi, "Design and stability analysis of networked predictive control systems," *IEEE Transaction on Control Systems Technology*, 2013.

[12] C. Lin, Z. Wang, and F. Yang, "Observer-based networked control for continuous-time systems with random sensor delays," *Automatica*, vol. 45, no. 2, pp. 578–584, 2009.

[13] S. Jiang and H.-J. Fang, "H_∞ static output feedback control for nonlinear networked control systems with time delays and packet dropouts," *ISA Transactions*, vol. 52, no. 2, pp. 215–222, 2013.

[14] Y.-L. Wang and G.-H. Yang, "H_∞ control of networked control systems with time delay and packet disordering," *IET Control Theory & Applications*, vol. 1, no. 5, pp. 1344–1354, 2007.

[15] D. Yue, Q. Han, and C. Peng, "State feedback controller design of networked control systems," *IEEE Transactions on Circuits and Systems II*, vol. 51, no. 11, pp. 640–644, 2004.

[16] D. Yue, Q.-L. Han, and J. Lam, "Network-based robust H_∞ control of systems with uncertainty," *Automatica*, vol. 41, no. 6, pp. 999–1007, 2005.

[17] X. Jiang, Q.-L. Han, S. Liu, and A. Xue, "A new H_∞ stabilization criterion for networked control systems," *IEEE Transactions on Automatic Control*, vol. 53, no. 4, pp. 1025–1032, 2008.

[18] Y. Zhao, G. Liu, and D. Rees, "Actively compensating for data packet disorder in networked control systems," *IEEE Transactions on Circuits and Systems II*, vol. 57, no. 11, pp. 913–917, 2010.

[19] J.-N. Li, Q.-L. Zhang, and M. Cai, "Modelling and robust stability of networked control systems with packet reordering and long delay," *International Journal of Control*, vol. 82, no. 10, pp. 1773–1785, 2009.

[20] J.-N. Li, Q.-L. Zhang, Y.-L. Wang, and M. Cai, "H_∞ control of networked control systems with packet disordering," *IET Control Theory & Applications*, vol. 3, no. 11, pp. 1463–1475, 2009.

[21] J.-N. Li, Q.-L. Zhang, H.-B. Yu, and M. Cai, "Real-time guaranteed cost control of MIMO networked control systems with packet disordering," *Journal of Process Control*, vol. 21, no. 6, pp. 967–975, 2011.

[22] J. Xiong, J. Lam, H. Gao, and D. W. C. Ho, "On robust stabilization of Markovian jump systems with uncertain switching probabilities," *Automatica*, vol. 41, no. 5, pp. 897–903, 2005.

[23] A. R. Fioravanti, A. P. C. Goncalves, and J. C. Geromel, "Discrete-Time H1 output feedback for Markov jump systems with uncertain transition probabilities," *International Journal Robust and Nonlinear Control*, vol. 23, no. 8, pp. 894–902, 2013.

[24] Y. Wang, L. Xie, and C. E. de Souza, "Robust control of a class of uncertain nonlinear systems," *Systems & Control Letters*, vol. 19, no. 2, pp. 139–149, 1992.

Hindawi Publishing Corporation
Mathematical Problems in Engineering
Volume 2013, Article ID 718759, 7 pages
http://dx.doi.org/10.1155/2013/718759

Research Article

Consensus of Continuous-Time Multiagent Systems with General Linear Dynamics and Nonuniform Sampling

Yanping Gao,[1] Bo Liu,[2] Min Zuo,[1] Tongqiang Jiang,[1] and Junyan Yu[3]

[1] *Beijing Technology and Business University, Beijing 100048, China*
[2] *North China University of Technology, Beijing 100144, China*
[3] *University of Electronic Science and Technology of China, Chengdu 610054, China*

Correspondence should be addressed to Bo Liu; boliu@ncut.edu.cn

Received 29 March 2013; Accepted 16 May 2013

Academic Editor: Wenwu Yu

This paper studies the consensus problem of multiple agents with general linear continuous-time dynamics. It is assumed that the information transmission among agents is intermittent; namely, each agent can only obtain the information of other agents at some discrete times, where the discrete time intervals may not be equal. Some sufficient conditions for consensus in the cases of state feedback and static output feedback are established, and it is shown that if the controller gain and the upper bound of discrete time intervals satisfy certain linear matrix inequality, then consensus can be reached. Simulations are performed to validate the theoretical results.

1. Introduction

Consensus is one of the fundamental issues in the study of distributed control of multiagent systems, and it has wide applications in formation control of multiple robots, communication among sensor networks, cooperative control of unmanned aerial vehicles, and so forth. Much research work on consensus has been emerged, and most of the existing work focuses on the consensus problems of multiple agents with special dynamics, such as first-order dynamics (or single integrator) [1–10], second-order dynamics (or double integrators) [11–19], and high-order dynamics [20, 21]. Consensus problems of second-order continuous-time multiagent systems are studied in [12–14], where the information transmission among agents is intermittent. In [15–17], only the partial state of second-order agent can be measured, and thus, some static or dynamic output feedback controllers are designed. In [20–22], consensus is studied for high-order and nonlinear multiagent systems, respectively.

In recent years, the consensus of multiple agents with general linear dynamics has been paid more and more attention, such as [23–28], and the analysis of such multiagent systems is more challenging than the case of special dynamics. In [24], consensus is considered in the case of static output feedback, and it is proved that the consensus is equivalent to the Hurwitz stable or Schur stable of a constant matrix, which is determined by the topology and the system dynamics. By studying the stability of the constant matrix, it is shown that consensus can be reached for continuous-time multiagent systems if and only if the system is stabilizable and detectable and the topology has a spanning tree under some rank constraints, and a necessary condition is also provided for consensus of discrete-time multiagent systems. In [25], consensus of continuous-time and discrete-time multiagent systems under a dynamic output feedback controller, which is actually a state estimator, is investigated, respectively. By applying the result in [29], some sufficient and necessary conditions are presented in [25]. In [26], the joint effect of network topology, agent dynamics, and communication data rate on consensus of discrete-time multiagent systems is analyzed, and it is shown that under perfect state feedback, consensus is reached if and only if the dynamics of each agent is stabilizable and the unstable eigenvalues of each agent satisfy some constraints. In [27], the H_∞ consensus problem of continuous-time multiagent systems is studied under dynamic output feedback by applying the robust

control theory and linear matrix inequality technique. In [28], consensus of discrete-time multiagent systems under a dynamic output feedback controller, which is actually an observer-type controller, is discussed, and the discrete-time consensus region is analyzed for neurally stable agents and unstable agents, respectively.

It should be mentioned that [23–25, 27] all study the consensus of continuous-time multiagent systems, and the information transmission among agents is continuous. However, due to the limitation of bandwidth, the cost of communication, the technique constraints, and so forth, it is possible to transmit information in the intermittent manner. In addition, sampled-data control has many favorable properties, such as flexibility, robustness, and low cost see [30] for further details. Hence, it is also necessary to study the consensus of general continuous-time multiagent systems with intermittent information transmission. To the authors' best knowledge, there is little research work reported on this problem. Based on the previous consideration, we analyze the consensus of continuous-time multiagent systems with general dynamics, where each agent can only obtain the information of other agents at discrete times. Moreover, the discrete time intervals may not be equal, which often occurs in the event-driven systems or networked control systems [31]. The sufficient condition for consensus and the method to design controller gain are presented.

This paper is organized as follows. In Section 2, we present some concepts in graph theory and formulate the model to be studied. In Section 3, main results are stated. In Section 4, simulations are provided to illustrate the effectiveness of the theoretical results. Conclusion remarks are made in Section 5.

Notations. Let I or $I_n \in \mathbb{R}^{n\times n}$ be an identity matrix, and $\mathbf{1}_n = [1,\ldots,1]^T \in \mathbb{R}^n$; for symmetric matrices A and B, $A < B$ (resp., $A \le B$) means that $A - B$ is a negative definite (resp., negative semidefinite) matrix; $\otimes$ denotes the Kronecker product operator, and $C \otimes D = [c_{ij}D]$, where $C = [c_{ij}]$ and $D = [d_{ij}]$ are two matrices.

2. Preliminaries

2.1. Graph Theory. Some basic definitions in graph theory [32] are first introduced.

A directed graph $\mathcal{G}$ consists of a vertex set $\mathcal{V}(\mathcal{G})$ and an edge set $\mathcal{E}(\mathcal{G})$, where $\mathcal{V}(\mathcal{G}) = \{v_1,\ldots,v_n\}$ and $\mathcal{E}(\mathcal{G}) \subset \{(v_j,v_i) : v_j, v_i \in \mathcal{V}(\mathcal{G})\}$. For edge (v_j,v_i), v_j is called the parent vertex of v_i and v_i is called the child vertex of v_j. The set of neighbors of vertex v_i is defined by $N(\mathcal{G},v_i) = \{v_j : (v_j,v_i) \in \mathcal{E}(\mathcal{G})$ and $j \ne i\}$, and the associated index set is denoted by $N(\mathcal{G},i) = \{j : v_j \in N(\mathcal{G},v_i)\}$. A (directed) path from v_{i_1} to v_{i_k} is a sequence, $v_{i_1},\ldots,v_{i_k}$, of distinct vertices such that $(v_{i_j},v_{i_{j+1}}) \in \mathcal{E}(\mathcal{G})$, $j = 1,\ldots,k-1$. A directed graph $\mathcal{G}$ is strongly connected if there is a path from every vertex to every other vertex. A directed tree is a directed graph, where every vertex except one special vertex has exactly one parent vertex, and the special vertex, called root vertex, has no parent vertices and can be connected to any other vertices via paths. A subgraph $\mathcal{G}_s$ of $\mathcal{G}$ is a graph such that $\mathcal{V}(\mathcal{G}_s) \subset \mathcal{V}(\mathcal{G})$ and $\mathcal{E}(\mathcal{G}_s) \subset \mathcal{E}(\mathcal{G})$. $\mathcal{G}_s$ is said to be a spanning subgraph if $\mathcal{V}(\mathcal{G}_s) = \mathcal{V}(\mathcal{G})$. For any $v_i, v_j \in \mathcal{V}(\mathcal{G}_s)$, if $(v_i,v_j) \in \mathcal{E}(\mathcal{G}_s) \Leftrightarrow (v_i,v_j) \in \mathcal{E}(\mathcal{G})$, then $\mathcal{G}_s$ is said to be an induced subgraph of $\mathcal{G}$ and $\mathcal{G}_s$ is also said to be induced by $\mathcal{V}(\mathcal{G}_s)$. A spanning tree of $\mathcal{G}$ is a directed tree which is a spanning subgraph of $\mathcal{G}$. $\mathcal{G}$ is said to have a spanning tree if some edges form a spanning tree of $\mathcal{G}$.

A matrix is called nonnegative if each of its elements is nonnegative. A weighted directed graph $\mathcal{G}(F)$ is a directed graph $\mathcal{G}$ plus a nonnegative matrix $F = [f_{ij}] \in \mathbb{R}^{n\times n}$, where $f_{ij} > 0 \Leftrightarrow (v_j,v_i) \in \mathcal{E}(\mathcal{G})$, and f_{ij} is called the weight of edge (v_j,v_i). The Laplacian matrix $L = [l_{ij}] \in \mathbb{R}^{n\times n}$ of $\mathcal{G}(f)$ is defined as

$$l_{ij} = \begin{cases} -f_{ij}, & i \ne j, \\ \displaystyle\sum_{s=1,s\ne i}^{n} f_{is}, & i = j. \end{cases} \tag{1}$$

The Laplacian matrix of $\mathcal{G}(F)$ has the following properties.

Lemma 1 (see [2]).

(i) *Zero is an eigenvalue of L, and* $\mathbf{1}_n$ *is the associated right eigenvector.*

(ii) *Zero is an algebraically simple eigenvalue of L, and all the other eigenvalues are with positive real parts if and only if* $\mathcal{G}(F)$ *has a spanning tree.*

2.2. Model. Consider a group of agents with the following general continuous-time dynamics:

$$\begin{aligned} \dot{x}_i(t) &= Ax_i(t) + Bu_i(t), \\ y_i(t) &= Cx_i(t), \quad i = 1,2,\ldots,n, \end{aligned} \tag{2}$$

where $x_i \in \mathbb{R}^m$, $u_i \in \mathbb{R}^p$ and $y_i \in \mathbb{R}^q$, are the state, control input, and output of agent i, respectively, and A, B, C are constant matrices.

Given u_i, $i = 1,\ldots,n$, we say that u_i or multiagent system (2) solves a consensus problem asymptotically if $\lim_{t\to\infty}(x_i(t) - x_j(t)) = 0$, $i,j = 1,2,\ldots,n$, for any initial states.

In this paper, we consider the case of intermittent information transmission; namely, each agent can only obtain the information of its neighbors at some discrete times $t_0, t_1, \ldots$, where $0 \le t_0 < t_1 < t_2 < \cdots$. Let $T_k = t_{k+1} - t_k$, and assume that $T_k \le d$, $k = 0,1,\ldots$; namely, all discrete time intervals have a common upper bound. Note that all T_k may not be equal.

In the case that the (relative) state of each agent can be measured directly, we consider the following control input:

$$\begin{aligned} u_i(t) &= K \sum_{j\in N(\mathcal{G},i)} a_{ij}\left(x_j(t_k) - x_i(t_k)\right), \\ t &\in [t_k, t_{k+1}), \quad i = 1,2,\ldots,n, \end{aligned} \tag{3}$$

where K is the controller gain to be designed.

In some times, the state of each agent cannot be measured directly, and thus, we also consider the following static output feedback controller:

$$u_i(t) = K \sum_{j \in N(\mathcal{G},i)} a_{ij}\left(y_j(t_k) - y_i(t_k)\right), \quad t \in [t_k, t_{k+1}),\ i = 1, 2, \ldots, n. \tag{4}$$

Remark 2. Obviously, if A is Hurwitz stable, then consensus can be reached for $K = 0$. Hence, we assume that A is not Hurwitz stable in this paper.

3. Main Results

In this section, we will present a sufficient condition for consensus under controllers (3) and (4), respectively, and the methods to design controller gains are also provided.

Let $X(t) = (x_1^T(t), x_2^T(t), \ldots, x_n^T(t))^T$, then multiagent system (2) under controller (3) can be written as

$$\dot{X}(t) = (I_n \otimes A) X(t) - (L \otimes (BK)) X(t_k), \quad t \in [t_k, t_{k+1}),\ k = 0, 1, \ldots. \tag{5}$$

By Lemma 1, there exists an invertible matrix U, the first column of which is $\mathbf{1}_n$, such that

$$U^{-1} L U = \begin{pmatrix} 0 & \alpha \\ 0 & H \end{pmatrix}, \tag{6}$$

where $H \in \mathbb{R}^{(n-1)\times(n-1)}$. Let $\delta(t) = (U^{-1} \otimes I_m)X(t)$; then

$$\dot{\delta}_1(t) = A\delta_1(t) - (\alpha \otimes (BK))\tilde{\delta}(t_k), \tag{7}$$

$$\dot{\tilde{\delta}}(t) = (I_{n-1} \otimes A)\tilde{\delta}(t) - (H \otimes (BK))\tilde{\delta}(t_k), \tag{8}$$

where $\delta(t) = (\delta_1(t)^T, \tilde{\delta}(t)^T)^T$, $\delta_1(t) \in \mathcal{R}^m$.

By the previous state transformation, it is easy to obtain the following lemma.

Lemma 3. *Controller* (3) *solves a consensus problem asymptotically if and only if system* (8) *is asymptotically stable.*

Proof. Sufficiency. Let $U = [\mathbf{1}_n, U_1]$, where $U_1 \in \mathcal{R}^{n\times(n-1)}$. By $X(t) = (U \otimes I_m)\delta(t)$, we have $X(t) = \mathbf{1}_n \otimes \delta_1(t) + (U_1 \otimes I_m)\tilde{\delta}(t)$. Clearly, if system (8) is asymptotically stable, namely, $\lim_{t\to\infty}\tilde{\delta}(t) = 0$, then $\lim_{t\to\infty}(x_i(t) - x_j(t)) = 0$, $i, j = 1, 2, \ldots, n$.

Necessity. Let $U^{-1} = (u_2, U_2^T)^T$, where $U_2 \in \mathcal{R}^{(n-1)\times n}$. From $U^{-1}U = I_n$, we have $u_2^T \mathbf{1}_n = 1$, $U_2 \mathbf{1}_n = 0$. Since consensus is reached, there exists $\phi(t) \in \mathcal{R}^m$ such that $\lim_{t\to\infty}(x_i(t) - \phi(t)) = 0$, $i = 1, 2, \ldots, n$. By $\delta(t) = (U^{-1} \otimes I_m)X(t)$,

$$\begin{aligned}
&\delta(t) - \left(U^{-1} \otimes I_m\right)\left(\mathbf{1}_n \otimes \phi(t)\right) \\
&\quad = \left(U^{-1} \otimes I_m\right)\left(X(t) - \mathbf{1}_n \otimes \phi(t)\right) \\
&\quad \Longrightarrow \delta(t) - \begin{pmatrix} u_2^T \mathbf{1}_n \\ U_2 \mathbf{1}_n \end{pmatrix} \otimes \phi(t) \\
&\quad = \left(U^{-1} \otimes I_m\right)\left(X(t) - \mathbf{1}_n \otimes \phi(t)\right) \\
&\quad \Longrightarrow \delta(t) - \begin{pmatrix} 1 \\ 0 \end{pmatrix} \otimes \phi(t) \\
&\quad = \left(U^{-1} \otimes I_m\right)\left(X(t) - \mathbf{1}_n \otimes \phi(t)\right) \\
&\quad \Longrightarrow \begin{pmatrix} \delta_1(t) - \phi(t) \\ \tilde{\delta}(t) \end{pmatrix} \\
&\quad = \left(U^{-1} \otimes I_m\right)\left(X(t) - \mathbf{1}_n \otimes \phi(t)\right) \\
&\quad \Longrightarrow \lim_{t\to\infty} \begin{pmatrix} \delta_1(t) - \phi(t) \\ \tilde{\delta}(t) \end{pmatrix} \\
&\quad = \begin{pmatrix} u_2^T \otimes I_m \\ U_2 \otimes I_m \end{pmatrix} \lim_{t\to\infty}\left(X(t) - \mathbf{1}_n \otimes \phi(t)\right).
\end{aligned} \tag{9}$$

By $\lim_{t\to\infty}(X(t) - \mathbf{1}_n \otimes \phi(t)) = 0$, it is easy to obtain $\lim_{t\to\infty}\tilde{\delta}(t) = 0$, which means that system (8) is asymptotically stable. □

By Lemma 3, we will analyze the stability of system (8) by applying the input delay approach [33], which is an effective method to deal with the stability of continuous-time systems with intermittent input.

Let $\tau(t) = t - t_k$, and let $t \in [t_k, t_{k+1})$; then $t_k = t - \tau(t)$, and system (8) can be rewritten as

$$\begin{aligned}
\dot{\tilde{\delta}}(t) &= (I_{n-1} \otimes A)\tilde{\delta}(t) - (H \otimes (BK))\tilde{\delta}(t - \tau(t)) \\
&= (I_{n-1} \otimes A - H \otimes (BK))\tilde{\delta}(t) \\
&\quad + (H \otimes (BK))\left(\tilde{\delta}(t) - \tilde{\delta}(t - \tau(t))\right) \\
&= \widetilde{A}\tilde{\delta}(t) + (H \otimes (BK))\xi(t),
\end{aligned} \tag{10}$$

where $\widetilde{A} = I_{n-1} \otimes A - H \otimes (BK)$, $\xi(t) = \tilde{\delta}(t) - \tilde{\delta}(t - \tau(t))$.

By $T_k \le d$, we have $0 \le \tau(t) \le d$, $k = 0, 1, \ldots$. Obviously, the stability of system (8) is equivalent to that of system (10). By analyzing the stability of system (10), we obtain the following main result.

Theorem 4. *Assume that* (A, B) *is stabilizable and the topology graph has a spanning tree. Controller* (3) *solves a consensus problem asymptotically if there exist positive definite matrices*

P, R such that K and d satisfy the following linear matrix inequality:

$$\begin{pmatrix} P\widetilde{A}+\widetilde{A}^T P & P(H\otimes(BK)) & \widetilde{A}^T R \\ * & -\frac{1}{d}R & (H\otimes(BK))^T R \\ * & * & -\frac{1}{d}R \end{pmatrix}. \quad (11)$$

Proof. Consider the following Lyapunov-Krasovskii functional for system (10):

$$V(t)=\widetilde{\delta}^T(t)P\widetilde{\delta}(t)+\int_{t-d}^{t}(s-t+d)\dot{\widetilde{\delta}}^T(s)R\dot{\widetilde{\delta}}(s)\,ds, \quad (12)$$

where $P>0$, $R>0$, and then

$$\begin{aligned}\dot{V}(t)&=2\widetilde{\delta}^T(t)P\dot{\widetilde{\delta}}(t)\\&\quad+\left(-\int_{t-d}^{t}\dot{\widetilde{\delta}}^T(s)R\dot{\widetilde{\delta}}(s)\,ds+d\dot{\widetilde{\delta}}^T(t)R\dot{\widetilde{\delta}}(t)\right).\end{aligned} \quad (13)$$

By Lemma 4 in [34],

$$\begin{aligned}&\int_{t-d}^{t}\dot{\widetilde{\delta}}^T(s)R\dot{\widetilde{\delta}}(s)\,ds\\&\quad\geq\frac{1}{d}\left(\widetilde{\delta}(t)-\widetilde{\delta}(t-\tau(t))\right)^T R\left(\widetilde{\delta}(t)-\widetilde{\delta}(t-\tau(t))\right),\end{aligned} \quad (14)$$

and thus,

$$\begin{aligned}\dot{V}(t)&\leq 2\widetilde{\delta}^T(t)P\dot{\widetilde{\delta}}(t)\\&\quad-\frac{1}{d}\left(\widetilde{\delta}(t)-\widetilde{\delta}(t-\tau(t))\right)^T R\left(\widetilde{\delta}(t)-\widetilde{\delta}(t-\tau(t))\right)\\&\quad+d\dot{\widetilde{\delta}}^T(t)R\dot{\widetilde{\delta}}(t)\\&=\left(\widetilde{\delta}^T(t),\xi^T(t)\right)Q\left(\widetilde{\delta}^T(t),\xi^T(t)\right)^T,\end{aligned} \quad (15)$$

where

$$\begin{aligned}Q&=\begin{pmatrix}P\widetilde{A}+\widetilde{A}^T P & P(H\otimes(BK))\\ * & -\frac{1}{d}R\end{pmatrix}\\&\quad+d\begin{pmatrix}\widetilde{A}^T\\(H\otimes(BK))^T\end{pmatrix}R\begin{pmatrix}\widetilde{A} & H\otimes(BK)\end{pmatrix}.\end{aligned} \quad (16)$$

By Schur complement, $Q<0$ if and only if (11) is satisfied. Hence, $\dot{V}(t)<0$; namely, system (10) is asymptotically stable. By Lemma 3, consensus is reached. □

Remark 5. By [24], if (A,B) is stabilizable and the topology graph has a spanning tree, then there exists K such that $\widetilde{A}$ is Hurwitz stable; namely, there exists $P>0$ such that $P\widetilde{A}+\widetilde{A}^T P<0$. Obviously, if $d>0$ is small enough, then (11) must be satisfied. Hence, by (11), we can find K and d which ensure consensus.

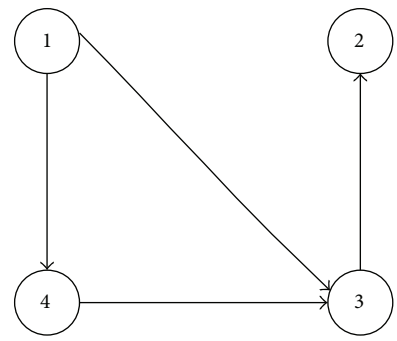

Figure 1: Topology.

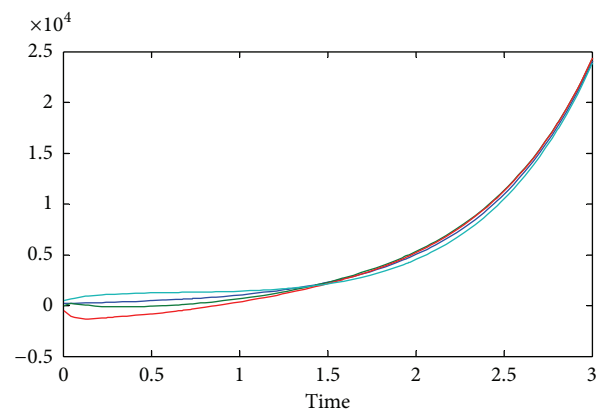

Figure 2: State trajectories x_{11}, x_{21}, x_{31}, x_{41} during time interval $[0,3]$.

Theorem 4 shows that if (A,B) is stabilizable and the topology graph has a spanning tree, then there exists controller gain K and discrete times $t_0,t_1,\ldots$, where $t_{k+1}-t_k\leq d$, $k=0,1,\ldots$, such that consensus is reached. Moreover, K and d can be obtained by (11), which can be solved easily by the feasp solver in Matlab LMI Toolbox.

Similar to the analysis in the case of state feedback, the consensus under controller (4) is equivalent to the asymptotic stability of the following system:

$$\dot{\widehat{\delta}}(t)=\widehat{A}\widehat{\delta}(t)+(H\otimes(BKC))\zeta(t), \quad (17)$$

where $\widehat{A}=I_{n-1}\otimes A-H\otimes(BKC)$, $\zeta(t)=\widehat{\delta}(t)-\widehat{\delta}(t-\tau(t))$. By analyzing the stability of system (17), we obtain the following result.

Theorem 6. *Assume that (A,B,C) is stabilizable and detectable and the topology graph has a spanning tree. Controller (4) solves a consensus problem asymptotically if there exist positive definite matrices P,R such that K and d satisfy the following LMI:*

$$\begin{pmatrix} P\widehat{A}+\widehat{A}^T P & P(H\otimes(BKC)) & \widehat{A}^T R \\ * & -\frac{1}{d}R & (H\otimes(BKC))^T R \\ * & * & -\frac{1}{d}R \end{pmatrix}. \quad (18)$$

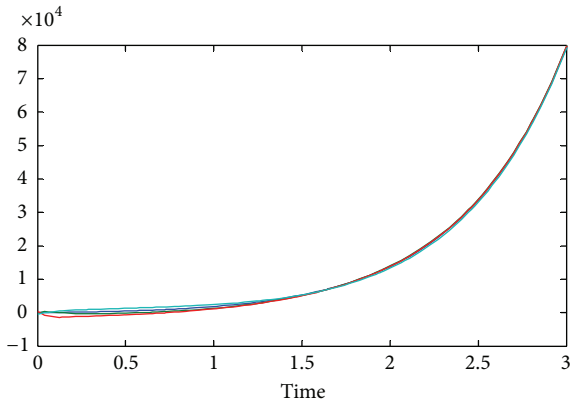

FIGURE 3: State trajectories x_{12}, x_{22}, x_{32}, x_{42} during time interval $[0, 3]$.

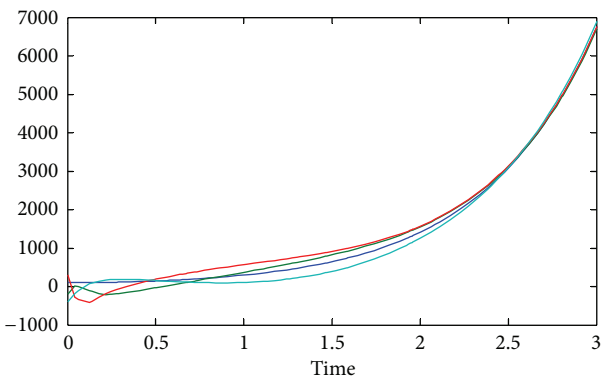

FIGURE 4: State trajectories x_{13}, x_{23}, x_{33}, x_{43} during time interval $[0, 3]$.

Remark 7. Although only the synchronous case is considered, the method in our paper can be applied to study the asynchronous case; namely, the discrete times of each agent are independent of the others.

4. Simulations

Consider the system of four agents, where the topology among four agents is shown in Figure 1. The dynamics of each agent are

$$\dot{x}_i = Ax_i + Bu_i, \quad i = 1, 2, 3, 4, \tag{19}$$

where $x_i = (x_{i1}, x_{i2}, x_{i3})^T$, and

$$A = \begin{pmatrix} 1 & 0 & 2 \\ 2 & 1 & 1 \\ 1 & 0 & -2 \end{pmatrix}, \qquad B = \begin{pmatrix} 1 \\ 2 \\ 1 \end{pmatrix}. \tag{20}$$

Since $\operatorname{rank}(B, AB, A^2B) = 3$, (A, B) is stabilizable. It is easy to verify that $\widetilde{A}$ is Hurwitz stable for $K = (-4, 5, 2)$. By using the feasp solver in Matlab LMI Toolbox, (11) is feasible for $d = 0.0625$ and it is infeasible for $d = 0.0626$, which means that for $K = (-4, 5, 2)$, the maximum d satisfying (11) is $d = 0.0625$.

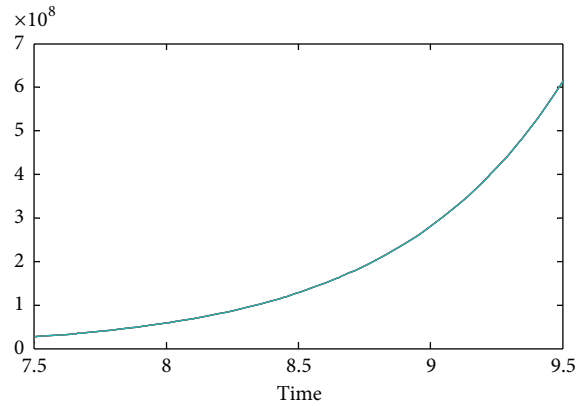

FIGURE 5: State trajectories x_{11}, x_{21}, x_{31}, x_{41} during time interval $[7.5, 9.5]$.

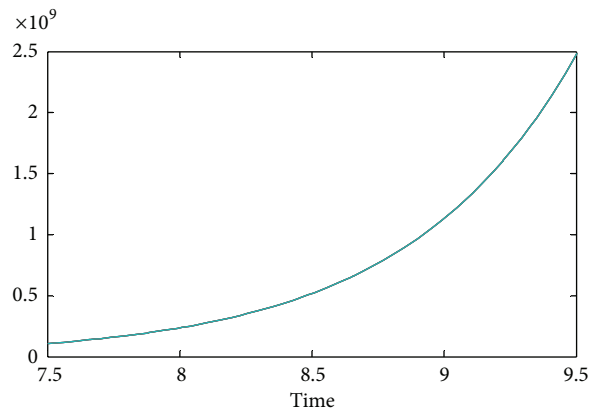

FIGURE 6: State trajectories x_{12}, x_{22}, x_{32}, x_{42} during time interval $[7.5, 9.5]$.

By Theorem 4, for $K = (-4, 5, 2)$, consensus can be reached if the maximum discrete time interval is not larger than 0.0625.

Without loss of generality, the discrete time intervals are chosen from $(0, 0, 0625]$ randomly. Then the state strategies of four agents during time interval $[0, 3]$ are shown in Figures 2, 3, and 4, and the state strategies of four agents during time interval $[7.5, 9.5]$ are shown in Figures 5, 6, and 7, which validate our theoretical results.

5. Conclusion

This paper has studied the consensus problem of continuous-time multiagent systems with general linear dynamics and nonuniform sampling. By applying a state transformation and the input-delay approach, the consensus under consideration is equivalent to the asymptotic stability of a continuous-time system with time-varying delay. By analyzing the asymptotic stability of the continuous-time system, it is shown that there exist a controller gain and discrete times such that consensus can be reached. Furthermore, the controller gain and the upper bound of discrete time intervals can be obtained easily by solving a linear matrix inequality.

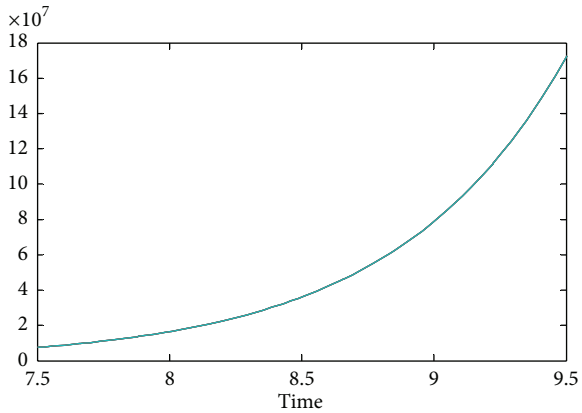

Figure 7: State trajectories x_{13}, x_{23}, x_{33}, x_{43} during time interval [7.5, 9.5].

Simulations have been provided to illustrate the effectiveness of the theoretical results.

Acknowledgments

This work was supported by the National Natural Science Foundation (61170113, 61203150, and 61104141), Beijing Natural Science Foundation (4122019), the Science and Technology Development Plan Project of Beijing Education Commission (no. KM201310009011), and the Funding Project for Academic Human Resources Development in Institutions of Higher Learning under the Jurisdiction of Beijing Municipality (PHR201108055).

References

[1] R. Olfati-Saber and R. M. Murray, "Consensus problems in networks of agents with switching topology and time-delays," *IEEE Transactions on Automatic Control*, vol. 49, no. 9, pp. 1520–1533, 2004.

[2] W. Ren and R. W. Beard, "Consensus seeking in multiagent systems under dynamically changing interaction topologies," *IEEE Transactions on Automatic Control*, vol. 50, no. 5, pp. 655–661, 2005.

[3] P. Frasca, "Continuous-time quantized consensus: convergence of Krasovskii solutions," *Systems & Control Letters*, vol. 61, no. 2, pp. 273–278, 2012.

[4] L. Wang and F. Xiao, "Finite-time consensus problems for networks of dynamic agents," *IEEE Transactions on Automatic Control*, vol. 55, no. 4, pp. 950–955, 2010.

[5] Y. Zheng, W. Chen, and L. Wang, "Finite-time consensus for stochastic multi-agent systems," *International Journal of Control*, vol. 84, no. 10, pp. 1644–1652, 2011.

[6] N. Abaid and M. Porfiri, "Consensus over numerosity-constrained random networks," *IEEE Transactions on Automatic Control*, vol. 56, no. 3, pp. 649–654, 2011.

[7] F. Xiao and L. Wang, "Asynchronous consensus in continuous-time multi-agent systems with switching topology and time-varying delays," *IEEE Transactions on Automatic Control*, vol. 53, no. 8, pp. 1804–1816, 2008.

[8] P. Lin and Y. Jia, "Multi-agent consensus with diverse time-delays and jointly-connected topologies," *Automatica*, vol. 47, no. 4, pp. 848–856, 2011.

[9] P. Lin, K. Qin, H. Zhao, and M. Sun, "A new approach to average consensus problems with multiple time-delays and jointly-connected topologies," *Journal of the Franklin Institute*, vol. 349, no. 1, pp. 293–304, 2012.

[10] Y. Sun, "Average consensus in networks of dynamic agents with uncertain topologies and time-varying delays," *Journal of the Franklin Institute*, vol. 349, no. 3, pp. 1061–1073, 2012.

[11] P. Lin and Y. Jia, "Consensus of a class of second-order multi-agent systems with time-delay and jointly-connected topologies," *IEEE Transactions on Automatic Control*, vol. 55, no. 3, pp. 778–784, 2010.

[12] H. Liu, G. Xie, and L. Wang, "Necessary and sufficient conditions for solving consensus problems of double-integrator dynamics via sampled control," *International Journal of Robust and Nonlinear Control*, vol. 20, no. 15, pp. 1706–1722, 2010.

[13] Y. Cao and W. Ren, "Multi-vehicle coordination for double-integrator dynamics under fixed undirected/directed interaction in a sampled-data setting," *International Journal of Robust and Nonlinear Control*, vol. 20, no. 9, pp. 987–1000, 2010.

[14] Y. Gao and L. Wang, "Consensus of multiple dynamic agents with sampled information," *IET Control Theory & Applications*, vol. 4, no. 6, pp. 945–956, 2010.

[15] A. Abdessameud and A. Tayebi, "On consensus algorithms for double-integrator dynamics without velocity measurements and with input constraints," *Systems & Control Letters*, vol. 59, no. 12, pp. 812–821, 2010.

[16] P. Lin and Y. Jia, "Further results on decentralised coordination in networks of agents with second-order dynamics," *IET Control Theory & Applications*, vol. 3, no. 7, pp. 957–970, 2009.

[17] F. Xiao, L. Wang, and J. Chen, "Partial state consensus for networks of second-order dynamic agents," *Systems & Control Letters*, vol. 59, no. 12, pp. 775–781, 2010.

[18] D. Xie and S. Wang, "Consensus of second-order discrete-time multi-agent systems with fixed topology," *Journal of Mathematical Analysis and Applications*, vol. 387, no. 1, pp. 8–16, 2012.

[19] Y. Zhao, Z. Duan, G. Wen, and Y. Zhang, "Distributed finite-time tracking control for multi-agent systems: an observer-based approach," *Systems & Control Letters*, vol. 62, no. 1, pp. 22–28, 2013.

[20] F. Jiang and L. Wang, "Consensus seeking of high-order dynamic multi-agent systems with fixed and switching topologies," *International Journal of Control*, vol. 83, no. 2, pp. 404–420, 2010.

[21] P. Lin, Z. Li, Y. Jia, and M. Sun, "High-order multi-agent consensus with dynamically changing topologies and time-delays," *IET Control Theory & Applications*, vol. 5, no. 8, pp. 976–981, 2011.

[22] G. Wen, Z. Duan, W. Yu, and G. Chen, "Consensus of multi-agent systems with nonlinear dynamics and sampled-data information: a delayed-input approach," *International Journal of Robust and Nonlinear Control*, vol. 23, no. 6, pp. 602–619, 2013.

[23] J. H. Seo, H. Shim, and J. Back, "Consensus of high-order linear systems using dynamic output feedback compensator: low gain approach," *Automatica*, vol. 45, no. 11, pp. 2659–2664, 2009.

[24] C.-Q. Ma and J.-F. Zhang, "Necessary and sufficient conditions for consensusability of linear multi-agent systems," *IEEE Transactions on Automatic Control*, vol. 55, no. 5, pp. 1263–1268, 2010.

[25] L. Cheng, Z.-G. Hou, Y. Lin, M. Tan, and W. Zhang, "Solving a modified consensus problem of linear multi-agent systems," *Automatica*, vol. 47, no. 10, pp. 2218–2223, 2011.

[26] K. You and L. Xie, "Network topology and communication data rate for consensusability of discrete-time multi-agent systems," *IEEE Transactions on Automatic Control*, vol. 56, no. 10, pp. 2262–2275, 2011.

[27] Y. Zhao, Z. Duan, G. Wen, and G. Chen, "Distributed H_∞ consensus of multi-agent systems: a performance region-based approach," *International Journal of Control*, vol. 85, no. 3, pp. 332–341, 2012.

[28] Z. Li, Z. Duan, and G. Chen, "Consensus of discrete-time linear multi-agent systems with observer-type protocols," *Discrete and Continuous Dynamical Systems B*, vol. 16, no. 2, pp. 489–505, 2011.

[29] F. Xiao and L. Wang, "Consensus problems for high-dimensional multi-agent systems," *IET Control Theory and Applications*, vol. 1, no. 3, pp. 830–837, 2007.

[30] T. Chen and B. Francis, *Optimal Sampled-Data Control Systems*, Springer, London, UK, 1996.

[31] W. P. M. H. Heemels, J. H. Sandee, and P. P. J. van den Bosch, "Analysis of event-driven controllers for linear systems," *International Journal of Control*, vol. 81, no. 4, pp. 571–590, 2008.

[32] C. Godsil and G. Royle, *Algebraic Graph Theory*, Springer, New York, NY, USA, 2001.

[33] X. Zhu, B. Chen, D. Yue, and Y. Wang, "An improved input delay approach to stabilization of fuzzy systems under variable sampling," *IEEE Transactions on Fuzzy Systems*, vol. 20, no. 2, pp. 330–341, 2012.

[34] Y. G. Sun, L. Wang, and G. Xie, "Average consensus in networks of dynamic agents with switching topologies and multiple time-varying delays," *Systems & Control Letters*, vol. 57, no. 2, pp. 175–183, 2008.

Hindawi Publishing Corporation
Mathematical Problems in Engineering
Volume 2013, Article ID 540687, 8 pages
http://dx.doi.org/10.1155/2013/540687

Research Article

Optimal Bandwidth Scheduling of Networked Learning Control System Based on Nash Theory and Auction Mechanism

Xiang Yan,[1] Hongbo Li,[2] Lide Wang,[1] and Ping Shen[1]

[1] *School of Electrical Engineering, Beijing Jiaotong University, Beijing 100044, China*
[2] *Department of Computer Science and Technology, State Key Laboratory of Intelligent Technology and Systems, Tsinghua University, Beijing 100084, China*

Correspondence should be addressed to Lide Wang; ldwang@bjtu.edu.cn

Received 29 March 2013; Accepted 15 May 2013

Academic Editor: Guanghui Wen

This paper addresses the optimal bandwidth scheduling problem for a double-layer networked learning control system (NLCS). To deal with this issue, auction mechanism is employed, and a dynamic bandwidth scheduling methodology is proposed to allocate the bandwidth for each subsystem. A noncooperative game fairness model is formulated, and the utility function of subsystems is designed. Under this framework, estimation of distribution algorithm (EDA) is used to obtain Nash equilibrium for NLCS. Finally, simulation and experimental results are given to demonstrate the effectiveness of the proposed approach.

1. Introduction

Networked control systems (NCSs) are the multiple feedback control loops closed via a serial communication channel. Compared with the traditional point-to-point control system, the advantages of NCSs are sharing of information resources, powerful system diagnosis, distributed remote control, modular design, configuration flexibility, and low cost [1–4]. As a result, NCSs have been widely used in national defense, aircraft, industrial automation, intelligent transportation, process control, and financial management [5]. And some useful results were reported on network protocol [6], network-induced delay [7–9], packet dropout [10–12], NCS structure [13], security [14, 15], scheduling [16–19], and network constraints [20].

It is notable that most of the aforementioned researches are focused on single-layer network structure; few results have been reported on NCSs with double-layer structure. As pointed out by [21, 22], a networked learning control system (NLCS) with double-layer structure can obtain better control performance and stronger robustness. Nonetheless, in real-time NLCS with limited network resources, random network-induced delay may have a significant impact on the performance and stability of the system [23]. The bandwidth availability is the major concern in many networking problems. A good schedule gives an appropriate resource allocation to network nodes and reduces packet collision. The performance of network applications is directly affected by the amount of available bandwidth and the sampling rate [24]. Therefore, the quality of service (QoS) and the quality of control (QoC) depend not only on the control algorithm and the system structure but also on the allocating and scheduling of the network resources. A more optimal allocation of the network bandwidth is the key to improve QoS and QoC. Due to the above discussion, bandwidth scheduling and optimizing is studied, based on the structure of the NLCS, in this paper.

We know that if each node is allowed to occupy network resource as much as possible according to its own requirements, the overall system performance will be very poor [25]. The limitations of the network resources cause the competition among many network nodes. These network nodes will maximize their own network utility, which forms a noncooperation game among them [26]. To meet the demands of individual and entirety in the NLCS, a network bandwidth scheduling strategy based on a noncooperation game model and auction mechanism is introduced. The auction mechanism will be used at the high-layer level in centralized control method, and the control system performance will be estimated by the cumulative amount of the output

errors of the closed control loops. Considering the difficulty of the precise calculation, EDA is applied to obtain an optimal solution.

The remainder of this paper is organized as follows: Section 2 describes NLCS and scheduling optimization schemes. Section 3 explains the auction-based methodology of bandwidth allocation and presents a fair noncooperative game model for scheduling in NLCS. Section 4 shows how to use the EDA-based optimization algorithm to find the equilibrium point of the game model. Simulation and experimental results are provided in Section 4. Finally, Section 5 concludes the results of this study.

Notation. Throughout this paper, $\mathfrak{R}^n$ denotes the n-dimensional Euclidean space. The superscript "T" denotes matrix transposition. And the notation $\mathbb{Z}^+$ stands for the set of nonnegative integers.

2. Problem Formulation

2.1. System Structure. A typical double-layer NLCS structure is shown in Figure 1 [21, 22]. Suppose that the number of closed-loop subsystems in the lower layer communication network (LLN) is M and there are two data transfer nodes (the sensor node and the controller node) in every closed-loop subsystem, the number of the total data transfer points will be $N = 2M$. In this figure, Ci, Ai, and Si represent ith controller, actuator, and sensor, respectively. The actuator is event driven, and the controller and sensor are time driven. The sampling period is longer than the polling period of the system. The data (sampling data, node identities, and others) are packed by sensors and sent to the controller. Then, such data will be used to calculate the control commands in the controller, which will be packed and sent to the actuator, then the actuator will update the control algorithm based on the new control commands. At the same time, the upper layer communication network (ULN) collects data of the control performance of the subsystems from the LLN controllers through shared network (LAN, WAN, or Internet) and then optimizes the sampling period and control parameters based on a self-adaptive and scheduling algorithm.

The timing diagram of bandwidth allocation is illustrated in Figure 2. The controllers report their bandwidth requirements to the learning and scheduling center through the ULN during T_P (the polling period). Then the center collects information and allocates bandwidths during T_A (the allocation period). According to the given bandwidth and the scheduling algorithm, all control loops send data during T_T (the transmission period). After T_O (the total operating period), a new period begins.

2.2. The Controlled Plants. The dynamics of the remote controlled plant is given by the following linear model:

$$\mathbf{x}(k+1) = \mathbf{F}\mathbf{x}(k) + \mathbf{G}\mathbf{u}(k), \tag{1}$$

where $k \in \mathbb{Z}^+$; $\mathbf{x}(k) \in \mathbb{R}^n$ is the plant state; $\mathbf{u}(k) \in \mathbb{R}^m$ is the control input; $\mathbf{F}$ and $\mathbf{G}$ are known matrices with appropriate dimensions. Suppose that the full state variables are available

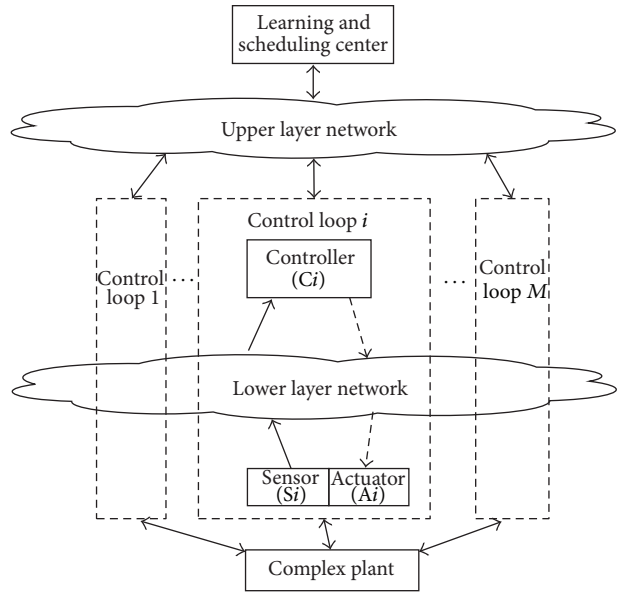

Figure 1: The structure of double-layer NLCS.

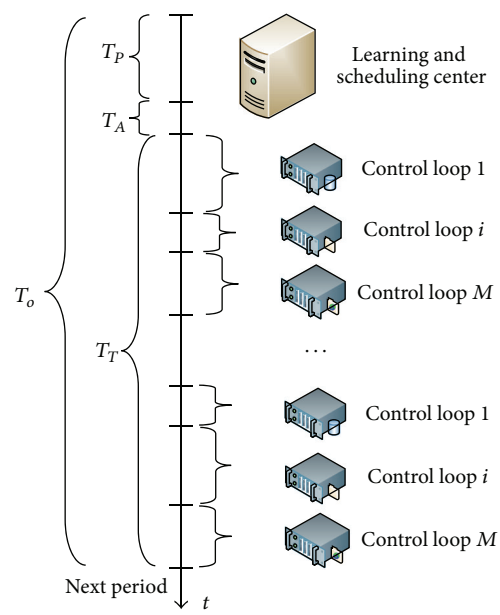

Figure 2: Timing diagram of bandwidth allocation.

in the networked subsystem. The sensor is time driven, that is, at time instant kh, it sends the most recent motor state and its timestamp to the controller via the network. Note that (1) can be considered as discretized from a continuous-time system given by

$$\dot{\mathbf{x}}_p(t) = \mathbf{A}\mathbf{x}_p(t) + \mathbf{B}\mathbf{u}(t), \tag{2}$$

with the sampling period h and

$$\mathbf{F} = e^{\mathbf{A}h}, \qquad \mathbf{G} = \int_0^h e^{\mathbf{A}\tau} d\tau \mathbf{B}. \tag{3}$$

The electromechanical dynamics of the networked dc-motor subsystem used in this paper can be described as

$$\begin{aligned} \dot{i}_a &= -\frac{R}{L} i_a - \frac{K_b}{L}\omega + \frac{1}{L}u, \\ \dot{\omega} &= \frac{K_t}{J} i_a - \frac{B}{J}\omega, \end{aligned} \tag{4}$$

where i_a is the armature winding current; ω is the rotor angular speed; u is the armature winding input voltage; R is the armature winding resistance; L is the armature winding inductance; K_b is the back-electromotive-force-(EMF-) constant; K_t is the torque constant; B is the system damping coefficient; J is the system moment of inertia. The parameters of the dc-motor subsystem are listed in Table 1.

By letting $x_p \triangleq [i_a, \omega]^T$ and the rotor angular speed $y = \omega$, the dc-motor subsystem as Loop 1 can be expressed by

$$\dot{x}_p(t) = \begin{bmatrix} -1579.9 & -4.1 \\ 430.3 & -0.1 \end{bmatrix} x_p(t) + \begin{bmatrix} 318.473 \\ 0 \end{bmatrix} u(t), \tag{5}$$

$$y(t) = \begin{bmatrix} 0 & 1 \end{bmatrix} x_p(t). \tag{6}$$

2.3. NLCS Performance Analysis. The performance of the NLCS can be demonstrated jointly by the subsystems, and the performance of the subsystem can be described by a function, such as the integral absolute error (IAE) [27]. The system error will be greater if some control loop is disturbed, indicating that the sampling frequency should be raised to a degree that enables the system to return to the equilibrium point rapidly. If the error is smaller, no higher sampling frequency is needed. Figure 3 shows the cumulative error of a rotor speed for a broad range of sampling rates from $h = 0.05 \cdots 0.5$ s. Integral absolute error $= \int_0^{t_e} |\dot{\theta}(t)| dt$, where t_e is the evaluation time interval. As it can be seen in Figure 3, the relation between control performance and a range of allowed periods can be approximated by a linear relationship [28] as (7). Consider the following

$$e_i(t_i) = \alpha_i + \beta_i t_i, \tag{7}$$

where α_i and β_i are specific for each control loop and can be determined prior to system run time. Due to the calculation of the gradient in solving optimization problems, α_i could be ignored.

For each control loop, the relation between sampling period t_i and allocation bandwidth x_i is given by [29]

$$t_i = \frac{c_i}{x_i}, \tag{8}$$

where c_i is the control time of the control loop (which may contain data exchange from sensor to controller and from controller to actuator, as well as the time spent to execute the controller); hypothetically c_i is within a sampling period.

On one hand, the QoC of each subsystem should be improved, on the other hand, the demands of network bandwidth of each subsystem should be reduced to provide more resources for extra subsystems. Due to the bandwidth limitations, a multiobjective optimization problem can be expressed as follows

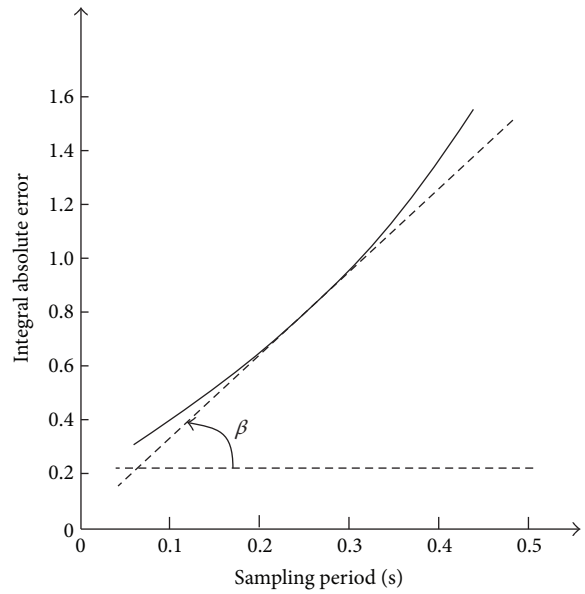

Figure 3: Sampling periods versus IAE.

Table 1: The parameters of the dc-motor subsystem.

R	Motor winding resistance	4.961 Ω
L	Motor winding inductance	3.14×10^{-3} H
K_b	Back-EMF constant	1.276×10^{-2} Vs/rad
K_t	Electric torque constant	7.105×10^{-2} N·m/A
J	Motor moment of inertia	1.6511×10^{-4} kg·m^2
B	Damping coefficient	$23.64 \times e^{-6}$ N·m·sec/rad

$$\begin{aligned} \mathbf{OP}: \ \min \ & \delta \mathbf{J_1} + (1-\delta)\mathbf{J_2} \\ \text{s.t.} \ & \sum_{i=1}^{M} x_i \le 1 - \gamma, \\ & x_i^{\min} \le x_i \le x_i^{\max}, \end{aligned} \tag{9}$$

where $\mathbf{J_1} = \sum_{i=1}^{M}(\alpha_i + \beta_i t_i) = \sum_{i=1}^{M}(\alpha_i + \beta_i c_i / x_i)$, $\mathbf{J_2} = \sum_{i=1}^{M} x_i$, $0 < \delta < 1$. To deal with the accidental overload and avoid the sudden deterioration of the system performance, the scale factor γ is introduced to retain part of the bandwidth. $x_i^{\min}$ and $x_i^{\max}$ can be calculated based on the resource constraints of the control loop and the maximum allowable delay bound (MADB) [30].

3. Main Results

The game model based on auction mechanism is discussed in this section. Auction theory is first proposed by Vickrey in 1961, which mainly includes four basic types: English auction (ascending-bid auction), Dutch Auction (descending-bid auction), and first price auction and second price auction (Vickrey auction). The highest offer will win the bid no matter

what type of auction is used, and the optimum outcome is that the price exactly equals what the second highest bidder can afford.

Remark 1. It is worth noting that the first two kinds of auction mechanism are bidding open, and the others are sealed. In sealed auction, each bidder submits his price without any information of others, then the auctioneer announces the winner who offers the highest bid. Both of them are suitable for bandwidth allocation in NLCS. The only difference between first and second price auction is the actual price that the winner paid. For second price auction, the winner just needs to pay the second highest bid of others instead of his own. For ease of operation, first price auction is applied in this paper.

The closed-loop control subsystem is modeled as a player. Every player is not explicitly aware of the existence of other players and their status. Each player puts forward its own bandwidth strategy denoted as x_i. Obviously, the bandwidth consumption of each player will affect the bandwidth allocation of other players, but it is impossible to improve the working performance by only increasing the bandwidth requirement. So, a noncooperative game is formed among the closed-loop control subsystems in NLCS. In the game, ULN plays the roll of auctioneer, and every player will pay the bandwidth based on their own bidding strategy and the final bandwidth they have got. The bidding and auction process is shown as follow.

Step 1. Every player has the same amount of money g before every round of bidding begins.

Step 2. Every player submits the price y_i ($y_i \in [0, g]$) based on their own bandwidth requirement.

Step 3. ULN will run the bandwidth allocation programs based on the bidding prices and allocate the bandwidth resources to each player.

Step 4. Every player will pay for the bandwidth they have got.

The price of bandwidth x_i defined as y_i which player i needs to pay can be calculated from

$$y_i = \lambda x_i, \tag{10}$$

where λ is the price of unity bandwidth. The revenue function of every player can be described as follow:

$$S_i(x_i) = \begin{cases} U_i(x_i) - y_i, & \text{if } y_i > 0, \\ U_i(0), & \text{if } y_i = 0. \end{cases} \tag{11}$$

Further, the revenue function based on auction theory and IAE evaluation method is shown as (12):

$$\begin{aligned} S_i(x_i) &= \ln\left(1 + \frac{1}{e_i}\right) - y_i \\ &= \ln\left(1 + \frac{1}{\beta_i t_i}\right) - \lambda x_i \\ &= \ln\left(1 + \frac{x_i}{\beta_i c_i}\right) - \lambda x_i. \end{aligned} \tag{12}$$

Obviously, the revenue of the player is determined by the received QoC and the payment under certain QoS. Every player will make the bidding strategy based on their own revenue and will not increase the price aimlessly. If a player overly spends its money for a much larger bandwidth than its actual need, it will only get a low payoff due to the reduced network utility. The money each player has to pay is based on the bandwidth they have got, which may not match the initial offer.

Every player in LLN wants to maximize their revenue under the framework of NLCS. ULN will make a network resources allocation strategy which makes it impossible to get more bandwidth resources through changing the offer. Generally speaking, the network utility of a single node depends on the scheduling strategy of others. If there is no node chooses other scheduling strategies when the scheduling strategies of other nodes that are decided, this equilibrium will not be broken in the network. This equilibrium is called Nash equilibrium (NE) [31]. Thus, the allocation problem of the network resources can be transformed into the solution of the Nash equilibrium with a noncooperation game model.

To address the modelling problem, we introduce the following definitions to prove the existence and uniqueness of Nash equilibrium in NLCS.

Definition 2. A noncooperative networked learning control game (NNLCG) with M players participated in, $NG = (\Gamma, \{X_i\}, \{S_i(\cdot)\})$, where $\Gamma = \{1, 2, \ldots, M\}$ is the index set of players, $\{X_i\}$ is a strategy profile, and $\{S_i(\cdot)\}$ is the revenue function set of players. If x_i^* is the best strategy of player i when other players choose strategies $x_{-i}^* = (x_1^*, \ldots, x_{i-1}^*, x_{i+1}^*, \ldots, x_M^*)$ which is shown in (13), $x^* = (x_1^*, \ldots, x_i^*, \ldots, x_M^*)$ will be a Nash equilibrium. One has the following:

$$S_i(x_i^*, x_{-i}^*) \geq S_i(x_i, x_{-i}^*), \quad \forall x_i \in X_i,\ i \in \Gamma. \tag{13}$$

Definition 3. The function $S_i(\cdot) : X_i \to \mathfrak{R}_+^1$ defined on the convex set X_i is quasi concave in x_i if and only if

$$S_i\left(\xi x_i + (1-\xi) x_i', x_{-i}\right) \geq \min\left(S_i(x_i, x_{-i}), S_i\left(x_i', x_{-i}\right)\right) \tag{14}$$

for all $x_i, x_i' \in X_i$ and $\xi \in [0, 1]$.

Theorem 4. *A Nash equilibrium exists in game $NG = (\aleph, \{P_j\}, \{u_j(\cdot)\})$ if for all $j \in \aleph$:*

(1) *P_j is a nonempty, convex, and compact subset of some Euclidean space $\mathfrak{R}^N$.*

(2) *$u_j(p)$ is continuous in p and quasi concave in p_j.*

Proof. Theorem 4 can be obtained using the classical Kakutani fixed-point theorem and in some sense generalizes Nash's

setting on the strategy space of the players. For the proof of this theorem, please refer to [32]. □

Theorem 5. *A Nash equilibrium exists in the NNLCG, NG* $= (\Gamma, \{X_i\}, \{S_i(\cdot)\})$.

Proof. By Theorem 4, we know that there exists a Nash equilibrium in NNLCG when the conditions in Theorem 4 are satisfied. Each player in NNLCG has a strategy space $[x_i^{\min}, x_i^{\max}]$, $x_i^{\min} > 0$, and $x_i^{\min} \leq x_i^{\max}$. Thus, the first condition is satisfied. It remains to prove that the revenue function $S_i(x)$ is quasi concave in x_i for all i in NNCG.

The first-order differential of the revenue function $S_i(\cdot)$ is

$$\frac{\partial S_i(x_i)}{\partial x_i} = \frac{1}{\beta_i c_i + x_i} - \lambda. \tag{15}$$

The second-order differential of the revenue function $S_i(\cdot)$ is

$$\frac{\partial S_i^2(x_i)}{\partial x_i^2} = -\frac{1}{(\beta_i c_i + x_i)^2} < 0. \tag{16}$$

Known from the above equations, the revenue function is continuous and differentiable in x and concave in x_i. A concave function $S_i(x)$ is quasi concave too. This completes the proof of the theorem. □

Theorem 6. *The NNLCG has a unique equilibrium.*

Proof. The proof of the unique equilibrium can be carried out by following similar lines as in the proof of Theorem 2 in [33] and is thus omitted here to avoid unnecessary repetition. □

Up to now, the problem of network resources allocation under a general framework of double-layer NLCS has be changed into the problem of Nash-equilibrium-point solving in the noncooperation game model. It is hard to solve the Nash equilibrium point by the traditional numerical method. So, estimation of distribution algorithm (EDA) is introduced in this paper to find the Nash equilibrium point. The EDA algorithm used in this paper is described as follows.

Rule 1. Initialization: generate gain candidates meeting the ratio of bandwidth (RoB) randomly to form an initial population.

Rule 2. Repeat the following steps until the termination criterion is met.

(a) Selection: select the best gain candidates from the parent generation.

(b) Updating: update using the selected promising gain candidates.

(c) Sampling: generate gain candidates meeting RoB based on the updated; copy the best gain candidate in the current population to the next population.

For more details about EDA, please refer to [34, 35], and the reference therein.

4. Experiments and Result Analysis

In this section, an illustrative example is presented to show the effectiveness of the proposed method. To this end, let us consider a double-layer NLCS as shown in Figure 1. The considered NLCS has three different networked dc-motor subsystems, where one takes the form (5) and the models of the rest two subsystems are listed in Table 2. Apparently, $\gamma = 0.1$, $T_O = 0.5$ s, $T_L = 0.005$ s, $T_P = 0.03$ s, and the rest of T_O is T_T. The allocation period T_A is very short compared to T_L so that T_A can be assumed to be zero.

Table 2: Parameters of the rest two subsystems.

	Parameter A	Parameter B
Loop 2	$\begin{bmatrix} 0 & 1 \\ 1 & -217.4 \end{bmatrix}$	$\begin{bmatrix} 0 \\ 1669.5 \end{bmatrix}$
Loop 3	$\begin{bmatrix} -579.9 & -4.1 \\ 30.3 & -0.01 \end{bmatrix}$	$\begin{bmatrix} 18.4713 \\ 0 \end{bmatrix}$

Table 3: Simulation results of comparison test.

	EBA		ABA	
	IAE	RoB	IAE	RoB
Loop 1	0.8199	0.30	0.9090	0.22
Loop 2	1.4720	0.30	1.2629	0.37
Loop 3	1.2310	0.30	1.1375	0.31
Total	3.5229	0.90	3.3094	0.90

Table 4: Statistics of the 30 simulation results.

	EBA	ABA
Mean value	1.9048	2.3154
Standard deviation	0.0603	0.0696

The auction-based bandwidth allocation (ABA) has an initial population of 100 solutions and ten generations. When the overall fitness value is stabilized, the Nash equilibrium point is reached. The bandwidth vector allocated by the ULN in this case is $x^* = [0.22\ 0.37\ 0.31]^T$. To illustrate the improving level of QoC and the bandwidth occupied, we compare ABA with equal bandwidth allocation (EBA), which is a simple static bandwidth allocation method. And the ratio of bandwidth given to player i can be quickly computed by $x_i = (1 - \gamma)/M$. The IAE and the RoB of two different strategies are given in Table 3. Accordingly, the step responses of three networked dc-motor subsystems with given corresponding RoB are shown in Figure 4.

As shown in Table 3 and Figure 4, the control performance of networked subsystem degrades when network conditions become worse (given less RoB). This phenomenon is reasonable, since each dc-motor subsystem performance worsens with longer time delays and more packet losses. It is notable that some loop has higher value of IAE in ABA than EBA; the ABA still gives the better overall performance according to the simulation results. So this equal bandwidth allocation method may be ineffective, since some loops may not receive enough bandwidth according to their demands, while others may receive unnecessary bandwidth compared to them.

Figure 5 shows the box-and-whisker diagram of system revenue over 30 paired simulation. And the statistics of the 30 simulation results are listed in Table 4. The same network condition is used in the simulation of networked

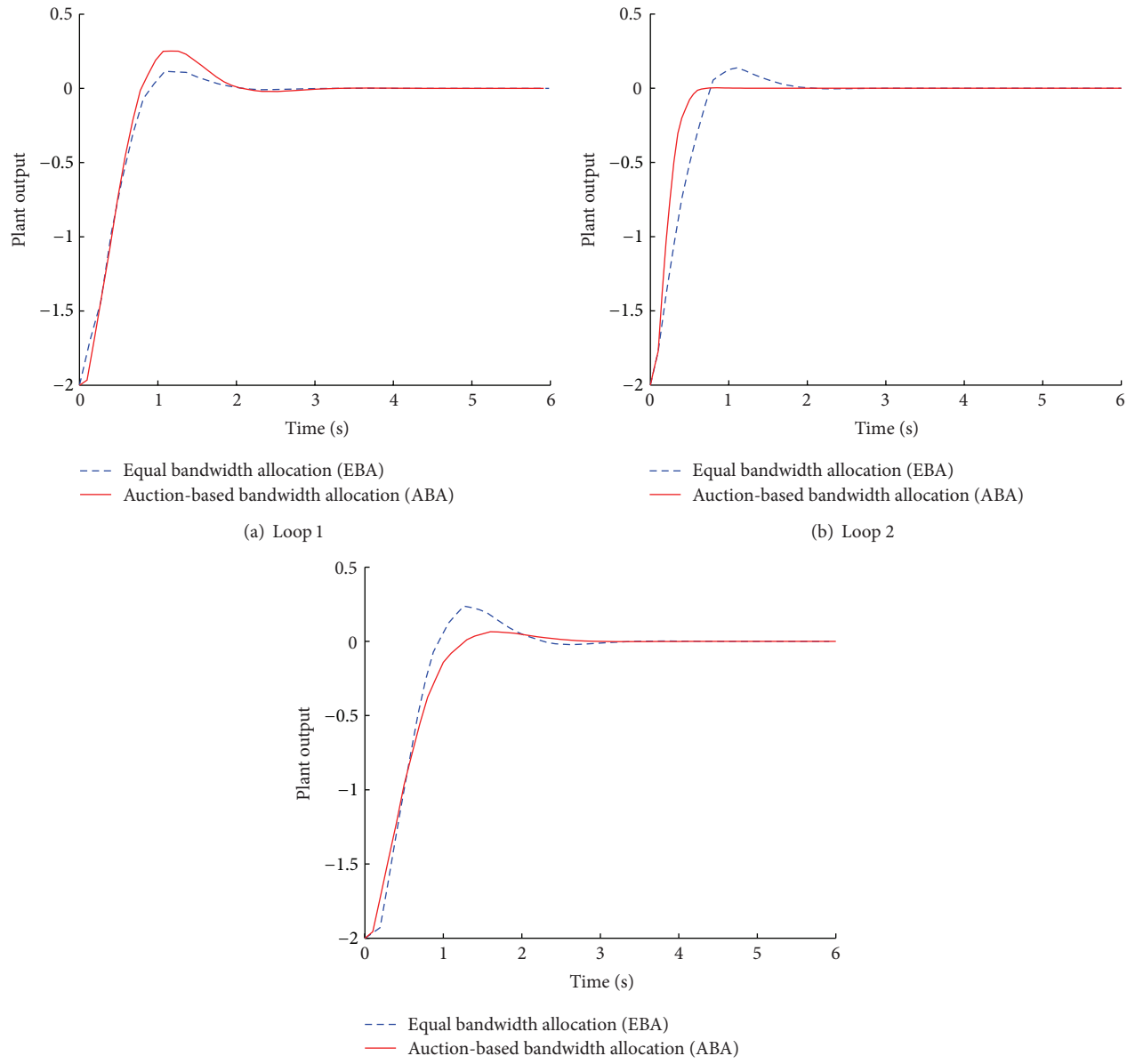

Figure 4: Different step responses of three networked dc-motor subsystems.

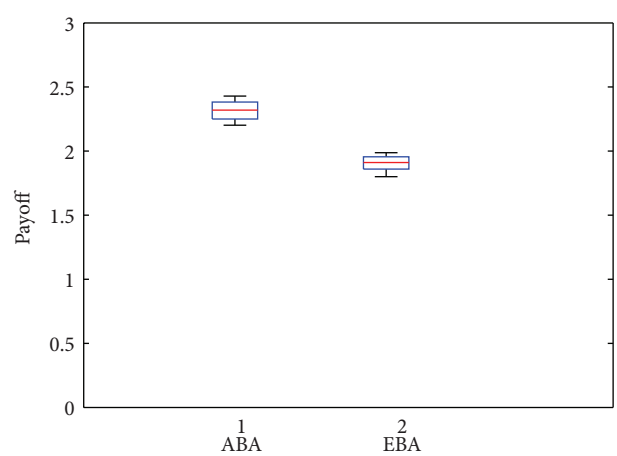

Figure 5: The box-and-whisker diagram.

system using the ABA and the EBA. Note that the 30 paired runs used 30 different network conditions and they were generated randomly under the given network constraints. Obviously, the overall payoff of ABA is higher than EBA. Based on the mean value of system payoff using ABA and EBA (denoted as $\bar{J}_{\mathrm{ABA}}$ and $\bar{J}_{\mathrm{EBA}}$, resp.), as listed in Table 4, we can further conclude that, comparing with EBA on the average, ABA method increases the system payoff by 21.56% $[(\bar{J}_{\mathrm{ABA}} - \bar{J}_{\mathrm{EBA}})100\%/\bar{J}_{\mathrm{EBA}}]$.

Motivated by the results, we found that auction-based bandwidth allocation that optimizes resource scheduling strategy can effectively meet the desired objectives in the resource-constrained NLCS.

5. Conclusion

This paper presents a noncooperation game model based on Nash theory and auction mechanism for bandwidth allocation in NLCS with limited resources. And the estimation of distribution algorithm is introduced to solve the problem effectively. The proposed method forces all players sharing the same network to have allocated bandwidths at Nash equilibrium point. Network resources are allocated in the optimum way to reduce delays and packet losses, and the overall performance of systems with communication constraints is significantly improved. The simulation and experiment results indicate the effectiveness and availability of the proposed approach.

Acknowledgments

The authors would like to thank C. Hao, D. W. Yang, and T. Tony for their valuable comments and suggestions to improve the quality of the paper. The work of X. Yan is supported by the Fundamental Research Funds for the Central Universities under Grant E11JB00310. The work of L. D. Wang and P. Shen is supported by the Fundamental Research Funds for the Central Universities under Grant E12JB00140. The work of H. Li is supported by National Basic Research Program of China (973 Program) under Grant 2012CB821206, the National Natural Science Foundation of China under Grant 61004021, and Beijing Natural Science Foundation (4122037).

References

[1] L. Zhang, H. Gao, and O. Kaynak, "Network-induced constraints in networked control systems—a survey," *IEEE Transactions on Industrial Informatics*, vol. 9, no. 1, pp. 403–416, 2013.

[2] M. Gholami, N. Cai, and R. W. Brennan, "An artificial neural network approach to the problem of wireless sensors network localization," *Robotics and Computer-Integrated Manufacturing*, vol. 29, no. 1, pp. 96–109, 2013.

[3] J. Yépez, P. Martí, and J. M. Fuertes, "Control loop scheduling paradigm in distributed control systems," in *Proceedings of the 29th Annual Conference of the IEEE Industrial Electronics Society (IECON '03)*, vol. 2, pp. 1441–1446, 2003.

[4] S. H. Hong, "Scheduling algorithm of data sampling times in the integrated communication and control systems," *IEEE Transactions on Control System Technology*, vol. 3, no. 2, pp. 225–231, 1995.

[5] M. N. Islam, N. Mandayam, and S. Kompella, "Optimal resource allocation and relay selection in bandwidth exchange based cooperative forwarding," in *Proceedings of the 10th International Symposium on Modeling and Optimization in Mobile, Ad Hoc and Wireless Networks (WiOpt '12)*, pp. 192–199, 2012.

[6] J. P. Hespanha, P. Naghshtabrizi, and Y. Xu, "A survey of recent results in networked control systems," *Proceedings of the IEEE*, vol. 95, no. 1, pp. 138–172, 2007.

[7] L. Zhang, Y. Shi, T. Chen, and B. Huang, "A new method for stabilization of networked control systems with random delays," *IEEE Transactions on Automatic Control*, vol. 50, no. 8, pp. 1177–1181, 2005.

[8] Y. Tipsuwan and M. Y. Chow, "Gain scheduler middleware: a methodology to enable existing controllers for networked control and teleoperation—part I: networked control," *IEEE Transactions on Industrial Electronics*, vol. 51, no. 6, pp. 1218–1227, 2004.

[9] C. Peng, Y. C. Tian, and M. O. Tadé, "State feedback controller design of networked control systems with interval time-varying delay and nonlinearity," *International Journal of Robust and Nonlinear Control*, vol. 18, no. 12, pp. 1285–1301, 2008.

[10] H. Li, M. Y. Chow, and Z. Sun, "Optimal stabilizing gain selection for networked control systems with time delays and packet losses," *IEEE Transactions on Control Systems Technology*, vol. 17, no. 5, pp. 1154–1162, 2009.

[11] J. Xiong and J. Lam, "Stabilization of linear systems over networks with bounded packet loss," *Automatica*, vol. 43, no. 1, pp. 80–87, 2007.

[12] M. Yu, L. Wang, T. Chu, and F. Hao, "An LMI approach to networked control systems with data packet dropout and transmission delays," in *Proceedings of the 43rd IEEE Conference on Decision and Control (CDC '04)*, vol. 4, pp. 3545–3550, December 2004.

[13] D. Du and M. Fei, "A two-layer networked learning control system using actor-critic neural network," *Applied Mathematics and Computation*, vol. 205, no. 1, pp. 26–36, 2008.

[14] W. Zeng and M. Y. Chow, "Optimal tradeoff between performance and security in networked control systems based on coevolutionary algorithms," *IEEE Transactions on Industrial Electronics*, vol. 59, no. 7, pp. 3016–3025, 2012.

[15] S. Vasudevan, D. Goeckel, and D. Towsley, "Security-capacity trade-off in large wireless networks using keyless secrecy," in *Proceedings of the 11th ACM International Symposium on Mobile Ad Hoc Networking and Computing (MobiHoc '10)*, pp. 21–30, September 2010.

[16] Z. Chunjie, X. Chunjie, C. Hui, and F. Huajing, "Genetic algorithm-based dynamic reconfiguration for networked control system," *Neural Computing and Applications*, vol. 17, no. 2, pp. 153–160, 2008.

[17] L. Tan, Z. Zhu, C. Yuan, and W. Zhang, "A novel approach for bandwidth allocation among soft QoS traffic in wireless networks," *Transactions on Emerging Telecommunications Technologies*, 2012.

[18] D. Xu, E. Jung, and X. Liu, "Efficient and fair bandwidth allocation in multichannel cognitive radio networks," *IEEE Transactions on Mobile Computing*, vol. 11, no. 8, pp. 1372–1385, 2012.

[19] U. Park, H. W. Kim, and D. S. Oh, "A dynamic bandwidth allocation scheme for a multi-spot-beam satellite system," *ETRI Journal*, vol. 34, no. 4, pp. 613–616, 2012.

[20] L. A. Montestruque and P. J. Antsaklis, "On the model-based control of networked systems," *Automatica*, vol. 39, no. 10, pp. 1837–1843, 2003.

[21] L. Xu, M. Fei, and T. Jia, "Bandwidth scheduling and optimization using non-cooperative game model-based shuffled frog leaping algorithm in a networked learning control system," *Neural Computing & Applications*, vol. 21, no. 6, pp. 1117–1128, 2012.

[22] D. Du, M. Fei, H. Hu, and L. Li, "Two-layer networked learning control using self-learning fuzzy control algorithms," *Chinese Journal of Scientific Instrument*, vol. 28, no. 12, pp. 2124–2131, 2007.

[23] Y. Tipsuwan, S. Kamonsantiroj, J. Srisabye, and P. Chongstitvattana, "An auction-based dynamic bandwidth allocation with sensitivity in a wireless networked control system," *Computers & Industrial Engineering*, vol. 57, no. 1, pp. 114–124, 2009.

[24] A. Dixit, B. Lannoo, and G. Das, "Dynamic bandwidth allocation with SLA awareness for QoS in ethernet passive optical networks," *Journal of Optical Communications and Networking*, vol. 5, no. 3, pp. 240–253, 2013.

[25] F. L. Lian, J. Moyne, and D. Tilbury, "Network design consideration for distributed control systems," *IEEE Transactions on Control Systems Technology*, vol. 10, no. 2, p. 297, 2002.

[26] G. C. M. Gabriel, E. V. Belmega, and M. Debbah, "Pricing and bandwidth allocation problems in wireless multi-tier networks," in *Proceedings of the 45th Asilomar Conference on Signals, Systems, and Computers (ASILOMAR '11)*, pp. 1633–1637, 2011.

[27] L. Xu and M. Fei, "A hybrid quantum clone evolutionary algorithm-based scheduling optimization in a networked learning control system," in *Proceedings of the Chinese Control and Decision Conference (CCDC '10)*, pp. 3632–3637, May 2010.

[28] A. Cervin, J. Eker, B. Bernhardsson, and K. E. Årzén, "Feedback-feedforward scheduling of control tasks," *Real-Time Systems*, vol. 23, no. 1-2, pp. 25–53, 2002.

[29] M. Velasco, P. Martí, and M. Frigola, "Bandwidth management for distributed control of highly articulated robots," in *Proceedings of IEEE International Conference on Robotics and Automation (ICRA '05)*, pp. 265–270, April 2005.

[30] D. S. Kim, Y. S. Lee, W. H. Kwon, and H. S. Park, "Maximum allowable delay bounds of networked control systems," *Control Engineering Practice*, vol. 11, no. 11, pp. 1301–1313, 2003.

[31] H. Yaïche, R. R. Mazumdar, and C. Rosenberg, "A game theoretic framework for bandwidth allocation and pricing in broadband networks," *IEEE/ACM Transactions on Networking*, vol. 8, no. 5, pp. 667–678, 2000.

[32] S.-P. Hsu, S.-L. Hsu, and A. S. Tsai, "A game-theoretic analysis of bandwidth allocation under a user-grouping constraint," *Journal of Applied Mathematics*, vol. 2013, Article ID 480962, 9 pages, 2013.

[33] C. U. Saraydar, N. B. Mandayam, and D. J. Goodman, "Efficient power control via pricing in wireless data networks," *IEEE Transactions on Communications*, vol. 50, no. 2, pp. 291–303, 2002.

[34] H. Li, M. Y. Chow, and Z. Sun, "EDA-based speed control of a networked DC motor system with time delays and packet losses," *IEEE Transactions on Industrial Electronics*, vol. 56, no. 5, pp. 1727–1735, 2009.

[35] P. A. N. Bosman and J. Grahl, "Matching inductive search bias and problem structure in continuous estimation-of-distribution algorithms," *European Journal of Operational Research*, vol. 185, no. 3, pp. 1246–1264, 2008.

Hindawi Publishing Corporation
Mathematical Problems in Engineering
Volume 2013, Article ID 979087, 12 pages
http://dx.doi.org/10.1155/2013/979087

Research Article

Distributed Robust H_∞ Consensus Control of Multiagent Systems with Communication Errors Using Dynamic Output Feedback Protocol

Xi Yang and Jinzhi Wang

State Key Laboratory for Turbulence and Complex System, Department of Mechanics and Aerospace Engineering, College of Engineering, Peking University, Beijing 100871, China

Correspondence should be addressed to Jinzhi Wang; jinzhiw@pku.edu.cn

Received 17 April 2013; Accepted 8 May 2013

Academic Editor: Guanghui Wen

This paper studies robust consensus problem for multiagent systems modeled by an identical linear time-invariant system under a fixed communication topology. Communication errors in the transferred data are considered, and only the relative output information between each agent and its neighbors is available. A distributed dynamic output feedback protocol is proposed, and sufficient conditions for reaching consensus with a prescribed H_∞ performance are presented. Numerical examples are given to illustrate the theoretical results.

1. Introduction

Consensus problem of multiagent systems has been a popular subject in system and control theory due to its widespread applications such as satellite formation flying, cooperative unmanned air vehicles, and mobile robots [1–3]. The study of consensus problem focuses on designing a distributed protocol using information which can only be obtained and shared locally to ensure that the resulting closed-loop system has the desired characteristics. A number of solutions that are based on relative states between each agent and its neighbors to the consensus problem have been proposed up to now. The theoretical framework of solving consensus for multiagent system was suggested by [4], providing the convergence analysis of a consensus protocol for a network of single integrators with directed fixed/switching topologies. Later, under different cases of communication topologies such as fixed, switching, and with communication delays, many different types of protocols have been proposed for different types of agent dynamics to reach global asymptotical consensus [2, 3, 5–16].

Recently, solving consensus problem for the multiagent systems by using output information has attracted particular attention due to its theoretical significance and wide applications. Reference [17] constructed a dynamic output feedback protocol based on a observer for the synchronization of a network of identical linear state space models under a possibly time-varying and directed interconnection, where each agent needs to obtain all the observer's state information of its neighbors. Based on the low gain approach, [18] proposed a consensus protocol which only used the relative outputs for N identical linear dynamics with fixed directed communication topologies. Consensus problem with $\mathscr{L}_2$ external disturbance under switching undirected communication topologies was studied by [19], where a dynamic output feedback protocol was proposed for subjecting the external disturbances. Reference [20] studied the output consensus problem for a class of heterogeneous uncertain linear SISO multiagent systems, where each agent's output information and the relative outputs with its neighbors were used to design the controller. Reference [21] designed robust static output feedback controllers to achieve consensus for undirected networks of heterogeneous agents modeled as nonlinear systems of relative degree two.

It can be seen that there is a common assumption in the literatures mentioned above that each agent can receive accurate measurements of relative states or outputs between its neighbors and itself all the time. However, in some practical situations, agents cannot perfectly sense their neighbors due

to the existence of sensor failures or some other communication constraints. In view of this, we consider the consensus problems for the multiagent systems with communication errors. It is required to point out that the measurement for communication errors we considered is limited to some errors in the transferred data not including loss of communication. The robustness analysis of first-/second-order leader-follower consensus with communication errors is studied by [22, 23]. Some robustness issues for systems with external disturbances or model uncertainties are investigated by some other researchers [19, 24–28], which are different from the robust consensus problem stated in this paper.

Motivated by the above-mentioned works, we study the consensus problem for linear multiagent systems to attenuate the communication errors by using dynamic output feedback controller. The agent dynamics considered here are general stabilizable and detectable linear systems, and a dynamic consensus protocol is proposed which uses only the relative output information between each agent and its neighbors. The main contributions of this paper can be summarized as two aspects. Firstly, in order to describe the effects of communication errors on consensus, a concept called consensus with H_∞ performance is introduced which can characterize the effects of communication errors on the difference between the state of each agent and the average of states of all agents. The problem of consensus with H_∞ performance is transmitted into an H_∞ control problem of another reduced-order system. It is shown that consensus with H_∞ performance can be achieved if there exists a common dynamic output feedback controller which can be realized by solving H_∞ problem for $N-1$ linear dynamic systems simultaneously, where N is the number of agents. Secondly, in terms of the $N-1$ linear systems, a sufficient condition based on linear matrix inequalities for the existence of the controller is provided, and the approach to construct the corresponding controller is given.

The rest of this paper is organized as follows. Section 2 introduces basic notations and reviews some useful results on graph theory and robust H_∞ control theory. Section 3 formulates the problem and conditions for reaching consensus with H_∞ performances that are derived. The existence for a dynamic output feedback protocol and a method to construct such controller are proposed in Section 4. Numerical simulations are provided in Section 5. Section 6 concludes the paper.

Notations. Let $\mathbb{R}^{n\times n}$ and $\mathbb{C}^{n\times n}$ be the set of $n\times n$ real matrices and $n\times n$ complex matrices, respectively. Matrices, if not explicitly stated, are assumed to have compatible dimensions. I_n and $0_{n\times m}$ are the $n\times n$ identity matrix and the $n\times m$ zero matrix, respectively. For a matrix A, $\|A\|_2$ is the induced 2-norm of the vector norm, and $\|A\|_2 \triangleq \sigma(A)$. The notation $\sigma(A)$ is the maximal singular value of matrix A. Notations A^T, A^{-1}, and A^* represent the transpose, the inverse, and the complex conjugate transpose of matrix A, respectively. Let $\mathrm{Im}(A)$ and $\ker(A)$ be the image space and kernel of A. $A<0$ ($A>0$) means that the matrix A is negative (positive) definite. $\mathrm{Span}\{v_1, v_2, \ldots v_m\}$ is a subspace of $\mathbb{R}^n$ spanned by $\{v_1, v_2, \ldots v_m\}$, where $v_i \in \mathbb{R}^n$, $i = 1, 2, \ldots, m$. The notation $\otimes$ represents the Kronecker product. For a vector $x \in \mathbb{C}^n$, $|x| \triangleq \sqrt{x^*x}$ is the Euclidean norm. $\mathbf{1}_N$ denotes the $N\times 1$ column vector whose elements are all ones. The space of piecewise continuous functions in $\mathbb{R}^m$ that are square integrable over $[0,+\infty)$ is denoted by $\mathscr{L}_2^m[0,\infty)$, for any $v(t) \in \mathscr{L}_2^m[0,\infty)$, and its normalized energy is defined by $\|v(t)\|_{\mathscr{L}_2} = \left(\int_0^\infty |v(t)|^2 dt\right)^{1/2}$. Let $\left[\begin{array}{c|c} A & B \\ \hline C & D \end{array}\right]$ be a state space realization of $G(s) = C(sI-A)^{-1}B + D$.

2. Preliminaries

2.1. Graph Theory. Directed graphs are used to model the information interaction among agents. Let $\mathscr{G}_N = (\mathscr{V}_N, \mathscr{E}_N, \mathscr{A}_N)$ be a directed weighted graph, where $\mathscr{V}_N = \{1, 2, \ldots, N\}$ is the node set, $\mathscr{E}_N \subseteq \mathscr{V}_N \times \mathscr{V}_N$ is the edge set, and $\mathscr{A}_N \in \mathbb{R}^{N\times N}$ is a weighted adjacency matrix with nonnegative elements a_{ij}. An edge of $\mathscr{G}_N$ is denoted by (i, j) which means that agent j can directly get information from agent i. $(j,i) \in \mathscr{E}_N$ if and only if $a_{ij} > 0$, otherwise $a_{ij} = 0$. If $(i,j) \in \mathscr{E}_N \Leftrightarrow (j,i) \in \mathscr{E}_N$, then $\mathscr{G}_N$ is said to be an undirected graph. In this paper, we assume that there are no self-cycles in $\mathscr{G}_N$; that is, $a_{ii} = 0$, $i = 1, 2, \ldots, N$. The in-degree and out-degree of the ith agent are, respectively, defined as $d_{\mathrm{in}}(i) = \sum_{j=1}^N a_{ij}$ and $d_{\mathrm{out}}(i) = \sum_{j=1}^N a_{ji}$. Let $d_{\max} = \max_i\{d_{\mathrm{in}}(i)\}$. Correspondingly, the Laplacian matrix of graph $\mathscr{G}_N$ is denoted by $L_N = \Delta_N - \mathscr{A}_N \in \mathbb{R}^{N\times N}$, where $\Delta_N = [\Delta_{ij}]$ is a diagonal matrix with $\Delta_{ii} = d_{\mathrm{in}}(i)$.

A sequence $(i_1, i_2), (i_2, i_3), \ldots, (i_{k-1}, i_k)$ of edges is called a directed path from node i_1 to node i_k. $\mathscr{G}_N$ is called a strongly connected digraph if for any $i, j \in \mathscr{V}_N$, there is a directed path from i to j. $\mathscr{G}_N$ has a directed spanning tree if there exists a node $r \in \mathscr{V}_N$ (a root) such that all other nodes can be linked to r via a directed path. A directed graph is called balanced if $\sum_{j\neq i} a_{ij} = \sum_{i\neq j} a_{ji}$ for all $i \in \mathscr{V}$.

Below are well-known results for the Laplacian matrix.

Lemma 1 (see [3]). *The Laplacian matrix L_N of a directed graph has at least one zero eigenvalue with an associated eigenvector $\mathbf{1}_N$.*

Lemma 2 (see [3]). *The Laplacian matrix L_N of a directed graph has a simple zero eigenvalue with an associated eigenvector $\mathbf{1}_N$, and all of the other eigenvalues have positive real parts if and only if the directed graph has a directed spanning tree.*

Lemma 3 (see [24]). *Let L_N be the Laplacian matrix of a directed graph $\mathscr{G}_N$, then there exists an orthogonal matrix $\overline{U} = [\mathbf{1}_N/\sqrt{N} \;\; U] \in \mathbb{R}^{N\times N}$ such that*

$$\overline{U}^T L_N \overline{U} = \begin{bmatrix} 0 & \dfrac{\mathbf{1}_N^T}{\sqrt{N}} LU \\ 0 & U^T L U \end{bmatrix}. \tag{1}$$

Furthermore, if $\mathscr{G}$ is a balanced graph, then

$$\overline{U}^T L_N \overline{U} = \begin{bmatrix} 0 & 0 \\ 0 & U^T L_N U \end{bmatrix}. \tag{2}$$

2.2. Robust H_∞ Control Theory. Consider that the nth-order linear time-invariant (LTI) system is described as follows:

$$\begin{aligned} \dot{x}(t) &= Ax(t) + B_1\omega(t) + B_2u(t), \\ z(t) &= C_1x(t) + D_{11}\omega(t) + D_{12}u(t), \\ y(t) &= C_2x(t) + D_{21}\omega(t) + D_{22}u(t), \end{aligned} \tag{3}$$

where $x(t) \in \mathbb{R}^n$ is the state, $\omega(t) \in \mathscr{L}_2^q[0,\infty)$ is the external disturbance, $u(t) \in \mathbb{R}^m$ is the control input, $z(t) \in \mathbb{R}^p$ is the regulated output, $y(t) \in \mathbb{R}^l$ is the measured output, and A, B_i, C_i, and D_{ij}, for $i, j = 1, 2$, are known real constant matrices of appropriate dimensions. Without loss of generality, we assume that $D_{22} = 0$, (A, B_2) is stabilizable and (C_2, A) is detectable.

The n_cth-order dynamic output feedback (DOF) controller is described as follows:

$$\begin{aligned} \dot{x}_c(t) &= A_kx_c(t) + B_ky(t), \\ u(t) &= C_kx_c(t) + D_ky(t), \end{aligned} \tag{4}$$

where $x_c(t) \in \mathbb{R}^{n_c}$ is the controller state and A_k, B_k, C_k, and D_k are constant matrices with appropriate dimensions.

Let $S_{pc}(s) = \left[\begin{array}{c|c} A_c & B_c \\ \hline C_c & D_c \end{array}\right]$ be the transfer function from $\omega(t)$ to $z(t)$ of the closed-loop system obtained from (3) and (4), where

$$\begin{gathered} A_c = A_0 + \overline{B}K\overline{C}, \qquad B_c = B_0 + \overline{B}K\overline{D}_{21}, \\ C_c = C_0 + \overline{D}_{12}K\overline{C}, \qquad D_c = D_{11} + \overline{D}_{12}K\overline{D}_{21}, \\ A_0 = \begin{bmatrix} A & 0 \\ 0 & 0 \end{bmatrix}, \qquad B_0 = \begin{bmatrix} B_1 \\ 0 \end{bmatrix}, \qquad C_0 = [C_1 \;\; 0], \\ \overline{B} = \begin{bmatrix} 0 & B_2 \\ I & 0 \end{bmatrix}, \qquad \overline{C} = \begin{bmatrix} 0 & I \\ C_2 & 0 \end{bmatrix}, \qquad \overline{D}_{12} = [0 \;\; D_{12}], \\ \overline{D}_{21} = \begin{bmatrix} 0 \\ D_{21} \end{bmatrix}, \qquad K = \begin{bmatrix} A_k & B_k \\ C_k & D_k \end{bmatrix}. \end{gathered} \tag{5}$$

The H_∞ problem for the given LTI system (3) is to find a DOF controller (4) such that the closed-loop system is internally stable and $\|S_{pc}(s)\|_\infty < \gamma$ for some constant $\gamma > 0$.

To facilitate the consensus protocol design and stability analysis, several results of the H_∞ problem are recalled as follows.

Lemma 4 (see [29]). *Given $\gamma > 0$, there exists a DOF controller (4) which can solve the H_∞ problem for the LTI system (3) if and only if there exist symmetric matrices $X > 0$ and $Y > 0$ such that*

$$\begin{aligned} &\text{(a)} \begin{bmatrix} N_X & 0 \\ 0 & I \end{bmatrix}^* \begin{bmatrix} XA + A^*X & XB_1 & C_1^* \\ B_1^*X & -\gamma I & D_{11}^* \\ C_1 & D_{11} & -\gamma I \end{bmatrix} \begin{bmatrix} N_X & 0 \\ 0 & I \end{bmatrix} < 0, \\ &\text{(b)} \begin{bmatrix} N_Y & 0 \\ 0 & I \end{bmatrix}^* \begin{bmatrix} YA^* + AY & YC_1^* & B_1 \\ C_1Y & -\gamma I & D_{11} \\ B_1^* & D_{11}^* & -\gamma I \end{bmatrix} \begin{bmatrix} N_Y & 0 \\ 0 & I \end{bmatrix} < 0, \\ &\text{(c)} \begin{bmatrix} X & I \\ I & Y \end{bmatrix} \geq 0, \end{aligned} \tag{6}$$

where N_X and N_Y are full-rank matrices whose images satisfy

$$\begin{aligned} \operatorname{Im}(N_X) &= \ker([C_2 \;\; D_{21}]), \\ \operatorname{Im}(N_Y) &= \ker([B_2^* \;\; D_{12}^*]). \end{aligned} \tag{7}$$

As the results shown by [29], the DOF controller (4) solving the H_∞ problem for the LTI system (3) can be constructed as follows.

(i) Find $X > 0$ and $Y > 0$ which satisfy Lemma 4.

(ii) Let $X_c = \left[\begin{smallmatrix} X & X_2 \\ X_2^* & I \end{smallmatrix}\right]$, where $X_2 \in \mathbb{R}^{n\times n_c}$ satisfying $X - Y^{-1} = X_2X_2^*$.

(iii) Solve the the following inequality:

$$H_{X_c} + Q^*K^*P_{X_c} + P_{X_c}^*KQ < 0. \tag{8}$$

For a feasible solution K, where

$$\begin{gathered} P_{X_c} = \left[\overline{B}^*X_c \;\; 0 \;\; \overline{D}_{12}^*\right], \qquad Q = \left[\overline{C} \;\; \overline{D}_{21} \;\; 0\right], \\ H_{X_c} = \begin{bmatrix} X_cA_0 + A_0^*X_c & X_cB_0 & C_0^* \\ B_0^*X_c & -\gamma_0 I & D_{11}^* \\ C_0 & D_{11} & -\gamma_0 I \end{bmatrix}, \end{gathered} \tag{9}$$

and A_0, B_0, C_0, $\overline{B}$, $\overline{C}$, $\overline{D}_{12}$, $\overline{D}_{21}$ are defined by (5). The solution K provides the state space realization for a feasible controller (4) which can solve H_∞ problem for system (3).

Lemma 5 (see [30]). *Let $\gamma > 0$, $G(s) = \left[\begin{array}{c|c} A & B \\ \hline C & D \end{array}\right]$ with A is Hurwitz stable, and*

$$H \triangleq \begin{bmatrix} A + BR^{-1}D^*C & BR^{-1}B^* \\ -C^*\left(I + DR^{-1}D^*\right)C & -\left(A + BR^{-1}D^*C^*\right)^* \end{bmatrix}, \tag{10}$$

where $R = \gamma^2 I - D^*D$. Then, the following conditions are equivalent:

(1) $\|G(s)\|_\infty < \gamma$,

(2) *$\sigma(D) < \gamma$ and H have no eigenvalues on the imaginary axis,*

(3) *there exists a matrix $X = X^* > 0$ such that*

$$\begin{bmatrix} XA + A^*X & XB & C^* \\ B^*X & -\gamma I & D^* \\ C & D & -\gamma I \end{bmatrix} < 0. \tag{11}$$

3. H_∞ Consensus Problem

Consider a multiagent system consisting of N identical agents with linear dynamics described by

$$\begin{aligned} \dot{x}_i(t) &= Ax_i(t) + Bu_i(t) \\ y_i(t) &= Cx_i(t) \end{aligned} \qquad i = 1, \ldots, N, \tag{12}$$

where $x_i(t) \in \mathbb{R}^n$ is the state, $u_i(t) \in \mathbb{R}^m$ is the control input, $y_i(t) \in \mathbb{R}^p$ is the measured output, and A, B, and C are constant matrices with compatible dimensions. It is assumed that (A, B) is stabilizable and (C, A) is detectable, and without loss of generality, B is of full column rank. We say that the control input $u_i(t)$ solves the consensus problem for the multiagent system (12) if the states of the agents satisfy

$$\lim_{t \to +\infty} \left[x_i(t) - x_j(t) \right] = 0, \quad \forall i, j \in \mathscr{V}_N \tag{13}$$

for any initial states.

Assume that the communication topology among the N agents is represented by a fixed directed graph $\mathscr{G}_N = (\mathscr{V}_N, \mathscr{E}_N, \mathscr{A}_N)$. Based on the relative output information between the agents, the following dynamic output feedback (DOF) control protocol is used by [18]:

$$\begin{aligned} \dot{v}_i(t) &= A_k v_i(t) + B_k \sum_{j=0}^{N} a_{ij} \left[y_j(t) - y_i(t) \right] \\ u_i(t) &= C_k v_i(t) + D_k \sum_{j=0}^{N} a_{ij} \left[y_j(t) - y_i(t) \right] \end{aligned} \qquad i = 1, \ldots, N, \tag{14}$$

where $v_i(t) \in \mathbb{R}^{n_c}$, n_c is a preassigned dimension of the coordinating law, and a_{ij} is the element of the corresponding adjacency matrix $\mathscr{A}_N$. The system matrix

$$K = \begin{bmatrix} A_k & B_k \\ C_k & D_k \end{bmatrix} \tag{15}$$

of the DOF control protocol (14) need to be designed to make the multiagent system (12) achieve consensus. A general method for constructing the system matrix K was presented by [18].

However, if there exist communication errors between the ith agent and the jth agent, $i, j = 1, 2, \ldots, N$, then the performance of consensus will be affect by these errors, as illustrated by the example given below.

Example 6. We consider double-integrator systems given by

$$\begin{aligned} \ddot{\xi}_i(t) &= u_i(t), \\ y_i(t) &= \xi_i(t), \end{aligned} \qquad i = 1, 2, \ldots, N, \tag{16}$$

where $\xi_i(t)$, $y_i(t) \in \mathbb{R}$. Let $\dot{\xi}_i(t) = \zeta_i(t)$. Then, the above system can be rewritten as the form of (12) with

$$\begin{gathered} x_i(t) = \begin{bmatrix} \xi_i(t) \\ \zeta_i(t) \end{bmatrix}, \qquad A = \begin{bmatrix} 0 & 1 \\ 0 & 0 \end{bmatrix}, \qquad B = \begin{bmatrix} 0 \\ 1 \end{bmatrix}, \\ C = \begin{bmatrix} 1 & 0 \end{bmatrix}. \end{gathered} \tag{17}$$

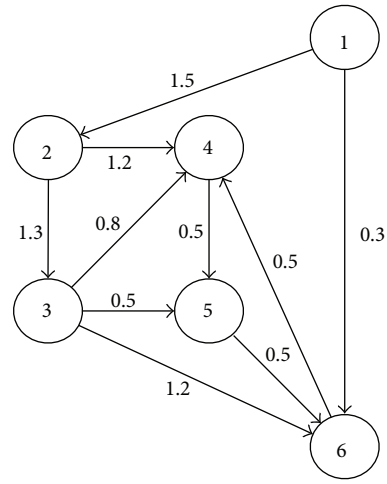

Figure 1: Communication topology.

The weighted communication topology with 6 agents is shown in Figure 1. Using the results presented in [18], the DOF control protocol (14) can be constructed with

$$\begin{gathered} A_k = \begin{bmatrix} -10 & -1 \\ -50.1039 & -0.485 \end{bmatrix}, \qquad B_k = \begin{bmatrix} 10 \\ 50 \end{bmatrix}, \\ C_k = \begin{bmatrix} 0.1039 & 0.485 \end{bmatrix}, \qquad D_k = 0. \end{gathered} \tag{18}$$

It is known that the consensus is asymptotically achieved when there are no communication errors with the designed protocol (see Figure 2(a)). However, communication errors are inevitable. Assume that a 1% error appears in all of the communication channels. Simulation results show that, under the same protocol, the system diverges in the sense that the position state of each agent is far away from the position state of leader (node 1) as can be seen in Figure 2(b).

Example 6 implies that, under the influence of communication errors, consensus cannot be achieved for each agent with the given control protocol. This provides motivation to design an appropriate DOF control protocol to attenuate the effects of communication errors on the consensus performance. In this paper, we assume that there exist communication errors in the transferred data; that is, the DOF control protocol takes the following form:

$$\begin{aligned} \dot{v}_i(t) &= A_k v_i(t) + B_k \sum_{j=0}^{N} a_{ij} \left[y_j(t) - y_i(t) + \omega_{ij}(t) \right], \\ u_i(t) &= C_k v_i(t) + D_k \sum_{j=0}^{N} a_{ij} \left[y_j(t) - y_i(t) + \omega_{ij}(t) \right] \end{aligned} \tag{19}$$

$$i = 1, \ldots, N,$$

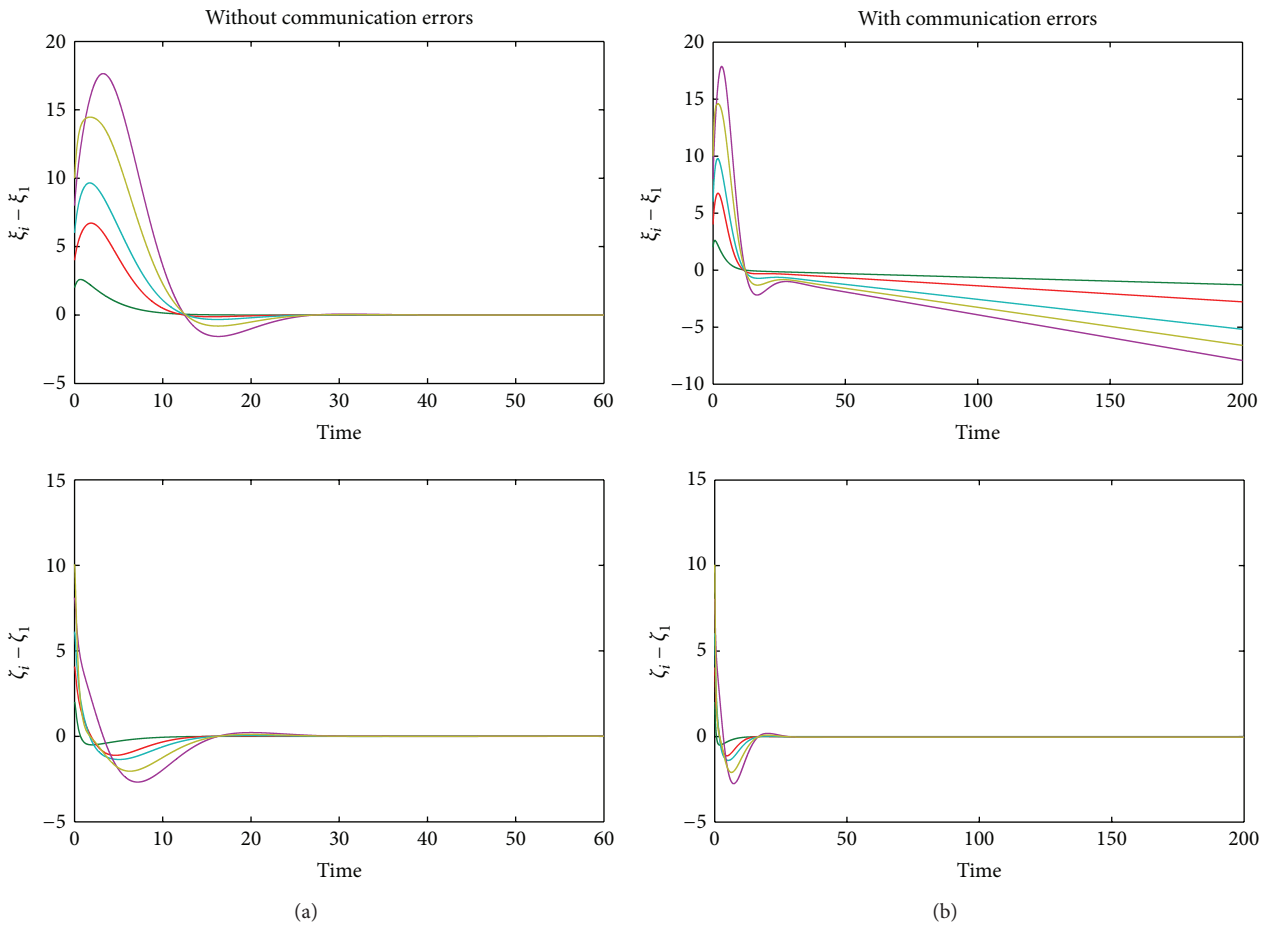

FIGURE 2: The disagreement states between x_i and x_1 without/with communication errors, $i = 2, 3, \ldots, 6$.

where $\omega_{ij} \in \mathscr{L}_2^p[0, +\infty)$ represents the communication error when the ith agent gets information from the jth agent. For convenience, denote

$$\begin{aligned}
\mathbf{x}(t) &= \left[\mathbf{x}_1^T(t), \ldots, \mathbf{x}_N^T(t)\right]^T \in \mathbb{R}^{N(n+n_c)}, \\
\mathbf{x}_i(t) &= \left[x_i^T(t), v_i^T(t)\right]^T \in \mathbb{R}^{n+n_c}, \quad i = 1, 2, \ldots, N, \\
\mathbf{y}(t) &= \left[y_1^T(t), y_2^T(t), \ldots, y_N^T(t)\right]^T \in \mathbb{R}^{Np}, \\
\mathbf{d}(t) &= \left[\mathbf{d}_1^T(t), \mathbf{d}_2^T(t), \ldots, \mathbf{d}_N^T(t)\right]^T \in \mathbb{R}^{N(N-1)p}, \\
\mathbf{d}_i(t) &= \left[\omega_{i1}^T(t), \ldots, \omega_{i(i-1)}^T(t), \omega_{i(i+1)}^T(t), \ldots, \omega_{iN}^T\right]^T(t) \\
&\in \mathbb{R}^{(N-1)p}, \quad i = 1, 2, \ldots, N.
\end{aligned} \tag{20}$$

Then, the overall dynamics result in the system (12) with the DOF control protocol (19) can be written as

$$\dot{\mathbf{x}}(t) = \left(I_N \otimes \overline{A} - L_N \otimes \overline{B}\,\overline{C}\right)\mathbf{x}(t) + \left(D_N \otimes \overline{B}\right)\mathbf{d}(t), \tag{21}$$

where

$$\begin{aligned}
&\overline{A} = \begin{bmatrix} A & BC_k \\ 0 & A_k \end{bmatrix}, \qquad \overline{B} = \begin{bmatrix} BD_k \\ B_k \end{bmatrix}, \qquad \overline{C} = \begin{bmatrix} C & 0 \end{bmatrix}, \\
&D_N = \begin{bmatrix} \delta_1 & 0_{1\times N-1} & \cdots & 0_{1\times N-1} \\ 0_{1\times N-1} & \delta_2 & \cdots & 0_{1\times N-1} \\ \vdots & \vdots & \ddots & \vdots \\ 0_{1\times N-1} & 0_{1\times N-1} & \cdots & \delta_N \end{bmatrix} \in \mathbb{R}^{N\times N(N-1)}, \\
&\delta_i = \begin{bmatrix} l_{i1} & \cdots & l_{i(i-1)} & l_{i(i+1)} & \cdots & l_{iN} \end{bmatrix}, \quad i = 1, \ldots, N,
\end{aligned} \tag{22}$$

and l_{ij} is the element of the Laplacian matrix L_N.

In order to characterize the effects of the communication errors on consensus performance, we need to define a controlled output for the multiagent system (12) as follows.

Assume that the fixed directed communication graph $\mathscr{G}_N$ has a spanning tree, and according to Lemma 2, the Laplacian matrix L_N of graph $\mathscr{G}_N$ has a simple zero, and all of the other eigenvalues are in the right half-plane. Let $e_1 = (1/\sqrt{N})\mathbf{1}_N$.

By Lemma 3, there exists an orthogonal matrix $[e_1 \ \ U] \in \mathbb{R}^{N\times N}$ such that

$$\begin{bmatrix} e_1^T \\ U^T \end{bmatrix} L_N \begin{bmatrix} e_1 & U \end{bmatrix} = \begin{bmatrix} 0 & e_1^T L_N U \\ 0 & \overline{L}_N \end{bmatrix}, \tag{23}$$

where $\overline{L}_N = U^T L_N U$. It is obvious that the eigenvalues of $\overline{L}_N$ are equal to the nonzero eigenvalues of L_N, which means that all of the eigenvalues of $\overline{L}_N$ are in the right half-plane. Here, the matrix U satisfies $U^T \mathbf{1}_N = 0$, $U^T U = I_{N-1}$, and $UU^T = I_N - (1/N)\mathbf{1}_N \mathbf{1}_N^T$ according to $[e_1 \ \ U]$ being an orthogonal matrix.

Let $C_0 = [I_n \ \ 0]$. Define an output vector $\mathbf{z}(t)$ as

$$\mathbf{z}(t) = \left(U^T \otimes C_0\right)\mathbf{x}(t) = \left(U^T \otimes I_n\right)x(t), \tag{24}$$

where $\mathbf{z}(t) = [\mathbf{z}_1^T(t), \ldots, \mathbf{z}_{N-1}^T(t)]^T \in \mathbb{R}^{(N-1)n}$, $\mathbf{z}_i(t) \in \mathbb{R}^n$, and $x(t) = [x_1^T(t), x_2^T(t), \ldots, x_N^T(t)]^T$. Then,

$$|\mathbf{z}(t)|^2 = \left|\left(U^T \otimes C_0\right)\mathbf{x}(t)\right|^2 = \left|x(t) - \mathbf{1}_N \otimes x_0(t)\right|^2, \tag{25}$$

where $x_0(t) = (1/N)\sum_{i=1}^N x_i(t)$, which means that $\mathbf{z}(t)$ can measure the difference between the state of each agent and the average state of all agents.

Let $\widehat{\mathbf{x}}(t) = (U^T \otimes I_{n+n_c})\mathbf{x}(t)$. Using the DOF control protocol (19), the system dynamics with the output $\mathbf{z}(t)$ can be represented as

$$\begin{aligned} \dot{\widehat{\mathbf{x}}}(t) &= \widetilde{A}\widehat{\mathbf{x}}(t) + \widetilde{B}\mathbf{d}(t), \\ \mathbf{z}(t) &= \widetilde{C}\widehat{\mathbf{x}}(t), \end{aligned} \tag{26}$$

where $\widetilde{A} = I_{N-1} \otimes \overline{A} - \overline{L}_N \otimes \overline{B}\,\overline{C}$, $\widetilde{B} = U^T D_N \otimes \overline{B}$, and $\widetilde{C} = I_{N-1} \otimes C_0$.

From the fact that the null-space of matrix $U^T \otimes I_n$ is Span $\{\mathbf{1}_N \otimes I_n\}$, we know that

$$\lim_{t\to+\infty} \mathbf{z}(t) = \lim_{t\to+\infty} \left(U^T \otimes I_n\right)x(t) = 0 \tag{27}$$

if and only if there exist $x_0(t) \in \mathbb{R}^n$ such that $\lim_{t\to+\infty} x_i(t) = x_0(t)$, which implies that consensus of the multiagent system (12) can be achieved asymptotically. However, it is obvious that $\mathbf{z}(t)$ cannot approach zero as t tending to infinity due to the existence of communication error $\mathbf{d}(t)$, which indicates that consensus cannot be achieved for the system (12) with the DOF control protocol (19). Inspired by the analysis above, it is reasonable to evaluate the effects of communication error on consensus of the system (12) with the DOF control protocol (19) by using the effects of communication error $\mathbf{d}(t)$ on the output $\mathbf{z}(t)$ of system (26). Notice that the latter can be quantitatively measured by the H_∞ norm of the transfer function matrix $G_{dz}(s)$ from $\mathbf{d}(t)$ to $\mathbf{z}(t)$, which is defined by $\|G_{dz}(s)\|_\infty = \sup_{\omega\in\mathbb{R}}\{\|G_{dz}(j\omega)\|_2\} = \sup_{\omega\in\mathbb{R}}\{\sigma(G_{dz}(j\omega))\}$, that results in the following definition.

Definition 7. Given a scalar $\gamma > 0$. The system (12) with the DOF control protocol (19) is called to achieve consensus with H_∞ performance if the following conditions hold.

(1) It can reach consensus when $\mathbf{d}(t) = 0$;

(2) $\|G_{dz}(s)\|_\infty < \gamma$, where $G_{dz}(s)$ is the transfer function matrix of system (26) from $\mathbf{d}(t)$ to $\mathbf{z}(t)$ and the output $\mathbf{z}(t)$ is defined by (24).

A sufficient condition is given in the following theorem to ensure that the multiagent system (12) with the DOF control protocol (19) can achieve consensus with H_∞ performance.

Theorem 8. *Given a scalar $\gamma > 0$. Assume that the fixed communication topology $\mathcal{G}_N$ has a spanning tree. The system* (12) *with the DOF control protocol* (19) *achieves consensus with H_∞ performance if there exists a matrix $X_c = X_c^* > 0$ such that*

$$\begin{bmatrix} X_c\left(\overline{A} - \lambda_i\overline{B}\,\overline{C}\right) + \left(\overline{A} - \lambda_i\overline{B}\,\overline{C}\right)^* X_c & X_c\overline{B} & C_0^* \\ \overline{B}^* X_c & -\gamma_0 I & 0 \\ C_0 & 0 & -\gamma_0 I \end{bmatrix} < 0, \tag{28}$$

where $\gamma_0 = d_{\max}^{-1}\gamma$ and λ_i is the nonzero eigenvalue of Laplacian matrix L_N, $i = 2, 3, \ldots, N$.

Proof. It is known that the system (12) with the DOF control protocol (19) achieves consensus with H_∞ performance if and only if $\widetilde{A}$ is Hurwitz and

$$\|G_{dz}(s)\|_\infty = \left\|\widetilde{C}\left(sI - \widetilde{A}\right)^{-1}\widetilde{B}\right\|_\infty < \gamma, \tag{29}$$

where $\widetilde{A}$, $\widetilde{B}$, and $\widetilde{C}$ are defined by (26).

According to Lemma 5 and (28), we have $\overline{A} - \lambda_i\overline{B}\,\overline{C}$ is Hurwitz stable, and

$$\overline{H}_i \triangleq \begin{bmatrix} \overline{A} - \lambda_i\overline{B}\,\overline{C} & \gamma_0^{-2}\overline{B}\,\overline{B}^* \\ -C_0^* C_0 & -\left(\overline{A} - \lambda_i\overline{B}\,\overline{C}\right)^* \end{bmatrix} \tag{30}$$

has no eigenvalues on the imaginary axis; that is, for any $\omega \in \mathbb{R}$,

$$\begin{aligned} \left(j\omega I - \left(A - \lambda_i\overline{B}\,\overline{C}\right)\right)\eta_1 - \left(\gamma_0^{-2}\overline{B}\,\overline{B}^*\right)\eta_2 &= 0, \\ C_0^* C_0\eta_1 + \left(j\omega I + \left(\overline{A} - \lambda_i\overline{B}\,\overline{C}\right)^*\right)\eta_2 &= 0, \end{aligned} \tag{31}$$

if and only if $\eta_1 = 0$ and $\eta_2 = 0$, where $\eta_1, \eta_2 \in \mathbb{C}^{n+n_c}$.

For matrix $\overline{L}_N$, there are two unitary matrices V_1 and V_2 such that

$$\begin{aligned} V_1^*\overline{L}_N V_1 &= T = \left[t_{ij}\right] \in \mathbb{R}^{(N-1)\times(N-1)}, \\ V_2^*\overline{L}_N^* V_2 &= S = \left[s_{ij}\right] \in \mathbb{R}^{(N-1)\times(N-1)}, \end{aligned} \tag{32}$$

where T and S are upper triangular, with diagonal entries $t_{ii} = \lambda_{i+1}$ and $s_{ii} = \lambda_{i+1}^*$, respectively, $i = 1, 2, \ldots, N-1$. Now, suppose that $j\omega_0$ is an eigenvalue of

$$H \triangleq \begin{bmatrix} I_{N-1} \otimes \overline{A} - T \otimes \overline{B}\,\overline{C} & \gamma_0^{-2} I_{N-1} \otimes \overline{B}\,\overline{B}^* \\ -I_{N-1} \otimes C_0^* C_0 & -\left(I_{N-1} \otimes \overline{A} - S^* \otimes \overline{B}\,\overline{C}\right)^* \end{bmatrix}. \tag{33}$$

Then, there exists a vector $\eta = [\eta_{1,1}^T, \eta_{1,2}^T, \ldots, \eta_{1,(N-1)}^T, \eta_{2,1}^T, \eta_{2,2}^T, \ldots, \eta_{2,(N-1)}^T]^T \neq 0$, where $\eta_{k,l} \in \mathbb{C}^{n+n_c}$, $k = 1, 2$, $l = 1, 2, \ldots, N-1$, such that

$$\begin{aligned} &\left(j\omega_0 I - \left(\overline{A} - \lambda_{i+1}\overline{B}\,\overline{C}\right)\right)\eta_{1,i} \\ &\quad + \sum_{j=i+1}^{N-1} t_{ij}\overline{B}\,\overline{C}\eta_{1,j} - \left(\gamma_0^{-2}\overline{B}\,\overline{B}^*\right)\eta_{2,i} = 0, \\ &C_0^* C_0 \eta_{1,i} + \left(j\omega_0 I + \left(\overline{A} - \lambda_{i+1}\overline{B}\,\overline{C}\right)^*\right)\eta_{2,i} \\ &\quad - \sum_{j=i+1}^{N-1} s_{ij}\left(\overline{B}\,\overline{C}\right)^* \eta_{2,j} = 0, \end{aligned} \tag{34}$$

where $i = 1, 2, \ldots, N-1$. When $i = N-1$, from (31), it is easy to get that $\eta_{1,N-1} = \eta_{2,N-1} = 0$. Then, when $i = N-2$, (34) can be rewritten as

$$\begin{aligned} &\left(j\omega_0 I - \left(A - \lambda_{N-1}\overline{B}\,\overline{C}\right)\right)\eta_{1,N-2} - \left(\gamma_0^{-2}\overline{B}\,\overline{B}^*\right)\eta_{2,N-2} = 0, \\ &C_0^* C_0 \eta_{1,N-2} + \left(j\omega_0 I + \left(\overline{A} - \lambda_{N-1}\overline{B}\,\overline{C}\right)^*\right)\eta_{2,N-2} = 0, \end{aligned} \tag{35}$$

which implies that $\eta_{1,N-2} = \eta_{2,N-2} = 0$. Similarly, it can be known that $\eta_{1,i} = \eta_{2,i} = 0$ for all $i = 1, 2, \ldots, N-1$. This contradicts our assumption, and hence matrix H has no eigenvalues on the imaginary axis.

Notice that

$$\begin{aligned} \widetilde{H} &\triangleq \begin{bmatrix} I_{N-1} \otimes \overline{A} - \overline{L}_N \otimes \overline{B}\,\overline{C} & \gamma_0^{-2} V_1 V_2^* \otimes \overline{B}\,\overline{B}^* \\ -V_2 V_1^* \otimes C_0^* C_0 & -\left(I_{N-1} \otimes \overline{A} - \overline{L}_N \otimes \overline{B}\,\overline{C}\right)^* \end{bmatrix} \\ &= \begin{bmatrix} V_1 \otimes I_{n+n_c} & 0 \\ 0 & V_2 \otimes I_{n+n_c} \end{bmatrix} H \begin{bmatrix} V_1^* \otimes I_{n+n_c} & 0 \\ 0 & V_2^* \otimes I_{n+n_c} \end{bmatrix}, \end{aligned} \tag{36}$$

which means that matrix $\widetilde{H}$ has no pure imaginary eigenvalues. Moreover, matrices $\overline{A} - \lambda_i \overline{B}\,\overline{C}$ are Hurwitz stable, $i = 2, 3, \ldots, N$, which implies that matrix $\widetilde{A} = I_{N-1} \otimes \overline{A} - \overline{L}_N \otimes \overline{B}\,\overline{C}$ is Hurwitz stable. Noting that V_1 and V_2 are unitary matrices, then there must exist two matrices Y_1 and Y_2 such that $Y_1 Y_1^* = V_1 V_2^*$, $Y_2^* Y_2 = V_2 V_1^*$, and $\|Y_1\|_2 = \|Y_2\|_2 = 1$. Thus, according to Lemma 5, it can be obtained that

$$\begin{aligned} &\left\|\left(Y_2 \otimes C_0\right)\left(sI - \left(I_{N-1} \otimes \overline{A} - \overline{L}_N \otimes \overline{B}\,\overline{C}\right)\right)^{-1}\left(Y_1 \otimes \overline{B}\right)\right\|_\infty \\ &\quad = \left\|\widetilde{C}\left(sI - \widetilde{A}\right)^{-1}\left(I_{N-1} \otimes \overline{B}\right)\right\|_\infty < \gamma_0. \end{aligned} \tag{37}$$

In addition, it is easy to know that

$$\left\|U^T D_N\right\|_2 \leq \|D_N\|_2 = \max_i \left\{\sqrt{\delta_i \delta_i^T}\right\} \leq d_{\max}. \tag{38}$$

Then, we have

$$\begin{aligned} \|G_{dz}(s)\|_\infty &= \left\|\widetilde{C}\left(sI - \widetilde{A}\right)^{-1}\widetilde{B}\right\|_\infty \\ &< d_{\max}\left\|\widetilde{C}\left(sI - \widetilde{A}\right)^{-1}\left(I_{N-1} \otimes \overline{B}\right)\right\|_\infty < \gamma. \end{aligned} \tag{39}$$

This completes the proof. □

Remark 9. If there are no communication errors, that is, $\mathbf{d}(t) = 0$, then from Theorem 8, it is only required that $\overline{A} - \lambda_i \overline{B}\,\overline{C}$ is Hurwitz for all nonzero eigenvalues λ_i of the Laplacian matrix L_N. In this case, consensus can be achieved asymptotically for the multiagent system (12) with the DOF control protocol (19), which is the result shown by [18].

Remark 10. In fact, from Lemma 5, there exists $X_c > 0$ such that the inequality (28) holds, $i = 2, 3, \ldots, N$, if and only if there exists a common n_cth-order DOF controller

$$\mathscr{K}(s) = \left[\begin{array}{c|c} A_k & B_k \\ \hline C_k & D_k \end{array}\right] \tag{40}$$

solving H_∞ problem with performance γ_0 for $N-1$ nth-order LTI systems

$$\Sigma_i(s) = \left[\begin{array}{c|cc} A & 0 & B \\ \hline I_n & 0 & 0 \\ -\lambda_i C & D_{21} & 0 \end{array}\right], \tag{41}$$

where A, B, and C are the state space matrices for system (12), $D_{21} = I_p$, and λ_i is the nonzero eigenvalue of Laplacian matrix L_N, $i = 2, 3, \ldots, N$.

4. Dynamic Output Feedback Design for H_∞ Consensus

In this section, we determine the system matrix K of the DOF control protocol (19) for the multiagent system (12) to achieve consensus with H_∞ performance. According to Remark 10, it is required to design a common DOF controller (40) to solve H_∞ problem for $N-1$ LTI systems. Notice that the common DOF controller is difficult to obtain; thus, we firstly consider the H_∞ problem for the systems $\Sigma_i(s)$, $i = 2, 3, \ldots, N$.

Let N_X and N_Y be full-rank matrices whose images satisfy

$$\operatorname{Im}(N_X) = \ker([C \;\; I_p]), \qquad \operatorname{Im}(N_Y) = \ker([B^* \;\; 0]). \tag{42}$$

Denote $N_X = [N_c^* \quad N_I^*]^*$, where N_c and N_I have n and p rows, respectively.

Lemma 11. *If there exist matrices $X = X^* > 0$ and $Y = Y^* > 0$ such that*

$$\text{(i)} \begin{bmatrix} N_c & 0 \\ 0 & I \end{bmatrix}^* \begin{bmatrix} XA + A^*X & I_n \\ I_n & -\gamma_0 I \end{bmatrix} \begin{bmatrix} N_c & 0 \\ 0 & I \end{bmatrix} - \begin{bmatrix} \gamma_m N_I^* N_I & 0 \\ 0 & 0 \end{bmatrix} < 0, \tag{43}$$

$$\text{(ii)} \quad N_Y^* \begin{bmatrix} YA^* + AY & Y \\ Y & -\gamma_0 I \end{bmatrix} N_Y < 0, \tag{44}$$

$$\text{(iii)} \quad \begin{bmatrix} X & I \\ I & Y \end{bmatrix} \geq 0, \tag{45}$$

where $\gamma_m = \gamma_0\{\min_i |\lambda_i|^2\}$, then there exists a DOF controller $\mathscr{K}_i(s) = \left[\begin{array}{c|c} A_k^i & B_k^i \\ \hline C_k^i & D_k^i \end{array}\right]$ which can solve the H_∞ problem with a given performance $\gamma_0 > 0$ for the LTI system $\Sigma_i(s)$ given by (41), *$i = 2, 3, \ldots, N$.*

Proof. According to Lemma 4, we have that there exists a DOF controller $\mathscr{K}_i(s)$ to solve the H_∞ problem for the LTI system $\Sigma_i(s)$ with a given index $\gamma_0 > 0$ if and only if there exist matrices $X_i = X_i^* > 0$ and $Y = Y^* > 0$ such that

$$\begin{aligned} &\text{(a)} \begin{bmatrix} N_X^i & 0 \\ 0 & I \end{bmatrix}^* \begin{bmatrix} X_iA + A^*X_i & 0 & I_n \\ 0 & -\gamma_0 I & 0 \\ I_n & 0 & -\gamma_0 I \end{bmatrix} \begin{bmatrix} N_X^i & 0 \\ 0 & I \end{bmatrix} < 0, \\ &\text{(b)} \begin{bmatrix} N_Y & 0 \\ 0 & I \end{bmatrix}^* \begin{bmatrix} YA^* + AY & Y & 0 \\ Y & -\gamma_0 I & 0 \\ 0 & 0 & -\gamma_0 I \end{bmatrix} \begin{bmatrix} N_Y & 0 \\ 0 & I \end{bmatrix} < 0, \\ &\text{(c)} \begin{bmatrix} X_i & I \\ I & Y \end{bmatrix} \geq 0, \end{aligned} \tag{46}$$

where N_X^i spans the kernel of $[-\lambda_i C \quad I_p]$. Notice the following facts:

$$[-\lambda_i C \quad I_p] \begin{bmatrix} N_c \\ -\lambda_i N_I \end{bmatrix} = -\lambda_i \left(CN_c + I_p N_I\right) = 0, \tag{47}$$

and, for all nonzero λ_i,

$$\operatorname{rank} \begin{bmatrix} N_c \\ -\lambda_i N_I \end{bmatrix} = \operatorname{rank} \begin{bmatrix} N_c \\ N_I \end{bmatrix}. \tag{48}$$

Thus, we can choose $N_X^i = \left[\begin{smallmatrix} N_c \\ -\lambda_i N_I \end{smallmatrix}\right]$. Let $X_i = X$ for all $i = 2, 3, \ldots, N$. Then, it is easy to obtain that

$$\begin{aligned} &\begin{bmatrix} N_X^i & 0 \\ 0 & I \end{bmatrix}^* \begin{bmatrix} X_iA + A^*X_i & 0 & I_n \\ 0 & -\gamma_0 I & 0 \\ I_n & 0 & -\gamma_0 I \end{bmatrix} \begin{bmatrix} N_X^i & 0 \\ 0 & I \end{bmatrix} \\ &= \begin{bmatrix} N_c & 0 \\ 0 & I \end{bmatrix}^* \begin{bmatrix} XA + A^*X & I_n \\ I_n & -\gamma_0 I \end{bmatrix} \begin{bmatrix} N_c & 0 \\ 0 & I \end{bmatrix} - \begin{bmatrix} \gamma_0 |\lambda_i|^2 N_I^* N_I & 0 \\ 0 & 0 \end{bmatrix} \\ &\leq \begin{bmatrix} N_c & 0 \\ 0 & I \end{bmatrix}^* \begin{bmatrix} XA + A^*X & I_n \\ I_n & -\gamma_0 I \end{bmatrix} \begin{bmatrix} N_c & 0 \\ 0 & I \end{bmatrix} - \begin{bmatrix} \gamma_m N_I^* N_I & 0 \\ 0 & 0 \end{bmatrix} < 0 \end{aligned} \tag{49}$$

and (b), (c) naturally hold from (44), (45), respectively. This completes the proof. □

Remark 12. Lemma 11 gives a sufficient condition for the existence of the controller $\mathscr{K}_i(s)$ which can solve the H_∞ problem for the system $\Sigma_i(s)$, $i = 2, 3, \ldots, N$. As the results stated in Section 2.2, if there exist $X = X^* > 0$ and $Y = Y^* > 0$ satisfying Lemma 11, then the DOF controller $\mathscr{K}_i(s)$ can be obtained by solving the following inequality:

$$H_{X_c} + Q(\lambda_i)^* K_i^* P_{X_c} + P_{X_c}^* K_i Q(\lambda_i) < 0, \tag{50}$$

for K_i, $i = 2, 3, \ldots, N$, where

$$H_{X_c} = \begin{bmatrix} X_cA_0 + A_0^*X_c & 0 & C_0^* \\ 0 & -\gamma_0 I & 0 \\ C_0 & 0 & -\gamma_0 I \end{bmatrix}, \tag{51}$$

$$\begin{aligned} &P_{X_c} = \begin{bmatrix} \widehat{B}^* X_c & 0 & 0 \end{bmatrix}, \qquad Q(\lambda_i) = \begin{bmatrix} \widehat{C}(\lambda_i) & \widehat{D} & 0 \end{bmatrix}, \\ &A_0 = \begin{bmatrix} A & 0 \\ 0 & 0 \end{bmatrix}, \qquad C_0 = [I \quad 0], \qquad \widehat{B} = \begin{bmatrix} 0 & B \\ I & 0 \end{bmatrix}, \\ &\widehat{C}(\lambda_i) = \begin{bmatrix} 0 & I \\ -\lambda_i C & 0 \end{bmatrix}, \qquad \widehat{D} = \begin{bmatrix} 0 \\ I \end{bmatrix}, \end{aligned} \tag{52}$$

$$\begin{aligned} &K_i = \begin{bmatrix} A_k^i & B_k^i \\ C_k^i & D_k^i \end{bmatrix}, \qquad X_c = \begin{bmatrix} X & X_2 \\ X_2^* & I \end{bmatrix}, \\ &X_2 X_2^* = X - Y^{-1}. \end{aligned} \tag{53}$$

Obviously, if there exists a common K that makes the inequality (50) hold for all $i = 2, 3, \ldots, N$, then there exists a common n_cth-order DOF controller $\mathscr{K}(s)$ which can solve the H_∞ problem for the LTI systems Σ_i, $i = 2, 3, \ldots, N$. Thus, we have the following result.

Theorem 13. *Given a scalar $\gamma > 0$, and let $\gamma_0 = d_{\max}^{-1}\gamma$. Assume that the fixed communication topology $\mathscr{G}_N$ has a spanning tree.*

Then, there exists a DOF control protocol (19) *for the system* (12) *achieving consensus with H_∞ performance if*

(i) *there exist matrices $X > 0$ and $Y > 0$ satisfying* (43), (44), *and* (45),

(ii) *there exists a matrix K satisfying the following LMIs:*

$$H_{X_c} + Q(\lambda_i)^* K^* P_{X_c} + P_{X_c}^* K Q(\lambda_i) < 0, \tag{54}$$

for all nonzero eigenvalues λ_i of Laplacian matrix L_N, where H_{X_c}, P_{X_c}, and $Q(\lambda_i)$ are given in (51) *and X_c is defined by* (53).

Proof. From the analysis above, the conditions (i) and (ii) hold which implies that there exist matrices K and $X_c > 0$ such that (28) holds due to the fact that (54) is exactly (28). The proof is completed by using Theorem 8 directly. □

Remark 14. If we want controllers of order n_c less than n, it is only required to add the additional constraint

$$\operatorname{rank}\begin{bmatrix} X & I \\ I & Y \end{bmatrix} \le n + n_c, \tag{55}$$

to (i) of Theorem 13, which can be obtained by using Corollary 7.8 given by [29] and Theorem 13 directly.

Remark 15. Theorem 13 gives the sufficient conditions under which there exists a DOF control protocol such that the multiagent system (12) achieve consensus with a given H_∞ performance. When the conditions are satisfied, the procedure to construct the DOF control protocol is presented as follows.

Sept 1: Solve LMIs (43), (44), and (45) for getting a solution: $X > 0$ and $Y > 0$.

Step 2: Construct $X_c > 0$ as (53).

Step 3: Solve the $N - 1$ LMIs (54) for a common feasible solution K.

Remark 16. Assume that there is no communication error in the system. As shown in Remark 9, in this case, the given problem is to design a stabilizing controller $\mathscr{K}(s)$ defined by (40) for the LTI systems (41) with $D_{21} = 0$. Using Theorem 5.8 given by [29] and the fact that the kernels of $\lambda_i C$ and C are exactly equal for all nonzero λ_i, reproducing the steps of the proof of Theorem 13, we have the following results. Assume that the fixed communication topology $\mathscr{G}_N$ has a spanning tree, then there exists a DOF control protocol (14) with order n_c for the system (12) achieving consensus if

(1) there exist matrices $X = X^* > 0$ and $Y = Y^* > 0$ such that

$$N_X^*(A^*X + XA)N_X < 0, \qquad N_Y^*(AY + YA^*)N_Y < 0,$$
$$\begin{bmatrix} X & I \\ I & Y \end{bmatrix} \ge 0, \qquad \operatorname{rank}\begin{bmatrix} X & I \\ I & Y \end{bmatrix} \le n + n_c, \tag{56}$$

where N_X and N_Y span the kernels of C and B^*, respectively,

(2) there exists a matrix K satisfying the following LMIs:

$$A_0^* P + PA_0 + \widehat{C}(\lambda_i)^* K^* \widehat{B}^* P + P\widehat{B}K\widehat{C}(\lambda_i) < 0, \tag{57}$$

for all nonzero eigenvalues λ_i of Laplacian matrix L_N, where

$$P = \begin{bmatrix} X & X_2 \\ X_2^* & I \end{bmatrix} \tag{58}$$

and X_2 satisfies $X_2 X_2^* = X - Y^{-1}$ and A_0, $\widehat{B}$, and $\widehat{C}(\lambda_i)$ are given in (51).

Moreover, using the method similar to that stated in Remark 15, we can construct the DOF controller for the multiagent system (12) reaching consensus.

Notice that condition (ii) in Theorem 13 implies that we need to solve $N - 1$ LMIs after constructing X_c, which increase the difficulty of the numerical calculation if the size of the multiagent system N is large. We give the following conditions, which can reduce the computational complexity for getting the DOF control protocol by solving four LMIs.

Denote that α_i and β_i are the real part and imaginary part of λ_i, respectively, where λ_i is the nonzero eigenvalue of Laplacian matrix L_N, $i = 2, 3, \ldots, N$. Let $\alpha_0 = \min_i\{\alpha_i\}$, $\overline{\alpha}_0 = \max_i\{\alpha_i\}$, $\beta_0 = \min_i\{\beta_i\}$, and $\overline{\beta}_0 = \max_i\{\beta_i\} = -\beta_0$.

Theorem 17. *Given a scalar $\gamma > 0$, and let $\gamma_0 = d_{\max}^{-1}\gamma$. Assume that the fixed communication topology $\mathscr{G}_N$ has a spanning tree. Then, there exists a DOF control protocol* (19) *for the system* (12) *achieving consensus with H_∞ performance if*

(i) *there exist matrices $X > 0$ and $Y > 0$ satisfying* (43), (44), *and* (45);

(ii) *there exists a matrix K such that*

$$H_{X_c} + Q(\alpha_k + j\beta_k)^* K^* P_{X_c} + P_{X_c}^* K Q(\alpha_k + j\beta_k) < 0 \tag{59}$$

for $(\alpha_k, \beta_k) \in \{(\alpha_0, \beta_0), (\alpha_0, \overline{\beta}_0), (\overline{\alpha}_0, \beta_0), (\overline{\alpha}_0, \overline{\beta}_0)\}$, where H_{X_c}, P_{X_c}, and $Q(\alpha_k + j\beta_k)$ are given in (51) *and X_c is defined by* (53).

Proof. To complete the proof, we only need to show that if LMI (59) holds for $(\alpha_k, \beta_k) \in \{(\alpha_0, \beta_0), (\alpha_0, \overline{\beta}_0), (\overline{\alpha}_0, \beta_0), (\overline{\alpha}_0, \overline{\beta}_0)\}$, then LMI (54) holds for all nonzero eigenvalues $\lambda_i = \alpha_i + j\beta_i$ of Laplacian matrix L_N, $i = 2, 3, \ldots, N$.

Notice that

$$H_{X_c} + Q(\alpha_i + j\beta_i)^* K^* P_{X_c} + P_{X_c}^* K Q(\alpha_i + j\beta_i)$$
$$= \begin{bmatrix} X_c\left(\overline{A} - (\alpha_i + j\beta_i)\overline{B}\,\overline{C}\right) + \left(\overline{A} - (\alpha_i + j\beta_i)\overline{B}\,\overline{C}\right)^* X_c & X_c\overline{B} & C_0^* \\ \overline{B}^* X_c & -\gamma_0 I & 0 \\ C_0 & 0 & -\gamma_0 I \end{bmatrix}$$
$$< 0 \tag{60}$$

which, in virtue of the Schur Complement Lemma, is equivalent to

$$X_c\left(\overline{A} - (\alpha_i + j\beta_i)\overline{B}\,\overline{C}\right) + \left(\overline{A} - (\alpha_i + j\beta_i)\overline{B}\,\overline{C}\right)^* X_c + \gamma_0^{-1}\left(X_c\overline{B}\,\overline{B}^* X_c + C_0^* C_0\right) < 0, \tag{61}$$

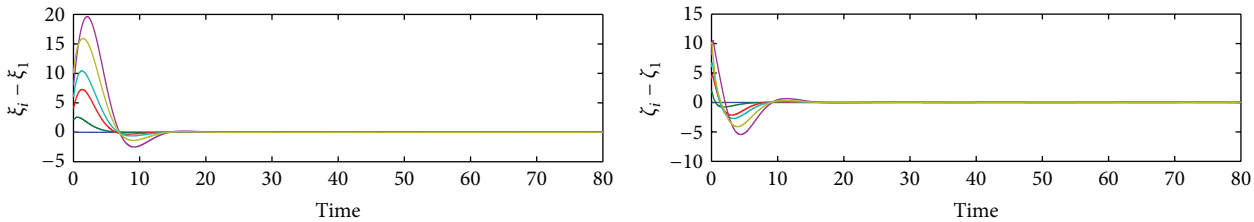

(a) Position states of the 6 agents (b) Velocity states of the 6 agents

FIGURE 3: The disagreement states between x_i and x_1 without communication error $\mathbf{d}(t)$, $i = 2, 3, \ldots, 6$.

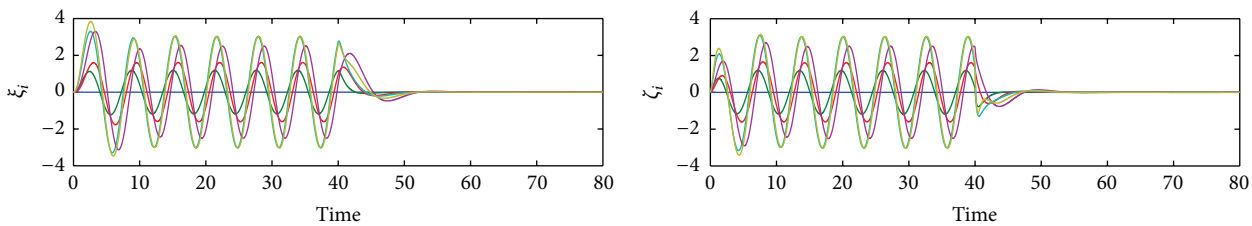

(a) Position states of the 6 agents (b) Velocity states of the 6 agents

FIGURE 4: The state trajectories of the multiagent system with communication error $\mathbf{d}(t)$.

where $\overline{A}$, $\overline{B}$, and $\overline{C}$ are defined by (22). For convenience, we denote

$$\begin{aligned}\mathscr{H}(\alpha_i, \beta_i) &= X_c\left(\overline{A} - (\alpha_i + j\beta_i)\overline{B}\,\overline{C}\right) \\ &\quad + \left(\overline{A} - (\alpha_i + j\beta_i)\overline{B}\,\overline{C}\right)^* X_c \\ &\quad + \gamma_0^{-1}\left(X_c\overline{B}\,\overline{B}^* X_c + C_0 C_0^*\right) \\ &= H_0 + \alpha_i H_1 + j\beta_i H_2,\end{aligned} \tag{62}$$

where $H_0 = X_c\overline{A} + \overline{A}^* X_c + \gamma_0^{-1} X_c\overline{B}\,\overline{B}^* X_c + \gamma_0^{-1} C_0 C_0^*$, $H_1 = -X_c\overline{B}\,\overline{C} - \overline{C}^*\overline{B}^* X_c$, and $H_2 = -X_c\overline{B}\,\overline{C} + \overline{C}^*\overline{B}^* X_c$.

In fact, there must exist $s \in [0, 1]$, $r \in [0, 1]$ such that $\alpha_i = s\alpha_0 + (1 - s)\overline{\alpha}_0$, $\beta_i = r\beta_0 + (1 - r)\overline{\beta}_0$. When $r \geq s$,

$$\begin{aligned}\mathscr{H}(\alpha_i, \beta_i) &= H_0 + \left[s\alpha_0 + (1 - s)\overline{\alpha}_0\right] H_1 \\ &\quad + j\left[r\beta_0 + (1 - r)\overline{\beta}_0\right] H_2 \\ &= s\mathscr{H}(\alpha_0, \beta_0) + (r - s)\mathscr{H}(\overline{\alpha}_0, \beta_0) \\ &\quad + (1 - r)\mathscr{H}\left(\overline{\alpha}_0, \overline{\beta}_0\right) < 0.\end{aligned} \tag{63}$$

Similarly, when $s \geq r$, we have

$$\begin{aligned}\mathscr{H}(\alpha_i, \beta_i) &= r\mathscr{H}(\alpha_0, \beta_0) + (s - r)\mathscr{H}\left(\alpha_0, \overline{\beta}_0\right) \\ &\quad + (1 - s)\mathscr{H}\left(\overline{\alpha}_0, \overline{\beta}_0\right) < 0.\end{aligned} \tag{64}$$

This completes the proof. □

5. Numerical Example

An example is shown to verify the results obtained in the above section. The agent dynamics and the communication topology are given in Example 6, and the H_∞ performance index is chosen as $\gamma = 10$. According to the results presented in Section 4, we have

$$X = \begin{bmatrix} 1.8218 & -1.2978 \\ -1.2978 & 3.6435 \end{bmatrix}, \qquad Y = \begin{bmatrix} 1.2145 & -0.9109 \\ -0.9109 & 3.6435 \end{bmatrix},$$
$$X_c = \begin{bmatrix} 1.8218 & -1.2978 & -0.8688 & 0.2312 \\ -1.2978 & 3.6435 & 1.8148 & 0.1107 \\ -0.8688 & 1.8148 & 1.0000 & 0 \\ 0.2312 & 0.1107 & 0 & 1.0000 \end{bmatrix}. \tag{65}$$

Then, by solving the LMIs (54), we can get a feasible controller (40) with

$$\begin{aligned} A_k &= \begin{bmatrix} -7.0377 & -5.6811 \\ -0.6005 & -5.2415 \end{bmatrix}, \qquad B_k = \begin{bmatrix} -9.5464 \\ -0.5110 \end{bmatrix}, \\ C_k &= \begin{bmatrix} 3.4520 & 2.9461 \end{bmatrix}, \qquad D_k = 4.9523, \end{aligned} \tag{66}$$

and the H_∞ norm of system (26) is $\|G_{dz}(s)\|_\infty = 3.0707$. With the designed DOF control protocol, the disagreement states between x_i and x_1 without communication error $\mathbf{d}(t)$ are shown in Figure 3, $i = 2, 3, \ldots, 6$, which implies that the consensus can be reached when $\mathbf{d}(t) = 0$. The communication error $\mathbf{d}(t) \in \mathscr{L}_2[0, \infty)$ is supposed to be

$$\mathbf{d}(t) = \begin{cases} \theta \sin(t), & t \in [0, 40], \\ 0, & t > 40, \end{cases} \tag{67}$$

where $\theta = [1.11 \;\; 0.58 \;\; 1.48 \;\; 1.59 \;\; 2.12 \;\; 2.53 \;\; 0.42 \;\; 1.31 \;\; 4.0 \;\; 0.14]^T$. Under zero initial condition, the state trajectories of the six agents are depicted in Figure 4, and the corresponding energy trajectories of $\mathbf{d}(t)$ and $\mathbf{z}(t)$ are given in Figure 5.

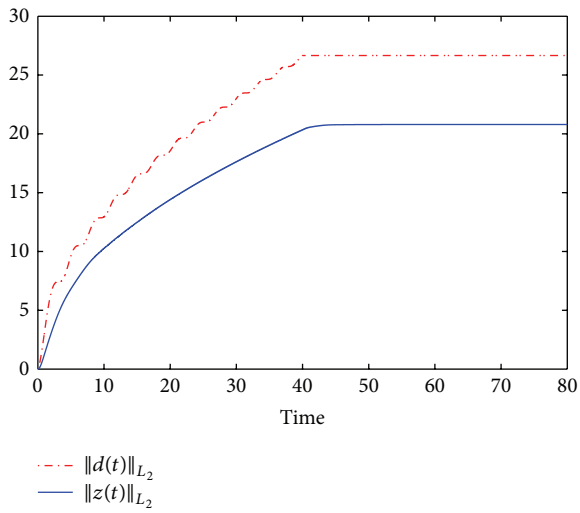

FIGURE 5: Energy trajectories of the controlled output $\mathbf{z}(t)$ and the communication error $\mathbf{d}(t)$.

It is noted obviously that $\|\mathbf{z}(t)\|_{\mathscr{L}_2} \leq \|\mathbf{d}(t)\|_{\mathscr{L}_2}$. Thus, the multiagent system with the given DOF controller can achieve the consensus with the given H_∞ performance, which validates the effectiveness of the proposed protocol and demonstrates the correctness of the obtained theoretical results.

6. Conclusions

This paper is devoted to the consensus problem for multiagent systems molded by linear time-invariant systems under fixed directed communication topologies and subject to communication errors in the transferred data. A dynamic output feedback control algorithm is proposed. The theoretical analysis shows that if there exists a common dynamic output feedback controller which can solve H_∞ problem for $N-1$ linear time-invariant systems of order n, then the consensus with a desired H_∞ level can be reached. By using H_∞ theory, a sufficient condition in terms of linear matrix inequalities is given to ensure the existence for such a controller. A procedure for the controller design is presented.

Acknowledgment

This work is supported by National Natural Science Foundation of China under Grants 90916003 and 61074026.

References

[1] J. A. Fax and R. M. Murray, "Information flow and cooperative control of vehicle formations," *IEEE Transactions on Automatic Control*, vol. 49, no. 9, pp. 1465–1476, 2004.

[2] R. Olfati-Saber, J. A. Fax, and R. M. Murray, "Consensus and cooperation in networked multi-agent systems," *Proceedings of the IEEE*, vol. 95, no. 1, pp. 215–233, 2007.

[3] W. Ren and R. W. Beard, *Distributed Consensus in Multi-Vehicle Cooperative Control: Theory and Applications*, Springer, London, UK, 2008.

[4] R. Olfati-Saber and R. M. Murray, "Consensus problems in networks of agents with switching topology and time-delays," *IEEE Transactions on Automatic Control*, vol. 49, no. 9, pp. 1520–1533, 2004.

[5] L. Moreau, "Stability of multiagent systems with time-dependent communication links," *IEEE Transactions on Automatic Control*, vol. 50, no. 2, pp. 169–182, 2005.

[6] K. L. Moore and D. Lucarelli, "Decentralized adaptive scheduling using consensus variables," *International Journal of Robust and Nonlinear Control*, vol. 17, no. 10-11, pp. 921–940, 2007.

[7] Z. Duan, J. Wang, G. Chen, and L. Huang, "Stability analysis and decentralized control of a class of complex dynamical networks," *Automatica*, vol. 44, no. 4, pp. 1028–1035, 2008.

[8] S. E. Tuna, "Conditions for synchronizability in arrays of coupled linear systems," *IEEE Transactions on Automatic Control*, vol. 54, no. 10, pp. 2416–2420, 2009.

[9] Z. Li, Z. Duan, G. Chen, and L. Huang, "Consensus of multiagent systems and synchronization of complex networks: a unified viewpoint," *IEEE Transactions on Circuits and Systems I*, vol. 57, no. 1, pp. 213–224, 2010.

[10] C.-Q. Ma and J.-F. Zhang, "Necessary and sufficient conditions for consensusability of linear multi-agent systems," *IEEE Transactions on Automatic Control*, vol. 55, no. 5, pp. 1263–1268, 2010.

[11] Z. Li, Z. Duan, and G. Chen, "Dynamic consensus of linear multi-agent systems," *IET Control Theory & Applications*, vol. 5, no. 1, pp. 19–28, 2011.

[12] W. Yu, G. Chen, W. Ren, J. Kurths, and W. X. Zheng, "Distributed higher order consensus protocols in multiagent dynamical systems," *IEEE Transactions on Circuits and Systems I*, vol. 58, no. 8, pp. 1924–1932, 2011.

[13] W. Yu, W. X. Zheng, G. Chen, W. Ren, and J. Cao, "Second-order consensus in multi-agent dynamical systems with sampled position data," *Automatica*, vol. 47, no. 7, pp. 1496–1503, 2011.

[14] G. Wen, Z. Duan, W. Yu, and G. Chen, "Consensus in multi-agent systems with communication constraints," *International Journal of Robust and Nonlinear Control*, vol. 22, no. 2, pp. 170–182, 2012.

[15] M. Arcak, "Passivity as a design tool for group coordination," *IEEE Transactions on Automatic Control*, vol. 52, no. 8, pp. 1380–1390, 2007.

[16] W. Yu, G. Chen, and M. Cao, "Consensus in directed networks of agents with nonlinear dynamics," *IEEE Transactions on Automatic Control*, vol. 56, no. 6, pp. 1436–1441, 2011.

[17] L. Scardovi and R. Sepulchre, "Synchronization in networks of identical linear systems," *Automatica*, vol. 45, no. 11, pp. 2557–2562, 2009.

[18] J. H. Seo, H. Shim, and J. Back, "Consensus of high-order linear systems using dynamic output feedback compensator: low gain approach," *Automatica*, vol. 45, no. 11, pp. 2659–2664, 2009.

[19] Y. Liu and Y. Jia, "H_∞ consensus control of multi-agent systems with switching topology: a dynamic output feedback protocol," *International Journal of Control*, vol. 83, no. 3, pp. 527–537, 2010.

[20] H. Kim, H. Shim, and J. H. Seo, "Output consensus of heterogeneous uncertain linear multi-agent systems," *IEEE Transactions on Automatic Control*, vol. 56, no. 1, pp. 200–206, 2011.

[21] U. Münz, A. Papachristodoulou, and F. Allgöwer, "Robust consensus controller design for nonlinear relative degree two multi-agent systems with communication constraints," *IEEE Transactions on Automatic Control*, vol. 56, no. 1, pp. 145–151, 2011.

[22] J. Wang, Y. Tan, and I. Mareels, "Robustness analysis of leader-follower consensus," *Journal of Systems Science & Complexity*, vol. 22, no. 2, pp. 186–206, 2009.

[23] X. Yang, J. Wang, and Y. Tan, "Robustness analysis of leader-follower consensus for multi-agent systems characterized by double integrators," *Systems & Control Letters*, vol. 61, no. 11, pp. 1103–1115, 2012.

[24] P. Lin, Y. Jia, and L. Li, "Distributed robust H_∞ consensus control in directed networks of agents with time-delay," *Systems & Control Letters*, vol. 57, no. 8, pp. 643–653, 2008.

[25] Z. Li, Z. Duan, and G. Chen, "On H_∞ and H_2 performance regions of multi-agent systems," *Automatica*, vol. 47, no. 4, pp. 797–803, 2011.

[26] G. Wen, Z. Duan, Z. Li, and G. Chen, "Consensus and its $\mathscr{L}_2$-gain performance of multi-agent systems with intermittent information transmissions," *International Journal of Control*, vol. 85, no. 4, pp. 384–396, 2012.

[27] Y. Zhao, Z. Duan, G. Wen, and G. Chen, "Distributed H_∞ consensus of multi-agent systems: a performance region-based approach," *International Journal of Control*, vol. 85, no. 3, pp. 332–341, 2012.

[28] H. Zhang and F. L. Lewis, "Adaptive cooperative tracking control of higher-order nonlinear systems with unknown dynamics," *Automatica*, vol. 48, no. 7, pp. 1432–1439, 2012.

[29] G. E. Dullerud and F. G. Paganini, *A Course in Robust Control Theory: A Convex Approach*, Springer, New York, NY, USA, 2000.

[30] K. M. Zhou and J. C. Doyle, *Essentials of Robust Control*, Prentice Hall, New York, NY, USA, 1998.

Hindawi Publishing Corporation
Mathematical Problems in Engineering
Volume 2013, Article ID 983637, 11 pages
http://dx.doi.org/10.1155/2013/983637

Research Article

A Distributed Flow Rate Control Algorithm for Networked Agent System with Multiple Coding Rates to Optimize Multimedia Data Transmission

Shuai Zeng, Lemin Li, and Dan Liao

School of Communication and Information Engineering, University of Electronic Science and Technology of China, Chengdu 611731, China

Correspondence should be addressed to Shuai Zeng; maillinger@gmail.com

Received 9 May 2013; Accepted 12 May 2013

Academic Editor: Guanghui Wen

With the development of wireless technologies, mobile communication applies more and more extensively in the various walks of life. The social network of both fixed and mobile users can be seen as networked agent system. At present, kinds of devices and access network technology are widely used. Different users in this networked agent system may need different coding rates multimedia data due to their heterogeneous demand. This paper proposes a distributed flow rate control algorithm to optimize multimedia data transmission of the networked agent system with the coexisting various coding rates. In this proposed algorithm, transmission path and upload bandwidth of different coding rate data between source node, fixed and mobile nodes are appropriately arranged and controlled. On the one hand, this algorithm can provide user nodes with differentiated coding rate data and corresponding flow rate. On the other hand, it makes the different coding rate data and user nodes networked, which realizes the sharing of upload bandwidth of user nodes which require different coding rate data. The study conducts mathematical modeling on the proposed algorithm and compares the system that adopts the proposed algorithm with the existing system based on the simulation experiment and mathematical analysis. The results show that the system that adopts the proposed algorithm achieves higher upload bandwidth utilization of user nodes and lower upload bandwidth consumption of source node.

1. Introduction

The considerable development of communication technologies has provided conditions for the application and popularization of mobile devices. In recent years, with diversification of access network, especially with the popularity of access technologies such as Wireless Local Area Network (WIFI) and the third generation mobile communication (3G), the scale of the mobile Internet rapidly expands [1, 2]. Compared with traditional terminal of PC-based user (fixed user), kinds of mobile devices such as smart phones, personal assistants, and tablet PCs begin to increasingly enter the Internet. At present, mobile users (as well as fixed users) more often use their terminals as enhanced application support platform to join some electronic social network, for example, content distribution tools, peer-to-peer multimedia players, Twitter clients, or web browsers [3]. These distributed and self-organizing networks can be seen as networked agent systems [4–8]. We are interested in the optimization of multimedia data transmission and bandwidth utilization in this kind of system [9–13].

Traditional multimedia data transmission or streaming system does not consider user access network morphology or the differences of terminal device but often simply ignores the existence of the user diversification and only provides multimedia data with a single coding rate data for users; in order to overcome this weakness, the current solution is to divide the system into multiple independent subsystems, with each subsystem covering part of the users and providing differentiated coding rate data for each part of the users. For example, the Cbox network television system [14] of CCTV provides two types of signals—SD and HD. The coding rate

of SD is 380 kbps, which is major for mobile users. And the coding rate of HD is 500 kbps, which is major for fixed users. Users can choose to watch based on access network morphologies or terminal conditions. From a technical point of view, the advantage of current solution is that the system provides different coding rate multimedia data for different users to meet individual needs of the user terminal and access network. However, because various subsystems are independent of each other in the design, the upload bandwidth among subsystem users cannot be shared, particularly that the upload, storage, and computing resources of user nodes with high performance and high bandwidth cannot be used by the system effectively.

This paper presents a distributed flow rate control algorithm for the mentioned networked agent system with coexisting multiple coding rates. On the one hand, it can provide distributed differentiated coding rate multimedia data to meet the different user needs. On the other hand, it can share and effectively use the user nodes upload bandwidth resources to reduce the upload bandwidth consumption of source node. The proposed algorithm can be part of agent-based framework and software infrastructure that improves the multimedia data transmission performance of the system.

In multimedia data transmission or streaming system studies, it is usually assumed that the download speed when user nodes acquire data from the system is not smaller than some rate (minimum flow rate), which means that the normal reception and play of multimedia data can be achieved [15–28]. The so-called flow rate control algorithm is a data transfer algorithm to satisfy the minimum flow rate of each user node [15]. Taking the application layer multicast form streaming system as the background, this paper presents a flow rate control algorithm of calculating minimum consumption of source node upload bandwidth required to support a certain flow rate. This paper presents the relationship among the tree depth, source node upload bandwidth consumption, and user nodes flow rate under this algorithm; [16] proposed a flow rate control algorithm of the streaming system to maximize the receiver flow rate under the conditions of a given source node upload bandwidth. It also analyzes the mathematical relationship between the source node upload bandwidth consumption and flow rate of a typical peer-to-peer streaming system; [19] taking the multimedia data transmission under the edge nodes constraints as the background, this paper analyzes the relationship between source node upload bandwidth consumption and user nodes flow rate in the model. In [20], it discusses the minimum source node upload bandwidth consumption and the maximum flow rate of user nodes of a given flow rate provided by streaming media system in the background of various random graph models and different connectivity constraints; [21] addresses the issue of rate allocation of multiple simultaneous multimedia data transmission sharing heterogeneous access networks; [22, 23] studies multimedia data transmission based on multichannel collaboration strategy and uses it as the background to study the corresponding flow rate control algorithm, and investigates the relationship between the source node upload bandwidth consumption and maximum user node flow rate under such systems and algorithms. In [24, 25], it compares several popular designs in the background of multichannel collaboration streaming media system and analyzes the minimum source node upload bandwidth consumption realized by each flow rate control algorithm and the performance differences and relationship of each system under the same conditions; [26] proposed a layer-based rate control algorithm for transporting multimedia data over multiple wireless links with heterogeneous reliability; [27] proposed an algorithm of joint path selection and source rate allocation to optimize the media quality on multipath networks streaming; [28] proposes a flow rate control algorithm with the background of multimedia data transmission based on network coding strategy and discusses the quantitative relationship between the system source node upload bandwidth consumption and user nodes flow rate under the proposed algorithm.

The difference between the proposed flow rate control algorithm in this paper and the previous studies lies in that previous algorithms treat the different coding rate data and the users as multiple independent subsystems, which can only provide multimedia data and flow rate support for one user needs in one subsystem; however, the proposed algorithm in this paper makes the different coding rate data and user nodes networked and makes use of the fixed nodes to provide coding rate conversion services for the mobile nodes and properly arranges the data transfer process before and after the coding rate conversion to realize the system to provide distributed differentiated coding rate data and desired flow rate for the needs of different users. The proposed algorithm in this paper more meets the multimedia data transmission in networked agent system with multiple coding rates. For example, there is a user class existing in the system to watch the program with PC (demanding for multimedia data with higher coding rate and larger minimum flow rate) and other two groups of users with different types of mobile phone models (demand for multimedia data with lower coding rate and smaller minimum flow rate). The current design establishes three independent subsystems for the three types of users to provide data and flow rate support, which cannot share the upload bandwidth among different users. However, the algorithm presented in this paper puts the three in the same networked system and through PC users provides coding rate conversion services for mobile users and appropriately arranges path and bandwidth for distributed multimedia data transmission, so that it can provide the corresponding data and flow rate support for the three types of users, and the efficient multimedia data transmission can be achieved. This paper conducts mathematical modeling and simulation for the proposed algorithm and demonstrates that, compared with the current design, the proposed algorithm has higher upload bandwidth utilization and lower source node upload bandwidth consumption.

The following part of this paper is organized as follows. Section 2 describes the background system of proposed algorithm; in Section 3, the system model is established, and

the algorithm is proposed; the performance comparison is given in Section 4; the final part is about the summary.

2. Systematic Overview

As shown in Figure 1(a), in the system that adopts the application of the proposed algorithm, the user nodes are divided into two major categories—fixed nodes and mobile nodes (mobile nodes can be divided into many subclasses). Fixed nodes mainly refer to the PC accessed to the Internet via a wired connection. Fixed nodes can be seen to possess larger upload bandwidth and higher computing power, with a larger viewing screen, more comprehensive multimedia player software, and large terminal with higher demand for multimedia quality. Fixed nodes in the system can be used as transcoding user nodes (i.e., it can convert the received multimedia data to a lower coding rate) [29–35]. In contrast, the mobile nodes mainly refer to wireless access equipment represented by mobile phone, Personal Digital Assistant (PDA), tablet PC, and other terminals. The mobile nodes are seen to relatively lack computing power with only limited access bandwidth and are weaker terminals in the performance and demand such as screen size, quality, and color depth. In system, mobile nodes are regarded as nontranscoding user nodes.

Intuitively, the mobile nodes lack conditions and are not necessary to receive multimedia data of the same coding rate of the fixed nodes. This on the one hand increases the bandwidth consumption and on the other hand causes the difficulties for the mobile nodes to receive and play. The current designs integrate fixed nodes and various mobile nodes into a lot of independent subsystems and, respectively, provide them with multimedia data of different coding rates. Different from this, the system that adopts the proposed algorithm in this paper integrates terminal with different demands for coding rate data into the same transmission network. The system uses computing resources and upload bandwidth of the fixed nodes to provide coding rate data that can be used by mobile nodes to receive and display. In Figure 1(a), the thicker line and the thinner line, respectively, signify that the different coding rate data demanded by fixed users and each subclass mobile users are simultaneously supported in the system; Figure 1(b) illustrates the coding rate conversion and multimedia sharing process: first, the source node provides a higher coding rate multimedia data for fixed nodes (thicker arrow in the figure). Then, the acquired data are shared among fixed nodes, and the data reception is completed. Second, the rest fixed nodes of the upload bandwidth convert the coding rate of the acquired data to the desired coding rate data of each subclass of mobile nodes and send it to the mobile nodes (thinner arrows in the figure). Meanwhile, if the upload bandwidth of fixed nodes is inadequate, the mobile nodes can also acquire the required data from the source node. Finally, the same subclass mobile nodes share the acquired data among each other and complete the data reception. The question is how to control and obtain proper receiving flow rate of different user nodes with distributed supply of upload bandwidth.

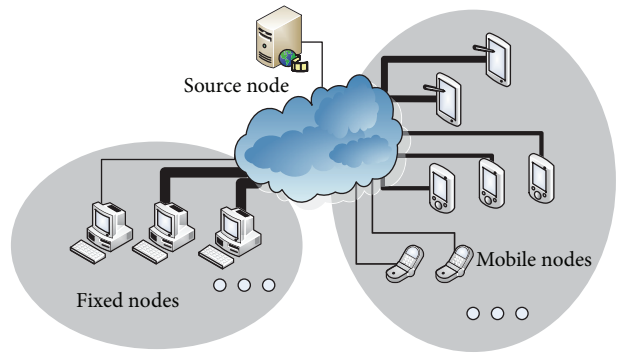

(a) Different coding rate data can be supported in the system

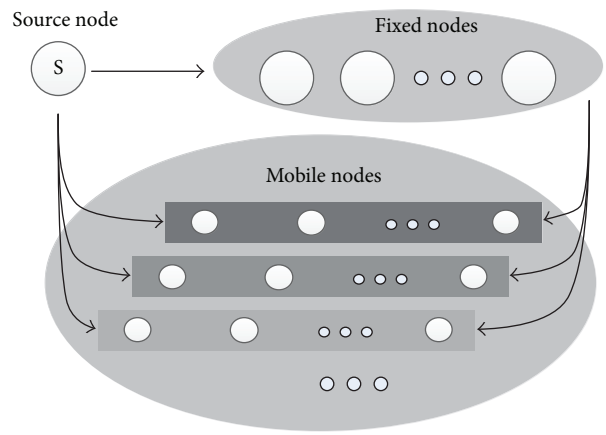

(b) Coding rate conversion and sharing process of multimedia data

Figure 1: Systematic structure and data transmission.

3. Mathematical Modeling and Algorithm Design

3.1. Initial Settings. Make some initial settings before modeling.

Firstly, each coding rate data corresponds to a minimum flow rate, and the sum of the user node reception rate of receiving a certain coding rate data is not less than the corresponding minimum flow rate, namely, it can play normally [15–28].

Secondly, discretionary communication is available among the nodes, and the upload bandwidth is the only restriction for data transmission [15–17, 28]. As mentioned previously, the proposed algorithm uses the computational capabilities of fixed nodes to provide coding rate conversion services for the mobile nodes. The algorithm improves the upload bandwidth utilization at the cost of the procedures and complexity of coding rate conversion. This paper only discusses the issue of data transmission, which does not limit specific multimedia codec algorithm or involves the discussion of the multimedia codec algorithm itself. It assumes that relative to the upload bandwidth, the coding rate conversion of data in the fixed nodes does not constitute the system bottleneck.

Thirdly, the coding rate conversion services can only come from the transcoding nodes (source node and fixed

Table 1: Mathematical symbols used in modeling and algorithm.

Symbols	Explanation
s	Source node.
p_i^f	The ith fixed nodes.
p_i^m	The ith mobile nodes.
$\mathbf{P}_f$	The set of fixed nodes.
$\mathbf{P}_m$	The set of mobile nodes.
n_f	Number of fixed nodes.
n_m	Number of fixed nodes.
r_f	Minimum flow rate of fixed node.
r_m	Minimum flow rate of mobile node.
u_i^f	Upload bandwidth of the ith fixed node.
u_i^m	Upload bandwidth of the ith mobile node.
$\overline{u_f}$	Average upload bandwidth of fixed nodes.
$\overline{u_m}$	Average upload bandwidth of mobile nodes.
$\mathrm{u}(\cdot)$	Function of upload bandwidth.
u_s	Design size of source node upload bandwidth.
$u_i'^f$	Remaining upload bandwidth of p_i^f after meeting the flow rate needs of $\mathbf{P}_f$.
u_s'	Remaining upload bandwidth of s after meeting the flow rate needs of $\mathbf{P}_f$.
u_{all}'	All the remaining upload bandwidth of the system after meeting the flow rate needs of $\mathbf{P}_f$.
s_{oi}^f	Multimedia data flow rate size that s sends to p_i^f.
s_{oi}^m	Multimedia data flow rate size that s transcodes for p_i^m and sends to p_i^m.
s_{ki}^t	Multimedia data flow rate size that p_k^f transcodes for p_i^m and sends to p_i^m.
tr_i^f	Total flow rate of multimedia data p_i^f received.
tr_i^m	Total flow rate of multimedia data p_i^m received.

nodes). Nontranscoding nodes can upload existing data but cannot convert the coding rate. Specifically, the sources of fixed nodes data may have two: the source node and other fixed nodes; the sources of mobile nodes data may have three: the source node, the fixed nodes, and other mobile nodes in the same subclass.

3.2. Mathematical Symbols. The main mathematical symbols used in modeling and algorithm are arranged into Table 1, and the symbols in the table will be further illustrated in subsequent reference.

3.3. Analysis and Modeling. This section will first analyze the flow rate control with only one mobile node subclass in the system. The complete flow rate algorithm can meet the case of multiple mobile nodes subclasses simply based on multiple cycles.

Set n_f as the number of the fixed nodes and n_m as the number of the mobile nodes (assuming that there is only one subclass). p_i^f $(i = 1, \ldots, n_f)$ denotes the ith fixed nodes, p_i^m $(i = 1, \ldots, n_m)$ the ith mobile nodes, s the source node, $\mathbf{P}_f$ the collection of fixed nodes, and $\mathbf{P}_m$ the collection of the mobile nodes; thereby,

$$\begin{aligned} \mathbf{P}_f &= \left\{p_i^f\right\}, \quad \left(i = 1, \ldots, n_f\right), \\ \mathbf{P}_m &= \left\{p_i^m\right\}, \quad \left(i = 1, \ldots, n_m\right). \end{aligned} \tag{1}$$

r_f denotes the minimum flow rate that supports the normal play of multimedia data at the fixed nodes. r_m denotes the minimum flow rate that supports the normal play of multimedia data at the mobile nodes. u_i^f $(i = 1, \ldots, n_f)$ denotes the upload bandwidth of the ith fixed node. u_i^m $(i = 1, \ldots, n_m)$ denotes the upload bandwidth of the ith mobile node. u_s means the size of upload bandwidth on the source node which makes all nodes play normally.

We first take $\mathbf{P}_f$ into consideration.

As for $\mathbf{P}_f$, the source of the multimedia data is s; thereby,

$$u_s \geq r_f. \tag{2}$$

Additionally, as for $\mathbf{P}_f$, the flow rate sum cannot be greater than the sum of all the upload bandwidth. For any node in $\mathbf{P}_f$ and other nodes with s as its multimedia data sources of s or other nodes in $\mathbf{P}_f$,

$$u_s + \sum_{\mathbf{P}_f} u_i^f \geq n_f r_f. \tag{3}$$

Function $\mathrm{u}(\cdot)$ denotes the result of upload bandwidth, for example, $\mathrm{u}(\mathbf{P}_f) = \sum_{\mathbf{P}_f} u_i^f = \sum_{i=1}^{n_f} u_i^f$ and $\overline{u_f}$ denote the average upload bandwidth of all the fixed nodes, $\overline{u_m}$ denotes the average upload bandwidth of all the mobile nodes

$$\begin{aligned} \overline{u_f} &= \frac{\mathrm{u}\left(\mathbf{P}_f\right)}{n_f} = \frac{\sum_{i=1}^{n_f} u_i^f}{n_f}, \\ \overline{u_m} &= \frac{\mathrm{u}\left(\mathbf{P}_m\right)}{n_m} = \frac{\sum_{i=1}^{n_m} u_i^m}{n_m}. \end{aligned} \tag{4}$$

(3) is rewritten as

$$u_s + n_f\left(\overline{u_f} - r_f\right) \geq 0. \tag{5}$$

Then we consider $\mathbf{P}_m$.

For $\mathbf{P}_m$, the multimedia data can be derived from s or the coding rate conversion of the data worked out by $\mathbf{P}_f$. The flow rate requirements should be first met if one succeeds in transcoding and uploading the $\mathbf{P}_f$. So the upload bandwidth got by the $\mathbf{P}_m$ from $\mathbf{P}_f$ is the remaining part after satisfying its own needs of $\mathbf{P}_f$; namely, the most upload bandwidth $\mathbf{P}_f$ can provide for $\mathbf{P}_m$ is $n_f(\overline{u_f} - r_f)$, and

$$u_s + n_f\left(\overline{u_f} - r_f\right) \geq r_m. \tag{6}$$

In addition, from the perspective of the entire system, the total uploads bandwidth must be greater than or equal to the total flow rate; thereby,

$$u_s + \sum_{\mathbf{P}_f} u_i^f + \sum_{\mathbf{P}_m} u_i^m \geq n_f r_f + n_m r_m. \tag{7}$$

Namely,

$$u_s + n_f\left(\overline{u_f} - r_f\right) + n_m\left(\overline{u_m} - r_m\right) \geq 0. \tag{8}$$

Equations (2), (5), (6), and (8) are organized as

$$\begin{aligned} u_s &\geq r_f, \\ u_s &\geq r_m + n_f\left(r_f - \overline{u_f}\right), \\ u_s &\geq n_f\left(r_f - \overline{u_f}\right) + n_m\left(r_m - \overline{u_m}\right). \end{aligned} \tag{9}$$

Set

$$\begin{aligned} \mathrm{MAX} = \ & \max\left(r_f, r_m + n_f\left(r_f - \overline{u_f}\right),\right. \\ & \left. n_f\left(r_f - \overline{u_f}\right) + n_m\left(r_m - \overline{u_m}\right)\right). \end{aligned} \tag{10}$$

Thereby,

$$u_s \geq \mathrm{MAX}. \tag{11}$$

Equations (10) and (11) show the consumption limit of upload bandwidth on the source node, when the system can support all mobile and fixed nodes to playback normally. Now we see whether we can design a flow rate control algorithm to approach as close as possible or even achieve this lower limit.

Set

$$u_s = \mathrm{MAX}. \tag{12}$$

s_{oi}^f $(i = 1, \ldots, n_f)$ denotes the flow rate of the multimedia data from the source node to p_i^f. s_{oi}^m $(i = 1, \ldots, n_m)$ denotes the flow rate of the multimedia data from the source node to p_i^m. s_{ki}^t $(i = 1, \ldots, n_m)$ denotes the flow rate of the multimedia data transcoded and transmitted by p_k^f for p_i^m. tr_i^f $(i = 1, \ldots, n_f)$ denotes the total flow rate of the multimedia data received by p_i^f. tr_i^m $(i = 1, \ldots, n_m)$ denotes the total flow rate of the multimedia data received by p_i^m.

First we consider $\mathbf{P}_f$.

When $r_f \geq n_f(r_f - \overline{u_f})$, namely, $r_f \leq n_f\overline{u_f}/(n_f - 1)$, s transmits the multimedia data for p_i^f $(i = 1, \ldots, n_f)$, and the flow rate is arranged as

$$s_{oi}^f = \frac{u_i^f r_f}{\mathrm{u}\left(\mathbf{P}_f\right)} = \frac{u_i^f r_f}{n_f\overline{u_f}}. \tag{13}$$

Notice that according to (12), $\sum_{\mathbf{P}_f} s_{oi}^f = r_f \leq u_s$, so s can achieve the transmitting with enough upload bandwidth, as

$$\begin{aligned} \left(n_f - 1\right) s_{oi}^f &= \frac{\left(n_f - 1\right) u_i^f}{n_f\overline{u_f}} \cdot r_f \\ &\leq \frac{\left(n_f - 1\right) u_i^f}{n_f\overline{u_f}} \cdot \frac{n_f\overline{u_f}}{\left(n_f - 1\right)} = u_i^f. \end{aligned} \tag{14}$$

p_i^f has enough upload bandwidth which can transmit the data in s_{oi}^f to other fixed nodes with the same flow rate; thereby p_i^f gets the total flow rate

$$\mathrm{tr}_i^f = s_{oi}^f + \sum_{\mathbf{P}_f}^{j \neq i} s_{oj}^f = r_f. \tag{15}$$

Thereby, p_i^f $(i = 1, \ldots, n_f)$ will get enough flow rate to ensure the normal play of the media.

When $r_f < n_f(r_f - \overline{u_f})$, s transmits the multimedia data twice for p_i^f $(i = 1, \ldots, n_f)$. And the flow rate arrangement of the first time (denoted by s_{oi}^{f1}) is

$$s_{oi}^{f1} = \frac{u_i^f}{n_f - 1}. \tag{16}$$

The second time is (denoted by s_{oi}^{f2})

$$s_{oi}^{f2} = r_f - \frac{\mathrm{u}\left(\mathbf{P}_f\right)}{n_f - 1} = r_f - \frac{n_f\overline{u_f}}{n_f - 1}. \tag{17}$$

According to (12), $\sum_{\mathbf{P}_f} s_{oi}^{f1} + \sum_{\mathbf{P}_f} s_{oi}^{f2} = n_f(r_f - \overline{u_f}) \leq u_s$; thereby, s has the enough upload bandwidth to achieve the previous transmitting. As

$$\left(n_f - 1\right) s_{oi}^{f1} = \left(n_f - 1\right) \cdot \frac{u_i^f}{n_f - 1} = u_i^f. \tag{18}$$

p_i^f has enough upload bandwidth which can transmit the data in s_{oi}^{f1} to other fixed nodes with the same flow rate. Then the total flow rate of p_i^f is

$$\mathrm{tr}_i^f = s_{oi}^{f1} + s_{oi}^{f2} + \sum_{\mathbf{P}_f}^{j \neq i} s_{oj}^{f1} = r_f. \tag{19}$$

Thereby, p_i^f $(i = 1, \ldots, n_f)$ will get enough flow rate to ensure the normal play of the media.

In conclusion, through the flow rate arrangement in the transmitting of the multimedia data, whether it is $r_f \geq n_f(r_f - \overline{u_f})$ or $r_f < n_f(r_f - \overline{u_f})$, all fixed nodes will play normally.

Then consider $\mathbf{P}_m$.

u_s' denotes the remaining upload bandwidth of s. $u_i'^f$ denotes the remaining upload bandwidth of p_i^f. u_{all}' denotes the remaining upload bandwidth of the system. Thereby,

$$u_{\mathrm{all}}' = u_s' + \sum_{\mathbf{P}_f} u_i'^f = u_s + n_f\left(\overline{u_f} - r_f\right). \tag{20}$$

Considering (12),

$$u_{\mathrm{all}}' \geq r_m. \tag{21}$$

When $r_m \geq n_m(r_m - \overline{u_m})$, namely, $r_m \leq n_m\overline{u_m}/(n_m - 1)$, s transmits the multimedia data for p_i^m $(i = 1, \ldots, n_m)$, and the flow rate arrangement is

$$\begin{aligned} s_{oi}^m &= \frac{u_i^m}{\mathrm{u}(\mathbf{P}_m)} \cdot \frac{u_s'}{u_{\mathrm{all}}'} \cdot r_m \\ &= \frac{u_i^m}{n_m\overline{u_m}} \cdot \frac{u_s'}{u_s + n_f\left(\overline{u_f} - r_f\right)} \cdot r_m. \end{aligned} \tag{22}$$

p_k^f $(k = 1, \ldots, n_f)$ transcodes and transmits the multimedia data for p_i^m $(i = 1, \ldots, n_m)$, and the flow rate is arranged as

$$\begin{aligned} s_{ki}^t &= \frac{u_i^m}{\mathrm{u}(\mathbf{P}_m)} \cdot \frac{u_k'^f}{u_{\mathrm{all}}'} \cdot r_m \\ &= \frac{u_i^m}{n_m\overline{u_m}} \cdot \frac{u_k'^f}{u_s + n_f\left(\overline{u_f} - r_f\right)} \cdot r_m. \end{aligned} \tag{23}$$

Notice that as $\sum_{\mathbf{P}_m} s_{oi}^m = u_s' \cdot r_m/u_{\mathrm{all}}'$, according to (21), we can get $\sum_{\mathbf{P}_m} s_{oi}^m \leq u_s'$, so s has enough upload bandwidth to achieve the previous transmitting. And as $\sum_{\mathbf{P}_m} s_{ki}^t = u_k'^f \cdot r_m/u_{\mathrm{all}}'$, according to (21), we can get $\sum_{\mathbf{P}_m} s_{ki}^t \leq u_k'^f$, so p_k^f $(k = 1, \ldots, n_f)$ has enough upload bandwidth to achieve the previous transmitting. Now the flow rate attained by p_i^m $(i = 1, \ldots, n_m)$ is

$$s_{oi}^m + \sum_{k=1}^{n_f} s_{ki}^t = \frac{u_i^m r_m}{\mathrm{u}(\mathbf{P}_m)} = \frac{u_i^m r_m}{n_m\overline{u_m}}. \tag{24}$$

As

$$\begin{aligned} (n_m - 1) \cdot \left(s_{oi}^m + \sum_{k=1}^{n_f} s_{ki}^t\right) &= \frac{(n_m - 1)\, u_i^m}{n_m\overline{u_m}} \cdot r_m \\ &\leq \frac{(n_m - 1)\, u_i^m}{n_m\overline{u_m}} \cdot \frac{n_m\overline{u_m}}{n_m - 1} = u_i^m. \end{aligned} \tag{25}$$

So p_i^m has enough upload bandwidth which can transmit the data in $s_{oi}^m + \sum_{k=1}^{n_f} s_{ki}^t$ to other fixed nodes with the same flow rate. Then the total flow rate of p_i^m is

$$\mathrm{tr}_i^m = s_{oi}^m + \sum_{k=1}^{n_f} s_{ki}^t + \sum_{\mathbf{P}_m}^{j \neq i} \left(s_{oj}^m + \sum_{k=1}^{n_f} s_{kj}^t\right) = r_m. \tag{26}$$

And p_i^m $(i = 1, \ldots, n_m)$ will get enough flow rate to ensure the normal play of the media.

When $r_m < n_m(r_m - \overline{u_m})$, s transmits the multimedia data for p_i^m $(i = 1, \ldots, n_m)$. And the flow rate arrangement of the first time (s_{oi}^{m1}) is

$$s_{oi}^{m1} = \frac{u_i^m}{n_m - 1} \cdot \frac{u_s'}{u_{\mathrm{all}}'} = \frac{u_i^m}{n_m - 1} \cdot \frac{u_s'}{u_s + n_f\left(\overline{u_f} - r_f\right)}. \tag{27}$$

And the second time (s_{oi}^{m2}) is

$$\begin{aligned} s_{oi}^{m2} &= \left(r_m - \frac{\mathrm{u}(\mathbf{P}_m)}{n_m - 1}\right)\left(\frac{u_s'}{u_{\mathrm{all}}'}\right) \\ &= \left(r_m - \frac{n_m\overline{u_m}}{n_m - 1}\right)\left(\frac{u_s'}{u_s + n_f\left(\overline{u_f} - r_f\right)}\right). \end{aligned} \tag{28}$$

p_k^f $(k = 1, \ldots, n_f)$ transcodes and transmits multimedia data for p_i^m $(i = 1, \ldots, n_m)$, and the flow rate arrangement of the first time (s_{ki}^{t1}) is

$$s_{ki}^{t1} = \frac{u_i^m}{n_m - 1} \cdot \frac{u_k'^f}{u_{\mathrm{all}}'} = \frac{u_i^m}{n_m - 1} \cdot \frac{u_k'^f}{u_s + n_f\left(\overline{u_f} - r_f\right)}. \tag{29}$$

And the second time (s_{ki}^{t2}) is

$$\begin{aligned} s_{ki}^{t2} &= \left(r_m - \frac{\mathrm{u}(\mathbf{P}_m)}{n_m - 1}\right)\left(\frac{u_k'^f}{u_{\mathrm{all}}'}\right) \\ &= \left(r_m - \frac{n_m\overline{u_m}}{n_m - 1}\right)\left(\frac{u_k'^f}{u_s + n_f\left(\overline{u_f} - r_f\right)}\right). \end{aligned} \tag{30}$$

Notice that as $\sum_{\mathbf{P}_m} s_{oi}^{m1} + \sum_{\mathbf{P}_m} s_{oi}^{m2} = n_m(r_m - \overline{u_m})/(u_s + n_f(\overline{u_f} - r_f)) \cdot u_s'$, according to (12), we can get $\sum_{\mathbf{P}_m} s_{oi}^{m1} + \sum_{\mathbf{P}_m} s_{oi}^{m2} \leq u_s'$, so s has enough upload bandwidth to achieve the previous transmitting, and as $\sum_{\mathbf{P}_m} s_{ki}^{t1} + \sum_{\mathbf{P}_m} s_{ki}^{t2} = n_m(r_m - \overline{u_m})/(u_s + n_f(\overline{u_f} - r_f)) \cdot u_k'^f$, according to (12), we can get $\sum_{\mathbf{P}_m} s_{ki}^{t1} + \sum_{\mathbf{P}_m} s_{ki}^{t2} \leq u_k'^f$, p_k^f $(k = 1, \ldots, n_f)$ has enough upload bandwidth to achieve the previous transmitting.

Moreover, as

$$(n_m - 1) \cdot \left(s_{oi}^{m1} + \sum_{k=1}^{n_f} s_{kj}^{t1}\right) = (n_m - 1) \cdot \frac{u_i^m}{n_m - 1} = u_i^m. \tag{31}$$

p_i^m has enough upload bandwidth which can transmit the data in $s_{oi}^{m1} + \sum_{k=1}^{n_f} s_{kj}^{t1}$ to other fixed nodes with the same flow rate. Then the total flow rate of p_i^m is

$$\begin{aligned} \mathrm{tr}_i^m &= s_{oi}^{m1} + s_{oi}^{m2} + \sum_{k=1}^{n_f} s_{ki}^{t1} + \sum_{k=1}^{n_f} s_{ki}^{t2} \\ &\quad + \sum_{\mathbf{P}_m}^{j \neq i} \left(s_{oj}^{m1} + \sum_{k=1}^{n_f} s_{kj}^{t1}\right) = r_m. \end{aligned} \tag{32}$$

Therefore, p_i^m $(i = 1, \ldots, n_m)$ will get enough flow rate to ensure the normal play of the media.

In conclusion, through the flow rate arrangement, whether it is $r_m \geq n_m(r_m - \overline{u_m})$ or $r_m < n_m(r_m - \overline{u_m})$, all mobile nodes will play normally.

Finally, according to the previous design, when u_s = MAX, the system can make all mobile and fixed nodes get the required coding rate of data and the flow rate.

3.4. Flow Rate Control. The previous analysis has attained a flow rate control algorithm for one mobile node subclass, and for multiple subclasses we should only do it for several cycles. Assume that the number of the fixed node is n_f, and there are l mobile node subclasses. The number of the node is n_i ($i = 1,\ldots,l$), and p_i^f ($i = 1,\ldots,n_f$) denotes the ith fixed node. p_{ij}^m ($i = 1,\ldots,l$; $j = 1,\ldots,n_i$) denotes the jth mobile node of the ith subclass, and s denotes the source node. r_f denotes the minimum flow rate which makes the multimedia data required by the fixed node normally broadcast. r_i ($i = 1,\ldots,l$) denotes the minimum flow rate which makes the multimedia data required by the ith subclass node normally broadcast. u_i^f ($i = 1,\ldots,n_f$) denotes the upload bandwidth of the ith fixed node. u_{ij}^m ($i = 1,\ldots,l$; $j = 1,\ldots,n_i$) denotes the upload bandwidth of the ith subclass node. u_s denotes the size of the upload bandwidth of the source node. $\overline{u_f}$ denotes the average upload bandwidth of all the fixed nodes. And tr_i^f ($i = 1,\ldots,n_f$) denotes the total flow rate of p_i^f when it receives the multimedia data. tr_{ij}^m ($i = 1,\ldots,l$; $j = 1,\ldots,n_i$) denotes the total flow rate of p_{ij}^m when it receives the multimedia data. According to flow rate arrangement attained by the previous analysis, as for the condition with multiple mobile subclasses, we can get that

$$u_s = \max\left(r_f, n_f\left(r_f - \overline{u_f}\right) + \sum_{i=1}^{l} \max\left(r_i, n_i\left(r_i - \overline{u_i}\right)\right)\right). \tag{33}$$

$f(x \to y) = z$ denotes that the node x transmits the required multimedia data to the node y with the flow rate of z. $f_t(x \to y) = z$ denotes that the node x provides y with coding rate conversion with the flow rate of z to transmit required multimedia data. The complete flow rate control algorithm is listed below.

The Flow Rate Control of Multimedia Data for Fixed Nodes

(1) attain the systematic information including $u_s, n_f, \overline{u_f}, r_f, n_i$ ($i = 1,\ldots,l$), $\overline{u_i}$ ($i = 1,\ldots,l$), r_i ($i = 1,\ldots,l$);

(2) if $(n_f - 1)r_f/n_f - \overline{u_f} > 0$, go to (6);

(3) make $u_s = r_f$, and transmit the following data;

(a) $f(s \to p_i^f) = u_i^f r_f / n_f \overline{u_f}$, ($i = 1,\ldots,n_f$);

(b) $f(p_j^f \to p_i^f) = u_j^f r_f / n_f \overline{u_f}$, ($j = 1,\ldots,n_f$; $i = 1,\ldots,n_f$; $j \neq i$);

(4) then the total flow rate of the required multimedia data for p_i^f is $\mathrm{tr}_i^f = r_f$, ($i = 1,\ldots,n_f$);

(5) go to (9);

(6) make $u_s = r_i + n_f(r_f - \overline{u_f})$, transmit the following data:

(a) $f(s \to p_i^f) = \overline{u_f}/(n_f - 1)$, ($i = 1,\ldots,n_f$);

(b) $f(p_j^f \to p_i^f) = \overline{u_f}/(n_f - 1)$, ($j = 1,\ldots,n_f$; $i = 1,\ldots,n_f$; $j \neq i$);

(c) $f(s \to p_i^f) = r_f - n_f\overline{u_f}/(n_f - 1)$, ($i = 1,\ldots,n_f$);

(7) then the total flow rate of the required multimedia data for p_i^f is $\mathrm{tr}_i^f = r_f$, ($i = 1,\ldots,n_f$);

(8) go to (9).

The Flow Rate Control of Multimedia Data for Mobile Nodes:

(9) make $i = 1$;

(10) if $i > l$, go to (18);

(11) if $(n_i - 1)r_i/n_i - \overline{u_i} > 0$, go to (15);

(12) the node with upload bandwidth above 0 initiates the following coding rate conversion and data transfer:

(a) $f_t(s \to p_{ij}^m) = u_{ij}^m / n_i\overline{u_i} \cdot u_s' / (u_s + n_f(\overline{u_f} - r_f)) \cdot r_i$, ($j = 1,\ldots,n_i$);

(b) $f_t(p_k^f \to p_{ij}^m) = u_{ij}^m / n_i\overline{u_i} \cdot u_k'^f / (u_s + n_f(\overline{u_f} - r_f)) \cdot r_i$, ($k = 1,\ldots,n_f$; $j = 1,\ldots,n_i$);

(c) $f(p_{ik}^m \to p_{ij}^m) = u_{ij}^m r_i / n_i\overline{u_i}$, ($k = 1,\ldots,n_i$; $j = 1,\ldots,n_i$; $k \neq j$);

(13) then the total flow rate of the required multimedia data for p_{ij}^m is $\mathrm{tr}_{ij}^m = r_i$, ($j = 1,\ldots,n_i$);

(14) $i = i + 1$ go to (10);

(15) make $u_s = n_f(r_f - \overline{u_f}) + n_i(r_i - \overline{u_i})$, the node with upload bandwidth above 0 initiates the following coding rate conversion and data transfer:

(a) $f_t(s \to p_{ij}^m) = u_{ij}^m / (n_i - 1) \cdot u_s' / (u_s + n_f(\overline{u_f} - r_f))$, ($j = 1,\ldots,n_i$);

(b) $f_t(p_k^f \to p_{ij}^m) = u_{ij}^m / (n_i - 1) \cdot u_k'^f / (u_s + n_f(\overline{u_f} - r_f))$, ($k = 1,\ldots,n_f$; $j = 1,\ldots,n_i$);

(c) $f(p_{ik}^m \to p_{ij}^m) = u_{ij}^m / (n_i - 1)$, ($k = 1,\ldots,n_i$; $j = 1,\ldots,n_i$; $k \neq j$);

(d) $f_t(s \to p_{ij}^m) = (r_i - n_i\overline{u_i}/(n_i - 1))(u_s' / (u_s + n_f(\overline{u_f} - r_f)))$, ($j = 1,\ldots,n_i$);

(e) $f_t(p_k^f \to p_{ij}^m) = (r_i - n_i\overline{u_i}/(n_i - 1))(u_k'^f / (u_s + n_f(\overline{u_f} - r_f)))$, ($k = 1,\ldots,n_f$; $j = 1,\ldots,n_i$);

(16) then the total flow rate of the required multimedia data for p_{ij}^m is $\mathrm{tr}_{ij}^m = r_i$, ($j = 1,\ldots,n_i$);

(17) go to (10);

(18) end.

3.5. Algorithm Instance. In the following, the algorithm will be demonstrated by an example. As shown in Figure 2(a), the system has two fixed nodes A and B, as well as two mobile nodes C and D. Wherein the multimedia data displayed by A and B requires a support of 800 kbps flow rate. And the multimedia data displayed by C and D requires a support of 600 kbps flow rate. The upload bandwidth of A is 1200 kbps; the upload bandwidth of B is 800 Kbps; the upload bandwidth of C is 200 Kbps; and the upload bandwidth of D is 100 kbps. According to (12) the upload bandwidth of s is set to 800 kbps. In Figure 2(b), the upload bandwidth and flow rate

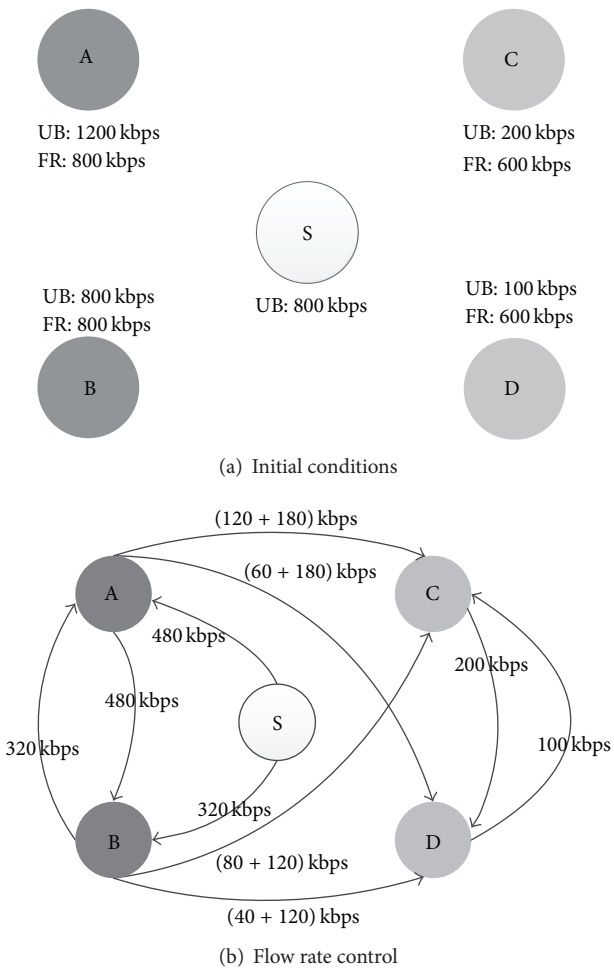

(a) Initial conditions

(b) Flow rate control

Figure 2: Algorithm instance.

requirements of each node are marked with UB and FR, respectively.

As shown in Figure 2(b), according to the flow rate control of the multimedia data required by fixed nodes in the algorithm, it provides flow rate for A and B. In the figure, the thick arrows mark the transmission path of multimedia data required by A and B, and the numbers mark the upload bandwidth. Then according to the flow rate control of the multimedia data required by mobile nodes in the algorithm, it provides the coding rate conversion and the flow rate for C and D. In the figure, the thin arrows mark the transmission path of multimedia data required by C and D, and the numbers mark the upload bandwidth (the plus sign between the numbers denotes twice transmission according to the algorithm). Finally, the entire system meets user needs for coding data and flow rate of all nodes by the distributed multimedia data transmission and flow rate control, which achieves the purpose of design.

4. Performance Comparison

As has been mentioned previously, current designs treat the fixed nodes and mobile nodes subclasses as multiple independent subsystems and, respectively, provides different coding rate of data and the corresponding flow rate control. Such systematic and typical flow rate control algorithm is proposed and analyzed in [15, 16]. This section first compares the upload bandwidth consumptions between the proposed algorithm of this paper and the algorithm of the references based on the simulation experiment and then further demonstrates the experimental results based on the mathematical analysis.

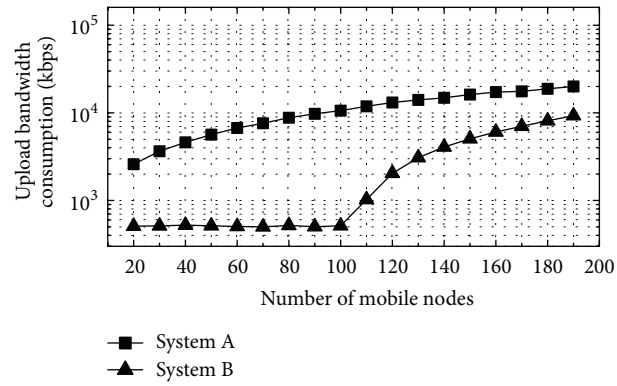

Figure 3: Comparison of u_s^A and u_s^B in the scenario of mobile node increase.

4.1. Simulation Experiment. Simulation platform generates the analog network environment with the commonly used Georgia Tech's Topology Generator [36, 37] in the multimedia data transmission and streaming system experiment. And on this basis, it achieves applying the system to simulate with the proposed algorithm in this paper and the references. For the convenience of description, in the following paragraphs, the system that adopts the algorithm of the references is referred to as system A, and the system that adopts the algorithm proposed in this paper is referred to as system B. u_s^A denotes the upload bandwidth consumption on the source node of system A. u_s^B denotes the upload bandwidth consumption on the source node of system B.

We make two experiments to compare the performance of u_s^A and u_s^B. First, assume that there are 20 fixed nodes and 20 mobile nodes in the system. The minimum flow rate of fixed node sets 500 kbps, and the minimum flow rate of mobile node sets 200 kbps. The upload bandwidth of fixed node sets 1000 kbps, and the upload bandwidth of mobile node sets 100 kbps. We increase the number of mobile nodes gradually and measure u_s^A and u_s^B in the same conditions. The results can be seen in Figure 3: the curve of u_s^B is below the curve of u_s^A (from 20 to 190 mobile nodes), which means that system B achieves lower upload bandwidth consumption of source node.

To be more fair, the random parameters are taken as the initial condition in the second experiment (the range is shown in Table 2), and it generates 500 sets of random initial conditions. In the same initial conditions, it tests

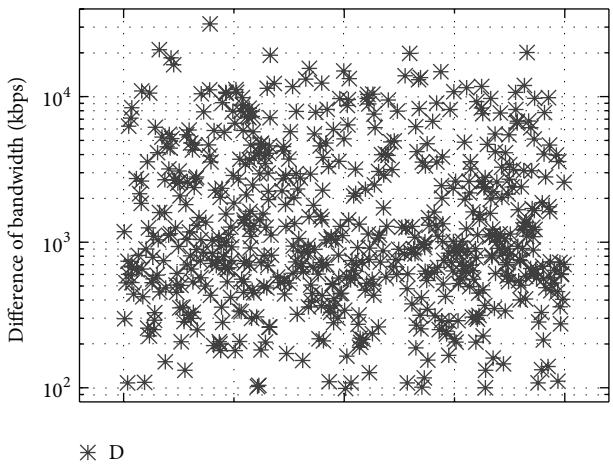

Figure 4: Upload bandwidth consumption difference of the source node in random setting.

Table 2: Range of randomly set initial conditions.

	Min	Max
Average upload bandwidth (kbps)	20	1000
Minimum flow rate (kbps)	100	1500
Amount of the mobile node subclasses	2	10
Amount of mobile nodes in one subclass	5	100

the difference of source node upload bandwidth consumption between system A and B, namely, $D = u_s^{\mathrm{A}} - u_s^{\mathrm{B}}$.

The experimental results can be seen in Figure 4: in the random test, D value ranges from about 100 kbps to about 10 Mbps; that is, the upload bandwidth consumption of the source node in system B is less than that in system A. As u_s^{A} and u_s^{B} are measured under the same conditions, it shows that the user nodes (especially the fixed nodes) in system B utilize upload bandwidth more fully than the system A, which alleviates the upload bandwidth consumption of the source node in system B. In fact, the result of this test is not accidental. In the following, it will demonstrate that the upload bandwidth consumption of the source node in system B is lower with mathematical analysis.

4.2. Mathematical Analysis. Assume that in the system there is only one mobile node subclass. Current design (system A) is divided into two separate subsystems, which, respectively, provide flow rates support for the fixed nodes and mobile nodes. The upload bandwidth consumption of the two subsystems is u_{sf}^{A} and u_{sm}^{A}, according to [15, 16],

$$\begin{aligned} u_{sf}^{\mathrm{A}} &= \max\left(r_f, n_f\left(r_f - \overline{u_f}\right)\right), \\ u_{sm}^{\mathrm{A}} &= \max\left(r_m, n_m\left(r_m - \overline{u_m}\right)\right). \end{aligned} \tag{34}$$

As the various subsystems of the current design are independent of each other, thereby

$$u_s^{\mathrm{A}} = u_{sf}^{\mathrm{A}} + u_{sm}^{\mathrm{A}}. \tag{35}$$

Equation (35) represents the upload bandwidth consumption of the source node with a given flow rate design. And combined with (33), it can quantitatively analyze upload bandwidth difference of the source node between system A and B in the same requirements and conditions. However, just by (35), it is not easy to see real relationship of the upload bandwidth consumption of the source node in the two systems.

Note that, according to (34),

$$\begin{aligned} u_{sf}^{\mathrm{A}} &\geq r_f, \\ u_{sf}^{\mathrm{A}} &\geq n_f\left(r_f - \overline{u_f}\right), \\ u_{sm}^{\mathrm{A}} &\geq r_m, \\ u_{sm}^{\mathrm{A}} &\geq n_m\left(r_m - \overline{u_m}\right), \end{aligned} \tag{36}$$

$$\begin{aligned} u_s^{\mathrm{A}} &= u_{sf}^{\mathrm{A}} + u_{sm}^{\mathrm{A}} \geq r_f, \\ u_s^{\mathrm{A}} &= u_{sf}^{\mathrm{A}} + u_{sm}^{\mathrm{A}} \geq r_m + n_f\left(r_f - \overline{u_f}\right), \\ u_s^{\mathrm{A}} &= u_{sf}^{\mathrm{A}} + u_{sm}^{\mathrm{A}} \geq n_f\left(r_f - \overline{u_f}\right) + n_m\left(r_m - \overline{u_m}\right). \end{aligned} \tag{37}$$

Comparing (37) with (9) and (10), it can be seen that

$$u_s^{\mathrm{A}} \geq \mathrm{MAX}. \tag{38}$$

The above has argued that with the proposed algorithm in this paper, system B can make all nodes play normally in the condition of $u_s^{\mathrm{B}} = \mathrm{MAX}$, so it is always true that $u_s^{\mathrm{B}} \leq u_s^{\mathrm{A}}$. For the multiple mobile node subclasses, the algorithm should be used for multiple cycles, and it is also true that $u_s^{\mathrm{B}} \leq u_s^{\mathrm{A}}$. As the upload bandwidth consumptions of the source node in system A and B are measured under the same initial conditions, u_s^{B} is lower, which shows that system B makes better use of upload bandwidth of user nodes.

5. Conclusion

In this paper, a distributed flow rate control algorithm for the optimization of multimedia data transmission in the networked agent system with multiple coding rates was put forward. The proposed algorithm makes the different coding rate data and user nodes networked to improve the upload bandwidth utilization of user nodes. It achieves personalized coding rate data transmission and the corresponding flow rate control for different user nodes. The paper uses the mathematical modeling to analyze the upload bandwidth consumption of the source node in the system that adopts the proposed algorithm. And it is compared with the current design. The paper demonstrates that the proposed algorithm makes the system achieves higher upload bandwidth utilization of user nodes and lower upload bandwidth consumption of source node compared with the current design through the simulation experiment and the mathematical analysis.

Acknowledgments

This work is partially supported by the National Natural Science Foundation of China (NSFC) Grant nos. 60972030 and 61001084 and Fundamental Research Funds for the Central Universities (ZYGX2010X001). The authors are grateful to the anonymous referee for a careful checking of the details and for helpful comments that improved this paper.

References

[1] IPOQUE, "Ipoque Internet Study 2008/2009," http://www.ipoque.com/.

[2] Y. Sun, Y. Guo, Z. Li et al., "The case for P2P mobile video system over wireless broadband networks: a practical study of challenges for a mobile video provider," *IEEE Network Magazine*, vol. 27, no. 2, pp. 22–27, 2013.

[3] G. Fortino and C. E. Palau, "An agent-based mobile social network," in *International Conference on Multimedia Computing and Systems (ICMCS '12)*, pp. 961–967, May 2012.

[4] H. Liang, B. J. Choi, W. Zhuang et al., "Multiagent coordination in microgrids via wireless networks," *IEEE Wireless Communications*, vol. 19, no. 3, pp. 14–22, 2012.

[5] L. Vasiu and Q. H. Mahmoud, "Mobile Agents in Wireless Devices," *Computer*, vol. 37, no. 2, pp. 104–105, 2004.

[6] G. Leetch and E. Mangina, "A multi-agent system to stream multimedia to handheld devices," in *Proceedings of the 6th International Conference on Computational Intelligence and Multimedia Applications (ICCIMA '05)*, pp. 2–10, August 2005.

[7] M. Adaçal and A. B. Benner, "Mobile web services: a new agent-based framework," *IEEE Internet Computing*, vol. 10, no. 3, pp. 58–65, 2006.

[8] Y. S. Kim and K. H. Lee, "A lightweight framework for mobile web services," *Computer Science-Research and Development*, vol. 24, no. 4, pp. 199–209, 2009.

[9] J. L. Hsiao, H. P. Hung, and M. S. Chen, "Versatile transcoding proxy for internet content adaptation," *IEEE Transactions on Multimedia*, vol. 10, no. 4, pp. 646–658, 2008.

[10] G. Wen, Z. Duan, W. Yu, and G. Chen, "Consensus in multi-agent systems with communication constraints," *International Journal of Robust and Nonlinear Control*, vol. 22, no. 2, pp. 170–182, 2012.

[11] G. Wen, Z. Duan, Z. Li, and G. Chen, "Consensus and its $\mathscr{L}_2$-gain performance of multi-agent systems with intermittent information transmissions," *International Journal of Control*, vol. 85, no. 4, pp. 384–396, 2012.

[12] J. Chakareski, "In-network packet scheduling and rate allocation: a content delivery perspective," *IEEE Transactions on Multimedia*, vol. 13, no. 5, pp. 1092–1102, 2011.

[13] C. M. Dobre, R. Voicu, A. Muram, and I. C. Legrand, "An agent based framework to monitor and control high performance data transfers," in *Proceedings of the International Conference on Computer as a Tool (EUROCON '07)*, pp. 453–458, September 2007.

[14] CNTV, http://cbox.cntv.cn/.

[15] S. Liu, R. Zhang-Shen, W. Jiang, J. Rexford, and M. Chiang, "Performance bounds for peer-assisted live streaming," in *Proceedings of the ACM SIGMETRICS International Conference on Measurement and Modeling of Computer Systems (SIGMETRICS '08)*, pp. 313–324, June 2008.

[16] R. Kumar, Y. Liu, and K. Ross, "Stochastic fluid theory for P2P streaming systems," in *Proceedings of the 26th IEEE International Conference on Computer Communications (INFOCOM '07)*, pp. 919–927, May 2007.

[17] M. Chen, M. Ponec, S. Sengupta et al., "Utility maximization in peer-to-peer systems with applications to video conferencing," *IEEE/ACM Transactions on Networking*, vol. 20, no. 6, pp. 1681–1694, 2012.

[18] T. Small, B. Li, and B. Liang, "Outreach: peer-to-peer topology construction towards minimized server bandwidth costs," *IEEE Journal on Selected Areas in Communications*, vol. 25, no. 1, pp. 35–45, 2007.

[19] S. Liu, M. Chiang, S. Sengupta, J. Li, and P. A. Chou, "P2P streaming capacity for heterogeneous users with degree bounds," in *Proceedings of the 46th Annual Allerton Conference on Communication, Control, and Computing*, pp. 968–976, September 2008.

[20] S. Sengupta, S. Liu, M. Chen, M. Chiang, J. Li, and P. A. Chou, "Peer-to-peer streaming capacity," *IEEE Transactions on Information Theory*, vol. 57, no. 8, pp. 5072–5087, 2011.

[21] X. Zhu, P. Agrawal, J. P. Singh, T. Alpcan, and B. Girod, "Distributed rate allocation policies for multihomed video streaming over heterogeneous access networks," *IEEE Transactions on Multimedia*, vol. 11, no. 4, pp. 752–764, 2009.

[22] C. Zhao, X. Lin, and C. Wu, "The streaming capacity of sparsely-connected P2P systems with distributed control," in *Proceedings of the IEEE International Conference on Computer Communications (INFOCOM '11)*, pp. 1449–1457, April 2011.

[23] C. Wu, B. Li, and S. Zhao, "On dynamic server provisioning in multichannel P2P live streaming," *IEEE/ACM Transactions on Networking*, vol. 19, no. 5, pp. 1317–1330, 2011.

[24] M. Wang, L. Xu, and B. Ramamurthy, "Linear programming models for multi-channel P2P streaming systems," in *Proceedings of the IEEE International Conference on Computer Communications (INFOCOM '10)*, March 2010.

[25] D. Wu, Y. Liu, and K. W. Ross, "Modeling and analysis of multichannel P2P live video systems," *IEEE/ACM Transactions on Networking*, vol. 18, no. 4, pp. 1248–1260, 2010.

[26] K. D. Lee and V. C. M. Leung, "Utility-based rate-controlled parallel wireless transmission of multimedia streams with multiple importance levels," *IEEE Transactions on Mobile Computing*, vol. 8, no. 1, pp. 81–92, 2009.

[27] D. Jurca and P. Frossard, "Media flow rate allocation in multipath networks," *IEEE Transactions on Multimedia*, vol. 9, no. 6, pp. 1227–1240, 2007.

[28] C. Feng and B. Li, "On large-scale peer-to-peer streaming Systems with Network Coding," in *Proceedings of the 16th ACM International Conference on Multimedia (MM '08)*, pp. 269–278, Vancouver, Canada, October 2008.

[29] D. Liu, E. Setton, B. Shen, and S. Chen, "PAT: peer-assisted transcoding for overlay streaming to heterogeneous devices," in *International Workshop on Network and Operating Systems Support for Digital Audio and Video*, 2007.

[30] S. R. Narayanan, D. Braun, J. Buford et al., "Peer-to-peer streaming for networked consumer electronics [Peer-to-peer multimedia streaming]," *IEEE Communications Magazine*, vol. 45, no. 6, pp. 124–131, 2007.

[31] M. Atenas, A. Canovas, M. Garcia, and J. Lloret, "IPTV transcoding to avoid network congestion," in *Proceedings of the 6th International Conference on Networking and Services (ICNS '10)*, pp. 36–41, March 2010.

[32] T. Wolf, "In-network services for customization in next-generation networks," *IEEE Network*, vol. 24, no. 4, pp. 6–12, 2010.

[33] S. Zeng, L. Li, and D. Liao, "Path selection and bandwidth allocation for fixed and mobile peers in P2P streaming system," *Journal of Computational Information Systems*, vol. 8, no. 17, 2012.

[34] H. Raja and S. B. Qaisar, "Rate-distortion optimized transcoder selection for multimedia transmission in heterogeneous networks," in *Computational Science and Its Applications—ICCSA 2012*, vol. 7335 of *Lecture Notes in Computer Science*, pp. 407–418, Springer, Berlin, Germany, 2012.

[35] J. C. Wu, P. Huang, J. J. Yao, and H. H. Chen, "A collaborative transcoding strategy for live broadcasting over peer-to-peer IPTV networks," *IEEE Transactions on Circuits and Systems for Video Technology*, vol. 21, no. 2, pp. 220–224, 2011.

[36] E. W. Zegura, K. L. Calvert, and S. Bhattacharjee, "How to model an internetwork," in *Proceedings of the 15th Annual Joint Conference of the IEEE Computer and Communications Societies (INFOCOM '96)*, pp. 594–602, March 1996.

[37] G. F. Riley, "The Georgia Tech network simulator," in *ACM SIGCOMM Workshop on Models, Methods and Tools for Reproducible Network Research (MoMeTools '03)*, pp. 5–12, August 2003.

Hindawi Publishing Corporation
Mathematical Problems in Engineering
Volume 2013, Article ID 326560, 6 pages
http://dx.doi.org/10.1155/2013/326560

Research Article

Absolute Stability and Master-Slave Synchronization of Systems with State-Dependent Nonlinearities

Rong Li,[1] Bo Liu,[2] and Chao Liu[3]

[1] *Department of Applied Mathematics, Shanghai Finance University, Shanghai 201209, China*
[2] *College of Sciences, North China University of Technology, Beijing 100144, China*
[3] *Department of Applied Mathematics, Shanghai University of Finance and Economics, Shanghai 200433, China*

Correspondence should be addressed to Rong Li; lirong@shfc.edu.cn

Received 3 April 2013; Accepted 7 May 2013

Academic Editor: Wenwu Yu

This paper is concerned with the problems of absolute stability and master-slave synchronization of systems with state-dependent nonlinearities. The Kalman-Yakubovich-Popov (KYP) lemma and the Schur complement formula are applied to get novel and less conservative stability conditions. A numerical example is presented to illustrate the efficiency of the stability criteria. Furthermore, a synchronization criterion is developed based on the proposed stability results.

1. Introduction and Preliminaries

This paper considers the problems of absolute stability and master-slave synchronization of dynamical systems described by the following differential equation:

$$\dot{x}_i = \sum_{j=1}^{n} a_{ij} f_j\left(x_j\right), \quad f_j(0) = 0, \quad j = 1, \ldots, n, \tag{1}$$

where $x = (x_1, \ldots, x_n)^T \in \mathbb{R}^n$ is the system state vector and $f_i : \mathbb{R} \to \mathbb{R}$, $i = 1, \ldots, n$, are time-invariant state-dependent nonlinearities with sector restrictions such as the following:

$$\gamma_i \tau^2 \le f_i(\tau)\tau \le \delta_i \tau^2, \quad i = 1, \ldots, n. \tag{2}$$

For convenience, system (1) will often be written by using the following compact notation:

$$\dot{x} = Af(x), \qquad f(\mathbf{0}) = \mathbf{0}, \tag{3}$$

where $A := (a_{ij})$ and $f(x) := (f_1, \ldots, f_n)^T$. And the sector conditions (2) will be denoted as follows:

$$\mathbf{F}(\Gamma, \Delta), \tag{4}$$

where $\Gamma := \operatorname{diag}(\gamma_1, \ldots, \gamma_n)$ and $\Delta := \operatorname{diag}(\delta_1, \ldots, \delta_n)$.

The problems of stability and synchronization of systems of form (3) play an important role in nonlinear systems theory. It has been found that system (3) has connections with problems in system theory and computation in fields as diverse as Hopfield neural networks [1], Lotka-Voltera ecosystems [2], and systems with saturation nonlinearities [3], among others. A rather recent contribution to the stability analysis of system (3) is [4].

As illustrated in [4], some well-known stability results, such as diagonal stability and passivity-based methods (the circle and the Popov criteria), can be used as stability criteria for system (3) with some particular sector conditions. However, while bringing simplicity, these stability criteria may also introduce conservativeness to the problem. By using a Lur'e function as a Lyapunov function candidate, [4] introduced a new absolute stability test for system (3) which was proved to be much less conservative than both diagonal stability and passivity-based methods. For the sake of convenience, we put this stability test in Lemma 1.

On the other hand, the problems of absolute stability and synchronization of Lur'e systems have been widely studied [5–15]. Thanks to the results of [9], we found that the stability criteria proposed in [4] can be further improved by relaxing the restriction of positiveness on matrix P in Lemma 1, which, as illustrated by a numerical example, can further reduce the

conservativeness of the stability test of [4]. Last but not least, a new synchronization criterion for systems of form (3) is developed based on the proposed stability results.

The Kalman-Yakubovic-Popov (KYP) lemma will be used in this paper to establish the equivalence relationship between the frequency-domain conditions and time-domain inequalities. The Schur complement formula will also be applied in the process of proof. They are both presented in lemmas below for the convenience of reading.

Lemma 1 (Theorem 2 of [4]). *The zero solution of system* (3) *is globally asymptotically stable (GAS) for all* $f \in \mathbf{F}(\Gamma, \Delta)$*, if there exist diagonal and positive-definite matrices* P *and* Q*, and a symmetric matrix* $W > -P\Gamma$ *such that the following LMI*

$$\begin{bmatrix} A^T P + PA - Q & A^T W + \frac{1}{2}(\Gamma + \Delta) Q \\ WA + \frac{1}{2} Q(\Gamma + \Delta) & -\Gamma\Delta Q \end{bmatrix} < 0 \quad (5)$$

is feasible, where $\Gamma := \operatorname{diag}(\gamma_1, \ldots, \gamma_n)$ *and* $\Delta := \operatorname{diag}(\delta_1, \ldots, \delta_n)$.

Lemma 2 (KYP lemma, Rantzer [16]). *Given* $A \in \mathbb{R}^{n\times n}$, $B \in \mathbb{R}^{n\times m}$, $\Pi = \Pi^T \in \mathbb{R}^{(n+m)\times(n+m)}$, *with* $\det(j\omega I - A) \neq 0$ *for all* $\omega \in \mathbb{R}$, *the following statements are equivalent.*

(i) $\begin{bmatrix} (j\omega I - A)^{-1} B \\ I \end{bmatrix}^* \Pi \begin{bmatrix} (j\omega I - A)^{-1} B \\ I \end{bmatrix} < 0$ *for all* $\omega \in \mathbb{R}$.

(ii) *There exists a matrix* $P = P^T \in \mathbb{R}^{n\times n}$ *such that*

$$\begin{bmatrix} A^T P + PA^T & PB \\ B^T P & 0 \end{bmatrix} + \Pi < 0. \quad (6)$$

Lemma 3 (Schur complement, Boyd et al. [17]). *The LMI*

$$\begin{bmatrix} S_{11} & S_{12} \\ S_{12}^T & -S_{22} \end{bmatrix} < 0 \quad (7)$$

with $S_{11} = S_{11}^T$ *and* $S_{22} = S_{22}^T$ *is equivalent to one of the following statements:*

(i) $S_{22} > 0$ *and* $S_{11} + S_{12} S_{22}^{-1} S_{12}^T < 0$;

(ii) $S_{11} < 0$ *and* $S_{22} + S_{12}^T S_{11}^{-1} S_{12} > 0$.

2. Absolute Stability Criteria

To analyze the absolute stability of system (3), a Lur'e function

$$V(x) = x^T W x + 2\sum_{i=1}^{n} p_i \int_0^{x_i} f_i(\tau)\, d\tau, \quad (8)$$

where $P = \operatorname{diag}(p_1, \ldots, p_n) > 0$ and $W > -P\Gamma$, was taken in [4] as a Lyapunov function candidate. The stability condition of Lemma 1 was then deduced by the analysis of the time derivative of (8) incorporating the S-procedure (see [4] for details).

Note that the diagonal matrix P in Lemma 1 is allowed to be only positive, so as to ensure the nonnegativeness of the Lyapunov function (6) in [4]. The main goal of this section is to prove that the restriction of positiveness on matrix P is unnecessary by finally showing that the Lur'e function $V(x)$ in (8) can still be taken as a Lyapunov candidate when some or even all entries p_i are nonpositive. We will start with a revised time-domain criterion for the absolute stability of system (3).

Theorem 4. *The zero solution of the nonlinear system* (3) *is GAS for all* $f \in \mathbf{F}(\Gamma, \Delta)$*, if* $A\Gamma$ *is stable and there exist diagonal matrices* P *and* Q *with* $Q > 0$ *and a symmetric matrix* W *such that the LMI* (5) *is feasible.*

Before proving this theorem, some needed results and some discussions on the frequency-domain interpretation to LMI (5) are first introduced.

Proposition 5. *Under the condition of inequality* (5)*, the following two statements are equivalent:*

(i) $A\Gamma$ *is stable;*

(ii) $W + P\Gamma > 0$.

Proof. Define

$$\Phi = \begin{bmatrix} A^T P + PA - Q & A^T W + \frac{1}{2}(\Gamma + \Delta) Q \\ WA + \frac{1}{2} Q(\Gamma + \Delta) & -\Gamma\Delta Q \end{bmatrix}. \quad (9)$$

Then the congruence transformation of Φ by the nonsingular matrix

$$T_1 = \begin{bmatrix} \Gamma & I \\ I & 0 \end{bmatrix} \quad (10)$$

provides an equivalent inequality to (5)

$$T_1 \Phi T_1^T = \begin{bmatrix} \Gamma A^T Y_1 + Y_1 A\Gamma & Y_1 A + \Gamma A^T P - \frac{1}{2}(\Gamma - \Delta) Q \\ A^T Y_1 + PA\Gamma - \frac{1}{2} Q(\Gamma - \Delta) & A^T P + PA - Q \end{bmatrix} < 0, \quad (11)$$

where $Y_1 = W + P\Gamma$. By the Schur complement (Lemma 3), (11) implies the following:

$$\Gamma A^T (W + P\Gamma) + (W + P\Gamma) A\Gamma < 0. \tag{12}$$

This inequality directly leads to the result of the proposition. □

Remark 6. Proposition 5 shows that the conditions of Theorem 4 guaranteeing the GAS of system (3) are consistent with Lemma 1, except for the restriction of positiveness on matrix P.

The next theorem reveals a frequency domain interpretation to the LMI (5).

Theorem 7. *Suppose that $A\Gamma$ is stable. Then, there exist diagonal matrices P and Q with $Q > 0$ and a symmetric matrix W such that the LMI (5) is feasible if, and only if,*

$$\operatorname{Re}\{(\Delta - \Gamma) QK_\Gamma (j\omega) + 2j\omega PK_\Gamma (j\omega) - Q\} < 0, \quad \forall \omega \in \mathbb{R}, \tag{13}$$

where $K_\Gamma(s) = (sI - A\Gamma)^{-1} A$.

Proof. Let

$$\Pi = \begin{bmatrix} 0 & \Gamma A^T P - \frac{1}{2}(\Gamma - \Delta) Q \\ PA\Gamma - \frac{1}{2} Q(\Gamma - \Delta) & A^T P + PA - Q \end{bmatrix}. \tag{14}$$

Then, inequality (11), which is equivalent to the LMI (5) as proved in Proposition 5, can be rewritten as follows:

$$\Pi + \begin{bmatrix} \Gamma A^T Y_1 + Y_1 A\Gamma & Y_1 A \\ A^T Y_1 & 0 \end{bmatrix} < 0. \tag{15}$$

From the KYP lemma (Lemma 2), (15) holds if, and only if,

$$\begin{bmatrix} (j\omega I - A\Gamma)^{-1} A \\ I \end{bmatrix}^* \Pi \begin{bmatrix} (j\omega I - A\Gamma)^{-1} A \\ I \end{bmatrix} < 0, \quad \forall \omega \in \mathbb{R}, \tag{16}$$

which is equivalent to inequality (13) through direct calculation.

Furthermore, noticing that

$$\begin{aligned} sPK_\Gamma(s) &= sP(sI - A\Gamma)^{-1} A \\ &= P\left(I - s^{-1} A\Gamma\right)^{-1} A \\ &= PA\left(I - s^{-1}\Gamma A\right)^{-1} \\ &= PA\left[I + s^{-1}\Gamma\left(I - s^{-1} A\Gamma\right)^{-1} A\right] \\ &= PA\left[I + \Gamma(sI - A\Gamma)^{-1} A\right], \end{aligned} \tag{17}$$

inequality (13) is equivalent to $\operatorname{Re}\{M(j\omega)\} > 0$, for all $\omega \in \mathbb{R}$, where

$$M(s) = \left[\frac{1}{2} Q(\Gamma - \Delta) - PA\Gamma\right](sI - A\Gamma)^{-1} A + \left(\frac{1}{2} Q - PA\right). \tag{18}$$

□

Remark 8. With the stability of $A\Gamma$, the frequency-domain inequality (FDI) (13) is equivalent to that the transfer function $M(s)$ as given in (18) is strictly positive real (SPR), which is consistent with the frequency-domain criterion of [4], except for the restriction of positiveness on matrix P.

Proposition 9. *Suppose that $A\Gamma$ is stable, then Theorem 4 (or equivalently Theorem 7) ensures that $A(\Gamma + \tilde{\Delta})$ is stable for any $0 \le \tilde{\Delta} \le \Delta - \Gamma$.*

Proof. Suppose to the contrary that there exists a $\tilde{\Delta}$, $0 \le \tilde{\Delta} \le \Delta - \Gamma$, such that $A(\Gamma + \tilde{\Delta})$ is not stable. Then, there exists a real number α, $0 \le \alpha \le 1$, such that $A(\Gamma + \alpha\tilde{\Delta})$ has at least an eigenvalue on the imaginary axis, which we denote by $j\omega_0, \omega_0 \in \mathbb{R}$. Then

$$\det\left(j\omega_0 I - A\Gamma - \alpha A\tilde{\Delta}\right) = 0. \tag{19}$$

Since $A\Gamma$ is stable, $\det(j\omega_0 I - A\Gamma) \neq 0$. It follows from (19) that

$$\det\left(I - \alpha(j\omega_0 I - A\Gamma)^{-1} A\tilde{\Delta}\right) = 0; \tag{20}$$

that is,

$$\det\left(I - \alpha K_\Gamma(j\omega_0)\tilde{\Delta}\right) = 0. \tag{21}$$

So there exists a vector $\eta \in \mathbb{C}^n$, $\eta \neq 0$, such that

$$\eta^*\left(I - \alpha\tilde{\Delta} K_\Gamma^*(j\omega_0)\right) = 0. \tag{22}$$

Thus $\eta^*\tilde{\Delta} \neq 0$, and

$$\begin{aligned} \eta^* &= \alpha\eta^*\tilde{\Delta} K_\Gamma^*(j\omega_0), \\ \eta &= \alpha K_\Gamma(j\omega_0)\tilde{\Delta}\eta. \end{aligned} \tag{23}$$

Equality (23) and the conditions $0 \le \tilde{\Delta} \le \Delta - \Gamma$ and $0 < \alpha \le 1$ indicate the following:

$$\begin{aligned} &\eta^*\tilde{\Delta}\left[-2Q + (\Delta - \Gamma) QK_\Gamma(j\omega_0) + K_\Gamma^*(j\omega_0) Q(\Delta - \Gamma)\right]\tilde{\Delta}\eta \\ &\quad = \eta^*\left[-2\tilde{\Delta} Q\tilde{\Delta} + \frac{2}{\alpha}(\Delta - \Gamma) Q\tilde{\Delta}\right]\eta \\ &\quad \ge 0. \end{aligned} \tag{24}$$

On the other hand, it follows from the FDI (13) that

$$\begin{aligned} &\eta^*\tilde{\Delta}\left[-Q + (\Delta - \Gamma) QK_\Gamma(j\omega_0) + 2j\omega_0 PK_\Gamma(j\omega_0)\right. \\ &\quad \left. -Q + K_\Gamma^*(j\omega_0) Q(\Delta - \Gamma) - 2j\omega_0 K_\Gamma^*(j\omega_0) P\right]\tilde{\Delta}\eta < 0. \end{aligned} \tag{25}$$

From (23),

$$\begin{aligned} \eta^*\tilde{\Delta} 2j\omega_0 PK_\Gamma(j\omega_0)\tilde{\Delta}\eta &= \frac{2}{\alpha} j\omega_0\eta^*\tilde{\Delta} P\eta, \\ \eta^*\tilde{\Delta} 2j\omega_0 K_\Gamma^*(j\omega_0) P\tilde{\Delta}\eta &= \frac{2}{\alpha} j\omega_0\eta^* P\tilde{\Delta}\eta, \end{aligned} \tag{26}$$

and since $\widetilde{\Delta}P = P\widetilde{\Delta}$, (25) indicates that

$$\eta^* \widetilde{\Delta}\left[-2Q+(\Delta-\Gamma)QK_\Gamma(j\omega_0)+K_\Gamma^*(j\omega_0)Q(\Delta-\Gamma)\right]\widetilde{\Delta}\eta<0. \tag{27}$$

It contradicts to (24). The proof is completed. □

Now, we are ready to prove Theorem 4.

Proof of Theorem 4. Take for Lyapunov function candidate

$$V(x) = x^T W x + 2\sum_{i=1}^{n} p_i \int_0^{x_i} f_i(\tau)\,d\tau, \tag{28}$$

where W is a symmetric matrix and p_i, $i = 1,\ldots,n$, need not to be positive.

The time derivative of $V(x)$ along any trajectory of system (3) is given by the following:

$$\dot{V}(x) = 2f(x)^T A^T W x + f(x)^T\left(A^T P + PA\right) f(x), \tag{29}$$

where $P = \operatorname{diag}(p_1,\ldots,p_n)$. For all $x_i \neq 0$, the sector condition (2) can be expressed as follows:

$$\begin{aligned} s_i(x_i) &:= \left(f_i(x_i)-\gamma_i x_i\right)\left(f_i(x_i)-\delta_i x_i\right) \le 0, \\ &\qquad \forall x_i \neq 0,\ i = 1,\ldots,n. \end{aligned} \tag{30}$$

Let $Q = \operatorname{diag}(q_1,\ldots,q_n)$, where $q_i > 0$, $i = 1,\ldots,n$; then

$$\begin{aligned} \sum_{i=1}^{n} q_i s_i(x_i) &= f(x)^T Q f(x) - f(x)^T(\Gamma+\Delta)Qx + x^T\Gamma\Delta Q x \\ &\le 0, \quad \forall\left(x, f(x)\right) \neq 0. \end{aligned} \tag{31}$$

Thus, if it is possible to show that

$$\dot{V}(x) < \sum_{i=1}^{n} q_i s_i(x_i), \quad \forall\left(x, f(x)\right) \neq 0, \tag{32}$$

it follows that $\dot{V}(x) < 0$, for all $x \neq 0$. Inequality (32) can be written as follows:

$$\begin{aligned} &\begin{pmatrix} f(x) \\ x \end{pmatrix}^T \begin{bmatrix} A^T P + PA - Q & A^T W + \frac{1}{2}(\Gamma+\Delta)Q \\ WA + \frac{1}{2}Q(\Gamma+\Delta) & -\Gamma\Delta Q \end{bmatrix} \\ &\times \begin{pmatrix} f(x) \\ x \end{pmatrix} < 0, \quad \forall \begin{pmatrix} f(x) \\ x \end{pmatrix} \neq 0, \end{aligned} \tag{33}$$

which is equivalent to the existence of a feasible solution to the LMI (5).

Then (5) guarantees the negative definiteness of $\dot{V}(x)$. In fact, (5) also guarantees that the Lyapunov candidate $V(x)$ defined in (28) is positive definite, even without the requirement of $P > 0$. Rewrite $V(x)$ in (28) as follows:

$$\begin{aligned} V(x) &= x^T W x + 2\sum_{i=1}^{n} p_i \int_0^{x_i} f_i(\tau)\,d\tau \\ &= x^T W x + 2\sum_{i=1}^{n} p_i \int_0^{x_i} \left(\gamma_i\tau + f_i(\tau) - \gamma_i\tau\right) d\tau \\ &= x^T(W + P\Gamma)x + 2\sum_{i=1}^{n} p_i \int_0^{x_i} \left(f_i(\tau) - \gamma_i\tau\right) d\tau. \end{aligned} \tag{34}$$

By Proposition 5, $W + P\Gamma > 0$. And $\int_0^{x_i}(f_i(\tau) - \gamma_i\tau)d\tau \ge 0$ because of the sector condition (2). So, $V(x) > 0$, for all $x \neq 0$, holds if $p_i \ge 0$, $i = 1,\ldots,n$. In the case that there exists $p_i < 0$, we suppose that $p_i < 0$, $i = 1,\ldots,k$, and $p_i \ge 0$, $i = k+1,\ldots,n$, without loss of generality. Then, we get the following inequality:

$$\begin{aligned} &V(x) \\ &\quad \ge x^T(W + P\Gamma)x + 2\sum_{i=1}^{k} p_i \int_0^{x_i} \left(\delta_i\tau - \gamma_i\tau\right) d\tau \\ &\qquad + 2\sum_{i=k+1}^{n} p_i \int_0^{x_i} \left(f_i(\tau) - \gamma_i\tau\right) d\tau \\ &\quad = x^T\left(W + P\Gamma + P_k\left(\Delta_k - \Gamma_k\right)\right)x \\ &\qquad + 2\sum_{i=k+1}^{n} p_i \int_0^{x_i} \left(f_i(\tau) - \gamma_i\tau\right) d\tau, \end{aligned} \tag{35}$$

where $P_k = \operatorname{diag}(p_1,\ldots,p_k,0,\ldots,0)$, $\Delta_k = \operatorname{diag}(\delta_1,\ldots,\delta_k, 0,\ldots,0)$, and $\Gamma_k = \operatorname{diag}(\gamma_1,\ldots,\gamma_k,0,\ldots,0)$. The congruence transformation of Φ in (9) defined by the nonsingular matrix

$$T_2 = \begin{bmatrix} \Gamma + \left(\Delta_k - \Gamma_k\right) & I \\ I & 0 \end{bmatrix} \tag{36}$$

provides an equivalent inequality to the LMI (5):

$$\Psi = T_2 \Phi T_2^T = \begin{bmatrix} \widetilde{A}^T Y_2 + Y_2\widetilde{A} & \Psi_{12} \\ \Psi_{12}^T & A^T P + PA - Q \end{bmatrix} < 0, \tag{37}$$

where $\widetilde{A} = A[\Gamma + (\Delta_k - \Gamma_k)]$, $Y_2 = W + P\Gamma + P_k(\Delta_k - \Gamma_k)$, and $\Psi_{12} = Y_2 A + \widetilde{A}^T P + (1/2)(\Delta - \Gamma)Q - (\Delta_k - \Gamma_k)Q$. From Proposition 9, $\widetilde{A}$ is stable; then it follows from (37) that

$$Y_2 = W + P\Gamma + P_k\left(\Delta_k - \Gamma_k\right) > 0. \tag{38}$$

Thus, by (35), $V(x) > 0$, for all $x \neq 0$. By the canonical Lyapunov theory, system (3) is absolutely stable. Now, we complete the proof of Theorem 4. □

Analogous to the proof of Theorem 4 while considering the stability of $A\Delta$ instead of $A\Gamma$, the following corollary can be deduced.

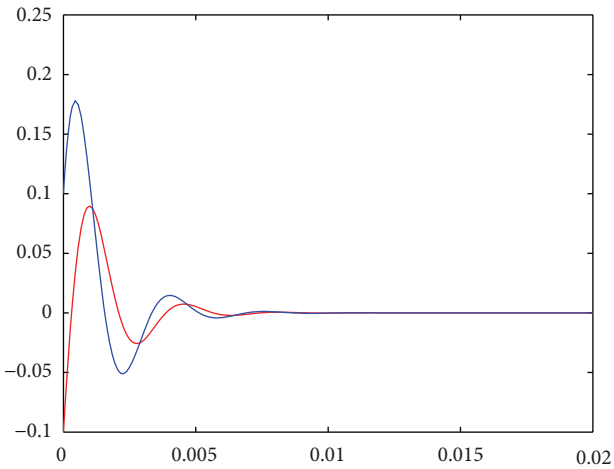

Figure 1: The state of system (39) with $A = \left[\begin{smallmatrix} 10 & -8 \\ 15 & -3 \end{smallmatrix}\right]$ and $\delta = 139.99$.

Table 1: The matrix A and the maximum allowed $\delta_{\max}$.

A	$\left[\begin{smallmatrix} 2 & -3 \\ 1 & -1 \end{smallmatrix}\right]$	$\left[\begin{smallmatrix} 5 & -4 \\ 5 & -3 \end{smallmatrix}\right]$	$\left[\begin{smallmatrix} 10 & -8 \\ 15 & -3 \end{smallmatrix}\right]$
$\delta_{\max}$ from [4]	86.85	71.65	93.33
$\delta_{\max}$ from Theorem 4	99.99	79.99	139.99

Corollary 10. *The zero solution of the nonlinear system* (3) *is GAS for all* $f \in \mathbf{F}(\Gamma, \Delta)$, *if* $A\Delta$ *is stable (or equivalently,* $W + P\Delta > 0$*) and there exist diagonal matrices* P *and* Q *with* $Q > 0$ *and a symmetric matrix* W *such that the LMI* (5) *is feasible.*

In the following, a numerical example is presented to illustrate the effectiveness of the proposed stability criteria.

Example 11. Consider the following system:

$$\dot{x}(t) = Af(x(t)), \qquad f(\mathbf{0}) = \mathbf{0}, \tag{39}$$

where

$$x(t) = \begin{bmatrix} x_1(t) \\ x_2(t) \end{bmatrix}, \qquad f(x(t)) = \begin{bmatrix} f_1(x_1(t)) \\ f_2(x_2(t)) \end{bmatrix}, \tag{40}$$

and A is given in Table 1. The nonlinear function f is supposed to belong to the sector $[\Gamma, \Delta]$, where

$$\Gamma = \begin{bmatrix} -200 & 0 \\ 0 & -200 \end{bmatrix}, \qquad \Delta = \Gamma + \begin{bmatrix} \delta & 0 \\ 0 & \delta \end{bmatrix}. \tag{41}$$

The purpose is to find a maximum upper bound $\delta_{\max}$ such that system (39) is absolute stable for all $\delta < \delta_{\max}$. Using Theorem 2 in [4] and Theorem 4 in this paper, the corresponding $\delta_{\max}$ for system (39) with different A is listed in Table 1, from which it is shown that Theorem 4 in this paper is less conservative than Theorem 2 in [4].

Take

$$f_i(x_i(t)) = G_{bi}x_i(t) + \frac{1}{2}(G_{ai} - G_{bi})(|x_i(t) + 1| - |x_i(t) - 1|), \quad i = 1, 2, \tag{42}$$

where $G_{a1} = -200$, $G_{b1} = -60.01$, $G_{a2} = -200$, and $G_{b2} = -60.01$. Then, the nonlinearity f belongs to the sector $[\Gamma, \Delta]$, where

$$\Gamma = \begin{bmatrix} -200 & 0 \\ 0 & -200 \end{bmatrix}, \qquad \Delta = \begin{bmatrix} -60.01 & 0 \\ 0 & -60.01 \end{bmatrix}; \tag{43}$$

that is, $\delta = 139.99$ in (41). The states of system (39) with $A = \left[\begin{smallmatrix} 10 & -8 \\ 15 & -3 \end{smallmatrix}\right]$ and f as given in (42) are presented in Figure 1, from which it is observed that the origin of the system is asymptotically stable.

3. Master-Slave Synchronization

The absolute stability criteria proposed in the last section can be applied to the master-slave synchronization of coupled systems of form (3). Using two identical systems in a master-slave synchronization scheme with linear full static state feedback, one has the following:

$$\begin{aligned} (M)\ \dot{x}(t) &= Af(x(t)), \\ (S)\ \dot{z}(t) &= Af(z(t)) + K(x(t) - z(t)), \end{aligned} \tag{44}$$

with master M, slave S, and feedback matrix $K \in R^{n\times n}$. The aim of synchronization is then to obtain $\|x(t) - z(t)\| \to 0$ for time $t \to \infty$. Defining the error signal $e = x - z$, one obtains the following error system:

$$\dot{e}(t) = A(\eta(e(t))) - K(e(t)), \tag{45}$$

where $\eta(e(t)) := f(z(t) + e(t)) - f(z(t))$. Assume a sector condition $(\overline{\Gamma}, \overline{\Delta})$ on $\eta(\cdot)$, with $\overline{\Gamma} = \operatorname{diag}(\overline{\gamma_1}, \ldots, \overline{\gamma_n})$ and $\overline{\Delta} = \operatorname{diag}(\overline{\delta_1}, \ldots, \overline{\delta_n})$, which gives the following inequalities for η:

$$\overline{\gamma_i}\tau^2 \le \eta_i(\tau)\tau \le \overline{\delta_i}\tau^2, \quad i = 1, \ldots, n. \tag{46}$$

Following a similar approach to the stability analysis, a synchronization criterion for the systems in (44) is obtained.

Theorem 12. *The zero solution of the error system* (45) *is GAS, which implies that system* (44) *synchronizes, if there exist diagonal matrices* P *and* Q *with* $Q > 0$, *a symmetric matrix* W, *and a feedback matrix* K *such that* $A\overline{\Gamma} - K$ *is stable, and*

$$\overline{\Phi} = \begin{bmatrix} A^TP + PA - Q & A^TW + \frac{1}{2}(\Gamma + \Delta)Q - PK \\ WA + \frac{1}{2}Q(\Gamma + \Delta) - K^TP & -(WK + K^TW) - \Gamma\Delta Q \end{bmatrix} < 0. \tag{47}$$

Proof. This theorem can be completed by the method analogous to that employed in the last section, so its proof is omitted here. □

Remark 13. For a given feedback matrix K, condition (47) is a linear matrix inequality problem (LMI) in P, Q, and W. The overall design problem can be formulated as the optimization problem [18]:

$$\min_{K,P,Q,W} \lambda_{\max}\left[\overline{\Phi}\right], \tag{48}$$

where $\lambda_{\max}[\cdot]$ denotes the maximal eigenvalue of a symmetric matrix. Comparing with the synchronization criteria given in the literature [10–15], Theorem 12 is less conservative by relaxing the restriction of positiveness on matrix P.

4. Conclusion

In this paper, the absolute stability criteria for systems with state-dependent sector nonlinearities provided in [4] are further studied. By relaxing some restrictions, revised stability criteria are proposed, which further reduce the conservativeness of the stability conditions as shown in a numerical example. In addition, the feasibility of the derived LMIs actually implies some FDI conditions bearing the same forms as those in the circle criterion and the Popov criterion. Finally, based on the proposed stability results, a synchronization criterion is developed in a master-slave synchronization scheme.

Acknowledgment

This work is supported by the National Science Foundation of China under Grant no. 11101256.

References

[1] E. Kaszkurewicz and A. Bhaya, "On a class of globally stable neural circuits," *IEEE Transactions on Circuits and Systems I*, vol. 41, no. 2, pp. 171–174, 1994.

[2] E. Kaszkurewicz and A. Bhaya, "Robust stability and diagonal Liapunov functions," *SIAM Journal on Matrix Analysis and Applications*, vol. 14, no. 2, pp. 508–520, 1993.

[3] F. Albertini and D. D'Alessandro, "Asymptotic stability of continuous-time systems with saturation nonlinearities," *Systems and Control Letters*, vol. 29, no. 3, pp. 175–180, 1996.

[4] M. C. de Oliveira, J. C. Geromel, and L. Hsu, "A new absolute stability test for systems with state-dependent perturbations," *International Journal of Robust and Nonlinear Control*, vol. 12, no. 14, pp. 1209–1226, 2002.

[5] Vl. Rasvan, D. Danciu, and D. Popescu, "On absolute (robust) stability: slope restrictions and stability multipliers," *International Journal of Robust and Nonlinear Control*, vol. 23, no. 1, pp. 77–103, 2013.

[6] J. Huang, Y. Yang, Z. Han, and J. Zhang, "Robust absolute stability criterion for uncertain Lur'e differential inclusion systems with time delay," *Circuits, Systems, and Signal Processing*, vol. 31, no. 6, pp. 2001–2017, 2012.

[7] Z. X. Gan and J. Q. Han, "Lyapunov function of general Lurie systems with multiple nonlinearities," *Applied Mathematics Letters*, vol. 16, no. 1, pp. 119–126, 2003.

[8] Q.-L. Han, "Absolute stability of time-delay systems with sector-bounded nonlinearity," *Automatica*, vol. 41, no. 12, pp. 2171–2176, 2005.

[9] J. Wang, Z. Duan, Y. Yang, and L. Huang, *Analysis and Control of Nonlinear Systems with Stationary Sets*, World Scientific Publishing, Singapore, 2009.

[10] G. Z. Feng and J. D. Cao, "Master-slave synchronization of chaotic systems with a modified impulsive controller," *Advances in Difference Equations*, vol. 2013, article 24, 2013.

[11] A. Proskurnikov, "Consensus in switching networks with sectorial nonlinear couplings: absolute stability approach," *Automatica*, vol. 49, no. 2, pp. 488–495, 2013.

[12] J. A. K. Suykens, P. F. Curran, and L. O. Chua, "Master-slave synchronization using dynamic output feedback," *International Journal of Bifurcation and Chaos*, vol. 7, no. 3, pp. 665–669, 1997.

[13] M. E. Yalçin, J. A. K. Suykens, and J. Vandewalle, "Master-slave synchronization of Lur'e systems with time-delay," *International Journal of Bifurcation and Chaos*, vol. 11, no. 6, pp. 1707–1722, 2001.

[14] X. Liao and G. Chen, "Chaos synchronization of general Lur'e systems via time-delay feedback control," *International Journal of Bifurcation and Chaos*, vol. 13, no. 1, pp. 207–213, 2003.

[15] J. Cao, H. X. Li, and D. W. C. Ho, "Synchronization criteria of Lur'e systems with time-delay feedback control," *Chaos, Solitons and Fractals*, vol. 23, no. 4, pp. 1285–1298, 2005.

[16] A. Rantzer, "On the Kalman-Yakubovich-Popov lemma," *Systems and Control Letters*, vol. 28, no. 1, pp. 7–10, 1996.

[17] S. Boyd, L. El Ghaoui, E. Feron, and V. Balakrishnan, *Linear Matrix Inequalities in System and Control Theory*, Society for Industrial and Applied Mathematics, Philadelphia, Pa, USA, 1994.

[18] R. Fletcher, *Practical Methods of Optimization*, John Wiley & Sons, Chichester, UK, 1987.

Hindawi Publishing Corporation
Mathematical Problems in Engineering
Volume 2013, Article ID 898375, 11 pages
http://dx.doi.org/10.1155/2013/898375

Research Article

Cooperative Control for Uncertain Multiagent Systems via Distributed Output Regulation

Lu Yu and Jinzhi Wang

State Key Laboratory for Turbulence and Complex Systems, Department of Mechanics and Aerospace Engineering, College of Engineering, Peking University, Beijing 100871, China

Correspondence should be addressed to Jinzhi Wang; jinzhiw@pku.edu.cn

Received 17 April 2013; Accepted 29 April 2013

Academic Editor: Guanghui Wen

The distributed robust output regulation problem for multiagent systems is considered. For heterogeneous uncertain linear systems and a linear exosystem, the controlling aim is to stabilize the closed-loop system and meanwhile let the regulated outputs converge to the origin asymptotically, by the help of local interaction. The communication topology considered is directed acyclic graphs, which means directed graphs without loops. With distributed dynamic state feedback controller and output feedback controller, respectively, the solvability of the problem and the algorithm of controller design are both investigated. The solvability conditions are given in terms of linear matrix inequalities (LMIs). It is shown that, for polytopic uncertainties, the distributed controllers constructed by solving LMIs can satisfy the requirements of output regulation property.

1. Introduction

Recently, there are amounts of researches on cooperative control for multiagent systems (MASs) because of broad applications. An MAS is a practical model to describe dynamic agents which can exchange information by communication, such as unmanned air vehicles and sensor networks. According to different control objectives, problems of consensus, tracking, formation, flocking and the rest have been widely studied.

Among those cooperative control problems, the consensus problem and the tracking problem share some common characteristics. The consensus problem requires the MAS to reach an agreement by protocols based on local information. In [1, 2], the consensus problem is primarily studied, and the basic problem framework is formed. The consensus problem has been investigated for different kinds of agents, such as first-order integrators in [3], second-order integrators in [4, 5], linear systems in [6–8], and nonlinear systems in [9–12]. Recently, the output consensus problem for heterogeneous systems also attracted researchers. The dynamics and even dimensions of the agents are possibly different, so it is desirable to focus on the synchronization of outputs. In [13], the consensus of a class of second-order integrators with unknown nonlinear dynamics is considered. As for high-order systems, the frequency domain approach is used to discuss the consensus of heterogenous linear systems in [14, 15]. Uncertain minimum-phase linear MASs are studied in [16], by a low-gain approach. In [7], general uncertain linear MASs are considered, and a sufficient and necessary condition for the solvability of the output consensus problem is proposed. It is admirable that Wieland et al. introduce an important concept of internal model to cooperative control, which is also fundamental in output regulation theory.

For the leader-follower consensus problem, also called consensus tracking problem, it involves one or multiple leaders and several followers. A leader is usually the target to be tracked, or the agent that directly receives the information of the target. Distributed controllers are designed to help all the agents to track one or multiple leaders by cooperation. The tracking problem for MASs has been studied in a lot of papers, such as [17–22]. Note that for heterogenous MASs, the outputs of all the agents are required to be synchronized in the issue of both consensus problem and tracking problem. To consider the two kinds of problems under a unified framework is one of the motivations to introduce distributed output regulation (DOR) problem.

According to [23], output regulation problem involves an exosystem and a regulated output defined by a combination of the measurement output and the output of the exosystem. Controllers are designed to stabilize the closed-loop system and modulate the regulated outputs to the origin. So, it has an attracting performance on solving a tracking problem in the presence of disturbances. The classic output regulation theory cannot directly be applied to MASs nevertheless. Actually the controllers obtained are probably not in a distributed form. So, a framework of DOR for MASs is introduced in [24–26]. What is mainly different from the classic theory is that the controllers have to be distributed, and only local information is available. In [24], homogenous linear MASs and a directed topology are considered, and dynamic state/output feedback controllers are designed. In [25], heterogenous MASs are challenged, and effective controllers are obtained under the directed acyclic topology. Different from the two works above, the limits on topology are dispelled in [26] by reconstructing the form of controllers. The communication of relative states of controllers replaces the communication of relative outputs.

This paper is basically motivated by [25]. In [25], the distributed controllers are robust to uncertain dynamics with sufficiently small uncertainties. However, more analyses based on information of the uncertainties are not involved in [25]. What we focus on in our paper is that how to design robust controllers if the uncertainty is structured. We suppose that the uncertainties are in a polytopic form. For the distributed robust output regulation problem, we give sufficient conditions of the solvability in terms of linear matrix inequalities (LMIs) and present an approach of controllers design.

An outline of this paper is as follows. In Section 2, some preliminaries and the problem statement are given. In Section 3, for distributed output regulation problem with polytopic uncertainties, the sufficient conditions of solvability and algorithms of both state and output feedback controllers design are proposed. In Section 4, a practical example is taken to show the control effect of our approach, which is compared with that of the algorithm given in [25]. In Section 5, a conclusion is given.

The following notations will be used throughout this paper. $\mathbb{R}$ is the set of real numbers. I_n is the n-dimensional identity matrix. $0_{m\times n}$ is the zero matrix with m rows and n columns, and 0 is the zero matrix with appropriate dimensions. For a symmetric matrix $M \in \mathbb{R}^{n\times n}$, $M > 0$ which means that M is positive definite. M^T is the transposition of the matrix M. diag block $(M_1, \ldots, M_p)$ means a block diagonal matrix with $M_1, \ldots, M_p$ as the diagonal entries. $\otimes$ denotes the Kronecker product.

2. Problem Statement

Let us begin with notations in graph theory [27]. A graph is denoted by $\mathcal{G} = (\mathcal{V}, \mathcal{E})$, where $\mathcal{V} = \{v_1, v_2, \ldots, v_N\}$ is the set of N nodes and $\mathcal{E} \subseteq \mathcal{V} \times \mathcal{V}$ is the set of edges. An edge from node v_j to node v_i is denoted by $(i, j) \in \mathcal{E}$. A subset of $\mathcal{E}\{(i_1, i_2), (i_2, i_3), \ldots, (i_k, i_{k+1})\}$ is called a path from $v_{i_{k+1}}$ to v_{i_1}. If $i_1 = i_{k+1}$, the path is called a loop. N_i denotes the neighbor set $\{j : (i, j) \in \mathcal{E}, 1 \le j \le N\}$, whose cardinality is $|N_i|$. A constant matrix $A_d = [a_{ij}] \in \mathbb{R}^{N\times N}$ is called the adjacency matrix of graph $\mathcal{G}$ if $a_{ij} = 1/|N_i|$ when $(i, j) \in \mathcal{E}$ and $a_{ij} = 0$ when $(i, j) \notin \mathcal{E}$. And a constant matrix $L = [l_{ij}] = I_N - A_d \in \mathbb{R}^{N\times N}$ is called the Laplacian matrix of graph $\mathcal{G}$. A graph is called an undirected graph if for all $1 \le i, j \le N$, $a_{ij} = a_{ji}$. Or else, it is called a directed graph. If a directed graph does not contain a loop, it is called a directed acyclic graph.

Consider an exosystem with $\omega \in \mathbb{R}^q$ as the state, whose dynamics can be described as follows:

$$\dot{\omega}(t) = S\omega(t), \tag{1}$$

where $S \in \mathbb{R}^{q\times q}$ is a constant matrix, satisfying the following assumption as that in [23, 25].

Assumption 1. S has no eigenvalues with negative real parts.

A MAS consists of N nonidentical dynamic agents which can exchange information among neighborhood. For $i = 1, \ldots, N$, the ith agent can be expressed by

$$\begin{aligned} \dot{x}_i(t) &= \overline{A}_i x_i(t) + \overline{B}_i u_i(t) + \overline{E}_i \omega(t), \\ y_i(t) &= \overline{C}_i x_i(t), \\ e_i(t) &= \overline{C}_i x_i(t) + F\omega(t), \end{aligned} \tag{2}$$

where $x_i \in \mathbb{R}^{p_i}$, $u_i \in \mathbb{R}^{m_i}$, $y_i \in \mathbb{R}^n$, and $e_i \in \mathbb{R}^n$ are, respectively, the state, the control input, the measurement output, and the regulated output of the ith agent. $F \in \mathbb{R}^{n\times q}$ is a certain constant matrix, while those matrices $\overline{A}_i \in \mathbb{R}^{p_i\times p_i}$, $\overline{B}_i \in \mathbb{R}^{p_i\times m_i}$, and $\overline{C}_i \in \mathbb{R}^{n\times p_i}$ are uncertain matrices represented as

$$\begin{aligned} \overline{A}_i &= \sum_{k=1}^{g_i} \lambda_{ki} A_{ki}, \\ \overline{B}_i &= \sum_{k=1}^{g_i} \lambda_{ki} B_{ki}, \\ \overline{C}_i &= \sum_{k=1}^{g_i} \lambda_{ki} C_{ki}, \end{aligned} \tag{3}$$

where A_{ki}, B_{ki}, and C_{ki} are known constant matrices, and λ_{ki} are nonnegative constants satisfying that $\sum_{k=1}^{g_i} \lambda_{ki} = 1$, for $i = 1, \ldots, N, k = 1, \ldots, g_i$. $\overline{E}_i \in \mathbb{R}^{p_i\times q}$ is an arbitrary constant matrix.

The controlling aim is to stabilize the closed-loop system and also to regulate $e_1, \ldots, e_N$ to the origin. For $i = 1, \ldots, N$, if e_i is available to the ith agent, the output regulation of the ith agent is simple to be achieved by classic output regulation theory. However, only some of the agents can get information of their own regulated outputs, which are called leader nodes. The set of their serial numbers is denoted by $\mathcal{L}$, while other agents utilize the relative output among neighbors to accomplish the output regulation property. To ensure that all the agents can receive the information of the exosystem by local interaction, the communication graph of the MAS satisfies the following assumption.

Assumption 2. Graph $\mathscr{G}$ is a directed acyclic graph. And for each nonleader node v_i, there exists a leader node v_j such that a path from node v_j to node v_i exists.

In this note, two kinds of distributed dynamic feedback controllers are considered.

(I) Distributed dynamic state feedback controller:

$$\begin{aligned} \dot{z}_i(t) &= G_1 z_i(t) + G_2 e_{i\omega}(t), \\ u_i(t) &= K_{1i} x_i(t) + K_{2i} z_i(t), \\ z_i(t) &\in \mathbb{R}^c, \quad q \le c, \quad i = 1, \ldots, N, \end{aligned} \tag{4}$$

where

$$e_{i\omega}(t) = \begin{cases} e_i(t) & i \in \mathscr{L} \\ \dfrac{1}{|N_i|} \displaystyle\sum_{j \in N_i} \left(y_i(t) - y_j(t)\right) & i \notin \mathscr{L}. \end{cases} \tag{5}$$

K_{1i}, K_{2i}, G_1, and G_2 are designed matrices with appropriate dimensions.

(II) Distributed dynamic output feedback controller:

$$\begin{aligned} \dot{z}_i(t) &= \overline{G}_{1i} z_i(t) + \overline{G}_{2i} e_{i\omega}(t), \\ u_i(t) &= K_i z_i(t), \\ z_i(t) &\in \mathbb{R}^{c+p_i}, \quad q \le c, \quad i = 1, \ldots, N. \end{aligned} \tag{6}$$

K_i, $\overline{G}_{1i}$, and $\overline{G}_{2i}$ are designed matrices with appropriate dimensions.

The variables $e_{i\omega}(t)$ in distributed feedback control laws (4) and (6) are measurable relative outputs. For $i \in \mathscr{L}$, $e_{i\omega}(t)$ is the regulated output $e_i(t)$. For $i \notin \mathscr{L}$, $e_{i\omega}(t)$ is the average of relative output errors between ith agent and its neighbors.

In the sequel, we rewrite the closed-loop system into a composite form. Let 1_N be a column vector with all the elements as 1. L_i and l_i, respectively, denote the ith row of L and $L1_N$. For $i \in \mathscr{L}$, $l_i = 1$, while for $i \notin \mathscr{L}$, $l_i = 0$. Let $\chi = (x_1^T, z_1^T, \ldots, x_N^T, z_N^T)^T$, $e = (e_1^T, \ldots, e_N^T)^T$,

$$\begin{aligned} \mathscr{A}_1 &= \text{diag block}\left(\mathscr{A}_{11}, \ldots, \mathscr{A}_{1N}\right), \\ \mathscr{A}_2 &= \text{diag block}\left(\mathscr{A}_{21}, \ldots, \mathscr{A}_{2N}\right), \\ \mathscr{C}_1 &= \text{diag block}\left(\left(\overline{C}_1 \ 0_{n\times c}\right), \ldots, \left(\overline{C}_N \ 0_{n\times c}\right)\right), \\ \mathscr{C}_2 &= \text{diag block}\left(\left(\overline{C}_1 \ 0_{n\times(c+p_1)}\right), \ldots, \left(\overline{C}_N \ 0_{n\times(c+p_N)}\right)\right), \\ \mathscr{G}_1 &= \begin{pmatrix} L_1 \otimes G_{21}' \\ \vdots \\ L_N \otimes G_{2N}' \end{pmatrix}, \qquad \mathscr{G}_2 = \begin{pmatrix} L_1 \otimes \overline{G}_{21}' \\ \vdots \\ L_N \otimes \overline{G}_{2N}' \end{pmatrix}, \\ \mathscr{E}_1 &= \begin{pmatrix} \overline{E}_1 \\ l_1 G_2 F \\ \vdots \\ \overline{E}_N \\ l_N G_2 F \end{pmatrix}, \qquad \mathscr{E}_2 = \begin{pmatrix} \overline{E}_1 \\ l_1 \overline{G}_{21} F \\ \vdots \\ \overline{E}_N \\ l_N \overline{G}_{2N} F \end{pmatrix}, \end{aligned} \tag{7}$$

where $\mathscr{A}_{1i} = \begin{pmatrix} \overline{A}_i + \overline{B}_i K_{1i} & \overline{B}_i K_{2i} \\ 0 & G_1 \end{pmatrix}$, $\mathscr{A}_{2i} = \begin{pmatrix} \overline{A}_i & \overline{B}_i K_i \\ 0 & \overline{G}_{1i} \end{pmatrix}$, $G_{2i}' = \begin{pmatrix} 0_{n\times p_i} \\ G_2 \end{pmatrix}$, and $\overline{G}_{2i}' = \begin{pmatrix} 0_{n\times p_i} \\ \overline{G}_{2i} \end{pmatrix}$, for $i = 1, \ldots, N$. Then, the closed-loop system (1), (2) with controllers (4) or (6) can be rewritten as

$$\begin{aligned} \dot{\omega}(t) &= S\omega(t), \\ \dot{\chi}(t) &= A_c \chi(t) + B_c \omega(t), \\ e(t) &= C_c \chi(t) + F_c \omega(t). \end{aligned} \tag{8}$$

With the controller (4),

$$\begin{aligned} A_c &= \mathscr{A}_1 + \mathscr{G}_1 \mathscr{C}_1, \qquad B_c = \mathscr{E}_1, \\ C_c &= \mathscr{C}_1, \qquad F_c = 1_N \otimes F, \end{aligned} \tag{9}$$

while with the controller (6),

$$\begin{aligned} A_c &= \mathscr{A}_2 + \mathscr{G}_2 \mathscr{C}_2, \qquad B_c = \mathscr{E}_2, \\ C_c &= \mathscr{C}_2, \qquad F_c = 1_N \otimes F. \end{aligned} \tag{10}$$

As a result, the distributed output regulation problem studied in this paper is given as follows.

Problem 3. Distributed output regulation problem: design controllers in the form of (4) or (6) such that the closed-loop system (8) has the following properties.

(i) It is exponentially stable at the origin with $\omega = 0$.

(ii) For all initial values $\chi(0)$ and $\omega(0)$, $\lim_{t\to\infty} e(t) = 0$.

3. Main Results

In this section, we give two theorems about the solvability of Problem 3 and the approach of controller design. First of all, we introduce the concept of quadratic stability and related lemmas, which will be used later.

Definition 4 (Amato [28]). Consider a parametric uncertain linear system given by

$$\dot{x}(t) = A(p_0)\, x(t), \quad t \in [0, +\infty), \tag{11}$$

where $x(t) \in \mathbb{R}^{n_0}$, $p_0 \in H \subset \mathbb{R}^{m_0}$ is the vector of uncertain parameters, where H is a hyperbox, and $A(\cdot)$ is continuous. This system is said to be quadratically stable (QS) in H if and only if there exists a symmetric positive definite matrix $P \in \mathbb{R}^{n_0\times n_0}$ such that for all $p_0 \in H$, $A^T(p_0)P + PA(p_0) < 0$.

Lemma 5 (Amato [28]). *Assume that the system* (11) *is QS. Then, for any function $p_0(\cdot)$ that is piecewise continuous on $\mathbb{R}^+$ and valued on W, the linear time-varying system $\dot{x}(t) = A(p_0(t))x(t)$ is exponentially stable.*

Lemma 6 (Amato [28]). *Assume that the uncertain system is in a polytopic form; that is,*

$$\dot{x}(t) = A(t)\, x(t), \quad A(t) \in \text{conv}\left\{A_1, A_2, \ldots, A_g\right\}, \tag{12}$$

where $A_1, \ldots, A_g \in \mathbb{R}^{n_0\times n_0}$ and conv$\{\cdot\}$ *represents the convex hull of the following matrices. It is QS if and only if there exists a positive definite symmetric matrix P such that for $k = 1, \ldots, g$, $A_k^T P + PA_k < 0$.*

Second, we need to recall the concept of internal model and its property.

Definition 7 (Huang [23]). Given any square matrix S, a pair of matrices $(\mathcal{G}_1, \mathcal{G}_2)$ is said to incorporate a p-copy internal model of the matrix S if the pair satisfies that

$$\mathcal{G}_1 = T\begin{pmatrix} S_1 & S_2 \\ 0 & G_1 \end{pmatrix}T^{-1}, \qquad \mathcal{G}_2 = T\begin{pmatrix} S_3 \\ G_2 \end{pmatrix}, \tag{13}$$

where S_1, S_2, and S_3 are arbitrary constant matrices of appropriate dimensions, T is any nonsingular matrix with the same dimension as $\mathcal{G}_1$, and G_1, G_2 are described as follows:

$$\begin{aligned} G_1 &= \text{block diag}\left(\beta_1, \ldots, \beta_p\right), \\ G_2 &= \text{block diag}\left(\sigma_1, \ldots, \sigma_p\right), \end{aligned} \tag{14}$$

where for $j = 1, \ldots, p$, β_j is a constant square matrix of dimension d_j for some integer d_j and σ_j is a constant column vector of dimension d_j such that

(i) β_i and σ_i are controllable,

(ii) the minimal polynomial of S divides the characteristic polynomial of β_i.

Lemma 8 (Huang [23]). *Under Assumption 1, assume that $(\mathcal{G}_1, \mathcal{G}_2)$ incorporates a p-copy internal model of S. Let*

$$\begin{bmatrix} \widehat{A} & \widehat{B} \\ \mathcal{G}_2\widehat{C} & \mathcal{G}_1 \end{bmatrix} \tag{15}$$

be exponentially stable, where $\widehat{A}$, $\widehat{B}$, and $\widehat{C}$ are any matrices with appropriate dimensions. Then, for any matrices $\widehat{E}$ and $\widehat{F}$ of appropriate dimensions, the following matrix equations

$$\begin{aligned} XS &= \widehat{A}X + \widehat{B}Z + \widehat{E}, \\ ZS &= \mathcal{G}_1 Z + \mathcal{G}_2\left(\widehat{C}X + \widehat{F}\right) \end{aligned} \tag{16}$$

have a unique solution X and Z. Moreover, X satisfies $\widehat{C}X + \widehat{F} = 0$.

Based on these preparations, theorems on solvability of Problem 3 with state/output feedback controllers are given as follows.

Theorem 9. *Suppose that Assumptions 1 and 2 hold and the pair (G_1, G_2) is a p-copy internal model of the exosystem* (1). *For $i = 1, \ldots, N$, if there exist a matrix Y_i and a positive definite matrix $\widetilde{P}_i$ satisfying that*

$$\widetilde{A}_{ki}\widetilde{P}_i + \widetilde{P}_i\widetilde{A}_{ki}^T + \widetilde{B}_{ki}Y_i + Y_i^T\widetilde{B}_{ki}^T < 0, \quad k = 1, \ldots, g_i, \tag{17}$$

where

$$\widetilde{A}_{ki} = \begin{pmatrix} A_{ki} & 0 \\ G_2C_{ki} & G_1 \end{pmatrix}, \qquad \widetilde{B}_{ki} = \begin{pmatrix} B_{ki} \\ 0 \end{pmatrix}, \tag{18}$$

Then, Problem 3 is solvable by a dynamic state feedback controller (4), *where $(K_{1i}, K_{2i}) = K_i = Y_i\widetilde{P}_i^{-1}$.*

Proof. Let $\gamma_i(t) = (x_i^T, z_i^T)^T$. Then, the subsystems of (8) with controller (4) can be written as follows: for $i \in \mathcal{L}$,

$$\dot{\gamma}_i(t) = \begin{pmatrix} \overline{A}_i + \overline{B}_iK_{1i} & \overline{B}_iK_{2i} \\ G_2\overline{C}_i & G_1 \end{pmatrix}\gamma_i(t) + \begin{pmatrix} \overline{E}_i \\ G_2F \end{pmatrix}w(t), \tag{19}$$

and for $i \notin \mathcal{L}$,

$$\begin{aligned} \dot{\gamma}_i(t) = &\begin{pmatrix} \overline{A}_i + \overline{B}_iK_{1i} & \overline{B}_iK_{2i} \\ G_2\overline{C}_i & G_1 \end{pmatrix}\gamma_i(t) + \begin{pmatrix} \overline{E}_i \\ 0 \end{pmatrix}w(t) \\ &+ \frac{1}{|N_i|}\sum_{j\in N_i}\begin{pmatrix} 0 & 0 \\ -G_2\overline{C}_j & 0 \end{pmatrix}\gamma_j(t). \end{aligned} \tag{20}$$

According to [29], by relabeling the nodes, a directed acyclic graph could be put into an ordered form. That is to say, for all edges $(i, j) \in \mathcal{E}$, $i > j$ holds. Notice that matrix A_c is consequently a block lower triangular matrix and system (8) with $w = 0$ is asymptotically stable if and only if all the subsystems below are asymptotically stable

$$\begin{aligned} \dot{\gamma}_i(t) &= \begin{pmatrix} \overline{A}_i + \overline{B}_iK_{1i} & \overline{B}_iK_{2i} \\ G_2\overline{C}_i & G_1 \end{pmatrix}\gamma_i(t) \\ &= \sum_{k=1}^{g_i}\lambda_{ki}\begin{pmatrix} A_{ki} + B_{ki}K_{1i} & B_{ki}K_{2i} \\ G_2C_{ki} & G_1 \end{pmatrix}\gamma_i(t) \\ &= \sum_{k=1}^{g_i}\lambda_{ki}\left(\widetilde{A}_{ki} + \widetilde{B}_{ki}K_i\right)\gamma_i(t). \end{aligned} \tag{21}$$

Consider LMI (17). When it holds for a symmetric positive definite matrix $\widetilde{P}_i$ and a matrix Y_i, let $P_i = \widetilde{P}_i^{-1}$, and let $K_i = Y_iP_i$. Pre- and postmultiplied by P_i, (17) is equivalent to the following inequality:

$$\left(\widetilde{A}_{ki} + \widetilde{B}_{ki}K_i\right)^T P_i + P_i\left(\widetilde{A}_{ki} + \widetilde{B}_{ki}K_i\right) < 0. \tag{22}$$

According to Lemma 6, when it holds, the subsystems (21) are all QS. And according to Lemma 5, for any polytopic uncertainties, the subsystems are exponentially stable. The system (8) with $w = 0$ is consequently exponentially stable. The condition (i) of Problem 3 has been satisfied. In the following, the error $e(t)$ is proved to converge to zero.

Since the matrix $\begin{pmatrix} \overline{A}_i + \overline{B}_iK_{1i} & \overline{B}_iK_{2i} \\ G_2\overline{C}_i & G_1 \end{pmatrix}$ is Hurwitz, according to Lemma 8, for any $\overline{E}_i$ and F_i, the following matrix equations

$$\begin{aligned} X_iS &= \left(\overline{A}_i + \overline{B}_iK_{1i}\right)X_i + \overline{B}_iK_{2i}Z_i + \overline{E}_i, \\ Z_iS &= G_1Z_i + G_2\left(\overline{C}_iX_i + F_i\right) \end{aligned} \tag{23}$$

have a unique solution X_i and Z_i, and at the same time, $\overline{C}_iX_i + F_i = 0$. For $i \in \mathcal{L}$, $F_i = F$, otherwise, $F_i = (-1/|N_i|)\sum_{j\in N_i}\overline{C}_jX_j$. Therefore, the N coupled matrix equations have a unique solution $(X_1, Z_1, \ldots, X_N, Z_N)$.

The proof will be given by induction. As mentioned earlier, each agent can only receive information from the agents with smaller labels, after appropriately relabeling the

directed acyclic graph. That is to say, for $i = 1, 2, \ldots, N$, $F_i = F$ or $F_i = (-1/|N_i|)\sum_{j=1, j\in N_i}^{i-1} \overline{C}_j X_j$. For $i = 1$, the first agent does not communicate with any other agents but the exosystem, so $F_1 = F$. And we can obtain a unique pair of (X_1, Z_1) that satisfies (23) and $\overline{C}_1 X_1 + F_1 = 0$. For $i = 2$, if it is a leader, then $F_2 = F$; or else, it can only communicate with the first agent, which means that $F_2 = -\overline{C}_1 X_1$. In both cases F_2 is a certain and known matrix, so there exists a unique solution (X_2, Z_2) of (23) and $\overline{C}_2 X_2 + F_2 = 0$. Suppose that for $i = 1, 2, \ldots, m$, the solution (X_i, Z_i) has already been obtained. And then for $i = m + 1$, either $F_i = F$ or $F_i = (-1/|N_i|)\sum_{j=1, j\in N_i}^{i-1} \overline{C}_j X_j$ is a certain and known matrix. So, the unique solution (X_{m+1}, Z_{m+1}) also exists. By induction, we can obtain the unique solution $(X_1, Z_1, \ldots, X_N, Z_N)$, and at the same time, $\overline{C}_1 X_1 + F_1 = \cdots = \overline{C}_N X_N + F_N = 0$.

Take notations $\Gamma_i = \begin{pmatrix} X_i \\ Z_i \end{pmatrix}$ and $\widetilde{\gamma}_i = \gamma_i - \Gamma_i \omega$, and substitute (23) into (19) and (20). It is obtained that

$$\begin{aligned}
\dot{\widetilde{\gamma}}_i(t) &= \dot{\gamma}_i(t) - \Gamma_i S\omega(t) \\
&= \begin{pmatrix} \overline{A}_i + \overline{B}_i K_{1i} & \overline{B}_i K_{2i} \\ G_2 \overline{C}_i & G_1 \end{pmatrix} \widetilde{\gamma}_i(t), \quad i \in \mathscr{L}, \\
\dot{\widetilde{\gamma}}_i(t) &= \dot{\gamma}_i(t) - \Gamma_i S\omega(t) \\
&= \begin{pmatrix} \overline{A}_i + \overline{B}_i K_{1i} & \overline{B}_i K_{2i} \\ G_2 \overline{C}_i & G_1 \end{pmatrix} \widetilde{\gamma}_i(t) \\
&\quad - \frac{1}{|N_i|} \sum_{j\in N_i} \begin{pmatrix} 0 & 0 \\ G_2 \overline{C}_j & 0 \end{pmatrix} \widetilde{\gamma}_j(t), \quad i \notin \mathscr{L}.
\end{aligned} \tag{24}$$

By the first part of the proof, the system above is exponentially stable; that is,

$$\lim_{t\to\infty} \widetilde{\gamma}_i(t) = 0, \quad i = 1, \ldots, N. \tag{25}$$

Since

$$\begin{aligned}
e_{i\omega}(t) &= \overline{C}_i x_i(t) + F\omega(t) \\
&= \left(\overline{C}_i \ 0\right) \widetilde{\gamma}_i(t) + \left(\overline{C}_i X_i + F\right) \omega(t), \quad i \in \mathscr{L}, \\
e_{i\omega}(t) &= \overline{C}_i x_i(t) - \frac{1}{|N_i|} \sum_{j\in N_i} \overline{C}_j x_j(t) \\
&= \left(\overline{C}_i \ 0\right) \widetilde{\gamma}_i(t) - \frac{1}{|N_i|} \sum_{j\in N_i} \left(\overline{C}_j \ 0\right) \widetilde{\gamma}_j(t) \\
&\quad + \left(\overline{C}_i X_i + F_i\right) \omega(t), \quad i \notin \mathscr{L},
\end{aligned} \tag{26}$$

it is obvious that

$$\lim_{t\to\infty} e_{i\omega}(t) = 0, \quad i = 1, \ldots, N. \tag{27}$$

Under Assumption 2, the statement (27) is equivalent to $\lim_{t\to\infty} e(t) = 0$. This completes the proof. □

Remark 10. When there is no uncertainty in the system (2), $\overline{A}_i = A_{1i}$, $\overline{B}_i = B_{1i}$, and $\overline{C}_i = C_{1i}$, $i = 1, \ldots, N$. Then, the conclusion of Theorem 9 still holds if the solvability of LMI (17) is replaced by the statement that the pair (A_{1i}, B_{1i}) is stabilizable. In fact, according to [23], from the two statements,

(i) the pair (A_{1i}, B_{1i}) is stabilizable,

(ii) Assumption 1 holds, and the pair (G_1, G_2) is an internal model of S; it is followed that the pair

$$\left(\begin{pmatrix} A_{1i} & 0 \\ G_2 C_{1i} & G_1 \end{pmatrix}, \begin{pmatrix} B_{1i} \\ 0 \end{pmatrix}\right) \tag{28}$$

is stabilizable. It is equivalent to LMI (17) that holds with $g_i = 1$, $i = 1, \ldots, N$. Specially, if for $i = 1, \ldots, N$, $A_{1i} = A$, $B_{2i} = B$, and $C_{1i} = C$, $g_i = 1$, then in Theorem 9, the solvability of LMI (17) can be replaced by the statement that the pair (A, B) is stabilizable.

Theorem 11. *Suppose that Assumptions 1 and 2 hold and the pair (G_1, G_2) is an internal model of the exosystem (1) if the following conditions are satisfied:*

(i) *For $i = 1, \ldots, N$, there exist a matrix Y_i and a symmetric positive definite matrix $\widetilde{P}_i$ satisfying LMI (17),*

(ii) *For $i = 1, \ldots, N$, and the matrices Y_i, $\widetilde{P}_i$ obtained in (i), let $P_i = \widetilde{P}_i^{-1}$, and let $K_i = (K_{1i}, K_{2i}) = Y_i P_i$, and there exist matrices M_{1i}, M_{2i}, M_{3i} and a symmetric positive definite matrix Q_i satisfying the following LMI:*

$$\begin{pmatrix} \overline{\Pi}_{11,ki} & \overline{\Pi}_{12,ki} \\ \overline{\Pi}_{12,ki}^T & \overline{\Pi}_{22,ki} \end{pmatrix} < 0, \tag{29}$$

where

$$\begin{aligned}
\overline{\Pi}_{11,ki} &= P_i \widetilde{A}_{ki} + \widetilde{A}_{ki}^T P_i + \widetilde{B}_{ki} K_i P_i + P_i K_i^T \widetilde{B}_{ki}^T, \\
\overline{\Pi}_{12,ki} &= P_i \begin{pmatrix} B_{ki} K_{1i} \\ 0 \end{pmatrix} \\
&\quad + \begin{pmatrix} -A_{ki}^T Q_i - K_{1i}^T B_{ki} Q_i + M_{1i}^T + C_{ki}^T M_{3i}^T \\ -K_{2i}^T B_{ki}^T Q_i + M_{2i}^T \end{pmatrix}, \\
\overline{\Pi}_{22,ki} &= -Q_i B_{ki} K_{1i} - K_{1i}^T B_{ki}^T Q_i + M_{1i} + M_{1i}^T, \\
&\qquad k = 1, \ldots, g_i.
\end{aligned} \tag{30}$$

Then, Problem 3 is solvable by a dynamic output feedback controller (6) with

$$\overline{G}_{1i} = \begin{pmatrix} T_{1i} & T_{2i} \\ 0 & G_1 \end{pmatrix}, \qquad \overline{G}_{2i} = \begin{pmatrix} T_{3i} \\ G_2 \end{pmatrix}, \tag{31}$$

where $T_{1i} = Q_i^{-1} M_{1i}$, $T_{2i} = Q_i^{-1} M_{2i}$, and $T_{3i} = Q_i^{-1} M_{3i}$.

Proof. For $i = 1, \ldots, N$, the subsystems of (8) with (6) and (31) can be written in such a form: for $i \in \mathscr{L}$,

$$\dot{\gamma}_i(t) = \begin{pmatrix} \overline{A}_i & \overline{B}_i K_{1i} & \overline{B}_i K_{2i} \\ T_{3i} \overline{C}_i & T_{1i} & T_{2i} \\ G_2 \overline{C}_i & 0 & G_1 \end{pmatrix} \gamma_i(t) + \begin{pmatrix} \overline{E}_i \\ T_{3i} F \\ G_2 F \end{pmatrix} w(t), \tag{32}$$

and for $i \notin \mathscr{L}$,

$$\dot{\gamma}_i(t) = \begin{pmatrix} \overline{A}_i & \overline{B}_i K_{1i} & \overline{B}_i K_{2i} \\ T_{3i}\overline{C}_i & T_{1i} & T_{2i} \\ G_2\overline{C}_i & 0 & G_1 \end{pmatrix} \gamma_i(t) + \begin{pmatrix} \overline{E}_i \\ 0 \\ 0 \end{pmatrix} w(t) - \frac{1}{|N_i|} \sum_{j \in N_i} \begin{pmatrix} 0 & 0 & 0 \\ T_{3i}\overline{C}_j & 0 & 0 \\ G_2\overline{C}_j & 0 & 0 \end{pmatrix} \gamma_j(t). \tag{33}$$

Similar to the proof of the previous theorem, the stability of the system (8) with $\omega = 0$ is dependent on the following subsystems:

$$\dot{\gamma}_i(t) = \begin{pmatrix} \overline{A}_i & \overline{B}_i K_{1i} & \overline{B}_i K_{2i} \\ T_{3i}\overline{C}_i & T_{1i} & T_{2i} \\ G_2\overline{C}_i & 0 & G_1 \end{pmatrix} \gamma_i(t) = \sum_{k=1}^{g_i} \lambda_{ki} \begin{pmatrix} A_{ki} & B_{ki}K_{1i} & B_{ki}K_{2i} \\ T_{3i}C_{ki} & T_{1i} & T_{2i} \\ G_2C_{ki} & 0 & G_1 \end{pmatrix} \gamma_i(t). \tag{34}$$

Let

$$\xi_i(t) = \begin{pmatrix} I_{p_i} & 0 & 0 \\ 0 & 0 & I_c \\ -I_{p_i} & I_{p_i} & 0 \end{pmatrix} \gamma_i(t). \tag{35}$$

Then, the subsystem (34) is similar to the following system:

$$\dot{\xi}_i(t) = \sum_{k=1}^{g_i} \lambda_{ki} \begin{pmatrix} A_{ki} + B_{ki}K_{1i} & B_{ki}K_{2i} & B_{ki}K_{1i} \\ G_2C_{ki} & G_1 & 0 \\ U_{ki} & V_{ki} & W_{ki} \end{pmatrix} \xi_i(t), \tag{36}$$

where

$$U_{ki} = T_{1i} + T_{3i}C_{ki} - A_{ki} - B_{ki}K_{1i}, \qquad V_{ki} = T_{2i} - B_{ki}K_{2i}, \qquad W_{ki} = T_{1i} - B_{ki}K_{1i}. \tag{37}$$

According to Lemma 6, the system (36) is QS if there exists a symmetric positive definite matrix $R_i > 0$ such that

$$\begin{pmatrix} A_{ki} + B_{ki}K_{1i} & B_{ki}K_{2i} & B_{ki}K_{1i} \\ G_2C_{ki} & G_1 & 0 \\ U_{ki} & V_{ki} & W_{ki} \end{pmatrix}^T R_i + R_i \begin{pmatrix} A_{ki} + B_{ki}K_{1i} & B_{ki}K_{2i} & B_{ki}K_{1i} \\ G_2C_{ki} & G_1 & 0 \\ U_{ki} & V_{ki} & W_{ki} \end{pmatrix} < 0. \tag{38}$$

Suppose that R_i is a block diagonal matrix, which means that $R_i = \begin{pmatrix} P_i & 0 \\ 0 & Q_i \end{pmatrix}$, $P_i \in \mathbb{R}^{(p_i+c)\times(p_i+c)}$, and $Q_i \in \mathbb{R}^{p_i \times p_i}$. Then, the inequality above can be rewritten as

$$\begin{pmatrix} \Pi_{11,ki} & \Pi_{12,ki} \\ \Pi_{12,ki}^T & \Pi_{22,ki} \end{pmatrix} < 0, \tag{39}$$

where

$$\Pi_{11,ki} = \left(\widetilde{A}_{ki} + \widetilde{B}_{ki}K_i\right)^T P_i + P_i\left(\widetilde{A}_{ki} + \widetilde{B}_{ki}K_i\right), \qquad \Pi_{12,ki} = P_i \begin{pmatrix} B_{ki}K_{1i} \\ 0 \end{pmatrix} + \begin{pmatrix} U_{ki}^T \\ V_{ki}^T \end{pmatrix} Q_i, \qquad \Pi_{22,ki} = W_{ki}^T Q_i + Q_i W_{ki}. \tag{40}$$

Notice that $\Pi_{11,ki} < 0$ is just the inequality (22), which is equivalent to LMI (17). When $\Pi_{11,ki} < 0$ holds, the matrices $\widetilde{P}_i$, Y_i, $P_i = \widetilde{P}_i^{-1}$, $K_i = (K_{1i}, K_{2i}) = Y_i\widetilde{P}_i$ have already been obtained. Let $Q_iT_{1i} = M_{1i}$, $Q_iT_{2i} = M_{2i}$, and $Q_iT_{3i} = M_{3i}$. We turn the inequality (39) into LMI (29). This implies that the system (8) with $\omega = 0$ is asymptotically stable.

The rest part of the proof is similar to that in Theorem 9. Recalling that $\begin{pmatrix} \overline{A}_i & \overline{B}_iK_i \\ \overline{G}_{2i}\overline{C}_i & \overline{G}_{1i} \end{pmatrix}$ is Hurwitz and $(\overline{G}_{1i}, \overline{G}_{2i})$ incorporates a p-copy internal model of S, we can obtain that for any matrices $\overline{E}_i$ and F_i, the following matrix equations

$$\overline{X}_iS = \overline{A}_i\overline{X}_i + \overline{B}_iK_i\overline{Z}_i + \overline{E}_i, \qquad \overline{Z}_iS = \overline{G}_{1i}\overline{Z}_i + \overline{G}_{2i}\left(\overline{C}_i\overline{X}_i + F_i\right) \tag{41}$$

have a unique solution $\overline{X}_i$ and $\overline{Z}_i$. And meanwhile, $\overline{C}_i\overline{X}_i + F_i = 0$. For $i \in \mathscr{L}$, $F_i = F$, otherwise $F_i = (-1/|N_i|)\sum_{j\in N_i}\overline{C}_j\overline{X}_j$.

Take notations $\overline{\Gamma}_i = \begin{pmatrix} \overline{X}_i \\ \overline{Z}_i \end{pmatrix}$ and $\overline{\gamma}_i(t) = \gamma_i(t) - \overline{\Gamma}_i\omega(t)$. By calculation, it can be verified that $\lim_{t\to\infty}\overline{\gamma}_i(t) = 0$. Consequently, $\lim_{t\to\infty}e_{i\omega}(t) = 0$. When Assumption 2 holds, the above statement is equivalent to $\lim_{t\to\infty}e(t) = 0$. This completes the proof. □

Remark 12. Consider the robust tracking problem for heterogenous MAS in the presence of disturbances. Suppose that an active leader is described as

$$\dot{x}_k(t) = A_kx_k(t), \qquad y_k(t) = C_kx_k(t), \tag{42}$$

and there is an environmental disturbance $d(t)$ satisfying

$$\dot{d}(t) = A_dd(t). \tag{43}$$

The model of the MAS can be given in

$$\dot{x}_i(t) = \overline{A}_ix_i(t) + \overline{B}_iu_i(t) + E_{di}d(t), \qquad y_i(t) = \overline{C}_ix_i(t), \qquad i = 1, \ldots, N, \tag{44}$$

where $\overline{A}_i$, $\overline{B}_i$, $\overline{C}_i$, and E_di are uncertain matrices with polytopic uncertainties. The control target is to design distributed controllers such that the outputs of followers track the output of the leader. That is to say, for $i = 1, \ldots, N$, $e_i(t) = y_i(t) - y_k(t)$ converges to zero. This problem is just Problem 3 with $\omega = (x_k^T, d^T)^T$, $S = \text{diag block}\,(A_k, A_d)$, $\overline{E} = \begin{pmatrix} 0 & E_{di} \end{pmatrix}$, and $F = \begin{pmatrix} -C_k & 0 \end{pmatrix}$. The robust tracking problem for the systems (44), therefore, can be studied under the framework of DOR problem. It can be solved by designing the controller (4) or (6) if the conditions in Theorems 9 or 11 are satisfied.

Remark 13. By Theorems 9 and 11, the sufficient condition of the solvability for Problem 3 depends on the dynamics of each agent. For a heterogenous MAS, N LMIs have to be solved to obtain appropriate distributed controllers, which limits scalability. When the agents share some common characteristics, such as nominal parts, the complexity of LMIs will decrease. Specially, if agents are identical in the sense of common nominal parts and common bounds of the uncertainties, the solution to one LMI will construct the required control law.

4. A Numerical Example

In this section, a numerical example of a heterogenous MAS consisting seven agents is given to show the control effect of controllers obtained by Theorems 9 and 11. A comparison is also given between our controllers and that of [25]. In the example, suppose that there is a constant environmental noise and the reference signal (the output of the tracking target) is a sinusoidal signal. Let $\omega = (\omega_1, \omega_2, \omega_3)^T$, where ω_1, ω_2 serve as the reference signals and ω_3 as the exogenous disturbance. Obviously, the differential equations about them are $\ddot{\omega}_1(t) = -\omega_1(t)$, $\ddot{\omega}_2(t) = -\omega_2(t)$, and $\ddot{\omega}_3(t) = 0$. Therefore, the exosystem can be described by (1) with

$$S = \begin{pmatrix} 0 & 1 & 0 \\ -1 & 0 & 0 \\ 0 & 0 & 0 \end{pmatrix}. \tag{45}$$

According to [23], we can immediately obtain a 1-copy internal model as follows:

$$G_1 = \begin{pmatrix} 0 & 1 & 0 \\ 0 & 0 & 1 \\ 0 & -1 & 0 \end{pmatrix}, \qquad G_2 = \begin{pmatrix} 0 \\ 0 \\ 1 \end{pmatrix}. \tag{46}$$

In the example, three kinds of linear agents with 2, 3, and 4 orders are considered. 2 or 3 basement matrices are randomly valued for each kind. We present the detailed description of basement matrices in the appendix.

And as for $\overline{E}_1, \ldots, \overline{E}_7$, their first two columns are zeros, noticing that only ω_3 refers to the disturbance, while the other elements are valued randomly. Finally, the regulated output, regarded as the tracking error between $y_i(t)$ and the sine reference signal $\omega_1(t)$, is defined as $e_i(t) = y_i(t) - \omega_1(t) = \overline{C}_i x_i(t) + F\omega(t)$, so, value $F = \begin{pmatrix} -1 & 0 & 0 \end{pmatrix}$.

The communication network is described by the directed acyclic graph shown in Figure 1, which satisfies Assumption 2. According to Theorem 11, by solving three kinds of LMIs as (17), we get control gains $K_1 = K_2 = (-6.3230, 28.5507, 2.6636, 0.9019, 6.8977)$, $K_3 = K_4 = K_5 = (0.9071, -9.9908, 10.4217, -1.2503, 0.9513, -3.1324)$, $K_6 = K_7 = (226.6539, 117.7418, -20.0749, -91.1218, 4.6064, -2.6648, 11.6774)$. If the states of each agent are measurable, then a candidate distributed controller can be chosen as (4) with the coefficients $K_1, \ldots, K_7$. Or else, one more group of LMIs (29) need to be solved to construct the output feedback controllers. In this situation, we obtain T_{1i}, T_{2i} and T_{3i} for $i = 1, \ldots, 7$, which are also listed in the appendix due to space limitation. And then the distributed dynamic output feedback controllers are given as (6). For simplicity, we denote this control law as controller C_a.

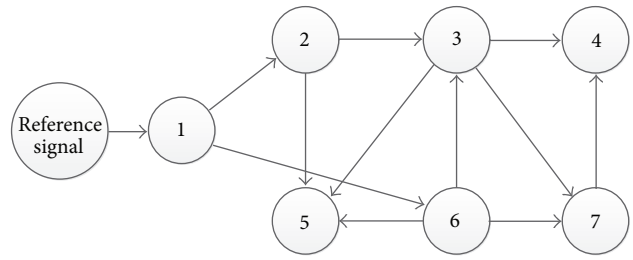

Figure 1: Information flow among exosystem and agents.

On the other hand, we translate the polytopic uncertainty into an equivalent form that consists of a nominal part and an uncertain part. In this case, the nominal part $A_1, \ldots, A_7$, $B_1, \ldots, B_7$, and $C_1, \ldots, C_7$ can be valued as the average of the basement matrices. Then, by the algorithm in [25], for $i = 1, \ldots, 7$, the candidate control law can be chosen as (6) with

$$\begin{gathered} \overline{G}_{1i} = \begin{pmatrix} A_i + B_i K_{1i} + L_i C_i & B_i K_{2i} \\ 0 & G_1 \end{pmatrix}, \\ \overline{G}_{2i} = \begin{pmatrix} -L_i \\ G_2 \end{pmatrix}, \qquad J_i = Q_i^{-1} Z_i, \end{gathered} \tag{47}$$

where $K_1 = K_2 = (-10, 0, 2, 1, -1)$, $L_1 = L_2 = (9.5, 10)^T$, $K_3 = K_4 = K_5 = (-9, -2, -4, 3, 2, 4)$, $L_3 = L_4 = L_5 = (30, -70, 28)^T$, $K_6 = K_7 = (10, 10, -2, 5, 1, 2, -2)^T$, $L_5 = L_6 = L_7 = (-69, -41, -10, -10)^T$. For simplicity, this control law obtained by [25] is denoted by controller C_b.

Note that both controllers C_a and C_b are robust controllers against the model uncertainty. To compare the effects, two cases of uncertainties are considered in the example. For one case, the model uncertainties denoted by Δ_1 are rather close to the "nominal part" set earlier. For $i = 1, \ldots, 7$, $k = 1, \ldots, g_i$, the values of λ_{ki} are randomly chosen around $1/g_i$, whose values are shown in the appendix. For another case, the model uncertainties denoted by Δ_2 are valued freely with reasonable coefficients, which are relatively farther from the "nominal part." With the same initial values, the numerical results of the regulated output for each agent are demonstrated in Figure 2 and Figure 3. Our controller C_a is effective in the presence of either Δ_1 or Δ_2. However, as for Controller C_b, when the uncertainty is relatively small, it can help to achieve the output regulation property. While in the case of Δ_2, the regulated errors diverge rapidly as shown in Figure 3(b). As a consequence of the above, for Problem 3 with polytopic uncertainties, Theorems 9 and 11 help construct distributed dynamic state/output feedback controllers of stronger robustness, at the price of increasing the calculation complexity.

5. Conclusions

In this paper, we consider the distributed robust output regulation problem for MASs under the topology of directed

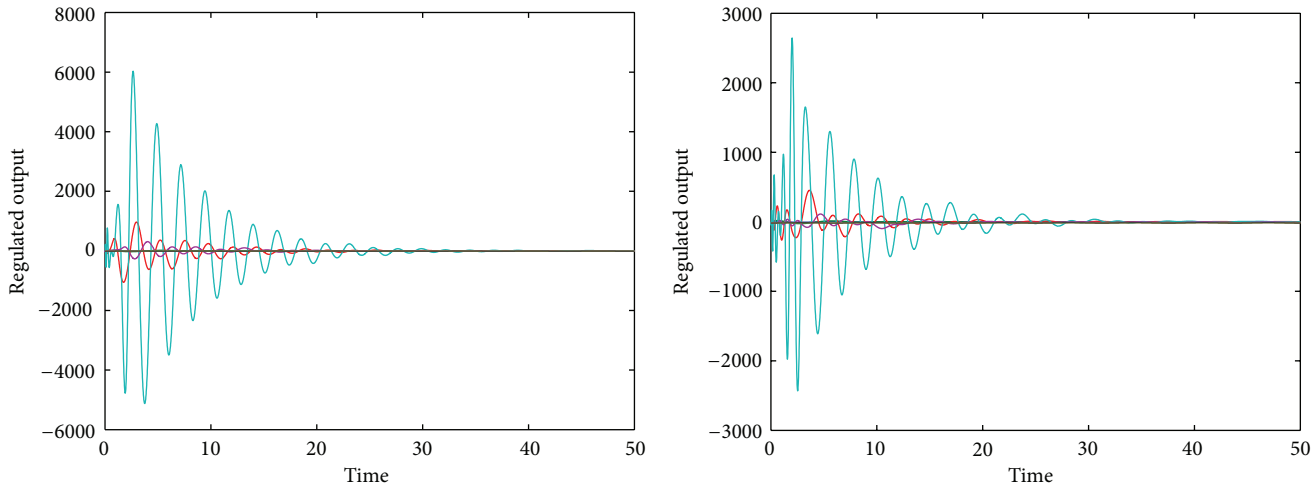

(a) For uncertainty Δ_1 (b) For uncertainty Δ_2

Figure 2: Regulated output of the MAS with the controller C_a.

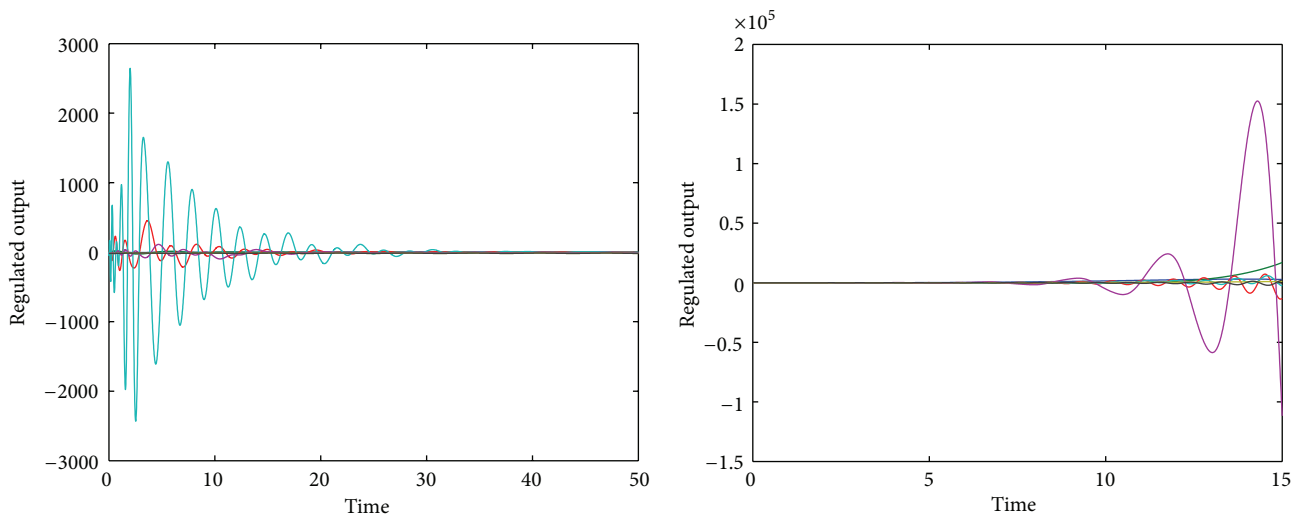

(a) For uncertainty Δ_1 (b) For uncertainty Δ_2

Figure 3: Regulated output of the MAS with the controller C_b.

acyclic graphs. As an extension of the existing results, we focus on a special class of parametric uncertainty. Assume that the dynamics of heterogeneous agents are in a polytopic form, and we study the solvability of the problem and the design of distributed controllers. Both dynamic state feedback controller and dynamic output feedback controller are under consideration. At last, a practical example is presented to validate our results. By local interaction, a team of heterogenous agents is required to achieve a common output, which is generated by an exosystem. The controller generated by our theorem can realize the property of output regulation and the performance of tracking the reference signal and rejecting the disturbances as a special case.

Appendix

Here are some detailed descriptions of the example in Section 4. Agents v_1 and v_2 are systems with 2 orders. And there are three basement matrices for an uncertain system, which means $g_1 = g_2 = 3$

$$A_{11} = A_{12} = \begin{pmatrix} -4.8512 & -8.9578 \\ -8.7108 & 7.4003 \end{pmatrix},$$

$$A_{21} = A_{22} = \begin{pmatrix} -4.5841 & -7.5263 \\ -9.3135 & 7.0596 \end{pmatrix},$$

$$A_{31} = A_{32} = \begin{pmatrix} -5.7140 & -8.2750 \\ -9.1175 & 7.0544 \end{pmatrix},$$

$$B_{11} = B_{12} = \begin{pmatrix} 1.6684 \\ -0.0861 \end{pmatrix},$$

$$B_{21} = B_{22} = \begin{pmatrix} 1.9897 \\ -0.7854 \end{pmatrix}, \qquad B_{31} = B_{32} = \begin{pmatrix} 1.8509 \\ -0.2403 \end{pmatrix},$$

$$C_{11} = C_{12} = (1.0614 \quad 0.8390),$$

$$C_{21} = C_{22} = (1.0102 \quad 0.9982),$$

$$C_{31} = C_{32} = (0.9283 \quad 0.7936). \tag{A.1}$$

Agents v_3, v_4, and v_5 are systems with 3 orders. And $g_3 = g_4 = g_5 = 2$

$$A_{13} = A_{14} = A_{15} = \begin{pmatrix} 2.5419 & -1.2319 & 4.7038 \\ 1.9598 & -1.9843 & -4.6719 \\ -2.6654 & -2.4159 & -4.6598 \end{pmatrix},$$

$$A_{23} = A_{24} = A_{25} = \begin{pmatrix} 1.1025 & -2.1701 & 3.6488 \\ 0.0927 & -0.1010 & -2.6299 \\ -3.4064 & -3.1707 & -3.2973 \end{pmatrix}, \tag{A.2}$$

$$B_{13} = B_{14} = B_{15} = \begin{pmatrix} 3.2738 \\ 2.3681 \\ -0.0088 \end{pmatrix},$$

$$B_{23} = B_{24} = B_{25} = \begin{pmatrix} 4.3570 \\ 1.9363 \\ -0.0489 \end{pmatrix},$$

$$C_{13} = C_{14} = C_{15} = (-2.9090 \quad -1.6423 \quad -0.6208), \tag{A.3}$$

$$C_{23} = C_{24} = C_{25} = (-3.5357 \quad -1.0246 \quad -2.3913). \tag{A.4}$$

Agents v_6 and v_7 are systems with 4 orders. And $g_6 = g_7 = 3$

$$A_{16} = A_{17} = \begin{pmatrix} 7.3858 & 7.0606 & -1.9638 & -6.3218 \\ 1.5941 & 2.4411 & -8.4807 & -5.2009 \\ 0.9972 & -2.9810 & -5.2017 & -1.6547 \\ -7.1009 & 0.2650 & -7.5336 & -9.0069 \end{pmatrix},$$

$$A_{26} = A_{27} = \begin{pmatrix} 5.7750 & 7.7097 & -3.0848 & -4.7077 \\ -0.1851 & 0.8409 & -8.0396 & -3.7288 \\ 1.0337 & -2.4579 & -4.1684 & -3.4229 \\ -7.0579 & 1.8202 & -7.1493 & -10.8314 \end{pmatrix},$$

$$A_{36} = A_{37} = \begin{pmatrix} 7.6867 & 8.3454 & -1.3674 & -6.1338 \\ -0.1668 & 0.5027 & -7.5538 & -6.0157 \\ -0.0637 & -4.8089 & -4.6107 & -0.6759 \\ -7.6883 & -1.0590 & -7.7299 & -10.2511 \end{pmatrix},$$

$$B_{16} = B_{17} = \begin{pmatrix} 0.0681 \\ 0.0862 \\ 2.5410 \\ 2.3587 \end{pmatrix},$$

$$B_{26} = B_{27} = \begin{pmatrix} -0.2206 \\ 0.3290 \\ 1.9179 \\ 2.2930 \end{pmatrix},$$

$$B_{36} = B_{37} = \begin{pmatrix} -0.2305 \\ 0.9642 \\ 3.2929 \\ 2.4590 \end{pmatrix},$$

$$C_{16} = C_{17} = (1.4942 \quad -2.5319 \quad -1.0521 \quad 1.0049),$$

$$C_{26} = C_{27} = (0.9337 \quad -1.6942 \quad -1.9109 \quad 0.4535),$$

$$C_{36} = C_{37} = (1.4678 \quad -2.6602 \quad -1.1586 \quad 0.6176). \tag{A.5}$$

Next, these are the matrices obtained according to the solution of LMIs (29)

$$T_{11} = T_{12} = \begin{pmatrix} 37.5608 & 109.7053 \\ -118.3196 & -149.5498 \end{pmatrix},$$

$$T_{21} = T_{22} = \begin{pmatrix} 4.8984 & 1.6586 & 12.6849 \\ -1.7007 & -0.5759 & -4.4042 \end{pmatrix},$$

$$T_{31} = T_{32} = \begin{pmatrix} -43.5409 & -74.3826 \\ 91.9349 & 157.0558 \end{pmatrix},$$

$$T_{13} = T_{14} = T_{15} = \begin{pmatrix} -6.8197 & -42.1931 & 33.9132 \\ 9.9034 & -14.7875 & 19.6377 \\ -2.6741 & -1.6089 & -3.5333 \end{pmatrix},$$

$$T_{23} = T_{24} = T_{25} = \begin{pmatrix} -4.2895 & 3.2637 & -10.7466 \\ -2.3038 & 1.7529 & -5.7718 \\ 0.1139 & -0.0867 & 0.2854 \end{pmatrix},$$

$$T_{33} = T_{34} = T_{35} = \begin{pmatrix} 11.1566 & 5.9291 & 5.2847 \\ -7.3616 & -3.9123 & -3.4871 \\ -0.3312 & -0.1760 & -0.1569 \end{pmatrix},$$

$$T_{16} = T_{17} = \begin{pmatrix} -167.8742 & 206.0977 & 254.4031 & -44.6630 \\ 15.0769 & 147.1908 & 106.7331 & -62.5135 \\ 462.5231 & 174.7488 & -97.4980 & -165.1735 \\ 532.2860 & 236.1899 & -93.3484 & -210.2411 \end{pmatrix},$$

$$T_{26} = T_{27} = \begin{pmatrix} -1.0162 & 0.5879 & -2.5760 \\ 1.5155 & -0.8767 & 3.8419 \\ 8.8346 & -5.1108 & 22.3961 \\ 10.5625 & -6.1104 & 26.7763 \end{pmatrix},$$

$$T_{36} = T_{37} = \begin{pmatrix} 123.6493 & -224.3619 & -253.0593 & 60.0567 \\ 59.3071 & -107.6129 & -121.3773 & 28.8056 \\ -26.7899 & 48.6103 & 54.8279 & -13.0119 \\ -19.6265 & 35.6123 & 40.1673 & -9.5326 \end{pmatrix}. \tag{A.6}$$

The coefficients in case of the uncertainty Δ_1 are as follows:

$$\begin{gathered}\lambda_{11} = 0.33, \qquad \lambda_{21} = 0.33, \qquad \lambda_{31} = 0.34,\\ \lambda_{12} = 0.4, \qquad \lambda_{22} = 0.3, \qquad \lambda_{32} = 0.3,\\ \lambda_{13} = 0.6, \qquad \lambda_{23} = 0.4,\\ \lambda_{14} = 0.45, \qquad \lambda_{24} = 0.55,\\ \lambda_{15} = 0.33, \qquad \lambda_{25} = 0.37, \qquad \lambda_{35} = 0.4,\\ \lambda_{16} = 0.35, \qquad \lambda_{26} = 0.36, \qquad \lambda_{36} = 0.39,\\ \lambda_{17} = 0.41, \qquad \lambda_{27} = 0.3, \qquad \lambda_{37} = 0.39.\end{gathered} \tag{A.7}$$

The coefficients in case of the uncertainty Δ_2 are as follows:

$$\begin{gathered}\lambda_{11} = 0.1, \qquad \lambda_{21} = 0.2, \qquad \lambda_{31} = 0.7,\\ \lambda_{12} = 0.5, \qquad \lambda_{22} = 0, \qquad \lambda_{32} = 0.5,\\ \lambda_{13} = 0, \qquad \lambda_{23} = 1,\\ \lambda_{14} = 0.81, \qquad \lambda_{24} = 0.19,\\ \lambda_{15} = 0.3, \qquad \lambda_{25} = 0.5, \qquad \lambda_{35} = 0.2,\\ \lambda_{16} = 0.02, \qquad \lambda_{26} = 0.13, \qquad \lambda_{36} = 0.85,\\ \lambda_{17} = 0.3, \qquad \lambda_{27} = 0.1, \qquad \lambda_{37} = 0.6.\end{gathered} \tag{A.8}$$

Acknowledgment

This work is supported by the National Natural Science Foundation of China under Grants 61074026 and 90916003.

References

[1] A. Jadbabaie, J. Lin, and A. S. Morse, "Coordination of groups of mobile autonomous agents using nearest neighbor rules," *IEEE Transactions on Automatic Control*, vol. 48, no. 6, pp. 988–1001, 2003.

[2] R. Olfati-Saber and R. M. Murray, "Consensus problems in networks of agents with switching topology and time-delays," *IEEE Transactions on Automatic Control*, vol. 49, no. 9, pp. 1520–1533, 2004.

[3] W. Ren and R. W. Beard, "Consensus seeking in multiagent systems under dynamically changing interaction topologies," *IEEE Transactions on Automatic Control*, vol. 50, no. 5, pp. 655–661, 2005.

[4] P. Lin and Y. Jia, "Further results on decentralised coordination in networks of agents with second-order dynamics," *IET Control Theory & Applications*, vol. 3, no. 7, pp. 957–970, 2009.

[5] G. Wen, Z. Duan, W. Yu, and G. Chen, "Consensus in multi-agent systems with communication constraints," *International Journal of Robust and Nonlinear Control*, vol. 22, no. 2, pp. 170–182, 2012.

[6] Z. Li, Z. Duan, G. Chen, and L. Huang, "Consensus of multiagent systems and synchronization of complex networks: a unified viewpoint," *IEEE Transactions on Circuits and Systems. I. Regular Papers*, vol. 57, no. 1, pp. 213–224, 2010.

[7] P. Wieland, R. Sepulchre, and F. Allgöwer, "An internal model principle is necessary and sufficient for linear output synchronization," *Automatica*, vol. 47, no. 5, pp. 1068–1074, 2011.

[8] G. Wen, Z. Li, Z. Duan, and G. Chen, "Distributed consensus control for linear multi-agent systems with discontinuous observations," *International Journal of Control*, vol. 86, no. 1, pp. 95–106, 2013.

[9] W. Yu, G. Chen, and M. Cao, "Consensus in directed networks of agents with nonlinear dynamics," *IEEE Transactions on Automatic Control*, vol. 56, no. 6, pp. 1436–1441, 2011.

[10] W. Ren and N. Sorensen, "Distributed coordination architecture for multi-robot formation control," *Robotics and Autonomous Systems*, vol. 56, no. 4, pp. 324–333, 2008.

[11] Z. Li and Z. Duan, "Distributed adaptive attitude synchronization of multiple spacecraft," *Science China Technological Sciences*, vol. 54, pp. 1992–11998, 2011.

[12] G. Wen, Z. Duan, Z. Li, and G. Chen, "Consensus and its $\mathscr{L}_2$-gain performance of multi-agent systems with intermittent information transmissions," *International Journal of Control*, vol. 85, no. 4, pp. 384–396, 2012.

[13] G. Hu, "Robust consensus tracking of a class of second-order multi-agent dynamic systems," *Systems & Control Letters*, vol. 61, no. 1, pp. 134–142, 2012.

[14] U. Münz, A. Papachristodoulou, and F. Allgöwer, "Delay robustness in non-identical multi-agent systems," *IEEE Transactions on Automatic Control*, vol. 57, no. 6, pp. 1597–1603, 2012.

[15] U. T. Jönsson and C.-Y. Kao, "Consensus of heterogeneous LTI agents," *IEEE Transactions on Automatic Control*, vol. 57, no. 8, pp. 2133–2138, 2012.

[16] H. Kim, H. Shim, and J. H. Seo, "Output consensus of heterogeneous uncertain linear multi-agent systems," *IEEE Transactions on Automatic Control*, vol. 56, no. 1, pp. 200–206, 2011.

[17] M. Ji, G. Ferrari-Trecate, M. Egerstedt, and A. Buffa, "Containment control in mobile networks," *IEEE Transactions on Automatic Control*, vol. 53, no. 8, pp. 1972–1975, 2008.

[18] Z. Li, W. Ren, X. Liu, and M. Fu, "Distributed containment control of multiagent systems with general linear dynamics in the presence of multiple leaders," *International Journal of Robust and Nonlinear Control*, vol. 23, no. 5, pp. 534–547, 2013.

[19] M. Porfiri, D. G. Roberson, and D. J. Stilwell, "Tracking and formation control of multiple autonomous agents: a two-level consensus approach," *Automatica*, vol. 43, no. 8, pp. 1318–1328, 2007.

[20] Q. Song, J. Cao, and W. Yu, "Second-order leader-following consensus of nonlinear multi-agent systems via pinning control," *Systems & Control Letters*, vol. 59, no. 9, pp. 553–562, 2010.

[21] G. Chen and F. L. Lewis, "Coordination of networked systems on digraphs with multiple leaders via pinning control," *International Journal of Systems Science*, vol. 43, no. 2, pp. 368–384, 2012.

[22] G. Chen and F. L. Lewis, "Leader-following control for multiple inertial agents," *International Journal of Robust and Nonlinear Control*, vol. 21, no. 8, pp. 925–942, 2011.

[23] J. Huang, *Nonlinear Output Reguation: Theory and Applications*, vol. 8, SIAM, Philadelphia, Pa, USA, 2004.

[24] Y. Hong, X. Wang, and Z. P. Jiang, "Distributed output regulation of leader-follower multi-agent systems," *International Journal of Robust and Nonlinear Control*, vol. 23, no. 1, pp. 48–66, 2013.

[25] X. Wang, Y. Hong, J. Huang, and Z.-P. Jiang, "A distributed control approach to a robust output regulation problem for multi-agent linear systems," *IEEE Transactions on Automatic Control*, vol. 55, no. 12, pp. 2891–2895, 2010.

[26] Y. Su and J. Huang, "Cooperative output regulation of linear multi-agent systems," *IEEE Transactions on Automatic Control*, vol. 57, no. 4, pp. 1062–1066, 2012.

[27] C. Godsil and G. F. Royle, *Algebraic Graph Theory*, Springer-Verlag, New York, NY, USA, 2001.

[28] F. Amato, *Robust Control of Linear Systems Subject to Uncertain Time-Varying Parameters*, Springer, Berlin, Germany, 2006.

[29] S. Dasgupta, C. H. Papadimitriou, and U. V. Vazirani, *Algorithms*, McGraw-Hill Science/Engineering/Math, New York, NY, USA, 2006.

Hindawi Publishing Corporation
Mathematical Problems in Engineering
Volume 2013, Article ID 315367, 8 pages
http://dx.doi.org/10.1155/2013/315367

Research Article

Bifurcation and Hybrid Control for A Simple Hopfield Neural Networks with Delays

Zisen Mao, Hao Wang, Dandan Xu, and Zhoujin Cui

College of Science, PLA University of Science and Technology, Nanjin 211101, China

Correspondence should be addressed to Zisen Mao; maozisen@126.com

Received 30 March 2013; Accepted 6 May 2013

Academic Editor: Guanghui Wen

A detailed analysis on the Hopf bifurcation of a delayed Hopfield neural network is given. Moreover, a new hybrid control strategy is proposed, in which time-delayed state feedback and parameter perturbation are used to control the Hopf bifurcation of the model. Numerical simulation results confirm that the new hybrid controller using time delay is efficient in controlling Hopf bifurcation.

1. Introduction

It is well known that neural networks are complex and large-scale nonlinear dynamical system. In the last decade, the dynamical characteristics (including stable, unstable, oscillatory, and chaotic behavior) of Hopfield neural networks (HNNs) with time delays have become a subject of intense research activities. Many stability criteria are obtained. We refer the reader to [1–8] and the references cited therein. However, the periodic nature of neural impulses is of fundamental significance in the control of regular dynamical functions such as breathing and heart beating. Neural networks involving persistent oscillations such as limit cycle may be applied to pattern recognition and associative memory. In differential equations with delays, periodic oscillatory behavior can arise through the Hopf bifurcation. Therefore, it is also very significant to study the class of problem. Olien and Bélair [9] investigated the bifurcation of the following HNNs system:

$$\begin{aligned}\dot{x}_1 &= -a_1 x_1(t) + b_{11} f_1(x_1(t-\tau_1)) \\ &\quad + b_{12} f_2(x_2(t-\tau_2)), \\ \dot{x}_2 &= -a_2 x_2(t) + b_{21} f_1(x_1(t-\tau_3)) \\ &\quad + b_{22} f_2(x_2(t-\tau_1)),\end{aligned} \tag{1}$$

in which $\tau_1 = \tau_2 = \tau_3 = \tau$, $a_i = 1$ and $f_i(0) = 0$, $i = 1, 2$, and Huang et al. [10] study further the bifurcation and periodic nature of system (1) with $2\tau_1 = \tau_2 + \tau_3$, $a_i = 1$ and $f_i(0) = 0$, $i = 1, 2$. Moreover, many authors also consider discrete form of system (1); we can see [11–13].

In recent years, bifurcation control has attracted many researchers from various disciplines. The aim of bifurcation control is to design a controller to modify the bifurcation properties of a given nonlinear system, thereby to achieve some desirable dynamical behaviors. After the pioneering work initiated by Ott et al. [14], there have been many ideas and methods of bifurcation control [15–20]. However, from the control theory point of view, we may classify the current methods into two main categories: the first one is feedback control where state feedback is applied to control bifurcation or chaos, and the other is nonfeedback methods. Recently, Luo et al. [21] proposed a new control strategy for period-doubling bifurcations in a discrete nonlinear dynamical system. Moreover, Liu and Chung [22] investigated the same control strategy in a continuous dynamical system without time delays. Now, we extend this strategy to deal with bifurcation control in HNNs system (1).

In the paper, we will propose a new hybrid control strategy in which the parameter perturbation and time-delayed state feedback are combined and used to control Hopf bifurcation in system (1). Simulation results demonstrate the correctness of our theoretical analysis. The comparison shows

that the control strategy is effective as it meets the purpose of retarding the occurrence of bifurcation.

2. Stability and Hopf Bifurcation of System (1) without Control

In this section, we will consider system (1) with $2\tau_1 = \tau_2 + \tau_3 \triangleq 2\tau$ and $f_i(0) = 0$, $i = 1, 2$. It is obviously that $(0, 0)$ is an equilibrium point of system (1).

To simplify, here we denote $c_{11} = b_{11}f_1'(0)$, $c_{12} = b_{12}f_2'(0)$, $c_{21} = b_{21}f_1'(0)$, $c_{22} = b_{22}f_2'(0)$, $a_1 = a_2 = b$. Consider the linearized system of system (1) at $(0, 0)$

$$\begin{aligned} \dot{x}_1 &= -bx_1(t) + c_{11}x_1(t-\tau) + c_{12}x_2(t-\tau_2), \\ \dot{x}_2 &= -bx_2(t) + c_{21}x_1(t-\tau_3) + c_{22}x_2(t-\tau). \end{aligned} \tag{2}$$

The characteristic equation of the linearized system (2) is

$$(\lambda + b)^2 - (c_{11} + c_{22})(\lambda + b)e^{-\lambda\tau} + (c_{11}c_{22} - c_{12}c_{21})e^{-2\lambda\tau} = 0, \tag{3}$$

which determines the local stability of the equilibrium solution. Thus, we will find some conditions which ensure that all roots of (3) have negative real parts. To facilitate the calculation in this paper, we rewrite the characteristic equation (3) as follows:

$$(\lambda + b)^2 e^{2\lambda\tau} - 2T(\lambda + b)e^{\lambda\tau} + D = 0, \tag{4}$$

where $D = c_{11}c_{22} - c_{12}c_{21}$, $T = (1/2)(c_{11} + c_{22})$. Obviously, (4) is a quadratic polynomial in the variable $(\lambda + b)e^{\lambda\tau}$ and has roots given by

$$(\lambda + b)e^{\lambda\tau} = T \pm \sqrt{T^2 - D}. \tag{5}$$

In the following, we distinguish two cases to discuss (5).

2.1. As $T^2 \geq D$. In this part, we state a result due to [23] as a lemma to analyze (5), which is, for the convenience of the reader, stated as follows.

Lemma 1. *For the transcendental equation*

$$\begin{aligned} &\lambda^n + p_1^{(0)}\lambda^{n-1} + \cdots + p_{n-1}^{(0)}\lambda + p_n^{(0)} \\ &\quad + \left[p_1^{(1)}\lambda^{n-1} + \cdots + p_{n-1}^{(1)}\lambda + p_n^{(1)}\right]e^{-\lambda\sigma_1} \\ &\quad + \cdots + \left[p_1^{(m)}\lambda^{n-1} + \cdots + p_{n-1}^{(m)}\lambda + p_n^{(m)}\right]e^{-\lambda\sigma_m} = 0, \end{aligned} \tag{6}$$

where $\sigma_i \geq 0$ $(i = 1, \ldots, m)$ and $p_j^{(i)}$ $(i = 1, \ldots, m; j = 1, \ldots, n)$ are constants. As $(\sigma_1, \ldots, \sigma_m)$ varies, the sum of the orders of the zeros of (6) in the open right half-plane can change only if a zero appears on or crosses the imaginary axis.

For convenience, we make the following assumptions:

(H1) $b > T \pm \sqrt{T^2 - D}$.

(H2) $b^2 > (T \pm \sqrt{T^2 - D})^2$.

(H3) $(T + \sqrt{T^2 - D})^2 < b^2 < (T - \sqrt{T^2 - D})^2$.

(H4) $b^2 < (T \pm \sqrt{T^2 - D})^2$.

Lemma 2. *If (H1) and (H2) hold, then all roots of (3) have negative real parts for every $\tau \in [0, +\infty)$.*

Proof. For (3), when $\tau = 0$, its roots can be expressed as $\lambda_{1,2} = -b + T \pm \sqrt{T^2 - D}$. Clearly, all roots of (3) are negative if (H1) holds. We want to determine if the real part of some root increases to reach zero and eventually becomes positive as $\tau \neq 0$. We can see that λ is a root of (3) if and only if λ is a root of (5).

We write $\lambda = \rho + i\omega$ for a root of the characteristic equations (5), separate the real and imaginary parts of the ensuing equations (5), and obtain

$$\begin{aligned} e^{\rho\tau}\left[(\rho + b)\cos(\omega\tau) - \omega\sin(\omega\tau)\right] &= T \pm \sqrt{T^2 - D}, \\ e^{\rho\tau}\left[(\rho + b)\sin(\omega\tau) + \omega\cos(\omega\tau)\right] &= 0. \end{aligned} \tag{7}$$

A change in the stability of the stationary solution can only occur when $\rho = 0$, that is,

$$\begin{aligned} b\cos(\omega\tau) - \omega\sin(\omega\tau) &= T \pm \sqrt{T^2 - D}, \\ b\sin(\omega\tau) + \omega\cos(\omega\tau) &= 0. \end{aligned} \tag{8}$$

By (8), we have

$$\omega^2 = \left(T \pm \sqrt{T^2 - D}\right)^2 - b^2. \tag{9}$$

By (9), if (H2) holds, we know that (5) has no purely imaginary roots, and then applying Lemma 1 one obtains that all roots of (3) have negative real parts. This completes the proof of lemma. □

Lemma 3. *For (5), one obtains the following results.*

(1) *If (H1) and (H3) hold, then (5) have a pair of purely imaginary roots $\pm i\omega_-$ at $\tau = \tau_{-,j}$.*

(2) *If (H1) and (H4) hold, then (5) have a pair of purely imaginary roots $\pm i\omega_+$ at $\tau = \tau_{+,j}$ and have another pair of purely imaginary roots $\pm i\omega_-$ at $\tau = \tau_{-,j}$,*

where

$$\omega_\pm^2 = \left(T \pm \sqrt{T^2 - D}\right)^2 - b^2, \tag{10}$$

$$\begin{aligned} \tau_{\pm,j} &= \frac{1}{\omega_\pm}\arctan\left(-\frac{\omega_\pm}{b}\right) + \frac{j\pi}{\omega_\pm}, \quad j = 0, 1, \ldots; \\ \tau_0 &= \min\{\tau_{+,0}, \tau_{-,0}\}. \end{aligned} \tag{11}$$

Here one denotes $\pm\omega_0$ especially as a pair of purely imaginary roots of (5) at $\tau = \tau_0$. To see if $\tau_{-,0}$ and τ_0 are bifurcation values, one needs to verify if the transversality conditions hold. In fact, one has the following.

Lemma 4. *The following transversality conditions:*

$$\operatorname{Re}\left(\frac{d\lambda}{d\tau}\right)\bigg|_{\tau_{\pm,j}} > 0 \tag{12}$$

are satisfied.

Proof. By (5), we have

$$\frac{d\lambda}{d\tau}e^{\lambda\tau} + (\lambda + b)\left(\tau e^{\lambda\tau}\frac{d\lambda}{d\tau} + \lambda e^{\lambda\tau}\right) = 0. \tag{13}$$

Hence,

$$\frac{d\lambda}{d\tau}(1 + (\lambda + b)\tau) = -\lambda(\lambda + b). \tag{14}$$

Obviously, we have

$$\left(\frac{d\lambda}{d\tau}\right)^{-1} = \frac{(1 + (\lambda + b)\tau)}{-\lambda(\lambda + b)} = -\frac{1}{\lambda(\lambda + b)} - \frac{\tau}{\lambda}, \tag{15}$$

then

$$\begin{aligned}
\operatorname{sign}\left(\operatorname{Re}\left(\frac{d\lambda}{d\tau}\right)\bigg|_{\tau_{\pm,j}}\right) &= \operatorname{sign}\left(\operatorname{Re}\left(\frac{d\lambda}{d\tau}\right)^{-1}\bigg|_{\tau_{\pm,j}}\right) \\
&= \operatorname{sign}\left(\operatorname{Re}\left(\frac{-1}{i\omega(i\omega + b)}\right)\right) \\
&= \operatorname{sign}\left(\operatorname{Re}\left(\frac{-1}{-\omega^2 + ib\omega}\right)\right) \\
&= \operatorname{sign}\left(\frac{-1\cdot -\omega^2}{\omega^4 + b^2\omega^2}\right) \\
&= \operatorname{sign}\left(\frac{1}{\omega^2 + b^2}\right) > 0.
\end{aligned} \tag{16}$$

We complete the proof of Lemma 4. □

From Lemmas 2–4, we can obtain the following theorem about the distribution of the characteristic roots of (3).

Theorem 5. *Let $\tau_{-,0}$, τ_0 be defined by* (11).

(i) *If (H1) and (H2) hold, then all roots of* (3) *have negative real parts for all $\tau \geq 0$.*

(ii) *If (H1) and (H3)((H4)) hold, then when $\tau < \tau_{-,0}$ ($\tau < \tau_0$), all roots of* (3) *have negative real parts, when $\tau = \tau_{-,0}$ ($\tau = \tau_0$),* (3) *has a pair of purely imaginary roots $\pm i\omega_-(\pm i\omega_0)$, and when $\tau > \tau_{-,0}$ ($\tau > \tau_0$),* (3) *has at least one root with positive real part.*

By using Theorem 5, the stability and bifurcation of system (1) can be summarized as the following theorem.

Theorem 6. *For system* (1), *let (H1) hold and let $\tau_{-,0}, \tau_0$ be defined by* (11).

(i) *If (H2) holds, then the equilibrium point* $(0, 0)$ *is asymptotically stable for discrete delays $\tau \geq 0$.*

(ii) *If (H3)((H4)) holds, there is a critical value $\tau = \tau_{-,0}$ ($\tau = \tau_0$) of the discrete delay so that if $\tau < \tau_{-,0}$ ($\tau < \tau_0$), then the equilibrium point* $(0, 0)$ *is asymptotically stable; if $\tau > \tau_{-,0}$ ($\tau > \tau_0$), then* $(0, 0)$ *is unstable; Hopf bifurcation occurs when $\tau = \tau_{-,0}$ ($\tau = \tau_0$).*

2.2. As $T^2 < D$. For convenience, we have the following assumptions:

(H5) $b > T$.

(H6) $b^2 > D$.

(H7) $b^2 < D$.

Similar to the deduction of Lemma 2, we have the following result.

Lemma 7. *If (H5) and (H6) hold, then all roots of* (3) *have negative real parts for every $\tau \in [0, +\infty)$.*

Proof. For (3), when $\tau = 0$, its roots can be expressed as $\lambda_{1,2} = -b + T \pm \sqrt{T^2 - D}$. Clearly, all roots of (3) have negative real parts if (H5) holds. We want to determine if the real part of some root increases to reach zero and eventually becomes positive as $\tau \neq 0$. We can see that λ is a root of (3) if and only if λ is a root of (5).

We write $\lambda = \rho + i\omega$ for a root of the characteristic equation (3), separate the real and imaginary parts of the ensuing equations (5), and obtain

$$\begin{aligned}
e^{\rho\tau}\left[(\rho + b)\cos(\omega\tau) - \omega\sin(\omega\tau)\right] &= T, \\
e^{\rho\tau}\left[(\rho + b)\sin(\omega\tau) + \omega\cos(\omega\tau)\right] &= \pm\sqrt{D - T^2}.
\end{aligned} \tag{17}$$

A change in the stability of the equilibrium point can only occur when $\rho = 0$, that is,

$$\begin{aligned}
b\cos(\omega\tau) - \omega\sin(\omega\tau) &= T, \\
b\sin(\omega\tau) + \omega\cos(\omega\tau) &= \pm\sqrt{D - T^2}.
\end{aligned} \tag{18}$$

Hence, we have

$$\omega^2 = D - b^2. \tag{19}$$

By (19), if (H6) holds, we know that (5) has no purely imaginary roots, and then applying Lemma 1 one obtains that all roots of (3) have negative real parts. This completes the proof of lemma. □

Lemma 8. *For* (3), *one obtains the following results.*

If (H5) and (H7) hold, then (3) *have a pair of purely imaginary roots $\pm i\omega$ at $\tau = \tau_{\pm,j}$, where*

$$\omega^2 = D - b^2, \tag{20}$$

$$\begin{aligned}
\tau_{\pm,j} &= \frac{1}{\omega}\arccos\left(\frac{bT \pm \omega\sqrt{D - T^2}}{b^2 + \omega^2}\right) + \frac{2j\pi}{\omega}, \qquad j = 0, 1, \ldots; \\
\tau_0 &= \min\{\tau_{+,0}, \tau_{-,0}\}.
\end{aligned} \tag{21}$$

According to Lemma 4, one knows that τ_0 is bifurcation values.

From Lemmas 1 and 2, one can obtain the following theorem about the distribution of the characteristic roots of (3).

Theorem 9. *Let τ_0 be defined by* (21).

(i) *If (H5) and (H6) hold, then all roots of* (3) *have negative real parts for all $\tau \geq 0$.*

(ii) *If (H5) and (H7) hold, then when $\tau < \tau_0$, all roots of* (3) *have negative real parts, when $\tau = \tau_0$,* (3) *has a pair of purely imaginary roots $\pm i\omega$, and when $\tau > \tau_0$,* (3) *has at least one root with positive real part.*

By using Theorem 9, the stability and bifurcation of system (1) can be summarized as the following theorem.

Theorem 10. *For system* (1)*, let (H5) hold and let τ_0 be defined by the following:* (21).

(i) *If (H6) holds, then the equilibrium point* $(0,0)$ *is asymptotically stable for discrete delays $\tau \geq 0$.*

(ii) *If (H7) holds, there is a critical value $\tau = \tau_0$ of the discrete delay so that if $\tau < \tau_0$, then the equilibrium point* $(0,0)$ *is asymptotically stable; if $\tau > \tau_0$, then* $(0,0)$ *is unstable; Hopf bifurcation occurs when $\tau = \tau_0$.*

3. Stability Analysis and Bifurcation with Hybrid Control

In this section, we will consider system (1) with hybrid control described by the following differential equation:

$$\begin{aligned}\dot{x}_1 &= \alpha\left(-a_1x_1(t) + b_{11}f_1\left(x_1(t-\tau_1)\right) + b_{12}f_2\left(x_2(t-\tau_2)\right)\right)\\ &\quad + \beta x_1(t-\tau_1),\\ \dot{x}_2 &= \alpha\left(-a_2x_2(t) + b_{21}f_1\left(x_1(t-\tau_3)\right) + b_{22}f_2\left(x_2(t-\tau_1)\right)\right)\\ &\quad + \beta x_2(t-\tau_1),\end{aligned} \tag{22}$$

where $\alpha > 0$ and $\beta \in R$. Obviously, $(0,0)$ is also an equilibrium point of system (22).

Linearizing the system (22) at the equilibrium point $(0,0)$, we obtain

$$\begin{aligned}\dot{x}_1 &= -\alpha b x_1(t) + (c_{11}\alpha + \beta)x_1(t-\tau_1) + c_{12}\alpha x_2(t-\tau_2),\\ \dot{x}_2 &= -\alpha b x_2(t) + c_{21}\alpha x_1(t-\tau_3) + (c_{22}\alpha + \beta)x_2(t-\tau_1).\end{aligned} \tag{23}$$

Then the characteristic equation for the linearized system around $(0,0)^T$ is given by

$$\begin{aligned}&(\lambda + \alpha b)^2 e^{2\lambda\tau} - (\alpha(c_{11}+c_{22}) + 2\beta)(\lambda + \alpha b)e^{\lambda\tau}\\ &\quad + \left((\alpha c_{11} + \beta)(\alpha c_{22} + \beta) - \alpha^2 c_{12}c_{21}\right) = 0,\end{aligned} \tag{24}$$

which is a quadratic polynomial in the variable $(\lambda + \alpha b)e^{\lambda\tau}$ and has roots given by

$$(\lambda + \alpha b)e^{\lambda\tau} = T' \pm \sqrt{(T')^2 - D'}, \tag{25}$$

where

$$D' = \alpha^2 D + 2\alpha\beta T + \beta^2, \qquad T' = \alpha T + \beta. \tag{26}$$

By (26), we know that $(T')^2 - D' = \alpha^2(T^2 - D)$, and thus, $(T')^2 \geq D'$ ($(T')^2 < D'$) holds if and only if $T^2 \geq D$ ($T^2 < D$) holds.

In the following, we also distinguish two cases to discuss (25).

3.1. As $T^2 \geq D$. Corresponding to Part I of Section 2, we make the following assumptions for convenience:

(H1)$'$ $b > T \pm \sqrt{T^2 - D} + (\beta/\alpha)$.

(H2)$'$ $b^2 > (T \pm \sqrt{T^2 - D} + (\beta/\alpha))^2$.

(H3)$'$ $(T + \sqrt{T^2 - D} + (\beta/\alpha))^2 < b^2 < (T - \sqrt{T^2 - D} + (\beta/\alpha))^2$.

(H4)$'$ $b^2 < (T \pm \sqrt{T^2 - D} + (\beta/\alpha))^2$.

Denote

$$\left(\omega'_{\pm}\right)^2 = \left(T' \pm \sqrt{(T')^2 - D'}\right)^2 - \alpha^2 b^2, \tag{27}$$

$$\begin{aligned}\tau'_{\pm,j} &= \frac{1}{\omega'_{\pm}}\arctan\left(-\frac{\alpha b}{\omega_{\pm}}\right) + \frac{j\pi}{\omega'_{\pm}}, \quad j = 0, 1, \ldots,\\ \tau'_0 &= \min\left\{\tau'_{+,0}, \tau'_{-,0}\right\}.\end{aligned} \tag{28}$$

Similarly, we can obtain the following theorem.

Theorem 11. *For system* (22)*, let $(H1)'$ hold and let $\tau'_{\pm,0}$, τ'_0 be defined by* (28).

(i) *If $(H2)'$ holds, then the equilibrium point* $(0,0)$ *is asymptotically stable for discrete delays $\tau \geq 0$.*

(ii) *If $(H3)'$($(H4)'$) holds, there is a critical value $\tau = \tau'_{-,0}$ ($\tau = \tau'_0$) of the discrete delay so that if $\tau < \tau'_{-,0}$ ($\tau < \tau'_0$), then the equilibrium point* $(0,0)$ *is asymptotically stable; if $\tau > \tau'_{-,0}$ ($\tau > \tau'_0$), then* $(0,0)$ *is unstable; Hopf bifurcation occurs when $\tau = \tau'_{-,0}$ ($\tau = \tau'_0$).*

3.2. As $T^2 < D$. Similar to deduction of Section 2.2, we have the following assumptions:

(H5)$'$ $b > T + (\beta/\alpha)$,

(H6)$'$ $b^2 > D + (2\beta/\alpha)T + (\beta/\alpha)^2$,

(H7)$'$ $b^2 < D + (2\beta/\alpha)T + (\beta/\alpha)^2$.

In this part, we denote

$$\left(\omega'\right)^2 = D' - \alpha^2 b^2, \tag{29}$$

$$\begin{aligned}\tau'_{\pm,j} &= \frac{1}{\omega'}\arccos\left(\frac{\alpha b T' \pm \omega'\sqrt{D' - (T')^2}}{\alpha^2 b^2 + (\omega')^2}\right)\\ &\quad + \frac{2j\pi}{\omega'}, \quad j = 0, 1, \cdots;\ \tau'_0 = \min\left\{\tau'_{+,j}, \tau'_{-,j}\right\}.\end{aligned} \tag{30}$$

Hence, we can obtain the following theorem.

Theorem 12. *For system* (22), *let* $(H5)'$ *hold and let* τ_0' *be defined by* (30).

(i) *If* $(H6)'$ *holds, then the equilibrium point* $(0,0)$ *is asymptotically stable for discrete delays* $\tau \geq 0$.

(ii) *If* $(H7)'$ *holds, there is a critical value* $\tau = \tau_0'$ *of the discrete delay so that if* $\tau < \tau_0'$ *then the equilibrium point* $(0,0)$ *is asymptotically stable; If* $\tau > \tau_0'$, *then* $(0,0)$ *is unstable; Hopf bifurcation occurs when* $\tau = \tau_0'$.

Remark 13. When $\alpha = 1-\gamma$ and $\beta = \gamma$ in the system (22), then we obtain the same hybrid control with [22]; however, a control model based on delayed feedback is proposed in this paper; it is well know that control theory should contain delay since any control action takes effect only after a certain delay. Hence, our hybrid control is more helpful than [22].

Remark 14. When $\alpha = 1$ in the system (23), then we obtain a control model only based on delayed feedback in this paper, it is clear that our hybrid control is more general than control strategy proposed by [17].

Remark 15. In [10], authors investigated the Hopf bifurcation of following HNNs with $\alpha = 1$ and $\beta = 0$:

$$\begin{aligned}\dot{x}_1 &= \alpha\left(-x_1(t) - \left(\sqrt{2}-1\right) f_1\left(x_1(t-\tau_1)\right)\right.\\ &\qquad \left. + b_{12} f_2\left(x_2(t-\tau_2)\right)\right) + \beta x_1(t-\tau_1),\\ \dot{x}_2 &= \alpha\left(-x_2(t) + b_{21} f_1\left(x_1(t-\tau_3)\right)\right.\\ &\qquad \left. - \left(\sqrt{2}-1\right) f_2\left(x_2(t-\tau_1)\right)\right) + \beta x_2(t-\tau_1),\end{aligned} \tag{31}$$

By choosing $\tau_1 = 3\pi/4$, $\tau_2 = \pi/8$, $\tau_3 = 11\pi/8$, the authors obtained that Hopf bifurcation occurs when $b_{12}b_{21} = 1$. However, if choosing the parameters $\alpha = 0.8$ and $\beta = 0$, by the hybrid control strategy of this paper, the Hopf bifurcation in [10] will be eliminated. We can see Figures 1 and 2.

Remark 16. It is known to all that neural networks are a special case of complex networks. Thus, it is interesting and important to further study how to expand the application of theoretical results in [24–27] and any other complex networks.

4. Examples

In this section, we give two examples to illustrate our results.

Example 1. Consider the following HNNs system with hybrid control:

$$\begin{aligned}\dot{x}_1 &= \alpha\left(-a_1 x_1(t) + b_{11} f_1\left(x_1(t-\tau_1)\right) + b_{12} f_2\left(x_2(t-\tau_2)\right)\right)\\ &\qquad + \beta x_1(t-\tau_1),\\ \dot{x}_2 &= \alpha\left(-a_2 x_2(t) + b_{21} f_1\left(x_1(t-\tau_3)\right) + b_{22} f_2\left(x_2(t-\tau_1)\right)\right)\\ &\qquad + \beta x_2(t-\tau_1),\end{aligned} \tag{32}$$

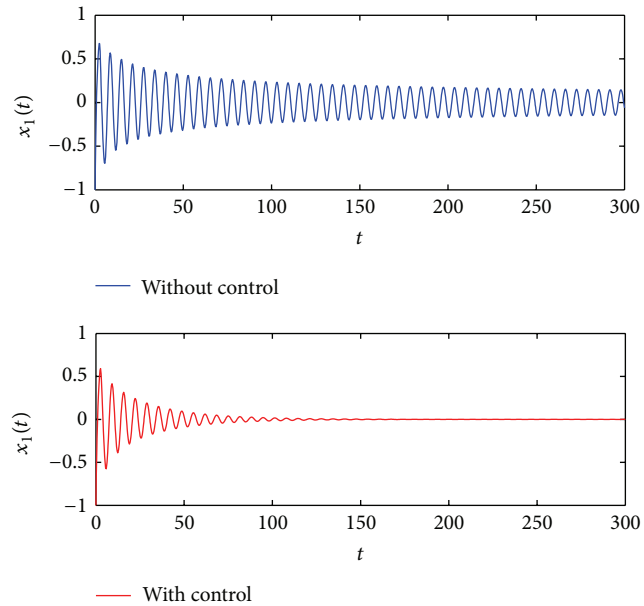

FIGURE 1: The trajectory of $x_1(t)$ versus time in the system (31) with $\tau = 3\pi/4$.

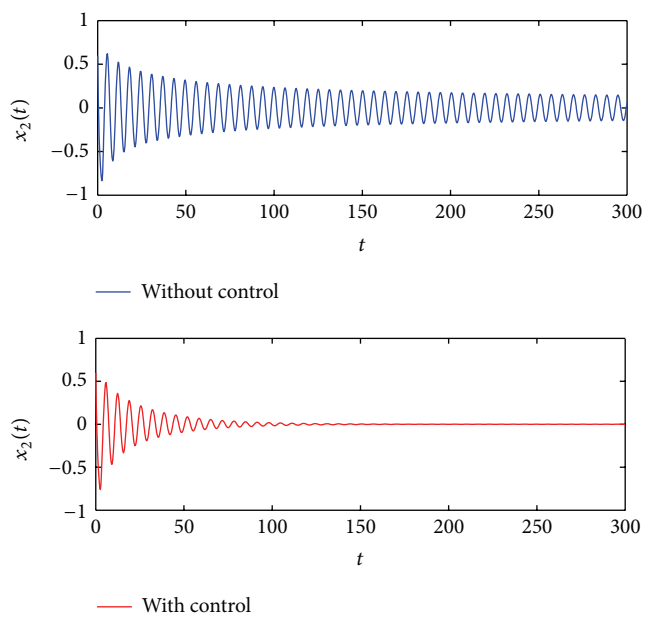

FIGURE 2: The trajectory of $x_2(t)$ versus time in the system (31) with $\tau = 3\pi/4$.

where $\tau_1 = \tau_2 = \tau_3 = \tau$, $a_i = 0.5$, $b_{ij} = -0.3$, and $f_i(x) = \tanh(x)$, $i, j = 1, 2$. It is obvious that $(0,0)$ is an equilibrium point of system (32). Choosing $\alpha = 1$, $\beta = 0$, by calculation, the periodic oscillatory behavior can arise through the Hopf bifurcation as $\tau_0 = 7.7063$; we can see Figures 3 and 5 ($\tau = 7.7063$, $\tau = 17.7063$). However, when $\alpha/5 < 2\beta < \alpha$, with complicated calculation, $(H2)'$ holds; by Theorem 11(i), the equilibrium point $(0,0)$ is asymptotically stable for any discrete delays $\tau \geq \tau_0$. For the convenience of numerical

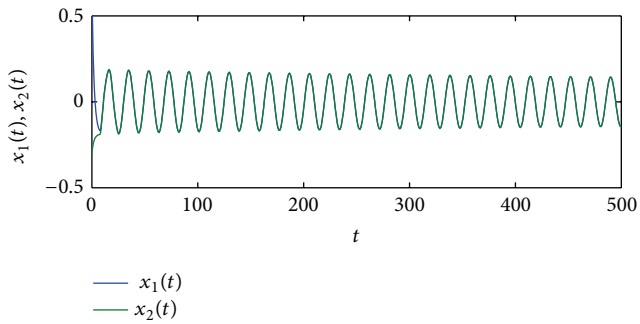

FIGURE 3: The trajectory of $x_1(t)$ and $x_2(t)$ versus time in the system (32) without control ($\tau = 7.7063$).

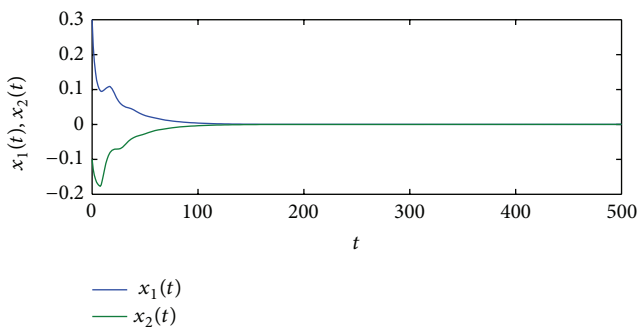

FIGURE 4: The trajectory of $x_1(t)$ and $x_2(t)$ versus time in the system (32) with control ($\tau = 7.7063$).

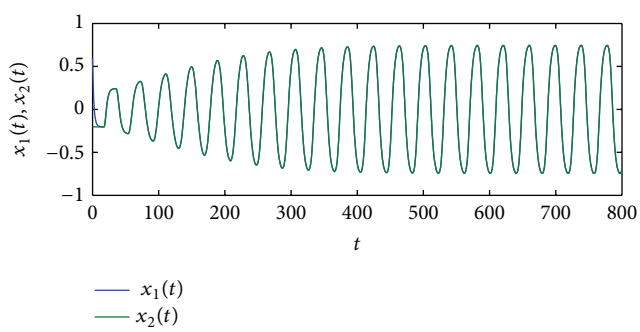

FIGURE 5: The trajectory of $x_1(t)$ and $x_2(t)$ versus time in the system (32) without control ($\tau > 7.7063$).

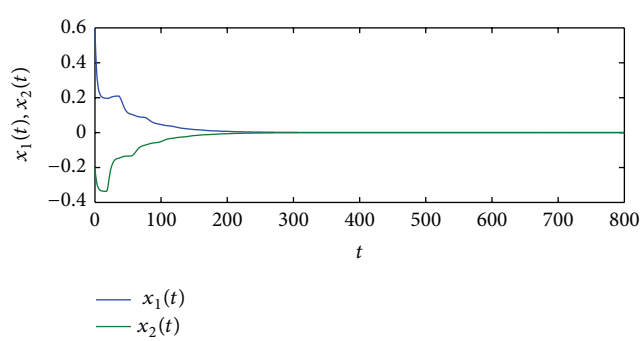

FIGURE 6: The trajectory of $x_1(t)$ and $x_2(t)$ versus time in the system (32) with control ($\tau > 7.7063$).

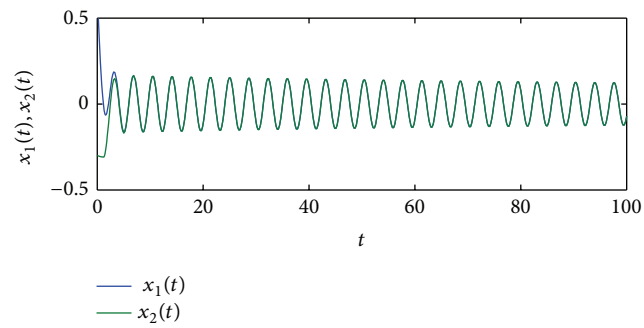

FIGURE 7: The trajectory of $x_1(t)$ and $x_2(t)$ versus time in the system (33) without control ($\tau = 1.2092$).

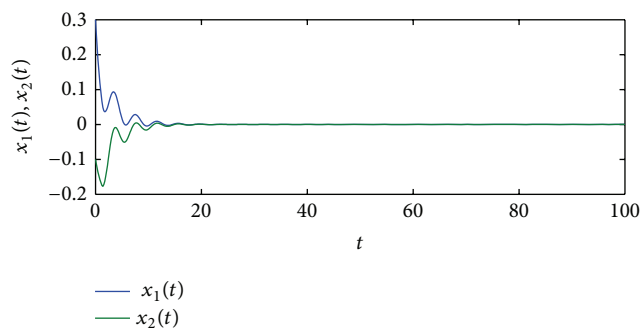

FIGURE 8: The trajectory of $x_1(t)$ and $x_2(t)$ versus time in the system (33) with control ($\tau = 1.2092$).

simulation, here we choose $\alpha = 0.75$, $\beta = 0.25$, and $\tau = 17.7063$ as an example. it can be seen in Figure 4 ($\tau = 7.7063$). Fix all coefficients of system (32) and let τ vary, and the waveforms $x_1(t)$, $x_2(t)$ without and with control are shown, respectively. Obviously, we obtain that the Hopf bifurcation in (32) without hybrid control could be eliminated by hybrid control; we can see Figure 6 ($\tau = 17.7063 > \tau_0$).

Example 2. Consider the following HNNs system with hybrid control:

$$\begin{aligned}\dot{x}_1 &= \alpha\left(-a_1 x_1(t) + b_{11} f_1\left(x_1(t-\tau_1)\right) + b_{12} f_2\left(x_2(t-\tau_2)\right)\right)\\ &\quad + \beta x_1(t-\tau_1),\\ \dot{x}_2 &= \alpha\left(-a_2 x_2(t) + b_{21} f_1\left(x_1(t-\tau_3)\right) + b_{22} f_2\left(x_2(t-\tau_1)\right)\right)\\ &\quad + \beta x_2(t-\tau_1),\end{aligned} \tag{33}$$

where $\tau_1 = \tau_2 = \tau_3 = \tau$, $a_i = 1$, $b_{ij} = -1$, and $f_i(x) = \tanh(x)$, $i, j = 1, 2$. It is obvious that $(0, 0)$ is an equilibrium point of system (33). Choosing $\alpha = 1$, $\beta = 0$, by calculation, we know $\tau_0 = 1.2092$. However, when $-\alpha < \beta < \alpha$, a family of periodic solutions bifurcates from $(0, 0)$ at τ_0' (see Figure 7). Choosing $\alpha = 0.75$ and $\beta = 0.25$, with complicated calculation, we know $\tau_0' = 2.2143$ (see Figure 8). Fix all coefficients of system (33) and let $\tau = \tau_0$; the waveforms $x_1(t)$, $x_2(t)$ without and with control are shown, respectively. However, the Hopf

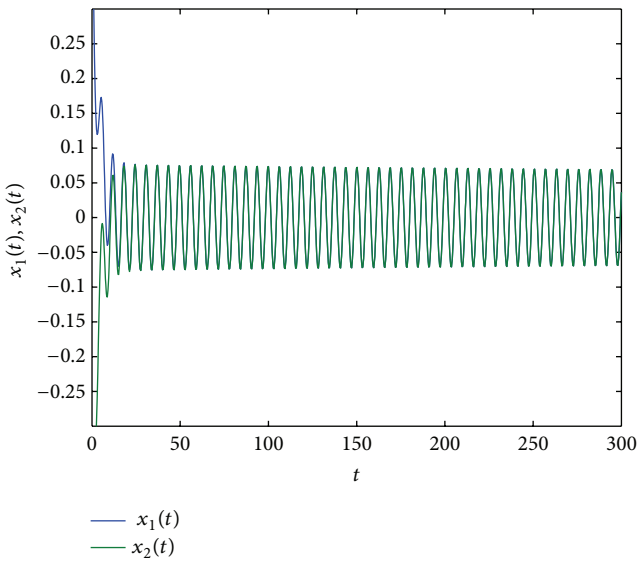

FIGURE 9: The trajectory of $x_1(t)$ and $x_2(t)$ versus time in the system (33) with control ($\tau = 2.2143$).

bifurcation in (33) could be delayed by hybrid control which could be seen by Figure 9.

5. Conclusions

In this paper, the bifurcation and the bifurcation control problems have further been investigated for a HNNs model with delays. For the model, hybrid control strategy in which the parameter perturbation and time-delayed state feedback are combined and used to control various bifurcations in a continuous nonlinear dynamical system. It should be pointed out that, although Liu also have dealt with hybrid control, the time delayed feedback control used in our paper is more helpful than the controller in [22]. On the other hand, using parameter perturbation in this paper, our control strategy is more general than the other feedback control. Numerical simulations are given to justify the validity of hybrid controller in bifurcation control.

Acknowledgments

This research was supported by the Pre-research Foundation of PLA University of Science and Technology. Youth Research Foundation of College of Science of PLA University of Science and Technology.

References

[1] J. J. Hopfield, "Neurons with graded response have collective computational properties like those of two-state neurons," *Proceedings of the National Academy of Sciences of the United States of America*, vol. 81, no. 10, pp. 3088–3092, 1984.

[2] C. Li, X. Liao, and K.-W. Wong, "Delay-dependent and delay-independent stability criteria for cellular neural networks with delays," *International Journal of Bifurcation and Chaos in Applied Sciences and Engineering*, vol. 16, no. 11, pp. 3323–3340, 2006.

[3] V. Singh, "On global robust stability of interval Hopfield neural networks with delay," *Chaos, Solitons and Fractals*, vol. 33, no. 4, pp. 1183–1188, 2007.

[4] L. Wan and J. Sun, "Mean square exponential stability of stochastic delayed Hopfield neural networks," *Physics Letters A*, vol. 343, no. 4, pp. 306–318, 2005.

[5] Z. Wang, Y. Liu, K. Fraser, and X. Liu, "Stochastic stability of uncertain Hopfield neural networks with discrete and distributed delays," *Physics Letters A*, vol. 354, no. 4, pp. 288–297, 2006.

[6] D.-Y. Xu and H.-Y. Zhao, "Invariant and attracting sets of Hopfield neural networks with delay," *International Journal of Systems Science*, vol. 32, no. 7, pp. 863–866, 2001.

[7] Z. Yuan, D. Hu, L. Huang, and G. Dong, "On the global asymptotic stability analysis of delayed neural networks," *International Journal of Bifurcation and Chaos in Applied Sciences and Engineering*, vol. 15, no. 12, pp. 4019–4025, 2005.

[8] H. Zhao, "Global asymptotic stability of Hopfield neural network involving distributed delays," *Neural Networks*, vol. 17, no. 1, pp. 47–53, 2004.

[9] L. Olien and J. Bélair, "Bifurcations, stability, and monotonicity properties of a delayed neural network model," *Physica D*, vol. 102, no. 3-4, pp. 349–363, 1997.

[10] C. Huang, Y. He, L. Huang, and Y. Zhaohui, "Hopf bifurcation analysis of two neurons with three delays," *Nonlinear Analysis. Real World Applications*, vol. 8, no. 3, pp. 903–921, 2007.

[11] W. He and J. Cao, "Stability and bifurcation of a class of discrete-time neural networks," *Applied Mathematical Modelling*, vol. 31, no. 10, pp. 2111–2122, 2007.

[12] Z. Yuan, D. Hu, and L. Huang, "Stability and bifurcation analysis on a discrete-time system of two neurons," *Applied Mathematics Letters*, vol. 17, no. 11, pp. 1239–1245, 2004.

[13] H. Zhao, L. Wang, and C. Ma, "Hopf bifurcation and stability analysis on discrete-time Hopfield neural network with delay," *Nonlinear Analysis. Real World Applications*, vol. 9, no. 1, pp. 103–113, 2008.

[14] E. Ott, C. Grebogi, and J. A. Yorke, "Controlling chaos," *Physical Review Letters*, vol. 64, no. 11, pp. 1196–1199, 1990.

[15] E. H. Abed, H. O. Wang, and R. C. Chen, "Stabilization of period doubling bifurcations and implications for control of chaos," *Physica D*, vol. 70, no. 1-2, pp. 154–164, 1994.

[16] Y. Braiman and I. Goldhirsch, "Taming chaotic dynamics with weak periodic perburbations," *Physical Review Letters*, vol. 66, no. 20, pp. 2545–2548, 1991.

[17] G. Chen, "On some controllability conditions for chaotic dynamics control," *Chaos, Solitons and Fractals*, vol. 8, no. 9, pp. 1461–1470, 1997.

[18] R. Lima and M. Pettini, "Suppression of chaos by resonant parametric perturbations," *Physical Review A*, vol. 41, no. 2, pp. 726–733, 1990.

[19] X. F. Wang and G. Chen, "Pinning control of scale-free dynamical networks," *Physica A*, vol. 310, no. 3-4, pp. 521–531, 2002.

[20] L. Yang, Z. Liu, and J. Mao, "Controlling hyperchaos," *Physical Review Letters*, vol. 84, pp. 67–70, 2000.

[21] X. S. Luo, G. Chen, B. H. Wang, and J. Q. Fang, "Hybrid control of period-doubling bifurcation and chaos in discrete nonlinear dynamical systems," *Chaos, Solitons and Fractals*, vol. 18, no. 4, pp. 775–783, 2003.

[22] Z. Liu and K. W. Chung, "Hybrid control of bifurcation in continuous nonlinear dynamical systems," *International Journal of Bifurcation and Chaos in Applied Sciences and Engineering*, vol. 15, no. 12, pp. 3895–3903, 2005.

[23] S. Ruan and J. Wei, "On the zeros of transcendental functions with applications to stability of delay differential equations with two delays," *Dynamics of Continuous, Discrete & Impulsive Systems A*, vol. 10, no. 6, pp. 863–874, 2003.

[24] W. Yu and J. Cao, "Synchronization control of stochastic delayed neural networks," *Physica A*, vol. 373, pp. 252–260, 2007.

[25] W. Yu, G. Chen, and J. Lü, "On pinning synchronization of complex dynamical networks," *Automatica*, vol. 45, no. 2, pp. 429–435, 2009.

[26] G. Wen, Z. Duan, W. Yu, and G. Chen, "Consensus in multi-agent systems with communication constraints," *International Journal of Robust and Nonlinear Control*, vol. 22, no. 2, pp. 170–182, 2012.

[27] G. Wen, Z. Duan, W. Yu, and G. Chen, "Consensus of second-order multi-agent systems with delayed nonlinear dynamics and intermittent communications," *International Journal of Control*, vol. 86, no. 2, pp. 322–331, 2013.

Hindawi Publishing Corporation
Mathematical Problems in Engineering
Volume 2013, Article ID 405034, 10 pages
http://dx.doi.org/10.1155/2013/405034

Research Article

Controllability of Weighted and Directed Networks with Nonidentical Node Dynamics

Linying Xiang,[1] Jonathan J. H. Zhu,[2] Fei Chen,[1] and Guanrong Chen[3]

[1] *Department of Automation, Xiamen University, Xiamen 361005, China*
[2] *Department of Media and Communication, City University of Hong Kong, Hong Kong*
[3] *Department of Electronic Engineering, City University of Hong Kong, Hong Kong*

Correspondence should be addressed to Linying Xiang; xiangly@xmu.edu.cn

Received 21 March 2013; Accepted 7 May 2013

Academic Editor: Wenwu Yu

The concept of controllability from control theory is applied to weighted and directed networks with heterogenous linear or linearized node dynamics subject to exogenous inputs, where the nodes are grouped into leaders and followers. Under this framework, the controllability of the controlled network can be decomposed into two independent problems: the controllability of the isolated leader subsystem and the controllability of the extended follower subsystem. Some necessary and/or sufficient conditions for the controllability of the leader-follower network are derived based on matrix theory and graph theory. In particular, it is shown that a single-leader network is controllable if it is a directed path or cycle, but it is uncontrollable for a complete digraph or a star digraph in general. Furthermore, some approaches to improving the controllability of a heterogenous network are presented. Some simulation examples are given for illustration and verification.

1. Introduction

Recent technological advances have stimulated broad interests in the notion of network controllability [1–12], which captures the ability to control aggregated dynamics of a networked system and guide it to a desired state by using limited external inputs [13, 14]. In most real dynamical networks, the nodes might have different dynamics. For example, the generators of a power network have different physical parameters and are certainly different from motors, which together form a heterogenous network with nonidentical node dynamics. Therefore, it is of both theoretical and practical importance to study the controllability of networked systems with nonidentical node dynamics, which can help develop a better understanding of the interplay between the complexity of the overall network topology and the collective dynamics of a networked system.

The controllability problem for a *leader-follower* multiagent system was proposed by Tanner [1], who formulated it as the classical controllability of a single-input linear system and then derived a necessary and sufficient algebraic condition in terms of the eigenvalues and eigenvectors of a submatrix of the graph's Laplacian matrix. Ji et al. [2] then gave a sufficient condition for multileader controllability based on the algebraic characteristics of a submatrix of the incidence matrix. Subsequently, Rahmani and Mesbahi [3, 4] discussed an intricate relationship between controllability and graph symmetry with respect to the leader and gave a sufficient condition for uncontrollability. Later, Ji et al. studied the controllability in the multileader setting via equitable partitions [5, 6]. It is worth noting that, in the above works [1–6], the interconnection graph is assumed to be connected. Ji et al. [7] introduced the concept of leader-follower connectedness and investigated the controllability of a multileader system that may not be connected. The work in [8] focused on the controllability of discrete-time single-leader switching networks, which was further extended to continuous-time single-leader switching networks [9]. Additionally, some sufficient algebraic conditions were derived for a multileader system with time delays in the states, where both single and double integrator dynamics were considered [10]. Moreover, Lou and Hong [11] employed a new equitable partition, that is,

weight-balanced partition, to classify interconnection graphs. Zhang et al. [12] established a bound on the controllable subspace for a given multiagent system using an almost equitable partition.

On the other hand, Liu et al. [15] developed some analytical tools to study the *structural controllability* of large-scale weighted and directed networks and solved the minimum input problem based on Lin's structural controllability theorem [16]. Wang et al. [17] further proposed a general approach to optimizing the structural controllability of a complex network by judiciously perturbing the network structure. Cowan et al. [18] pointed out that the main results in [15] hinge on a critical modeling assumption: the results (implicitly) require that the "default" structures of the dynamical systems at the nodes of the network have infinite time constants, which do not reflect the dynamics of real physical and biological systems. It is important to emphasize that the controllability addressed in the present paper is fundamentally different from the "structural controllability" [15–18] and "*pinning controllability*" [19]. In fact, structural controllability is a weaker notion than the classical controllability, whereas pinning controllability discussed in [19] is essentially "synchronizability".

To summarize, the previous works [1–15, 17, 20], except for [18], did not consider the situation where the nodes have *internal dynamics*. However, many real networks including social networks, power grids, food webs, regulatory networks, and neuronal networks manifest intrinsic dynamics at each living node. Additionally, all the works in [1–12, 15, 17, 18] assumed that the dimension of the state of each node is one. Although Cai and Zhong [20] studied the controllability of a swarm system with higher-dimensional agent dynamics, they did not consider the nodal intrinsic dynamics. The introduction of higher-dimensional heterogenous node dynamics makes the controllability of the entire system more complicated since, apart from the complexity of the network structure, the complexity of the dynamics of the nodes has to be considered simultaneously.

The contributions of this paper are as follows. The classic concept of controllability from control theory is extended to weighted and directed complex networks with nonidentical node dynamics in a systematic way. The leader-follower structure is introduced to characterize a network where a few nodes take a leader's role and are subject to external signals while the remaining nodes simply follow the leaders. Necessary and/or sufficient conditions on node dynamics and network topology for controllability are given in either algebraic or graph-theoretic forms. Furthermore, some approaches to improving the controllability are presented.

2. Notation and Preliminaries

2.1. Notation. Throughout the paper, $\mathbb{R}(\mathbb{C})$ denotes the set of real (complex) numbers and $\mathbb{R}^m(\mathbb{C}^m)$ the space of real (complex) m-vectors. The $n \times n$ unit (zero) matrix is denoted by $I_n(0_n)$. $\mathbf{1}_n$ denotes the n-dimensional column vector of ones and $\mathbf{0}_n$ the column vector of zeroes. The subscript n might be omitted if it is clear from the context. $A^T(a^T)$ stands for the transpose (conjugate transpose) of matrix $A \in \mathbb{R}^{n\times n}$ (vector $a \in \mathbb{C}$). $\mathrm{diag}\{a_1, \ldots, a_n\}$ denotes the $n \times n$ diagonal matrix with its diagonal elements being $a_1, \ldots, a_n$. $\mathrm{Re}(\cdot)$ is the real part of a complex number and $\mathrm{Im}(\cdot)$ the imaginary part. $\otimes$ denotes the Kronecker product.

Lemma 1 (see [21]). *For real matrices A, B, C, and D with compatible dimensions, one has the following.*

(i) $(A + B) \otimes C = A \otimes C + B \otimes C$.

(ii) $(A \otimes B)(C \otimes D) = (AC) \otimes (BD)$.

(iii) $(A \otimes B)^T = A^T \otimes B^T$.

(iv) *Let A be an $m \times m$ matrix with left eigenvectors $\alpha_1, \ldots, \alpha_m$ corresponding to its eigenvalues $\lambda_1, \ldots, \lambda_m$, and B an $n \times n$ matrix with left eigenvectors $\beta_1, \ldots, \beta_n$ corresponding to its eigenvalues $\mu_1, \ldots, \mu_n$. Then, $\alpha_i \otimes \beta_j$ are left eigenvectors of $A \otimes B$ corresponding to its eigenvalues $\lambda_i\mu_j$ $(i = 1, \ldots, m,\ j = 1, \ldots, n)$.*

2.2. Graphs and Their Algebraic Representations. A *weighted digraph* (or a *weighted directed graph*) [22] $\mathcal{G} = (\mathcal{V}, \mathcal{E}, \mathcal{W})$ consists of a node set $\mathcal{V} = \{1, \ldots, n\}$, an edge set $\mathcal{E} \subset \mathcal{V} \times \mathcal{V}$, and a weight set $\mathcal{W}$. An edge, denoted by (i, j), is an ordered pair of distinct nodes of $\mathcal{V}$. $(i, j) \in \mathcal{E}$ means that there is a direct edge from node i to node j. In this paper, simple weighted digraphs are considered. That is, self-loops and multiple edges are precluded.

A sequence of edges, (v_j, v_{j+1}), $j = 1, \ldots, k-1$, is called a *directed path* and is denoted by $\mathcal{P} = v_1 \to \cdots \to v_k$, where all the nodes $v_1, \ldots, v_k$ are distinct. Node v_1 is called the *beginning node* and v_k the *end node* of the path. In this case, node v_k is said to be *reachable* from node v_1. A *directed cycle* is a closed directed path of the form $\mathcal{P}_c = v_1 \to \cdots \to v_k \to v_1$, where the beginning node and end node are the same.

If $\mathcal{V}' \subset \mathcal{V}$ and $\mathcal{E}' \subset \mathcal{E}$, then $\mathcal{G}' = (\mathcal{V}', \mathcal{E}')$ is called a *subgraph* of $\mathcal{G} = (\mathcal{V}, \mathcal{E})$, written as $\mathcal{G}' \subset \mathcal{G}$. In addition, if $\mathcal{G}'$ contains all the edges $(i, j) \in \mathcal{E}$ with $i, j \in \mathcal{V}'$, then $\mathcal{G}'$ is called an *induced subgraph* of $\mathcal{G}$. Graphs $\mathcal{G}_1 = (\mathcal{V}_1, \mathcal{E}_1)$ and $\mathcal{G}_2 = (\mathcal{V}_2, \mathcal{E}_2)$ are said to be *disjoint* if $\mathcal{V}_1 \bigcap \mathcal{V}_2 = \emptyset$.

The *adjacency* matrix of a weighted directed graph $\mathcal{G}$, $\mathcal{A}(\mathcal{G}) \in \mathbb{R}^{n\times n}$ is defined by [23]

$$[\mathcal{A}(\mathcal{G})]_{ij} = \begin{cases} \omega_{ij}, & (j, i) \in \mathcal{E}, \\ 0, & \text{otherwise}, \end{cases} \tag{1}$$

where $\omega_{ij} > 0$ is the weight of edge (j, i).

Remark 2. An unweighted digraph (or digraph) is a weighted digraph with $\omega_{ij} = 1$ for $i, j = 1, \ldots, n$.

The graph *Laplacian* is defined by

$$[\mathcal{L}(\mathcal{G})]_{ij} = \begin{cases} \displaystyle\sum_{j=1, j\neq i}^{n} \omega_{ij}, & i = j, \\ -\omega_{ij}, & i \neq j. \end{cases} \tag{2}$$

The sum of all entries in any row of $\mathcal{L}(\mathcal{G})$ is zero.

3. Problem Description

Consider a weighted and directed networked system consisting of n nodes with linear or linearized nonidentical dynamics, described by

$$\dot{x}_i(t) = c_i\Gamma x_i(t) + \sum_{j=1}^{n}\mathscr{L}_{ij}\Gamma\left(x_i(t) - x_j(t)\right) + \delta_i B u_i(t), \quad i = 1,\ldots,n, \tag{3}$$

where $x_i \in \mathbb{R}^m$ is the state vector of the ith node, $u_i \in \mathbb{R}^p$ the control input of node i, and $B \in \mathbb{R}^{m\times p}$ the control input matrix. One has $\delta_i = 1$ if node i is subject to an exogenous control signal and $\delta_i = 0$ otherwise. Here, $c_i\Gamma x_i$ ($c_i \in \mathbb{R}$ and $c_i \neq 0$) describes the intrinsic dynamics of node i, $\Gamma = (\gamma_{ij}) \in \mathbb{R}^{m\times m}$ is a constant matrix indicating the inner-coupling between different components, and the Laplacian matrix $\mathscr{L} = (\mathscr{L}_{ij}) \in \mathbb{R}^{n\times n}$ denotes the outer-coupling among the nodes, which contains all the weights of the network.

Remark 3. Network model (3) describes a generic networked system. Several models considered previously can be seen as special cases of (3). For example, in [1–7, 11, 12, 15, 17], $c_i = 0$, $m = 1$, and $\Gamma = B = 1$, in [18], $m = 1$ and $\Gamma = B = 1$, and in [20], $c_i = 0$.

The nodes in the network can be divided into two different groups: *leaders* and *followers*, where external control inputs are injected only at the leaders. Denote the set of controlled nodes as the leader set, $\mathscr{V}_l$, and the remaining nodes as the follower set, $\mathscr{V}_f$. Herein, the subscripts l and f denote the leaders and followers, respectively. It follows that $\mathscr{V}_l \bigcup \mathscr{V}_f = \mathscr{V}$ and $\mathscr{V}_l \bigcap \mathscr{V}_f = \emptyset$. Define the *follower graph* $\mathscr{G}_f$ to be the subgraph induced by $\mathscr{V}_f$ and the *leader graph* $\mathscr{G}_l$ the subgraph induced by $\mathscr{V}_l$. Obviously, $\mathscr{G}_l$ and $\mathscr{G}_f$ are disjoint.

Without loss of generality, one can reorganize the indices of the nodes in such a way that the first q ($1 \le q < n$) nodes are chosen to be controlled. That is, one can label the leaders from 1 to q and the followers from $q+1$ to n. The associated Laplacian matrix $\mathscr{L}$ is thereby partitioned as

$$\mathscr{L} = \begin{bmatrix} L_l & L_{lf} \\ L_{fl} & L_f \end{bmatrix}, \tag{4}$$

where L_l and L_f are $q\times q$ and $(n-q)\times(n-q)$ matrices, respectively. However, they generally no longer have the Laplacian matrix properties. Moreover, L_{fl} denotes the information flow from the leaders to the followers and L_{lf} the flow from the followers to the leaders.

Defining $X(t) = [x_1^T(t),\ldots,x_n^T(t)]^T \in \mathbb{R}^{mn}$ and $U(t) = [u_1^T(t),\ldots,u_q^T(t),\mathbf{0}^T,\ldots,\mathbf{0}^T]^T \in \mathbb{R}^{pn}$, system (3) can be rewritten in a matrix form as

$$\dot{X}(t) = [(\mathscr{C} - \mathscr{L}) \otimes \Gamma]\, X(t) + (\Delta \otimes B)\, U(t), \tag{5}$$

where $\mathscr{C} = \mathrm{diag}\{c_1,\ldots,c_n\}$ and $\Delta = \mathrm{diag}\{\overbrace{1,\ldots,1}^{q},\overbrace{0,\ldots,0}^{n-q}\}$.

Some definitions and lemmas are introduced below.

Definition 4. The system (5) is said to be *controllable* if, for any initial state $X(0)$ and target state $X(T)$ in the state space, there exists an input signal $U(t)$ such that the driven system can be steered from $X(0)$ to $X(T)$ in finite time.

The classical controllability theorem [24] asserts the equivalence of the following statements.

Lemma 5. *Given system $\dot{x}(t) = A_0x(t) + B_0u(t)$, where $x \in \mathbb{R}^N$, $u \in \mathbb{R}^P$, and A_0 and B_0 are matrices with appropriate dimensions, the following statements are equivalent.*

(i) *The system is completely controllable.*

(ii) *The controllability matrix*

$$\mathbb{Q} = \begin{bmatrix} B_0 & A_0B_0 & \cdots & A_0^{N-1}B_0 \end{bmatrix} \tag{6}$$

is of full row rank.

(iii) *The relationship $v^TA_0 = \lambda v^T$ implies $v^TB_0 \neq \mathbf{0}^T$, where v is the nonzero left eigenvector of A_0 corresponding to the eigenvalue λ.*

Conditions (ii) and (iii) in Lemma 5 are referred to as the controllability rank criterion and PBH eigenvector test, respectively.

4. Controllability Analysis

In this section, the controllability of system (5) is analyzed in detail. Before proceeding, some definitions are given.

Definition 6. A graph $\mathscr{G}$ with the Laplacian matrix $\mathscr{L}$ is said to be a controllable graph if and only if $[L_f \;\; L_{fl}]$ is a controllable matrix pair.

Definition 7. Define the extended graph $\overline{\mathscr{G}}$ as the graph with the extended Laplacian matrix

$$\overline{\mathscr{L}} = \mathscr{L} - \mathscr{C} = \begin{bmatrix} L_l - \mathscr{C}_l & L_{lf} \\ L_{fl} & L_f - \mathscr{C}_f \end{bmatrix}, \tag{7}$$

where $\mathscr{C}_l = \mathrm{diag}\{c_1,\ldots,c_q\}$ and $\mathscr{C}_f = \mathrm{diag}\{c_{q+1},\ldots,c_n\}$. Moreover,

$$L_f - \mathscr{C}_f = M\overline{\mathscr{L}}M^T, \qquad L_{fl} = M\overline{\mathscr{L}}N, \tag{8}$$

where $M = [0_{(n-q)\times q} \;\; I_{n-q}]$ and $N = [I_q \;\; 0_{q\times(n-q)}]^T$.

A sufficient and necessary condition for the controllability of system (5) is now established.

Theorem 8. *The system* (5) *is controllable if and only if the following two conditions are satisfied simultaneously:*

(i) *$[\Gamma \;\; B]$ is a controllable matrix pair;*

(ii) *there exists no left eigenvector of $\overline{\mathscr{L}}$ with the first q entries being all zeroes.*

Proof. It follows from Lemma 5(iii) that the system (5) is uncontrollable if and only if there exists a nonzero left eigenvector $\nu \in \mathbb{C}^{mn}$ of $(\mathscr{C} - \mathscr{L}) \otimes \Gamma$ such that $\nu^T(\Delta \otimes B) = \mathbf{0}^T$. According to Lemma 1, there exist two nonzero vectors $\nu_1 \in \mathbb{C}^n$ and $\nu_2 \in \mathbb{C}^m$, which are left eigenvectors of $\mathscr{C} - \mathscr{L}$ and Γ, respectively, such that $\nu = \nu_1 \otimes \nu_2$ and $(\nu_1^T \otimes \nu_2^T)(\Delta \otimes B) = \mathbf{0}^T$. Furthermore, one has

$$\left(\nu_1^T \Delta\right) \otimes \left(\nu_2^T B\right) = \mathbf{0}^T. \tag{9}$$

It follows that (9) is true if and only if either

(i) $\nu_1^T \Delta = \mathbf{0}^T$, that is, there exists a left eigenvector of $\overline{\mathscr{L}}$ with the first q elements being all zeroes, or

(ii) $\nu_2^T B = \mathbf{0}^T$, that is, $[\Gamma \;\; B]$ is an uncontrollable matrix pair.

The proof is thus completed. □

Remark 9. By Theorem 8, the controllability of system (5) is decoupled into two independent problems: one is to analyze the controllability of the isolated leader subsystem $\dot{x} = \Gamma x + Bu$, which depends only on the intrinsic dynamics of the isolated node, and the other is to identify whether there exists a left eigenvector of $\overline{\mathscr{L}}$ with the first q entries being all zeroes, which is determined by $\overline{\mathscr{G}}$.

4.1. Controllability of the Isolated Leader Subsystem. Consider the system

$$\dot{x} = \Gamma x + Bu, \tag{10}$$

where $\Gamma \in \mathbb{R}^{m\times m}$ and $B \in \mathbb{R}^{m\times p}$ are defined in (3).

In general, the controllability of system (10) can be derived by using the classic controllability rank criterion or PBH eigenvector test. In this subsection, two special cases of Γ are further discussed below, since it characterizes the inner-coupling among different components.

First, consider the fully diagonal inner-coupling $\Gamma = I_m$.

Theorem 10. *The system* (10) *is controllable if and only if* $m \le p$ *and* $\operatorname{rank}(B) = m$.

Proof. Since $\Gamma = I_m$, the controllability matrix of the pair $[\Gamma \;\; B]$ is

$$\mathbb{Q} = \left[B \;\; \Gamma B \;\; \cdots \;\; \Gamma^{m-1}B\right] = \left[B \;\; B \;\; \cdots \;\; B\right]. \tag{11}$$

According to the second statement of Lemma 5, $[\Gamma \;\; B]$ is controllable if and only if $m \le p$ and $\operatorname{rank}(B) = m$. The proof is thus completed. □

Remark 11. From Theorem 10, all the leaders' states should be controlled in order to render the system controllable.

Secondly, assume Γ is symmetric and the sum of all entries in each row of Γ is zero.

Theorem 12. *The system* (10) *is uncontrollable if* $\mathbf{1}_m^T B = \mathbf{0}^T$.

Proof. Since Γ is symmetric, for each eigenvalue, its left and right eigenvectors are the same. Additionally, the sum of all elements in any row of Γ is zero. Therefore, 0 is an eigenvalue of Γ associated with eigenvector $\mathbf{1}_m = [1, \ldots, 1]^T$. It follows from PBH eigenvector test that if $\mathbf{1}_m^T B = \mathbf{0}^T$, then $[\Gamma \;\; B]$ is uncontrollable. The proof is thus completed. □

4.2. Controllability of the Extended Graph. It follows from Theorem 8 that if condition (i) of Theorem 8 is already satisfied, then the controllability of system (5) is reduced to the controllability of the extended graph $\overline{\mathscr{G}}$.

Consider the system

$$\dot{x} = (\mathscr{C} - \mathscr{L})\, x, \tag{12}$$

or equivalently,

$$\begin{bmatrix} \dot{x}_l \\ \dot{x}_f \end{bmatrix} = \begin{bmatrix} \mathscr{C}_l - L_l & -L_{lf} \\ -L_{fl} & \mathscr{C}_f - L_f \end{bmatrix} \begin{bmatrix} x_l \\ x_f \end{bmatrix}, \tag{13}$$

where $x_l = [x_1^T, \ldots, x_q^T]^T$ denotes the states of the leaders and $x_f = [x_{q+1}^T, \ldots, x_n^T]^T$ those of the followers.

From (13), the dynamics of the $n - q$ followers can be rewritten as

$$\dot{x}_f = \left(\mathscr{C}_f - L_f\right) x_f - L_{fl} x_l. \tag{14}$$

Remark 13. By Definitions 6 and 7, that $\overline{\mathscr{G}}$ is controllable is equivalent to that the system (14) is controllable through x_l. Therefore, the controllability of $\overline{\mathscr{G}}$ is reduced to the problem whether the leaders can drive the followers from any configuration to any other configuration in finite time. This question will be answered next. It should be emphasized that parameter c_i of node i makes the controllability of $\overline{\mathscr{G}}$ more challenging than the question based on the original graph $\mathscr{G}$.

4.2.1. Algebraic Criteria. In this section, the controllability of $\overline{\mathscr{G}}$ is discussed.

Theorem 14. *$\overline{\mathscr{G}}$ is controllable if and only if there exists no left eigenvector of $\overline{\mathscr{L}}$ with the first q entries being all zeroes.*

Proof. This theorem reveals that $\overline{\mathscr{G}}$ is uncontrollable if and only if there exists a left eigenvector of $\overline{\mathscr{L}}$ with the first q entries being all zeroes.

Necessity. Let $\overline{\nu} \in \mathbb{C}^n$ be a left eigenvector of $\overline{\mathscr{L}}$ corresponding to the eigenvalue $\overline{\lambda} \in \mathbb{C}$ with the first q elements being zeros. From (7) and (8), one has $L_f - \mathscr{C}_f = M\overline{\mathscr{L}}M^T$ and $L_{fl} = M\overline{\mathscr{L}}N$, where $M = [0_{(n-q)\times q} \;\; I_{n-q}]$ and $N^T = [I_q \;\; 0_{q\times(n-q)}]$. Since $M^T M = \operatorname{diag}\{0_q, I_{n-q}\}$, it follows that $M^T M\overline{\nu} = \overline{\nu}$. From $\overline{\nu}^T\overline{\mathscr{L}} = \overline{\lambda}\overline{\nu}^T$, one has $(M\overline{\nu})^T(L_f - \mathscr{C}_f) = \overline{\nu}^T M^T(M\overline{\mathscr{L}}M^T) = \overline{\lambda}(M\overline{\nu})^T$ and $(M\overline{\nu})^T L_{fl} = (M\overline{\nu})^T M\overline{\mathscr{L}}N = \mathbf{0}^T$. Let $\nu = M\overline{\nu}$. Then, $\nu^T(L_f - \mathscr{C}_f) = \overline{\lambda}\nu^T$ and $\nu^T L_{fl} = \mathbf{0}^T$. According to (iii) of Lemma 5, $\overline{\mathscr{G}}$ is uncontrollable.

Sufficiency. Assume that $\overline{\mathscr{G}}$ is not controllable. By the PBH eigenvector criterion, $\overline{\mathscr{G}}$ is uncontrollable if there exist a nonzero eigenvector $\nu \in \mathbb{C}^{n-q}$ and a corresponding eigenvalue $\lambda \in \mathbb{C}$ such that $\nu^T(L_f - \mathscr{C}_f) = \lambda\nu^T$ and $\nu^T L_{fl} = \mathbf{0}^T$. Construct a new vector

$$\overline{\nu} = \begin{bmatrix} \mathbf{0} \\ \nu \end{bmatrix}. \tag{15}$$

Then, one has

$$\begin{aligned} \overline{\nu}^T\overline{\mathscr{L}} &= \begin{bmatrix} \mathbf{0}^T & \nu^T \end{bmatrix} \begin{bmatrix} L_l - \mathscr{C}_l & L_{lf} \\ L_{fl} & L_f - \mathscr{C}_f \end{bmatrix} \\ &= \begin{bmatrix} \nu^T L_{fl} & \nu^T\left(L_f - \mathscr{C}_f\right) \end{bmatrix} \\ &= \begin{bmatrix} \mathbf{0}^T & \lambda\nu^T \end{bmatrix} \\ &= \lambda\overline{\nu}^T. \end{aligned} \tag{16}$$

This implies that $\overline{\nu}$ is a left eigenvector of $\overline{\mathscr{L}}$ with the first q elements being zeros. The proof is thus completed. □

Theorem 15. *The system* (14) *is controllable if $L_f - \mathscr{C}_f$ and $\overline{\mathscr{L}}$ have no common eigenvalues.*

Proof. It suffices to prove that if the system is uncontrollable then there exists at least one common eigenvalue between $L_f - \mathscr{C}_f$ and $\overline{\mathscr{L}}$.

Assume that the system (14) is not controllable. From (iii) of Lemma 5, there exists a vector $\nu \in \mathbb{C}^{n-q}$ such that $\nu^T(L_f - \mathscr{C}_f) = \lambda\nu^T$ for some $\lambda \in \mathbb{C}$, with $\nu^T L_{fl} = \mathbf{0}^T$. Moreover,

$$\begin{aligned} \begin{bmatrix} \mathbf{0}^T & \nu^T \end{bmatrix} \begin{bmatrix} L_l - \mathscr{C}_l & L_{lf} \\ L_{fl} & L_f - \mathscr{C}_f \end{bmatrix} &= \begin{bmatrix} \nu^T L_{fl} & \nu^T\left(L_f - \mathscr{C}_f\right) \end{bmatrix} \\ &= \lambda \begin{bmatrix} \mathbf{0}^T & \nu^T \end{bmatrix}, \end{aligned} \tag{17}$$

which implies that λ is also an eigenvalue of $\overline{\mathscr{L}}$ with eigenvector $[\mathbf{0}^T \quad \nu^T]^T$. The proof is thus completed. □

Note that Theorem 15 is only a sufficient condition. Therefore, the system might be controllable even if $L_f - \mathscr{C}_f$ and $\overline{\mathscr{L}}$ have common eigenvalues, which is different from the results for undirected graphs [5, 6]. This can be verified by a special case that there is no edge from the followers to the leaders. The following result is given for further explanation.

Theorem 16. *If there is no edge from the followers to the leaders in the system* (14)*, then $L_f - \mathscr{C}_f$ and $\overline{\mathscr{L}}$ have common eigenvalues.*

Proof. In this case, $\overline{\mathscr{L}}$ can be rewritten as

$$\overline{\mathscr{L}} = \begin{bmatrix} L_l - \mathscr{C}_l & 0_{q\times(n-q)} \\ L_{fl} & L_f - \mathscr{C}_f \end{bmatrix}. \tag{18}$$

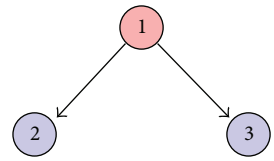

Figure 1: A digraph with $c_2 \neq c_3$.

Since $L_f - \mathscr{C}_f$ is a principal diagonal submatrix of $\overline{\mathscr{L}}$, it can be described by $M^T(L_f - \mathscr{C}_f) = \overline{\mathscr{L}}M^T$, where $M = [0_{(n-q)\times q} \quad I_{n-q}]$ is an $(n-q)\times n$ matrix. Let ν be the right eigenvector of $L_f - \mathscr{C}_f$ corresponding to λ. Then, one has $\overline{\mathscr{L}}(M^T\nu) = (\overline{\mathscr{L}}M^T)\nu = M^T(L_f - \mathscr{C}_f)\nu = M^T(\lambda\nu) = \lambda(M^T\nu)$. That is, $M^T\nu$ is the right eigenvector of $\overline{\mathscr{L}}$ corresponding to the common eigenvalue λ. The proof is thus completed. □

4.2.2. Example 1. As shown in Figure 1, node 1 is selected to be the leader and $c_2 \neq c_3$. It can be verified that $\overline{\mathscr{L}}$ and $L_f - \mathscr{C}_f$ have two common eigenvalues $1 - c_2$ and $1 - c_3$, and the rank of the controllability matrix $[L_{fl} \quad (L_f - \mathscr{C}_f)L_{fl}]$ is 2. By (ii) of Lemma 5, the graph is still controllable, although $\overline{\mathscr{L}}$ and $L_f - \mathscr{C}_f$ have common eigenvalues.

Now, consider the special case with $c_1 = c_2 = \cdots = c_n = c$.

Corollary 17. *A directed path is controllable if the beginning node is selected to be the only leader.*

Proof. The extended Laplacian matrix of a directed path (Figure 2(a)) is given by

$$\overline{\mathscr{L}} = \begin{bmatrix} -c & 0 & 0 & \cdots & 0 \\ -1 & 1-c & 0 & \cdots & 0 \\ 0 & -1 & 1-c & \cdots & 0 \\ \vdots & \vdots & \ddots & \ddots & \vdots \\ 0 & 0 & \cdots & -1 & 1-c \end{bmatrix}. \tag{19}$$

By direct calculation, the eigenvalues of $\overline{\mathscr{L}}$ are $-c$ and $1 - c$ with the left eigenvectors $[1, 0, \ldots, 0]^T$ and $[1, -1, 0, \ldots, 0]^T$, respectively. It follows from Theorem 14 that the graph is controllable. □

Corollary 18. *A directed cycle with a single leader is controllable.*

Proof. For a directed cycle (Figure 2(b)), the extended Laplacian matrix is given by

$$\overline{\mathscr{L}} = \begin{bmatrix} 1-c & 0 & 0 & \cdots & -1 \\ -1 & 1-c & 0 & \cdots & 0 \\ 0 & -1 & 1-c & \cdots & 0 \\ \vdots & \vdots & \ddots & \ddots & \vdots \\ 0 & 0 & \cdots & -1 & 1-c \end{bmatrix}. \tag{20}$$

The real and imaginary parts of the eigenvalues λ satisfy the elliptic relationship $[\mathrm{Re}(\lambda) + c - 1]^2 + [\mathrm{Im}(\lambda)]^2 = 1$. However, all the eigenvalues of $L_f - \mathscr{C}_f$ are equal to $1 - c$. Thus, it follows from Theorem 15 that the graph is controllable. □

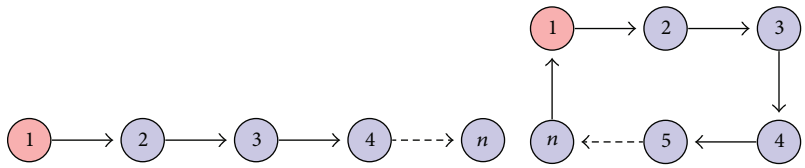

(a) A directed path (b) A directed cycle

Figure 2: Illustration of network topologies.

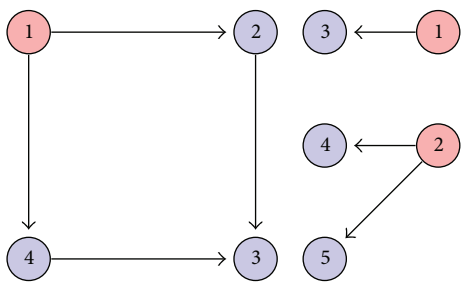

(a) $c_2 = c_4$ (b) $c_4 = c_5$

Figure 3: The digraphs that are leader symmetric: (a) with respect to node $\{1\}$, (b) with respect to nodes $\{1, 2\}$.

4.2.3. Graph Theoretical Criteria. So far, some sufficient and/or necessary conditions for network controllability have been derived. However, these conditions are basically algebraic, which remains elusive on the exact graphical interpretation. In fact, the study of the graph associated with a controlled system is equivalent to the study of the underlying algebraic system, which motivates us to study the controllability from a graph-theoretic perspective. It turns out that the graph-theoretic conditions are indeed more intuitive and easier to evaluate.

First, some definitions are introduced.

Definition 19. A permutation matrix $P \in \mathbb{R}^{n\times n}$ is a 0-1 matrix with a single nonzero element in each row and column.

Definition 20. The system (14) is leader symmetric with respect to the leaders if there exists a nonidentity permutation matrix P such that

$$P\left(L_f - \mathscr{C}_f\right) = \left(L_f - \mathscr{C}_f\right)P, \qquad PL_{fl} = L_{fl}. \tag{21}$$

Remark 21. Definition 20 is an extension of Definition 5.7 in [6]. The main differences are twofold.

(i) Definition 5.7 in [6] is applicable only to single-leader systems and unweighted graphs, whereas Definition 20 works also for multiple-leader systems and weighted digraphs.

(ii) Because of the nonidentical node dynamics, $\mathscr{C}_f$ must satisfy certain conditions in addition to that the original graph is leader symmetric.

Some examples are given here for illustration.

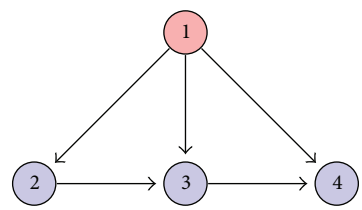

Figure 4: The digraph that is leader asymmetric with respect to node $\{1\}$: $c_2 = c_3 \neq c_4$.

Example 22. Figure 3(a) shows a directed leader-follower network with $\mathscr{V}_l = \{1\}$ and $\mathscr{V}_f = \{2, 3, 4\}$. It can be verified that

$$\overline{\mathscr{L}} = \begin{bmatrix} -c_1 & 0 & 0 & 0 \\ -1 & 1-c_2 & 0 & 0 \\ 0 & -1 & 2-c_3 & -1 \\ -1 & 0 & 0 & 1-c_4 \end{bmatrix}, \tag{22}$$

with

$$L_f - \mathscr{C}_f = \begin{bmatrix} 1-c_2 & 0 & 0 \\ -1 & 2-c_3 & -1 \\ 0 & 0 & 1-c_4 \end{bmatrix}, \qquad L_{fl} = \begin{bmatrix} -1 \\ 0 \\ -1 \end{bmatrix}. \tag{23}$$

Assuming $c_2 = c_4$, one can find a nonidentity permutation matrix

$$P = \begin{bmatrix} 0 & 0 & 1 \\ 0 & 1 & 0 \\ 1 & 0 & 0 \end{bmatrix}, \tag{24}$$

satisfying (21). As a result, it is leader symmetric with respect to $\{1\}$. Likewise, the digraph of Figure 3(b) is leader symmetric about $\{1, 2\}$.

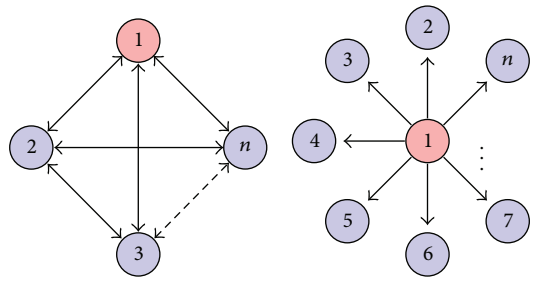

(a) A complete digraph (b) A star digraph

Figure 5: Illustration of network topologies.

Theorem 23. *The system* (14) *is uncontrollable if it is leader symmetric.*

Proof. If system (14) is leader symmetric, then there exists a nonidentity permutation matrix P such that $P(L_f - \mathscr{C}_f) = (L_f - \mathscr{C}_f)P$. Let λ and ν be the corresponding eigenvalue and left eigenvector of $L_f - \mathscr{C}_f$, respectively, satisfying $\nu^T(L_f - \mathscr{C}_f) = \lambda\nu^T$. As a result, $\nu^T(L_f - \mathscr{C}_f)P = \lambda\nu^T P = \lambda(P^T\nu)^T$. Using (21), $(P^T\nu)^T(L_f - \mathscr{C}_f) = \nu^T P(L_f - \mathscr{C}_f) = \nu^T(L_f - \mathscr{C}_f)P = \lambda(P^T\nu)^T$. This implies that $P^T\nu$ is also a left eigenvector of $L_f - \mathscr{C}_f$ corresponding to the eigenvalue λ. Furthermore, one has $\nu - P^T\nu$ is also a left eigenvector of $L_f - \mathscr{C}_f$. By (21), it follows that $(\nu - P^T\nu)^T L_{fl} = \nu^T L_{fl} - \nu^T P L_{fl} = \nu^T L_{fl} - \nu^T L_{fl} = \mathbf{0}^T$. This suggests that the eigenvector $\nu - P^T\nu$ of $L_f - \mathscr{C}_f$ is orthogonal to L_{fl}, which does not satisfy the controllability condition in (iii) of Lemma 5. Therefore, the system (14) is uncontrollable. The proof is completed. □

Remark 24. Theorem 23 provides a graph-theoretic result for the uncontrollability of system (14). Note that leader symmetry is only a sufficient condition rather than a necessary one. For example, the graph shown in Figure 4 is asymmetric about the leader {1}, but it is uncontrollable.

Consider the case of $c_1 = c_2 = \cdots = c_n = c$. Some corollaries can be easily derived from Theorem 23.

Corollary 25. *A complete digraph with a single leader is uncontrollable.*

Proof. It is well known that each node in a complete digraph (Figure 5(a)) has an in-degree (or out-degree) $n - 1$. Corollary 25 is a direct consequence of Theorem 23 because of its leader symmetry. □

Corollary 26. *A star digraph is uncontrollable with respect to the center node.*

Proof. A star digraph is symmetric about the center node (Figure 5(b)). If one chooses the center node as the leader, the graph is leader symmetric. It thus follows that a star digraph with the center node being the leader is uncontrollable. □

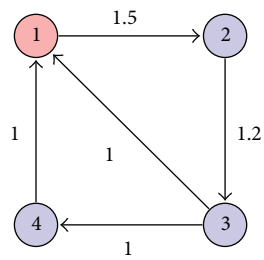

Figure 6: Illustration of a network topology.

5. Controllability Improvement of Heterogenous Networked Systems

There exists a fundamental and yet challenging problem in the study of the controllability of complex networks: how to improve the controllability of an uncontrollable networked system? In this section, some approaches to improving the controllability are suggested.

5.1. Increasing the Number of Leaders. It can be verified that *leader reachable* is a necessary condition for being controllable. That is, the graph is uncontrollable if there exist followers who are isolated or have no incoming edge from any leader or other follower. Therefore, the isolated nodes and the nodes without incoming edge should be first selected to be the leaders. As shown in Figure 3(a), node 1 has no incoming edge from other nodes and is thus chosen to be a leader. It follows that the graph is leader symmetric about the leader node 1 and is, therefore, uncontrollable when $c_2 = c_4$. However, if node 2 or node 4 is also selected to be a leader, the leader symmetry property does not hold anymore. It follows from (ii) of Lemma 5 that the system becomes controllable. This example shows that increasing the number of leaders may improve the controllability.

5.2. Changing the Nodal Parameters. Nodal intrinsic dynamics is considered for the system (5). It follows that parameter c_i of node i is an important quantity determining the controllability of the networked system. For example, in Figure 3(b), if $c_4 \neq c_5$, then the leader symmetry property is not satisfied. It follows from (ii) of Lemma 5 that the system is controllable, which implies that changing the nodal intrinsic parameters may improve the controllability.

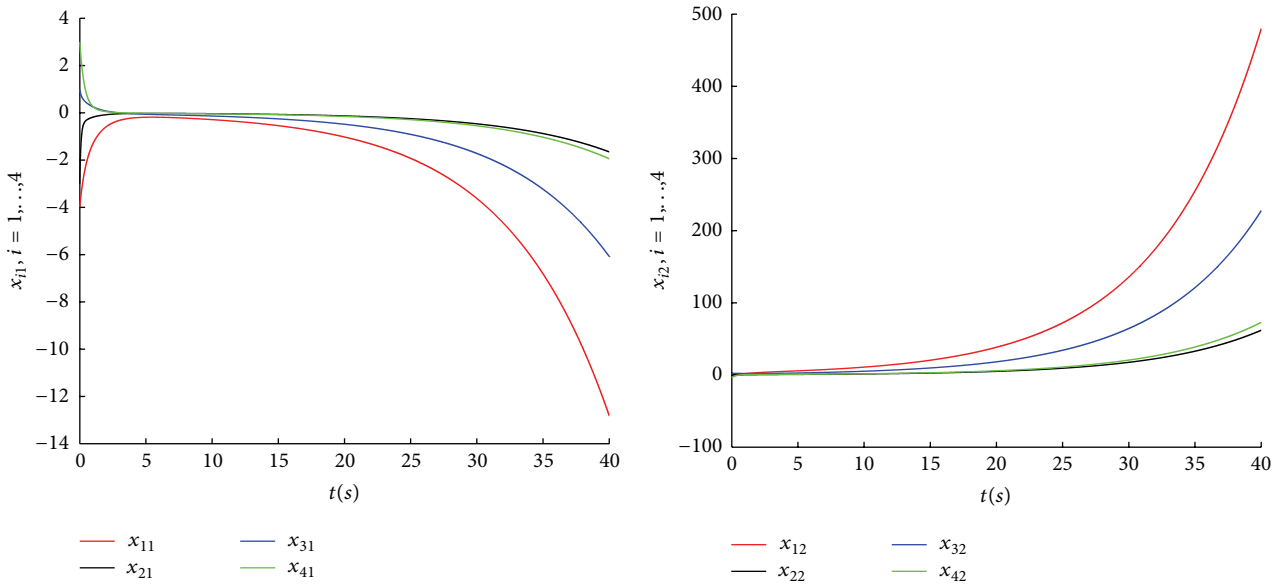

(a) $x(0) = [-4 \quad -3 \quad 1 \quad 3]^T$ (b) $x(0) = [1 \quad 3.5 \quad 2 \quad -4]^T$

Figure 7: The evolution of node states without control.

5.3. Changing the Edge Weights. Note that the edge weights in the system (5) can be different, indicating that one can change the weights to possibly improve the controllability of the system. For instance, in Figure 3(b), by assigning different weights of the edges $(2, 4)$ and $(2, 5)$, the leader symmetry property is also violated so that the digraph becomes controllable.

5.4. Example 2. To verify the theoretical results, consider a directed and weighted network with four different nodes, as shown in Figure 6. Let $m = p = 2$, $\Gamma = I_2$, and $B = \mathrm{diag}\{1, 2\}$. The local dynamics of the nodes are given by

$$\dot{x}_1 = 1.5x_1, \qquad \dot{x}_2 = -10x_2, \qquad \dot{x}_3 = x_3, \qquad \dot{x}_4 = -2x_4. \tag{25}$$

Node 1 is selected to be a leader, so one has

$$\mathscr{L} = \begin{bmatrix} 2 & 0 & -1 & -1 \\ -1.5 & 1.5 & 0 & 0 \\ 0 & -1.2 & 1.2 & 0 \\ 0 & 0 & -1 & 1 \end{bmatrix}, \qquad L_f = \begin{bmatrix} 1.5 & 0 & 0 \\ -1.2 & 1.2 & 0 \\ 0 & -1 & 1 \end{bmatrix}. \tag{26}$$

It follows from Theorem 10 that $[\Gamma \quad B]$ is controllable. Furthermore, one can calculate the eigenvalues of $L_f - \mathscr{C}_f$ and $\overline{\mathscr{L}}$, obtaining $\{0.2, 3, 11.5\}$ and $\{-0.1263, 0.8709, 2.9681, 11.4872\}$, respectively. By Theorem 15, the extended digraph is controllable.

The evolution of the states of the network without control input is depicted in Figures 7(a) and 7(b). The whole network is unstable. Design the control law $u_1 = -10x_1$. Then, as shown in Figures 8(a) and 8(b), all the nodes are controlled to zeroes.

6. Conclusions

In this paper, the controllability of a weighted and directed network with nonidentical node dynamics has been investigated, where the network has a leader-follower structure. The controllability of the controlled network is converted to two subproblems. The first subproblem is to analyze the controllability of the isolated leader subsystem. The second subproblem is to examine the controllability of the extended follower subgraph. A set of conditions for assessing network controllability and identifying nodes playing a key role in network controllability have been established based on matrix theory. Additionally, by using graph theory, several controllability properties have been translated into graph conditions, which are generally more intuitive and informative, therefore, easier to use for applications.

It is found that the controllability of a controlled network with heterogeneous node dynamics is determined by both the node local dynamics and the graph topology including the number of leaders, the location of leaders, and the connection pattern among followers. This result is constructive since it allows for selecting leaders to render the system controllable. Under this framework, the notion of controllability of complex networks with various essentially different structures has been generalized. It has been shown that a single-leader network is controllable if it is a directed path or cycle, otherwise uncontrollable if it is a complete digraph or a star digraph. It has also been shown that the controllability of the system can be improved by increasing the number of leaders, changing the nodal local parameters, or assigning different weights to the edges.

The main difference between our work and the previous works lies in the introduction of different kinetic constants for the uncoupled nodes. The results obtained here are merely the first step in the study on controllability of complex networks

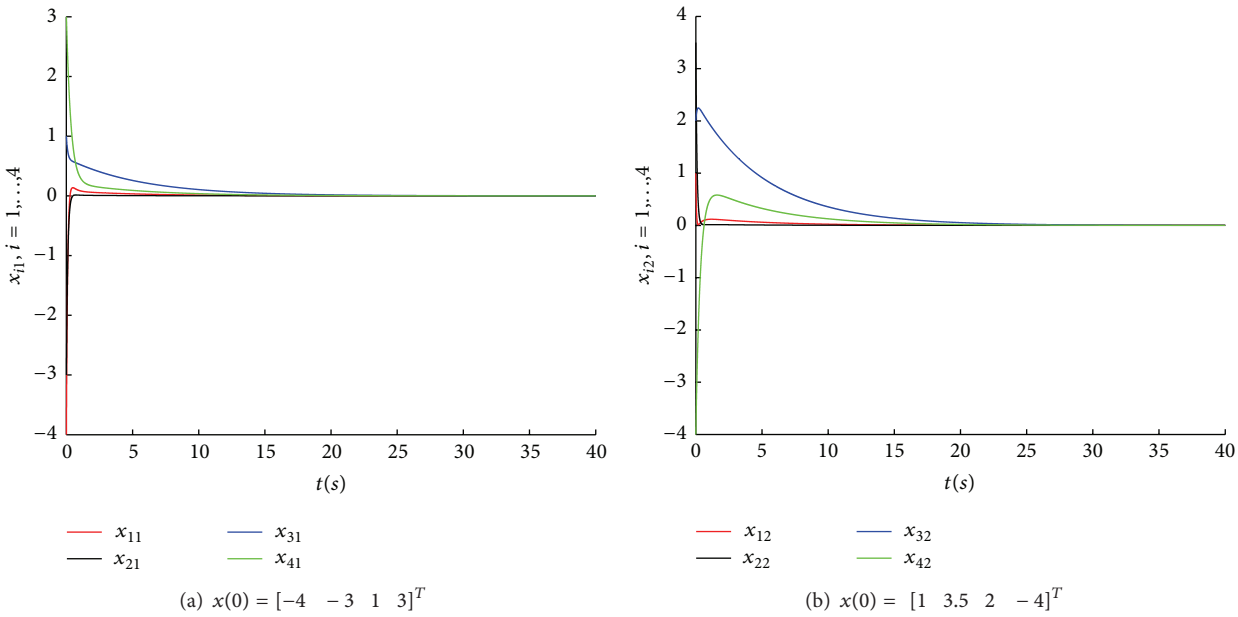

(a) $x(0) = [-4 \quad -3 \quad 1 \quad 3]^T$ (b) $x(0) = [1 \quad 3.5 \quad 2 \quad -4]^T$

Figure 8: The evolution of node states under control.

with heterogenous node dynamics. Future research along the same line might include the cases of noise, uncertainties, and time-varying topology. In addition, the dual property of the observability of complex networks is worthy of future investigation. The concept of "structural observability" [25] may help build up a general framework for future research on this topic.

Acknowledgments

The authors are grateful to the editor and anonymous reviewers for their valuable suggestions and comments, which have led to the improved version of this paper. This work was partially supported by the National Natural Science Foundation of China under Grants 61104151 and 61104018, the Science Foundation of Fujian Province under Grant 2012J01289, and the Hong Kong Research Grants Council under the GRF Grants City University of Hong Kong 1109/12 and 1544/12.

References

[1] H. G. Tanner, "On the controllability of nearest neighbor interconnections," in *Proceedings of the 43rd IEEE Conference on Decision and Control (CDC '04)*, pp. 2467–2472, December 2004.

[2] M. Ji, A. Muhammad, and M. Egerstedt, "Leader-based multi-agent coordination: controllability and optimal control," in *Proceedings of the American Control Conference (ACC '06)*, pp. 1358–1363, June 2006.

[3] A. Rahmani and M. Mesbahi, "On the controlled agreement problem," in *Proceedings of the American Control Conference (ACC '06)*, pp. 1376–1381, June 2006.

[4] A. Rahmani and M. Mesbahi, "Pulling the strings on agreement: anchoring, controllability, and graph automorphisms," in *Proceedings of the American Control Conference (ACC '07)*, pp. 2738–2743, July 2007.

[5] M. Ji and M. Egerstedt, "A graph-theoretic characterization of controllability for multi-agent systems," in *Proceedings of the American Control Conference (ACC '07)*, pp. 4588–4593, July 2007.

[6] A. Rahmani, M. Ji, M. Mesbahi, and M. Egerstedt, "Controllability of multi-agent systems from a graph-theoretic perspective," *SIAM Journal on Control and Optimization*, vol. 48, no. 1, pp. 162–186, 2009.

[7] Z. Ji, Z. Wang, H. Lin, and Z. Wang, "Interconnection topologies for multi-agent coordination under leader-follower framework," *Automatica*, vol. 45, no. 12, pp. 2857–2863, 2009.

[8] B. Liu, T. Chu, L. Wang, and G. Xie, "Controllability of a leader-follower dynamic network with switching topology," *IEEE Transactions on Automatic Control*, vol. 53, no. 4, pp. 1009–1013, 2008.

[9] B. Liu, T. Chu, L. Wang, Z. Zuo, G. Chen, and H. Su, "Controllability of switching networks of multi-agent systems," *International Journal of Robust and Nonlinear Control*, vol. 22, no. 6, pp. 630–644, 2012.

[10] Z. Ji, Z. Wang, H. Lin, and Z. Wang, "Controllability of multi-agent systems with time-delay in state and switching topology," *International Journal of Control*, vol. 83, no. 2, pp. 371–386, 2010.

[11] Y. Lou and Y. Hong, "Controllability analysis of multi-agent systems with directed and weighted interconnection," *International Journal of Control*, vol. 85, no. 10, pp. 1486–1496, 2012.

[12] S. Zhang, M. K. Camlibel, and M. Cao, "Controllability of diffusively-coupled multi-agent systems with general and distance regular coupling topologies," in *Proceedings of the 50th IEEE Conference on Decision and Control and European Control Conference (CDC-ECC '11)*, pp. 759–764, December 2011.

[13] X. Li, X. Wang, and G. Chen, "Pinning a complex dynamical network to its equilibrium," *IEEE Transactions on Circuits and Systems. I. Regular Papers*, vol. 51, no. 10, pp. 2074–2087, 2004.

[14] F. Chen, Z. Chen, L. Xiang, Z. Liu, and Z. Yuan, "Reaching a consensus via pinning control," *Automatica*, vol. 45, no. 5, pp. 1215–1220, 2009.

[15] Y. Y. Liu, J. J. Slotine, and A. L. Barabási, "Controllability of complex networks," *Nature*, vol. 473, no. 7346, pp. 167–173, 2011.

[16] C. T. Lin, "Structural controllability," *IEEE Transactions on Automatic Control*, vol. AC-19, no. 3, pp. 201–208, 1974.

[17] W. X. Wang, X. Ni, Y. C. Lai, and C. Grebogi, "Optimizing controllability of complex networks by minimum structural perturbations," *Physical Review E*, vol. 85, no. 2, Article ID 026115, 2012.

[18] N. J. Cowan, E. J. Chastain, D. A. Vilhena, J. S. Freudenberg, and C. T. Bergstrom, "Nodal dynamics, not degree distributions, determine the structural controllability of complex networks," *PLoS ONE*, vol. 7, no. 6, article e38398, 2012.

[19] F. Sorrentino, M. Di Bernardo, F. Garofalo, and G. Chen, "Controllability of complex networks via pinning," *Physical Review E*, vol. 75, no. 4, Article ID 046103, 2007.

[20] N. Cai and Y.-S. Zhong, "Formation controllability of high-order linear time-invariant swarm systems," *IET Control Theory and Applications*, vol. 4, no. 4, pp. 646–654, 2010.

[21] R. A. Horn and C. R. Johnson, *Matrix Analysis*, Cambridge University Press, Cambridge, UK, 1985.

[22] J. Bang-Jensen and G. Gutin, *Digraphs: Theory, Algorithms and Applications*, Springer, New York, NY, USA, 2009.

[23] C. Godsil and G. Royle, *Algebraic Graph Theory*, vol. 207, Springer, New York, NY, USA, 2001.

[24] W. J. Rugh, *Linear System Theory*, Prentice Hall, Englewood Cliffs, NJ, USA, 1996.

[25] Y. Y. Liu, J. J. Slotine, and A. L. Barabási, "Observability of complex systems," *Proceedings of the National Academy of Sciences of the United States of America*, vol. 110, no. 7, pp. 2460–2465, 2013.

Hindawi Publishing Corporation
Mathematical Problems in Engineering
Volume 2013, Article ID 268063, 8 pages
http://dx.doi.org/10.1155/2013/268063

Research Article

Feature Selection in Decision Systems: A Mean-Variance Approach

Chengdong Yang,[1] Wenyin Zhang,[1] Jilin Zou,[2] Shunbo Hu,[1] and Jianlong Qiu[3]

[1] *School of Informatics, Linyi University, Linyi 276005, China*
[2] *Key Laboratory of Child Development and Learning Science of Ministry of Education, Southeast University, Nanjing 211189, China*
[3] *School of Science, Linyi University, Linyi 276005, China*

Correspondence should be addressed to Jianlong Qiu; qiujianlong@lyu.edu.cn

Received 6 April 2013; Accepted 24 April 2013

Academic Editor: Guanghui Wen

Uncertainty measure is an important implement for characterizing the degree of uncertainty. It has been extensively applied in pattern recognition and data clustering. Because of instability of traditional uncertainty measures, mean-variance measure (MVM) is utilized to perform feature selection, which could depress disturbances and noises effectively. Thereby, a novel evaluation function based on MVM is designed. The forward greedy search algorithm (FGSA) with the proposed evaluation function is exploited to perform feature selection. Experiment analysis shows the validity and effectiveness of MVM.

1. Introduction

Rough sets, originated by Pawlak [1] in 1980s, is a powerful mathematical tool to deal with inexact, uncertain, and vague knowledge in information systems. It has been drawing extensive attention in theory and applications in artificial intelligence, pattern recognition, data mining, intelligence information processing, decision support, image processing, feature selection, neural computing, conflict analysis, and knowledge discovery [2–10].

Uncertainty measure is an important implement for characterizing the degree of uncertainty in rough set theory. It has been extensively applied in pattern recognition and data clustering. However, this paper reveals the issue that classical uncertainty measures are sensitive to disturbances or noises. Therefore, a novel uncertainty measure, called mean-variance measure (MVM), was proposed to characterize the degree of uncertainty of rough sets in paper [11]. Since it takes fully information in the boundary region into account, MVM is more robust and effective than classical uncertainty measures in depressing disturbances and noises.

As an important application of rough sets in artificial intelligence and machine learning, feature selection or attribute reduction in information systems has been drawing wide attention. due to the fact that excessive features or attributes usually confuse learning algorithms, cause significant slowdowns in learning processes, and increase risks of learned classifiers to over-fit the training data [4, 12].

Unfortunately, it has been proved that finding all reducts or finding an optimal reduct (a reduct with the least number of attributes) is an NP-complete problem [13]. Many researchers devote themselves to finding an efficient reduct by optimization techniques. The forward greedy search algorithm (FGSA), also called hill-climbing algorithm or greedy algorithm, is such an optimal technique for finding one reduct quickly and has been extensively investigated [14–16]. A key ingredient of FGSA lies in establishing an evaluation function to examine importance of each feature or attribute in databases. The evaluation function induced by the classical uncertainty measure, that is, the Pawlak's roughness or dependency, has been successfully applied in rough sets based feature selection [17, 18]. Along with the development of rough sets, attribute reduction has been studied extensively in the past decade, such as fuzzy rough sets based attribute reduction [19–23], neighborhood rough sets based attribute reduction [24], cross-entropy based attribute reduction [25], tolerance rough sets based attribute reduction [26], cost based attribute reduction [27, 28], and dynamic attribute reduction

[29, 30], and extended rough set based attribute reduction [31], cover rough sets based attribute reduction [14, 32], covering generalized rough sets based attribute reduction [33], variable precision rough sets based attribute reduction [34]. Nevertheless, the classical uncertainty measure is not robust and maybe fluctuates largely only with minor disturbances. Even a little change in information systems may produce an unpredictable fluctuation of this uncertainty measure.

The mean value and variance in probability theory, able to be used to analyze preciously data, have been widely discussed in portfolio optimization and portfolio selection [35–38]. They are considered as an arbitrator which is used to determine whether a group of data is robust and stable. For example, two shooters obtain the same score (mean value). If one has to be chosen to take part in a tournament, which one should be chosen reasonably? Apparently, the one with a less variance score would like to be chosen. In this paper, the notions of mean value and variance are introduced into information systems as an arbitrator to evaluate the uncertainty degree. A novel uncertainty measure, called mean-variance measure (MVM), is proposed. MVM firstly calculates the mean of every object, and then all objects' variances are taken into account. The effect caused by disturbances of data in decision systems on MVM will decrease, since a tiny alteration of values will not result in a large change of variance.

Based on the new notion of MVM, an evaluation function called D-MVM in decision systems is further designed. The designed evaluation function takes full information in positive region and boundary region into account.

This paper is organized as follows. Some elementary concepts on rough sets and MVM are reviewed in Section 2. Section 3 investigates the issue on feature selection in decision systems by MVM. Experimental results and analysis are given in Section 4, and Section 5 concludes this paper.

2. Preliminaries

2.1. Rough Sets. This section briefly outlines some basic notions on rough sets.

Definition 1. An information system is a pair $S = (U, \mathrm{AT})$ satisfying

(1) U is a nonempty finite set of objects;

(2) AT is a nonempty finite set of attributes;

(3) for every $a \in \mathrm{AT}$, there is a mapping $a : U \to V_a$, where V_a is the set of values.

Definition 2. Given an information system $S = (U, \mathrm{AT})$ and $P \subseteq \mathrm{AT}$, an indiscernibility relation on U is defined by

$$R_P = \{(x, y) \in U \times U \mid a(x) = a(y),\ \forall a \in P\}. \quad (1)$$

Obviously, R_P is an equivalent relation induced by the attribute set P. $[x]_{R_P} = \{y \in U \mid (x, y) \in R_P\}$ is referred to as the equivalence class of x with respect to R_P. A partition of U induced by the equivalent relation R_P can be denoted by

$$\frac{U}{R_P} = \{P_1, P_2, \ldots, P_n\}, \quad (2)$$

where P_i is some equivalence class of R_P in U, $i = 1, 2, \ldots, n$. U/R_P and $[x]_{R_P}$ are, respectively, denoted by U/P and $[x]_P$, for short, when no ambiguity arises in this paper.

Definition 3. Given an information system $S = (U, \mathrm{AT})$, $P \subseteq \mathrm{AT}$, and $X \subseteq U$, the lower approximation and the upper approximation of X with respect to P are defined, respectively, by

$$\begin{aligned} \underline{P}(X) &= \bigcup \left\{P_i \in \frac{U}{P} \mid P_i \subseteq X\right\}, \\ \overline{P}(X) &= \bigcup \left\{P_i \in \frac{U}{P} \mid P_i \cap X \neq \emptyset\right\}. \end{aligned} \quad (3)$$

Definition 4. Given an information system $S = (U, \mathrm{AT})$, a partial ordering relation $\preceq$ in the family $\{U/B \mid B \subseteq \mathrm{AT}\}$ is defined as

$$\frac{U}{P} \preceq \frac{U}{Q}, \quad (4)$$

if and only if for any $P_i \in U/P$, there exists a $Q_j \in U/Q$ such that $P_i \subseteq Q_j$, where $U/P = \{P_1, P_2, \ldots, P_n\}$ and $U/Q = \{Q_1, Q_2, \ldots, Q_m\}$ are partitions induced by $P, Q \subseteq A$, respectively.

Q is said to be coarser than P, or P is finer than Q, if $U/P \preceq U/Q$. P is said to be strictly finer than Q, denoted by $U/P \prec U/Q$, if $U/P \preceq U/Q$ but $U/P \neq U/Q$.

Proposition 5. *Given an information system $S = (U, \mathrm{AT})$, $P, Q \subseteq AT$, and if $P \subseteq Q$, then $U/Q \preceq U/P$.*

From Proposition 5, the more attributes an information system contains, the finer the corresponding partition is. Therefore, U/AT is the finest one among partitions induced by all subsets of AT.

The classical uncertainty measure is defined as follows.

Definition 6. Given an information system $S = (U, \mathrm{AT})$ or an incomplete information system $IS = (U, \mathrm{AT})$, $P \subseteq \mathrm{AT}$, and $X \subseteq U$, the roughness of X is defined as

$$\rho_P(X) = 1 - \frac{|\underline{P}(X)|}{|\overline{P}(X)|}. \quad (5)$$

The quantity $\rho_P(X)$ characterizes the uncertainty degree of X with respect to P. When $\rho_P(X) = 0$, X is said to be definable; otherwise, it is said to be rough.

When AT is divided into two nonempty sets C and D such that $C \cap D = \emptyset$, then $S = (U, \mathrm{AT})$, denoted by $S = (U, C \cup D)$, is called a decision system, C is called the conditional attribute set, and D is called the decision attribute set.

x_1	x_2	x_5	x_6	x_9	x_{10}
x_3	x_4	x_7	x_8	x_{11}	x_{12}
x_{13}	x_{14}	x_{17}	x_{18}	x_{21}	x_{22}
x_{15}	x_{16}	x_{19}	x_{20}	x_{23}	x_{24}
x_{25}	x_{26}	x_{29}	x_{30}	x_{33}	x_{34}
x_{27}	x_{28}	x_{31}	x_{32}	x_{35}	x_{36}

X

(a) X

0	0	0	0	0	0
0	1	1	1	1	0
0	1	1	1	1	1
0	1	1	1	1	0
0	1	1	1	1	0
0	0	0	0	0	0

X

(b) $A(X)$

1/4	1/4	1/2	1/2	1/4	1/4
1/4	1/4	1/2	1/2	1/4	1/4
1/2	1/2	1	1	3/4	3/4
1/2	1/2	1	1	3/4	3/4
1/4	1/4	1/2	1/2	1/4	1/4
1/4	1/4	1/2	1/2	1/4	1/4

X

(c) $A_R(X)$

Figure 1: X, $A(X)$, and $A_R(X)$.

Definition 7. Given a decision system $S = (U, C \cup D)$, the dependency degree of D on C is defined by

$$\gamma(C, D) = \frac{|\mathrm{POS}_C(D)|}{|U|}, \tag{6}$$

where $\mathrm{POS}_C(D) = \cup_{X \in U/D} \underline{C}(X)$ is the positive region of D with respect to C and $|*|$ denotes the cardinality of $*$.

Definition 8. Given a decision system $S = (U, C \cup D)$ and $B \subseteq C$, B is independent if

$$\gamma(B - a, D) < \gamma(B, D), \quad \forall a \in B. \tag{7}$$

Attribute reduction in decision systems is defined as follows.

Definition 9. Given a decision system $S = (U, C \cup D)$ and $B \subseteq C$, B is called a reduct if

(1) $\gamma(B, D) = \gamma(C, D)$,

(2) $\gamma(B - \{a\}, D) < \gamma(B, D)$ for any $a \in B$.

2.2. A Novel Uncertainty Measure of Rough Sets. Given an information system $S = (U, \mathrm{AT})$ and $X \subseteq U$, the characteristic function of X on U can be denoted by

$$A(x) = \begin{cases} 1, & \text{if } x \in X, \\ 0, & \text{if } x \notin X, \end{cases} \tag{8}$$

where $x \in U$.

Let $A(X) = \{A(x)/x \mid x \in U\}$, then $A(X)$ can be considered as a special fuzzy set derived from X on U.

In rough set theory, objects in the same equivalent class cannot be distinguished for each other, since they have the same characteristic. However, in the boundary region of a rough set, objects in the same class have different characteristics. In this case, their mean value of objects in a class is generally used to characterize each object.

Definition 10. Given an information system $S = (U, \mathrm{AT})$, $X \subseteq U$, $P \subseteq \mathrm{AT}$, and $x \in U$, the mean value of x in X, denoted by $A_P(x)$, is defined by

$$A_P(x) = \frac{|[x]_P \cap X|}{|[x]_P|}. \tag{9}$$

We denote $\{A_R(x)/x \mid x \in U\}$ by $A_P(X)$. It is evident that $A_P(X)$ is a fuzzy set on U. As an example, given $U = \{x_1, x_2, \ldots, x_{36}\}$, $U/P = \{\{x_1, x_2, x_3, x_4\}, \{x_5, x_6, x_7, x_8\}, \ldots, \{x_{33}, x_{34}, x_{35}, x_{36}\}\}$, and $X = \{u_8, \ldots, x_{11}, u_{14}, \ldots, x_{17}, u_{20}, \ldots, x_{24}, u_{26}, \ldots, x_{29}\}$, seen in Figure 1(a), then $A(x)$ and $A_P(x)$ are calculated by (8) and (9), respectively, as shown in Figures 1(b) and 1(c).

As mentioned above, when an object x is not in X, its mean value is non-zero if and only if its equivalent class has non-empty intersection with X; when x is in X, its mean value is 1 if and only if its its equivalent class is contained in X. From Definition 10, it is easy to verify that the mean value $A_P(x)$ is an inclusion degree $D(X/[x]_P)$ of $[x]_P$ being included in X.

Proposition 11. *Given an information system $S = (U, \mathrm{AT})$, $X \subseteq U$, $P \subseteq AT$, and $x \in U$, the following conclusions hold:*

(1) *if $x \in \underline{P}(X)$, then $A_P(x) = 1$;*

(2) *if $x \notin \overline{P}(X)$, then $A_P(x) = 0$;*

(3) *if $x \in \overline{P}(X) - \underline{P}(X)$, then $0 < A_P(x) < 1$.*

Note that $A_P(x) = A(x)$ when x is in the positive region and the negative region. It is obvious that $A_P(x) \neq A(x)$ only when x is in the boundary region.

Definition 12. Given an information system $S = (U, \mathrm{AT})$, $P \subseteq \mathrm{AT}$, and $X \subseteq U$, the mean-variance uncertainty measure (MVM) of X with respective to P, denoted by $\sigma_P(X)$, is defined as

$$\sigma_P(X) = \sqrt{\frac{\sum_{x \in U} (A(x) - A_P(x))^2}{|U|}}. \tag{10}$$

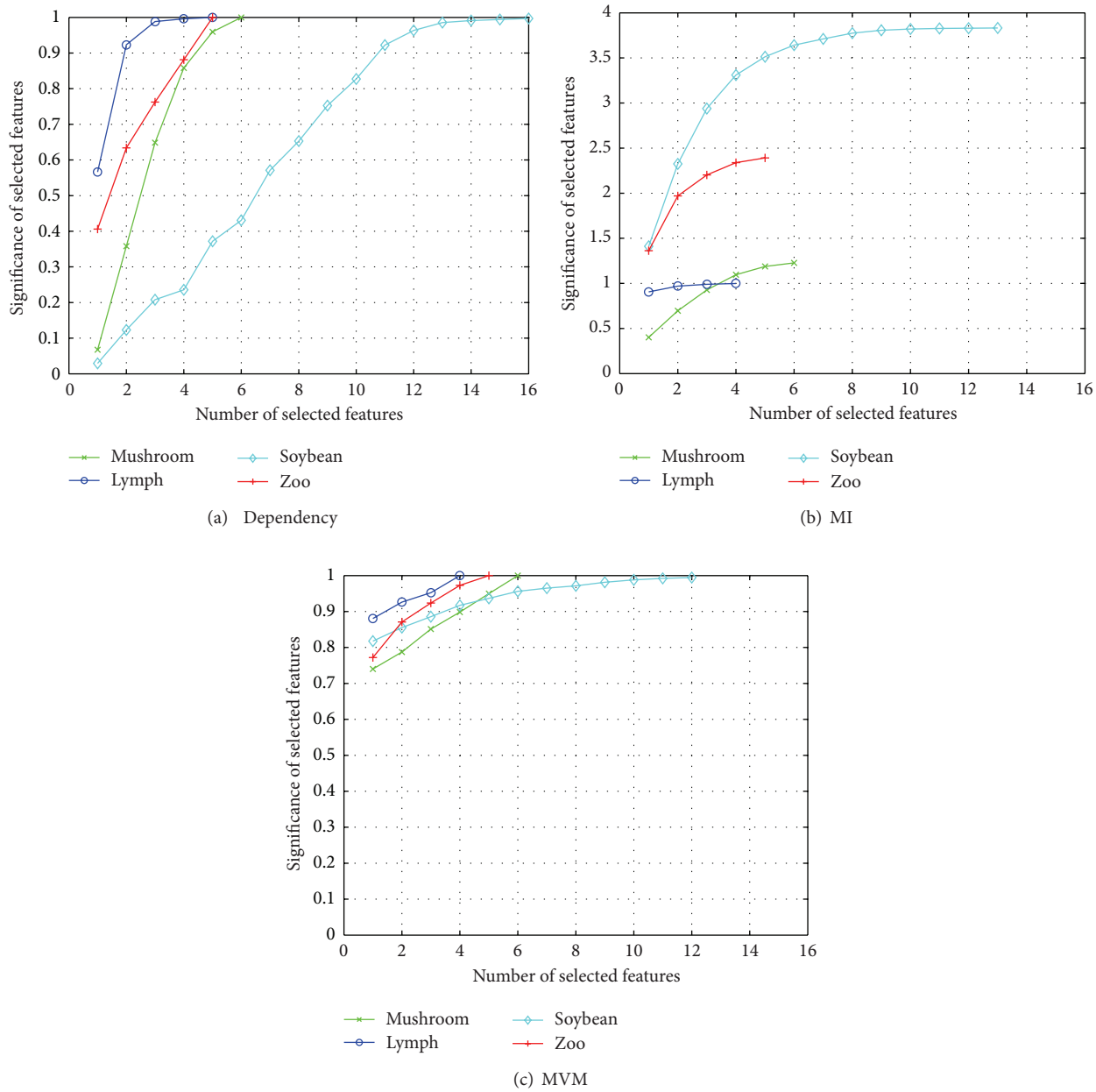

Figure 2: Comparison of convergence among three methods.

It is clear that

$$\sigma_P(X) = \sqrt{\frac{\sum_{x\in X}\left(1 - A_P(x)\right)^2 + \sum_{x\in U-X}\left(A_P(x)\right)^2}{|U|}}. \tag{11}$$

Assume $\sigma_P(X) = 0$ when $X = \emptyset$ or $P = \emptyset$. From Definition 12 one can see that only objects in the boundary region of X contribute to the value of $\sigma_P(X)$. In this sense, $\sigma_P(X)$ takes fully information in the boundary region into account. Therefore, it is a proper measure to evaluate the uncertainty of X.

Definition 13. Given an information system $S = (U, \mathrm{AT})$, $P, Q \subseteq \mathrm{AT}$, and $X, Y \subseteq U$,

(1) X is said to be σ-definable if $\sigma_P(X) = 0$;

(2) X is said to be σ-rough if $\sigma_P(X) \neq 0$;

(3) X is said to be coarser with respect to P than Y with respect to Q if $\sigma_P(X) < \sigma_Q(Y)$, in which case, Y is called finer with respect to Q than X with respect to P.

Next, we investigate properties of $\sigma_P(X)$ and show its efficiencies in evaluating uncertainty of a set in information systems.

Proposition 14. *Given an information system $S = (U, \mathrm{AT})$, $P \subseteq AT$, and $X \subseteq U$, the following conclusions hold:*

(1) $\sigma_P(X) = 0 \Leftrightarrow \rho_P(X) = 0$;

(2) *if $U/P = \omega$, then $\sigma_P(X) = 0$, where $\omega = \{\{x\} \mid x \in U\}$ is the finest partition of U;*

(3) *if $U/P = \delta$, then $\sigma_P(X) = \sqrt{|X|/|U| - (|X|/|U|)^2}$, where $\delta = \{U\}$ is the coarsest partition of U.*

3. Feature Selection in Decision Systems

In this section, the proposed uncertainty measure is further investigated to perform feature selection in decision systems.

Definition 15. Given a decision system $S = (U, C \cup D)$ and $B \subseteq C$, MVM of the decision attribute set D with respect to the conditional attribute subset B, called D-MVM, or an evaluation function, is defined by

$$\sigma(B, D) = \frac{1}{N}\left(\sigma_B(D_1) + \sigma_B(D_2) + \cdots + \sigma_B(D_N)\right), \quad (12)$$

where N is the number of the decision classes induced by the decision attribute set D, $\sigma_B(D_i)$, $i = 1, 2, \ldots, N$, reflect the uncertainty measure of each decision class, and $\sigma(B, D)$ describes the integrated uncertainty degree of blocks $D_1, D_2, \ldots, D_N$.

In the following, some properties of $\sigma(B, D)$ are studied.

Proposition 16. *Given a decision system $S = (U, C \cup D)$ and $B \subseteq C$, the following conclusions hold:*

(1) $\sigma(B, D) = 0 \Leftrightarrow \rho(B, D) = 0$;

(2) *if $U/B = \omega$, then $\sigma(B, D) = 0$;*

(3) *if $U/B = \delta$, then $\sigma(B, D) = (1/N)\sum_{i=1}^{N}\sqrt{|D_i|/|U| - (|D_i|/|U|)^2}$.*

Proof. The proof is analogous to that of ([11], property 2.14). □

Definition 17. Given a decision system $S = (U, C \cup D)$ and $B \subseteq C$, B is independent if

$$\sigma(B, D) < \sigma(B - a, D), \quad \forall a \in B. \quad (13)$$

By D-MVM, a relative reduct can be defined as follows.

Definition 18. Given a decision system $S = (U, C \cup D)$ and $B \subseteq C$, B is a relative reduct of C with respective to D if and only if

(1) $\sigma(B, D) = \sigma(C, D)$,

(2) $\sigma(B, D) < \sigma(B - a, D)$ for any $a \in B$.

A relative reduct is a minimal subset which has the same discriminating power as the raw decision systems.

Table 1: Data sets.

	Data sets	Abbreviation	Samples	Features	Class
1	Lymphography	Lymph	148	19	4
2	Mushroom	Mush	8124	23	2
3	Soybean	Soybean	683	36	19
4	Zoo	Zoo	101	17	7

Definition 19 (significance based on D-MVM). Given a decision system $S = (U, C \cup D)$, $B \subseteq C$, and a feature $a \in C - B$, the significance of a is defined as

$$\mathrm{Sig}_\sigma(a, B, D) = \sigma(B \cup a, D) - \sigma(B, D). \quad (14)$$

Notice that if B is an empty set, $\sigma(B, D) = 0$, and $\mathrm{Sig}_\sigma(a, B, D)$ is a nonnegative real number; otherwise, $\mathrm{Sig}_\sigma(a, B, D) \leq 0$.

With the proposed evaluation function, a forward greedy search algorithm for feature selection can be designed as follows.

In the first iteration, we start with an empty set specified with $\sigma(B, D) = 0$. The quantity $\mathrm{Sig}_\sigma(a, B, D)$ is negative in every iteration except the first one. The rest features in each iteration are all evaluated, and the one with the minimal significance will be chosen. The algorithm does not stop until adding any of the rest features to selected feature set will not bring a change larger than threshold ε in Algorithm 1, where ε controls the precision of the algorithm.

There is no doubt that FGSA-MVM is for the sake of searching a subset of conditional attributes with minimal positive real D-MVM. We obverse step 7 of FGSA-MVM. In the first iteration, we choose the minimal significance because $\mathrm{Sig}_\sigma(a, \emptyset, D)$ is a positive number. In the rest iterations, we also select the minimal significance with the biggest step length since $\mathrm{Sig}_\sigma(a, B, D)$ is nonpositive for any $B \neq \emptyset$.

4. Experiments and Analysis

In order to test the validity of the proposed method for feature selection, comparative experiments have been implemented in efficiency and convergence of proposed algorithm with two of the most important methods, feature selection based on dependence [39] and mutual information [40].

As shown in Table 1, four standard data sets, cited from the machine learning data repository, University of California, Irvine, CA, USA [41], are employed in our experiments.

CART and RBF-support vector machine (SVM) learning algorithms are introduced to test the classification performances of feature selection for raw sets and for selected feature sets. As a widely used technique to evaluate classification performances in machine learning, 10-fold cross-validation [42] is carried out in our experiments by dividing the samples into 10 subsets. Nine of them are used as training set, and the rest one is used as the test set. After 10 rounds, the average value and variation are computed as the final classification performance.

Classification performances are evaluated by CART in Table 2 and by RBF-SVM in Table 3. "Hold" marks the highest classification performances among these obtained

Forward Greedy Search Algorithm of Feature Selection based on Mean-Variable in Decision Systems (FGSA-MVM):
Input: $(U, C \cup D, V, f), \varepsilon$
Output: red
(1) $\emptyset \rightarrow red$
(2) while $C - red \neq \emptyset$
(3) for each $a_i \in C - red$
(4) compute $\mathrm{Sig}_\sigma(a_i, B, D) = \sigma(B \cup a_i, D) - \sigma(B, D)$
(5) end for
(6) select the attribute a_k such that
(7) $\mathrm{Sig}_\sigma(a_k, red, D) = \min_i \mathrm{Sig}_\sigma(a_i, red, D)$
(8) if $|\mathrm{Sig}_\sigma(a_k, red, D)| < \varepsilon$
(9) $red \cup a_k \rightarrow red$
(10) else
(11) break
(12) end if
(13) end while
(14) return red

Algorithm 1

Table 2: Comparison of classification performance of reducts based on different uncertainty measures with CART.

Data sets	Raw data	Dependency	MI	MVM
Lymph	0.6994 ± 0.2195	**0.6825 ± 0.1822**	**0.6825 ± 0.1822**	**0.6825 ± 0.1822**
Mush	0.9637 ± 0.0990	0.9637 ± 0.0990	**0.9685 ± 0.0996**	**0.9685 ± 0.0996**
Soybean	0.9174 ± 0.0507	0.8485 ± 0.0700	0.8780 ± 0.0629	**0.9192 ± 0.0490**
Zoo	0.9065 ± 0.0913	0.8329 ± 0.0676	**0.9276 ± 0.0987**	**0.9276 ± 0.0987**
Aver.	0.8567	0.8439	0.8672	0.8676

Table 3: Comparison of classification performance of reducts based on different uncertainty measures with SVM.

Data sets	Raw data	Dependency	MI	MVM
Lymph	0.5623 ± 0.0583	**0.8448 ± 0.0940**	**0.8448 ± 0.0940**	**0.8448 ± 0.0940**
Mush	0.9587 ± 0.0984	**0.9587 ± 0.0984**	**0.9587 ± 0.0984**	**0.9587 ± 0.0984**
Soybean	0.5445 ± 0.0649	0.6041 ± 0.0723	0.6239 ± 0.0683	**0.6566 ± 0.0817**
Zoo	0.8615 ± 0.0901	**0.9239 ± 0.0924**	**0.9239 ± 0.0924**	**0.9239 ± 0.0924**
Aver.	0.7181	0.8435	0.8523	0.8549

by the methods based on three uncertainty measures. The number of selected features with the highest classification performance by the new measure is larger than that by dependency and by MI. It is 12, 4, and 12, respectively, via CART algorithm, whereas it is 14, 8, and 11 via SVM algorithm.

From the experiments one can see that the proposed measure outperforms not only in the smallest average number of selected features in reducts but also in the highest classification performance in feature selection.

In the remainder of this section, we pay attention to the convergence of the proposed method. Figure 2 shows the fluctuations of evaluation functions with respect to the number of selected features. The significance of selected features is calculated based on dependency, on MI, and on MVM, respectively. The four data sets are used to show the convergence of different techniques. The selected orders of the four data sets based on different evaluation functions are shown in Table 4, in which the sequences of selected features are different, even the number of selected features in the optimal reducts may be the same. As a whole, significance degrees based on dependency and MI increase, while significance based on MVM decreases. With MVM, all four evaluation functions decrease fast at the beginning of the selection process. The evaluation function of credit data slowly decreases, and this result constitutes a different pattern of behavior compared with the three other data sets. Feature selection algorithms may stop very early if we specify a threshold to stop the search in this case. The convergence and good classification performances are observed in the results.

Table 4: Comparison of selected features by different uncertainty measures.

Data sets	Dependency	Mutual information	MVM
Lymph	18 2 13 14 15 16	13 18 14 2 15 16	13 18 14 2 15 16
Mush	5 20 8 12 3	5 20 22 21	5 20 22 21
Soybean	18 26 11 12 35 29 22 1	29 15 22 1 18 3 7 6	28 26 22 15 1 18 3 7
	3 6 7 10 4 5 9 16	10 4 9 16 5	10 6 14 4
Zoo	4 13 12 6 8	13 4 6 8 3	13 4 6 8 3

5. Conclusion

This contribution studied feature selection based on MVM in decision information systems, which is one of the most important applications of rough set theory. A novel approach to feature selection was proposed by introducing an evaluation function based on MVM. Theoretical analysis and experimental results concluded that the performances of proposed method are outperformed by dependency and by MI not only in the number of selected features but also in the classification precision.

Acknowledgments

This work is supported by the National Natural Science Foundation of China under Grant 61273012 and 61102040, and the Shandong Province College Science and Technology Plan Project under Grant J12LN91, and the Shandong Natural Science Foundation of China under Grant ZR2011FL014, and the Shandong Province Science and Technology Development Plan Projects under Grant 2012YD01052.

References

[1] Z. Pawlak, "Rough sets," *International Journal of Computer and Information Sciences*, vol. 11, no. 5, pp. 341–356, 1982.

[2] P. Fortemps, S. Greco, and R. Słowiński, "Multicriteria decision support using rules that represent rough-graded preference relations," *European Journal of Operational Research*, vol. 188, no. 1, pp. 206–223, 2008.

[3] T. Deng, Y. Chen, W. Xu, and Q. Dai, "A novel approach to fuzzy rough sets based on a fuzzy covering," *Information Sciences*, vol. 177, no. 11, pp. 2308–2326, 2007.

[4] W. Z. Wu, "Attribute reduction based on evidence theory in incomplete decision systems," *Information Sciences*, vol. 178, no. 5, pp. 1355–1371, 2008.

[5] M. C. Lee, "Using support vector machine with a hybrid feature selection method to the stock trend prediction," *Expert Systems with Applications*, vol. 36, no. 8, pp. 10896–10904, 2009.

[6] Z. Pawlak, "Some remarks on conflict analysis," *European Journal of Operational Research*, vol. 166, no. 3, pp. 649–654, 2005.

[7] H. Xiumei, F. Haiyan, and S. Kaiquan, "S-rough sets and the discovery of F-hiding knowledge," *Journal of Systems Engineering and Electronics*, vol. 19, no. 6, pp. 1171–1177, 2008.

[8] C. Wang, C. Wu, D. Chen, Q. Hu, and C. Wu, "Communicating between information systems," *Information Sciences*, vol. 178, no. 16, pp. 3228–3239, 2008.

[9] D. Chen, Y. Yang, and X. Zhang, "Parameterized local reduction of decision systems," *Journal of Applied Mathematics*, vol. 2012, Article ID 857590, 14 pages, 2012.

[10] Md. M. Kabir, Md. Shahjahan, and K. Murase, "A new local search based hybrid genetic algorithm for feature selection," *Neurocomputing*, vol. 74, no. 17, pp. 2914–2928, 2011.

[11] C. Yang, W. Zhang, J. Zou et al., "A novel uncertainty measure on rough sets: a mean-variance approach," in *Proceedings of the 9th International Conference on Fuzzy Systems and Knowledge Discovery*, pp. 900–904, 2012.

[12] L. Yu and H. Liu, "Efficiently handling feature redundancy in highdimensional data," in *Proceedings of the 9th ACM SIGKDD International Conference on Knowledge Discovery and Data Mining (KDD '03)*, pp. 685–690, Washington, DC, USA, August 2003.

[13] S. K. M. Wong and W. Ziarko, "On optimal decision rules in decision tables," *Bulletin of the Polish Academy of Sciences*, vol. 33, no. 11-12, pp. 693–696, 1985.

[14] F. Li and Y. Yin, "Approaches to knowledge reduction of covering decision systems based on information theory," *Information Sciences*, vol. 179, no. 11, pp. 1694–1704, 2009.

[15] J. Guan and D. Bell, "Rough computational methods for information systems," *Artificial Intelligence*, vol. 105, pp. 77–103, 1998.

[16] Z. Geng and Q. Zhu, "Rough set-based heuristic hybrid recognizer and its application in fault diagnosis," *Expert Systems with Applications*, vol. 36, no. 2, pp. 2711–2718, 2009.

[17] Z. Pawlak, "Rough sets and fuzzy sets," *Fuzzy Sets and Systems in Information Science and Engineering*, vol. 17, no. 1, pp. 99–102, 1985.

[18] X. Hu and N. Cercone, "Learning in relational databases: a rough set approach," *Computational Intelligence*, vol. 11, no. 2, pp. 323–338, 1995.

[19] Q. Shen and R. Jensen, "Selecting informative features with fuzzy-rough sets and its application for complex systems monitoring," *Pattern Recognition*, vol. 39, no. 7, pp. 1351–1363, 2004.

[20] Q. Hu, Z. Xie, and D. Yu, "Hybrid attribute reduction based on a novel fuzzy-rough model and information granulation," *Pattern Recognition*, vol. 40, no. 12, pp. 3509–3521, 2007.

[21] R. Jensen and Q. Shen, "New approaches to fuzzy-rough feature selection," *IEEE Transactions on Fuzzy Systems*, vol. 17, no. 4, pp. 824–838, 2009.

[22] Q. He, C. Wu, D. Chen, and S. Zhao, "Fuzzy rough set based attribute reduction for information systems with fuzzy decisions," *Knowledge-Based Systems*, vol. 24, no. 5, pp. 689–696, 2011.

[23] D. Zhang, Y. Wang, and H. Huang, "Rough neural network modeling based on fuzzy rough model and its application to texture classification," *Neurocomputing*, vol. 72, no. 10–12, pp. 2433–2443, 2009.

[24] Q. Hu, D. Yu, J. Liu, and C. Wu, "Neighborhood rough set based heterogeneous feature subset selection," *Information Sciences*, vol. 178, no. 18, pp. 3577–3594, 2008.

[25] J. Zheng and R. Yan, "Attribute reduction based on cross entropy in rough set theory," *Journal of Information & Computational Science*, vol. 9, no. 3, pp. 745–750, 2012.

[26] N. M. Parthaláin and Q. Shen, "Exploring the boundary region of tolerance rough sets for feature selection," *Pattern Recognition*, vol. 42, no. 5, pp. 655–667, 2009.

[27] X. Jia, W. Liao, Z. Tang, and L. Shang, "Minimum cost attribute reduction in decision-theoretic rough set models," *Information Sciences*, vol. 219, pp. 151–167, 2013.

[28] F. Min, H. He, Y. Qian, and W. Zhu, "Test-cost-sensitive attribute reduction," *Information Sciences*, vol. 181, no. 22, pp. 4928–44942, 2011.

[29] F. Wang, J. Liang, and C. Dang, "Attribute reduction for dynamic data sets," *Applied Soft Computing*, vol. 13, no. 1, pp. 676–6689, 2013.

[30] J. Zhang, T. Li, D. Ruan, and D. Liu, "Rough sets based matrix approaches with dynamic attribute variation in set-valued information systems," *International Journal of Approximate Reasoning*, vol. 53, no. 4, pp. 620–635, 2012.

[31] Z. Meng and Z. Shi, "Extended rough set-based attribute reduction in inconsistent incomplete decision systems," *Information Sciences*, vol. 204, pp. 44–69, 2012.

[32] W. Zhu and F. Y. Wang, "Reduction and axiomization of covering generalized rough sets," *Information Sciences*, vol. 152, pp. 217–230, 2003.

[33] E. C. C. Tsang, C. Degang, and D. S. Yeung, "Approximations and reducts with covering generalized rough sets," *Computers & Mathematics with Applications*, vol. 56, no. 1, pp. 279–289, 2008.

[34] J. S. Mi, W. Z. Wu, and W. X. Zhang, "Approaches to knowledge reduction based on variable precision rough set model," *Information Sciences*, vol. 159, no. 3-4, pp. 255–272, 2004.

[35] X. T. Deng, Z. F. Li, and S. Y. Wang, "A minimax portfolio selection strategy with equilibrium," *European Journal of Operational Research*, vol. 166, no. 1, pp. 278–292, 2005.

[36] X. Huang, "Mean-variance model for fuzzy capital budgeting," *Computers and Industrial Engineering*, vol. 55, no. 1, pp. 34–47, 2008.

[37] P. Gupta, M. K. Mehlawat, and A. Saxena, "Asset portfolio optimization using fuzzy mathematical programming," *Information Sciences*, vol. 178, no. 6, pp. 1734–1755, 2008.

[38] X. Y. Zhou and G. Yin, "Markowitz's mean-variance portfolio selection with regime switching: a continuous-time model," *SIAM Journal on Control and Optimization*, vol. 42, no. 4, pp. 1466–1482, 2003.

[39] M. Modrzejewski, "Feature selection using rough sets theory," in *Proceedings of the European Conference on Machine Learning*, pp. 213–226, Vienna, Austria, 1993.

[40] F. F. Xu, D. Q. Miao, and L. Wei, "Fuzzy-rough attribute reduction via mutual information with an application to cancer classification," *Computers and Mathematics with Applications*, vol. 57, no. 6, pp. 1010–1017, 2009.

[41] D. J. Newman, S. Hettich, C. L. Blake, and C. J. Merz, "UCI Repository of Machine Learning Databases," University of California, Department of Information and Computer Science, 1998, http://mlearn.ics.uci.edu/MLRepository.html.

[42] M. van der Gaag, T. Hoffman, M. Remijsen et al., "The five-factor model of the positive and negative syndrome scale II: a ten-fold cross-validation of a revised model," *Schizophrenia Research*, vol. 85, no. 1–3, pp. 280–287, 2006.

Hindawi Publishing Corporation
Mathematical Problems in Engineering
Volume 2013, Article ID 742765, 6 pages
http://dx.doi.org/10.1155/2013/742765

Research Article

Synchronization of N Different Chaotic Systems Based on Antisymmetric Structure

Xiangyong Chen and Jianlong Qiu

School of Sciences, Linyi University, Linyi 276005, China

Correspondence should be addressed to Xiangyong Chen; cxy8305@163.com

Received 4 April 2013; Accepted 10 May 2013

Academic Editor: Wenwu Yu

The problem of synchronization of N different chaotic systems is investigated. By using the direct design control method, the synchronization controler is designed to transform the error system into a nonlinear system with a special antisymmetric structure. The sufficient stability conditions are presented for such systems, and the complete synchronization of chaotic systems is realized. Finally, the corresponding numerical simulations demonstrate the effectiveness of the proposed schemes.

1. Introduction

Since Pecora and Carroll have synchronizes two identical chaotic systems with different initial conditions [1], chaotic synchronization has been intensively and extensively investigated due to its potential applications in many fields [2–4]. And most of research efforts have been done about some synchronization phenomena, such as phase synchronization [5], antisynchronization [6], and projective synchronization [7]. Many techniques have been developed to realize chaos synchronization which includes sliding mode control [8], direct design control method [9], and backstepping method [10]. However, most of researches mentioned above mainly concentrated on synchronizing two identical or different chaotic systems.

In fact, more and more applications of chaos synchronization in secure communication make it much more important to synchronize multiple chaotic systems. It can satisfy the synchronization of multiple chaotic communication systems with a lower cost, and it can make it possible to realize multiparty communications simultaneously. Therefore, the synchronization of multiple chaotic systems has become a hot topic. It is more essential and useful in real-life applications. For example, Yu and Zhang studied the global synchronization of three coupled chaotic systems with ring connection in [11]. The adaptive coupled synchronization among multi-Lorenz systems family is investigated in [12]. The synchronization of N different coupled chaotic systems with ring and chain connection was proposed in [13]. The synchronization of N-coupled fractional-order chaotic systems with ring connection was investigated using the stability criteria of fractional-order system in [14]. Zhang studied the synchronization of multi-chaotic systems based on the impulsive control theory in [15]. Grassi researched the propagation of projective synchronization in a series connection of N chaotic discrete-time drive systems and N response systems in [16]. Yang and Zhang studied the synchronization of three identical systems and its application for secure communication with noise perturbation in [17].

However, the realization of synchronization of N identical or nonidentical chaotic systems is much more difficult, so it is necessary to find an easy method to realize such synchronization of multiple chaotic systems. Motivated by the above discussions, in this paper, we consider the problem of synchronization of N different chaotic systems. With the active control method, the synchronization controller is designed to transform the error system into a nonlinear system with the special antisymmetric structure. The complete synchronization of multiple chaotic systems is realized.

This paper is organized as follows. In Section 2, the synchronization of N different chaotic systems is theoretically analyzed. A stability theorem for N different chaotic systems with a special antisymmetric structure is given. In Section 3, the proposed synchronization schemes with the direct design

control method are applied to three different chaotic systems, that is, New system, Lorenz system and Rössler system. The simulations demonstrate the effectiveness of proposed schemes. And finally some concluding remarks are given in Section 4.

2. Synchronization of N Different Chaotic Systems and Controllers Design

Consider the following chaotic systems:

$$\begin{aligned} \dot{x}_1 &= A_1 x_1 + g_1(x_1), \\ \dot{x}_2 &= A_2 x_2 + g_2(x_2), \\ &\vdots \\ \dot{x}_N &= A_N x_N + g_n(x_N), \end{aligned} \tag{1}$$

where $x_1, x_2, \ldots, x_N \in \mathbb{R}^n (N > 2)$ represent state vectors of the chaotic systems; $g : \mathbb{R}^n \to \mathbb{R}^n$ is a continuous nonlinear function; $A_1, A_2, \ldots, A_N$ are constant matrices. For $i, j = 1, \ldots, N$, and $i \neq j$, if

$$A_i \neq A_j, \quad g_i(\cdot) \neq g_j(\cdot), \tag{2}$$

then the systems (1) are the different chaotic systems.

We consider N different chaotic systems. The drive systems and the controled response systems are described as follows:

$$\begin{aligned} \dot{x}_1 &= A_1 x_1 + g_1(x_1), \\ \dot{x}_2 &= A_2 x_2 + g_2(x_2) + u(x_1, x_2), \\ &\vdots \\ \dot{x}_N &= A_N x_N + g_n(x_N) + u(x_1, x_N). \end{aligned} \tag{3}$$

Let us define the errors systems between response systems and drive systems as $\dot{e}_i = \dot{x}_i - \dot{x}_1, (i = 2, \ldots, N)$, then the dynamics of the synchronization errors can be expressed as

$$\dot{e} = \begin{bmatrix} \dot{e}_2 \\ \dot{e}_3 \\ \vdots \\ \dot{e}_N \end{bmatrix} = \begin{bmatrix} A_2 e_2 + (A_2 - A_1) x_1 + g_2(x_2) - g_1(x_1) + u(x_2, x_1) \\ A_3 e_3 + (A_3 - A_1) x_1 + g_3(x_3) - g_1(x_1) + u(x_3, x_1) \\ \vdots \\ A_N e_N + (A_N - A_1) x_1 + g_N(x_N) - g_1(x_1) + u(x_N, x_1) \end{bmatrix}. \tag{4}$$

Our purpose is to design the appropriate controllers $u(x_i, x_1)$ for the response systems such that the error systems (4) are asymptotically stable, which implies that the complete synchronization of N different chaotic systems (3) is realized; that is,

$$\lim_{t \to \infty} \|e_i\| = \lim_{t \to \infty} \|x_i - x_1\| = 0. \tag{5}$$

Here, the direct design control method is used to achieve the objective. In accordance to the active control design strategy, we choose the control input $u(x_i, x_1)$ to eliminate all known items that cannot be shown in the form of the error system e_i. The controller can be given by

$$u(x_i, x_1) = u_i - (A_i - A_1) x_1 - g_i(x_i) + g_1(x_1), \quad i = 2, \ldots, N. \tag{6}$$

The error systems (4) can be rewritten as

$$\dot{e} = \begin{bmatrix} \dot{e}_2 \\ \dot{e}_3 \\ \vdots \\ \dot{e}_N \end{bmatrix} = \begin{bmatrix} A_2 & 0 & \cdots & 0 \\ 0 & A_3 & \cdots & 0 \\ \vdots & \vdots & \vdots & \vdots \\ 0 & 0 & \cdots & A_N \end{bmatrix} \begin{bmatrix} e_2 \\ e_3 \\ \vdots \\ e_N \end{bmatrix} + \begin{bmatrix} u_2 \\ u_3 \\ \vdots \\ u_N \end{bmatrix}. \tag{7}$$

Defining $u_i = p_i e_i$, we can get the error systems (8) as follows:

$$\dot{e} = \begin{bmatrix} \dot{e}_2 \\ \dot{e}_3 \\ \vdots \\ \dot{e}_N \end{bmatrix} = \begin{bmatrix} A_2 + p_2 & 0 & \cdots & 0 \\ 0 & A_3 + p_3 & \cdots & 0 \\ \vdots & \vdots & \vdots & \vdots \\ 0 & 0 & \cdots & A_N + p_N \end{bmatrix} \begin{bmatrix} e_2 \\ e_3 \\ \vdots \\ e_N \end{bmatrix}. \tag{8}$$

There are many possible choices for p_i, as long as it assures that the error dynamic system (8) is asymptotically stable at the origin. Without loss of generality, let us define p_i as a state-dependent coefficient matrix, then the error systems (8) can be rewritten as

$$\dot{e} = \begin{bmatrix} B_2(e_2) & 0 & \cdots & 0 \\ 0 & B_3(e_3) & \cdots & 0 \\ \vdots & \vdots & \vdots & \vdots \\ 0 & 0 & \cdots & B_N(e_N) \end{bmatrix} \begin{bmatrix} e_2 \\ e_3 \\ \vdots \\ e_N \end{bmatrix}. \tag{9}$$

The sufficient stability conditions of the systems (9) will be given by transforming it into a stable system with a special antisymmetric structure. The main result is described as follows.

Theorem 1. *Consider the systems* (9) *with the state-dependent coefficient matrices* $B_i(e_i) = B_{i1}(e_i) + B_{i2}$. *If the matrices* $B_{i1}(e_i)$ *and* B_{i2} *satisfy the assumptions that*

$$\begin{aligned} B_{i1}^T(e_i) &= -B_{i1}(e_i), \quad (i = 2, \ldots, N), \\ B_{i2} &= \operatorname{diag}(b_{i1}, \ldots, b_{in}), \quad b_{ij} < 0, (j = 1, \ldots, n), \end{aligned} \tag{10}$$

and the invariant set of the system (9) *only includes the origin, then the system* (9) *is asymptotically stable.*

Proof. Choose Lyapunov function as follows:

$$V = \frac{1}{2} e^T e. \tag{11}$$

Then

$$\begin{aligned}
\dot{V} &= \frac{1}{2}\left(\dot{e}^T e + e^T \dot{e}\right) \\
&= \frac{1}{2} e^T \left(\begin{bmatrix} B_2(e_2) & 0 & \cdots & 0 \\ 0 & B_3(e_3) & \cdots & 0 \\ \vdots & \vdots & \vdots & \vdots \\ 0 & 0 & \cdots & B_N(e_N) \end{bmatrix}^T + \begin{bmatrix} B_2(e_2) & 0 & \cdots & 0 \\ 0 & B_3(e_3) & \cdots & 0 \\ \vdots & \vdots & \vdots & \vdots \\ 0 & 0 & \cdots & B_N(e_N) \end{bmatrix} \right) e \\
&= \frac{1}{2} e^T \left(\begin{bmatrix} B_{21}(e_2) + B_{22}(e_2) & 0 & \cdots & 0 \\ 0 & B_{31}(e_3) + B_{32}(e_3) & \cdots & 0 \\ \vdots & \vdots & \vdots & \vdots \\ 0 & 0 & \cdots & B_{N1}(e_N) + B_{N2}(e_N) \end{bmatrix}^T \right. \\
&\qquad \left. + \begin{bmatrix} B_{21}(e_2) + B_{22}(e_2) & 0 & \cdots & 0 \\ 0 & B_{31}(e_3) + B_{32}(e_3) & \cdots & 0 \\ \vdots & \vdots & \vdots & \vdots \\ 0 & 0 & \cdots & B_{N1}(e_N) + B_{N2}(e_N) \end{bmatrix} \right) e,
\end{aligned} \tag{12}$$

where $B_{i1}^T(e_i) = -B_{i1}(e_i)$, $(i = 2, \ldots, N)$, and $B_{i2}^T(e_i) = B_{i2}(e_i)$. So we get that

$$\dot{V} = e^T \begin{bmatrix} B_{22}(e_2) & 0 & \cdots & 0 \\ 0 & B_{32}(e_3) & \cdots & 0 \\ \vdots & \vdots & \vdots & \vdots \\ 0 & 0 & \cdots & B_{N2}(e_N) \end{bmatrix} e, \tag{13}$$

where, for $j = 1, \ldots, n$ and $b_{ij} < 0$, $B_{i2} = \mathrm{diag}(b_{i1}, \ldots, b_{in})$ is negative definite. Therefore, $\dot{V}$ is negative definite. According to Lyapunov asymptotical stability theory, the complete synchronization of the different chaotic systems is achieved. □

Remark 2. The system (9) is transformed into the system $\dot{e}_i = B_i(e_i)e_i$ under the control law $u(x_i, x_1)$, where $B_i(e_i)$ possesses the antisymmetric structure; then the error system (4) is asymptotically stable at the origin according to the Theorem 1.

Remark 3. The antisymmetric structures in Theorem 1 are the generalization of the tridiagonal structures. The error system constructed with the antisymmetric structure is more convenient than the one with tridiagonal structure, if the original system has some zero elements at the tridiagonal position and nonzero elements at other positions.

The selecting of the coefficient matrices with antisymmetric structure is an important and difficult technique, which relates to the coefficient matrices and the states of the original system. In the following section, we will demonstrate the proposed approaches for the special structure with an example.

3. Applications of Synchronization Control Schemes

In this section, we employ a simulation example to illustrate the effectiveness of the proposed schemes. The synchronization is simulated for three different chaotic systems. We choose New system as drive system, and we consider Lorenz system and Rössler system as the response systems. They are described as follows:

$$\begin{aligned}
\dot{x}_{11} &= 5x_{11} - x_{12}x_{13}, \\
\dot{x}_{12} &= -10x_{12} + x_{11}x_{13}, \\
\dot{x}_{13} &= -3.8x_{13} + \frac{1}{3}x_{11}x_{12},
\end{aligned} \tag{14}$$

$$\begin{aligned}
\dot{x}_{21} &= -10x_{21} + 10x_{22} + u_{21}, \\
\dot{x}_{22} &= 28x_{21} - x_{22} - x_{21}x_{23} + u_{22}, \\
\dot{x}_{23} &= -\frac{8}{3}x_{23} + x_{21}x_{22} + u_{23},
\end{aligned} \tag{15}$$

$$\begin{aligned}
\dot{x}_{31} &= -x_{32} - x_{33} + u_{31}, \\
\dot{x}_{32} &= x_{31} + 0.2x_{32} + u_{32}, \\
\dot{x}_{33} &= -5.7x_{33} + 0.2 + x_{31}x_{33} + u_{33},
\end{aligned} \tag{16}$$

where

$$A_1 = \begin{bmatrix} 5 & 0 & 0 \\ 0 & -10 & 0 \\ 0 & 0 & -3.8 \end{bmatrix}, \qquad A_2 = \begin{bmatrix} -10 & 10 & 0 \\ 28 & -1 & 0 \\ 0 & 0 & -\frac{8}{3} \end{bmatrix},$$

$$A_3 = \begin{bmatrix} 0 & -1 & -1 \\ 1 & 0.2 & 0 \\ 0 & 0 & -5.7 \end{bmatrix}, \qquad g_1(x_1) = \begin{bmatrix} -x_{12}x_{13} \\ x_{11}x_{13} \\ \frac{1}{3}x_{11}x_{12} \end{bmatrix},$$
$$g_2(x_2) = \begin{bmatrix} 0 \\ -x_{21}x_{23} \\ x_{21}x_{22} \end{bmatrix}, \qquad g_3(x_3) = \begin{bmatrix} 0 \\ 0 \\ 0.2 + x_{31}x_{33} \end{bmatrix}. \tag{17}$$

Let the synchronization error state be $\dot{e}_i = \dot{x}_i - \dot{x}_1$, $(i = 2, 3)$, then the error dynamical states can be written as

$$\begin{aligned} \dot{e}_{21} &= -10e_{21} + 10e_{22} + u_{21} + x_{12}x_{13} - 15x_{11} + 10x_{12}, \\ \dot{e}_{22} &= 28e_{21} - e_{22} + u_{22} - x_{21}x_{23} - x_{11}x_{13} + 28x_{11} + 9x_{12}, \\ \dot{e}_{23} &= -\frac{8}{3}e_{23} + u_{23} + x_{21}x_{22} - \frac{1}{3}x_{11}x_{12} + \left(3.8 - \frac{8}{3}\right)x_{13}, \end{aligned} \tag{18}$$

$$\begin{aligned} \dot{e}_{31} &= -e_{32} - e_{33} + u_{31} + x_{12}x_{13} - 5x_{11} - x_{12} - x_{13}, \\ \dot{e}_{32} &= e_{31} + 0.2e_{32} + u_{32} + x_{11} + 10.2x_{12} - x_{11}x_{13}, \\ \dot{e}_{33} &= -5.7e_{33} + u_{33} - 1.9x_{13} + 0.2 + x_{31}x_{33} - \frac{1}{3}x_{11}x_{12}. \end{aligned} \tag{19}$$

Then the controllers are designed as follows,

$$\begin{aligned} u(x_2, x_1) &= \begin{bmatrix} u_{21} \\ u_{22} \\ u_{23} \end{bmatrix} \\ &= p_1 \begin{bmatrix} e_{21} \\ e_{22} \\ e_{23} \end{bmatrix} - \begin{bmatrix} 15 & -10 & 0 \\ 28 & 9 & 0 \\ 0 & 0 & \left(3.8 - \frac{8}{3}\right) \end{bmatrix} \begin{bmatrix} x_{11} \\ x_{12} \\ x_{13} \end{bmatrix} \\ &\quad - g_2(x_2) + g_1(x_1), \\ u(x_3, x_1) &= \begin{bmatrix} u_{31} \\ u_{32} \\ u_{33} \end{bmatrix} \\ &= p_2 \begin{bmatrix} e_{31} \\ e_{32} \\ e_{33} \end{bmatrix} - \begin{bmatrix} -5 & -1 & -1 \\ 1 & 10.2 & 0 \\ 0 & 0 & -1.9 \end{bmatrix} \begin{bmatrix} x_{11} \\ x_{12} \\ x_{13} \end{bmatrix} \\ &\quad - g_3(x_3) + g_1(x_1), \end{aligned} \tag{20}$$

where

$$p_1 = \begin{bmatrix} 0 & 0 & -x_{12} \\ -18 & 0 & -(x_{11} + e_{21}) \\ x_{12} & (x_{11} + e_{21}) & 0 \end{bmatrix}, \qquad p_2 = \begin{bmatrix} -1 & 0 & 0 \\ 0 & -1.2 & -(x_{11} + e_{31}) \\ 1 & (x_{11} + e_{31}) & 0 \end{bmatrix}. \tag{21}$$

Then the error systems (18) can be rewritten as

$$\begin{aligned} \dot{e} &= \begin{bmatrix} \dot{e}_2 \\ \dot{e}_3 \end{bmatrix} = \begin{bmatrix} \dot{e}_{21} & \dot{e}_{22} & \dot{e}_{23} & \dot{e}_{31} & \dot{e}_{32} & \dot{e}_{33} \end{bmatrix}^T \\ &= \begin{bmatrix} -10 & -10 & -x_{12} & 0 & 0 & 0 \\ 10 & -1 & -(x_{11} + e_{21}) & 0 & 0 & 0 \\ x_{12} & (x_{11} + e_{21}) & -\frac{8}{3} & 0 & 0 & 0 \\ 0 & 0 & 0 & -1 & -1 & -1 \\ 0 & 0 & 0 & 1 & -1 & -(x_{11} + e_{31}) \\ 0 & 0 & 0 & 1 & (x_{11} + e_{31}) & -5.7 \end{bmatrix} \begin{bmatrix} e_{21} \\ e_{22} \\ e_{23} \\ e_{31} \\ e_{32} \\ e_{33} \end{bmatrix}. \end{aligned} \tag{22}$$

Let us define $B_2(e_2)$ and $B_3(e_3)$ as follows:

$$\begin{aligned} B_{21}(e_2) &= \begin{bmatrix} 0 & -10 & -x_{12} \\ 10 & 0 & -(x_{11} + e_{21}) \\ x_{12} & (x_{11} + e_{21}) & 0 \end{bmatrix} \\ &\quad + \begin{bmatrix} -10 & 0 & 0 \\ 0 & -1 & 0 \\ 0 & 0 & -\frac{8}{3} \end{bmatrix}, \\ B_3(e_3) &= \begin{bmatrix} 0 & -1 & -1 \\ 1 & 0 & -(x_{11} + e_{31}) \\ 1 & (x_{11} + e_{31}) & 0 \end{bmatrix} \\ &\quad + \begin{bmatrix} -1 & 0 & 0 \\ 0 & -1 & 0 \\ 0 & 0 & -5.7 \end{bmatrix}. \end{aligned} \tag{23}$$

Then we declare that the error systems (18) and (19) are asymptotically stable at the origin under the controllers (20)

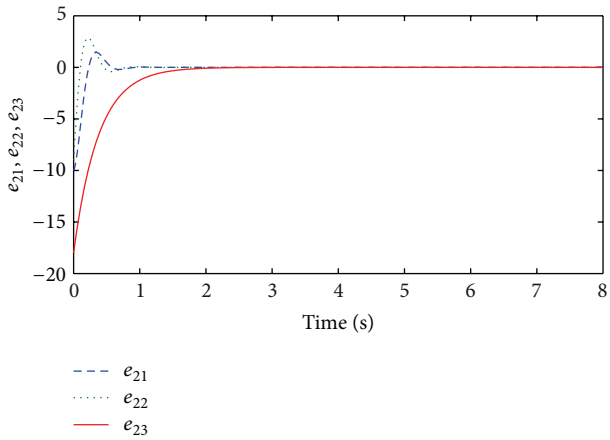

FIGURE 1: Dynamics of the variables e_{21}, e_{22}, and e_{23} of the error system (18) with time t.

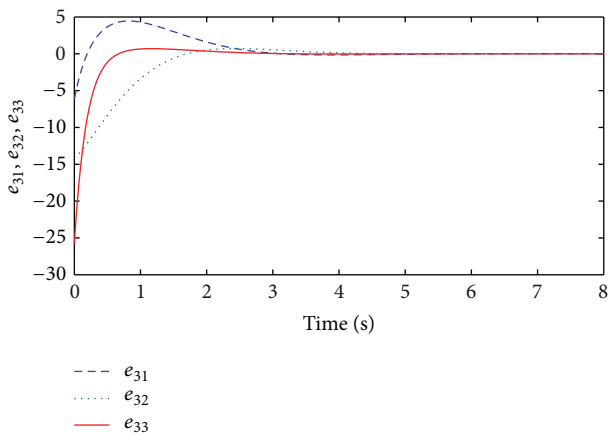

FIGURE 2: Dynamics of the variables e_{31}, e_{32}, and e_{33} of the error system (19) with time t.

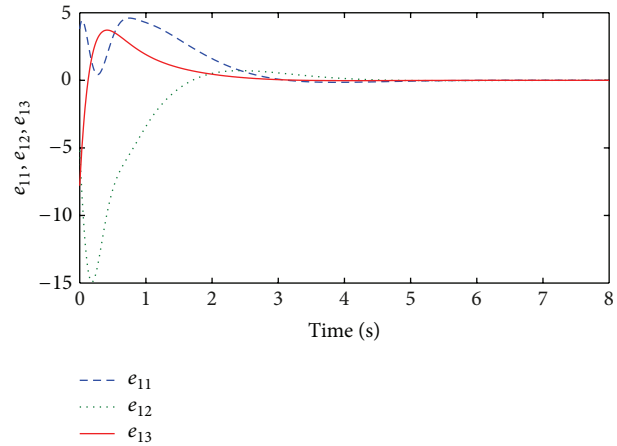

FIGURE 3: Dynamics of the variables of the error system between the response systems (15) and (16) with time t.

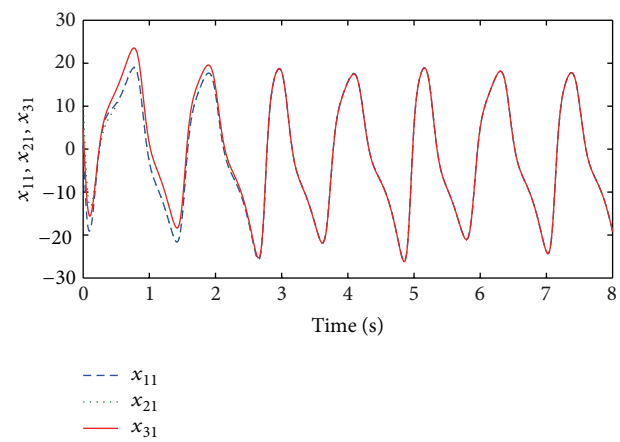

FIGURE 4: The state trajectories x_{11}, x_{21}, and x_{31} of the chaotic systems with time t.

according to Theorem 1. Then the synchronization between the response systems and the drive system is realized.

The fourth-order Runge-Kutta integration method is used to numerical simulation with time step size 0.001s. Let the initial conditions of the drive system and the response systems be $(x_{11}(0), x_{12}(0), x_{13}(0))^T = (11, 15, 26)^T$, $(x_{21}(0), x_{22}(0), x_{23}(0))^T = (1, 6, 8)^T$, and $(x_{31}(0), x_{32}(0), x_{33}(0))^T = (4.8, 0.8, 0.2)^T$, respectively. Then the initial values of the error states are $(e_{21}(0), x_{22}(0), x_{23}(0))^T = (-10, -9, -18)^T$ and $(e_{31}(0), x_{32}(0), x_{33}(0))^T = (-6.2, -14.2, -25.8)^T$. The state trajectories of the error systems are shown in Figures 1, 2, and 3, and the state trajectories of 3 different chaotic systems are shown in Figures 4, 5, and 6. We can make out that, from Figures 1–6, the state trajectories asymptotically converge to zero near 2.5 s, 4.5 s, and 5 s under the controllers, and the state vectors of the different chaotic systems achieve the complete synchronization. The numerical simulations demonstrate that the proposed design method is feasible and effective to realize the complete synchronization of N different chaotic systems which satisfy Theorem 1.

4. Conclusions

In this paper, the synchronization problem of N different chaotic systems is investigated. The direct design method is adopted to realize the complete synchronization of N different chaotic systems according to the proposed theorems. And then the stability theorems about the error systems with the special antisymmetric structure are presented. Numerical simulations of the synchronization about the different chaotic systems, respectively, illustrate the validity of the proposed schemes. How to realize other types of synchronization of N-coupled chaotic systems is our further work. Inspired by the studies [18–20], how to extend the current results to chaotic systems with discontinuous functions is also our future research directions.

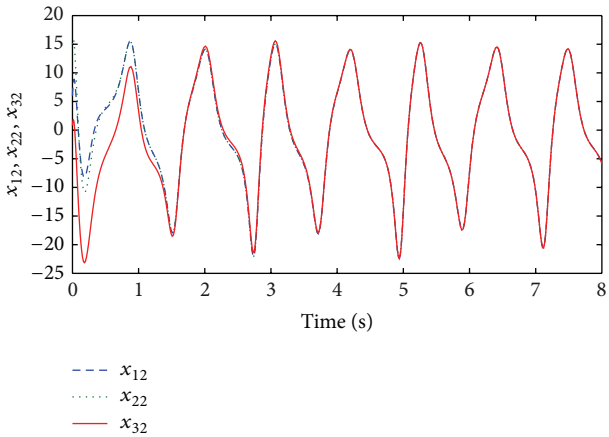

FIGURE 5: The state trajectories x_{12}, x_{22}, and x_{32} of the chaotic systems with time t.

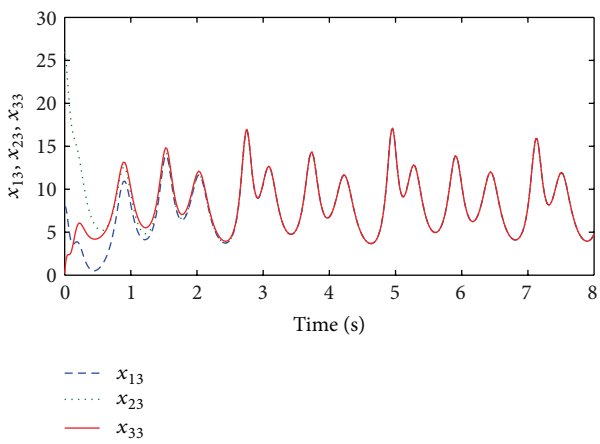

FIGURE 6: The state trajectories x_{13}, x_{23}, and x_{33} of the chaotic systems with time t.

Acknowledgments

The authors' work was supported in part by the National Natural Science Foundation of China, nos. 61273012, 11201212, and a Project of Shandong Province Higher Educational Science and Technology Program, nos. J13LI11, J12LI58. The authors would like to express their thanks to the gratefully acknowledged suggestions and comments made by the referees.

References

[1] L. M. Pecora and T. L. Carroll, "Synchronization in chaotic systems," *Physical Review Letters*, vol. 64, no. 8, pp. 821–824, 1990.

[2] B. Nana, P. Woafo, and S. Domngang, "Chaotic synchronization with experimental application to secure communications," *Communications in Nonlinear Science and Numerical Simulation*, vol. 14, no. 5, pp. 2266–2276, 2009.

[3] C. Aguirre, D. Campos, P. Pascual, and E. Serrano, "Synchronization effects using a piecewise linear map-based spiking-bursting neuron model," *Neurocomputing*, vol. 69, no. 10–12, pp. 1116–1119, 2006.

[4] S. Tang and J. M. Liu, "Chaos synchronization in semiconductor lasers with optoelectronic feedback," *IEEE Journal of Quantum Electronics*, vol. 39, no. 6, pp. 708–715, 2003.

[5] S. Guan, C.-H. Lai, and G. W. Wei, "Phase synchronization between two essentially different chaotic systems," *Physical Review E*, vol. 72, no. 1, article 016205, 8 pages, 2005.

[6] N. Cai, Y. W. Jing, and S. Y. Zhang, "Adaptive synchronization and anti-synchronization of two different chaotic systems," *Acta Physica Sinica*, vol. 58, no. 2, pp. 802–813, 2009.

[7] N. Cai, Y. Jing, and S. Zhang, "Generalized projective synchronization of different chaotic systems based on antisymmetric structure," *Chaos, Solitons and Fractals*, vol. 42, no. 2, pp. 1190–1196, 2009.

[8] N. Cai, Y. Jing, and S. Zhang, "Modified projective synchronization of chaotic systems with disturbances via active sliding mode control," *Communications in Nonlinear Science and Numerical Simulation*, vol. 15, no. 6, pp. 1613–1620, 2010.

[9] M. Yahyazadeh, A. R. Noei, and R. Ghaderi, "Synchronization of chaotic systems with known and unknown parameters using a modified active sliding mode control," *ISA Transactions*, vol. 50, no. 2, pp. 262–267, 2011.

[10] M. T. Yassen, "Controlling, synchronization and tracking chaotic Liu system using active backstepping design," *Physics Letters A*, vol. 360, no. 4-5, pp. 582–587, 2007.

[11] Y. Yu and S. Zhang, "Global synchronization of three coupled chaotic systems with ring connection," *Chaos, Solitons and Fractals*, vol. 24, no. 5, pp. 1233–1242, 2005.

[12] J.-a. Lu, X.-p. Han, Y.-t. Li, and M.-h. Yu, "Adaptive coupled synchronization among multi-Lorenz systems family," *Chaos, Solitons and Fractals*, vol. 31, no. 4, pp. 866–878, 2007.

[13] Y. Liu and L. Lü, "Synchronization of N different coupled chaotic systems with ring and chain connections," *Applied Mathematics and Mechanics*, vol. 29, no. 10, pp. 1299–1308, 2008.

[14] Y. Tang and J.-a. Fang, "Synchronization of N-coupled fractional-order chaotic systems with ring connection," *Communications in Nonlinear Science and Numerical Simulation*, vol. 15, no. 2, pp. 401–412, 2010.

[15] Q. L. Zhang, "Synchronization of multi-chaotic systems via ring impulsive control," *Journal of Control Theory and Applications*, vol. 27, no. 2, pp. 226–232, 2010.

[16] G. Grassi, "Propagation of projective synchronization in a series connection of chaotic systems," *Journal of the Franklin Institute*, vol. 347, no. 2, pp. 438–451, 2010.

[17] L. X. Yang and J. Zhang, "Synchronization of three identical systems and its application for secure communication with noise perturbation," in *Proceedings of the International Conference on Information Engineering and Computer Science (ICIECS '09)*, Wuhan, China, December 2009.

[18] X. Liu and J. Cao, "Robust state estimation for neural networks with discontinuous activations," *IEEE Transactions on Systems, Man, and Cybernetics B*, vol. 40, no. 6, pp. 1425–1437, 2010.

[19] X. Liu, J. Cao, and G. Huang, "Complete periodic synchronization of delayed neural networks with discontinuous activations," *International Journal of Bifurcation and Chaos in Applied Sciences and Engineering*, vol. 20, no. 7, pp. 2151–2164, 2010.

[20] X. Y. Liu, J. D. Cao, and W. W. Yu, "Filippov systems and quasi-synchronization control for switched networks," *Chaos*, vol. 22, no. 3, pp. 1–12, 2012.

Hindawi Publishing Corporation
Mathematical Problems in Engineering
Volume 2013, Article ID 906785, 7 pages
http://dx.doi.org/10.1155/2013/906785

Research Article

The Effects of Decision-Making Processes and Population Turnover on the Formation of Social Networks

Zhijing Xu, Zhenghu Zu, Tao Zheng, Wendou Zhang, and Qing Xu

Beijing Institute of Biotechnology, 20 East Avenue, Fengtai District, Beijing 100071, China

Correspondence should be addressed to Tao Zheng; zt19721@hotmail.com

Received 13 March 2013; Accepted 28 April 2013

Academic Editor: Guanghui Wen

The researchs on the structure and formation mechanism of social networks lead to several models with differences in the attachment patterns of new links (edges). In fact, the driving factor behind the addition of new links is just as important as the attachment patterns, while very little attention has been devoted so far to this exploration. We present an agent-based model which could successfully reproduce large-scale social networks. We find that the structure of social networks is a consequence of continuous individuals' decision-making processes based on self-evaluations and the turnover of the population. The individuals' self-evaluation processes are key motivating factors for the addition of new links, while the attachment patterns and the turnover of the population should be responsible for the topology of social networks. The resulting networks of our model display dynamics between order and randomness, which is greatly consistent with current observations and research achievements of social networks. We also find that some plausible properties of empirical data are actually artifacts due to the boundedness of sampling. Our research has revealed the driving factors behind the evolution of social networks as well as the underlying evolving patterns. These findings will lead to a better understanding of social structures.

1. Introduction

Complex networks have gained increasing enthusiasm in various fields ranging from natural science to social science in the last few years. The achievements of data acquisition make it possible to calibrate some hypotheses once supposed to be reasonable in people's mind, one of which is networks of complex topology described with the random graph theory of Erdös-Rényi (ER) [1], whose degree obeys a Gaussian distribution. Barabási and Albert (BA) have developed a growing network model to interpret the emergence of scaling in networks, known as BA model [2], which leads to a degree distribution $P(k) \sim k^{-3}$. However, it is obviously inappropriate for applying it mechanically to social networks for two reasons: first, the population is relatively constant, which does not conform with the hypothesis of unceasing increasing of nodes; second, individuals could not be present in all the lifetime of social networks, instead, the living individuals will die after a few years' survival.

Researchers had realized these problems not long after BA model was proposed [3–7]. Furthermore, the analysis of empirical data [8, 9] shows that some social networks exhibit single-scale properties for the degree distribution rather than power law regime. So González et al. [5] and Singer et al. [7] introduce constraints named "aging effect" to limit the addition of new links and the results indicate that these new observations are well fitted. However, there are still some problems with these models: (i) the empirical networks used in these models come from an in-school questionnaire among junior high school students from the USA (for acquaintance network, it comes from a questionnaire among 43 Utah Mormons), so are these social networks from specific groups universal and representative? Furthermore, could these models be used to explain the formation of large-scale social networks? (ii) Constraints introduced by these researches are more passive responses to the dilemma of continuous addition of new links, which could not lead to a deep understanding of the driving factors behind the addition of new links. We have developed a new agent-based model for large-scale friendship networks, which successfully reproduces acceptable properties of social networks such as small-world phenomenon and community structures [10, 11]. We also find that the resulting degree distribution of social networks displays obvious scale-free regime, indicating that the observed

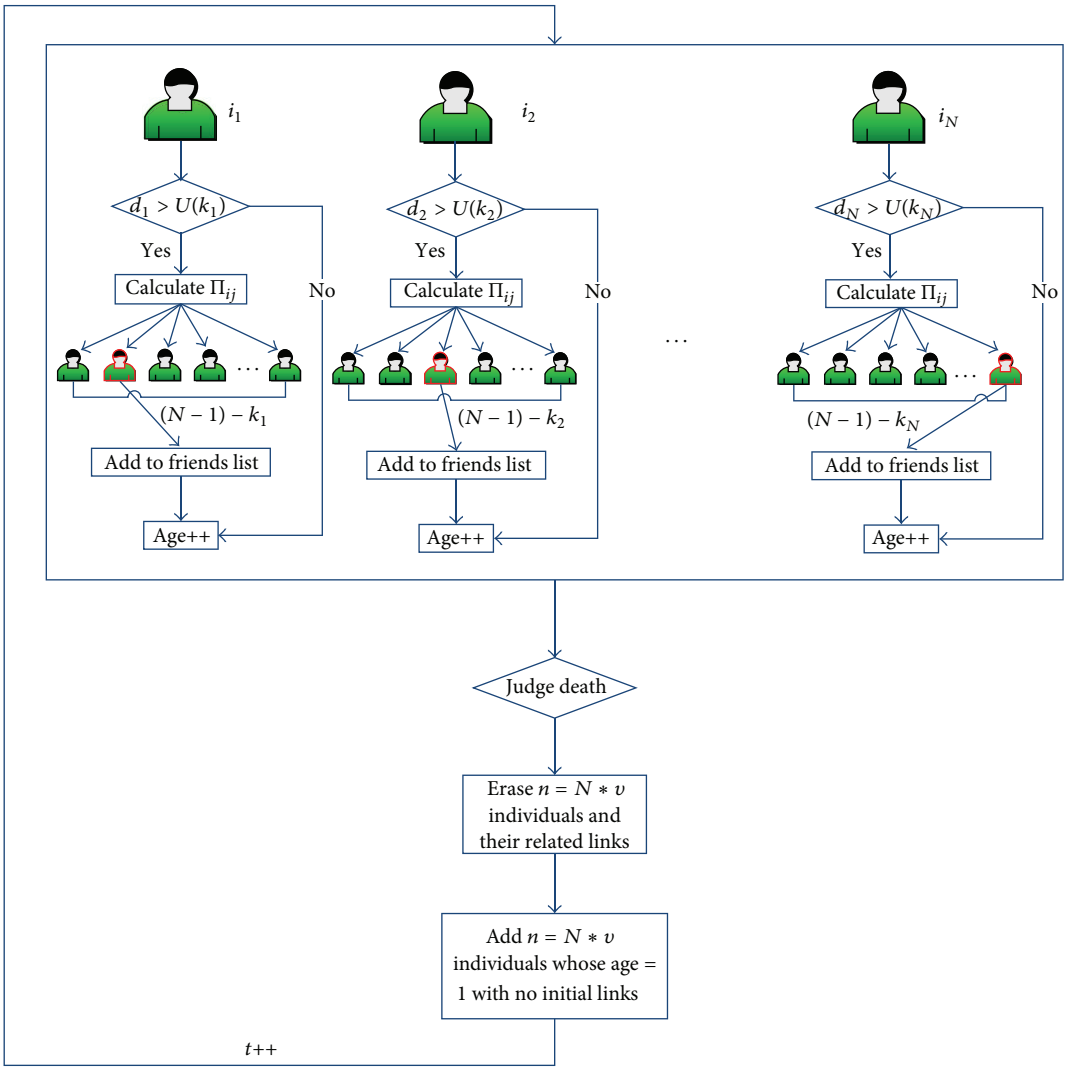

Figure 1: The model framework. At each time step t, every individual i will evaluate his satisfaction based on current friend circles. Here, we simply generate a random number d ranging from 0 to 1. If $d > U(k)$, individual i is not satisfied with current situation, and so he chooses a new friend j from those used to be strangers (the red individual) and adds j into his friends list. Meanwhile, j also adds i into his friends list. After all the individuals complete the decision-making processes independently, the network updates with $n = N * v$ aged individuals along with their links removed from the network and the same number of newborns with no initial links added into the network. Then time step t increases by 1.

single-scale properties of empirical networks are artifacts resulting from the boundedness of sampling. These findings give a clear answer to the questions above and confirm the drawbacks in the previous models.

2. Materials and Methods

There are two key features of real social networks neglected by foregoing researches: (i) the continuous turnover of the population—in real worlds, the aged die at a certain rate while new individuals are born at an appropriate rate resulting in an almost unchanged number of individuals present at the networks over time; (ii) on-going individuals' decision-making processes—the living individuals carry out social activities based on their current neighbors in the network including families, schoolmates, colleagues, and sometimes strangers and in the case of dissatisfaction with current circles of friends, they will try to build new relationships with some strangers. These ingredients are incorporated into our model framework. We also introduce an index named social activeness index, which is a comprehensive measurement about individual's activeness in social networks, denoted by λ. An active individual will be likely to make more friends. Integrated with the definition of natural attributes, we finally get an agent-base model in which individuals are characterized by a set of natural and social attributes, including identity number, age, residence, and social activeness index, along with behavioral rules.

At the beginning of the modeling, there are N individuals (agents) with no initial connections, who are randomly placed into an area of $x * y$ grids. This is close to the reality that the city is usually composed of a number of communities

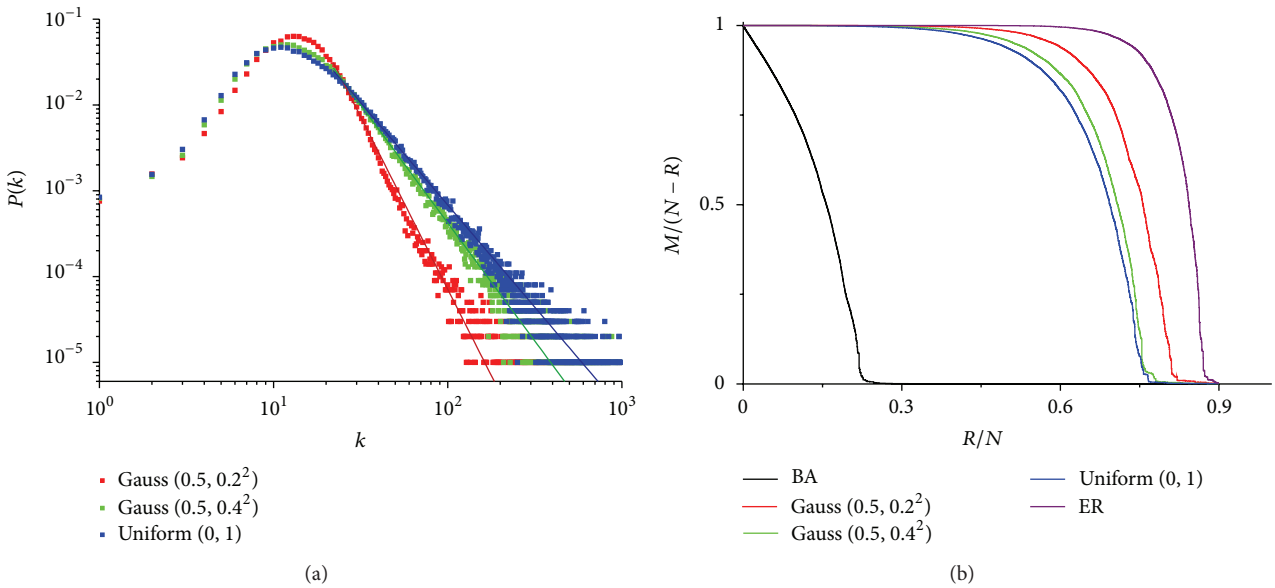

Figure 2: The resulting networks at $t = 2000$ for $N = 100000$, $\upsilon = 0.0005$, $\alpha = 0.2$, $\beta = 4$, $\gamma = 4$, and $p = 0.0001$ within an area of $10 * 10$ grids. (a) The distribution functions of connectivity: for red and green squares, $\rho(\lambda)$ is of truncated normal distribution Gauss (μ, σ^2); for blue squares, $\rho(\lambda)$ is of uniform distribution Uniform $(0, 1)$. The red, green, and blue lines have respectively slopes 4.02, 2.75, and 2.38. (b) The robustness of obtained networks: for red and green curves, $\rho(\lambda)$ is of truncated normal distribution Gauss (μ, σ^2). The red curve has $\zeta = 0.82$ while the green one has $\zeta = 0.76$; for blue curve, $\rho(\lambda)$ is of uniform distribution Uniform $(0, 1)$ and $\zeta = 0.74$; purple curve for ER, $\zeta = 0.92$, and black curve for BA, $\zeta = 0.16$.

and different individuals share the same community. For simplicity, we assume that the identity number of individuals increases from 0, so an elder individual will get a smaller identity number. Each individual's age is an integer selected randomly from 1 to max_age (max_age $= 1/\upsilon$, where υ is the death rate of the population). Social activeness index (λ) is an important parameter indicating individual's social activeness, which is assigned a value ranging from 0 to 1 generated from a specific distribution $\rho(\lambda)$ when an individual is born. Figure 1 illustrates our model framework. At each time step, every individual will evaluate the situation of his social contacts based on the current number of neighbors in the network (degree). Here, we introduce the utility function [12] which is widely used to quantify consumer's total satisfaction from consuming a good or service in economics because of the observed striking similarities among many collective human activities [13–17]. We employ an exponential utility function $U(k) = 1 - e^{-\lambda k}$, where k is individual's degree and λ is the social activeness index. So $U(k)$ decreases with the decreasing of λ, that is, the individual would be more dissatisfied with the current situation and more likely to make a new contact. Under the circumstance of dissatisfaction, individual i will make a new friend with j based on three criteria: age difference (a_{ij}), grid distance (d_{ij}), and the number of shared friends (m_{ij}). These criteria have been observed in many social networks and employed by some foregoing studies [3, 5, 11, 18], while never integrated into a single model. So the probability i making a new contact with j is given by

$$\prod_{ij} = \frac{R_{ij}}{\sum_{l \neq i} R_{il}}, \tag{1}$$

where

$$R_{ij} = \begin{cases} p \cdot e^{-(\beta a_{ij} + \gamma d_{ij})} & k_i = 0, \\ \left(\left(\dfrac{m_{ij}}{k_i} \right)^{\alpha} (1 - p) + p \right) \cdot e^{-(\beta a_{ij} + \gamma d_{ij})} & k_i \neq 0, \end{cases} \tag{2}$$

where k_i is the degree of i, α, β, γ are scale factors, and $p \ll 1$. Obviously, the effects of age difference and grid distance on social networks increase with the increasing of α and β, while γ does the opposite to m_{ij}/k_i. After every individual makes his decision independently, the network updates. We assume that the friendship is reciprocal, when i adds j into his friends list and so does j. Then a small number (n) of individuals are removed from the network along with the links with them and the same amount of individuals with no initial links is added, respectively, corresponding to individual's death and birth in real world. The number is determined by the death rate υ with $n = N * \upsilon$ (noticing that we assume that the population is relatively constant, so υ is also the birth rate).

3. Results and Discussion

In Figure 2(a), we show the degree distributions of truncated normal distribution $\rho(\lambda)$ with different μ and σ (the uniform distribution could be regarded as a limit form of truncated normal distribution with a large σ). Note that λ is the individual's social activeness index, so a normal distribution implies that most of individuals have similar social activeness, while only few of them are very active or inactive. With the increasing of σ, λ will be much more diverse. Our modeling suggests that the heavy tail will be more straightforward with

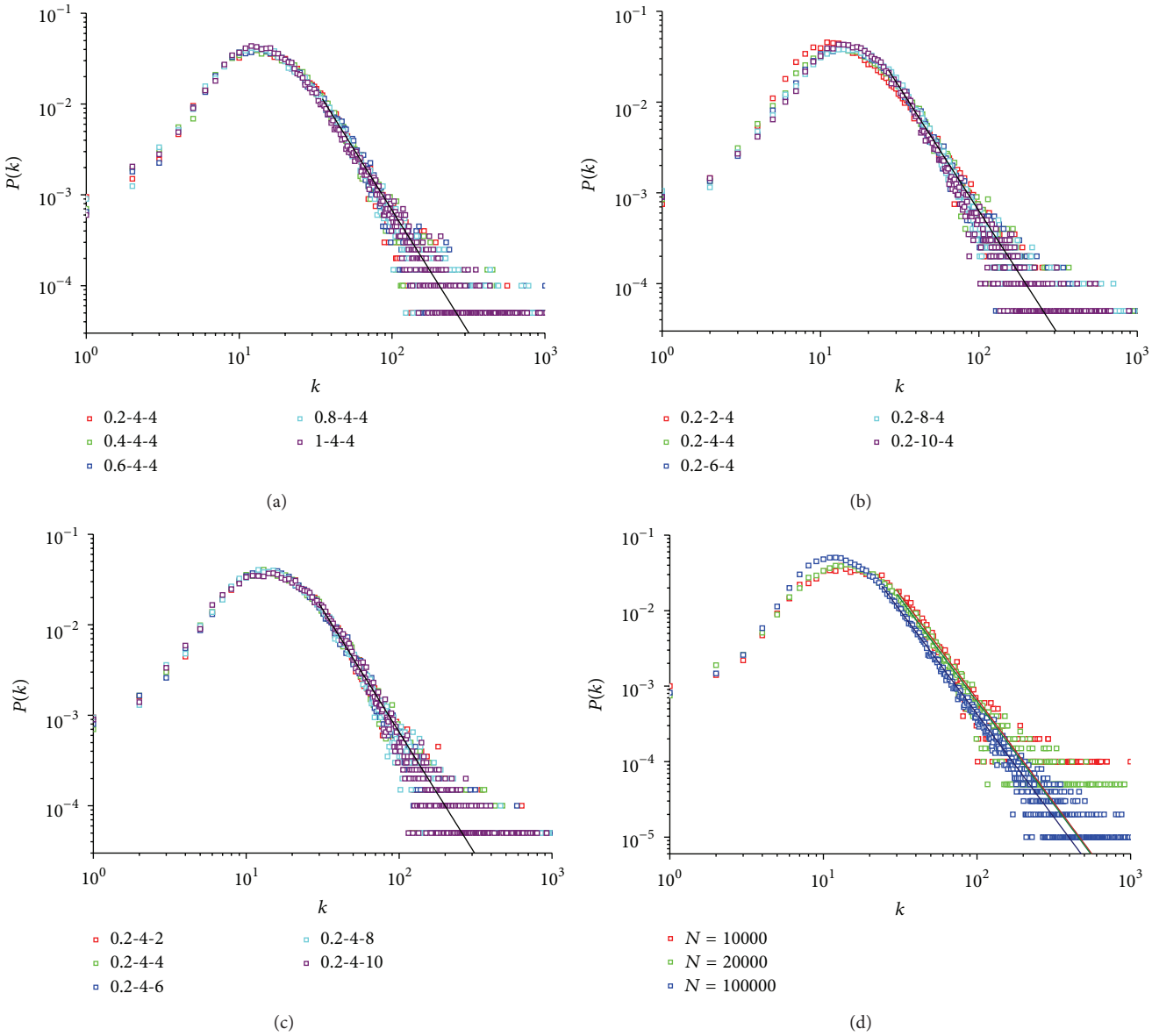

FIGURE 3: The sensitivity analysis. (a) $\rho(\lambda) = \text{Gauss}\ (0.5, 0.40^2)$ with different α. The black solid line has slope 2.69. (b) $\rho(\lambda) = \text{Gauss}\ (0.5, 0.40^2)$ with different β. The black solid line has slope 2.72. (c) $\rho(\lambda) = \text{Gauss}\ (0.5, 0.40^2)$ with different γ. The black solid line has slope 2.71. (d) $\rho(\lambda) = \text{Gauss}\ (0.5, 0.20^2)$. The black solid line has slope 4.01.

a decreasing of the scaling exponent. When coming to the uniform distribution, the scaling exponent is approximately equal to 2.38. Sensitivity analyses of N, α, β, and γ show that they do not significantly change the scaling exponent (see Figure 3).

When exploring various complex networks, we have a gut feeling that social networks are of strong robustness. It is easily accountable—individuals' death should not greatly shatter social networks, although they are hubs (people with a lot of links). So we compare the output of our model to some other networks, for example, random network from ER theory and scale-free network from BA model. As Figure 2(b) shows, the obtained network's robustness is between BA and ER. If we regard the BA network as a well-ordered network and correspondingly the ER network as a random network, the obtained networks will be between order and randomness, just as Watts [18] described. In order to make the contrast of different networks more clearly, we define a shatter index ζ as

$$\zeta = \frac{1}{N}\sum_{R=1}^{N}\frac{M}{(N-R)}, \tag{3}$$

where R denotes the number of nodes removed, and M is the nodes' number of the maximal connected subnetwork in the remained network after R nodes have been removed. Noticing that $\zeta = 1$ for a full connected network, the geometric meaning of ζ is actually the area enclosed by curves in Figure 2(b) and the coordinate axes.

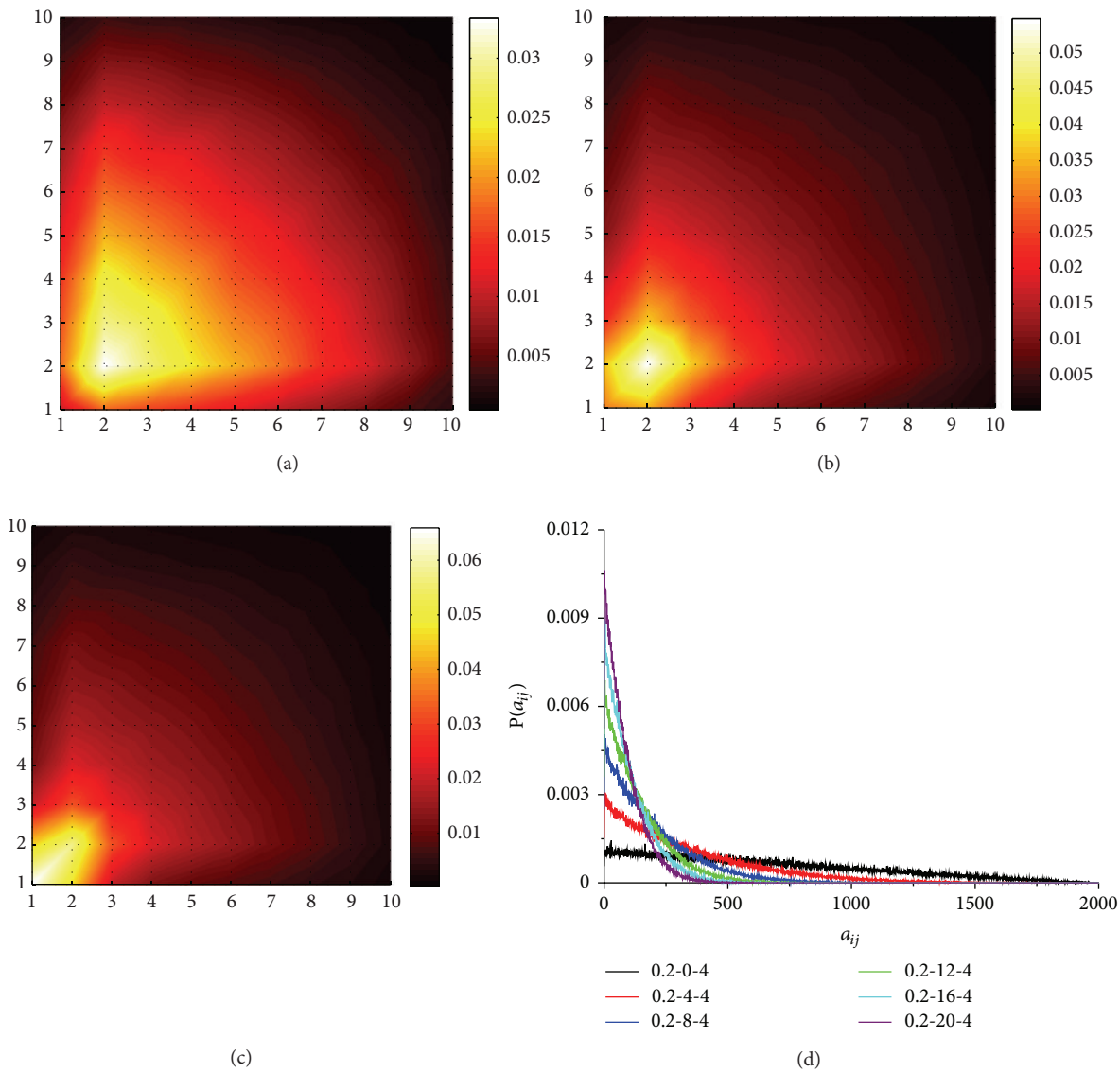

Figure 4: The grid distance and age difference between connected nodes at $t = 2000$ for $N = 20000$, $\upsilon = 0.0005$, and $p = 0.0001$ and $\rho(\lambda)$ is of truncated normal distribution with $\mu = 0.5$, $\sigma = 0.20$ within an area of $10 * 10$ grids. In (a), (b), and (c), the color denotes the proportion of node pairs with grid distance (x, y) in total nodes pairs. All of them use $\alpha = 0.2$ and $\beta = 4$, while $\gamma = 0$ for (a), 10 for (b), and 20 for (c). (d) The age difference between connected node pairs uses $\alpha = 0.2$, $\gamma = 4$, and different β (see the legend α-β-γ). The horizontal axis denotes age difference, while the vertical axis denotes the proportion of node pairs with age difference a_{ij} in total node pairs.

We also check the grid distance and age difference between friends in the networks. As Figures 4(a), 4(b), and 4(c) show, the regional structure will be more conspicuous with the increasing of γ. Figure 4(d) gives the analysis result of age difference between node pairs in obtained networks with different β. A significant positive correlation between the age effect and β emerges from the comparison of different curves.

The shortage of empirical large-scale social networks makes a straightforward verification of the obtained networks from comparison impossible. However, researches in related areas have provided some strong circumstantial evidences. In the past few years, the tight correlation between the spreading of infectious diseases and social networks has aroused widespread concerns. Eubank et al. [19] proposed a large-scale simulation framework based on realistic urban social networks. Though edges in their networks are defined as contacts between individuals, they also give a lot of valuable information about friendship networks because of the interplay between contact network and friendship network. Namely, close friends tend to make more contacts, while frequent contacts will lead to an intimate relationship. Their studies show that real networks are strongly connected small-world graphs with a well-defined scale for the degree

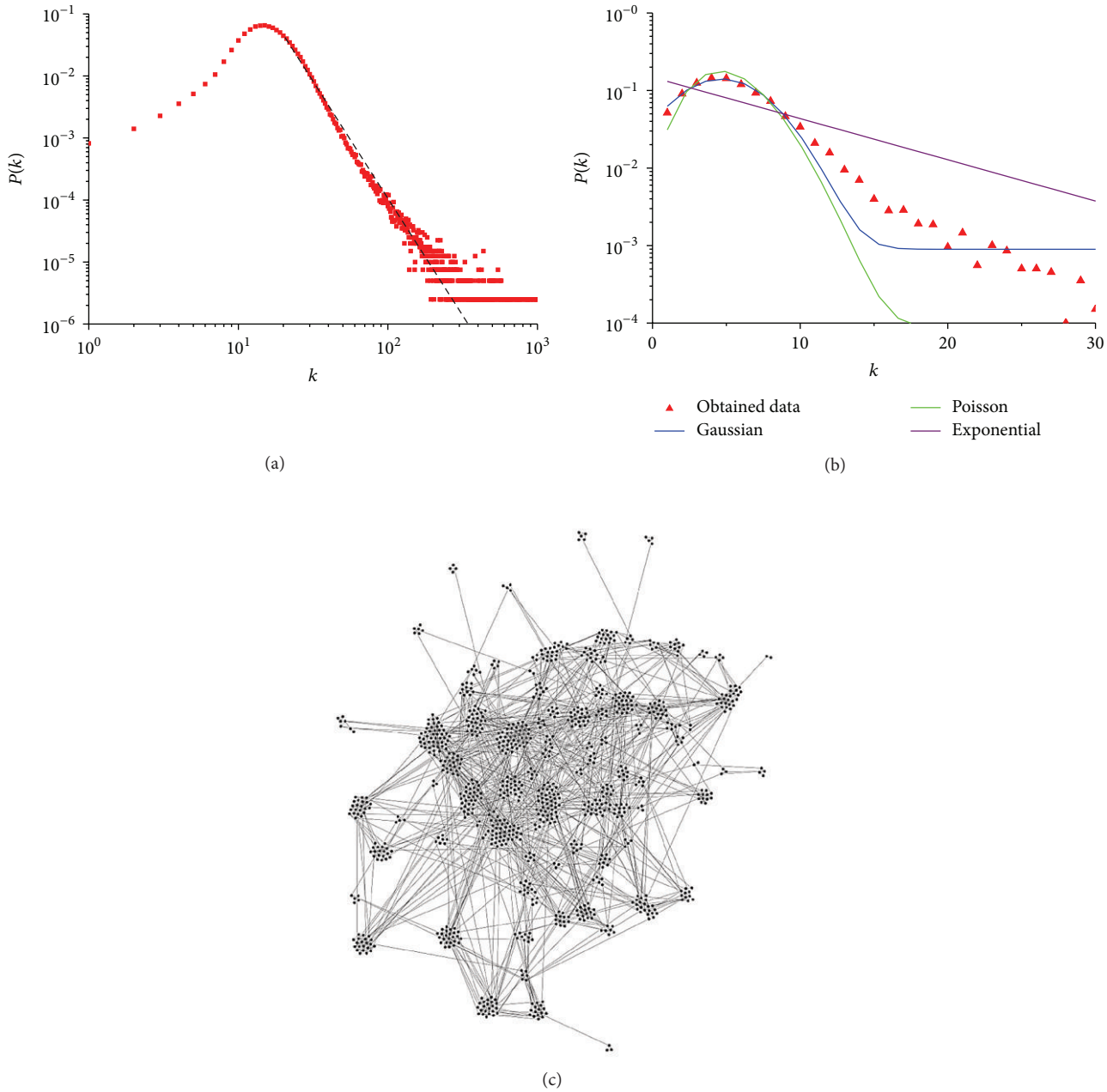

Figure 5: The in-school friendship networks at $t = 2000$ using $N = 20000$, $\upsilon = 0.0005$, $p = 0.0001$, $\mu = 0.5$, $\sigma = 0.20$, $\alpha = 0.8$, $\beta = 16$, and $\gamma = 2$ within an area of $10 * 10$ grids. The results have been averaged over 20 realizations. (a) The degree distribution of obtained full social networks. The dashed line has slope 4.02. (b) The degree distribution of sampled in-school friendship network. (c) A snapshot of the in-school friendship networks visualized with the Gephi software.

distribution and could not be shattered by removing a small number of high-degree vertices, which coincides with the obtained network of our model.

Next, we will show by sampling individuals from the obtained social networks and reconstructing their interconnections that our model successfully reproduces the observed single-scale properties in the in-school friendship networks. Owing to the obvious age effect in in-school friendship networks, we employ a large β, indicating that when individual makes a new friend, there is an obvious tendency to individuals from the same generation. After evolution over few time steps, we pick up a group of individuals of similar age as well as their interconnections. In this way, we get a subnetwork corresponding to in-school friendship network, as shown in Figure 5(c). It is visually apparent that the obtained in-school friendship network is composed of a number of different size communities. Figure 5(b) shows the connectivity distribution of in-school friendship network, a striking similarity between with them and the observations [5, 7, 20] could easily be detected; however, the degree

distribution of the full social network exhibits a visible heavy tail property (Figure 5(a)), indicating that the observed single-scale properties in empirical in-school friendship and acquaintance networks are more artifacts than universal phenomena, leading to an inability of foregoing models to describe social systems.

4. Conclusions

In this study, we have uncovered the structure and formation of social networks by capturing some important features of real world. This has significant potential in interpreting lots of social phenomena related to human activities. Further study will focus on the effects of social networks on individual's migration, which may help understand heterogeneity of human geographical distribution.

Conflict of Interest

The authors declare that they have no conflict of interests.

Acknowledgments

This study was funded by the Ministry of Science and Technology of China Grant 2013ZX10004605 and the National Natural Science Foundation of China (NSFC) Grant 90924019.

References

[1] P. Erdös and A. Rényi, *On the Evolution of Random Graphs*, Akad. Kiadó, 1960.

[2] A.-L. Barabási and R. Albert, "Emergence of scaling in random networks," *American Association for the Advancement of Science. Science*, vol. 286, no. 5439, pp. 509–512, 1999.

[3] L. A. N. Amaral, A. Scala, M. Barthélémy, and H. E. Stanley, "Classes of small-world networks," *Proceedings of the National Academy of Sciences*, vol. 97, no. 21, pp. 11149–11152, 2000.

[4] G. Caldarelli, A. Capocci, P. De Los Rios, and M. A. Muñoz, "Scale-free networks from varying vertex intrinsic fitness," *Physical Review Letters*, vol. 89, no. 25, Article ID 258702, 4 pages, 2002.

[5] M. C. González, P. G. Lind, and H. J. Herrmann, "System of mobile agents to model social networks," *Physical Review Letters*, vol. 96, no. 8, Article ID 88702, 4 pages, 2006.

[6] J. M. Kumpula, J. P. Onnela, J. Saramäki, K. Kaski, and J. Kertész, "Emergence of communities in weighted networks," *Physical Review Letters*, vol. 99, no. 22, Article ID 228701, 4 pages, 2007.

[7] H. M. Singer, I. Singer, and H. J. Herrmann, "Agent-based model for friendship in social networks," *Physical Review E*, vol. 80, no. 2, Article ID 026113, 5 pages, 2009.

[8] H. R. Bernard, P. D. Killworth, M. J. Evans, C. McCarty, and G. A. Shelley, "Studying social relations cross-culturally," *Ethnology*, vol. 27, no. 2, pp. 155–179, 1988.

[9] T. J. Fararo and M. H. Sunshine, *A Study of a Biased Friendship Net*, Youth Development Center, Syracuse University, 1964.

[10] G. Palla, I. Derényi, I. Farkas, and T. Vicsek, "Uncovering the overlapping community structure of complex networks in nature and society," *Nature*, vol. 435, no. 7043, pp. 814–818, 2005.

[11] G. Palla, A. L. Barabasi, and T. Vicsek, "Quantifying social group evolution," *Nature*, vol. 446, no. 7136, pp. 664–667, 2007.

[12] J. E. Ingersoll, *Theory of Financial Decision Making*, Rowman & Littlefield Pub Inc, 1987.

[13] P. W. Anderson, "Nonlinear dynamics, mathematical biology, and social science," *Complexity*, vol. 3, no. 2, pp. 50–51, 1997.

[14] T. Lux, M. Marchesi, and B. Universität, "Scaling and criticality in a stochastic multi-agent model of a financial market," *Nature*, vol. 397, no. 6719, pp. 498–500, 1999.

[15] X. Gabaix, P. Gopikrishnan, V. Plerou, and H. E. Stanley, "A theory of power-law distributions in financial market fluctuations," *Nature*, vol. 423, no. 6937, pp. 267–270, 2003.

[16] A. L. Barabasi, "The origin of bursts and heavy tails in human dynamics," *Nature*, vol. 435, no. 7039, pp. 207–211, 2005.

[17] J. C. Bohorquez, S. Gourley, A. R. Dixon, M. Spagat, and N. F. Johnson, "Common ecology quantifies human insurgency," *Nature*, vol. 462, no. 7275, pp. 911–914, 2009.

[18] D. J. Watts, *Small Worlds: The Dynamics of Networks between Order and Randomness*, Princeton University Press, 1999.

[19] S. Eubank, H. Guclu, V. S. Kumar et al., "Modelling disease outbreaks in realistic urban social networks," *Nature*, vol. 429, no. 6988, pp. 180–184, 2004.

[20] K. M. Harris and J. R. Udry, *National Longitudinal Study of Adolescent Health (Add Health), 1994–2008*, Inter-University Consortium for Political and Social Research (ICPSR), 2012.

Hindawi Publishing Corporation
Mathematical Problems in Engineering
Volume 2013, Article ID 248153, 7 pages
http://dx.doi.org/10.1155/2013/248153

Research Article

Delayed Antiwindup Control Using a Decoupling Structure

Huawei Zhu,[1] Guozheng Qin,[1] Yingxin Yan,[2] Zhichao Jiang,[2] and Zhisheng Duan[1]

[1] *State Key Lab for Turbulence and Complex Systems, Department of Mechanics and Aerospace Engineering, College of Engineering, Peking University, Beijing 100871, China*
[2] *Beijing Institute of Near-Space Vehicle's System Engineering, Beijing 100076, China*

Correspondence should be addressed to Zhisheng Duan; duanzs@pku.edu.cn

Received 28 March 2013; Accepted 29 April 2013

Academic Editor: Guanghui Wen

This paper investigates the antiwindup (AW) control problem for plants with input saturation. The AW compensator is not activated as soon as input saturation occurs as usual. A delayed decoupling structure is first proposed. Then, appropriate linear matrix inequalities (LMIs) are developed to determine a plant-order AW compensator. Effectiveness of the presented AW technique is illustrated by a fighter aircraft model.

1. Introduction

Input saturation is one of the most frequently encountered nonlinearities in control design for linear plants. Most controllers are designed assuming that the inputs have no limits. If input saturation appears, output performance often deteriorates. Slight performance degradation could be large overshoot or sluggish response. Severe performance deterioration could be persistent oscillation, sometimes even instability.

Multiagent control has become a hot topic of academic research in recent years. This is because it can be used in various fields, such as physics, biology, industry, and military applications. The two main applications of multiagent control in industry and military are the multirobot cooperative control and the multivehicle flight control, respectively. Although these two applications have been intensively studied, however, few results consider the case when actuators are limited [1]. The well-known AW control is one of the most successful methodologies applied in practice to deal with plants with input saturation. As summed in [2, 3], the essential idea of AW control is adding control modification to a nominal linear controller. The nominal linear controller is first synthesized for the plant ignoring saturation, and then an AW compensator is designed to improve output performance when saturation occurs. Sufficient conditions to design a static AW compensator were provided in [4] in terms of LMIs. Necessary and sufficient conditions for the existence of a plant-order AW compensator were given in [5]. A novel, less conservative sector condition was presented in [6], and a static AW compensator for both stable and unstable plants was obtained therein. A switching AW design using multiple Lyapunov functions was proposed in [7]. In [4, 5], attention was focused on minimizing the influence of a generic disturbance signal w in the output. In [6, 7], concern was on maximization of the region of attraction. Innovatively in [8], Weston and Postlethwaite proposed a structure, which established a specific formulation of the error between the plant outputs with and without input saturation. Then, in [9], two different AW compensators were designed to make the error as small as possible based on the structure.

Usually, the AW compensator was activated as soon as input saturation occurs. However, a static AW compensator designed in [10] was not activated immediately but belatedly. It was found in [10] that delayed activation of AW compensator can lead to a better performance compared with the immediate one. In order to improve AW control performance and derive a simpler LMI condition for the AW compensator construction, motivated by the structure proposed in [8], a modified delayed decoupling structure is developed in this paper. Then, sufficient conditions in terms of LMIs are obtained to minimize the error between the plant outputs with and without input saturation.

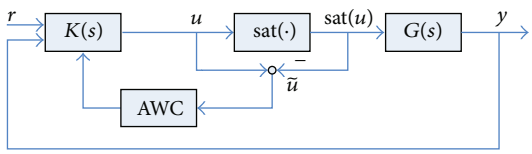

Figure 1: General structure of AW control.

The remainder of this paper is organized as follows. In Section 2, the structure, which has a decoupling feature, is introduced. Main results of this paper are presented in Section 3. A new modified delayed AW decoupling structure is first proposed. And the AW compensator is constructed for single-input plants by making a set of LMIs feasible. It is also extended to multi-input plants. A fighter craft model is used to illustrate the proposed AW technique. Conclusions are given in Section 4.

2. A Decoupling Structure

A general AW control structure is shown in Figure 1, where $G(s)$ is the plant, $K(s)$ is the nominal linear controller, $\mathrm{sat}(\cdot)$ is the input saturation function, and block AWC is the AW compensator. $G(s)$ is a stable linear plant subject to input saturation as

$$G(s) \sim \begin{cases} \dot{x}_p = A_p x_p + B_p \,\mathrm{sat}(u), \\ y = C_p x_p + D_p \,\mathrm{sat}(u), \end{cases} \tag{1}$$

where (A_p, B_p) is stabilizable, $x_p \in \mathbb{R}^n$, $y \in \mathbb{R}^q$, $u \in \mathbb{R}^p$, and $\mathrm{sat}(u)$ is the saturated input. The saturation function $\mathrm{sat}(\cdot)$ satisfies $\mathrm{sat}(u) = [\mathrm{sat}(u_1), \mathrm{sat}(u_2), \ldots, \mathrm{sat}(u_p)]^T$, $\mathrm{sat}(u_i) = \mathrm{sign}(u_i)\min(|u_i|, \overline{u}_i)$. $\overline{u}_i$ is the amplitude limit, $\overline{u}_i > 0$, $i = 1, 2, \ldots, p$. The state-space descriptions of $K(s)$ and AW compensator are, respectively

$$\begin{aligned} K(s) &\sim \begin{cases} \dot{x}_c = A_c x_c + B_c e, \\ u = C_c x_c + D_c e, \end{cases} \\ \mathrm{AWC} &\sim \begin{cases} \dot{x}_{\mathrm{aw}} = A_{\mathrm{aw}} x_{\mathrm{aw}} + B_{\mathrm{aw}} \tilde{u}, \\ \eta = \left(\eta_1^T, \eta_2^T\right)^T = C_{\mathrm{aw}} x_{\mathrm{aw}} + D_{\mathrm{aw}} \tilde{u}, \end{cases} \end{aligned} \tag{2}$$

where $\tilde{u} := u - \mathrm{sat}(u)$ is the error between the unsaturated input and saturated input, $e := r - y$ is the tracking error, and r is the reference to be tracked. The AW compensator is activated only when input saturation occurs. As mentioned earlier, the essential idea of AW control is adding control modification to $K(s)$. The state and output equations of $K(s)$ are modified by the AWC's output $\eta = (\eta_1^T, \eta_2^T)^T$ as

$$\begin{aligned} \dot{x}_c &= A_c x_c + B_c e + \eta_1, \\ u &= C_c x_c + D_c e + \eta_2. \end{aligned} \tag{3}$$

An appealing AW structure, which is a special case of the general structure, proposed by Weston and Postlethwaite in [8], is shown in Figure 2(a), where the design of AW compensator turns into the conditioning of a transfer function $M(s)$. With all signals labeled the same, the structure in Figure 2(a) can be equivalently redrawn as in Figure 2(b). Note that in Figure 2(b), a dead-zone function $dz(\cdot)$ is introduced, which maps the unsaturated input u to the input error $\tilde{u}$; that is, $dz(u) = \tilde{u}$. If $u \in \mathcal{U}$, where $\mathcal{U} \in \mathbb{R}^p$ is a compact set defined as $\mathcal{U} = [-\overline{u}_1, \overline{u}_1] \times [-\overline{u}_2, \overline{u}_2] \times \cdots \times [-\overline{u}_p, \overline{u}_p]$, then $dz(u) = 0$. What is fascinating about the structure in Figure 2(b) is that it can be seen as two decoupled subsystems: the nominal linear closed-loop system (NLCS) and the nonlinear path. If NLCS and the nonlinear path are stable, respectively, the stability of the overall system in Figure 2(b) follows. The NLCS is stable, as it is guaranteed by $K(s)$. The NLCS's output y_{lin} is what one tries to recover when input saturation occurs. Thus, the AW compensator should be designed to ensure stability of the nonlinear path, further on, if possible, to make the output difference $y_d = y_{\mathrm{lin}} - y$ as small as possible.

One selection for $M(s)$ in Figure 2(a) is a right coprime factor of $G(s)$; that is, $G(s) = N(s)M^{-1}(s)$. The state space descriptions of $M(s)$ and $N(s)$ can be chosen as

$$\begin{pmatrix} M(s) \\ N(s) \end{pmatrix} \sim \left[\begin{array}{c|c} A_p + B_p F & B_p \\ \hline F & I \\ C_p + D_p F & D_p \end{array}\right]. \tag{4}$$

The conditioning with $M(s)$ turns into the design of matrix F. $G(s)M(s) = N(s)$, and the state space description of AW compensator is

$$\begin{aligned} \dot{x}_{\mathrm{aw}} &= \left(A_p + B_p F\right) x_{\mathrm{aw}} + B_p \tilde{u}, \\ u_d &= F x_{\mathrm{aw}}, \\ y_d &= \left(C_p + D_p F\right) x_{\mathrm{aw}} + D_p \tilde{u}. \end{aligned} \tag{5}$$

Remark 1. Note that all the initial states and the control inputs of $M(s)$ and $N(s)$ are equal. Therefore the states of $M(s)$ and $N(s)$ are identical. Under this circumstance, although $M(s)$ and $N(s)$ are different transfer functions, they can still share the same state x_{aw}.

Define the distance between a vector x and a compact set $\mathcal{S}$ as $\mathrm{dist}(x, \mathcal{S}) := \inf_{y \in \mathcal{S}} \|x - y\|$. Then, the objective of this paper, which is based on the decoupling AW structure proposed in [8], is to solve the AW control problem defined as follows.

Definition 2 (see [9]). The AW compensator (5) is said to solve the AW control problem for plant (1) if the closed-loop system in Figure 2(a) is well posed and the following conditions hold.

(1) If $\mathrm{dist}(u_{\mathrm{lin}}, \mathcal{U}) = 0$ for all $t \geq 0$, then $y_d = 0$ for all $t \geq 0$ (assuming zero initial condition for AW compensator).

(2) If $\mathrm{dist}(u_{\mathrm{lin}}, \mathcal{U}) \in \mathcal{L}_2$, then $y_d \in \mathcal{L}_2$.

The AW compensator (5) is said to solve the strong AW control problem if in addition, the following condition is satisfied.

(3) The operator $\tau : u_{\mathrm{lin}} \mapsto y_d$ is well defined and the $\mathcal{L}_2$ gain from u_{lin} to y_d is less than γ; namely, $\|y_d\|_2 < \gamma \|u_{\mathrm{lin}}\|_2$.

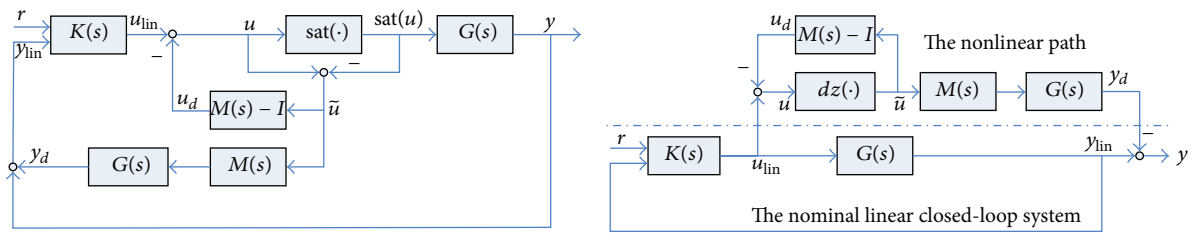

(a) Conditioning with $M(s)$

(b) An equivalent decoupling structure

Figure 2: A decoupling structure.

Remark 3. Note that condition 3 in Definition 2 implies condition 2. In this paper, only the strong AW control problem is considered.

3. Main Results

Immediate AW compensation may increase safety of the overall system, being away from instability, for example, but the performance may be no better than leaving the controller uncompensated during some moderate input saturation, as the numerical example demonstrated in [10]. If the nominal controller is robust, the system still demonstrates good performance during this modest saturation stage. Thus, the delayed activation of AW compensation is considered.

3.1. Delayed Decoupling AW Structure. To realize certain delay in activating the AW compensator, an artificial saturation function is added after the controller, and thus the structure in Figure 2(a) becomes as in Figure 3. This structure has two saturation nonlinearities, and thus it is not equivalent to the decoupling structure in Figure 2(b). In order to sustain a decoupling feature, Figure 3 needs to be modified. A new decoupling structure with delayed saturation is therefore presented in Figure 4(a). Note that a time-varying gain $G_d = \mathrm{diag}[g_1(t), g_2(t), \ldots, g_p(t)]$ is introduced in Figure 4(a), where $g_i(t)$ is defined as

$$g_i(t) = \begin{cases} 1, & |u_i| \le \bar{u}_i, \\ \dfrac{\mathrm{sgn}(u_i)\,\bar{u}_i}{u_i}, & \bar{u}_i < |\bar{u}_i| < \dfrac{\bar{u}_i}{g_d}, \\ g_d, & |u_i| \ge \dfrac{\bar{u}_i}{g_d}. \end{cases} \tag{6}$$

Here g_d is the delayed saturation index, $0 < g_d < 1$. The AW compensator is activated when the input magnitude is higher than the delayed saturation level $\bar{u}_i/g_d$, rather than $\bar{u}_i$. Now treat $\widehat{G}(s) := G(s)G_d$ as a new plant, which is linear parameter-varying (LPV). The time varying matrix gain G_d is continuous in the known bounds, $G_d \in [g_d, 1]$. Since the expressions for u, y, $\tilde{u}$ are the same in Figures 4(a) and 4(b), the two figures are mathematically equivalent if the following equation holds:

$$\widehat{G}u_{\mathrm{lin}} = \widehat{N}\tilde{u} + \widehat{G}\left(u_{\mathrm{lin}} - \widehat{M}\tilde{u}\right). \tag{7}$$

Taking the same steps as in [11], where the decoupling AW structure is extended to LPV system, the equivalence between

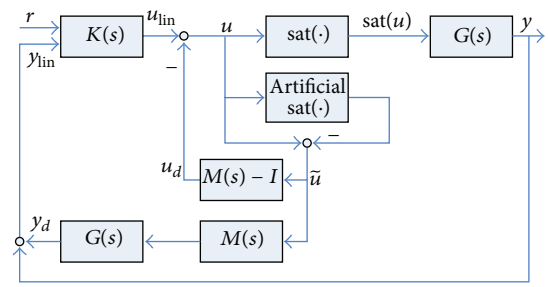

Figure 3: Conditioning with $M(s)$ (delayed).

Figures 4(a) and 4(b) follows. Note that in the nonlinear path, $\widehat{G}(s)$ replaces the original $G(s)$. Therefore, the state space description of the AW compensator becomes

$$\begin{aligned} \dot{x}_{\mathrm{aw}} &= \left(A_p + B_p G_d F\right) x_{\mathrm{aw}} + B_p G_d \tilde{u}, \\ u_d &= F x_{\mathrm{aw}}, \\ y_d &= \left(C_p + D_p G_d F\right) x_{\mathrm{aw}} + D_p G_d \tilde{u}. \end{aligned} \tag{8}$$

3.2. Delayed AW Synthesis Using LMI. In order to analyze the behavior of the new system, for intuitiveness, single-input ($p = 1$) plants are considered first. And one has the following theorem.

Theorem 4. *For a single-input saturated plant, the strong AW control problem in Definition 2 is solved if there exist a symmetric positive definite matrix $Q \in \mathbb{R}^{n\times n}$, a diagonal positive definite matrix $S \in \mathbb{R}^{1\times 1}$, a matrix $R \in \mathbb{R}^{1\times n}$, and a positive real scalar γ such that*

$$\begin{pmatrix} A_pQ + QA_p^T + B_pG_dR + R^TG_dB_p^T & * & * \\ 0 & -\gamma I & * \\ C_pQ + D_pG_dR & 0 & -\gamma I \end{pmatrix} < 0 \tag{9}$$

for $G_d = 1$ and

$$\begin{pmatrix} A_pQ + QA_p^T + B_pG_dR + R^TG_dB_p^T & * & * & * \\ 0 & -\gamma I & * & * \\ C_pQ + D_pG_dR & 0 & -\gamma I & * \\ SG_dB_p^T - R & I & \left(D_pG_dS\right)^T & -2S \end{pmatrix} < 0 \tag{10}$$

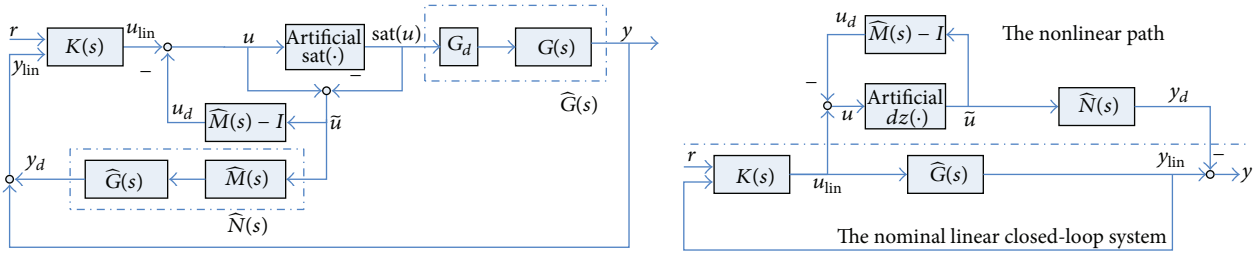

(a) Conditioning with $M(s)$ (modified)

(b) The equivalent decoupling structure (modified)

Figure 4: The delayed decoupling structure.

for $G_d = g_d$. Furthermore, the designing matrix F for AW compensator (8) to guarantee $\mathscr{L}_2$ performance requirement $\|y_d\|_2 < \gamma\|u_{\text{lin}}\|_2$ is given by $F = RQ^{-1}$.

Proof. The operation of the saturated plant with delayed activation of AW compensator can be separated into two stages.

Stage 1 ($|u| \le \bar{u}/g_d$). The input is below the artificial saturation level. The input to AW compensator is zero, namely, $\tilde{u} = 0$, and $G_d \in [g_d, 1]$. Then, following the standard approach, if inequality

$$\dot{V} + \gamma^{-1} y_d^T y_d - \gamma u_{\text{lin}}^T u_{\text{lin}} < 0 \tag{11}$$

holds, it gives $\|y_d\|_2 < \gamma\|u_{\text{lin}}\|_2$, and the strong AW control problem is solved. Choose the Lyapunov function in (11) as $V = x_{\text{aw}}^T P x_{\text{aw}}$ where $P = P^T > 0$, and substitute (8) into inequality (11); one has

$$\begin{aligned}&\left[\left(A_p + B_p G_d F\right) x_{\text{aw}}\right]^T P x_{\text{aw}} + x_{\text{aw}}^T P \left[\left(A_p + B_p G_d F\right) x_{\text{aw}}\right] \\ &\quad + \gamma^{-1}\left[\left(C_p + D_p G_d F\right) x_{\text{aw}}\right]^T \left[\left(C_p + D_p G_d F\right) x_{\text{aw}}\right] \\ &\quad - \gamma u_{\text{lin}}^T u_{\text{lin}} < 0.\end{aligned} \tag{12}$$

Then, by Schur complement and congruency transformation, inequality (12) becomes LMI (9) in Theorem 4 with $Q = P^{-1}$, $R = FQ$; thus, $F = RQ^{-1}$. Because $G_d \in [g_d, 1]$ at Stage 1, it suffices to check LMI (9) for G_d at the vertices, namely for $G_d = g_d$ and $G_d = 1$. The stability of the nonlinear path is thus ensured. Note that during this stage, the "nominal" closed-loop system is linear time-varying as shown in Figure 4(b). Leaving the nominal controller $K(s)$ undisturbed when $|u| \in (\bar{u}, \bar{u}/g_d]$, the stability of new NCLS is preserved by the robustness of controller $K(s)$. With the two subsystems being stable, the stability of the overall closed-loop system at Stage 1 follows.

Stage 2 ($|u| > \bar{u}/g_d$). During this stage, the controller's output exceeds the delayed saturation level $\bar{u}/g_d$. As a result, $\tilde{u}$ is nonzero, the AW compensator is activated, and $G_d = g_d$. Due to $\tilde{u}^T u \ge \tilde{u}^T \tilde{u}$, the sector condition $2\tilde{u}^T W(u - \tilde{u}) \ge 0$ always holds, where W is a diagonal positive definite matrix. Then, a sufficient condition for inequality (11) is

$$\dot{V} + \gamma^{-1} y_d^T y_d - \gamma u_{\text{lin}}^T u_{\text{lin}} + 2\tilde{u}^T W (u - \tilde{u}) < 0. \tag{13}$$

Then, following the similar steps as [9], if inequality (13) holds, the strong AW control problem is solved. Substitute (8) into inequality (13); one has

$$\begin{aligned}&\left[\left(A_p + B_p G_d F\right) x_{\text{aw}} + B_p G_d \tilde{u}\right]^T P x_{\text{aw}} \\ &\quad + x_{\text{aw}}^T P \left[\left(A_p + B_p G_d F\right) x_{\text{aw}} + B_p G_d \tilde{u}\right] \\ &\quad + \gamma^{-1}\left[\left(C_p + D_p G_d F\right) x_{\text{aw}} + D_p G_d \tilde{u}\right]^T \\ &\quad \times \left[\left(C_p + D_p G_d F\right) x_{\text{aw}} + D_p G_d \tilde{u}\right] \\ &\quad - \gamma u_{\text{lin}}^T u_{\text{lin}} + 2\tilde{u}^T W \left(u_{\text{lin}} - F x_{\text{aw}} - \tilde{u}\right) < 0.\end{aligned} \tag{14}$$

Inequality (14) can be rewritten as

$$\begin{pmatrix} x_{\text{aw}}^T & \tilde{u}^T & u_{\text{lin}}^T \end{pmatrix} \left[X - Y^T(-\gamma)^{-1} Y\right] \begin{pmatrix} x_{\text{aw}} \\ \tilde{u} \\ u_{\text{lin}} \end{pmatrix} < 0, \tag{15}$$

where

$$X = \begin{pmatrix} \left(A_p + B_p G_d F\right)^T P + P\left(A_p + B_p G_d F\right) & * & * \\ B_p^T G_d P - WF & -2W & * \\ 0 & W & -\gamma I \end{pmatrix},$$
$$Y = \begin{pmatrix} C_p + D_p G_d F & D_p G_d & 0 \end{pmatrix}. \tag{16}$$

According to the standard Schur complement and exerting congruency transformation, one has LMI (10) with $Q = P^{-1}$, $S = W^{-1}$, $R = FQ$; thus, $F = RQ^{-1}$. Similar to Stage 1, with the two subsystems being stable, the stability of the overall closed-loop system at Stage 2 follows.

Note that LMI (10) for $G_d = g_d$ implies that LMI (9) for $G_d = g_d$, thus only $G_d = 1$ is checked for LMI (9) in the theorem. And this completes the proof. □

The section of the delayed saturation index g_d can be determined by an iterative algorithm, starting at an initial

value and stopping at a point when the $\mathscr{L}_2$ gain γ is optimized. By applying the AW compensator designed using Theorem 4, the nominal linear performance is recovered as much as possible. The static and dynamic AW compensators designed in [10, 12] used the states $x = (x_p^T, x_c^T)^T$ and $x = (x_p^T, x_c^T, x_{\text{aw}}^T)^T$ respectively, in the Lyapunov function for LMI derivation. In this paper, only x_{aw} is used, and thus the LMIs to be solved here are much simpler than the resulting LMIs in [10, 12].

For a multi-input plant, G_d is no longer a scalar, but a $p \times p$ diagonal matrix. Because each diagonal element of G_d varies between g_d and 1, thus G_d can be expressed as a linear combination of the vertices as follows:

$$G_d = \sum_{j=1}^{2^p} \alpha_j G_d^j, \qquad \sum_{j=1}^{2^p} \alpha_j = 1, \tag{17}$$
$$\alpha_j \in [0,1], \; G_d^j \in \mathscr{G}, \; j = 1, 2, \ldots, 2^p,$$

where $\mathscr{G} = \{\text{diag}[g_1, g_2, \ldots, g_p] : g_i = g_d \text{ or } 1, \; i = 1, 2, \ldots, p\}$. Let $G_d^1 = \text{diag}[1, 1, \ldots, 1]$; similarly, one has the following theorem.

Theorem 5. *For a multi-input saturated plant, the strong AW control problem in Definition 2 is solved if there exist a symmetric positive definite matrix $Q \in \mathbb{R}^{n\times n}$, a diagonal positive definite matrix $S \in \mathbb{R}^{p\times p}$, a matrix $R \in \mathbb{R}^{p\times n}$, and a positive real scalar γ such that LMI (9) holds for $G_d = G_d^1$ and*

$$\begin{pmatrix} A_pQ + QA_p^T + B_pG_d^jR + R^TG_d^jB_p^T & * & * & * \\ 0 & -\gamma I & * & * \\ C_pQ + D_pG_d^jR & 0 & -\gamma I & * \\ SG_d^jB_p^T - R & I & \left(D_pG_d^jS\right)^T & -2S \end{pmatrix} < 0 \tag{18}$$

for all $j = 2, 3, \ldots, 2^p$. Furthermore, the designing matrix F for AW compensator (8) to guarantee $\mathscr{L}_2$ performance requirement $\|y_d\|_2 < \gamma\|u_{\text{lin}}\|_2$ is given by $F = RQ^{-1}$.

Proof. The proof follows the same steps as Theorem 4, and thus it is omitted here. □

3.3. Application Example. Consider a linearized fighter aircraft model (matrices A_p, B_p, and C_p can be found from equations (A.2)–(A.4) in Yee et al. [13]). The aircraft has six states (u, v, w, p, q, r). The first three states are airspeed in the X-, Y-, and Z-axes of the body frame, respectively. The last three states are roll, pitch, and yaw rates about X-, Y-, and Z-axes. The outputs $(\dot{\mu}\alpha\beta)$ are, respectively, stability-axis roll rate, angle-of-attack, and sideslip angle. The inputs (δ_h, δ_a, δ_r) are elevator, aileron, and rudder deflection angles, with control surface constraints $-25^\circ \le \delta_h \le 25^\circ$, $-20^\circ \le \delta_a \le 20^\circ$, and $-30^\circ \le \delta_r \le 30^\circ$. The reference to be tracked is shown in Figure 5.

Without consideration of input saturation, the aircraft demonstrates precise and fast tracking response, as shown in Figure 6(a), using a continuous-time robust $\mathscr{H}_\infty$ controller designed in [13] (matrices A_c, B_c, C_c, and D_c are obtained

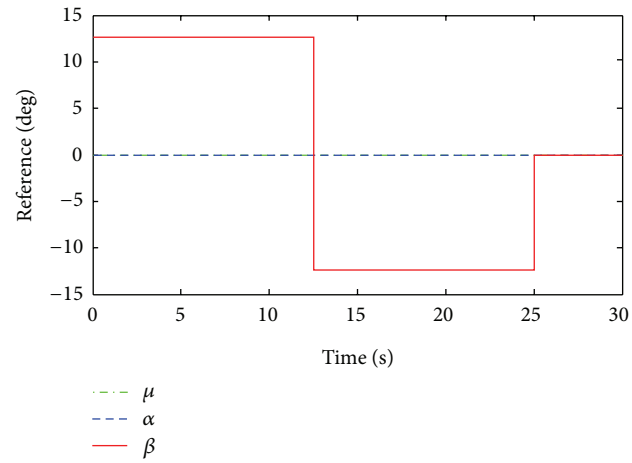

Figure 5: Reference.

by using the robust control toolbox). But the control inputs δ_a and δ_r actually exceed their amplitude limits as Figure 6(b) displays. Imposing amplitude limits at the aircraft's inputs in the simulation, the tracking performance deteriorates, as shown in Figure 7(a). Thus, AW compensation should be considered. Using Theorem 5 and taking the delayed saturation index $g_d = 0.65$, the designing matrix is

$$F = \begin{pmatrix} -1.6399 & 0.0327 & 0.6927 & -0.2444 & 241 & 3.8841 \\ 0.0219 & -0.2281 & 0.0013 & 45.841 & 0.0003 & 38.787 \\ 0.0155 & -0.2099 & 0.0010 & -10.303 & 0.1976 & 174.09 \end{pmatrix}, \tag{19}$$

and the obtained optimal $\mathscr{L}_2$ gain is $\gamma = 5.7294$. The corresponding tracking performance is shown in Figure 8(a). The AW compensator designed in [14] which is based on immediate activation is further presented here for comparison. Solving LMI (13) in [14], the designing matrix is

$$F = \begin{pmatrix} -731.13 & 16.222 & 425.51 & -106.50 & 98175 & 1634.7 \\ 31.960 & -329.78 & 2.4337 & 54547 & -76.769 & 59246 \\ 11.554 & -123.60 & 1.0543 & -5903.4 & 79.153 & 10750 \end{pmatrix}, \tag{20}$$

and the optimal $\mathscr{L}_2$ gain is $\gamma = 5.7298$. The corresponding tracking performance is shown in Figure 7(b). Our method is also compared with the delayed AW compensator proposed in [10]. Using the method of [10], the tracking performance is shown in Figure 8(b).

Comparing the tracking performance in Figure 8(a) with the uncompensated one as in Figure 7(a), fluctuation in μ channel decreases significantly in Figure 8(a). The AW compensator plays its role. From Figures 8(a) and 7(b) which are based on the immediate AW compensation, the output dynamic property in Figure 8(a) is preferable. This is because modest saturation can be seen as a small amount of plant uncertainty, and since the nominal controller is robust, the system still demonstrates good performance during this modest saturation stage. Immediate AW compensation may destroy this equilibrium. From Figures 8(a) and 8(b) with the static delayed AW compensator, the output performance in Figure 8(a) is no worse. This is because the AW compensator

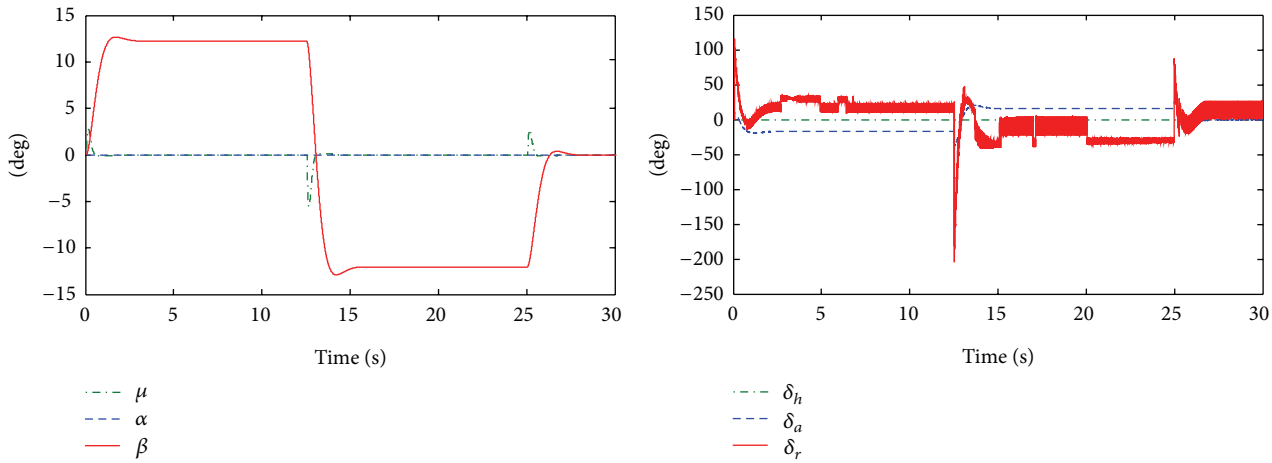

(a) Output response (b) Control inputs

Figure 6: Linear tracking response with pulse reference in β (no saturation).

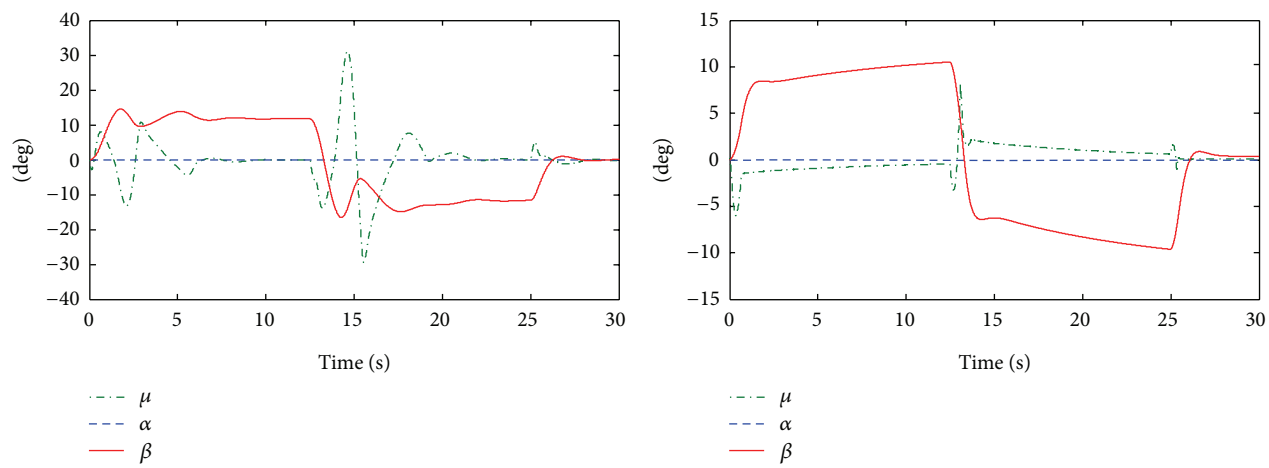

(a) Without AW compensator (b) With AW compensator

Figure 7: Saturated tracking response with pulse reference in β (with saturation).

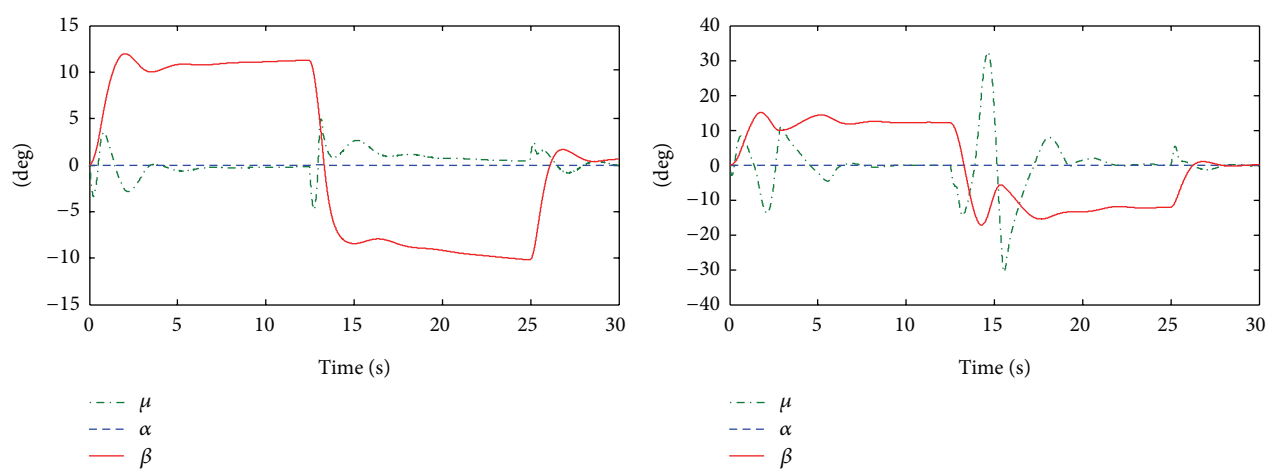

(a) Delayed AW compensator (b) Delayed AW compensator proposed in [10]

Figure 8: Saturated tracking response with delayed AW compensator.

is a plant-order dynamic one, while the delayed AW compensator proposed in [10] is static.

4. Conclusion

In this paper, the AW control problem based on the decoupling structure proposed by Weston and Postlewaite is investigated. Based on the decoupling AW structure, matrix F is to be designed to determine $M(s)$, which is a right coprime factor of the plant $G(s)$. Motivated by the novel idea of delaying the activation of the AW compensator, a new decoupling structure with delayed activation of AW compensator is developed. A time-varying gain G_d is introduced, and $\widehat{G}(s) = G(s)G_d$ is treated as a new quasi-LPV plant to deal with the delayed AW control problem. For both single-input and multi-input plants, a set of small scale LMIs are derived to calculate the designing matrix F for AW compensator. Only simple LMIs are needed to be solved, while the LMIs in [14] to be solved are large. Most of all, the AW technique proposed here has a better performance applied in the application example than in [14] and has no worse performance than [10].

Acknowledgments

This work is jointly supported by National Science Foundation of China under Grants 60974078 and 90916003 and Foundation of National Defense B0320110023.

References

[1] K. Peng, H. S. Su, and Y. P. Yang, "Coordinated control of multi-agent systems with a varying-velocity leader and input saturation," *Communications in Theoretical Physics*, vol. 52, no. 3, pp. 449–456, 2009.

[2] M. V. Kothare, P. J. Campo, M. Morari, and C. N. Nett, "A unified framework for the study of anti-windup designs," *Automatica*, vol. 30, no. 12, pp. 1869–1883, 1994.

[3] S. Tarbouriech and M. Turner, "Anti-windup design: an overview of some recent advances and open problems," *IET Control Theory & Applications*, vol. 3, no. 1, pp. 1–19, 2009.

[4] E. F. Mulder, M. V. Kothare, and M. Morari, "Multivariable anti-windup controller synthesis using linear matrix inequalities," *Automatica*, vol. 37, no. 9, pp. 1407–1416, 2001.

[5] G. Grimm, J. Hatfield, I. Postlethwaite, A. R. Teel, M. C. Turner, and L. Zaccarian, "Antiwindup for stable linear systems with input saturation: an LMI-based synthesis," *IEEE Transactions on Automatic Control*, vol. 48, no. 9, pp. 1509–1525, 2003.

[6] J. M. Gomes da Silva Jr. and S. Tarbouriech, "Antiwindup design with guaranteed regions of stability: an LMI-based approach," *IEEE Transactions on Automatic Control*, vol. 50, no. 1, pp. 106–111, 2005.

[7] L. Lu and Z. Lin, "A switching anti-windup design using multiple Lyapunov functions," *IEEE Transactions on Automatic Control*, vol. 55, no. 1, pp. 142–148, 2010.

[8] P. F. Weston and I. Postlethwaite, "Linear conditioning for systems containing saturating actuators," *Automatica*, vol. 36, no. 9, pp. 1347–1354, 2000.

[9] M. C. Turner and I. Postlethwaite, "A new perspective on static and low order anti-windup synthesis," *International Journal of Control*, vol. 77, no. 1, pp. 27–44, 2004.

[10] S. Sajjadi-Kia and F. Jabbari, "Modified anti-windup compensators for stable plants," *IEEE Transactions on Automatic Control*, vol. 54, no. 8, pp. 1934–1939, 2009.

[11] E. Prempain, M. C. Turner, and I. Postlethwaite, "Coprime factor based anti-windup synthesis for parameter-dependent systems," *Systems & Control Letters*, vol. 58, no. 12, pp. 810–817, 2009.

[12] S. Sajjadi-Kia and F. Jabbari, "Modified anti-windup compensators for stable plants: dynamic anti-windup case," in *Proceedings of the 48th IEEE Conference on Decision and Control Held Jointly with the 28th Chinese Control Conference (CDC/CCC '09)*, pp. 2795–2800, Shanghai, China, December 2009.

[13] J. S. Yee, J. L. Wang, and N. Sundararajan, "Robust sampled-data H_∞-flight-controller design for high α stability-axis roll maneuver," *Control Engineering Practice*, vol. 8, no. 7, pp. 735–747, 2000.

[14] M. C. Turner, G. Herrmann, and I. Postlethwaite, "Anti-windup compensation using a decoupling architecture," in *Advanced Strategies in Control Systems with Input and Output Constraints*, vol. 346 of *Lecture Notes in Control and Information Sciences*, pp. 121–171, Springer, Berlin, Germany, 2007.

Hindawi Publishing Corporation
Mathematical Problems in Engineering
Volume 2013, Article ID 384654, 8 pages
http://dx.doi.org/10.1155/2013/384654

Research Article

Hybrid Synchronization of General T-S Fuzzy Complex Dynamical Networks with Time-Varying Delay

Degang Xu, Weihua Gui, Panlei Zhao, and Chunhua Yang

College of Information Science and Engineering, Central South University, Changsha 410083, China

Correspondence should be addressed to Degang Xu; dgxu@csu.edu.cn

Received 5 April 2013; Accepted 28 April 2013

Academic Editor: Wenwu Yu

We propose and investigate a new general model of fuzzy complex network systems described by Takagi-Sugeno (T-S) fuzzy model with time-varying delays. Hybrid synchronization problem is discussed for this general T-S fuzzy complex dynamical network with nondelayed and delayed coupling between nodes. Utilizing Lyapunov-Krasovskii functional method, synchronization stability criteria for the networks are established in terms of linear matrix inequalities (LMIs). These criteria reveal the relationship between coupling matrices with time-varying delays and synchronization stability of the dynamical network. Numerical simulation is provided to illustrate the effectiveness and advantage of derived theoretical results.

1. Introduction

In recent years, complex dynamical networked agent systems have attracted a great deal of attention in various engineering fields from physics to biology, chemistry, and computer science [1–3]. The reason can be attributed to their flexibility and generality for representing virtually any natural and man-made systems. Such systems in the real world usually consist of a large number of highly interconnected dynamical units. Transportation networks, coupled biological and chemical engineering systems, neural networks in human brains, and the Internet are only a few of such examples [4].

Synchronization is one of the most significant and interesting collective behaviors in complex networked agent systems due to its potential applications in many fields including secure communization, parallel image processing, and information science [5–7]. On the other hand, time delays occur commonly in complex networks because of the finite speed of signal transmission over the links [8]. Since the time delay often causes undesirable performance and instability of the network, various approaches to synchronization analysis for complex dynamical networks with time delay have been investigated in the literature [9–12]. Therefore, synchronization criteria of complex networks with delays have become a topic of practical importance. The stability criteria for time delay systems include two categories: delay-dependent ones and delay-independent ones. Since delay-dependent stability criteria include the information on the size of delay, delay-dependent stability criteria are generally less conservative than delay-independent ones [10]. Moreover, many real-world networks are not static but more likely to be time-varying evolving, particularly in biological and physical networks. Commonly, time-varying delays are general form of time delays. There are a few research works [13–15] considering the time-varying coupling for complex agent systems of dynamical networks.

Furthermore, the uncertainty or vagueness is unavoidable in real modeling problems of agent systems. Fuzzy theory as an efficient tool in approximating a complex nonlinear system is a feasible method to take vagueness into consideration [16]. There are some research works investigating the problem of delay-dependent robust controllers and filtering design for a class of uncertain state-delayed Takagi-Sugeno (T-S) fuzzy systems [17–20]. Recently, the problems of stability analysis, approximation, and stabilization for Takagi-Sugeno fuzzy systems with time-varying state delay are investigated [21–24]. So, fuzzy complex networks have advantages over pure complex networks since they incorporate the capability of fuzzy reasoning in handling uncertain information. In this regard, the fuzzy models to describe complex dynamical

networks which are subjected to nonlinearity and have time-varying delays are introduced. The synchronization problem for T-S fuzzy stochastic discrete-time complex networks with mixed time-varying delays is discussed in a recent work [25]. By employing the information of probability distribution of time delays, the original system is transformed into a T-S fuzzy model with stochastic parameter [26, 27]. But how to solve the synchronization problem for general fuzzy complex networks still remains largely unsolved and challenging. To the best of our knowledge, time-varying delay [28, 29] synchronization analysis of general fuzzy complex dynamical networks has not been reported in the literature.

Besides, it is noticed that most of the studies on synchronization of dynamical networks have been performed under some implicit assumptions that there exists the information communication of nodes via the edges only at time t or at time t_τ [30]. However, in many circumstances, this simplification does not match satisfactorily the peculiarities of real networks; there exists the information communication of nodes not only at time t but also at time t_τ. More recently, coexistence of the hybrid synchronization in chaotic systems was investigated intensively [31]. However, our generalized dynamical network model has different coupling strengths for different connections. So it is complex and extended comparing with the simplified network model in [32]. So our conclusion is more compact and more meaningful for the generalized network models. To the best of our knowledge, there are very few studies on the hybrid synchronization of general coupled complex dynamical networks with nondelayed and delayed coupling in the literature.

Motivated by the previous discussions, in this paper, we attempt to introduce some more general time-varying dynamical network models based on the T-S fuzzy model and investigate the synchronization properties of this model. Based on the Lyapunov-Krasovskii functional method, we use a linearized method to solve the problem of synchronization for fuzzy complex networks with time-varying coupling delay and derive hybrid synchronization conditions for delay-dependent stabilities in terms of LMIs, the time-varying network model. A numerical example is given to demonstrate the effectiveness and the advantage of the proposed method.

The rest of this paper is organized as follows. In Section 2, we present some preliminaries for proving the proof and the fuzzy time-varying coupled dynamical network model. Hybrid synchronization criterions are derived in Section 3. In Section 4, we provide a numerical simulation to verify the correctness and effectiveness of the derived results. Conclusions are presented in Section 5.

2. Problem Formulation

Consider the following model of general continuous-time complex networks with time-varying coupling delays which can be represented by a T-S fuzzy model.

Rule l: If $\theta_1(t)$ is F_{l1}, $\theta_2(t)$ is F_{l2},..., $\theta_g(t)$ is F_{lg}, then

$$\begin{aligned}\dot{x}_i(t) &= f(x_i(t)) + \varepsilon\sum_{j=1}^{N} c_{ij}\Gamma_l x_j(t) \\ &\quad + \varepsilon\sum_{j=1}^{N}\widetilde{c}_{ij}\widetilde{\Gamma}_l x_j(t-\tau(t)), \\ &\quad t>0,\ i=1,2,\ldots,N, \\ x(t) &= \phi(t), \quad t\in[-h,0],\end{aligned} \tag{1}$$

where F_{lj} ($l = 1,\ldots,r$; $j = 1,\ldots,g$) are the fuzzy sets; r is the number of rules and θ_j ($j = 1,\ldots,g$) are the premise variables; N is the number of agent nodes, where each agent node is an n-dimensional dynamical system with node dynamics $\dot{x} = f(x,t)$; $x_i = (x_{i1}, x_{i2},\ldots,x_{in})^T \in R^n$ are the state variables of node i; $f : R^n \to R^n$ is continuously differentiable; Γ_l and $\widetilde{\Gamma}_l$ are the constant inner-coupling matrices of the nodes; the constant $\varepsilon > 0$ is the coupling strength; $C = (c_{ij})_{N\times N}$ and $\widetilde{C} = (\widetilde{c}_{ij})_{N\times N}$ are the outer-coupling matrices of the network, in which c_{ij} is defined, as follows: if there is a connection between node i and node j ($j \neq i$), then $c_{ij} = c_{ji} = 1$; otherwise, $c_{ij} = c_{ji} = 0$, $\widetilde{c}_{ij}$ is similar defined and the diagonal elements of matrices C and $\widetilde{C}$ are defined by

$$\begin{aligned}c_{ij} &= -\sum_{j=1,i\neq j}^{N} c_{ij} = -\sum_{j=1,i\neq j}^{N} c_{ji}, \\ \widetilde{c}_{ij} &= -\sum_{j=1,i\neq j}^{N}\widetilde{c}_{ij} \\ &= -\sum_{j=1,i\neq j}^{N}\widetilde{c}_{ji}, \quad i=1,\ldots,N.\end{aligned} \tag{2}$$

Suppose that C and $\widetilde{C}$ are irreducible matrices. Time-varying delay $\tau(t)$ satisfies

$$0 \le \tau(t) \le h, \quad \dot{\tau}(t) \le \gamma, \tag{3}$$

in which h and γ are constants. The initial function $\phi(t)$ is a continuous and differentiable vector-valued function.

By using the standard fuzzy inference method, the T-S fuzzy network (1) can be expressed by the following model:

$$\begin{aligned}\dot{x}_i(t) = \sum_{l=1}^{r}\mu_l(\theta(t))\Bigg[& f(x_i(t)) + \varepsilon\sum_{j=1}^{N} c_{ij}\Gamma_l x_j(t) \\ & + \varepsilon\sum_{j=1}^{N}\widetilde{c}_{ij}\widetilde{\Gamma}_l x_j(t-\tau(t))\Bigg],\end{aligned} \tag{4}$$

where $\theta(t) = [\theta_1(t), \theta_2(t),\ldots,\theta_g(t)]$, and $\mu_l(\theta(t)) = \omega_l(\theta(t))/\sum_{l=1}^{r}\omega_l(\theta(t))$, in which $F_{lj}(\theta_j(t))$ is the grade of membership

of $\theta_j(t)$ in F_{lj}. It is obvious that the fuzzy weighting functions $\mu_l(\theta(t))$ satisfy

$$\mu_l(\theta(t)) \geq 0, \qquad \sum_{l=1}^{r} \mu_l(\theta(t)) = 1. \tag{5}$$

In the following, some elementary situations are introduced, which play an important role in proving the main result.

Definition 1. The dynamical networked agent system (1) is said to achieve asymptotic synchronization if

$$x_1(t) = x_2(t) = \cdots = x_N(t) = s(t), \quad t \to \infty, \tag{6}$$

where $s(t)$ is a solution of an isolate node, satisfying $\dot{s}(t) = f(s(t))$.

Lemma 2 (see [7]). *If $C = (c_{ij})_{N\times N}$ satisfies the aforementioned defined conditions, then there exists a unitary matrix, $\phi = (\phi_1, \ldots, \phi_N)$, such that $C^T\phi_k = \lambda_k\phi_k$, $k = 1, 2, \ldots, N$, where λ_k, $k = 1, 2, \ldots, N$, are the eigenvalues of matrix C.*

Lemma 3 (see [12]). *Let X and Y be arbitrary n-dimensional real vectors, and let K be an $n \times n$ positive definite matrix. $P \in R^{n\times n}$ is an arbitrary real matrix. Then, the following matrix inequality holds:*

$$2X^TPY \leq X^TPK^{-1}P^TX + Y^TKY. \tag{7}$$

The aim of this paper is to investigate synchronization problem of the fuzzy complex dynamical network with time-varying delay (4).

3. Main Results

In this section, we focus on investigating the hybrid synchronization problem of fuzzy complex dynamical networks with nondelayed and delayed coupling. Before deriving our main results, the following lemma will be utilized.

Lemma 4. *Consider the T-S fuzzy dynamical network* (4). *Let $0 = \lambda_1 > \lambda_2 \geq \cdots \geq \lambda_N$ and $0 = \widetilde{\lambda}_1 > \widetilde{\lambda}_2 \geq \cdots \geq \widetilde{\lambda}_N$, respectively, be the eigenvalues of outer coupling matrix C and $\widetilde{C}$. If the following $N-1$ time-varying delayed differential equations are asymptotically stable about their zero solution:*

$$\begin{aligned}\dot{w}_k(t) = \sum_{l=1}^{r}\mu_l(\theta(t))\big[\big(J(t) + \varepsilon\lambda_k\Gamma_l\big)w_k(t) \\ +\varepsilon\widetilde{\lambda}_k\widetilde{\Gamma}_l w_k(t-\tau(t))\big], \\ k = 2, 3, \ldots, N,\end{aligned} \tag{8}$$

where $J(t)$ is the Jacobin of $f(x(t))$ at $s(t)$, then synchronized states in fuzzy complex networks (1) *are asymptotically stable.*

Proof. For the synchronized states of complex networks (4), we have

$$x_i(t) = s(t) + e_i(t), \quad i = 1, 2, \ldots, N. \tag{9}$$

Substituting (9) into (4), we obtain

$$\begin{aligned}\dot{e}_i(t) = \sum_{l=1}^{r}\mu_l(\theta(t))\Bigg[& f(s(t) + e_i(t)) - f(s(t)) \\ & + \varepsilon\sum_{j=1}^{N} c_{ij}\Gamma_l e_j(t) \\ & + \varepsilon\sum_{j=1}^{N}\widetilde{c}_{ij}\widetilde{\Gamma}_l e_j(t-\tau(t))\Bigg].\end{aligned} \tag{10}$$

Considering that $f(s(t))$ is continuous differentiable, it is easy to know that the origin of the complex networks (8) is an asymptotically stable equilibrium point for the following linear time delay systems:

$$\begin{aligned}\dot{e}_i(t) &= \sum_{l=1}^{r}\mu_l(\theta(t))\Bigg[J(t)e_i(t) + \varepsilon\sum_{j=1}^{N}c_{ij}\Gamma_l e_j(t) \\ &\qquad + \varepsilon\sum_{j=1}^{N}\widetilde{c}_{ij}\widetilde{\Gamma}_l e_j(t-\tau(t))\Bigg] \\ &= \sum_{l=1}^{r}\mu_l(\theta(t)) \\ &\qquad \times \Big[J(t)e_i(t) + \varepsilon\Gamma_l\big(e_1(t), \ldots, e_N(t)\big)(c_{i1}, \ldots, c_{iN})^T \\ &\qquad + \varepsilon\widetilde{\Gamma}_l\big[e_1(t-\tau(t)), \ldots, e_N(t-\tau(t)\big] \\ &\qquad \times (\widetilde{c}_{i1}, \ldots, \widetilde{c}_{iN})^T\Big].\end{aligned} \tag{11}$$

Let $e(t) = (e_1(t), \ldots, e_N(t)) \in R^{N\times N}$; we can obtain

$$\begin{aligned}&\dot{e}_i(t) \\ &= \sum_{l=1}^{r}\mu_l(\theta(t))\big[J(t)e_i(t) + \varepsilon\Gamma_l e(t)C^T + \varepsilon\widetilde{\Gamma}_l e(t-\tau(t))\widetilde{C}^T\big].\end{aligned} \tag{12}$$

According to Lemma 2, there exist nonsingular matrices, $\Phi_1 = (\phi_{11}, \ldots, \phi_{1N})$, $\Phi_2 = (\phi_{21}, \ldots, \phi_{2N})$, such that $C^T\Phi_1 = \Phi_1\Lambda_1$ and $\widetilde{C}^T\Phi_2 = \Phi_2\Lambda_2$, with $\Lambda_1 = \mathrm{diag}(\lambda_1, \ldots, \lambda_N)$, $\Lambda_2 = \mathrm{diag}(\widetilde{\lambda}_1, \ldots, \widetilde{\lambda}_N)$. Using the nonsingular transform $e(t)\Phi = w(t)$, $e(t-\tau)\Phi = w(t-\tau)$, then we obtain

$$\begin{aligned}\dot{w}_k(t) = \sum_{l=1}^{r}\mu_l(\theta(t))\big[\big(J(t) + \varepsilon\lambda_k\Gamma_l\big)w_k(t) \\ +\varepsilon\widetilde{\lambda}_k\widetilde{\Gamma}_l w_k(t-\tau(t))\big], \\ k = 1, \ldots, N.\end{aligned} \tag{13}$$

Note that $\lambda_1 = 0$, $\widetilde{\lambda}_1 = 0$ correspond to the synchronization of the network states (4), where the state $s(t)$ is an orbital

stable solution of the isolate node as assumed before in (4). If the following $N-1$ pieces of n-dimensional linear multiple time delay differential equations

$$\begin{aligned}\dot{w}_k(t) = \sum_{l=1}^{r}\mu_l(\theta(t))\left[\left(J(t)+\varepsilon\lambda_k\Gamma_l\right)w_k(t)\right.\\ \left.+\varepsilon\widetilde{\lambda}_k\widetilde{\Gamma}_l w_k(t-\tau(t))\right],\\ k=1,\ldots,N\end{aligned} \tag{14}$$

are asymptotically stable, then $e(t)$ will tend to the origin asymptotically, which implies that synchronized states of complex networks (8) are asymptotically stable.

The proof is thus completed. □

Remark 5. We use Lemma 4 to linearize the complicated system to deal with the complex networks by using fuzzy theory. It is an available way to investigate the interconnected dynamical agents of complex networks. Then some new subsystems can be obtained, which are easy to be analyzed.

Now, the main result is stated in the following theorem.

Theorem 6. *If there exist positive definite symmetric matrices $P_k = P_k^T > 0$, $Q_k = Q_k^T > 0$, $R_k = R_k^T > 0$, and $Z_k = Z_k^T > 0$, such that the following LMI holds for all $l = 1, 2, \ldots, r$:*

$$\begin{bmatrix}\Theta_k & h\Omega_{1k} & h\Omega_{2k} & h\Omega_{3k} & h\Pi_k^T Z_k\\ * & -hZ_k & 0 & 0 & 0\\ * & * & -hZ_k & 0 & 0\\ * & * & * & -hZ_k & 0\\ * & * & * & * & -hZ_k\end{bmatrix} < 0, \tag{15}$$

where

$$\Omega_{1k} = \begin{bmatrix}N_{1k}^1\\ N_{1k}^2\\ N_{1k}^2\end{bmatrix},\quad \Omega_{2k} = \begin{bmatrix}N_{2k}^1\\ N_{2k}^2\\ N_{2k}^2\end{bmatrix},\quad \Omega_{3k} = \begin{bmatrix}N_{3k}^1\\ N_{3k}^2\\ N_{3k}^2\end{bmatrix},$$

$$\text{for } k = 2, 3, \ldots, N,$$

$$\Theta_k = \Theta_{k1} + \Theta_{k2} + \Theta_{k2}^T,$$

$$\Theta_{k1} = \begin{bmatrix}P_k\left(J(t)+\varepsilon\lambda_k\Gamma_l\right) + \left(J(t)+\varepsilon\lambda_k\Gamma_l\right)^T P_k & \varepsilon\widetilde{\lambda}_k\widetilde{\Gamma}_l P_k & 0\\ * & -(1-\gamma) & 0\\ * & * & -R_k\end{bmatrix},$$

$$\Theta_{k2} = \left[\Omega_{k1}+\Omega_{k3}\quad -\Omega_{k1}+\Omega_{k2}\quad -\Omega_{k2}-\Omega_{k3}\right],$$

$$\Pi_k = \left[J(t)+\varepsilon\lambda_k\Gamma_l\quad \varepsilon\widetilde{\lambda}_k\widetilde{\Gamma}_l\quad 0\right], \tag{16}$$

where $*$ denotes the symmetric terms in a symmetric matrix, then the asymptotic synchronization of complex network system (8) can be achieved.

Proof. Construct a Lyapunov-Krasovskii function as

$$\begin{aligned}V_k(t) = {} & w_k^T(t)P_k w_k(t) + \int_{t-\tau(t)}^{t} w_k^T(s)Q_k w_k(s)\,ds\\ & + \int_{t-h}^{t} w_k^T(s)R_k w_k(s)\,ds\\ & + \int_{-h}^{0}\int_{t+\theta}^{t}\dot{w}_k^T(s)Z_k\dot{w}_k(s)\,ds\,d\theta.\end{aligned} \tag{17}$$

According to Lemma 4, calculating the time derivative of $V_k(t)$ along the trajectories of complex networks (8), we obtain

$$\begin{aligned}\dot{V}_k(t) = {} & 2w_k^T(t)P_k\dot{w}_k(t) + w_k^T(t)Q_k w_k(t)\\ & -(1-\dot{\tau}(t))w_k^T(t-\tau(t))Q_k w_k(t-\tau(t))\\ & + w_k^T(t)R_k w_k(t) - w_k^T(t-h)R_k\dot{w}_k(t-h)\\ & + h\dot{w}_k^T(s)Z_k\dot{w}_k(s) - \int_{t-h}^{t}\dot{w}_k^T(s)Z_k\dot{w}_k(s)\\ \le {} & 2w_k^T(t)P_k\dot{w}_k(t) + w_k^T(t)Q_k w_k(t)\\ & -(1-\gamma)w_k^T(t-\tau(t))Q_k w_k(t-\tau(t))\\ & + w_k^T(t)R_k w_k(t) - w_k^T(t-h)R_k\dot{w}_k(t-h)\\ & + h\dot{w}_k^T(s)Z_k\dot{w}_k(s) - \int_{t-h}^{t}\dot{w}_k^T(s)Z_k\dot{w}_k(s).\end{aligned} \tag{18}$$

Based on the Newton-Leibniz formula, the following equations can be obtained for arbitrary matrices Ξ_k with appropriate dimensions:

$$2\xi_k^T(t)\Xi_k\left[w_k(t) - w_k(t-\tau) - \int_{t-\tau}^{t}\dot{w}_k(s)\,ds\right] = 0, \tag{19}$$

where $\varsigma_k^T(t) = (w_k^T(t), w_k^T(t-\tau))$ and $\Xi_k^T = (X_1^T, X_2^T)$.

Therefore, using Lemma 3, we have

$$\begin{aligned}\dot{V}_k(t) = {} & 2w_k^T(t)P_k\dot{w}_k(t) + w_k^T(t)\left(Q_k+R_k\right)w_k(t)\\ & -(1-\gamma)w_k^T(t-\tau(t))Q_k w_k(t-\tau(t))\\ & - w_k^T(t-h)R_k\dot{w}_k(t-h) + h\dot{w}_k^T(t)Z_{k1}\dot{w}_k(t)\\ & - \int_{t-\tau(t)}^{t}\dot{w}_k^T(s)Z_{k1}(s)\,ds\\ & - \int_{t-h}^{t-\tau(t)}\dot{w}_k^T(s)Z_{k1}\dot{w}_k(s)\,ds\\ & - \int_{t-h}^{t}\dot{w}_k^T(s)Z_{k1}\dot{w}_k(s)\,ds\\ & + 2\Delta_k^T(t)\Omega_{1k}\left[w_k(t) - w_k(t-\tau(t))\right.\\ & \left. - \int_{t-\tau(t)}^{t}\dot{w}_k^T(s)\,ds\right]\end{aligned}$$

$$
\begin{aligned}
&+ 2\Delta_k^T(t)\,\Omega_{2k}\left[w_k(t-\tau(t)) - w_k(t-h) - \int_{t-h}^{t-\tau(t)} \dot{w}_k^T(s)\,ds\right] \\
&+ 2\Delta_k^T(t)\,\Omega_{3k}\left[w_k(t) - w_k(t-h) - \int_{t-h}^{t} \dot{w}_k^T(s)\,ds\right] \\
&< \sum_{i=1}^{r}\mu_l(\theta(t))\Big\{\Phi_k^T(t)\Big[\Theta_k + h\widetilde{\Gamma}_k^T Z_k \widetilde{\Gamma}_k + h\Omega_{1k}Z_k^{-1}\Omega_{1k}^T + h\Omega_{2k}Z_k^{-1}\Omega_{2k}^T + h\Omega_{3k}Z_k^{-1}\Omega_{3k}^T\Big]\Phi_k(t) \\
&\quad - \int_{t-\tau(t)}^{t}\left[\Phi_k^T(t)\,\Omega_{1k} + \dot{w}_k^T(s)\,Z_k\right]Z_k^{-1} \times \left[\Omega_{1k}^T\Phi_k(t) + Z_k\dot{w}_k(s)\right]ds \\
&\quad - \int_{t-h}^{t-\tau(t)}\left[\Phi_k^T(t)\,\Omega_{2k} + \dot{w}_k^T(s)\,Z_k\right]Z_k^{-1} \times \left[\Omega_{2k}^T\Phi_k(t) + Z_k\dot{w}_k(s)\right]ds \\
&\quad - \int_{t-h}^{t}\left[\Phi_k^T(t)\,\Omega_{3k} + \dot{w}_k^T(s)\,Z_k\right]Z_k^{-1} \times \left[\Omega_{3k}^T\Phi_k(t) + Z_k\dot{w}_k(s)\right]ds\Big\},
\end{aligned}
\tag{20}
$$

where $\Delta_k^T(t) = [w_k^T(t), w_k^T(t-\tau), w_k^T(t-h)]^T$. Because the last three terms are all less than zero, if

$$
\begin{aligned}
&\Theta_k + h\widetilde{\Gamma}_k^T Z_k \widetilde{\Gamma}_k + h\Omega_{1k}Z_k^{-1}\Omega_{1k}^T + h\Omega_{2k}Z_k^{-1}\Omega_{2k}^T \\
&\quad + h\Omega_{3k}Z_k^{-1}\Omega_{3k}^T < 0,
\end{aligned}
\tag{21}
$$

then $\dot{V}_k(t) < -\kappa\|w(t)\|^2$ for sufficiently small $\kappa > 0$. It is easy to see that system (8) is globally synchronized. By Schur complements, we know that the function (21) is equivalent to the function (15).

The proof is thus completed. □

Remark 7. For the delay-dependent synchronization problems of complex networks, the Lyapunov-Krasovskii condition has been attracted owing to the structural advantage. The key point is the introduction of the integral inequality technique, a fundamental trick to derive delay-dependent stability criteria containing the size or the bounds of delays and their derivatives. However, almost results in this field have employed partial information on the relationship among delay-related terms. Being differently from the common construction, we use not only the time-varying-delayed state but also the delay-upper-bounded state to exploit all possible information when constructing the Lyapunov-Krasovskii functional. Our approach in Theorem 6 reduces the conservatism of the existing methods to a certain extent.

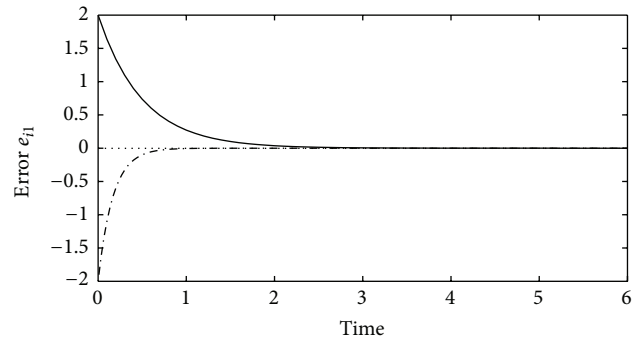

Figure 1: Synchronization error e_{i1} for the coupling delayed networks with $h = \gamma = 0.5$.

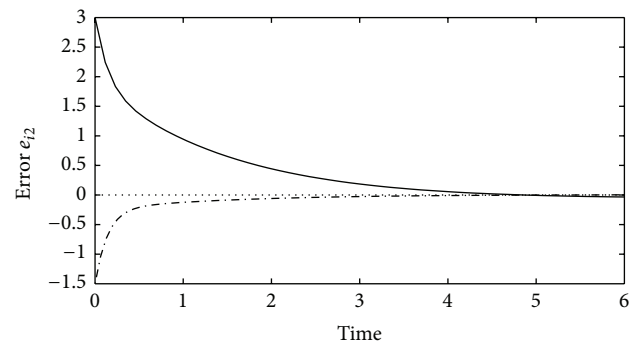

Figure 2: Synchronization error e_{i1} for the coupling delayed networks with $h = \gamma = 0.5$.

The aforementioned results can be extended to the case of bound constant time delay. If the time-varying delay $\tau(t)$ is a constant time delay in system (1), then fuzzy system (4) can be expressed in the following model:

$$
\dot{x}_i(t) = \sum_{l=1}^{r}\mu_l(\theta(t))\left[f(x_i(t)) + \varepsilon\sum_{j=1}^{N}c_{ij}\Gamma_l x_j(t) + \varepsilon\sum_{j=1}^{N}\widetilde{c}_{ij}\widetilde{\Gamma}_l x_j(t-\tau)\right].
\tag{22}
$$

We obtain the following corollary.

Corollary 8. *If there exist positive definite symmetric matrices P_k, Q_k, and R_k $(2 \le k \le N)$ and two arbitrary matrices N_1,*

Table 1: Upper bounds of h for different ε and γ.

Coupling strength ε	0.3	0.4	0.5	0.6
$\gamma = 0$	1.832	1.136	0.813	0.637
$\gamma = 0.2$	1.461	1.053	0.716	0.562
$\gamma = 0.5$	1.263	0.851	0.641	0.514
$\gamma = 0.9$	0.953	0.710	0.560	0.473

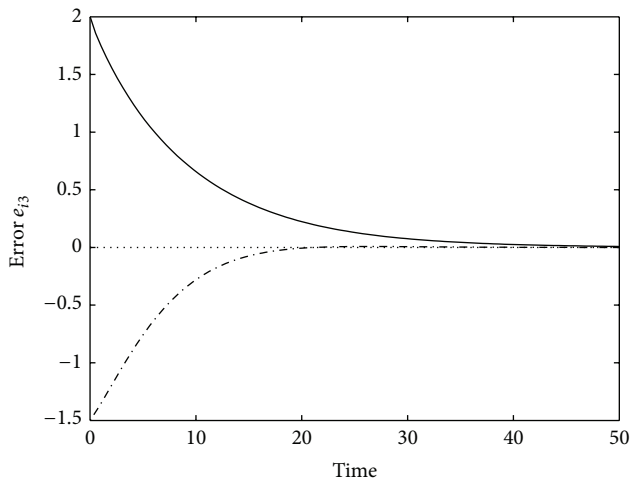

Figure 3: Synchronization error e_{i3} for the coupling delayed networks with $h = \gamma = 0.5$.

N_2 with appropriate dimensions, such that the following LMIs hold for all $l = 1, 2, \ldots, r$:

$$\Omega_k = \begin{bmatrix} \Theta & \widetilde{\lambda}_k \varepsilon P_k \widetilde{\Gamma}_l - N_1 + N_2^T & \tau J^T(t) R_k & \tau N_1 \\ * & -Q_k - N_2 - N_2^T & \tau c \widetilde{\lambda}_k \widetilde{\Gamma}_l^T R_k & \tau N_2 \\ * & * & -\tau R_k & 0 \\ * & * & * & -\tau R_k \end{bmatrix} < 0, \tag{23}$$

where

$$\Theta = P_k \left(J(t) + \varepsilon \lambda_k \Gamma_l\right) + \left(J(t) + \varepsilon \lambda_k \Gamma_l\right)^T P_k + Q_k + N_1^T + N_1, \tag{24}$$

then the asymptotic synchronization of system (22) *in Definition 1 can be achieved.*

Proof. Select a Lyapunov-Krasovskii function as

$$V_k(t) = w_k^T(t) P_k w_k(t) + \int_{t-\tau}^{t} w_k^T(s) Q_k w_k(s)\, ds + \int_{t-\tau}^{t} \int_{\theta}^{t} \dot{w}_k^T(s) R_k \dot{w}_k(s)\, ds\, d\theta. \tag{25}$$

The rest of the proof is similar to that of Theorem 6; thus one can easily obtain the result. Thus it is omitted here. The proof is completed. □

Remark 9. Corollary 8 presents new hybrid synchronization conditions for fuzzy complex networks with constant delays. We consider the delay which involve general form of delays. Based on Lyapunov-Krasovskii function method, stability criteria are obtained in the form of LMIs which can be easily solved. And the results are usually less conservative than delay-independent ones especially when the size of the time delay is small.

4. Numerical Example

To illustrate the previous results we obtain, we consider the following complex dynamical networks with time-varying delays consisting of three nodes:

$$\begin{bmatrix} \dot{x}_1(t) \\ \dot{x}_2(t) \\ \dot{x}_3(t) \end{bmatrix} = \begin{bmatrix} -x_1 \\ -2x_2 \\ -3x_3 \end{bmatrix} \tag{26}$$

which is asymptotically stable at $s(t) = 0$, with Jacobin given by $J = \mathrm{diag}\{-1, -2, -3\}$. Assume that inner-coupling matrices are $\Gamma = \widetilde{\Gamma} = \mathrm{diag}\{1, 1, 1\}$, and the coupling configuration matrices are

$$C = \widetilde{C} = \begin{bmatrix} -1 & 0.5 & 0.5 \\ 0.5 & -1 & 0.5 \\ 0.5 & 0.5 & -1 \end{bmatrix}, \quad \mu_1(\theta(t)) = \sin^2(x_1(t)), \quad \mu_2(\theta(t)) = \cos^2(x_1(t)). \tag{27}$$

The eigenvalues of C and $\widetilde{C}$ are $\lambda(C) = \widetilde{\lambda}(\widetilde{C}) = \{0, -1.5, -1.5\}$.

Using MATLAB LMI toolbox, the upper bounds on the time delay for different values of the coupling strength ε can be obtained from Theorem 6. A detailed comparison is given in Table 1, where the achieved upper bounds of time delay in the previous system are listed for their respective lower bounds.

Assume that the coupling strength is $\varepsilon = 0.4$; it is found that the maximum delay bound is $h = 0.73$ in [27], for which the synchronized states of the network are asymptotically stable. By Theorem 6 in this paper, however, it is found that the maximum delay bound for the synchronized states to be asymptotically stable is $h = 0.851$. It can be seen that the method proposed in this paper is better.

For example, when the delay is $\gamma = 0.5$, by employing the LMI Toolbox in Matlab, we simulate system (26) for given chosen initial parameter $\varepsilon = 0.3$. We define the errors of synchronization as follows:

$$e_{ij}(t) \triangleq x_{ij}(t) - x_{(i+1)j}(t), \quad i = 1, 2, \quad j = 1, 2, 3. \tag{28}$$

For random initial conditions, Figures 1, 2, and 3 show the synchronization errors between the states of node i and node $i+1$ with $h = 0.5$. We find that the synchronization errors converge to zero under the previous conditions.

5. Conclusions

In this paper, we have proposed a class of general complex dynamical network models based on T-S fuzzy theory and investigated hybrid synchronization of the proposed complex dynamical networks. Time-varying delays in network couplings of dynamical nodes have been considered. New delay-dependent synchronization criteria in terms of LMIs have been derived based on an appropriate Lyapunov functional. Synchronization criteria are obtained in this paper which can be applicable to networks with different topologies and different sizes. Numerical simulation is also provided to illustrate the usefulness and advantage of the synchronization criteria.

Acknowledgments

This research was partially supported by the National Natural Science Foundation of PR China (Grant nos. 61104135, 61025015, 61174132, and 61134006), China Postdoctoral Science Fund (Grant no. 2012T50705), and Postdoctoral Fund of the Central South University. The authors also gratefully thank the Editor and the reviewers for their helpful comments and suggestions, which have improved the quality of this paper.

References

[1] A.-L. Barabási and R. Albert, "Emergence of scaling in random networks," *Science*, vol. 286, no. 5439, pp. 509–512, 1999.

[2] R. Albert and A.-L. Barabási, "Statistical mechanics of complex networks," *Reviews of Modern Physics*, vol. 74, no. 1, pp. 47–97, 2002.

[3] S. Boccaletti, V. Latora, Y. Moreno, M. Chavez, and D.-U. Hwang, "Complex networks: structure and dynamics," *Physics Reports*, vol. 424, no. 4-5, pp. 175–308, 2006.

[4] M. Newman, A.-L. Barabási, and D.J. Watts, Eds., *The Structure and Dynamics of Networks*, Princeton University Press, Princeton, NJ, USA, 2006.

[5] A. Arenas, A. Díaz-Guilera, and C. J. Pérez-Vicente, "Synchronization processes in complex networks," *Physica D*, vol. 224, no. 1-2, pp. 27–34, 2006.

[6] J. Lü, H. Leung, and G. Chen, "Complex dynamical networks: modeling, synchronization and control," *Dynamics of Continuous, Discrete and Impulsive Systems B*, vol. 11, pp. 70–77, 2004.

[7] J. Lü, X. Yu, and G. Chen, "Chaos synchronization of general complex dynamical networks," *Physica A*, vol. 334, no. 1-2, pp. 281–302, 2004.

[8] W. Lu and T. Chen, "Synchronization analysis of linearly coupled networks of discrete time systems," *Physica D*, vol. 198, no. 1-2, pp. 148–168, 2004.

[9] C. Li and G. Chen, "Synchronization in general complex dynamical networks with coupling delays," *Physica A*, vol. 343, no. 1–4, pp. 263–278, 2004.

[10] Z. Wang, Y. Wang, and Y. Liu, "Global synchronization for discrete-time stochastic complex networks with randomly occurred nonlinearities and mixed time delays," *IEEE Transactions on Neural Networks*, vol. 21, no. 1, pp. 11–25, 2010.

[11] J. Cao, Z. Wang, and Y. Sun, "Synchronization in an array of linearly stochastically coupled networks with time delays," *Physica A*, vol. 385, no. 2, pp. 718–728, 2007.

[12] D. Xu and Z. Su, "Synchronization criterions and pinning control of general complex networks with time delay," *Applied Mathematics and Computation*, vol. 215, no. 4, pp. 1593–1608, 2009.

[13] J. Lü and G. Chen, "A time-varying complex dynamical network model and its controlled synchronization criteria," *IEEE Transactions on Automatic Control*, vol. 50, no. 6, pp. 841–846, 2005.

[14] Z. Fei, H. Gao, and W. X. Zheng, "New synchronization stability of complex networks with an interval time-varying coupling delay," *IEEE Transactions on Circuits and Systems II*, vol. 56, no. 6, pp. 499–503, 2009.

[15] J. H. Koo, D. H. Ji, and S. C. Won, "Synchronization of singular complex dynamical networks with time-varying delays," *Applied Mathematics and Computation*, vol. 217, no. 8, pp. 3916–3923, 2010.

[16] T. Takagi and M. Sugeno, "Fuzzy identification of systems and its applications to modeling and control," *IEEE Transactions on Systems, Man and Cybernetics*, vol. 15, no. 1, pp. 116–132, 1985.

[17] J. Qiu, G. Feng, and J. Yang, "A new design of delay-dependent robust H∞ filtering for discrete-time T-S fuzzy systems with time-varying delay," *IEEE Transactions on Fuzzy Systems*, vol. 17, no. 5, pp. 1044–1058, 2009.

[18] J. Qiu, G. Feng, and H. Gao, "Fuzzy-model-based piecewise $\mathscr{H}\infty$ static-output-feedback controller design for networked nonlinear systems," *IEEE Transactions on Fuzzy Systems*, vol. 18, no. 5, pp. 919–934, 2010.

[19] J. Qiu, G. Feng, and H. Gao, "Nonsynchronized-State estimation of multichannel networked nonlinear systems with multiple packet dropouts Via TS Fuzzy-Affine dynamic models," *IEEE Transactions on Fuzzy Systems*, vol. 19, no. 1, pp. 75–90, 2011.

[20] L. Wu and D. W. C. Ho, "Fuzzy filter design for Itô stochastic systems with application to sensor fault detection," *IEEE Transactions on Fuzzy Systems*, vol. 17, no. 1, pp. 233–242, 2009.

[21] L. Wu and W. X. Zheng, "L2-L∞ control of nonlinear fuzzy itô stochastic delay systems via dynamic output feedback," *IEEE Transactions on Systems, Man, and Cybernetics B*, vol. 39, no. 5, pp. 1308–1315, 2009.

[22] L. Wu, X. Su, P. Shi, and J. Qiu, "Model approximation for discrete-time state-delay systems in the TS fuzzy framework," *IEEE Transactions on Fuzzy Systems*, vol. 19, no. 2, pp. 366–378, 2011.

[23] L. Wu and W. X. Zheng, "Weighted H_∞ model reduction for linear switched systems with time-varying delay," *Automatica*, vol. 45, no. 1, pp. 186–193, 2009.

[24] L. Wu, X. Su, P. Shi, and J. Qiu, "A new approach to stability analysis and stabilization of discrete-time T-S fuzzy time-varying delay systems," *IEEE Transactions on Systems, Man, and Cybernetics B*, vol. 41, no. 1, pp. 273–286, 2011.

[25] Y. Tang, J. Fang, and M. Xia, "Synchronization of Takagi-Sugeno fuzzy stochastic complex networks with mixed delays," in *Proceedings of the 2nd International Conference on Intelligent Computation Technology and Automation (ICICTA '09)*, vol. 2, pp. 810–813, 2009.

[26] Y. Tang, J.-A. Fang, M. Xia, and X. Gu, "Synchronization of Takagi-Sugeno fuzzy stochastic discrete-time complex networks with mixed time-varying delays," *Applied Mathematical Modelling*, vol. 34, no. 4, pp. 843–855, 2010.

[27] H. Li, "Delay-distribution-dependent synchronization of T-S fuzzy stochastic complex networks with mixed time delays," in *Proceedings of the Control and Decision Conference (CCDC)*, pp. 1629–1634, 2011.

[28] K. Gu, "An integral inequality in the stability problem of time-delay systems," in *Proceedings of the 39th IEEE Confernce on Decision and Control*, pp. 2805–2810, December 2000.

[29] S. M. Lee, O. M. Kwon, and J. H. Park, "A novel delay-dependent criterion for delayed neural networks of neutral type," *Physics Letters A*, vol. 374, no. 17-18, pp. 1843–1848, 2010.

[30] X. J. Wu and H. T. Lu, "Hybrid synchronization of the general delayed and non-delayed complex dynamical networks via pinning control," *Neurocomputing*, vol. 89, no. 15, pp. 168–177, 2012.

[31] S. Wang, Y. Yu, and M. Diao, "Hybrid projective synchronization of chaotic fractional order systems with different dimensions," *Physica A*, vol. 389, no. 21, pp. 4981–4988, 2010.

[32] Y. Dai, Y. Cai, and X. Xu, "Synchronization criteria for complex dynamical networks with neutral-type coupling delay," *Physica A*, vol. 387, no. 18, pp. 4673–4682, 2008.

Hindawi Publishing Corporation
Mathematical Problems in Engineering
Volume 2013, Article ID 812032, 7 pages
http://dx.doi.org/10.1155/2013/812032

Research Article

A Multiagent Dynamic Assessment Approach for Water Quality Based on Improved Q-Learning Algorithm

Jianjun Ni,[1] Li Ren,[2] Minghua Liu,[1] and Daqi Zhu[3]

[1] *College of IOT Engineering, Hohai University, Changzhou 213022, China*
[2] *College of Hydrology and Water Resources, Hohai University, Nanjing 210098, China*
[3] *Laboratory of Underwater Vehicles and Intelligent Systems, Shanghai Maritime University, Shanghai 200135, China*

Correspondence should be addressed to Jianjun Ni; njjhhuc@gmail.com

Received 30 March 2013; Revised 17 April 2013; Accepted 18 April 2013

Academic Editor: Guanghui Wen

The dynamic water quality assessment is a challenging and critical issue in water resource management systems. To deal with this complex problem, a dynamic water assessment model based on multiagent technology is proposed, and an improved Q-learning algorithm is used in this paper. In the proposed Q-learning algorithm, a fuzzy membership function and a punishment mechanism are introduced to improve the learning speed of Q-learning algorithm. The dynamic water quality assessment for different regions and the prewarning of water pollution are achieved by using an interaction factor in the proposed approach. The proposed approach can deal with various situations, such as static and dynamic water quality assessment. The experimental results show that the water quality assessment based on the proposed approach is more accurate and efficient than the general methods.

1. Introduction

The assessment of water quality plays an essential role whether in engineering applications or in scientific research. However, due to the frequent occurrence of abrupt water pollution accident [1, 2], the general static assessment of water quality cannot meet the actual requirements any more. So, it is very important to assess the water quality of different regions accurately and dynamically, which is a hot field in water environment management system. The dynamic assessment of water quality can give out alarm timely before the pollutant reaches to some sensitive water regions. It is very helpful for these regions to make preparations and control water pollution effectively.

Various methods have been proposed to deal with the problem of water quality evaluation [3–5]. The main methods of the static water quality assessment include the comprehensive index method [6], fuzzy comprehensive evaluation method [7], BP neural network [8], and comprehensive water quality identification index method [9]. Although these methods have their own advantages, there are some shortcomings of these methods. For example, the calculation of the comprehensive index assessment method is complex. The accuracy of the fuzzy comprehensive evaluation method is lower, which cannot give out the assessment for water in worse than Grade V level. The calculation model based on BP neural network is very complex, and the choice of training samples for BP neural network is difficult. The general comprehensive water quality identification index method cannot make specific analysis according to the characteristics of different water bodies because various indicators are considered to have the same effects in the water quality assessment.

The static evaluation methods can just assess water quality after the occurrence of water pollution. To solve this problem, more and more research has been focused on dynamic water quality assessment methods. For example, Yun et al. [10] evaluated the changes in river water quality during a period of time by using the probability transition matrix. Su et al. [11] studied the spatiotemporal patterns and source apportionment of pollution in Qiantang River (China) using neural-based modeling and multivariate statistical techniques. There is much research on dynamic water quality assessment methods, but few considered the problem of quick perception

for the abrupt water pollution. The methods to determine water quality of other regions according to the water quality change of a region in the same basin are few.

To control water pollution and improve water environment quality effectively, the trend of water pollution should be predicted accurately when water pollution accident occurs [12, 13]. Because it is a problem of complex system, the general method cannot deal with it efficiently. Recently, more and more focus has been put on the agent-based method, which is not only a feasible solution but also an efficient one [14, 15]. For example, Wen et al. [16] studied the problem of consensus in directed networks of multiple agents with intrinsic nonlinear dynamics and sampled-data information. Leon [17] proposed an interaction protocol for a task allocation system, which can reveal the emergent behaviors in social networks of adaptive agents. In the multiagent system, agent is defined as an entity, which has the capabilities of environment perception, problem solving, and communication with the outside world. Based on these features, the agent can be used to solve the complex problems in practice by sharing knowledge with each other [18]. To solve the problem of dynamic water quality assessment, a multiagent model of water environment is set up [19, 20], where different regions in the water environment are abstracted as various agents. An improved Q-learning algorithm is proposed to deal with the cooperation of multiagents and carry out the task of dynamic water quality assessment.

The paper is organized as follows. In Section 2, the dynamic assessment model for water quality based on multiagent technology is introduced. Section 3 presents the proposed Q-learning algorithm for water quality assessment. Some experiments are conducted, and the results are discussed in Section 4. At last, the conclusions are given in Section 5.

2. The Multiagent Dynamic Assessment Model for Water Quality

In this paper, the dynamic assessment for water quality is studied. The dynamic water quality assessment has attracted much attention due to its complexity and significance. There are two main problems that need to be solved in the task of dynamic water quality assessment. The first one is how to assess the water quality of different regions efficiently, when the indicators of water quality in all these regions are obtained. The other one is how to assess the water quality of other regions, when the indicators of water quality in only one region are obtained.

To achieve the task of dynamic water quality assessment, an assessment model for water quality based on multiagent technology is proposed in this paper, where the water environment is divided into different regional agents based on the requirement of administration. By the information exchange among these regional agents, the task of dynamic water quality assessment can be accomplished efficiently. In each agent, there is a water quality assessment model, which is defined as follows in this study:

$$P = \omega_1 P_1 + \omega_2 P_2 + \cdots + \omega_n P_n, \tag{1}$$

where P is the level of water quality, $P_1, P_2, \ldots, P_n$ are various indicators used to assess the water quality and $\omega_1, \omega_2, \ldots, \omega_n$ are the weights for these indicators.

To assess water quality, more accurately, the water quality level P is defined as the following form:

$$P = X_1 \cdot X_2, \tag{2}$$

where $X_1 \in \{1, 2, \ldots, 6\}$ is the water quality level, which is determined by the Chinese national standard for water quality (see the Environmental Quality Standards for Surface Water in China (GB3838-2002)), X_2 is the relative position of the water quality level between two adjacent water quality grades, and the symbol $\{\cdot\}$ is a separating character, which has the same function as plus. For example, when the water quality level $P = 2.5$, the mean is that the grade of this water quality is Grade II by the national standard, and the relative grade of the water quality is 0.5; namely, the water quality is at a relatively intermediate location between Grade II and Grade III. When the value of X_1 is 6, the water quality is worse than Grade V. To reduce the computation complexity, the value of X_2 is designed as a discrete value in this paper, namely, $X_2 \in \{0.0, 0.1, \ldots, 0.9\}$.

In the water quality assessment model above, the weight for the ith indicator needs to be optimized based on the dynamic change of water environment. In this study, a Q-learning-based algorithm is proposed to deal with this problem, which will be introduced in detail at Section 3.

3. The Proposed Multiagent Q-Learning Algorithm

In the assessment model, the weights of various indicators need to be obtained. In general water quality assessment methods, these weights are always set by the experience. Recently, some artificial intelligent methods are introduced to optimize these weights, such as genetic algorithms and neural networks. However, those approaches cannot realize the information transmission and exchange among different regions. So, the weights obtained by those approaches are intrinsically static. To deal with this problem, the multiagent-based technology is introduced into the water quality assessment, and an improved Q-learning algorithm is proposed to realize the cooperation of multiagents. In general multiagent reinforcement learning, the Markov decision process is extended to realize the exchange learning for multiagent systems. In most of algorithms of multiagent reinforcement learning, it is required that each agent should know what action will be taken by other agents before it takes action. Thus, with the increase of the number of agents or the actions of each agent, it will cause that the state space of agent grows exponentially [21]. To solve these problems introduced above, an improved multiagent Q-learning algorithm is proposed in this study.

The Q-learning algorithm is a kind of reinforcement learning method by the trial-and-error method. Compared with other machine learning methods, the Q-learning algorithm can initiatively find which action will produce the greatest reward, instead of being told which action should

be done [22–24]. To improve the learning efficiency of the Q-learning algorithm, the number of action-state pairs and the searching in the action-state pairs should be reduced. In a multiagent system, an agent needs to keep track of its environment as well as other agents, so the convergency and learning speed are the problems that need to be solved at first in the multiagent Q-learning algorithm [25, 26]. Some improvements have been done on the multiagent Q-learning to deal with the convergence problem [27, 28]. However, there are still some problems of those approaches in the literatures such that most of those approaches do not consider the interactions among the agents. In this study, a fuzzy membership function with distinguish weight [29] is used to reduce the size of the action-state set. And a punishment mechanism [30] is used in the proposed algorithm to reduce the searching frequency. The proposed algorithm has some better performances than the general Q-learning algorithm such as the high learning speed and good convergence rate. Furthermore, an interactive factor is introduced into the proposed Q-learning algorithm, to realize the information transmission and the interaction among the agents in the system. The flow chart of the proposed Q-learning is shown in Figure 1. The proposed approach is presented in detail as follows.

3.1. The State Reduction Based on Fuzzy Membership Function. In the state preprocessing module of the proposed Q-learning algorithm, a fuzzy membership function with distinguish weight is used to reduce the size of sate-action sets by removing the superfluous or unrelated information from the system. The membership function is defined as follows in this paper:

$$y = \begin{cases} 0, & x \le x_b \text{ or } x \ge x_{b+1}, \\ \dfrac{x_{b+1} - x}{x_{b+1} - x_b}, & x_b < x < x_{b+1}, \end{cases} \tag{3}$$

where x is the original state (namely, the evaluation indicator for water quality in this study), y is the distinguish weight value of the indicator within its membership domain (namely, the parameter X_2 in (2)), x_b is the demarcation point of a grade, and x_{b+1} is the demarcation point of the next grade. When the grade of x_b is g (namely, the parameter X_1 in (2)), the membership value of the evaluation indicator is $v = g + y$. Because the size of the distinguish weight value y is 10 and the number of the grade g is 6 in this paper, the total number of states is $z = 10 * 6 = 60$. By this way, the state space can be reduced obviously.

3.2. The Information Transmission Based on Interaction Factor. To transfer the information among these agents in the system, a concept of the interaction factor (denoted by σ) is proposed in this paper, which can transfer the information of the key state to other agents for water quality assessment. In practice, the value of the interaction factor σ should be learnt by experience. In this paper, it is calculated by

$$\sigma = \exp(-Kd), \tag{4}$$

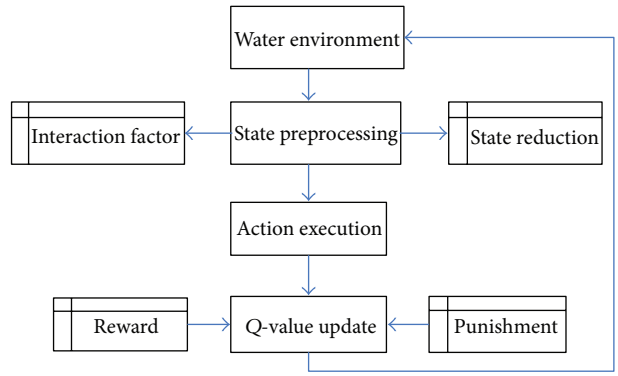

Figure 1: Flowchart of the proposed Q-learning algorithm for multiagent system.

where d is the distance between two agents, which can be an abstract concept or an actual physical distance and K is the attenuation coefficient, which can be calculated by the least square method:

$$\operatorname*{Min}_{K} F = \sqrt{\sum (s_c - s_r)^2}, \tag{5}$$

where s_c is the value of next state obtained by the proposed algorithm at the given K. Moreover s_r is the actual value of the next state. The value of K obtained is the attenuation coefficient, when the function F arrives to the minimum value. Based on (4) and (5), the time when the water quality grade of one region will be reached to the highest value (namely, the water quality will be worst) can be obtained. Then, we can make some preparations to prevent the water pollution for some sensitive areas.

3.3. The Action Execution Module. In the action execution module, the regional agents select their actions by the soft-max strategy [31], which is defined as

$$P(a \mid s, Q) = \frac{e^{Q(s,a)/\tau}}{\sum_{a' \in A} e^{Q(s,a')/\tau}}, \tag{6}$$

where a is the action of agents, which is to increase or decrease the weights of indicators in this study, τ is the simulated annealing temperature parameter, which is used to control the searching rate, and $Q(s, a)$ is the Q-value function for the action-state pair. To reduce the searching times in the action-state set and accelerate the learning rate of the proposed algorithm, a punishment mechanism is introduced into the proposed algorithm. Then, the Q-value function $Q(s, a)$ is separated into a punishment Q-value and a reward Q-value function, respectively. The update algorithm of the punishment Q-value is

$$Q_c(s_t, a_t) = (1 - \alpha) Q_c(s_t, a_t) + \alpha [c + \gamma Q_{c\max}(s_{t+1}, b)]. \tag{7}$$

And the update algorithm for the cumulative reward Q-value is:

$$Q_r(s_t, a_t) = (1-\alpha) Q_r(s_t, a_t) + \alpha \left[r + \gamma Q_{r\max}(s_{t+1}, b) \right], \tag{8}$$

where $\alpha \in (0,1)$ is learning rate, $\gamma \in (0,1)$ is discount factor, and r and c are the reward value and the punishment value, respectively.

3.4. The Work Flow of the Proposed Approach. The work flow of the proposed approach for dynamic water quality assessment is summarized as follows.

(1) The initial state sets should be obtained from the water quality monitoring system, which is denoted as $S_1 = \{S_{11}, S_{12}, \ldots, S_{1n}\}$, where S_{1i} is the actual concentration value of the ith indicator. The action set of agent is $A = \{\omega_i + 1, \omega_i - 1\}$, where ω_i is the weight of the ith indicator.

(2) Initialize the value of Q_c and Q_r to 0, select a key state from the state sets, and initialize the interaction factor σ for this state to 0.

(3) Reduce the initial sate sets by (3), and a new state set can be obtained, which is denoted as $S_2 = \{S_{21}, S_{22}, \ldots, S_{2n}\}$, where S_{2i} is the concentration value of the ith indicator after being processed.

(4) Each agent calculates the real-time state P_{key} for the key state, based on the state sets after being processed. To easily compute and without losing generality, the state P_{key} is calculated by $P_{\text{key}} = S_{2\text{key}} + \sigma$, where $S_{2\text{key}}$ is the key state after being processed. The interaction factor σ can be obtained by (4) and (5).

(5) Each agent selects the optimal action under current state s according to (6) and gets the next state s' after executing the action a. Then, a reward r and punishment c can be obtained from the environment feedback.

(6) Calculate the cumulative punishment value Q_c by (7). If $Q_c \geq \theta$, then select a new action from the action sets (where θ is the upper limit for the punishment value and $\theta = 50$ in this paper). If $Q_c < \theta$, then set $Q_r(s_{t+1}, b)_{\max} = \max \sum_{b \in A} Q_r(s_{t+1}, b)$. By (8), the value of Q_r can be obtained.

(7) Repeat steps (5) and (6) to find out the weights of each group indicators, and calculate the average value of the weight for each indicator. Then, the water quality can be assessed by (1).

4. Experimental Studies

In order to test the performance of the proposed approach, some experiments are conducted. In these experiments, a water area of a lake is studied, which has six different regions (see Figure 2). The task of these experiments is to assess the water quality of the six regions. The pollution sources include the industrial pollution source, the agricultural pollution source, and the domestic pollution source. According to the characteristics of the water area, it is assumed that the main pollution indicators are Permanganate Index (COD_{Mn}), Total Nitrogen (TN), and Total Phosphorus (TP); namely, the initial state set is $S_1 = \{S_{1C}, S_{1N}, S_{1P}\}$. Then, the reduced state sets can be obtained based on the membership function (3); that is, $S_2 = \{S_{2C}, S_{2N}, S_{2P}\}$. The assessment model for water quality is $P = \omega_1 P_C + \omega_2 P_N + \omega_3 P_P$. In this paper, two experiments were conducted, where the interaction factor σ is set as $\sigma = 0$ and $\sigma \neq 0$ to test the performance of the proposed approach in the static and dynamic assessment, respectively.

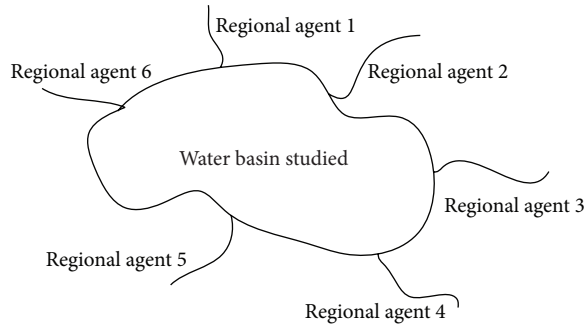

Figure 2: The schematic drawing of the water area studied.

4.1. Static Water Quality Assessment ($\sigma = 0$). In this experiment, the interaction factor σ is set as 0, which means that there is no information transmission among these regional agents in the water area. Each regional agent assesses its own water quality based on the monitoring data of various indicators. The training data set for the Q-learning algorithm is shown in Table 1, which is used to learn the weights ω_1, ω_2, and ω_3 for COD_{Mn}, TN, and TP, respectively.

The training data of S_{1C}, S_{1N}, and S_{1P} in Table 1 are collected from the monitoring points for each regional agent. The value of the S_{2C}, S_{2N}, and S_{2P} is the corresponding value of the three indicators reduced by the membership function. P is the water quality assessed by water quality experts. From these training data, the optimal weights for the three indicators can be obtained, which are $\omega_1 = 0.5$, $\omega_2 = 0.3$, and $\omega_3 = 0.2$. Based on these optimal weights above, the water quality of different regional agents can be assessed. To show the advantages of the proposed Q-learning approach (QL), it is compared with the approach based on the fuzzy comprehensive evaluation method (FC) and the comprehensive identification index evaluation method (CI). The test data and the water quality assessment results are shown in Table 2, where the test date are the indicator data collected in each monitoring point.

The results in Table 2 show that the assessment results of the water quality are almost the same by the three methods (see the water quality of the regional agent 1, agent 2, agent 3, and agent 4). The water quality assessment result for the regional agent 5 shows that the water quality assessment by the proposed method is more accurate than the method based on the fuzzy comprehensive evaluation method (FC). The proposed approach can not only give out the water quality

Table 1: The training data set for the Q-learning algorithm.

S_{1C}	S_{1N}	S_{1P}	$P_C = S_{2C}$	$P_N = S_{2N}$	$P_P = S_{2P}$	P
1.2	0.1	0.01	1.4	1.5	1.5	1.5
2.4	0.4	0.08	2.4	2.7	2.5	2.5
4.6	0.6	0.12	3.6	3.4	3.4	3.6
6.8	1.3	0.23	4.4	4.8	4.6	4.5
10.5	1.6	0.34	5.2	5.4	5.8	5.4
16.9	2.8	0.68	6.3	6.8	6.6	6.4

Table 2: The test data and results of water quality assessment.

Regional agent	COD_{Mn} (mg/L)	TN (mg/L)	TP (mg/L)	The assessment results		
				QL	FC	CI
Agent 1	2.605	0.356	0.056	2.5	II	2.4
Agent 2	2.597	0.481	0.123	2.6	II	2.8
Agent 3	2.536	0.224	0.124	2.6	II	2.5
Agent 4	6.625	1.434	0.321	4.4	IV	4.7
Agent 5	17.603	2.741	0.646	6.5	V	6.5
Agent 6	10.618	1.914	0.788	5.4	V	6.0

grade but also evaluate the pollution degree of the water in this grade. In addition, the proposed approach can assess the water quality which is worse than Grade V (see the assessment results for agent 5 in Table 2). The assessment results for agent 6 show that the assessment based on the comprehensive water quality identification index method will become incorrect, when some indicators exceed the range in the national standard. Because the weight of each indicator is considered in the assessment model, the results based on the proposed approach are more accurate.

The results of this experiment show that the proposed Q-learning approach can assess the water quality accurately and can deal with some abnormal conditions such that some indicators become abnormal. Furthermore, the proposed approach can assess the water quality of worse Grade V.

4.2. Dynamic Water Quality Assessment ($\sigma \neq 0$). To test the performance of the proposed approach in the dynamic water quality assessment task, this experiment is conducted. In this experiment, an abrupt water pollution occurs in the regional agent 1, which is an industrial pollution, and the main contamination in the waste water is COD_{Mn}. So, the interaction factor σ is used to transfer the concentration information of COD_{Mn} among these regional agents. In the dynamic water quality assessment model, $P_C = S_{2C} + \sigma$, $P_N = S_{2N}$, and $P_P = S_{2P}$, respectively.

In order to have an easy analysis, the assumptions in this experiment are as follows. (1) The value of σ is only related to the physical distance among the regional agents. (2) The change step of K in (4) is assumed as 0.1. (3) The water speed is set as 0.02 km/h and assumed as fixed. (4) The water quality of each regional agent is known before the occurrence of the abrupt water pollution accident, which is set as the same data in the first experiment (see the water quality assessed by the proposed approach in Table 2).

Table 3: The actual monitoring concentration of COD_{Mn} for each agent.

Regional agent	The distance d To agent 1 (km)	The actual concentration of COD_{Mn} (mg/L)
Agent 1	0	6.00
Agent 2	2	3.08
Agent 3	4	1.84
Agent 4	6	0.48
Agent 5	5	1.10
Agent 6	3	2.33

In this experiment, the actual concentration of COD_{Mn} in the six regional agents before this abrupt water pollution accident and the physical distance between other agents to agent 1 are listed in Table 3. The value of K can be calculated by (5) based on the information of Table 3, where K is 0.4. With this K and d, the interaction factor σ of each agent can be obtained by (4). After the water pollution accident occurs, the concentration of COD_{Mn} in the regional agent 1 increases by 1.8 mg/L. Based on the proposed approach, the change of the COD_{Mn} concentration in other regional agents and the time when the COD_{Mn} concentration reaches to the highest value are shown in Figure 3. The results of the dynamic water quality assessment for each regional agent are shown in Figure 4.

The results in Figure 4 show that the water quality becomes worse too, when the concentration of COD_{Mn} in the regional agent 1 increased. This experimental results show that the proposed approach can give out the water quality assessment for different regions in the same water area, when there is just some information about the concentration of indicator in one region. Furthermore, the proposed approach can calculate the time when the concentration of the indicator will reach to the highest value. This performance is very

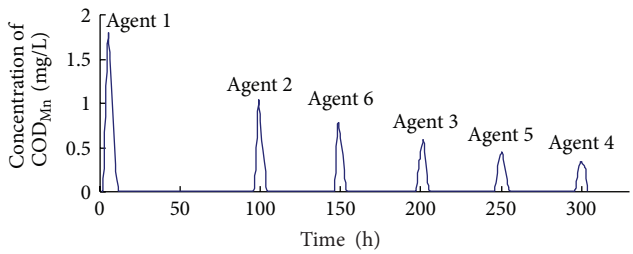

Figure 3: Changes of water quality and the diffusion time of pollutant in each agent.

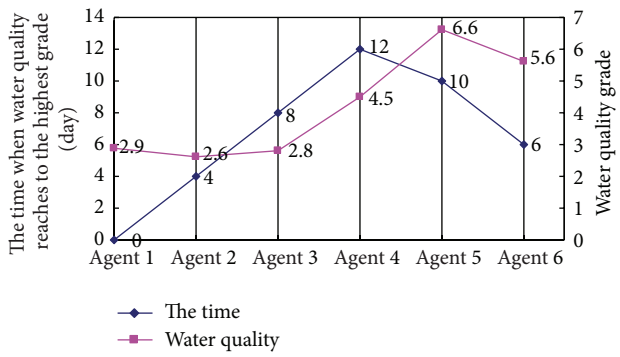

Figure 4: The dynamic assessment results of water quality for different agents.

important for the sensitive regions to prepare for the water pollution control.

5. Conclusions

The dynamic water quality assessment for a whole water basin has been investigated. A water assessment model based on multiagent technology is set up, and an improved multiagent Q-learning algorithm is proposed. The proposed approach can deal with various situations. It can deal with the water quality assessment at the static situations, and the assessment results are more accurately than the general methods. In addition, it can deal with the dynamic water quality assessment, which is very important for the water pollution prewarning and control. The feasibility and efficiency of the proposed approach have been discussed and illustrated through experimental studies. The results show that the proposed approach can assess the water quality efficiently, without any complex mathematical model nor any prior knowledge about the water environment. The proposed approach is applicable to other real-time cooperative tasks of multiagent systems, such as the fire disaster response for wide tracts of forest.

Acknowledgments

This work was supported by the National Natural Science Foundation of China (61203365), the Jiangsu Province Natural Science Foundation (BK2012149), the Open Fund of Changzhou Key Laboratory of Sensor Networks and Environmental Sensing (CZSN201102), and the Yangtze River Delta Region scientific and technological project (1259-5810200).

References

[1] Q.-G. Wang, X.-H. Zhao, W.-J. Wu, M.-S. Yang, Q. Ma, and K. Liu, "Advection-diffusion models establishment of water-pollution accident in middle and lower reaches of Hanjiang river," *Advances in Water Science*, vol. 19, no. 4, pp. 500–504, 2008.

[2] P. Tang, L. Zhao, L. Ren, Z. Zhao, and Y. Yao, "Real time monitoring of surface water pollution using microwave system," *Journal of Electromagnetic Waves and Applications*, vol. 22, no. 5-6, pp. 767–774, 2008.

[3] N. Pochai, "A numerical treatment of nondimensional form of water quality model in a nonuniform flow stream using Saulyev scheme," *Mathematical Problems in Engineering*, vol. 2011, Article ID 491317, 15 pages, 2011.

[4] S. Rodgher, H. de Azevedo, C. R. Ferrari et al., "Evaluation of surface water quality in aquatic bodies under the influence of uranium mining (MG, Brazil)," *Environmental Monitoring and Assessment*, vol. 185, no. 3, pp. 2395–2406, 2013.

[5] L. KeGang and H. KePeng, "Dynamic extension evaluation of soil and water environmental quality in metal mine and its improvement measures," *Research Journal of Chemistry and Environment*, vol. 16, no. 2, pp. 97–101, 2012.

[6] Q. Wu, C. Zhao, and Y. Zhang, "Landscape river water quality assessment by nemerow pollution index," in *Proceedings of the International Conference on Mechanic Automation and Control Engineering (MACE '10)*, pp. 2117–2120, Wuhan, China, June 2010.

[7] J. Shu, M. Hong, L. Liu, and Y. Chen, "A water quality monitoring method based on fuzzy comprehensive evaluation in wireless sensor networks," *Journal of Networks*, vol. 7, no. 1, pp. 195–202, 2012.

[8] S. Ni and Y. Bai, "Application of BP neural network model in groundwater quality evaluation," *System Engineering Theory and Practice*, vol. 20, no. 8, pp. 124–127, 2000.

[9] Z.-X. Xu, "Comprehensive water quality identification index for environmental quality assessment of surface water," *Journal of Tongji University*, vol. 33, no. 4, pp. 482–488, 2005.

[10] Y. Yun, Z. Zou, W. Feng, and M. Ru, "Quantificational analysis on progress of river water quality in China," *Journal of Environmental Sciences*, vol. 21, no. 6, pp. 770–773, 2009.

[11] S. Su, J. Zhi, L. Lou, F. Huang, X. Chen, and J. Wu, "Spatio-temporal patterns and source apportionment of pollution in Qiantang River (China) using neural-based modeling and multivariate statistical techniques," *Physics and Chemistry of the Earth*, vol. 36, no. 9–11, pp. 379–386, 2011.

[12] W. Sun and Z. Zeng, "City optimal allocation of water resources research based on sustainable development," *Advanced Materials Research*, vol. 446–449, pp. 2703–2707, 2012.

[13] G.-H. Wei, F. Liu, and L. Ma, "Fuzzy optimization of water resources project scheme based on improved grey relation analysis," in *Proceedings of the 3rd International Conference on Computer Research and Development*, vol. 4, pp. 333–336, Shanghai, China, 2011.

[14] Y. Cao, W. Yu, W. Ren, and G. Chen, "An overview of recent progress in the study of distributed multi-agent coordination," *IEEE Transactions on Industrial Informatics*, vol. 9, no. 1, pp. 427–438, 2013.

[15] C. Li, F. Wang, X. Wei, and Z. Ma, "Solution method of optimal scheme set for water resources scheduling group decision-making based on multi-agent computation," *Intelligent Automation and Soft Computing*, vol. 17, no. 7, supplement 1, pp. 871–883, 2011.

[16] G. Wen, Z. Duan, W. Yu, and G. Chen, "Consensus of multi-agent systems with nonlinear dynamics and sampled-data information: a delayed-input approach," *International Journal of Robust and Nonlinear Control*, vol. 23, no. 6, pp. 602–619, 2013.

[17] F. Leon, "Emergent behaviors in social networks of adaptive agents," *Mathematical Problems in Engineering*, vol. 2012, Article ID 857512, 19 pages, 2012.

[18] J. Wang, K. Gwebu, M. Shanker, and M. D. Troutt, "An application of agent-based simulation to knowledge sharing," *Decision Support Systems*, vol. 46, no. 2, pp. 532–541, 2009.

[19] J. Ni, C. Zhang, and L. Ren, "An intelligent decision support system of lake water pollution control based on multi-agent model," in *Proceedings of the International Conference on Computational Intelligence and Security (CIS '09)*, vol. 1, pp. 217–221, Beijing, China, December 2009.

[20] J. Ni, M. Liu, J. Fei, and H. Ma, "Reinforcement learning based multi-agent cooperation for water price forecasting decision support system," *Information-An International Interdisciplinary Journal*, vol. 15, no. 5, pp. 1889–1899, 2012.

[21] M.-L. Xu and W.-B. Xu, "Fuzzy Q-learning in continuous state and action space," *Journal of China Universities of Posts and Telecommunications*, vol. 17, no. 4, pp. 100–109, 2010.

[22] S. Zheng, J. Han, X. Luo, and J. Jiang, "Research on cooperation and reinforcement learning algorithm in multi-agent systems," *Pattern Recognition and Artificial Intelligence*, vol. 15, no. 4, pp. 453–457, 2002.

[23] A. Bonarini, A. Lazaric, F. Montrone, and M. Restelli, "Reinforcement distribution in fuzzy Q-learning," *Fuzzy Sets and Systems*, vol. 160, no. 10, pp. 1420–1443, 2009.

[24] X. Xu, C. Liu, S. X. Yang, and D. Hu, "Hierarchical approximate policy iteration with binarytree state space decomposition," *IEEE Transactions on Neural Networks*, vol. 22, no. 12, part 1, pp. 1863–1877, 2011.

[25] M. L. Littman, "Value-function reinforcement learning in Markov games," *Cognitive Systems Research*, vol. 2, no. 1, pp. 55–66, 2001.

[26] X. Xu, D. Hu, and X. Lu, "Kernel-based least squares policy iteration for reinforcement learning," *IEEE Transactions on Neural Networks*, vol. 18, no. 4, pp. 973–992, 2007.

[27] J. Wu, X. Xu, P. Zhang, and C. Liu, "A novel multi-agent reinforcement learning approach for job scheduling in Grid computing," *Future Generation Computer Systems*, vol. 27, no. 5, pp. 430–439, 2011.

[28] K. Fujita and H. Matsuo, "Multiagent reinforcement learning with the partly high-dimensional state space," *Systems and Computers in Japan*, vol. 37, no. 9, pp. 22–31, 2006.

[29] K.-D. Liu, Y.-J. Pang, and W.-G. Li, "Membership transforming algorithm in multi-index decision and its application," *Acta Automatica Sinica*, vol. 35, no. 3, pp. 315–319, 2009.

[30] X.-H. Zhao, K.-K. Zhao, Q.-Q. Wang, and F.-Q. Ma, "Research and application of reinforcement learning based on constraint MDP in coal mine," in *Proceedings of the WRI World Congress on Computer Science and Information Engineering (CSIE '09)*, vol. 4, pp. 687–691, Los Angeles, Calif, USA, March 2009.

[31] V. Derhami, V. J. Majd, and M. N. Ahmadabadi, "Exploration and exploitation balance management in fuzzy reinforcement learning," *Fuzzy Sets and Systems*, vol. 161, no. 4, pp. 578–595, 2010.

Hindawi Publishing Corporation
Mathematical Problems in Engineering
Volume 2013, Article ID 978251, 7 pages
http://dx.doi.org/10.1155/2013/978251

Research Article

Second-Order Consensus in Multiagent Systems via Nonlinear Protocol

Huan Pan,[1] Xiaohong Nian,[2] and Ling Guo[2]

[1] *School of Physics Electrical Information Engineering, Ningxia University, Yinchuan 750021, China*
[2] *School of Information Science and Engineering, Central South University, Changsha 410075, China*

Correspondence should be addressed to Huan Pan; pan198303@gmail.com

Received 8 February 2013; Accepted 15 April 2013

Academic Editor: Wenwu Yu

This paper focuses on theoretical analysis of second-order consensus in multiagent system. As an extension of the general linear protocol, a nonlinear protocol is designed for multiagent system with undirected communication topology. The nonlinear protocol is also applied to achieve reference velocity consensus. Through choosing the appropriate Lyapunov functions and using LaSalle's invariance principle, some consensus conditions are derived. Simulation examples are provided to demonstrate the effectiveness of the proposed results.

1. Introduction

Recently, consensus problems have been investigated extensively in the content of distributed coordinated control of dynamic agents, partly owning to the potential broad application in various areas. A basic and fundamental question in consensus is how to design the effective protocols (or algorithms) such that each agent can achieve a common target. Most of the consensus literatures mainly considered general linear protocols for multiagent systems. However, the relation between agents is usually not linear. In some situations, the states of multiagent systems cannot be observed directly, and some nonlinear functions about the states can be observed. Therefore, it is necessary to design nonlinear protocols for multiagent systems.

Nonlinear functions are always used to describe the coupling relations of nodes in complex networks [1–6]. On the other hand, some scholars have paid attentions to nonlinear protocols for multiagent systems recently. Bauso et al. [7] designed the distributed nonlinear protocols and proposed a game theoretical approach to solve consensus problems. Xiao et al. [8] presented a new nonlinear protocol for state consensus of multiagent system which provides faster convergence rate than the typical linear protocol [9]. Liu et al. [10] discussed the consensus problem under two nonlinear protocols with directed topology. Hui and Haddad [11] developed a thermodynamic framework for addressing consensus for nonlinear multiagent dynamical systems. Shang [12] proposed some sufficient criteria guaranteeing multiagent systems to reach a consensus in finite time under nonlinear protocols. Li and Guan [13] investigated nonlinear consensus protocols for dynamic directed networks of multiagent systems based on the central manifold reduction technique. Shi and Hong [14] considered a group of continuous-time agents with nonlinear agent dynamics and concluded that the agents can flock to a convex target set. Sepulchre [15] introduced consensus problems whose underlying state space is not a linear space but a nonlinear space. Yu et al. [16] studied the consensus problem for cooperative agents with nonlinear dynamics in a directed network. Zhou and Wang [17] derived some sufficient conditions for (global/exponential) semistability for general discrete-time nonlinear protocols.

However, it is worthwhile to note that the above-mentioned nonlinear protocols [7–13, 17] are all proposed for the first-order multiagent systems. As we all know, first-order consensus problems are mainly relative to communication topologies, but, for second-order consensus, both the interaction graph and the coupling strength affect the convergence result. Therefore, the consensus of second-order multiagent systems is more challenging and interesting and

attracts researchers' broad attention. For example, Yu et al. [18] considered a second-order consensus problem for multiagent systems with nonlinear dynamics. Furthermore, Song et al. [19] studied the second-order leader-following consensus problem of nonlinear multiagent systems. Ren [20] proposed and analyzed a consensus algorithm for double-integrator dynamics with a bounded control input under an undirected interaction graph. Though [20] extended some existing results in consensus algorithms to account for actuator saturation, saturation function which is assumed to be the hyperbolic tangent function is concrete and simple. So far as we know, there is no result about designing some nonlinear protocols for second-order multiagent systems. For this purpose, this paper mainly designs a nonlinear protocol for second-order dynamics with an undirected communication topology as an extension of the linear protocol. Then, the consensus protocol for second-order multiagent system with a group reference velocity available to each individuality is proposed.

The rest of this paper is organized as follows. Section 2 provides some preliminary graph theory, the proposed nonlinear protocol, and two useful lemmas. In Section 3, consensus problem and reference velocity consensus of a second-order multiagent system with an undirected communication topology are analyzed, respectively. Some numerical examples are given to show the effectiveness and advantage of the theoretical results in Section 4. Finally, a conclusion is provided in Section 5.

2. Notation and Preliminaries

2.1. Graph Theory. In this paper, the communication topology among n multiagents is assumed to be an undirected graph $\mathscr{G} = (\mathscr{V}, \mathscr{E}, \mathscr{A})$, where $\mathscr{V} = \{v_1, \ldots, v_n\}$ is the set of nodes, $\mathscr{E} \subseteq \mathscr{V} \times \mathscr{V}$ is the set of edges, and $\mathscr{A} = [a_{ij}] \in \mathbb{R}^{n\times n}$ represents the weighted adjacency matrix with nonnegative adjacency elements a_{ij}. The node or multiagent indexes belong to a finite index set $\mathscr{I} = \{1, 2, \ldots, n\}$. An edge $e_{ij} = (v_i, v_j) \in \mathscr{E}$ in weighted undirected graph $\mathscr{G}$ denotes that node j can receive information from i each other. The adjacency elements associated with the edges of an undirected graph are positive $a_{ij} > 0$ if $e_{ij} \in \mathscr{E}$, $a_{ij} = 0$ otherwise, and have the property that $a_{ij} = a_{ji}$, for all $i \neq j$, since e_{ij} implies e_{ji}. A path on $\mathscr{G}$ from node i_1 to i_l is a sequence of undirected edges in the form of (i_k, i_{k+1}), $k = 1, \ldots, l-1$. An undirected graph is called connected if there exists a path from any node i to any other node j.

2.2. Nonlinear Protocols for Second-Order Dynamics. Consider a second-order multiagent system with the following dynamics:

$$\begin{aligned} \dot{x}_i(t) &= v_i(t), \\ \dot{v}_i(t) &= u_i(t), \end{aligned} \quad i \in \mathscr{I}, \tag{1}$$

where $x_i(t) \in \mathbb{R}$ is the position state, $v_i(t) \in \mathbb{R}$ is the velocity state, and $u_i(t) \in \mathbb{R}$ is the control input (or protocol). Given the dynamical system (1), it is said that protocol $u_i(t)$ asymptotically solves the consensus problem, if the states of agents satisfy

$$\begin{aligned} &\lim_{t\to+\infty} \left|x_i(t) - x_j(t)\right| \\ &\quad = 0, \lim_{t\to+\infty} \left|v_i(t) - v_j(t)\right| = 0, \quad \forall i \neq j, \end{aligned} \tag{2}$$

for any $x_i(0)$ and $v_i(0)$.

The linear protocol [21, 22] is proposed as follows:

$$u_i(t) = -\sum_{j=1}^{n} a_{ij} \left[\alpha\left(x_i(t) - x_j(t)\right) + \beta\left(v_i(t) - v_j(t)\right)\right], \tag{3}$$

where a_{ij} is the (i, j) entry of the weighted adjacency matrix $\mathscr{A} \in \mathbb{R}^{n\times n}$, and parameters α, β are the coupling strengths.

It is clear that protocol (3) is based on a linear function of difference between each agent and other ones. Linear protocol (3) is simple and easy to use. However, sometimes in order to improve convergence rate or model a bounded control input, the linear protocol is often needed to be extended. Furthermore, in some cases, the state feedback $x_i(t) - x_j(t)$ may be unobservable; instead, we can observe a nonlinear function $\phi(x_i(t) - x_j(t))$ of $x_i(t) - x_j(t)$. Naturally, a nonlinear protocol for second-order system (1) is designed as follows:

$$\begin{aligned} u_i(t) = &-\sum_{j=1}^{n} a_{ij} \left(\phi\left(x_i(t) - x_j(t)\right)\right. \\ &\left. + \psi\left(v_i(t)\right) - \psi\left(v_j(t)\right)\right), \end{aligned} \tag{4}$$

where a_{ij} is the (i, j) entry of the weighted adjacency matrix $\mathscr{A}$ and $\phi(\cdot)$ and $\psi(\cdot)$ are two continuous functions.

In order to ensure existence, uniqueness of solution, and the operative property of nonlinear functions $\phi(\cdot)$ and $\psi(\cdot)$, the following sets are defined.

Definition 1. Define two function sets $\Phi = \{\phi(x) \mid \phi(x)$ is an odd function, $\phi(x)x > 0$, $\phi(x) = 0$ if and only if $x = 0\}$, and $\Psi = \{\psi(x) \mid \psi(x)$ is a continuous function and increasing about x, $\psi(x) = \psi(y)$ if and only if $x = y\}$.

At the end of this section, two useful lemmas about $\phi(\cdot)$ and $\psi(\cdot)$ are introduced.

Lemma 2. *Letting* $\mathbf{a} = [a_1 \ a_2 \ \cdots \ a_n]^T \in \mathbb{R}^n$, $\mathbf{b} = [b_1 \ b_2 \ \cdots \ b_n]^T \in \mathbb{R}^n$, *and* $C = [c_{ij}] \in \mathbb{R}^{n\times n}$, *if matrix* C *is symmetrical, that is,* $c_{ij} = c_{ji}$, *and odd function* $\phi(x) \in \Phi$, *then it is derived that*

$$\begin{aligned} &\frac{1}{2}\sum_{i=1}^{n}\sum_{j=1}^{n} c_{ij}\left(a_i - a_j\right)\phi\left(b_i - b_j\right) \\ &\quad = \sum_{i=1}^{n}\sum_{j=1}^{n} c_{ij} a_i \phi\left(b_i - b_j\right). \end{aligned} \tag{5}$$

Proof. Consider that

$$\begin{aligned}
&\frac{1}{2}\sum_{i=1}^{n}\sum_{j=1}^{n}c_{ij}\left(a_i-a_j\right)\phi\left(b_i-b_j\right)\\
&\quad=\frac{1}{2}\sum_{i=1}^{n}\sum_{j=1}^{n}c_{ij}a_i\phi\left(b_i-b_j\right)\\
&\qquad-\frac{1}{2}\sum_{i=1}^{n}\sum_{j=1}^{n}c_{ij}a_j\phi\left(b_i-b_j\right)\\
&\quad=\frac{1}{2}\sum_{i=1}^{n}\sum_{j=1}^{n}c_{ij}a_i\phi\left(b_i-b_j\right)\\
&\qquad+\frac{1}{2}\sum_{j=1}^{n}\sum_{i=1}^{n}c_{ji}a_j\phi\left(b_j-b_i\right)\\
&\quad=\sum_{i=1}^{n}\sum_{j=1}^{n}c_{ij}a_i\phi\left(b_i-b_j\right),
\end{aligned}\tag{6}$$

where the facts that $c_{ij}=c_{ji}$ and $\phi(\cdot)$ is an odd function that is, $\phi(b_j-b_i)=-\phi(b_i-b_j)$, are used to obtain the equalities. □

Using the same proof and the fact that $\psi(b_j)-\psi(b_i)=-(\psi(b_i)-\psi(b_j))$, the following lemma is obvious.

Lemma 3. *Letting* $\mathbf{a}=[a_1\ a_2\ \cdots\ a_n]^T\in\mathbb{R}^n$, $\mathbf{b}=[b_1\ b_2\ \cdots\ b_n]^T\in\mathbb{R}^n$, *and* $C=[c_{ij}]\in\mathbb{R}^{n\times n}$, *if matrix* C *is symmetrical, function* $\psi(x)\in\Psi$, *then it follows that*

$$\begin{aligned}
&\frac{1}{2}\sum_{i=1}^{n}\sum_{j=1}^{n}c_{ij}\left(a_i-a_j\right)\left(\psi\left(b_i\right)-\psi\left(b_j\right)\right)\\
&\quad=\sum_{i=1}^{n}\sum_{j=1}^{n}c_{ij}a_i\left(\psi\left(b_i\right)-\psi\left(b_j\right)\right).
\end{aligned}\tag{7}$$

3. Consensus Analysis

In this section, the consensus and reference velocity consensus of second-order multiagent system (1) with the designed nonlinear protocol will be analyzed.

3.1. Consensus with Nonlinear Protocol. Second-order multiagent system (1) with protocol (4) is written as

$$\begin{aligned}
\dot{x}_i(t)&=v_i(t),\\
\dot{v}_i(t)&=-\sum_{j=1}^{n}a_{ij}\left[\phi\left(x_i(t)-x_j(t)\right)\right.\\
&\qquad\left.+\left(\psi\left(v_i(t)\right)-\psi\left(v_j(t)\right)\right)\right].
\end{aligned}\tag{8}$$

Theorem 4. *For nonlinear protocol* (4), *suppose that functions* $\phi(\cdot)\in\Phi$ *and* $\psi(\cdot)\in\Psi$. *If information topology graph* $\mathcal{G}$ *is undirected and connected, then it is held that* $x_i(t)\to x_j(t)$, $v_i(t)\to v_j(t)$, *as* $t\to\infty$; *that is to say, multiagent system* (8) *achieves consensus asymptotically.*

Proof. Choose the following Lyapunov function:

$$V(t)=\frac{1}{2}\sum_{i=1}^{n}\sum_{j=1}^{n}a_{ij}\int_0^{x_i(t)-x_j(t)}\phi(s)\,ds+\frac{1}{2}\sum_{i=1}^{n}v_i^2(t).\tag{9}$$

The time derivative of the Lyapunov function (9) along any trajectory of (8) is

$$\begin{aligned}
&\dot{V}(t)\\
&\quad=\frac{1}{2}\sum_{i=1}^{n}\sum_{j=1}^{n}a_{ij}\left(v_i(t)-v_j(t)\right)\phi\left(x_i(t)-x_j(t)\right)\\
&\qquad-\sum_{i=1}^{n}v_i(t)\left(\sum_{j=1}^{n}a_{ij}\left[\phi\left(x_i(t)-x_j(t)\right)\right.\right.\\
&\qquad\qquad\left.\left.+\left(\psi\left(v_i(t)\right)-\psi\left(v_j(t)\right)\right)\right]\right)\\
&\quad=\sum_{i=1}^{n}\sum_{j=1}^{n}a_{ij}v_i(t)\ \phi\left(x_i(t)-x_j(t)\right)\\
&\qquad-\sum_{i=1}^{n}\sum_{j=1}^{n}a_{ij}v_i(t)\left[\phi\left(x_i(t)-x_j(t)\right)\right.\\
&\qquad\qquad\left.+\left(\psi\left(v_i(t)\right)-\psi\left(v_j(t)\right)\right)\right]\\
&\quad=-\frac{1}{2}\sum_{i=1}^{n}\sum_{j=1}^{n}a_{ij}\left(v_i(t)-v_j(t)\right)\left(\psi\left(v_i(t)\right)-\psi\left(v_j(t)\right)\right),
\end{aligned}\tag{10}$$

where the second equality and the last equality are derived from Lemmas 2 and 3, respectively. Since $(v_i(t)-v_j(t))(\psi(v_i(t))-\psi(v_j(t)))\geq 0$ and the information topology graph $\mathcal{G}$ is connected, it is derived that

$$-\frac{1}{2}\sum_{i=1}^{n}\sum_{j=1}^{n}a_{ij}\left(v_i(t)-v_j(t)\right)\left(\psi\left(v_i(t)\right)-\psi\left(v_j(t)\right)\right)\leq 0;\tag{11}$$

that is to say, $\dot{V}(t)\leq 0$. Letting $\dot{V}(t)\equiv 0$, it is easily seen that $v_i(t)\equiv v_j(t)$ and $\dot{v}_i(t)\equiv\dot{v}_j(t)$. Therefore, it follows that $\dot{v}(t)\in\mathrm{Span}(\mathbf{1}\times\varsigma)$, where ς is a constant and $v(t)=[v_1(t)\ v_2(t)\ \cdots\ v_n(t)]^{\mathrm{T}}$. Furthermore, from $v_i(t)\equiv v_j(t)$, it is obtained that

$$\dot{v}_i(t)\equiv-\sum_{j=1}^{n}a_{ij}\left(\phi\left(x_i(t)-x_j(t)\right)\right),\tag{12}$$

$$(\mathbf{1}\times\varsigma)^{\mathrm{T}}\dot{v}_i(t)\equiv-\varsigma\sum_{i=1}^{n}\sum_{j=1}^{n}a_{ij}\left(\phi\left(x_i(t)-x_j(t)\right)\right).\tag{13}$$

Since information topology graph is undirected, that is, $a_{ij}=a_{ji}$, and $\phi(x_i(t)-x_j(t))=-\phi(x_j(t)-x_i(t))$, it is held that

$$\sum_{i=1}^{n}\sum_{j=1}^{n}a_{ij}\phi\left(x_i(t)-x_j(t)\right)\equiv 0,\tag{14}$$

which implies that $(\mathbf{1} \times \varsigma)^{\mathrm{T}} \dot{v}(t) \equiv 0$. Thus, it means that $\dot{v}(t)$ is orthogonal to $\mathbf{1} \times \varsigma$. From the above discussion, it is concluded that $\dot{v}(t) \equiv 0$ which in turn implies that $-\sum_{j=1}^{n} a_{ij}\phi(x_i(t) - x_j(t)) \equiv 0$ from (12). Furthermore, it is obtained that $-\sum_{i=1}^{n} x_i(t) \sum_{j=1}^{n} a_{ij}\phi(x_i(t) - x_j(t)) \equiv 0$ which implies that

$$-\frac{1}{2}\sum_{i=1}^{n}\sum_{j=1}^{n} a_{ij}\left(x_i(t) - x_j(t)\right)\phi\left(x_i(t) - x_j(t)\right) \equiv 0, \tag{15}$$

from Lemma 2. For $\phi(x)x > 0$ and information topology graph is connected, from (15), it is derived that

$$a_{ij}\left(x_i(t) - x_j(t)\right)\phi\left(x_i(t) - x_j(t)\right) \equiv 0, \quad \forall i \neq j. \tag{16}$$

As a result, it follows that $x_i(t) \equiv x_j(t)$, for all $i \neq j$. By LaSalle's invariance principle, it is concluded that $x_i(t) \to x_j(t)$, $v_i(t) \to v_j(t)$, for all $i \neq j$, as t $\to \infty$. The proof is ended. □

When nonlinear protocol (4) is simplified as follows:

$$u_i(t) = -\psi\left(v_i(t)\right) - \sum_{j=1}^{n} a_{ij}\phi\left(x_i(t) - x_j(t)\right), \tag{17}$$

and the Lyapunov function (9) is chosen, the following conclusion is easily obtained.

Corollary 5. *If the information topology graph $\mathcal{G}$ is undirected and connected, nonlinear functions $\phi(\cdot) \in \Phi$ and $\psi \in \Psi$, then the multiagent system* (1) *with protocol* (17) *can achieve consensus, namely, $x_i(t) \to x_j(t)$, $v_i(t) \to v_j(t) \to 0$, asymptotically as $t \to \infty$.*

In practice, since the position of each agent is easily measured relatively, nonlinear function $\phi(x)$ in protocol (4) *can be assumed to be $\phi(x) = x$. Therefore, letting $\phi(x_i(t) - x_j(t)) = x_i(t) - x_j(t)$, protocol* (4) *is reduced to*

$$u_i(t) = -\sum_{j=1}^{n} a_{ij}\left(x_i(t) - x_j(t) + \psi\left(v_i(t)\right) - \psi\left(v_j(t)\right)\right). \tag{18}$$

Applying protocol (18) *to system* (1), *the following corollary is derived from Theorem 4 directly.*

Corollary 6. *For nonlinear protocol* (18), *suppose the function $\psi(\cdot) \in \Psi$. If the information topology graph $\mathcal{G}$ is undirected and connected, multiagent system* (1) *with protocol* (18) *achieves consensus asymptotically, namely, $x_i(t) \to x_j(t)$, $v_i(t) \to v_j(t)$, as $t \to \infty$.*

Remark 7. The second-order multiagent system with linear protocol can be written as compact matrix form, and the consensus conditions can be derived by analysing the eigenvalues of the compact matrix [22]. When the second-order multiagent system achieves consensus, the positions and velocities will, respectively, converge to a constant value which is relative to the initial position and velocity and the left eigenvector of the Laplacian matrix (see [21, 22]).

However, the nonlinear protocol is different from the linear protocol. The second-order multiagent system with nonlinear protocol cannot be written as a compact matrix form. So, the proof of consensus is different from the method used in the linear protocol and is more difficult. When the consensus of the second-order multiagent system with nonlinear protocol is reached, the value which the positions and velocities converge to cannot be decided. The value is relative to the nonlinear function, the communication graph, and the initial position and velocity.

3.2. Consensus with Group Reference Velocity. In practice, given a reference velocity $v^*(t)$, the positions and velocities of the agents in multiagent system (1) are often required to achieve consensus and converge to $v^*(t)$; that is, $x_i(t) \to x_j(t)$, $v_i(t) \to v_j(t) \to v^*(t)$, for all $i \neq j$. Hence, the following nonlinear protocol is designed with a group reference velocity $v^*(t)$ as

$$\begin{aligned} u_i(t) = {} & \dot{v}^*(t) - \left(\psi\left(v_i(t)\right) - \psi\left(v^*(t)\right)\right) \\ & - \sum_{j=1}^{n} a_{ij}\left(\phi\left(x_i(t) - x_j(t)\right)\right. \\ & \left. + \psi\left(v_i(t)\right) - \psi\left(v_j(t)\right)\right). \end{aligned} \tag{19}$$

Given a group reference velocity $v^*(t)$, second-order multiagent system (1) with protocol (19) is expressed as

$$\begin{aligned} \dot{x}_i(t) &= v_i(t), \\ \dot{v}_i(t) &= \dot{v}^*(t) - \left(\psi\left(v_i(t)\right) - \psi\left(v^*(t)\right)\right) \\ &\quad - \sum_{j=1}^{n} a_{ij}\left(\phi\left(x_i(t) - x_j(t)\right)\right. \\ &\quad \left. - \left(\psi\left(v_i(t)\right) - \psi\left(v_j(t)\right)\right)\right). \end{aligned} \tag{20}$$

Theorem 8. *For nonlinear protocol* (19), *consider functions $\phi(\cdot) \in \Phi$ and $\psi(\cdot) \in \Psi$. When information topology graph $\mathcal{G}$ is undirected and connected, multiagent system* (20) *achieves consensus; that is, $x_i(t) \to x_j(t)$, $v_i(t) \to v_j(t) \to v^*(t)$, as $t \to \infty$.*

Proof. Letting $\tilde{v}_i(t) = v_i(t) - v^*(t)$, $\tilde{x}_i(t) = x_i(t) - \int_0^t v^*(s)ds$, system (20) is rewritten as

$$\begin{aligned} \dot{\tilde{x}}_i(t) &= \tilde{v}_i(t), \\ \dot{\tilde{v}}_i(t) &= -\left(\psi\left(v_i(t)\right) - \psi\left(v^*(t)\right)\right) \\ &\quad - \sum_{j=1}^{n} a_{ij}\left(\phi\left(\tilde{x}_i(t) - \tilde{x}_j(t)\right)\right. \\ &\quad \left. - \left(\psi\left(v_i(t)\right) - \psi\left(v_j(t)\right)\right)\right). \end{aligned} \tag{21}$$

Choose the following Lyapunov function:

$$V(t) = \frac{1}{2}\sum_{i=1}^{n}\sum_{j=1}^{n} a_{ij}\int_0^{\tilde{x}_i(t)-\tilde{x}_j(t)} \phi(s)\,ds + \frac{1}{2}\sum_{i=1}^{n}\tilde{v}_i^2(t). \tag{22}$$

Taking the derivative of the Lyapunov function (22) with respect to t along the trajectory of (21) yields

$$\begin{aligned}\dot{V}(t) &= \frac{1}{2}\sum_{i=1}^{n}\sum_{j=1}^{n}a_{ij}\left(\tilde{v}_i(t)-\tilde{v}_j(t)\right)\phi\left(\tilde{x}_i(t)-\tilde{x}_j(t)\right) \\ &\quad -\sum_{i=1}^{n}\tilde{v}_i(t)\Bigg(\left(\psi\left(v_i(t)\right)-\psi\left(v^*(t)\right)\right) \\ &\qquad +\sum_{j=1}^{n}a_{ij}\left(\phi\left(\tilde{x}_i(t)-\tilde{x}_j(t)\right)\right. \\ &\qquad\qquad \left.+\left(\psi\left(v_i(t)\right)-\psi\left(v_j(t)\right)\right)\right)\Bigg).\end{aligned} \tag{23}$$

From Lemma 2, it is obtained that

$$\begin{aligned}\dot{V}(t) &= \frac{1}{2}\sum_{i=1}^{n}\sum_{j=1}^{n}a_{ij}\left(\tilde{v}_i(t)-\tilde{v}_j(t)\right)\phi\left(\tilde{x}_i(t)-\tilde{x}_j(t)\right) \\ &\quad -\frac{1}{2}\sum_{i=1}^{n}\sum_{j=1}^{n}a_{ij}\left(\tilde{v}_i(t)-\tilde{v}_j(t)\right)\phi\left(\tilde{x}_i(t)-\tilde{x}_j(t)\right) \\ &\quad -\sum_{i=1}^{n}\tilde{v}_i(t)\left(\psi\left(v_i(t)\right)-\psi\left(v^*(t)\right)\right) \\ &\quad -\frac{1}{2}\sum_{i=1}^{n}\sum_{j=1}^{n}a_{ij}\left(\tilde{v}_i(t)-\tilde{v}_j(t)\right) \\ &\quad \times\left(\psi\left(v_i(t)\right)-\psi\left(v_j(t)\right)\right) \\ &= -\sum_{i=1}^{n}\left(v_i(t)-v^*(t)\right)\left(\psi\left(v_i(t)\right)-\psi\left(v^*(t)\right)\right) \\ &\quad -\frac{1}{2}\sum_{i=1}^{n}\sum_{j=1}^{n}a_{ij}\left(v_i(t)-v_j(t)\right) \\ &\quad \times\left(\psi\left(v_i(t)\right)-\psi\left(v_j(t)\right)\right).\end{aligned} \tag{24}$$

Since function $\psi(\cdot)\in\Psi$ and the information topology graph $\mathcal{G}$ is undirected and connected, there exist the following facts that

$$\begin{aligned}&-\sum_{i=1}^{n}\left(v_i(t)-v^*(t)\right)\left(\psi\left(v_i(t)\right)-\psi\left(v^*(t)\right)\right)\le 0, \\ &-\frac{1}{2}\sum_{i=1}^{n}\sum_{j=1}^{n}a_{ij}\left(v_i(t)-v_j(t)\right)\left(\psi\left(v_i(t)\right)-\psi\left(v_j(t)\right)\right)\le 0.\end{aligned} \tag{25}$$

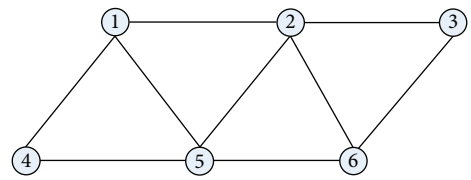

Figure 1: Communication topology graph.

Combing (25), it follows that $\dot{V}(t)\le 0$. When $\dot{V}(t)\equiv 0$, it is clear that $v_i(t)\equiv v_j(t)$, $v_i(t)\equiv v^*(t)$. Then, it is derived that

$$-\sum_{j=1}^{n}\phi\left(\tilde{x}_i(t)-\tilde{x}_j(t)\right)\equiv 0, \tag{26}$$

$$-\sum_{i=1}^{n}\tilde{x}_i(\mathrm{t})\sum_{j=1}^{n}a_{ij}\phi\left(\tilde{x}_i(t)-\tilde{x}_j(t)\right)\equiv 0. \tag{27}$$

Note that (27) implies that

$$-\frac{1}{2}\sum_{i=1}^{n}\sum_{j=1}^{n}a_{ij}\left(\tilde{x}_i(t)-\tilde{x}_j(t)\right)\phi\left(\tilde{x}_i(t)-\tilde{x}_j(t)\right)\equiv 0, \tag{28}$$

from Lemma 2. Due to the connected information graph $\mathcal{G}$, it is derived from (28) that

$$\left(\tilde{x}_i(t)-\tilde{x}_j(t)\right)\phi\left(\tilde{x}_i(t)-\tilde{x}_j(t)\right)\equiv 0. \tag{29}$$

As a result, it is concluded that $\tilde{x}_i(t)\equiv\tilde{x}_j(t)$ which is equivalent to $x_i(t)\equiv x_j(t)$. Making use of LaSalle's invariance principle, it is concluded that $x_i(t)\to x_j(t)$, $v_i(t)\to v_j(t)\to v^*(t)$, as $t\to\infty$. The proof is completed. □

4. Numerical Examples

In this section, a number of simulations are given to illustrate the effectiveness of the results proposed in the paper.

Example 9. Consider the communication topology graph $\mathcal{G}$ as described in Figure 1. Graph $\mathcal{G}$ has eight nodes, and the edges denote the information interchange between agents. For simplicity, it is assumed that graph $\mathcal{G}$ has 0-1 weights. To simulate numerical examples, choose

$$\phi(x)=\begin{cases}x^2 & \text{if } x>1,\\ \sqrt{x} & \text{if } 0<x\le 1,\\ -\sqrt{-x} & \text{if } -1<x\le 0,\\ -x^2 & \text{if } x\le -1,\end{cases} \tag{30}$$

and $\psi(x)=x^3$ in the nonlinear protocol (4), and it is clear that $\phi\in\Phi$ and $\psi\in\Psi$. Therefore, the nonlinear protocol (4) can be achieved asymptotically for multiagent system (1) from Theorem 4. Figure 2 shows that the velocity and position trajectories of second-order multiagent system (8) converge to consensus, respectively. In addition, Figure 3 describes that both the velocity and position trajectories of second-order multiagent system (1) with protocol (18) achieve consensus.

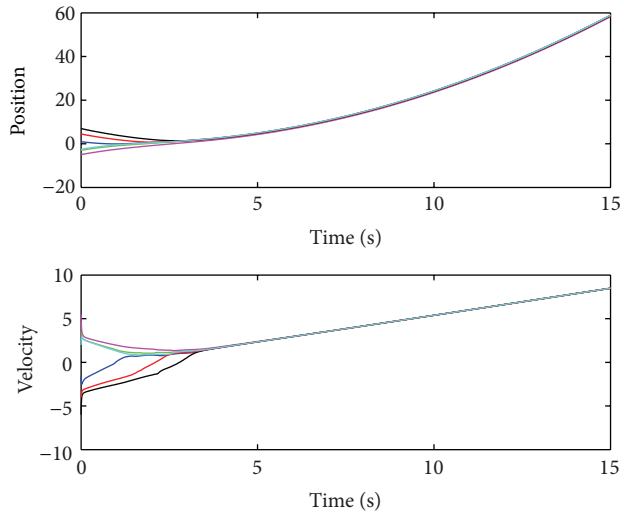

Figure 2: State trajectories of multiagent system (8).

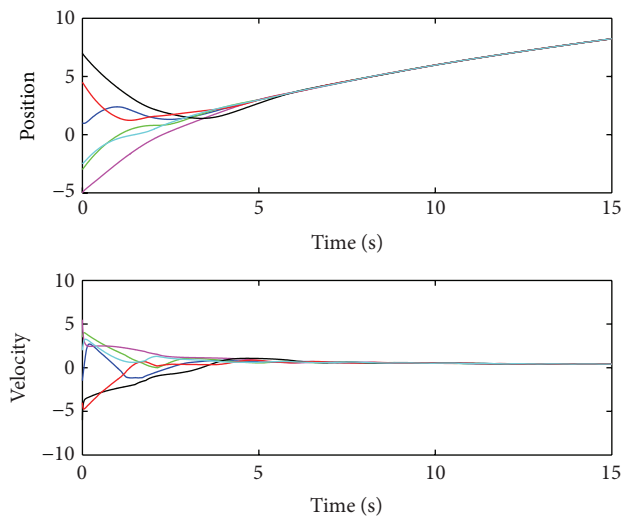

Figure 3: State trajectories of multiagent system (1) with protocol (18).

Choose a reference velocity $v^*(t) = \sin(3 * t) + \cos(t)$, and using protocol (19), multiagent system (1) can achieve consensus asymptotically. Figure 4 describes the trajectories of velocity and position of multiagent system (1) with protocol (19), respectively. It is seen that the trajectories of velocity follow the reference velocity $v^*(t)$ successfully.

5. Conclusions

This paper provided consensus analysis for the second-order multiagent system with nonlinear protocol. As an extension of linear protocols, a nonlinear protocol was designed to achieve consensus. In addition, the protocol was also used to achieve reference velocity consensus for second-order multiagent system. The analysis mainly relied on some tools from algebraic graph and control theory. Through using the Lyapunov theory and LaSalle's invariance principle, sufficient conditions for consensus are derived. Simulation examples show that when the nonlinear function satisfies the assumption, the second-order multiagent can achieve consensus and reference velocity consensus.

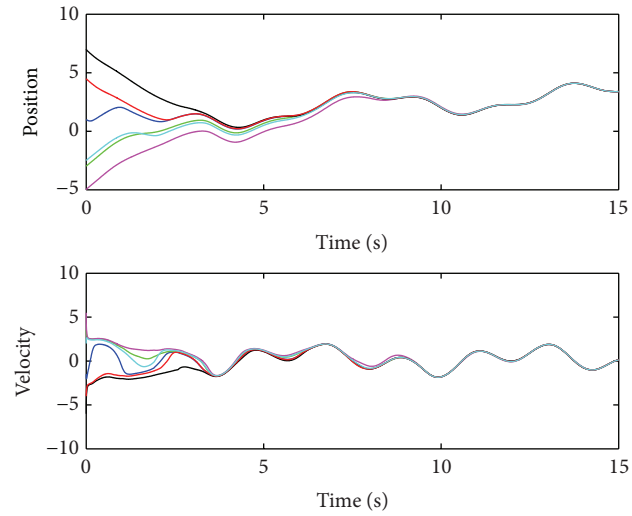

Figure 4: State trajectories of multiagent system (20).

Acknowledgment

This work was supported by the Research Funds of Ningxia University Introducing Talent (no. BQD2012004).

References

[1] W. Lu, F. Atay, and J. Jost, "Synchronization of discrete-time dynamical networks with time-varying couplings," *SIAM Journal on Mathematical Analysis*, vol. 39, no. 2, pp. 1231–1259, 2007.

[2] S. Barbarossa and G. Scutari, "Decentralized maximum-likelihood estimation for sensor networks composed of nonlinearly coupled dynamical systems," *IEEE Transactions on Signal Processing*, vol. 55, no. 7, part 1, pp. 3456–3470, 2007.

[3] T. Chen and Z. Zhu, "Exponential synchronization of nonlinear coupled dynamical networks," *International Journal of Bifurcation and Chaos in Applied Sciences and Engineering*, vol. 17, no. 3, pp. 999–1005, 2007.

[4] W. Lu and T. Chen, "Synchronization of coupled connected neural networks with delays," *IEEE Transactions on Circuits and Systems. I.*, vol. 51, no. 12, pp. 2491–2503, 2004.

[5] X. Liu and T. Chen, "Exponential synchronization of nonlinear coupled dynamical networks with a delayed coupling," *Physica A*, vol. 381, no. 15, pp. 82–92, 2007.

[6] W. Yu, G. Chen, J. Lü, and J. Kurths, "Synchronization via pinning control on general complex networks," *SIAM Journal on Control and Optimization*, vol. 51, no. 2, pp. 1395–1416, 2013.

[7] D. Bauso, L. Giarré, and R. Pesenti, "Non-linear protocols for optimal distributed consensus in networks of dynamic agents," *Systems & Control Letters*, vol. 55, no. 11, pp. 918–928, 2006.

[8] F. Xiao, L. Wang, and Y. Jia, "Fast information sharing in networks of autonomous agents," in *Proceedings of the American*

Control Conference (ACC '08), pp. 4388–4393, Seattle, Wash, USA, June 2008.

[9] R. Olfati-Saber and R. M. Murray, "Consensus problems in networks of agents with switching topology and time-delays," *IEEE Transactions on Automatic Control*, vol. 49, no. 9, pp. 1520–1533, 2004.

[10] X. Liu, T. Chen, and W. Lu, "Consensus problem in directed networks of multi-agents via nonlinear protocols," *Physics Letters A*, vol. 373, no. 35, pp. 3122–3127, 2009.

[11] Q. Hui and W. M. Haddad, "Distributed nonlinear control algorithms for network consensus," *Automatica*, vol. 44, no. 9, pp. 2375–2381, 2008.

[12] Y. Shang, "On consensus of nonlinear multi-agent systems under directed interaction topologies," in *Proceedings of the International Conference on Cyber-Enabled Distributed Computing and Knowledge Discovery (CyberC '09)*, pp. 128–131, Beijing, China, October 2009.

[13] M. Li and X. Guan, "Nonlinear consensus protocols for multi-agent systems based on centre manifold reduction," *Chinese Physics B*, vol. 18, no. 8, pp. 3355–3366, 2009.

[14] G. Shi and Y. Hong, "Global target aggregation and state agreement of nonlinear multi-agent systems with switching topologies," *Automatica*, vol. 45, no. 5, pp. 1165–1175, 2009.

[15] R. Sepulchre, "Consensus on nonlinear spaces," *Annual Reviews in Control*, vol. 35, no. 1, pp. 56–64, 2011.

[16] W. Yu, G. Chen, and M. Cao, "Consensus in directed networks of agents with nonlinear dynamics," *IEEE Transactions on Automatic Control*, vol. 56, no. 6, pp. 1436–1441, 2011.

[17] J. Zhou and Q. Wang, "Distributed discrete-time nonlinear consensus protocols," in *Proceedings of the 48th IEEE Conference on Decision and Control and 28th Chinese Control Conference (CDC/CCC '09)*, pp. 4759–4764, Shanghai, China, December 2009.

[18] W. Yu, G. Chen, M. Cao, and J. Kurths, "Second-Order consensus for multiagent systems with directed topologies and nonlinear dynamics," *IEEE Transactions on Systems, Man, and Cybernetics B*, vol. 40, no. 3, pp. 881–891, 2010.

[19] Q. Song, J. Cao, and W. Yu, "Second-order leader-following consensus of nonlinear multi-agent systems via pinning control," *Systems & Control Letters*, vol. 59, no. 9, pp. 553–562, 2010.

[20] W. Ren, "On consensus algorithms for double-integrator dynamics," *IEEE Transactions on Automatic Control*, vol. 53, no. 6, pp. 1503–1509, 2008.

[21] W. Ren and E. Atkins, "Distributed multi-vehicle coordinated control via local information exchange," *International Journal of Robust and Nonlinear Control*, vol. 17, no. 10-11, pp. 1002–1033, 2007.

[22] W. Yu, G. Chen, and M. Cao, "Some necessary and sufficient conditions for second-order consensus in multi-agent dynamical systems," *Automatica*, vol. 46, no. 6, pp. 1089–1095, 2010.